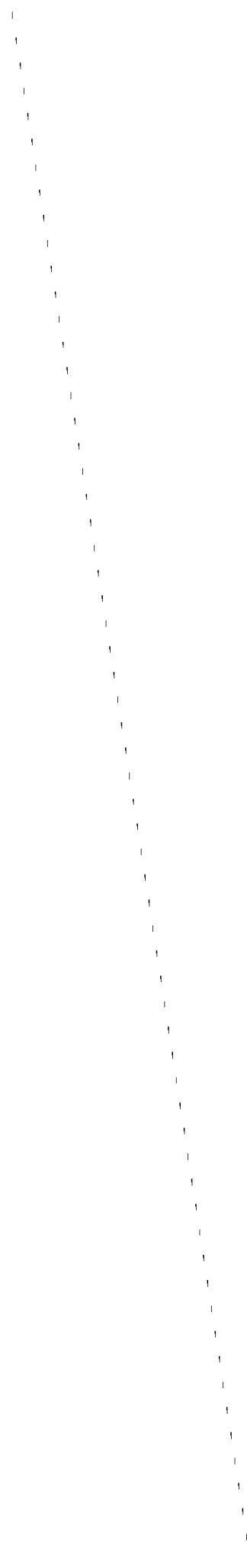


Proceedings of the
REVIEW MEETING
U.S.-Japan Cooperative Research Program in
EARTHQUAKE ENGINEERING
with Emphasis on
THE SAFETY OF SCHOOL BUILDINGS

August 18-20, 1975
Honolulu, Hawaii, U.S.A.

Handwritten notes or scribbles in the top left corner of the page.



Proceedings
of the
REVIEW MEETING
U.S.-Japan Cooperative Research Program
in
EARTHQUAKE ENGINEERING
with Emphasis on
THE SAFETY OF SCHOOL BUILDINGS

August 18-20, 1975
Honolu'u, Hawaii, U.S.A.

Compiled by
THE JAPAN EARTHQUAKE ENGINEERING PROMOTION SOCIETY
Tokyo, Japan
1976

Any opinions, findings, conclusions
or recommendations expressed in this
publication are those of the author(s)
and do not necessarily reflect the views
of the National Science Foundation.

The statements made and the opinions expressed in the following papers are those of the authors, each of whom is alone responsible for his particular contribution.

Published by

THE JAPAN EARTHQUAKE ENGINEERING PROMOTION SOCIETY
c/o INTERNATIONAL INSTITUTE OF SEISMOLOGY
AND EARTHQUAKE ENGINEERING
3-28-8, Hyakunin-cho, Shinjuku-ku, Tokyo 160, Japan

Printed by and also purchasable at

ASSOCIATION FOR SCIENCE DOCUMENTS INFORMATION
c/o TOKYO INSTITUTE OF TECHNOLOGY
2-12-1, Oh-okayama, Meguro-ku, Tokyo 152, Japan

PREFACE

A few preliminary remarks are in order to introduce these PROCEEDINGS of the REVIEW MEETING of the U.S.-JAPAN COOPERATIVE RESEARCH PROGRAM IN EARTHQUAKE ENGINEERING WITH EMPHASIS ON THE SAFETY OF SCHOOL BUILDINGS.

This cooperative program was initiated following the 1968 Tokachi-Oki earthquake in Hokkaido, Japan, during which numerous reinforced concrete school buildings of modern design suffered heavy damages. The design of these school buildings, based on a seismic coefficient of 0.18 which is very high in comparison with world standards, more than satisfied all of the earthquake requirements of California schools at that time. Thus, it was apparent that every effort should be made to improve new designs through (1) learning as much as possible from the experience of the Tokachi-Oki earthquake, (2) reviewing and considering possible changes in building codes, (3) improving design and construction practices, and (4) initiating programs of needed research.

In the interest of improving seismic safety of school buildings, a joint seminar under the sponsorship of the U.S.-Japan Cooperative Science Program was held in Sendai, Japan, during the period 21-26 September 1970 for the purpose of (1) reviewing, in depth, the causes of damage sustained by modern school buildings during the Tokachi-Oki earthquake, (2) examining design and construction methods, and (3) identifying and defining needed programs of research which would be conducted most effectively on a cooperative basis. The official participants of this seminar were H. Aoyama, University of Tokyo, R. Hanson, University of Michigan, P. Jennings, California Institute of Technology, H. Kobayashi, Tokyo Institute of Technology, K. Lee, University of California, Los Angeles, K. Ogura, Meiji University, K. Ohno, Hokkaido University, J. Penzien, University of California, Berkeley, J. Roesset, Massachusetts Institute of Technology, T. Shiga, Tohoku University, M. Sozen, University of Illinois, H. Umemura, University of Tokyo, and M. Wakabayashi, Kyoto University. J. Penzien and H. Umemura served as coordinators of the seminar. The proceedings of this seminar (Proceedings of the U.S.-Japan Seminar on Earthquake Engineering with emphasis on the Safety of School Buildings - 466 pgs.) were published by the Japan Earthquake Engineering Promotion Society.

A second joint seminar under the sponsorship of the U.S.-Japan Cooperative Science Program was held in Berkeley, California, during the period 4-8 September 1973 for purposes of reviewing (1) the causes of damages sustained by reinforced concrete structures during the 1971 San Fernando earthquake, (2) current research on earthquake resistant design, (3) the safety of existing structures and means of upgrading their resistance, and (4) post-earthquake damage and adequacy of repaired structures. The official participants of this seminar were H. Aoyama, University of Tokyo, V. Bertero, University of California, Berkeley, B. Bresler, University of California, Berkeley, W. Corley, Portland Cement Association, C. A. Cornell, Massachusetts Institute of Technology, R. Hanson, University of Michigan, M. Hirose, Building Research Institute, S. Ikeda, Tokyo Metropolitan University, P. Jennings, California Institute of Technology, J. Jirsa, University of Texas, K. Kubo, University of Tokyo, A. Mattock, University of Washington, J. Penzien, University of California, Berkeley, Y. Ozaka, Tohoku University, M. Sozen, University of Illinois, and M. Wakabayashi, Kyoto University. B. Bresler and K. Kubo served as coordinators of the seminar.

Prompted by informal discussions held at the Sendai seminar, a U.S.-Japan Cooperative Research Program on Earthquake Engineering with Emphasis on the Safety of School Buildings was later established under the U.S.-Japan Cooperative Science Program for the period May 1973 - October 1975. The cooperative research in this program was conducted by B. Bresler, T. Okada, J. Penzien, and M. Murakami at the University of California, Berkeley, by A. Shibata and M. Sozen at the University of Illinois, and by R. Hanson and T. Nishikawa at the University of Michigan. J. Penzien and H. Umemura served as coordinators of this program. Also under the U.S.-Japan Cooperative Science program, J. Penzien and H. Umemura conducted a 6-month cooperative research program at the University of Tokyo.

Since the ultimate objective of the cooperative research program was to propose advanced earthquake resistant design procedures for reinforced concrete school buildings, a review meeting was held at the East-West Center, University of Hawaii during the period 18-20 August 1975 to review the results of the program and to formulate seismic design criteria and procedures. The 19 technical papers included in these proceedings were presented at the meeting to form a basis for the review. The official participants of this meeting were H. Aoyama, University of Tokyo, B. Bresler, University of California, Berkeley, R. Hanson, University of Michigan, P. Jennings, California Institute of Technology, S. Kokusho, Tokyo Institute of Technology, T. Okada, University of Tokyo, J. Penzien, University of California, Berkeley, A. Shibata, Tohoku University, M. Sozen, University of Illinois, and H. Umemura, University of Tokyo. J. Penzien and H. Umemura served as coordinators of this meeting.

On behalf of all participants of the joint seminars, the cooperative research program, and the review meeting, we wish to express our sincere thanks and appreciation to the National Science Foundation and the Japan Society for the Promotion of Science for their financial support of all activities mentioned above which were sponsored under the U.S.-Japan Cooperative Science Program.

J. Penzien

H. Umemura

CLOSING REMARKS

by

Hajime Umemura^I

The objective of the U.S.-Japan Cooperative Research Program on the Earthquake Engineering With Emphasis on Safety of School Buildings was to propose a rational method for the earthquake resistant design of reinforced concrete school buildings. For this purpose, the U.S.-Japan joint projects as well as the projects on individual basis in each country have been carried out since 1973.

In order to review the progress of the program, the Review Meeting was held at Honolulu, Hawaii, U.S.A., during August 18-20, 1975, and 19 papers were presented and discussed by both U.S. and Japanese participants in the following five sessions:

- Session I: Earthquake Ground Motion for Seismic Design
- Session II: Dynamic Testing and Response of Reinforced Concrete Buildings
- Session III: Evaluation of the Seismic Safety of Existing Reinforced Concrete School Buildings (A)
- Session IV: Evaluation of the Seismic Safety of Existing Reinforced Concrete School Buildings (B)
- Session V: Strengthening of Existing Buildings and Repair of Damaged Buildings

The presented papers were refined after the discussions at the review meeting and compiled in these proceedings. The proceedings are the final results of the program and our proposal for the future earthquake resistant design of the buildings, while they do not appear in a familiar form like a building code.

At the beginning stage of the program, our attention was paid to the design of new buildings, the evaluation of the seismic safety of existing buildings and the strengthening and repair of existing or damaged buildings, independently. However, we gradually recognized that a common important problem was hidden among them, i.e., "how to evaluate the seismic safety of buildings". The discussion at the review meeting was done from this point of view and all papers were related with solving the common problem. This is why the proceedings are the proposal for the future earthquake resistant design.

The following is a brief summary of each session with emphasis on the relationship with the earthquake resistant design of buildings:

-
1. Professor, Faculty of Engineering, University of Tokyo, Tokyo, Japan

Three papers presented in the session I deal with the characteristics of the earthquake ground motions which are important to decide the criteria for evaluating the seismic safety.

Five papers in the session II which discuss the structural performance of reinforced concrete members and buildings subjected to earthquake ground motion contribute to determine the criteria, to make reasonable analytical models of buildings and to develop analytical methods for earthquake response of buildings.

The recent trend in developing the earthquake resistant design method in Japan is reported in the session III. The methodologies for evaluating the seismic safety of existing buildings are also discussed in the session III. They have been developed independently, but based on the similar concept which starts from a simple method like field investigation or estimation of a seismic safety index as wall-column area ratio and gradually employs more elaborated analysis considering the strength and ductility of the buildings. The methods are applicable also to the design of new buildings with some modifications.

Four practical methods for evaluating the non-linear response of buildings are proposed in the session IV, which are useful both for the design of new buildings and for the evaluation of seismic safety of existing buildings.

The methods for strengthening the buildings which are evaluated unsafe and the method for repairing the earthquake damaged buildings are suggested in the session V.

Another successful result of the program was the exchange of the researchers between U.S. and Japan greatly contributed to the progress of the program. Six of nineteen papers presented to the review meeting were based on the joint projects performed by the exchanges of the researchers.

I, as one of the coordinators, express my sincere gratitude to the National Science Foundation and the Japan Society for the Promotion of Science.

REVIEW MEETING

U.S. - JAPAN COOPERATIVE RESEARCH PROGRAM IN EARTHQUAKE
ENGINEERING WITH EMPHASIS ON THE SAFETY OF SCHOOL BUILDINGS

East-West Center
Honolulu, Hawaii, August 18-20, 1975

Sunday, August 17, 1975

6:30 - 8:30 p.m. Reception

SESSION I

Monday, August 18, 9:30 - 12:00 noon
Co-Chairmen: H. Aoyama and M. Sozen

9:30 - 9:40 a.m. Welcome - N. Nielsen

9:40 - 10:00 a.m. Opening Remarks - H. Umemura and J. Penzien

EARTHQUAKE GROUND MOTION FOR SEISMIC DESIGN

10:00 - 10:40 a.m. (1) Strong Ground Motion and Seismic Design
Criteria - P. Jennings

10:40 - 11:20 a.m. (2) Earthquake Motion Measurements and Analysis
of Pile-Supported Building and Its Surrounding
Soil - S. Kawamura

11:20 - 12:00 p.m. (3) Characteristics of Three-Dimensional Ground
Motions, San Fernando Earthquake - T. Kubo

12:00 - 1:20 p.m. Lunch

SESSION II

Monday, August 18, 1:20 - 5:00 p.m.
Co-Chairmen: B. Bresler and S. Kokusho

1:20 - 2:00 p.m. (4) Inelastic Cyclic Behavior of Reinforced
Concrete Flexural Members - J. Penzien

2:00 - 2:40 p.m. (5) Seismic Design Implications of Hysteretic
Behavior of Reinforced Concrete Elements
under High Shear - V. Bertero

2:40 - 3:20 p.m. (6) Hysteretic Behavior of Reinforced Concrete
Shear Walls - A. Shibata

3:20 - 3:40 p.m. Coffee Break

- 3:40 - 4:20 p.m. (7) Structural Walls Subjected to Simulated Earthquakes - M. Sozen
- 4:20 - 5:00 p.m. (8) Experimental and Analytical Study of Reinforced Concrete Chimneys - Y. Omote

SESSION III

Tuesday, August 19, 9:00 - 12:00 noon
Co-Chairmen: R. Hanson and A. Shibata

EVALUATION OF THE SEISMIC SAFETY OF EXISTING REINFORCED CONCRETE SCHOOL BUILDINGS

- 9:00 - 9:40 a.m. (9) Aseismic Measures for Reinforced Concrete Structures — In View of Damage from Oita Earthquake of 1975 — H. Umemura
- 9:40 - 10:20 a.m. (10) An Evaluation Method of Earthquake Resistant Properties of Existing Reinforced Concrete School Buildings - S. Kokusho
- 10:20 - 10:40 a.m. Coffee Break
- 10:40 - 11:20 a.m. (11) Assessment of Earthquake Safety and of Hazard Abatement - B. Bresler
- 11:20 - 12:00 p.m. (12) Seismic Safety of Existing Low-Rise Reinforced Concrete Buildings — Screening Method — T. Okada
- 12:00 - 1:20 p.m. Lunch

SESSION IV

Tuesday, August 19, 1:20 - 4:20 p.m.
Co-Chairmen: V. Bertero and T. Okada

EVALUATION OF THE SEISMIC SAFETY OF EXISTING REINFORCED CONCRETE SCHOOL BUILDINGS

- 1:20 - 2:00 p.m. (13) Nonlinear Response Spectra for Probabilistic Seismic Design of Reinforced Concrete Structures - M. Murakami
- 2:00 - 2:40 p.m. (14) Use of Linear Models in Design to Reflect the Effect of Nonlinear Response - A. Shibata
- 2:40 - 3:00 p.m. Coffee Break
- 3:00 - 3:40 p.m. (15) Simple Nonlinear Models for the Seismic Response of Reinforced Concrete Buildings - H. Aoyama

3:40 - 4:20 p.m. (16) Nonlinear Building Response by the Characteristics Method - R. Hanson

SESSION V

Wednesday, August 20, 9:00 - 12:00 noon
Co-Chairmen: P. Jennings and T. Katayama

STRENGTHENING OF EXISTING BUILDINGS AND REPAIR OF
DAMAGED BUILDINGS

- 9:00 - 9:40 a.m. (17) The Strengthening Method of Existing Reinforced Concrete Buildings - S. Kokusho
- 9:40 - 10:20 a.m. (18) An Experimental Study on Earthquake Resistant Strengthening Work for Existing Reinforced Concrete Buildings - H. Aoyama
- 10:20 - 10:40 a.m. Coffee Break
- 10:40 - 11:20 a.m. (19) Repair and Rehabilitation of Reinforced Concrete Structures - J. Wight
- 11:20 - 12:00 p.m. General Discussion
- 12:00 - 1:00 p.m. Lunch

SESSION VI

Wednesday, August 20, 1:00 - 3:00 p.m.
Co-Chairmen: H. Umemura and J. Penzien

FORMULATION OF JOINT RECOMMENDATION ON FUTURE RESEARCH

Closing Remarks

REVIEW MEETING

U.S. - JAPAN COOPERATIVE RESEARCH PROGRAM IN EARTHQUAKE
ENGINEERING WITH EMPHASIS ON THE SAFETY OF SCHOOL BUILDINGS

East-West Center
Honolulu, Hawaii, August 18-20, 1975

Official Participants

Professor Hiroyuki Aoyama
Department of Architecture
University of Tokyo
7-3-1 Hongo
Bunkyo-ku, Tokyo 113, Japan

Professor Boris Bresler
Department of Civil Engineering
University of California
Berkeley, California 94720, USA

Professor Robert D. Hanson
Department of Civil Engineering
University of Michigan
Ann Arbor, Michigan 48104, USA

Professor Paul C. Jennings
Division of Engineering and Applied Science
California Institute of Technology
Pasadena, California 91109, USA

Professor Seiji Kokusho
Department of Architecture
Tokyo Institute of Technology
2-12-1 Ohokayama
Meguro-ku, Tokyo 152, Japan

Professor Tsuneo Okada
Institute of Industrial Science
University of Tokyo
7-22-1 Roppongi
Minato-ku, Tokyo 106, Japan

Professor Joseph Penzien
Department of Civil Engineering
University of California
Berkeley, California 94720, USA

Professor Akenori Shibata
Department of Architecture
Tohoku University
Aoba, Aramaki
Sendai 980, Japan

Professor Mete A. Sozen
Department of Civil Engineering
University of Illinois
Urbana, Illinois 61801, USA

Professor Hajime Umemura
Department of Architecture
University of Tokyo
7-3-1 Hongo
Bunkyo-ku, Tokyo 113, Japan

Observers

Professor Vitelmo V. Bertero
Department of Civil Engineering
University of California
Berkeley, California 94720, USA

Professor Tsuneo Katayama
Institute of Industrial Science
University of Tokyo
7-22-1 Roppongi
Minato-ku, Tokyo 106, Japan

Dr. Soichi Kawamura
Technical Development Department
Taisei Corporation
1-4-28 Mita, Kokusai Bldg.
Minato-ku, Tokyo 108, Japan

Mr. Tetsuo Kubo
Earthquake Engineering Research Center
University of California
1301 South 46th Street
Richmond, California 94804, USA
Department of Architecture
University of Tokyo
7-3-1 Hongo
Bunkyo-ku, Tokyo 113, Japan

Mr. Duane L. N. Lee
Department of Civil Engineering
University of Michigan
Ann Arbor, Michigan 48104, USA

Dr. Masaya Murakami
Department of Civil Engineering
University of California
Berkeley, California 94720, USA
Department of Architecture
Chiba University
1-33 Yayoi-cho, Chiba 280, Japan

Professor N. Norby Nielsen
Department of Civil Engineering
University of Hawaii
Honolulu, Hawaii 96822, USA

Dr. Yutaro Omote
Earthquake Engineering Research Center
University of California
1301 South 46th Street
Richmond, California 94804, USA
Ohbayashi-gumi Technical Research Laboratory
4-640 Shimo-kiyoto
Kiyose, Tokyo 180-04, Japan

Professor Shunsuke Otani
Department of Civil Engineering
University of Toronto
Toronto, Ontario, Canada

Dr. Haruo Takizawa
Division of Engineering and Applied Science
California Institute of Technology
Pasadena, California 91109, USA
Department of Architectural Engineering
Hokkaido University
Kita 13, Nishi 8
Kita-ku, Sapporo 060, Japan

Professor James K. Wight
Department of Civil Engineering
University of Michigan
Ann Arbor, Michigan 48104, USA

TABLE OF CONTENTS

	Page
1. Strong Ground Motion and Seismic Design Criteria by Paul C. Jennings	1
2. Earthquake Motion Measurements and Analysis of Pile-Supported Building and Its Surrounding Soil by Soichi Kawamura, Yutaka Osawa and Hajime Umemura	12
3. Characteristics of Three-Dimensional Ground Motions, San Fernando Earthquake by Tetsuo Kubo and Joseph Penzien	35
4. Inelastic Cyclic Behavior of Reinforced Concrete Flexural Members by J. Penzien, V. Bertero and B. Atalay	52
5. Seismic Design Implications of Hysteretic Behavior of Reinforced Concrete Elements under High Shear by Vitelmo V. Bertero, Egor P. Popov and Tsan-Yuan Wang	75
6. Hysteretic Behavior of Reinforced Concrete Shear Walls by Toshio Shiga, Akenori Shibata and Junichi Takahashi	107
7. Structural Walls Subjected to Simulated Earthquakes by Mete A. Sozen and Shunsuke Otani	118
8. Experimental and Analytical Study on Reinforced Concrete Chimneys by Yutaro Omote and Toshikazu Takeda	135
9. Aseismic Measures for Reinforced Concrete Structures — In View of Damage from Oita Earthquake of 1975 — by Hajime Umemura	164
10. An Evaluation Method of Earthquake Resistant Properties of Existing Reinforced Concrete School Buildings by Masaya Hirose, Yōichi Higashi, Kōichirō Ogura and Seiji Kokusho	174
11. Assessment of Earthquake Safety and of Hazard Abatement by Boris Bresler, Tsuneo Okada and David Zisling	188
12. Seismic Safety of Existing Low-Rise Reinforced Concrete Buildings — Screening Method — by Tsuneo Okada and Boris Bresler	210
13. Nonlinear Response Spectra for Probabilistic Seismic Design of Reinforced Concrete Structures by Masaya Murakami and Joseph Penzien	247

	Page
14. Use of Linear Models in Design to Reflect the Effect of Nonlinear Response by Akenori Shibata and Mete A. Sozen	274
15. Simple Nonlinear Models for the Seismic Response of Reinforced Concrete Buildings by Hiroyuki Aoyama	291
16. Nonlinear Building Response by the Characteristics Method by Takao Nishikawa, Martin E. Batts and Robert D. Hanson	310
17. The Strengthening Method of Existing Reinforced Concrete Buildings by Yōichi Higashi and Seiji Kokusho	333
18. An Experimental Study on Earthquake Resistant Strengthening Work for Existing Reinforced Concrete Buildings by Tetsuya Sasaki, Atsusi Hattori, Naoharu Mori, Kohichi Nonaka and Tatsuo Suenaga	352
19. Repair and Rehabilitation of Reinforced Concrete Structures by Duane L. N. Lee, James K. Wight and Robert D. Hanson	371

STRONG GROUND MOTION AND SEISMIC DESIGN CRITERIA

by Paul C. Jennings^I

INTRODUCTION

The purpose of this paper is to summarize the status of measurements of strong ground motion in the United States and to discuss how the data are being used to determine seismic design criteria. The statistical data concerning the strong-motion records and the measurement programs are drawn from a series of papers by D. E. Hudson and his coworkers (1, 2, 3, 4); these references can be consulted for additional information. Almost all of the accelerograph networks in the United States are maintained by the Seismic Engineering Branch of the U.S. Geological Survey, or are coordinated with the program of this agency. The instruments are owned by a wide variety of organizations, including federal and state agencies, universities, public utilities and building owners. The Seismic Engineering Branch, however, services many of the instruments owned by others and acts as a central repository for the records and the digitized data.

STRONG-MOTION DATA

Of the estimated 4000 strong-motion accelerographs installed at present in the world, about 1000 are located in the United States. All but a very few are in the western part of the country, with the large majority in California. The number of instruments has increased dramatically from a level of about 100 in 1965, largely because of the introduction at that time of a requirement in the Los Angeles Building Code that three accelerographs be installed in all major buildings (essentially those above 10 stories), and the establishment by the State of California in 1972 of the Strong-Motion Instrumentation Program. The later program is funded by a 7 cent per \$1000 assessment on building permits and has already resulted in the installation of a few hundred accelerographs.

The instruments are of various types and use different recording techniques (5), including photosensitive paper, film and magnetic tape. The majority of the instruments installed in the United States are of the film-recording type in which a mechanical-optical system is used to generate a trace on 70-mm film. Experience with this type of instrument has shown it to have a resolution of about 0.001 g and a dynamic range of about 1000. The combination of dynamic range and resolution, simplicity, and field reliability obtained by the mechanical-optical instruments has not yet been achieved by instruments recording electronically. The velocities and displacements associated with the recorded accelerations

^IProfessor of Applied Mechanics, California Institute of Technology, Pasadena, California 91125.

are found from integration of the accelerograms after some needed filtering has been performed. (6) The resulting ground displacements are thought to be reliable to about ± 1 centimeter in the 5 to 8-second period range and to about ± 2 centimeters in the 10-second period range. Components of the motion with periods longer than 15 seconds have been removed by filtering, as these periods are beyond the accurate recording range of the instrument.

Nearly all of the significant U. S. records have been digitized and analyzed in a multiyear project at the California Institute of Technology, under the sponsorship of the National Science Foundation. The project has resulted in a voluminous set of reports containing uncorrected accelerograms, corrected accelerograms, velocities and displacements, response spectra and Fourier spectra. (6) The basic information is also available on punched cards and on computer compatible magnetic tapes. Detailed information about the availability of the data can be obtained from the National Information Service for Earthquake Engineering, Thomas Laboratory, 104-44, California Institute of Technology, Pasadena, California 91125.

This data bank contains 381, 3-component accelerograms and their derived velocities, displacements, response spectra and Fourier spectra. One hundred eighty seven of the records were obtained on the ground, mainly in basements of buildings with the rest from upper floors of buildings. These records were obtained from 57 different earthquakes ranging in Magnitude from 3 to 7.7, but 241 records, including 98 at ground level, were obtained from the Magnitude 6.4 San Fernando earthquake of 1971. The $M = 6.4$ Borrego Mountain earthquake in 1968 generated 13 records and the Lytle Creek earthquake of 1970 ($M = 5.4$) produced 7 records. All of these are southern California earthquakes. The site producing the most records from different shocks is El Centro, California, where the well-known accelerogram of 1940 was recorded. There are 16 different records from this site. Of the records obtained at ground level, 60 percent have been categorized as being recorded on alluvium, 30 percent on intermediate sites, including sedimentary rock, and 10 percent on hard, crystalline bedrock.

Figure 1 illustrates the Magnitudes of earthquakes from which accelerograms have been obtained. This figure makes it clear that there are very few records from truly great earthquakes. The strong ground motion from a Magnitude 8.0 or greater earthquake has not yet been recorded and only a few records from Magnitude 7.0 shocks are available, none of these from the area of strongest shaking. The records of most severe shaking were obtained during the San Fernando earthquake and at El Centro in 1940. In particular, the record at Pacoima dam in the San Fernando earthquake was recorded almost directly over the geometric center of the area of fault rupture and showed about 8 seconds of very intense motion, including high-frequency peaks in the horizontal components that exceeded 1 g.

The strength of the record from Pacoima dam and the general lack of other records obtained near the fault in major shocks has led to a wide difference of opinion among researchers concerning the strength of

shaking to be expected in large earthquakes. Obtaining the measurements of ground shaking in the near field in major earthquakes, which are required to resolve the different viewpoints on this important practical problem, represents the highest priority of the strong-ground motion program in the author's judgment. The next largest gap in the data is the lack of enough records to determine the nature and amount of effects that different local soil conditions and geologic settings can have upon the motion.

CHARACTERISTICS OF PEAK GROUND MOTION

The principal use of the strong-motion records for engineering is to determine appropriate design criteria for future construction. The understanding of the ground motion and the resulting structural response made possible by the accelerograms is essential to rational earthquake-resistant design. One of the most common ways to present the data for this purpose is to plot the peak values of the ground motion as functions of distance from the source area and Magnitude of the earthquake. The peak values of horizontal acceleration, velocity and displacement are plotted this way in figures 2, 3 and 4. The data points are the selected records tabulated by Hudson (2) with minor modifications as indicated below. Each of the figures has the same horizontal scale, and uses the same symbols for Magnitude. Of the 93 accelerograms included in the plot, 60 are from the San Fernando earthquake, and this dominance of the data by the one earthquake must be considered when interpreting the trends.

The peak accelerations are plotted in figure 2. A plot of this data emphasizes the high-frequency content of the motion. The points are those given by Hudson (2) plus the Melendy ranch record (0.69 g and 0.47 g) from the Magnitude 4.7 Bear Valley earthquake of September 1972. (7) In figure 2, both components of acceleration have been plotted for those records with a peak horizontal acceleration greater than 0.20 g, or which were recorded at distances less than 20 kilometers. In the case of smaller or more distant records, only the larger of the two horizontal components has been plotted. The distances used are the epicentral distance given in reference 2, with the following exceptions: The records obtained from the Parkfield earthquake are plotted at the distance from the fault, as given by Page et al (8); and the Pacoima dam record is plotted at a distance of 1 kilometer. The symbols used to denote Magnitudes are the same as used by the USGS in reference 8, and the sets of data overlap to the extent that they are substantially the same. The only major difference is that figure 2 is a linear plot, whereas two-way logarithmic graphs are used in reference 8.

It is difficult to identify trends in figure 2 because of the variability of the data and the scarcity of measurements for distances less than 20 kilometers. For this reason, no curves or formulas have been applied to the data. It does seem possible, however, to make the following observations: 1) The variability in the peak acceleration is larger in the

near field (< 20 kilometers) than it is further away from the source; 2) There appears to be a weak dependence on Magnitude in the near field which grows stronger with distance; 3) The data suggest a rapid attenuation with distance in the near field, followed by a more gradual decay thereafter; 4) In terms of trends so far apparent in the data, the Pacoima dam record lies well above the rest of the data.

A similar plot of velocity is given in figure 3. The ground velocity tends to emphasize middle frequencies and is preferred by some investigators over peak acceleration as an indicator of the strength of ground motion. Both components of ground velocity are plotted in figure 3 for records with peaks greater than 20 centimeters per second, and for records obtained at distances less than 20 kilometers. The data are from reference 2 with the changes noted above, with the exception that ground velocities are not available for the Melendy ranch record. Again the dispersion in the data is apparent, with an even wider variation than seen in the previous figure, particularly for those records obtained closest to the fault. There is also the impression that other factors beside distance are of major importance. For example, the ground velocities appear to increase going from 25 to 40 kilometers. This effect is a result of the data from the San Fernando earthquake and reflects the growth of surface waves as the motion traversed the deep sediments of the Los Angeles basin. In addition to such effects of travel paths and local geology, it is also believed that the high velocities recorded near the source at Parkfield ($M = 5.6$, $v = 78$ centimeters per second) and at Pacoima dam ($M = 6.4$, $v = 113$ and 57.7 centimeters per second) are a reflection of the source mechanisms. The data tentatively suggest that these high velocities attenuate rapidly with increasing distance.

The peak displacements, which are most indicative of the low-frequency components of the ground motion are plotted in figure 4. The records used are the same as for figure 3. There is an even wider variation in the data than in the previous figures and if it were not for the Parkfield record ($d = 26.4$ centimeters) and that from Pacoima dam ($d = 37.6$ and 10.8 centimeters), it would be difficult to identify any attenuation of peak displacement with distance within the first 60 kilometers. As was the case for ground velocities, these two records obtained very near the fault appear anomalous with respect to the other data.

The lack of data in the near field and the variability of what data there are show clearly that many more records are needed to define trends in peak ground-motion parameters close to the causative fault. Unfortunately this is also the region of most importance to engineering; in the more seismic regions of the country, especially California and Nevada, a given site is almost always within 20 kilometers of an active fault, and the characteristics of the motion in the near field are of critical importance in the earthquake-resistant design of major structures and facilities. The situation is complicated further by the fact that in the near field the appropriate distance to use becomes hard to determine and the Magnitude, the most common single index of the size of the earthquake, becomes a less reliable measure of the energy released at frequencies of importance to engineering.

IMPLICATIONS FOR EARTHQUAKE-RESISTANT DESIGN

All of these points argue strongly for looking beyond peaks of ground-motion parameters when determining earthquake-resistant design criteria. It is much more logical, from the viewpoint of engineers, to try to use the existing near-field data to a much greater extent, to seek better measures of the strength of the shaking and to supplement these efforts by analyses.

As has long been recognized, some of the disadvantages of using peak ground-motion parameters can be overcome by using response spectra. In one such approach (9), response spectra recorded under conditions comparable to those of the design earthquake are used in an empirical manner to determine the level of the design spectra. It would also seem possible to use Fourier spectra to advantage in setting earthquake-resistant design criteria. The spectral methods have the advantage of treating the range of periods of interest in the problem simultaneously and consistently. They have the disadvantage of being a nonunique representation of the motion and as a result the spectra do not always reflect features of the ground motion, particularly the duration of shaking, in the most meaningful way. Even with this limitation, however, the spectral methods are thought to be much superior to methods based on peaks of ground motion parameters.

The inadequacies of peak values of ground motion, especially peak acceleration, as measures of the strength of shaking have led to the development of other indices of the intensity of the motion. The most promising of these is thought to be the integral of the square of the acceleration over the duration of strong shaking. This measure, which has been related to the energy input to an ensemble of simple linear oscillators by Arias and his coworkers (10, 11) has the advantages of simplicity and physical significance, and fits well into the theoretical framework of random vibrations. (12) To improve substantially on this single measure of the motion it seems necessary to use more than one parameter. For example, the integral of the acceleration squared could be supplemented by the duration of the strong shaking, thereby describing both the total amount and average rate of energy input. Similarly, the peak acceleration, velocity and displacement together have been suggested as a three-parameter measure of the shaking. The description of those characteristics of the ground motion of importance to engineers by more than one parameter and the relation of these parameters as directly as possible to earthquake design criteria seems to be the most promising direction for work in this area.

The importance of the earthquake problem and the lack of data in the near field have led to a large number of analytical attempts to increase the understanding of the characteristics of strong-ground motion. These studies include deterministic analyses using the seismological concepts of seismic moment, stress drop, etc., or the related quantities in the frequency domain. Some of these analyses employ finite-element models of the source region, while others use analytical results from dynamic elasticity. These efforts are directed at exploiting the advantages of a more detailed description of the mechanics of energy

release than is given by the single number, the Magnitude. It is expected that the results of studies of this type will be increasingly useful to engineering.

Statistical analyses of the existing strong-motion data are also used to try to identify trends and levels that may be valid in the near field. These analyses are most commonly done using logarithmic values of peak ground-motion parameters and distances, in addition to Magnitude (also a logarithmic parameter) and such variables as site conditions or Modified-Mercalli intensity. The statistical studies can provide valuable insight into the nature of the earthquake motion (e. g. reference 13), but the lack of data in the near field, the wide dispersion of the data, usually describable by a log-normal statistical distribution, and the necessity of using simple, but limited parameters such as peak acceleration tend to restrict the engineering utility of these studies, in the author's opinion.

The concentration of attention on the strong shaking near the fault and the discussion of how strong the shaking might be in the strongest credible case tend to give an imbalance to the problem of determining earthquake-resistance design criteria. These very large motions must, by definition, occur very rarely and the data so far recorded indicate that the areal extent of the extremely strong motion is confined to within several kilometers of the source. Earthquake experience also indicates that energy is not released at maximum intensity everywhere along the fault. Under these circumstances, a structure has a very small chance of receiving such intense motion during its useful lifetime, and in all but the most exceptional cases the only reasonable limitation on response is that the structure should not suffer damage so severe as to be in imminent danger of collapse. Determining the level of the strongest credible motion and the assessment of the capacity of structures to resist such shaking by nonlinear, yielding response are both tasks full of major uncertainties and important assumptions, without the essential backup of experimental data. It therefore seems important when the earthquake design problem is approached in this manner to make an additional comparison of the response of the structure at lower levels, for example at yield point stresses, in response to more moderate shaking. At this lower level of response, both the excitation and the behavior of the structure are much better understood and it is possible to obtain a better evaluation of the adequacy of the design under more probable excitation.

REFERENCES

1. Hudson, D. E. et al, (1975), "Index of Digitized Strong Motion Accelerograms and Standardized Processed Data," National Information Service for Earthquake Engineering, Earthquake Engineering Research Laboratory, California Institute of Technology, Pasadena.
2. Hudson, D. E., (1974), "Destructive Earthquake Ground Motions," in Applied Mechanics in Earthquake Engineering, W. D. Iwan (Ed.) American Society of Mechanical Engineers, New York.

3. Hudson, D. E. (1975a), "The Strong-Motion Data Bank," Earthquake Research Affiliates Conference, California Institute of Technology, Pasadena.
4. Hudson, D. E., (1975b), "The Characteristics of Strong Ground" Motion as Revealed by Accelerograph Records," presented at the 70th annual meeting of the Seismological Society of America, California State University, Los Angeles.
5. Halvorsen, H., (1974), "A Technical Review of Recent Strong Motion Accelerographs," Proceedings of the Fifth World Conference on Earthquake Engineering, Vol. I., Edigraf, Rome.
6. Hudson, D. E., M. D. Trifunac, and A. G. Brady, (1969-1975), "Strong-Motion Earthquake Accelerograms; Vol. I, parts A-Y Uncorrected Accelerograms; Vol. II, parts A-Y, Corrected Accelerograms and Integrated Velocity and Displacement Curves; Vol. III, parts A-Y, Response Spectra; Vol. IV, parts A-Y, Fourier Amplitude Spectra," California Institute of Technology, Earthquake Engineering Research Laboratory, Pasadena.
7. Morrill, B. J. and R. B. Matthiesen, (1972), "Strong-Motion Accelerograph Records from 4 September 1972 Stone Canyon Earthquake," Earthquake Notes, Vol. XLIII, No. 3.
8. Page, R. A., Boore, D. M., Joyner, W. B., and H. W. Coulter, (1972), "Ground Motion Values for Use in the Seismic Design of the Trans-Alaska Pipeline System," U.S. Geological Survey Circular 672, Washington, D. C.
9. Jennings, P. C. and R. A. Guzmán, (1975), "Seismic Design Criteria for Nuclear Powerplants," Proceedings of the U. S. National Conference on Earthquake Engineering, Edward Brothers, Ann Arbor, Michigan.
10. Lange, J. G., (1968), "Una Medida de Intensidad Sismica," Departamento de Obras Civiles, University of Chile, Santiago, Chile.
11. Arias, A., (1970), "A Measure of Earthquake Intensity," in Seismic Design for Nuclear Power Plants, M.I.T. Press, Cambridge, Massachusetts.
12. Housner, G. W. and P. C. Jennings, (1975), "The Capacity of Extreme Earthquake Motions to Damage Structures," Proceedings of the Symposium on Structural and Geotechnical Mechanics, University of Illinois, Urbana-Champaign.
13. Berrill, J. B., (1975). "A Study of High-Frequency Strong Ground Motion from the San Fernando Earthquake," California Institute of Technology, Soil Mechanics Laboratory, Pasadena.

NUMBER OF OCCURRENCES
INSTRUMENTED
STRONG MOTION EARTHQUAKES

—
8
—

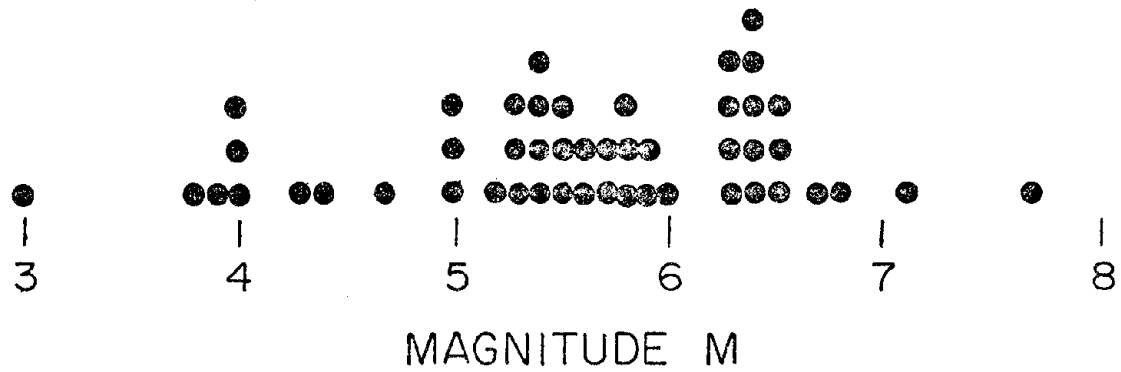


Figure 1.

Distribution of Magnitudes of Earthquakes with Recorded Strong Ground Motion (Hudson, 1975b).

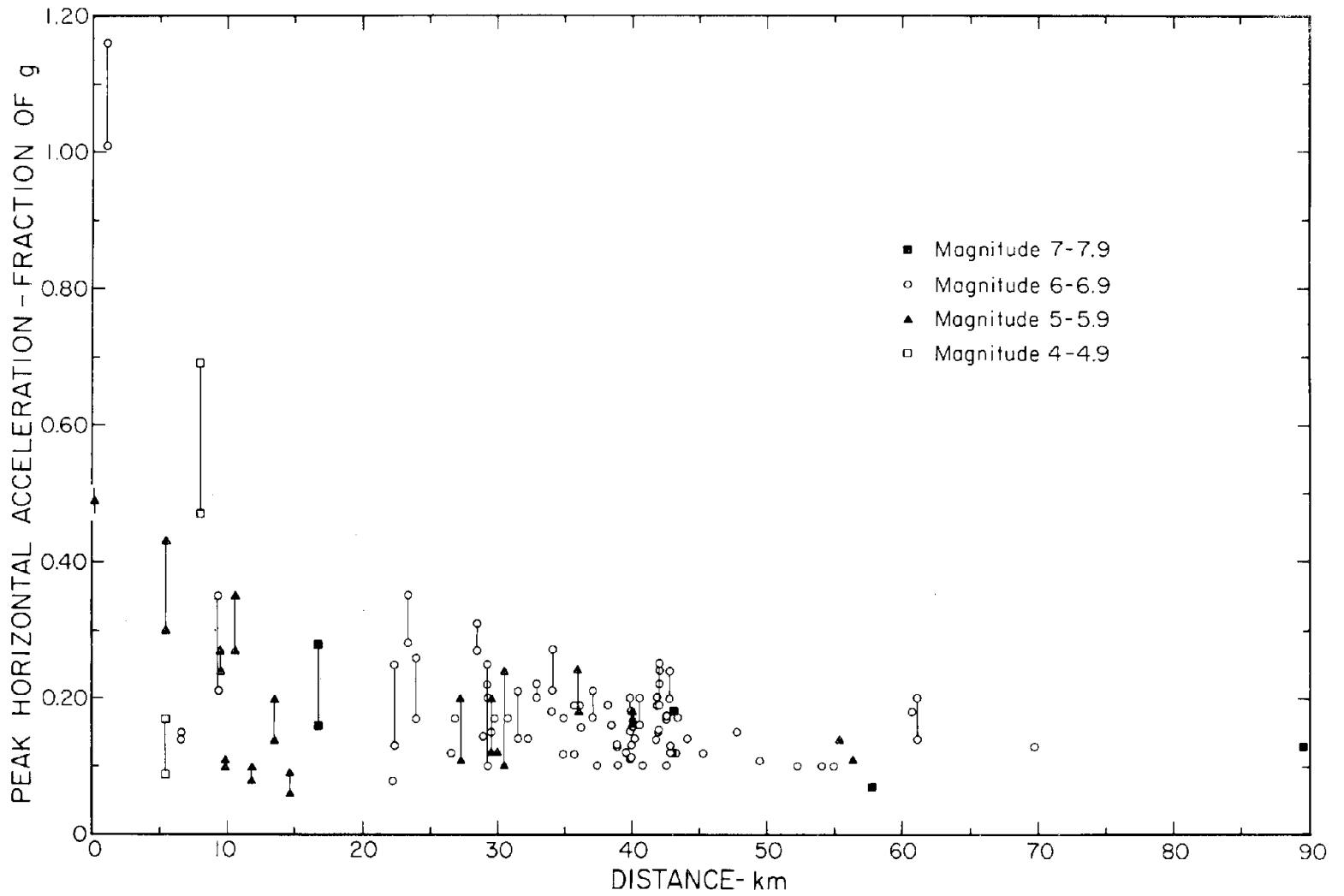


Figure 2.

Peaks of Recorded Ground Acceleration, Horizontal Components.

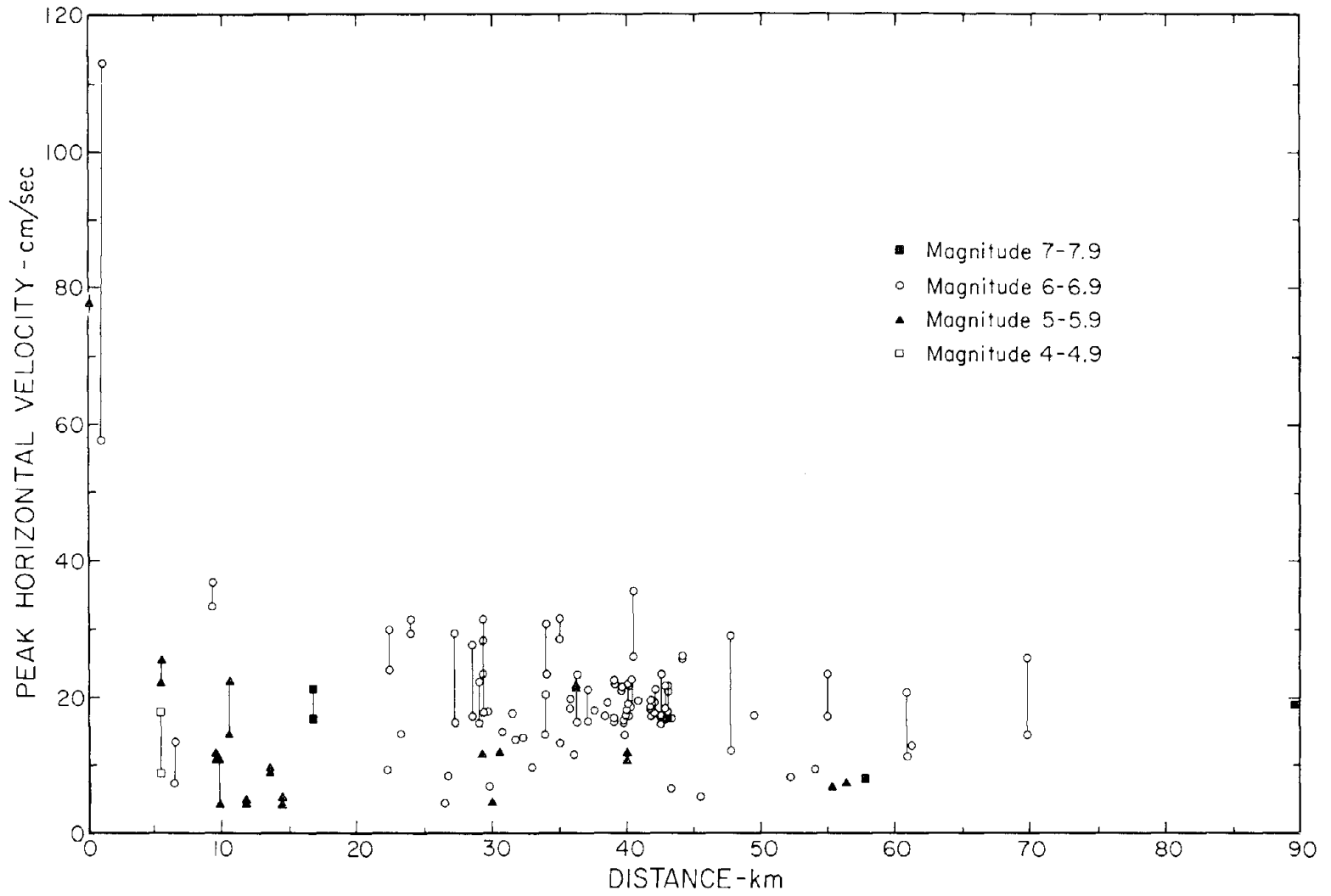


Figure 3.

Peaks of Computed Ground Velocity, Horizontal Components.

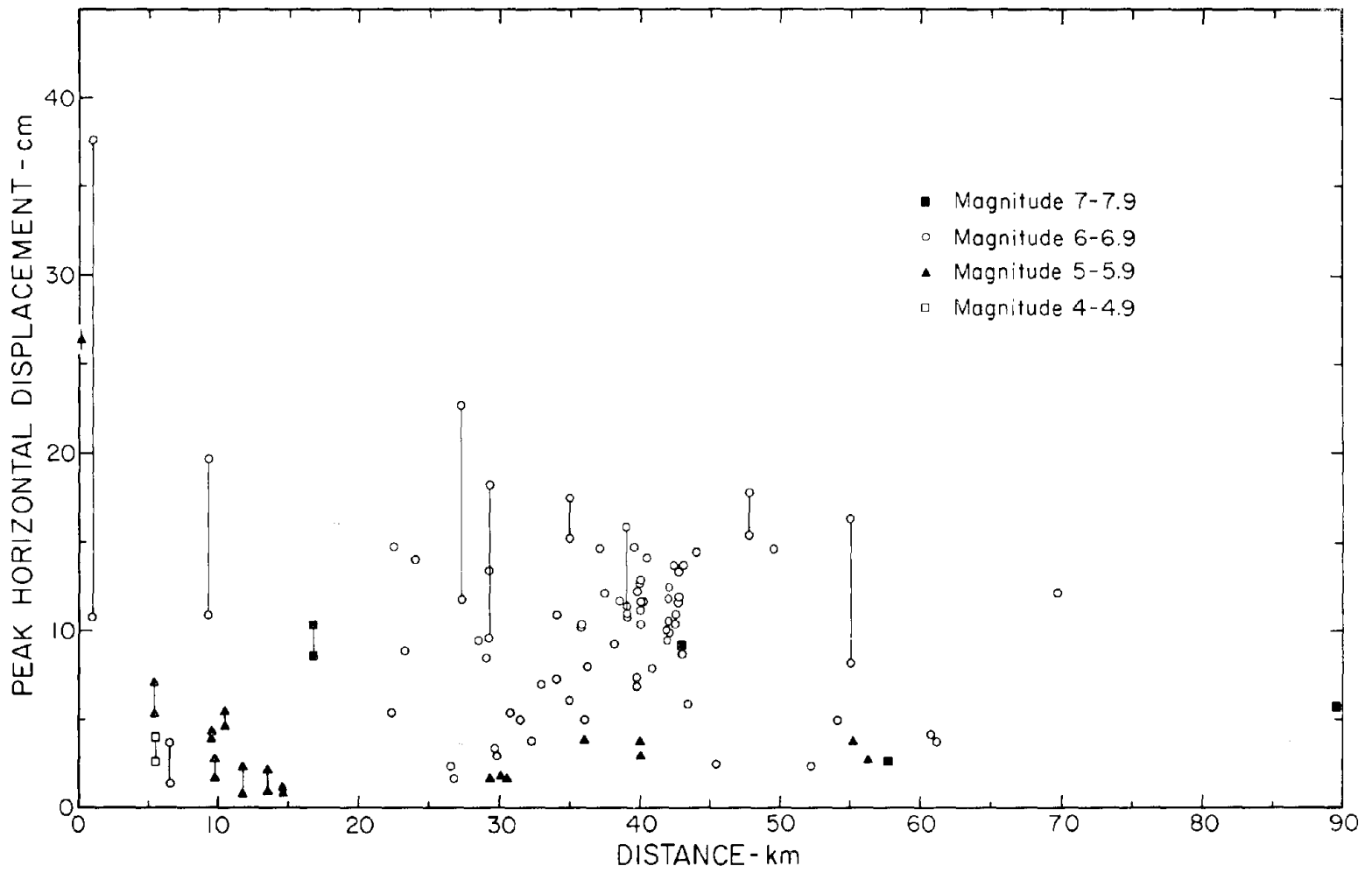


Figure 4.

Peaks of Computed Ground Displacement, Horizontal Components.

2 Earthquake Motion Measurement and Analysis of Pile-Supported Building and Its Surrounding Soil

Soichi KAWAMURA *
Yutaka OFAWA **
Hajime UMEMURA ***

Synopsis

The interaction effects between a structure and its surrounding soil are considered to be significant especially when the structure is stiffer than the soil. Since most of the structures built on the very soft ground such as reclaimed ground are supported on piles, the soil-structure interaction becomes more important and complicate. However the real comprehension of the effects by way of field research was not enough up to the present.

This report describes the outline of earthquake-motion measurements in pile supported 7-storied apartmenthouse and its surrounding soil as well as the analytical results. The earthquakes measured were not so intense but through their analysis many characteristics were recognized regarding the soil-structure vibration. Theoretical analysis was made in the elastic range and the results were compared with observed values. The volume of surrounding soil which cooperate with piles and modal damping factors of soil and structure could be obtained.

1. Outline of the Measurement System

1.1 Building

The building where earthquake-motion measurement has been carried out is 7-storied apartmenthouse made of precast light-weight concrete as is shown in Photo.1 and Figs. 1 and 2. It is supported on P.C. piles which are driven into a dense sandy layer 12m below surface. The main structural components are walled frames in longitudinal direction and shear walls in transverse direction. The dimensions are 55.8 m in Y direction, 13.6 m in X direction and 19.1 m in Z direction excluding penthouse.

The natural periods of the building obtained from the forced vibration tests are 0.19 sec in X and 0.24 sec in Y direction. Translational and rotational displacements at the base are quite large and occupy about half of the top displacement.

* Taisei Corporation
** Professor, Earthquake Research Institute, University of Tokyo
*** Professor, University of Tokyo

1.2 Soil

The surrounding soil is mainly consisted of sand and partly of silt or clay. The N-value distribution is shown in Fig. 3 and the shape varies place by place. The thickness of reclaimed layer is as shallow as 4 - 5 m.

The predominant periods observed in microtremor at the ground surface (GL) are 0.2 - 0.4 sec, 0.7 sec and 1.2 sec.

1.3 Measurement System

The location of pick-ups is shown in Fig. 3 together with soil profile. They are separated into two groups, building line and soil line, which are denoted by filled circle and empty circle respectively. Building line consists of 5 points, RF and LF in the building, GL-4 m, - 12 m and - 24 m just below the building. Soil line is parallel to the building line and consists of 4 points at the same level: GL, GL-4 m, - 12 m and - 24 m about 15 m distant from the building. Each point has three components, two in the horizontal (X, Y) and one in the vertical (Z) direction. The natural period of the pendulum is 0.2 sec or 0.33 sec and acceleration is recorded. In addition to them 5.0 sec pick-ups are placed in three direction on the RF only and velocity is recorded at the same time. The number of recording channels is 30 in all. The recorder is optical type and triggered when acceleration over 1 gal acts at GL-12 m below the building.

2. Outline of Observed Earthquakes

2.1 Intensity and Epicenter

Since the measurement was begun in Dec. 1971 more than 80 earthquakes have been observed. All of them belong to small or middle class of intensity, IV or less in Japanese Meteorological Agency scale. Epicenters of them mostly lie on the side of the Pacific Ocean and above all in the north-eastern Kwanto district. The distances to the epicenters are distributed in quite wide range, but more than half of them are less than 80 km.

Most of the focal depths are around 50 km and 90% of them are less than 100 km. Magnitudes are mostly below 6.0 with a few exceptions like 7.2 or 6.8.

2.2 Observed Records

Figs. 4 and 5 show examples of the observed records in horizontal direction. Amplification from the lower point to the upper point is clear, but the times when maximum amplitudes occur do not always coincide. The record at RF oscillates somewhat harmonically.

To compare the records of building line and soil line at the same level conspicuous difference can not be found at the lower two levels GL-12 m and - 24 m. However at GL of the soil line rather shorter periods are contained considerably and its maximum amplitude is greater compared with 1F of the building line.

Fig. 6 shows vertical records of the same earthquake shown in Fig. 5. Compared with horizontal motions vertical ones have relatively flat envelopes. Very short periods are predominant at the beginning of records and especially upper points have the feature all the more remarkably.

3. Amplitude Characteristics of Observed Records

3.1 Amplification of Horizontal Motion

The average amplitude ratios of maximum accelerations for 20 earthquakes regulating 1F to unity in three directions are shown in Fig. 7, where the thick continuous line and broken line denote building line and soil line respectively both with standard deviations shown by lateral bars.

In horizontal directions amplification is remarkable above GL-4 m where was the ancient sea bed and N-value is a little high, and below that point amplification is small. The difference between the building line and the soil line can be seen only between 1F and GL. Maximum amplitude of GL is about 1.5 times that of 1F. At lower levels both lines are almost equal, especially at GL-24 m and - 12 m. Horizontal motion is amplified 2.52 and 2.83 times from 1F to RF each in X and Y direction.

Average amplification factors from GL-24 m are shown in Table 1, which are calculated independently for building line and soil line. Amplification factors of horizontal motion from GL-24 m to 1F are 2.45 in X and 2.34 in Y direction, which are nearly equal to those from 1F to RF. Consequently from GL-24 m to RF amplification factors are 6.19 in X and 6.64 in Y direction. In the soil line from GL-24 m to GL they are 3.61 in X and 3.24 in Y direction.

3.2 Vertical Amplitude

As shown in Fig. 7 amplification in the vertical direction is not so large as in horizontal directions. Average amplification factors are 1.48 from 1F to RF, 1.64 from GL-24 m to 1F and 2.43 from GL-24 m to RF in the building line. In the soil line amplitude grows 1.96 times from GL-24 m to GL.

Fig. 8 shows the result of comparison of the vertical and horizontal motions at three points: GL of the soil line, GL-12 m and GL-24 m of the building line. Though at GL vertical motion is 27 - 34% of horizontal motions the ratio increases to 45 - 49% at GL-12 m and as large as 61 - 73% at GL-24 m. The change of the value is explained

by the fact that the vertical amplification is not so large as the horizontal. Anyhow it should be noted that such a quite large value as 61 - 73% is observed at the bottom.

4. Period Characteristics of Observed Records

4.1 Fourier Spectrum Analysis

Fourier amplitude spectra and their ratios in the horizontal directions are shown in Figs. 9 and 10. Though amplitude spectra are influenced by the epicentral distance or magnitude of earthquakes common tendency can be observed as follows. The spectra of RF and LF have relatively simple peaks about 0.32 sec in X and 0.34 sec in Y direction which are considered to be the primary periods of coupled building-pile-soil system. At GL, such shorter periods as 0.14 sec and 0.20 sec are predominant rather than 0.30 sec which is considered to be the primary period of the soil column above GL-24 m. On the contrary at GL-12 m and - 24 m longer periods like 0.5 sec or 0.7 sec are predominant.

Transfer characteristics represented by Fourier amplitude ratio have relatively constant peaks irrespective of the difference of earthquakes as shown in Table 2. The primary periods of the building with base rotation included are judged 0.24 sec in X and 0.27 sec in Y direction, and also that of the soil above GL-24 m is 0.30 sec from GL/GL-24 m. 0.14 sec and 0.20 sec in the spectra of GL are revealed to be the characteristics of the layer above GL-4 m and - 12 m respectively. The predominant period of RF can be explained by taking the system above GL-24 m. The shift of the period characteristics in accordance with time elapse can be seen using running Fourier spectrum. Figs. 11 and 12 are the amplitude spectra and amplitude-ratio spectra, where the time duration of a unit block and time interval between blocks were selected so as that the blocks are not wrapped too much. Based on these analyses general tendency that the longer periods dominate in the latter part of a record was affirmed. The transfer function shown by amplitude ratio spectrum is almost unvaried irrespective of time elapse and amplitude variation.

4.2 Comparison between Building Line and Soil Line

Fig. 13 shows the Fourier amplitude ratio spectra between the building line and the soil line. From the ratio LF/GL it is clear that with about 0.3 sec as the boundary in longer period range both amplitudes are nearly equal but in shorter period range LF is half of GL on an average. This means that the short period elements have large amplitude at GL but they are reduced acting on the building. The average maximum amplitude ratio 1.5 shown in the section 3.1 can be explained by these short period elements.

Such a tendency is weakened according as the depth from the ground surface increases. The ratio at GL-24 m is around unity though with some fluctuation, and it coincides with the fact that both amplitudes are nearly equal. In the ratio at GL-12 m quite large and stable fluctuation is conspicuous, though both lines were shown to have nearly equal amplitudes.

4.3 Period Characteristics of Vertical Motion

In Fig. 14 are shown the Fourier spectra and its ratios of vertical motions. Compared with the horizontal spectra the period characteristics of vertical motions are not necessarily different from the horizontal ones, though the transfer function is biased to the very short period.

5. Lumped Mass Models and Damping Factor for Building and Soil

5.1 Building

The natural periods of lumped mass models for three directions are shown in Table 3 compared with observed values. Though in Y direction good coincidence are obtained analytical results are quite shorter than the observed in X and Z directions.

In X direction wall was calculated as a continuous cantilever, but as a result it overestimated the stiffness and the loosening of joints between precast pannels should be considered. In Z direction axial stiffness of walls and columns were adopted, but also in this case reduction factor should be introduced though it may be difficult to get the value theoretically.

5.2 Soil

The natural periods of the lumped mass models for the soil column above GL-4 m, - 12 m and - 24 m are shown in Table 4 with observed values. They coincides quite well and the lumped mass model was proved to be enough for the analysis of soil. Fig. 15 shows the participation function of the model above GL-24m. The whiplash-like amplification in the reclaimed layer should be noted.

5.3 Damping Factor Obtained by Spectrum-Fitting Method

Modal damping factors were obtained by spectrum fitting method, using the lumped mass models whose natural periods are justified. As shown in Fig. 16 modal damping factors are assumed first and response calculation is made with the observed record at the base as an input wave. Then calculate the transfer function of the model from the top response and input record, and compare it with the observed one. If they do not coincide new values should be assumed and the procedure is repeated. Thus fitting the analytical transfer function to the observed one modal damping factors are obtained iteratively.

The results are shown in Table 5. Damping factors of the soil column above GL-24m are calculated using averaged spectrum of five earthquakes. There is a remarkable trend that the damping factor decreases in higher modes, and the value 8.5% for the first mode is quite large.

In Fig. 17 maximum response is shown. Large amplification of acceleration and high strain in the reclaimed layer are obvious.

For the building conventional frequency proportional damping factors are adequate taking 1% for the first mode in X and Y direction.

6. Lumped Mass Model for Building-Pile-Soil System

6.1 Model Composition and Equation of Motion

Lumped mass model adopted to simulate the building-pile-soil interaction is shown in Fig. 18. This is similar to that which Dr. Penzien ¹⁾ originally used in 1964, but in some points they differs. In the model used herein the surrounding soil within some area is treated as real additive masses which move together with piles, and shear-type springs are inserted between these masses. In the original model the mass effect of the surrounding soil is considered to be virtual and shear-type springs which connect the masses are not included. The pressure-type spring connecting the building line and the soil line laterally is common to both models and calculated by Mindlin's equations ²⁾ as shown in Fig. 19. In the original model the additive masses are also evaluated from Mindlin's equations on the conception of energy balance, but in the modified model they should be assumed parametrically.

The equation of motion for the modified model neglecting the damping term is as follows:

Building Line

$$([M_T] + [M_C]) (\{\ddot{u}_t\} + \{\ddot{u}_g\}) + ([K_T] + [K_{SE}]) \{U_t\} + [K_E] \{U_t\} - \{U_s\} = \{0\} \dots\dots\dots 1$$

M_T : Mass of Structure, M_C : Additive Mass, K_T : Stiffness of Structure

K_{SE} : Shear Spring between Additive Mass, K_E : Interaction Spring

U_t : Displacement of Structure, U_s : Displacement of Soil

U_g : Ground Motion

Soil Line

$$[M_s] (\{\ddot{u}_s\} + \{\ddot{u}_g\}) + [K_s] \{U_s\} = \{0\} \dots\dots\dots 2$$

M_s : Mass of Soil Column, K_s : Spring of Soil Column

Coupled System (for undamped free vibration)

$$\left[\begin{array}{cc|c} [M_B] & 0 & \\ \hline 0 & [M_p + M_c] & \\ \hline 0 & 0 & [M_s] \end{array} \right] \begin{Bmatrix} \{\ddot{u}_t\} \\ \{\ddot{u}_s\} \end{Bmatrix} + \left[\begin{array}{cc|c} [K_B] & 0 & 0 \\ \hline 0 & [K_p + K_{SE} + K_E] & - [K_E] \\ \hline 0 & - [K_E] & [K_s + K_E] \end{array} \right] \begin{Bmatrix} \{U_t\} \\ \{U_s\} \end{Bmatrix} = \begin{Bmatrix} 0 \\ 0 \end{Bmatrix} \dots\dots\dots 3$$

M_B : Mass of Building, M_p : Mass of Pile

K_B : Stiffness of Building, K_p : Stiffness of Pile

In the coupled system total masses of the soil line should be taken enoughly larger than that of the building line in order that the soil line is not affected by the building line.

6.2 The Volume of Additive Mass

The primary period of the coupled system was almost equal to that of the building line with the soil line fixed. The appropriate volume of additive mass was obtained by changing the volume parametrically and comparing the primary period with the observed one. As shown in Fig. 20 the primary period becomes shorter according to the increase of the additive mass in both X and Y directions. However the slope is gentle and the cross point of the calculated line and the observed one shifts sensitively if a slight error is considered. Then additive mass ratio against the building mass was counted with wide range as 0.7 - 2 in X and 3 - 10 in Y direction, which is in area ratio 0.2 - 0.6 in X and 0.9 - 3 in Y. In Fig. 21 participation function of the coupled system is shown for X direction with the mass ratio of 1.0.

6.3 Damping Factor and Response Results

For this model the modal damping factor was calculated applying spectrum-fitting method as mentioned before. First the damping factors for the soil line were decided and then those for the building line including the neighbouring soil were obtained. Response calculation for the coupled system was not by modal synthesis but by direct integration, when the modal damping factors were translated into orthogonal damping matrix.³⁾

Table 6 shows the obtained damping factors for two earthquakes which have different period characteristics. The values for the soil column above GL-12m have same tendency as mentioned before, quite large for the first mode and lesser for higher modes. In the building line large values are obtained for the second mode though not so large for the first mode. The spectrum comparison and wave form comparison are shown in Figs. 22 and 23 respectively. Fig. 24 shows the result of response. More than 50% of base shear of the building is resisted by the surrounding soil. The stress of pile is maximum at the top and reduces to the bottom. Relative displacement between the building line and the soil line is amplified in the reclaimed layer.

SUMMARY

Based on the observed records in the pile supported building and its surrounding soil dynamic characteristics of the coupled building-pile-soil system have been studied and some facts were pointed out.

- 1) Large amplification was observed in the reclaimed layer.
- 2) Maximum acceleration at the ground surface was about 1.5 times that of the building base on an average. But it mainly depends on the short period elements.

- 3) The ratio of the vertical acceleration to the horizontal was as large as 61 - 73% at the deep point (GL - 24m).
- 4) The motion of the structure and that of the soil were nearly equal in the deep layer (GL-12m, - 24m).
- 5) Base rotation and translation occupied quite large part of the top displacement, and elongation of the period was accordingly conspicuous.
- 6) Modal damping factor of soil obtained by spectrum fitting method had a conspicuous tendency of decrease in higher modes. For the soil column above GL-24m they were 3.50%, 1.85%, 1.90% and 1.15% in the order from the first to higher-modes.
- 7) The damping factor of the building was frequency proportional and for the first mode 1% was adequate.
- 8) The damping factor of the coupled building-pile-soil system did not show clear tendency. For the first mode it was 2.5 - 5% but for the second mode larger value than 10% was obtained.
- 9) The additive mass which moves together with piles was estimated to be 0.7 - 2 in transverse direction and 3 - 10 in longitudinal direction expressed in the ratio to the total mass of building.

REFERENCES

- 1) Penzien, J., Scheffey, C.F., Parmelee, R.A.
"Seismic Analysis of Bridges on Long Piles"
A.S.C.E. (1964)
- 2) Mindlin, R.D
"Force at a Point in the Interior of a Semi-Infinite Solid"
Physics, vol. 7 (1936)
- 3) Wilson, E.L., Penzien, J.
"Evaluation of Orthogonal Damping Matrices"
International Journal of Numerical Methods in
Engineering, vol. 4 (1972)

Table 1 Amplification Factor from GL-24m

Position		X		Y		Z	
Building Line	Soil Line	B-Line	S-Line	B-Line	S-Line	B-Line	S-Line
RF		6.19		6.64		2.43	
1F	S00	2.45	3.61	2.34	3.24	1.64	1.96
04	S04	1.32	1.68	1.70	1.72	1.55	2.20
12	S12	1.09	1.20	1.22	1.05	1.16	1.54
24	S24	1.00	1.00	1.00	1.00	1.00	1.00

Table 2 Peak Periods in Fourier Amplitude Ratio

Building Line	Ratio	X			Y			Z		
		1	2	3	1	2	3	1	2	3
Building Line	RF/1F	0.24	-	-	0.27	0.23	0.10	0.06	-	-
	RF/04	0.27	0.14	-	0.30	0.28	0.15	0.07	-	-
	RF/12	0.30	0.21	-	0.32	0.28	0.20	(0.07)	-	-
	RF/24	0.32	0.28	0.15	0.34	0.28	-	0.07	-	-
Soil Line	S00/S04	0.14	-	-	0.14	-	-	-	-	-
	S00/S12	0.21	0.12	-	0.22	0.12	-	-	-	-
	S00/S24	0.14	0.33	0.20	0.14	0.28	0.088	0.07	-	-

(The order is from higher to lower peak)

Table 3 Primary Periods of the Building

	Analytical	Observed
X	0.12 sec	0.19 sec
Y	0.23	0.24
Z	0.045	0.06

Table 4 Primary Periods of Soil Column

	Analytical	Observed
GL-4m	0.12 sec	0.14 sec
-12m	0.20	0.21-0.22
-24m	0.30	0.28-0.33

Table 5 Modal Damping Ratio of Soil Column above GL-24m

1st	2nd	3rd	4th
0.085	0.0185	0.0190	0.0115

Table 6 Modal Damping Ratio of Soil Column above GL-12m and Structure with Additive Mass

		Earthq. No.	1st	2nd	3rd
Soil	X	07	0.081	0.050	0.015
		14	0.050	0.048	0.020
	Y	07	0.11	0.030	0.020
		14	0.10	0.055	0.047
Structure	X	07	0.026	0.054	0.050
		14	0.042	0.061	0.033
	Y	07	0.027	0.12	0.090
		14	0.039	0.13	0.085

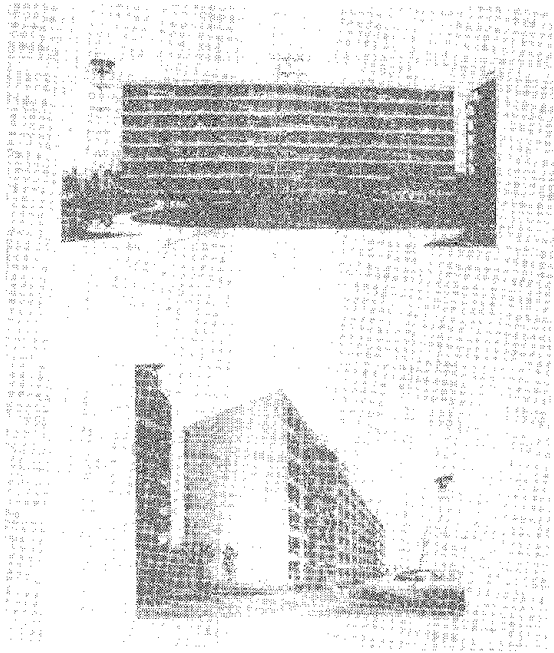


Photo.1 Outside View of the Building

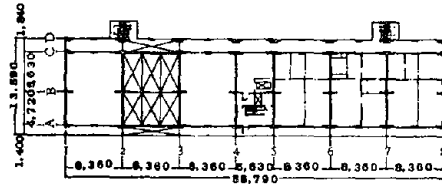


Fig.1 Plan 平面図

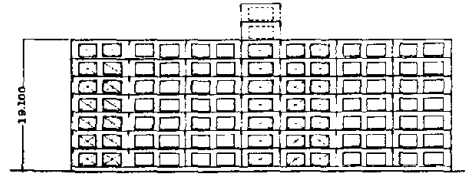


Fig.2 Section 断面図

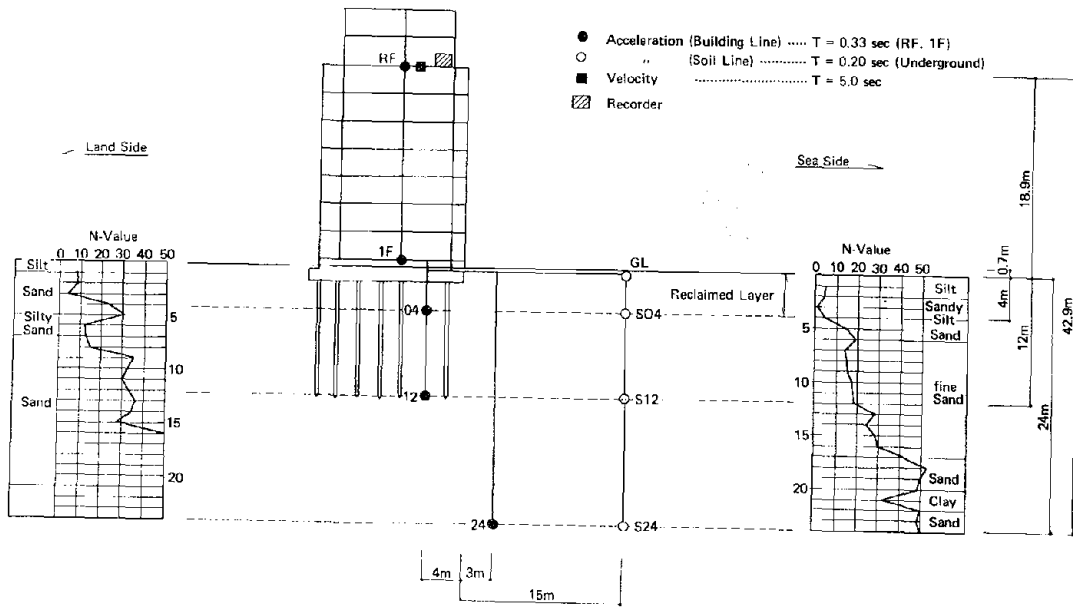


Fig.3 Pick-up Location and Soil Profile

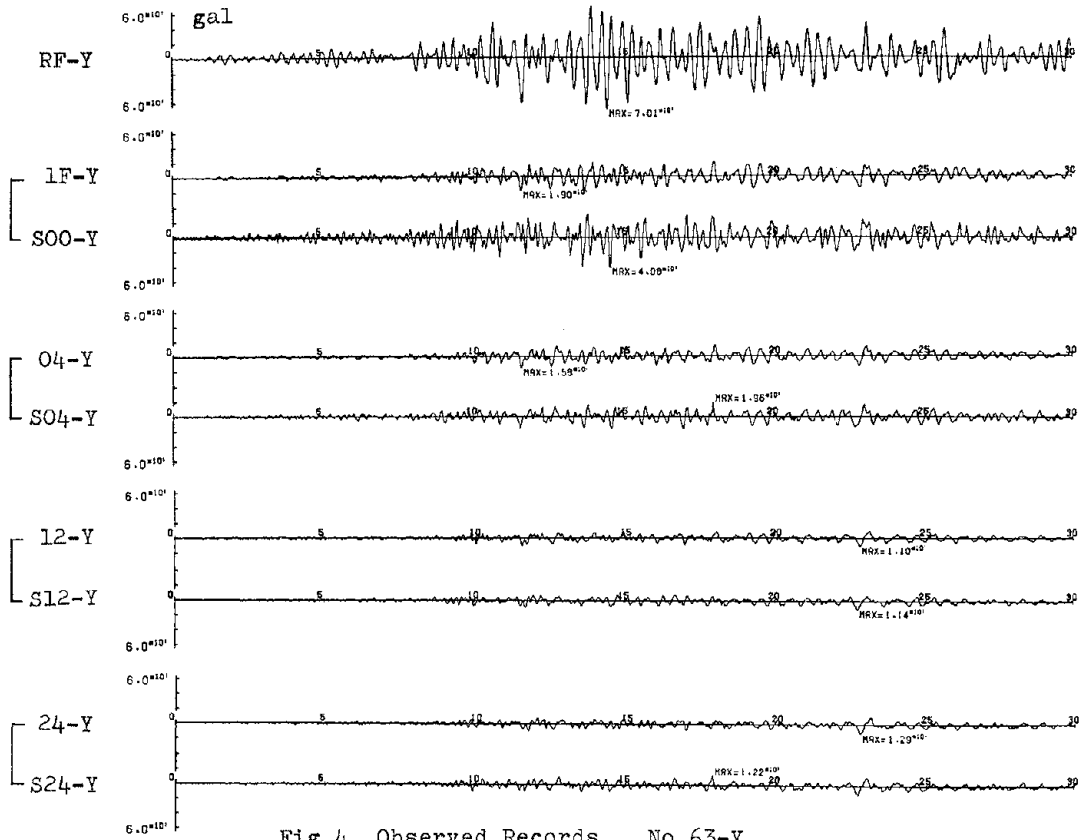


Fig.4 Observed Records No.63-Y

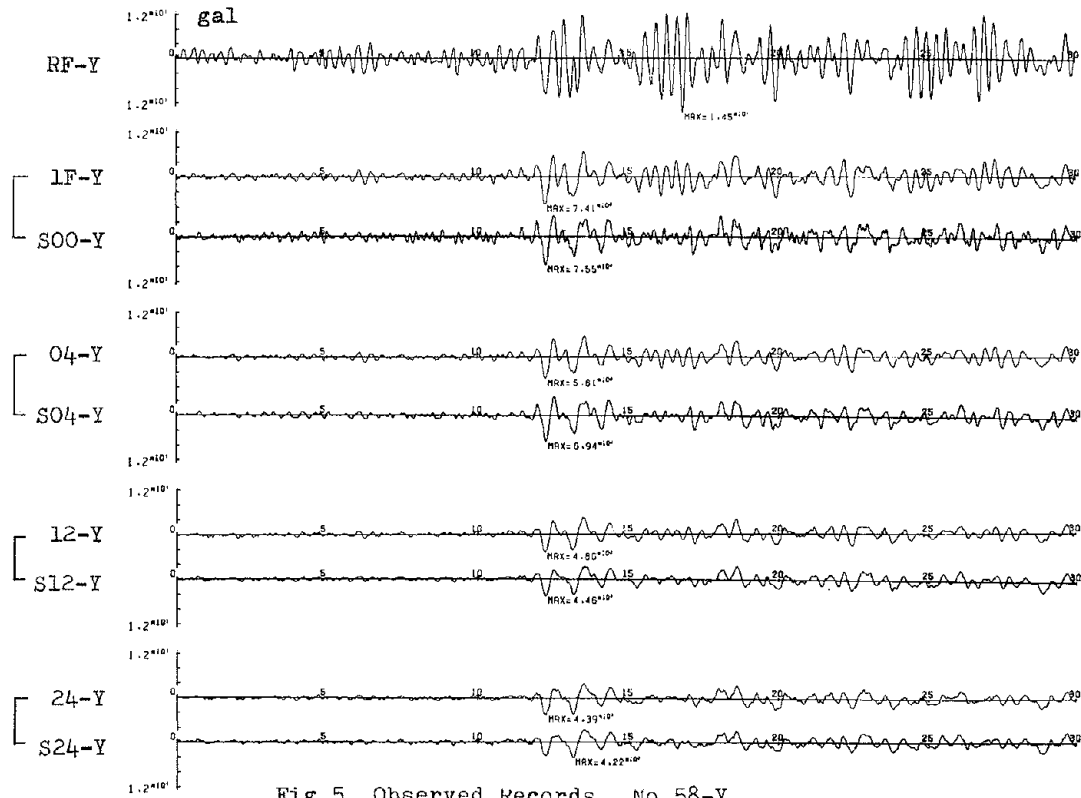


Fig.5 Observed Records No.58-Y

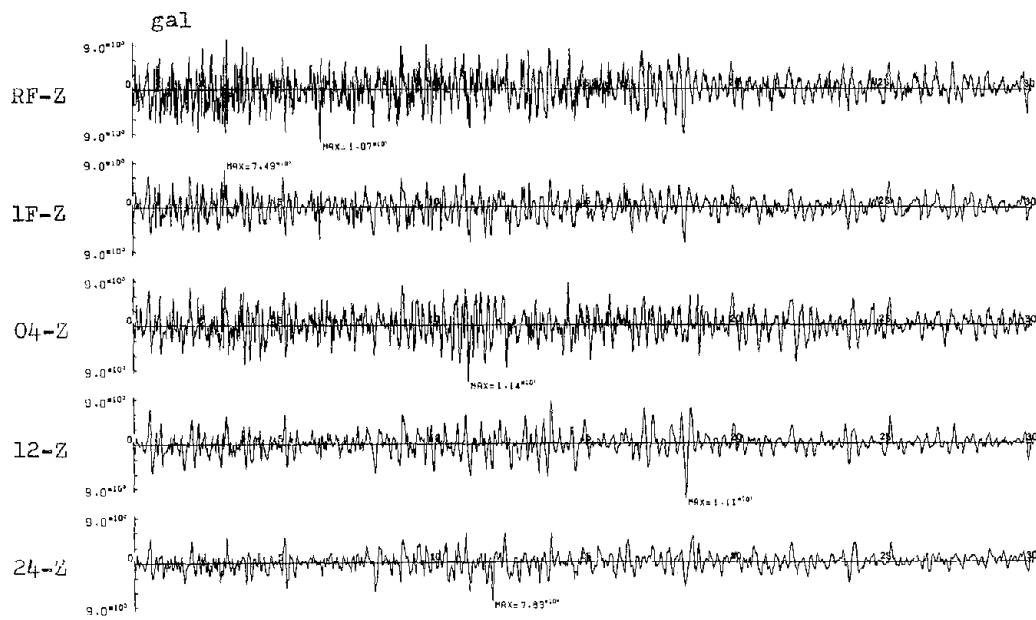


Fig.6 Observed Records No.63-Z

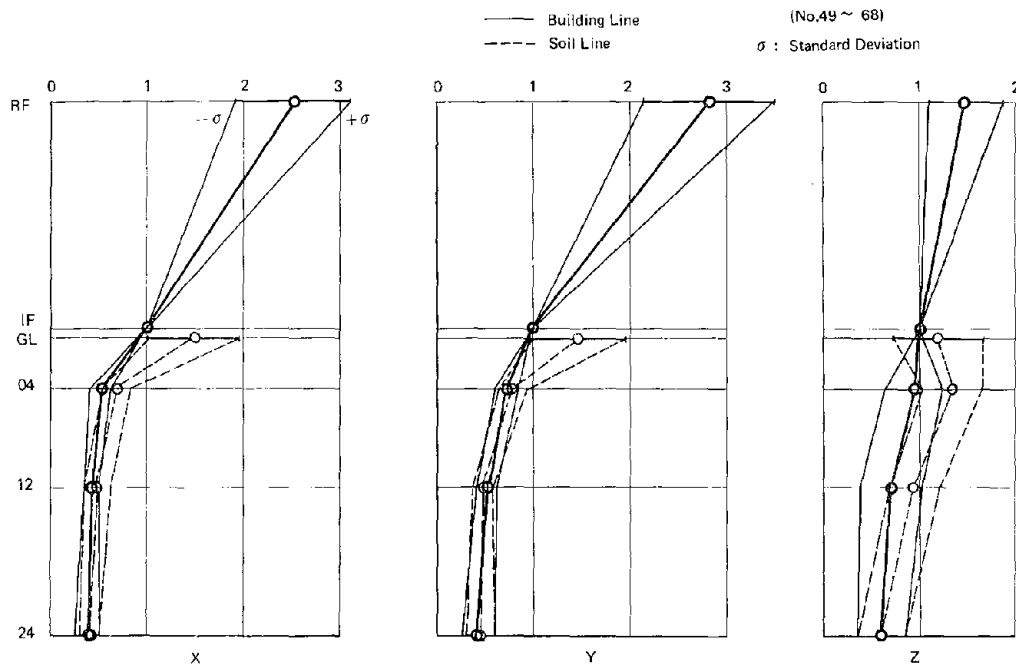


Fig.7 Average Maximum Acceleration Pattern

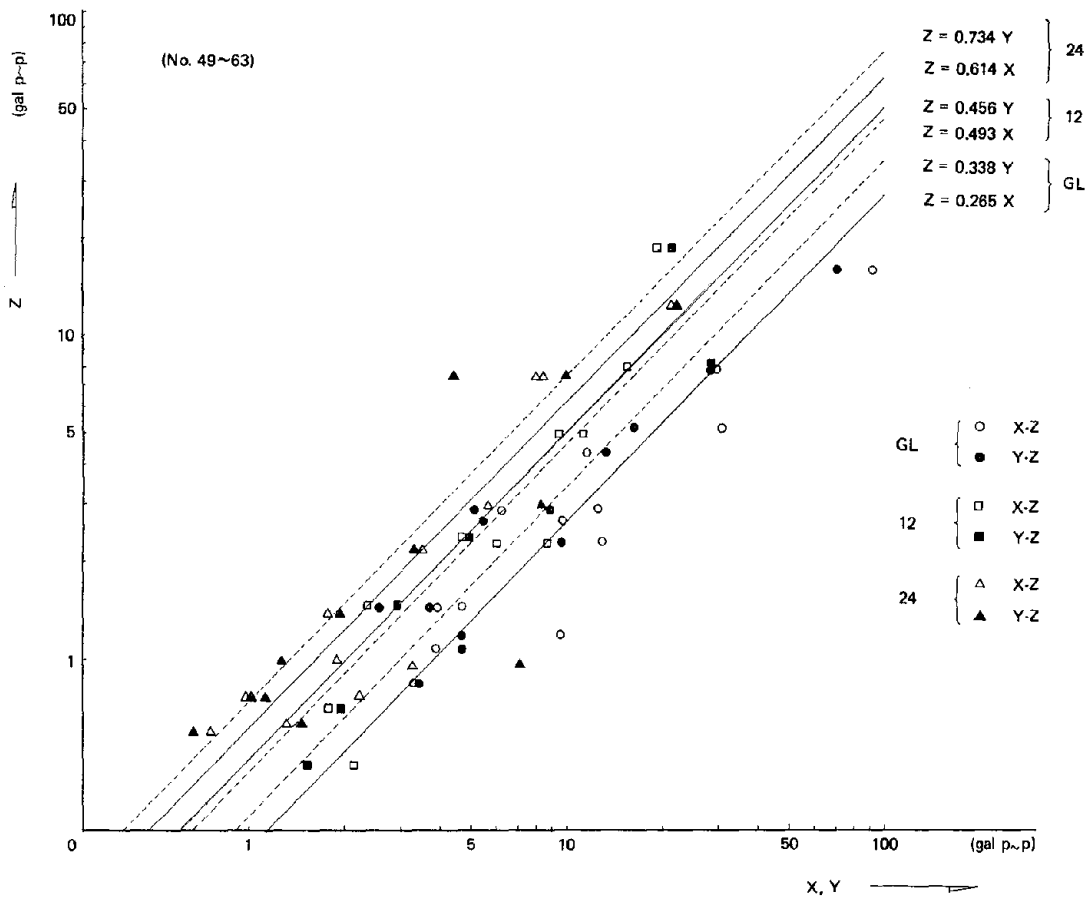


Fig.8 Comparison between Vertical & Horizontal Amplitudes

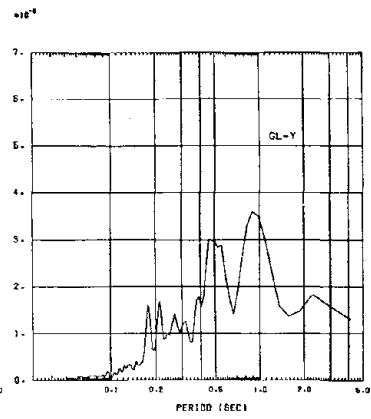
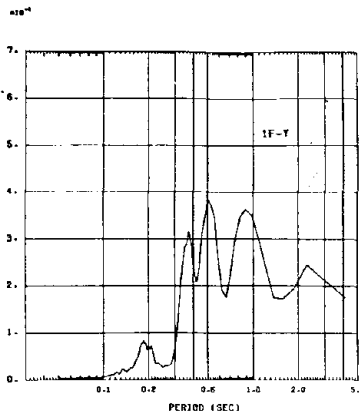
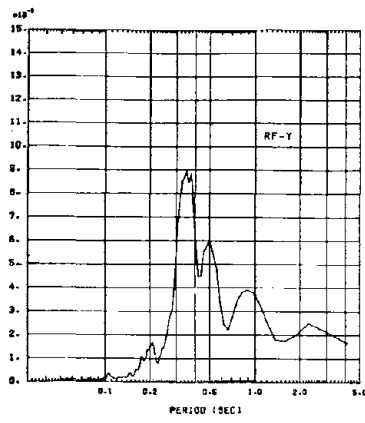


Fig.9 Fourier
Amplitude Spectra
No.58-Y

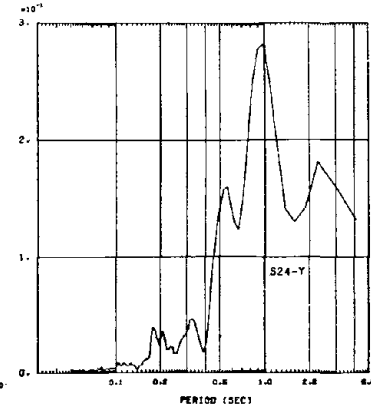
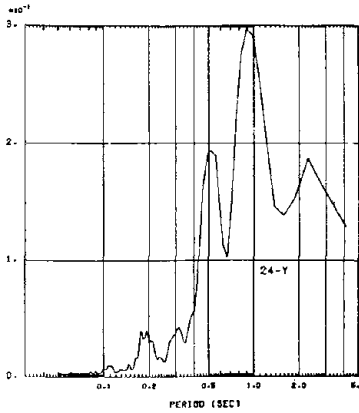
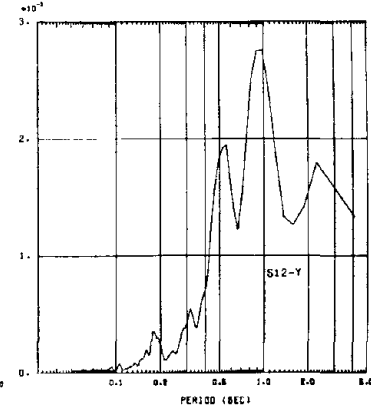
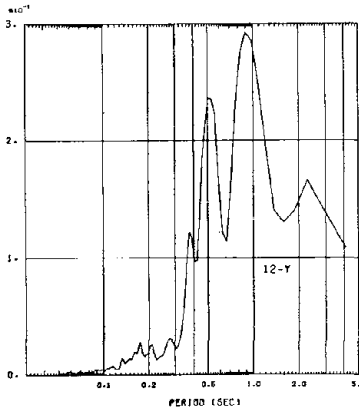
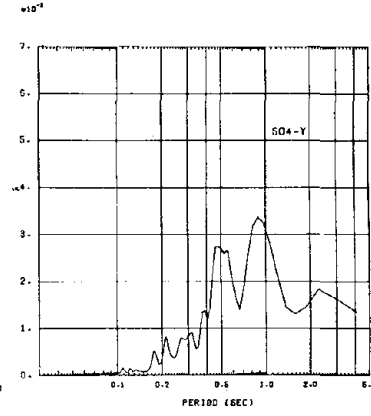
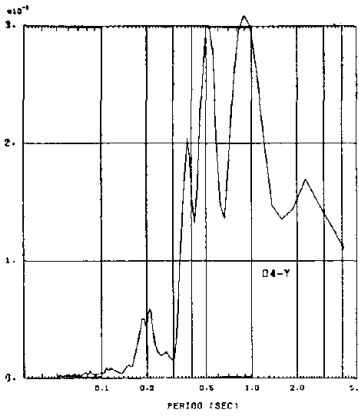
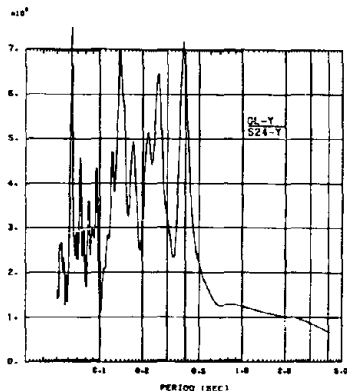
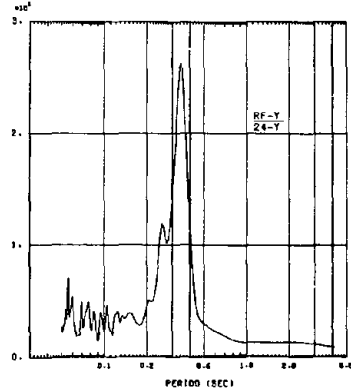
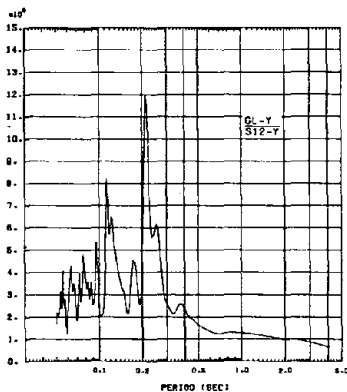
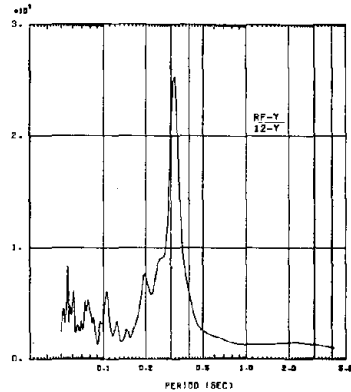
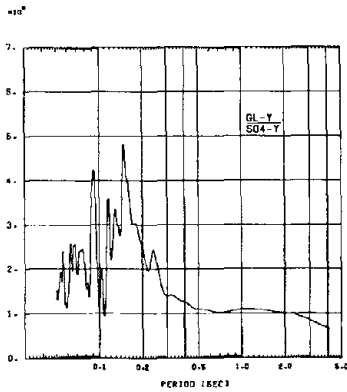
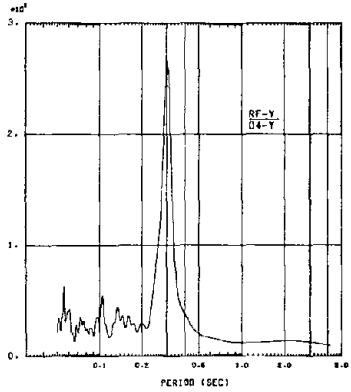
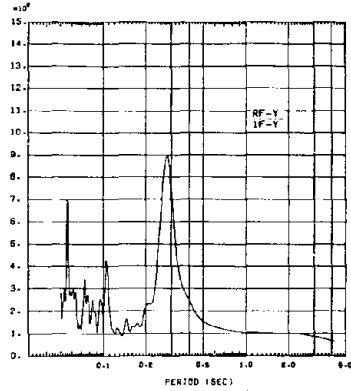


Fig.10 Fourier Amplitude Ratios

No.58-Y



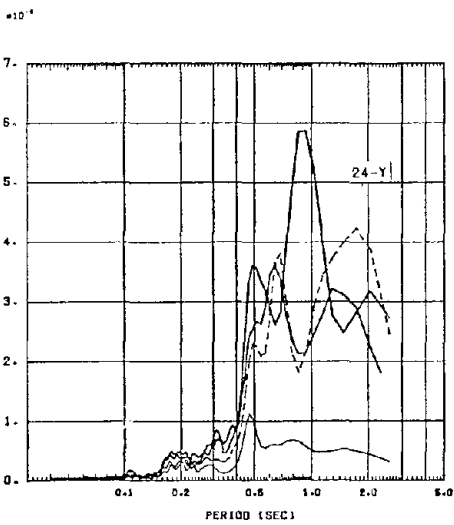
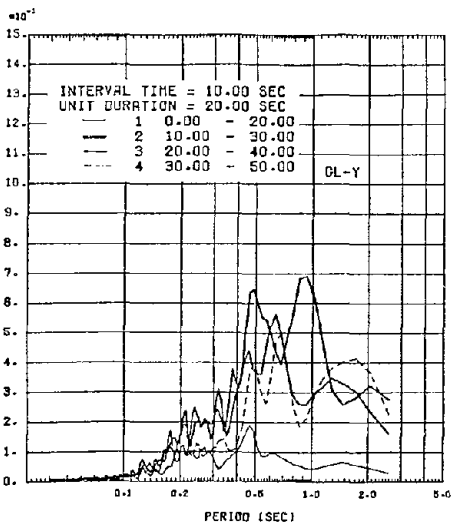
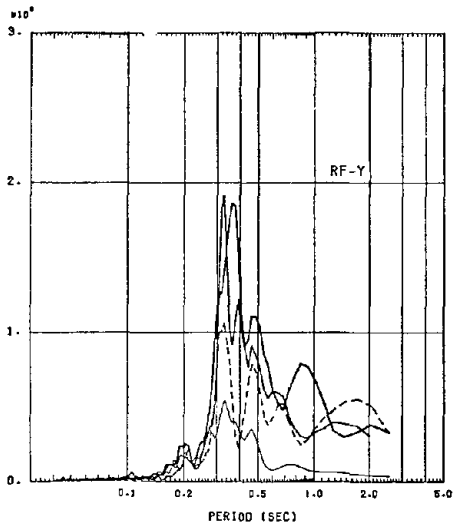


Fig.11 Stepwise Running Fourier Amplitude Spectra No.58-Y

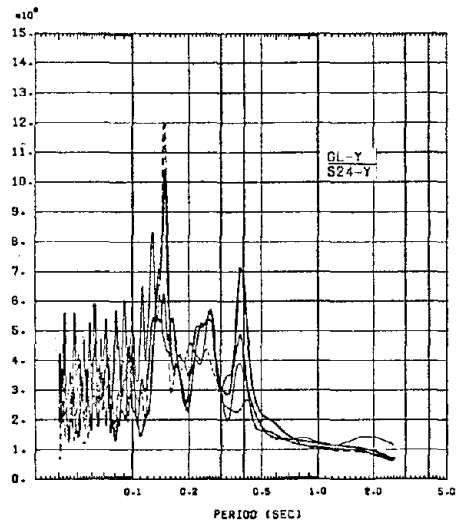
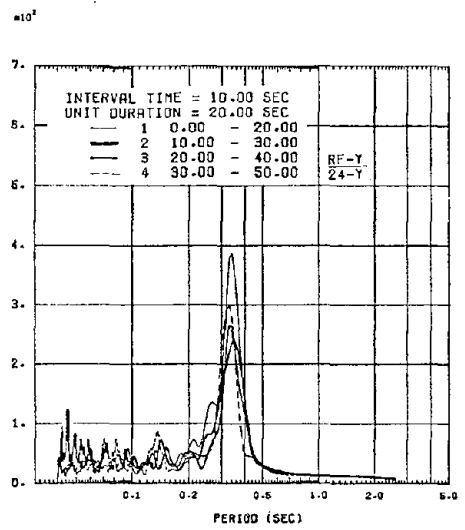
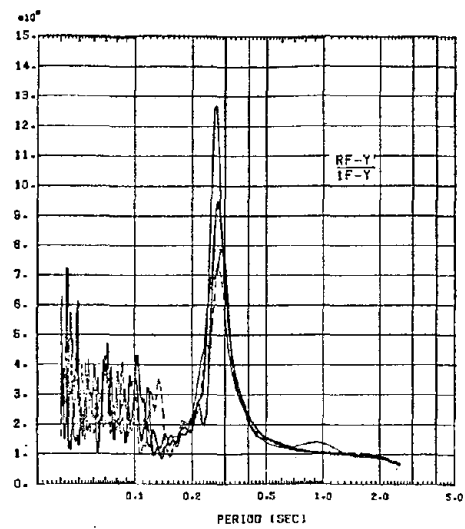


Fig.12 Stepwise Running Fourier Amplitude Ratios No.58-Y

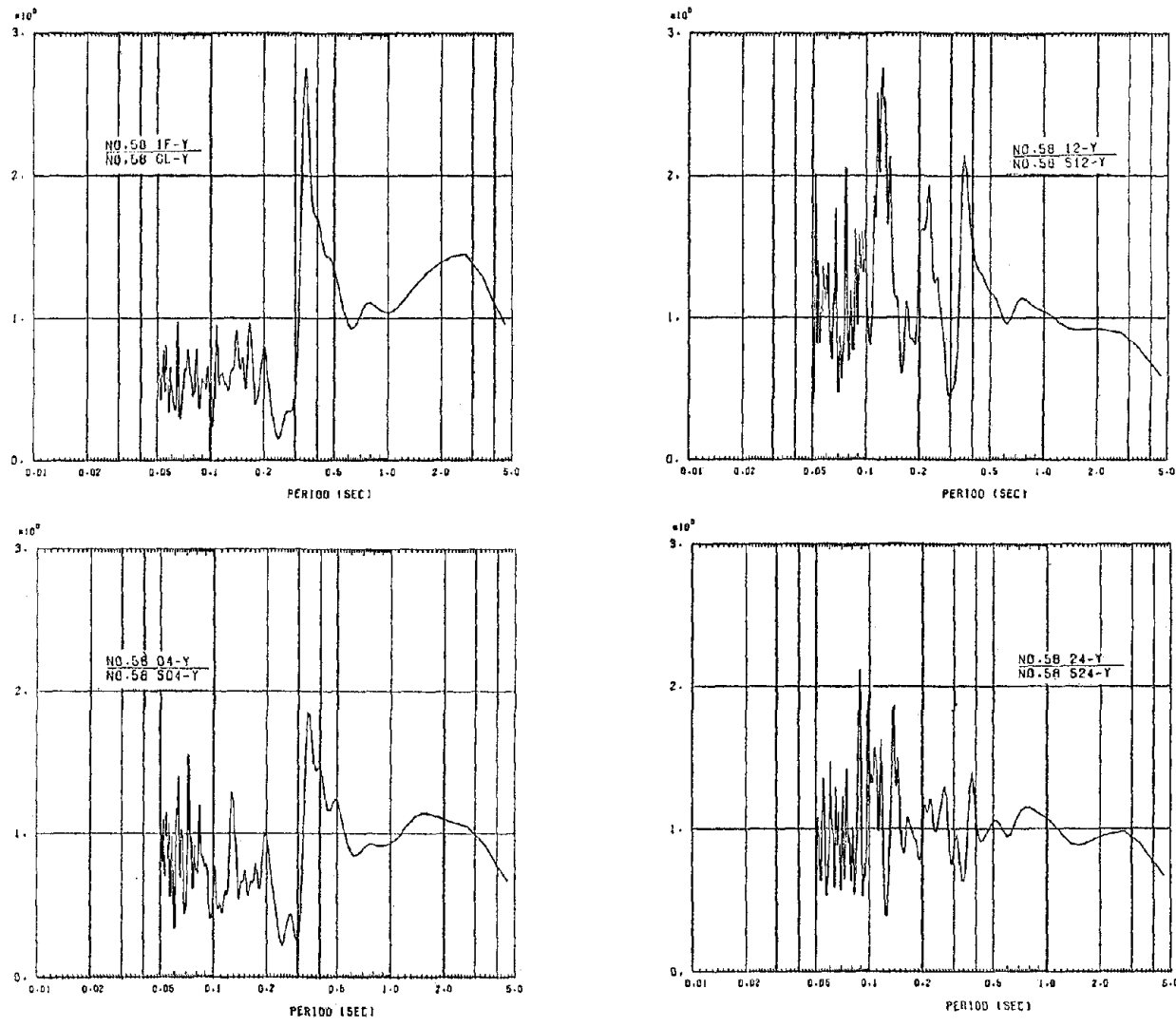


Fig.13 FOURIER SPECTRUM RATIO BETWEEN BUILDING LINE & SOIL LINE

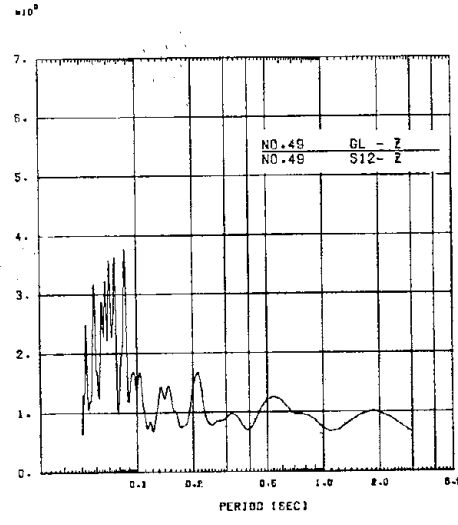
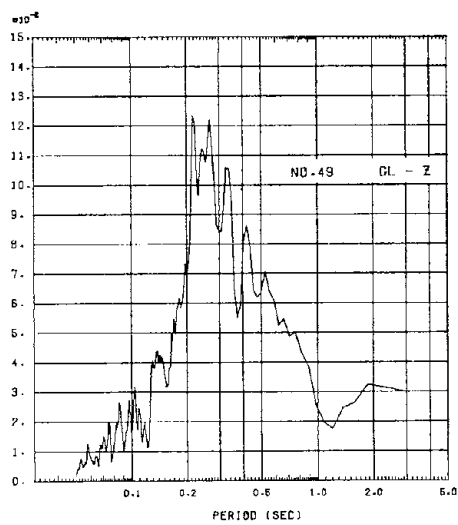
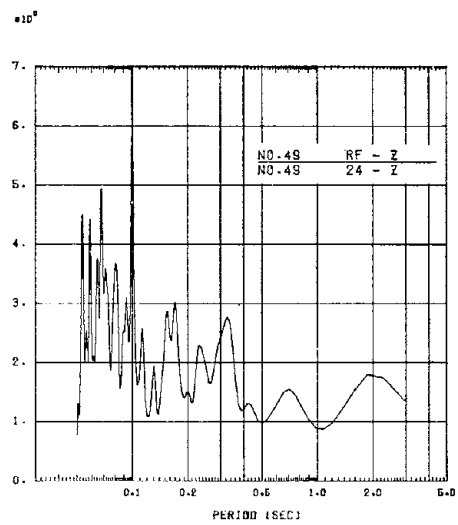
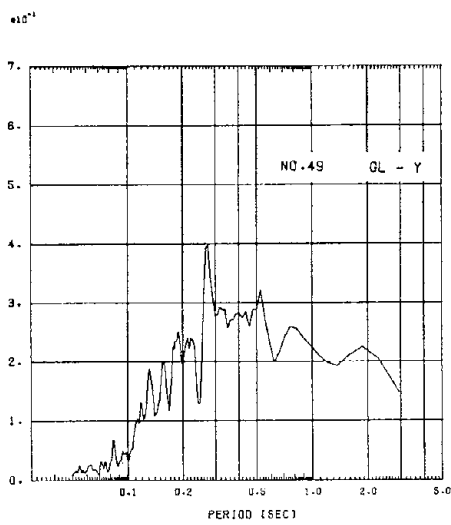
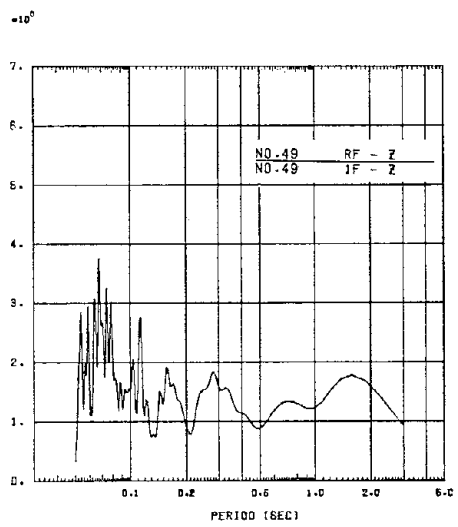
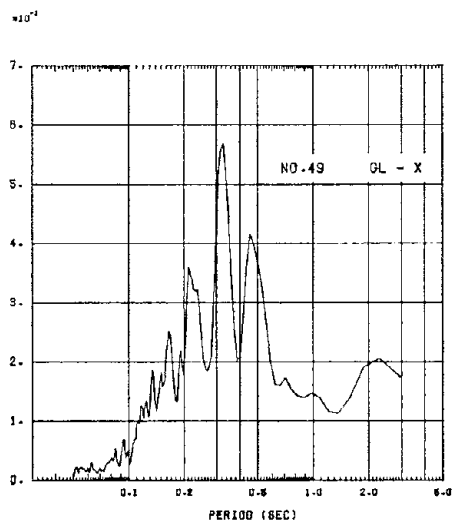
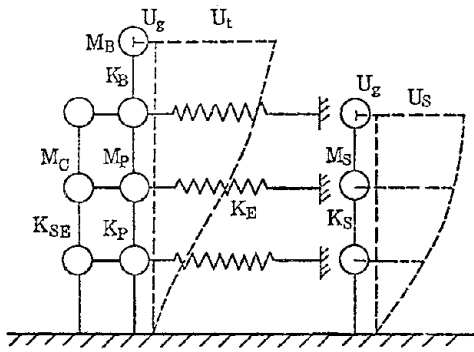


Fig.14 Fourier Amplitude Spectra and Ratios Compared with Horizontal Ones



M_B : Mass of Building, M_P : Mass of Pile
 M_C : Additive Mass, M_S : Mass of Soil Column
 K_B : Stiffness of Building
 K_P : Stiffness of Pile
 K_S : Stiffness of Soil Column
 K_E : Interaction Spring
 K_{SE} : Shear Spring between Additive Masses
 U_g : Ground Motion
 U_t : Displacement of Structure
 U_s : Displacement of Soil Column

Fig.18 Model Composition of Building-Pile-Soil System

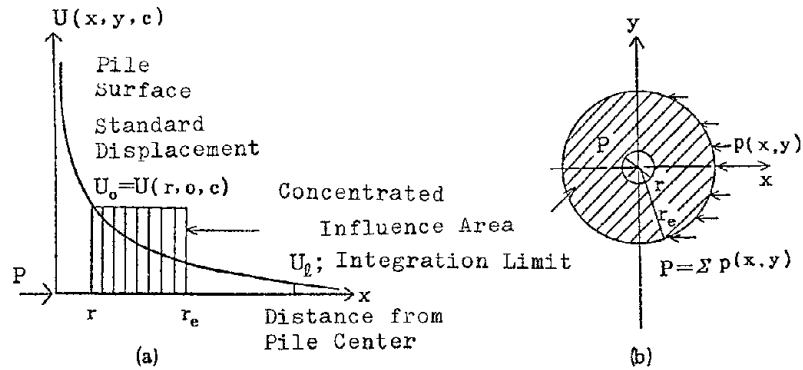


Fig.19 Calculation of Interaction Spring & Additive Mass

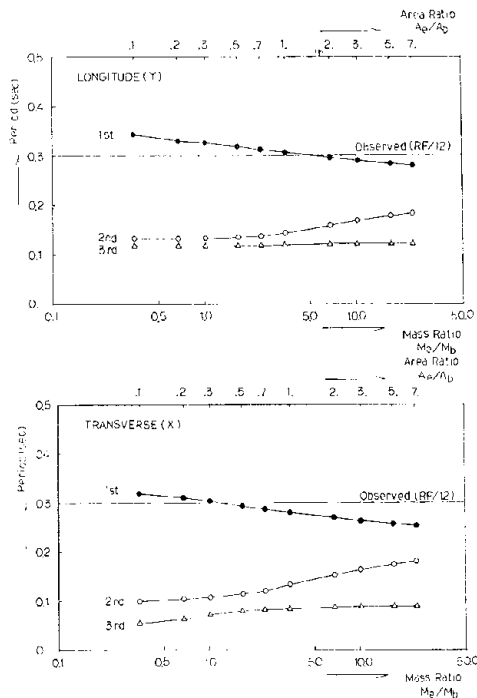


Fig.20 Period Variation due to Additive Mass

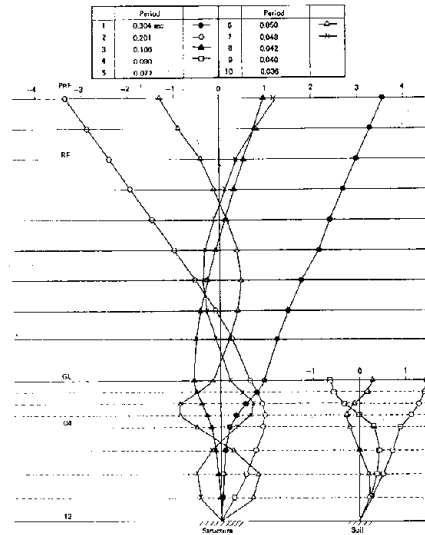


Fig.21 Participation Function of Coupled System - X

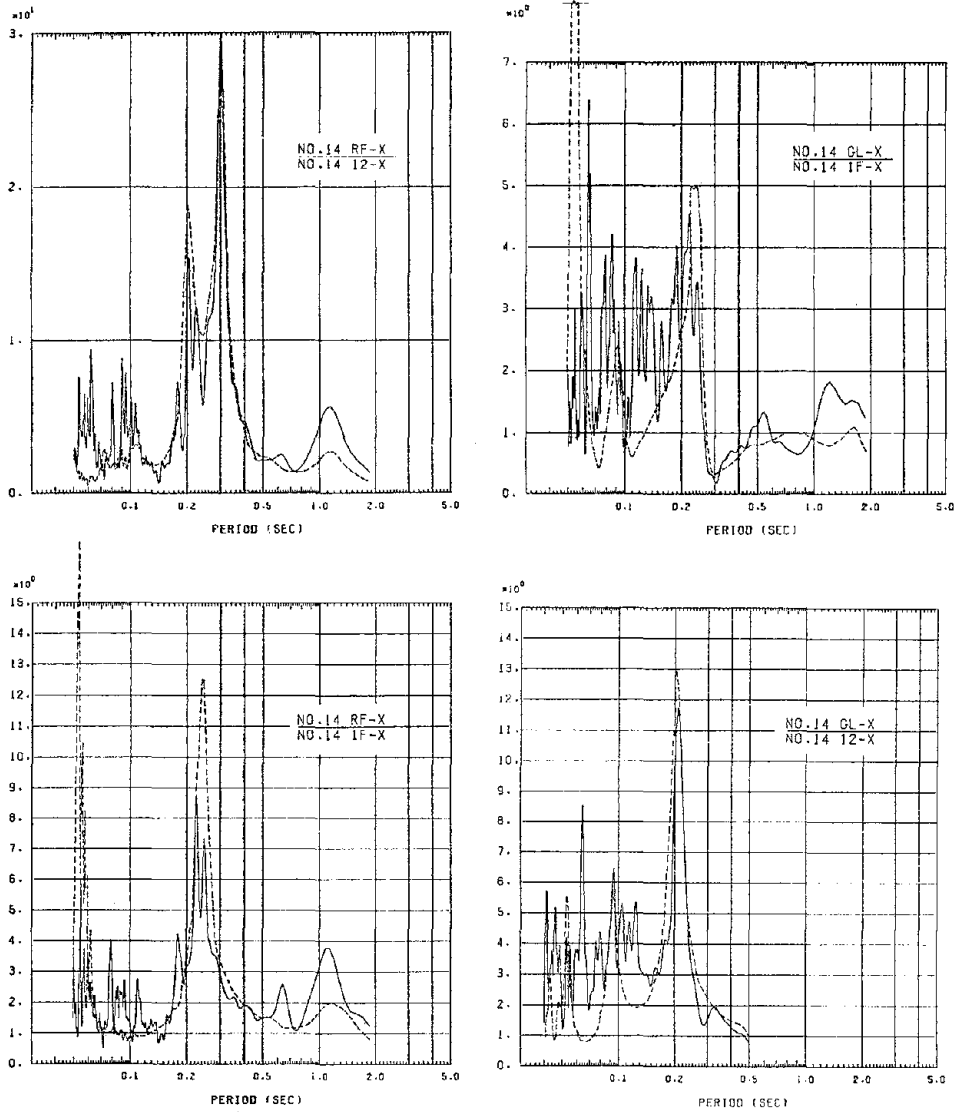


Fig.22 Comparison between Analytical & Observed Spectra

Observed ———
 Analytical - - - - -

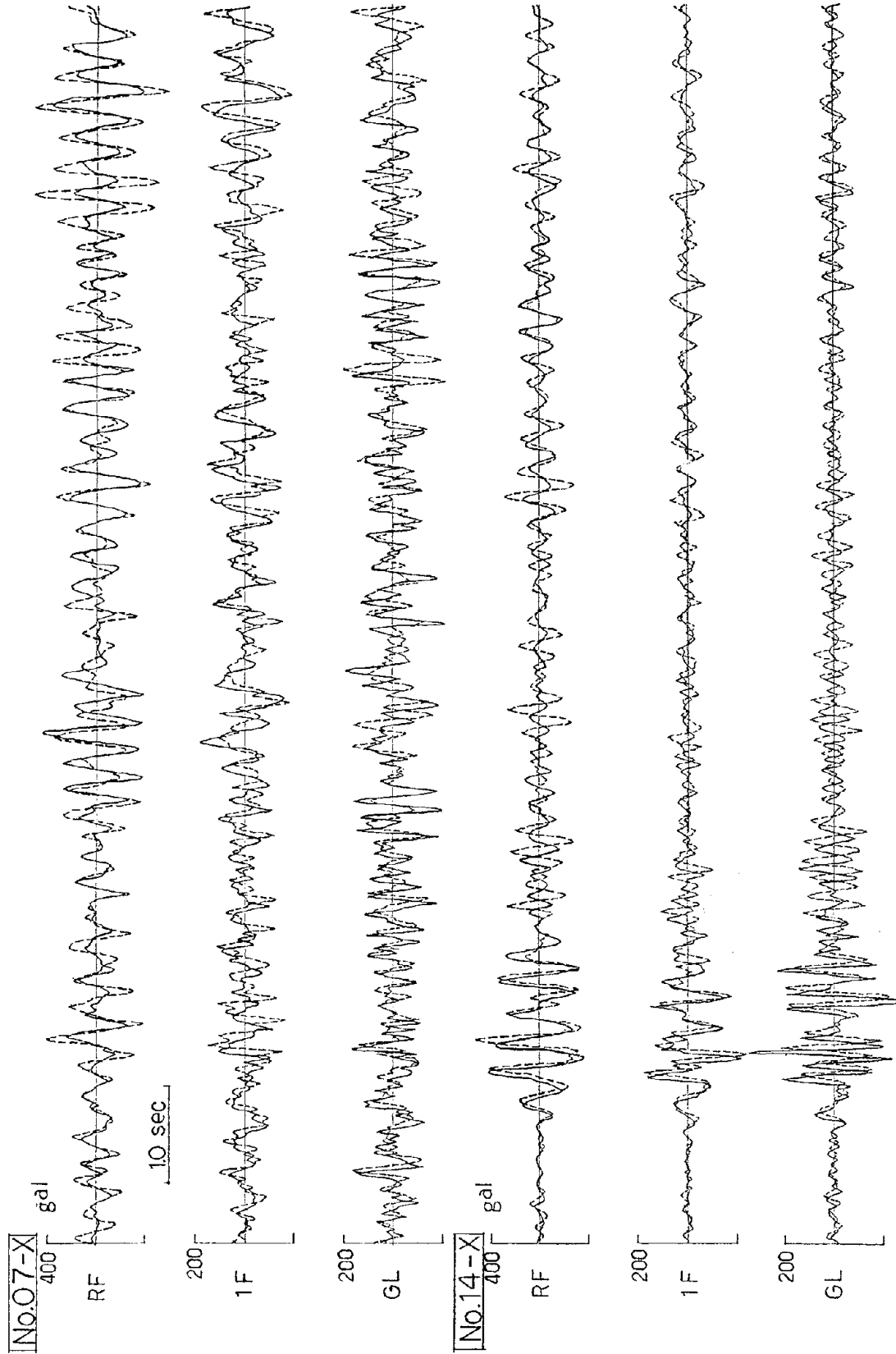


Fig. 23 COMPARISON BETWEEN OBSERVED & CALCULATED WAVES

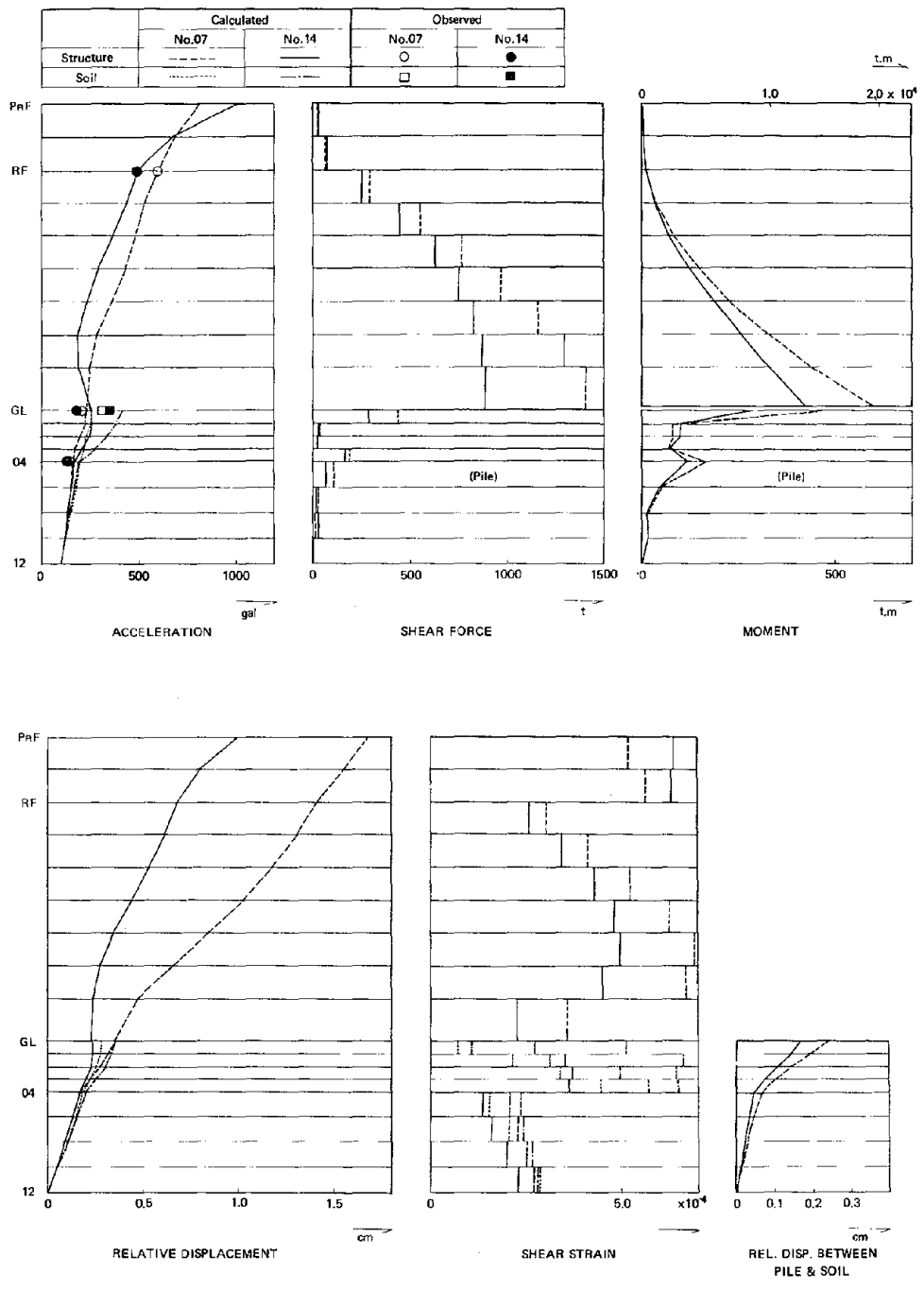


Fig.24 Maximum Response of Coupled System - Y

CHARACTERISTICS OF THREE-DIMENSIONAL
GROUND MOTIONS, SAN FERNANDO EARTHQUAKE

by

Tetsuo Kubo* and Joseph Penzien†

SYNOPSIS

Using the concept of an orthogonal set of principal axes for earthquake ground motions [1], characteristics of the three-dimensional motions produced by the San Fernando, California, earthquake of February 9, 1971, are determined. These principal axes are defined such that the corresponding variances of motions have maximum, minimum, and intermediate values and their covariances equal zero. Results of the analyses indicate a significant correlation of directions of principal axes with directions to the fault zone. It is concluded that three-dimensional ground motions which are generated artificially can be uncorrelated statistically provided the components are directed along principal axes.

INTRODUCTION

In the past, most analytical investigations of the dynamic response of structural systems to strong earthquake motions have considered only one component of ground motion. It is becoming increasingly evident, however, that the responses of some important structural systems such as three-dimensional piping systems, certain nuclear reactor facilities, highway bridges, and earth dams are significantly affected by more than one component of motion. While ground motion at a point has six components, three translational and three rotational [2], it is usually sufficient to consider only the three translational components. Obviously, because of the multi-component influence of ground motion on some systems, there will be an increasing demand in the future for dynamic response analyses using three-dimensional ground motion excitations.

A very simple approach to defining the three translational components of motion would be to assume that certain recorded ground motions of a past earthquake are representative of future site ground motions. This simple approach is subject to question, however, as two recorded accelerograms, even for the same site location, often have quite dissimilar characteristics.

Recognizing that seismic waves are initiated by irregular slippage along faults followed by numerous random reflections, refractions, and attenuations within the complex ground formations through which they pass,

* Assistant Specialist, Earthquake Engineering Research Center, University of California, Berkeley, and Graduate Student, University of Tokyo, Tokyo, Japan.

† Professor of Structural Engineering, University of California, Berkeley, California.

stochastic modelling of strong ground motions is a realistic form which can be applied in practice. Defining earthquake inputs to a structural system in this manner has the distinct advantage that analyses yield mean values and variances of response consistent with the variations to be expected in ground motion characteristics. A number of stochastic models, representing both stationary and nonstationary random processes, have been employed. Some of these models have been extended to multi-components of motion [1,3].

Representative stochastic models for earthquake ground motions could be established directly by statistical analyses if unlimited data were available. Unfortunately, strong motion data in the form of accelerograms are quite limited. Therefore, one is forced to hypothesize model forms, and to use the available strong motion data primarily in checking the appropriateness of these forms. One such model, commonly used in its one-dimensional form [4,5], defines ground accelerations at a point along three orthogonal coordinate axes (usually two being horizontal and one vertical) through the relations

$$\begin{aligned}
 a_x(t) &= \zeta_x(t) b'_x(t) \\
 a_y(t) &= \zeta_y(t) b'_y(t) \\
 a_z(t) &= \zeta_z(t) b'_z(t)
 \end{aligned}
 \tag{1}$$

where $b'_x(t)$, $b'_y(t)$, and $b'_z(t)$ are stationary random processes and $\zeta_x(t)$, $\zeta_y(t)$, and $\zeta_z(t)$ are deterministic intensity functions giving appropriate nonstationarity to their respective ground motion processes.

The use of Eqs.(1) requires that the intensity functions be obtained by statistical analyses of real accelerograms and that realistic power spectral density functions, or corresponding autocorrelation functions, be established by similar means for processes $b'_x(t)$, $b'_y(t)$ and $b'_z(t)$. The question which immediately arises when extending the use of Eqs. (1) to the two- and three-dimensional forms is "Should the components of motions be cross correlated statistically?". If so, one must establish appropriate cross-spectral density functions or corresponding cross-correlation functions.

In a previous paper, it was suggested that the stochastic model [1]

$$\begin{aligned}
 a_x(t) &= \zeta(t) b_x(t) \\
 a_y(t) &= \zeta(t) b_y(t) \\
 a_z(t) &= \zeta(t) b_z(t)
 \end{aligned}
 \tag{2}$$

be used. This model represents an approximation to that defined by Eqs. (1) in that it assumes intensity functions $\zeta_x(t)$, $\zeta_y(t)$, and $\zeta_z(t)$ vary with time in identically the same manner even though they may have different magnitudes, i.e. any two of these intensity functions differ from each other by a fixed constant only. Thus stationary processes $b_x(t)$, $b_y(t)$ and $b_z(t)$ differ from $b'_x(t)$, $b'_y(t)$ and $b'_z(t)$, respectively, by a

corresponding set of constants. Principal axes exist for this model along which the components of ground motion have maximum, minimum, and intermediate values of variance and have zero values of covariance. This property suggests that components of motion generated in accordance with Eqs. (2) need not be cross correlated provided the x, y and z axes are treated as principal axes. It is the purpose of this paper to provide additional evidence in support of this suggestion as obtained from a study of accelerograms recorded during the San Fernando, California, earthquake.

CHARACTERISTICS OF GROUND MOTION HAVING FIXED PRINCIPAL AXES

Suppose $a_x(t)$, $a_y(t)$, and $a_z(t)$ shown in Eqs. (2) represent the components of ground motion at point 0 along an arbitrary set of orthogonal axes x, y and z, respectively. Considering recorded earthquake motions, these components would normally represent accelerations measured along the instrument axes of accelerometers. For purpose of discussion here, however, these motions could equally well represent velocities or displacements.

If $a_x(t)$, $a_y(t)$ and $a_z(t)$ of Eqs. (2) are considered to be zero-mean processes, covariance functions defined by

$$E[a_i(t) a_j(t + \tau)] = \zeta(t) \zeta(t + \tau) E[b_i(t) b_j(t + \tau)] \quad i, j = x, y, z \quad (3)$$

where E denotes ensemble average, can be used to characterize the complete ground motion process. If this process is Gaussian, these covariance functions completely characterize the process in a probabilistic sense [6].

Since random processes $b_x(t)$, $b_y(t)$ and $b_z(t)$ are stationary, all ensemble averages on the right hand side of Eqs. (3) are independent of time t; therefore, showing dependence only upon the time difference τ . Since real earthquake accelerograms can be approximately represented by shot noise [7], they demonstrate a very rapid loss in correlation with increasing values of τ . Therefore, the influence of coordinate directions on the covariance functions can be investigated using the relations.

$$E[a_i(t) a_j(t)] = \zeta(t)^2 E[b_i(t) b_j(t)] \quad i, j = x, y, z \quad (4)$$

Adopting matrix notation, Eqs. (4) can be written in the more compact form

$$\underline{\mu}(t) = \zeta(t)^2 \underline{\beta} \quad (5)$$

where

$$\mu_{ij}(t) = E[a_i(t) a_j(t)] \quad (6)$$

$$\beta_{ij} = E[b_i(t) b_j(t)] \quad (7)$$

Note that because random processes $b_x(t)$, $b_y(t)$ and $b_z(t)$ are stationary, all nine coefficients in matrix $\underline{\beta}$ are time invariant.

If the components of ground motion at point 0 are transformed from coordinate system x, y, z to a new orthogonal coordinate system x', y', z' through the relation

$$\begin{pmatrix} a_{x'}(t) \\ a_{y'}(t) \\ a_{z'}(t) \end{pmatrix} = \underline{a} \begin{pmatrix} a_x(t) \\ a_y(t) \\ a_z(t) \end{pmatrix} \quad (8)$$

where the transformation matrix \underline{a} satisfies the condition

$$\underline{a}^T \underline{a} = \underline{I} \text{ (identity matrix)} \quad (9)$$

relations identical to Eqs. (5)-(7) can be written for the new coordinate system with

$$\underline{\beta}' = \underline{a}^T \underline{\beta} \underline{a} \quad (10)$$

$$\underline{\mu}' = \zeta(t)^2 \underline{a}^T \underline{\beta} \underline{a} \quad (11)$$

This transformation of ground motion is identical to the transformation of a three-dimensional state of stress; therefore, it is apparent that a set of principal axes exist along which the component variances of motion have maximum, minimum, and intermediate values. The directions of these principal axes are found in exactly the same manner as locating the directions of principal stresses, i.e. by obtaining the eigen value formulation. The resulting three vectors define the principal transformation matrix \underline{P} ; thus, permitting the components of ground motion along principal axes, 1, 2, 3 to be given by

$$\begin{pmatrix} a_1(t) \\ a_2(t) \\ a_3(t) \end{pmatrix} = \underline{P} \begin{pmatrix} a_x(t) \\ a_y(t) \\ a_z(t) \end{pmatrix} \quad (12)$$

where

$$\underline{P}^T \underline{P} = \underline{I} \quad (13)$$

the corresponding covariance matrix for ground motion becomes

$$\underline{\mu}_P(t) = \zeta(t)^2 \underline{\beta}_P = \zeta(t)^2 \underline{P}^T \underline{\beta} \underline{P} = \zeta(t)^2 \begin{bmatrix} \beta_{11} & 0 & 0 \\ 0 & \beta_{22} & 0 \\ 0 & 0 & \beta_{33} \end{bmatrix} \quad (14)$$

A procedure similar to that above can be used to determine the coordinate transformations which yield maximum covariances of ground motion. When transforming from principal axes 1, 2, 3, this procedure leads to the following orthogonal transformation matrices.

$$\underline{S}_1 = \begin{bmatrix} \pm\sqrt{1/2} & 0 & \pm\sqrt{1/2} \\ 0 & \pm 1 & 0 \\ \pm\sqrt{1/2} & 0 & \mp\sqrt{1/2} \end{bmatrix} \quad \underline{S}_2 = \begin{bmatrix} \pm 1 & 0 & 0 \\ 0 & \pm\sqrt{1/2} & \pm\sqrt{1/2} \\ 0 & \mp\sqrt{1/2} & \pm\sqrt{1/2} \end{bmatrix} \quad (15)$$

$$\underline{S}_3 = \begin{bmatrix} \pm\sqrt{1/2} & \pm\sqrt{1/2} & 0 \\ \pm\sqrt{1/2} & \mp\sqrt{1/2} & 0 \\ 0 & 0 & \pm 1 \end{bmatrix}$$

Substituting Eqs. (15) separately into the relation

$$\underline{\mu}_C(t) = \underline{S}^T \underline{\mu}_P(t) \underline{S} \quad (16)$$

gives maximum covariances equal to $\pm 1/2[\mu_{11}(t) - \mu_{33}(t)]$, $\pm 1/2[\mu_{22}(t) - \mu_{33}(t)]$, and $\pm 1/2[\mu_{11}(t) - \mu_{22}(t)]$ where $\mu_{ii} = \zeta(t)^2 \beta_{ii}$ ($i=1,2,3$). The corresponding variances are $\pm 1/2[\mu_{11} + \mu_{33}(t)]$, $\pm 1/2[\mu_{22}(t) + \mu_{33}(t)]$, and $\pm 1/2[\mu_{11}(t) + \mu_{22}(t)]$, respectively.

Fortunately in practice, stationary processes $b_x(t)$, $b_y(t)$, and $b_z(t)$ can often be considered as ergodic processes in which case the covariances can be obtained by time averaging over any single member of the ensemble, say the r th member. In this case β_{ij} as defined by Eqs. (7) can be obtained using the relation

$$\beta_{ij} = \langle b_{ir}(t) b_{jr}(t) \rangle \quad \begin{matrix} i,j = x,y,z \\ r = 1,2,3,\dots \end{matrix} \quad (17)$$

where the triangular brackets denote time average.

CHARACTERISTICS OF GROUND MOTIONS FROM MOVING-WINDOW ANALYSIS

In a previous paper [1], variances and covariances of recorded ground motions were obtained for successive time intervals using the relation

$$\mu_{ij} = \langle [a_i(t) - \bar{a}_i] [a_j(t) - \bar{a}_j] \rangle_{t_1}^{t_2} \quad (18)$$

in which the time average is taken over the interval $t_1 < t < t_2$ but where the mean values \bar{a}_i and \bar{a}_j are found by averaging $a_i(t)$ and $a_j(t)$ over the entire duration of motion. Locations of principal axes and magnitudes of corresponding variances were obtained for earthquake motions recorded at three stations in California and three stations in Japan.

In the present paper, variances and covariances are obtained as continuous functions of time t_0 using the so-called "moving-window" technique, i.e. using the relation

$$\mu_{ij}(t_0, \Delta t) = \langle [a_i(t) - \bar{a}_i] [a_j(t) - \bar{a}_j] \rangle_{t_0 - \frac{\Delta t}{2}}^{t_0 + \frac{\Delta t}{2}} \quad (19)$$

where the time average is taken over the interval Δt centered on time t_0 [8]. As the value of Δt is taken shorter and shorter, increased fluctuations in $\mu_{ij}(t_0, \Delta t)$ and the corresponding directions of principal axes will, of course, occur. In fact, as $\Delta t \rightarrow 0$, the major principal axis of ground motion coincides with the instantaneous resultant acceleration vector which changes its direction rapidly in a random fashion over the entire sphere of space. Therefore, Δt should be taken sufficiently long so that the higher frequency fluctuations are essentially removed. In the present investigation, Δt is taken as five seconds and all time averages are evaluated for discrete values of t_0 spaced one-half second apart.

Having obtained all nine covariance functions for the recorded components of motion in accordance with Eq. (19), the corresponding time dependent directions of principal axes can be obtained; thus, giving the principal transformation matrix \underline{P} as a function of time t_0 , i.e. $\underline{P} = \underline{P}(t_0)$. This time dependent transformation matrix then allows one to obtain the principal components of motion $a_1(t)$, $a_2(t)$, and $a_3(t)$, and their corresponding variances $\sigma_1^2(t_0)$, $\sigma_2^2(t_0)$, and $\sigma_3^2(t_0)$. If the intensity functions of all recorded components of motion vary with time in the same manner, i.e. satisfy Eqs. (2), any two of these variance functions differ from each other by a fixed constant only in which case the directions of principal axes are time invariant.

The above described moving-window technique, as applied in the time domain, can also be applied in the frequency domain. In this case, the variances and covariances are obtained as continuous functions of frequency f_0 using the relation

$$\mu_{ij}(f_0, \Delta f) = \left\langle \left[\int_{-f_0 - \frac{\Delta f}{2}}^{-f_0 + \frac{\Delta f}{2}} A_i(2\pi if) e^{2\pi ift} df + \int_{f_0 - \frac{\Delta f}{2}}^{f_0 + \frac{\Delta f}{2}} A_i(2\pi if) e^{2\pi ift} df \right] \cdot \right. \\ \left. \left[\int_{-f_0 - \frac{\Delta f}{2}}^{-f_0 + \frac{\Delta f}{2}} A_j(2\pi if) e^{2\pi ift} df + \int_{f_0 - \frac{\Delta f}{2}}^{f_0 + \frac{\Delta f}{2}} A_j(2\pi if) e^{2\pi ift} df \right] \right\rangle_0^T \quad (20)$$

$$\text{where } A_i(2\pi if) = \int_0^T a_i(t) e^{-2\pi ift} dt ; \quad A_j(2\pi if) = \int_0^T a_j(t) e^{-2\pi ift} dt$$

and where T equals the total duration of ground motion. This formulation allows one to investigate the directions of principal axes, variances, covariances, etc. associated with only those frequencies of ground motion in the range $(f_0 - \Delta f/2) < f < (f_0 + \Delta f/2)$. Hopefully, this approach can be used to reveal certain characteristic features of the various types of seismic waves associated with strong ground motions.

RESULTS OF MOVING-WINDOW ANALYSIS

The time domain moving-window analysis described above has been applied to the ground motions recorded at numerous stations during the San Fernando earthquake of February 9, 1971.

Directions of principal axes and the corresponding principal variances are obtained as functions of time t_0 using Δt equal to five seconds. The direction of each principal axis is given by angles ϕ and θ as shown in Fig. 1. Angle ϕ is the declination of the principal axis from the vertical axis through point O ; thus, its value falls in the range $0 \leq \phi \leq 90^\circ$. Angle θ is measured from the North axis to the projection of the northerly extension of the principal axis on a horizontal plane containing point O . By this definition, θ lies in the range $-90^\circ < \theta \leq +90^\circ$. The angle θ_E in Fig. 1 represents the horizontal direction of an axis passing through the instrument location (point O) and the reported epicenter. Since this angle is measured similar to angle θ , it also lies in the range $-90 < \theta_E \leq +90^\circ$. Length OA in Fig. 1 represents magnitude of the variance of principal ground motion. The square root of this quantity (sigma) can be used to represent the intensity function of the corresponding nonstationary process [9].

Direction angles ϕ (phi) and θ (theta) and the square root of the variance (sigma) have been obtained as functions of t_0 (time) for the major, minor, and intermediate principal axes of the ground motions recorded at numerous stations. The results for stations Nos. 241, 264, 475, 287, and 103 are shown in Figs. 2-6, respectively. The solid, short-dashed, and intermediate-dashed curves in these figures represent the major, minor, and intermediate axes, respectively, and the horizontal long-dashed straight lines represent the directions θ_E to the reported epicenter. The site locations of these particular stations are shown in Figs. 7 and 8 and certain data associated with each are given in Table 1. It should be noted from the definition of θ that as the horizontal direction of a principal axis rotates in a continuous manner through the East-West direction, the value of θ changes instantaneously by 180° , i.e. changes from $+90^\circ$ to -90° or from -90° to $+90^\circ$ depending upon whether the horizontal projection of the principal axis is rotating clockwise or counterclockwise. This explains the sudden jumps which appear in the functions of θ which take place over single spacings of the prescribed discrete values of t_0 , namely over one-half second spacings.

Although the functions shown in Figs. 2-6 have numerous unexplainable features, certain correlations should be noted as follows:

- (1) Usually during the early period of low intensity motion, either the major or the intermediate principal axis is nearly vertical

but later shifts towards a horizontal position with the minor principal axis taking the vertical position.

- (2) Following the shift of the major principal axis towards a horizontal position, the horizontal directions of the major and intermediate axes are sometimes suddenly interchanged.
- (3) After the major and intermediate axes have moved to their nearly horizontal positions, it is common for the minor and intermediate axes to have approximately the same horizontal directional angles θ over large time intervals.
- (4) For motions measured in many high rise buildings, some of the more common correlative features of motion related to principal axes are eliminated due to soil-structure interaction.
- (5) Usually during the periods of high intensity motions, the horizontal direction of either the major or the intermediate principal axis is towards the fault zone.

Further studies are required to explain the physical phenomena associated with these correlations. Hopefully they can be related to the various types of seismic waves producing the motions.

Figures 7, 8 and 9 are maps of areas in southern California showing the horizontal directions of the major and intermediate principal axes during the periods of high intensity motions at numerous recording stations, including stations Nos. 241, 264, 475, 287, and 103. The map in Fig. 8 is an enlargement of the small rectangular area in Fig. 7 showing the extended Los Angeles and San Fernando regions. Similarly, the map in Fig. 9 is an enlargement of the small rectangular area in Fig. 8 showing the cities of Los Angeles, Hollywood, and Beverly Hills. While the correlation is not strong, there is a tendency of the directions of the major principal axis or, in some cases, the intermediate axis to point in the general direction of the fault slip zone as shown in Fig. 8 [10] which is also the general direction towards the previously reported locations of surface fault traces south of the epicenter [11]. One can speculate that this direction coincides with the direction to maximum energy release in the fault zone. Obviously, the closeness of the recording stations to the fault slip zone, local geological conditions and soil-structure interaction effects weaken this correlation in the case of motions produced by the San Fernando earthquake. It should be pointed out that the horizontal directions of major and intermediate axes obtained from time averaging over the entire durations of motions are quite similar to those shown in Figs. 7, 8, and 9.

CONCLUDING REMARKS

Examination of ground motions recorded during the San Fernando earthquake of February 9, 1971, reveals a correlation between the horizontal directions of the major and intermediate principal axes and the directions from the recording stations to the fault slip zone. While in this case there is a definite tendency for one of these principal axes, most often the major axis, to line up with direction to the fault slip zone, the correlation is not as strong as previously reported for ground motions

produced by other earthquakes [1]. Several possible reasons exist for this weaker correlation:(1) closeness of the recording stations to the fault slip zone, (2) local geologic conditions, and (3) soil-structure interaction.

In view of the existance of the above correlation, it is believed that the stochastic three-dimensional ground motion model defined by Eqs. (2) is reasonable for practical use at this time. The components of motion generated from this model need not be correlated statistically; however, the uncorrelated components should be directed along a set of principal axes. If the decision is made that the radial motions are to be higher intensity than the transverse motions, then the major principal axis should be directed towards the most probable epicenter location and the minor axis should be directed vertically. Unfortunately, evidence in support of this decision is weak. Therefore, one may decide to use the same intensity in both the radial and transverse directions in which case the major and intermediate axes are interchangeable. The uncorrelated components can, of course, be transformed to principal axes of structural systems for use in dynamic analyses.

It is quite apparent that further investigations are needed, using both the time domain and frequency domain moving-window analysis technique, to establish better definitions of the frequency contents of expected ground motions and better descriptions of the intensity functions to be used in three-coordinate directions. The results of such analyses should be interpreted with full consideration given to the contributions of the various types of seismic waves present in the ground motions.

ACKNOWLEDGMENT

The study presented herein is an extension of an investigation previously conducted by the authors in collaboration with Dr. M. Watabe, Mr. R. Iwasaki, and Mr. K. Ishida at the University of Tokyo. The financial support provided by the National Science Foundation under Grant No. GI-36387 is hereby acknowledged with sincere thanks and appreciation.

BIBLIOGRAPHY

- [1] J. Penzien and M. Watabe, "Characteristics of 3-Dimensional Earthquake Ground Motions", *Earthquake Engineering and Structural Dynamics*, Vol. 3, No. 4, April-June 1975.
- [2] E. Rosenblueth, "The Six Components of Earthquakes", *Proceedings of the Australian and New Zealand Conference on the Planning and Design of Tall Buildings*, Sydney, Australia, August 14-17, 1973.
- [3] M. Shinozuka and C.-M. Jan, "Simulation of Multivariate and Multidimensional Processes II", Technical Report No. 12, Department of Civil Engineering and Engineering Mechanics, Columbia University.
- [4] P. C. Jennings, G. W. Housner and N. C. Tsai, "Simulated Earthquake Motions", Report of Earthquake Engineering Research Laboratory, California Institute of Technology, Pasadena, California, April 1968.
- [5] P. Ruiz and J. Penzien, "Probabilistic Study of Behavior of Structures during Earthquakes", Report of Earthquake Engineering Research Center, EERC 69-3, University of California, Berkeley, California, March 1969.
- [6] J. S. Bendat and A. G. Piersal, "Random Data: Analysis and Measurement Procedures", Wiley-Interscience, 1971.
- [7] G. W. Housner, "Characteristics of Strong-Motion Earthquakes", *Bulletin of Seismological Society of America*, Vol. 37, No. 1, 1947.
- [8] M. Both, "Spectral Analysis in Geophysics", *Developments in Solid Earth Geophysics* 7, Elsevier, 1974.
- [9] R. N. Iyengar and K. T. S. R. Iyengar, "A Nonstationary Random Process Model for Earthquake Accelerograms", *Bulletin of Seismological Society of America*, Vol. 59, No. 3, June 1969.
- [10] G. W. Housner, "General Features of the San Fernando Earthquake", from *Engineering Features of the San Fernando Earthquake, February 9, 1971*", edited by P. C. Jennings, Report of Earthquake Engineering Research Laboratory, California Institute of Technology, EERC 71-02, Pasadena, California, June 1971.
- [11] J. A. Johnson and C. M. Duke, "Subsurface Geology of Portions of San Fernando Valley and Los Angeles Basin", from *"San Fernando, California, Earthquake of February 9, 1971"*, U.S. Department of Commerce, National Oceanic and Atmospheric Administration.
- [12] R. P. Maley and W. K. Cloud, "Strong-Motion Accelerograph Record", from *"San Fernando, California, Earthquake of February 9, 1971"*, U.S. Department of Commerce, National Oceanic and Atmospheric Administration.

TABLE 1
Accelerograph Site Information [12]

Station No	Station Location	Positive Directions of Recorded Accelerograph	Peak Accelerations (gal)	Approximate Distance to Epicenter (km)	Direction to Epicenter (degree)	Building Structural Type	Geology
241	Los Angeles 8244 Orion Blvd. 1st Floor	N00W S90W DOWN	-250.0 -131.7 167.5	21	19	7-story RC Building	Alluvium
264	Pasadena Millikan Library Basement CALTECH	N00E N90E DOWN	-198.0 -181.6 - 91.2	38	-40	9-story RC Building	Approx. 1,000 of Alluvium upon Granite
475	Pasadena Athenaeum CALTECH	N00E N90E DOWN	93.5 -107.3 - 92.9	38	-41	2-story RC Building	Approx. 1,000 of Alluvium upon Granite
287	Upland San Antonio Dam Crest	N15E N75W DOWN	- 55.7 75.9 - 28.3	71	-68	Earthfill Dam	Shallow Layer of Alluvium over Granitics
103	Anza Post Office Storage	N45E N45W DOWN	- 25.6 - 35.4 14.0	184	-60	Small Building	Alluvium

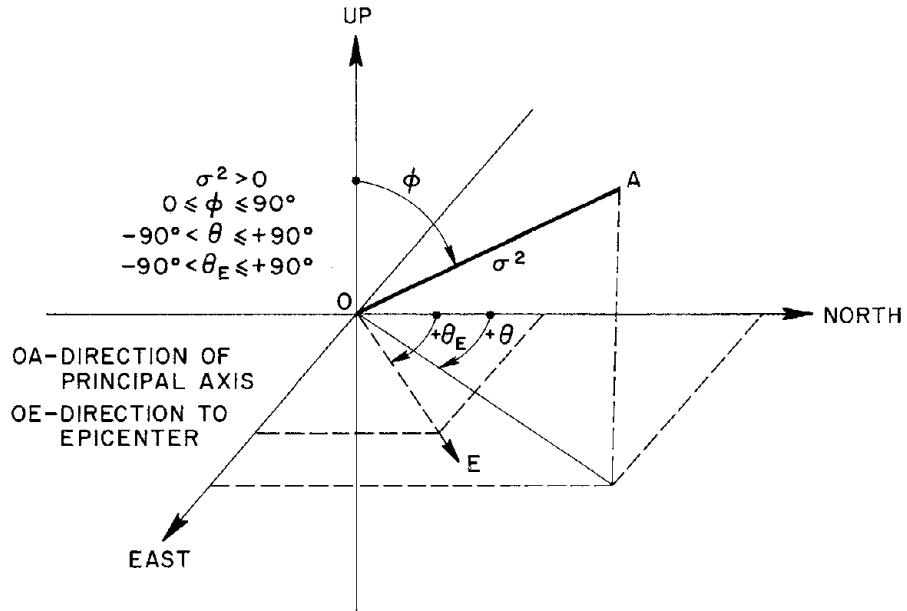


Fig. 1 Directions of principal axis in three-dimensional space.

STATION NO. 241 34 13 16N, 118 28 16W
 8244 ORION BLVD. 1ST FLOOR, LOS ANGELES, CAL.

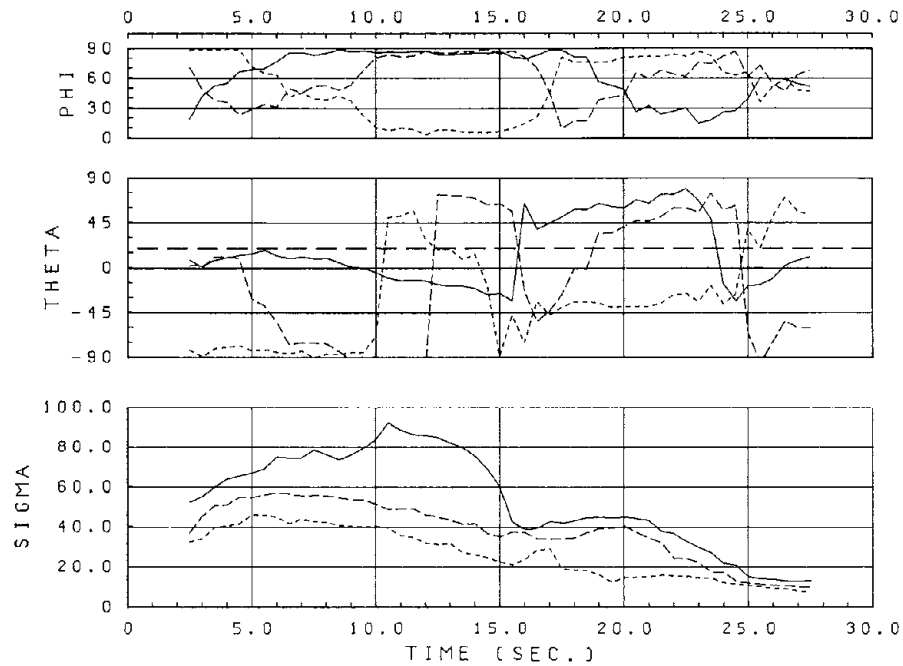


Fig. 2 Time dependent directions of principal axes and square root of principal variances.

STATION NO. 264 34 08 12N, 118 07 30W
CALTECH MILLIKAN LIBRARY, BASEMENT, PASADENA, CAL.

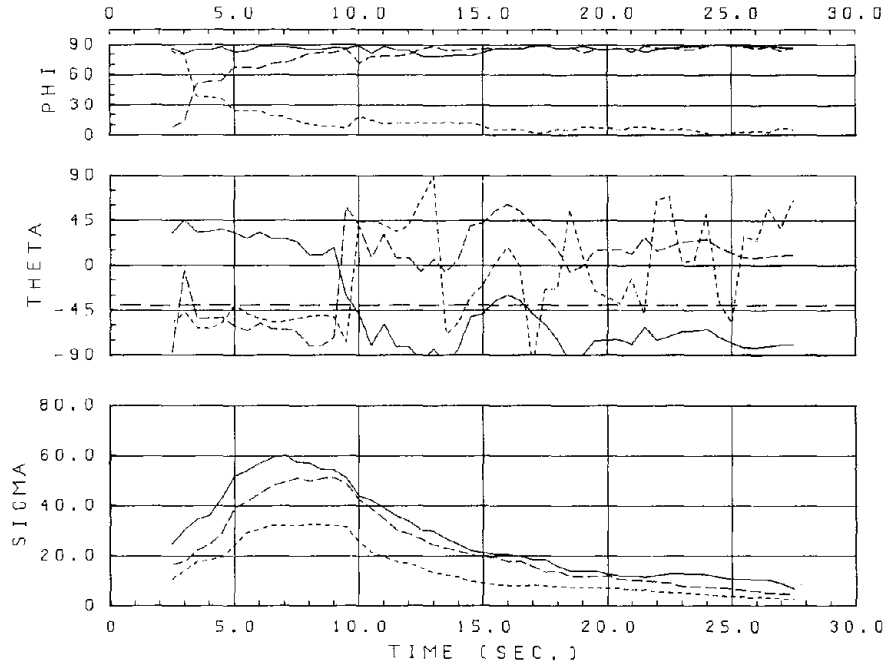


Fig. 3 Time dependent directions of principal axes and square root of principal variances.

STATION NO. 475 34 08 20N, 118 07 17W
CALTECH ATHENAEUM, PASADENA, CAL.

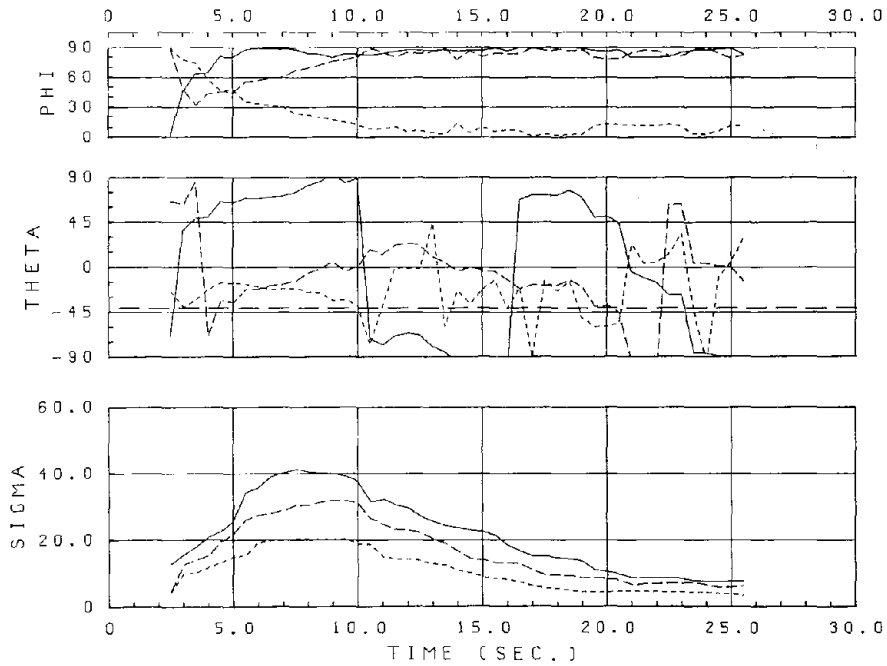


Fig. 4 Time dependent directions of principal axes and square root of principal variances.

STATION NO. 287 34 09 26N, 117 40 47W
SAN ANTONIO DAM, UPLAND, CAL.

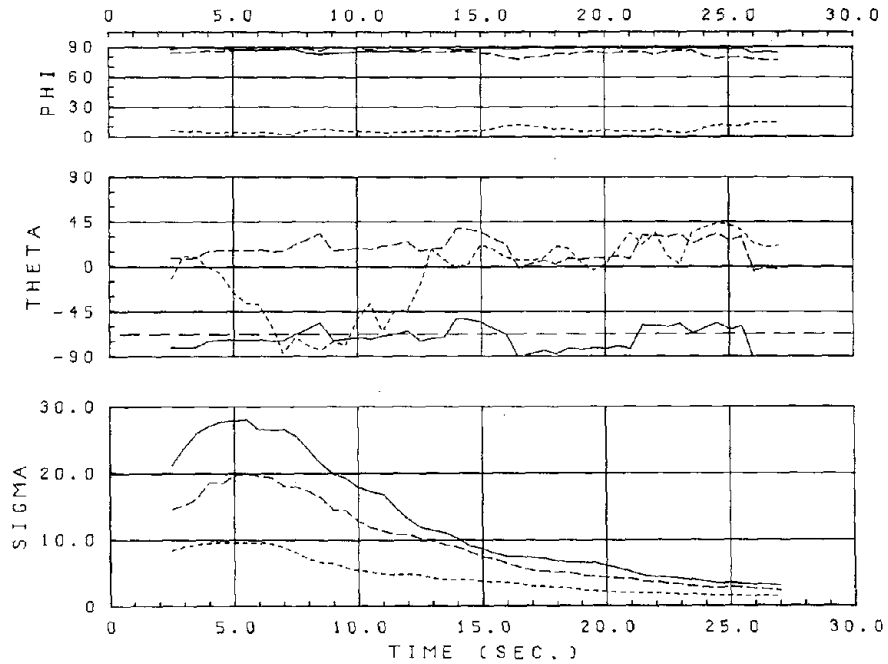


Fig. 5 Time dependent directions of principal axes and square root of principal variances.

STATION NO. 103 33 33 20N, 116 40 25W
ANZA POST OFFICE, STORAGE ROOM, ANZA, CAL.

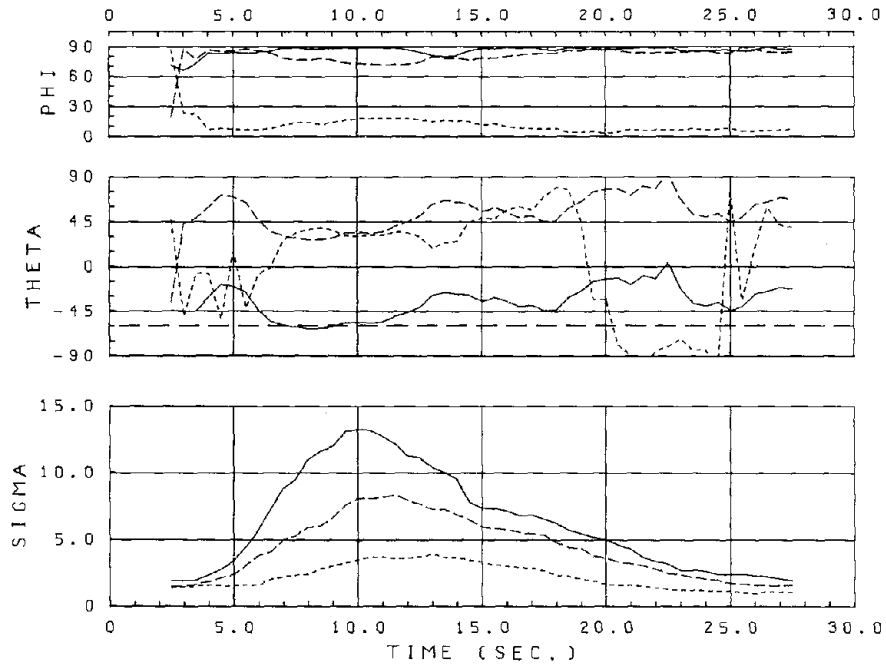


Fig. 6 Time dependent directions of principal axes and square root of principal variances.

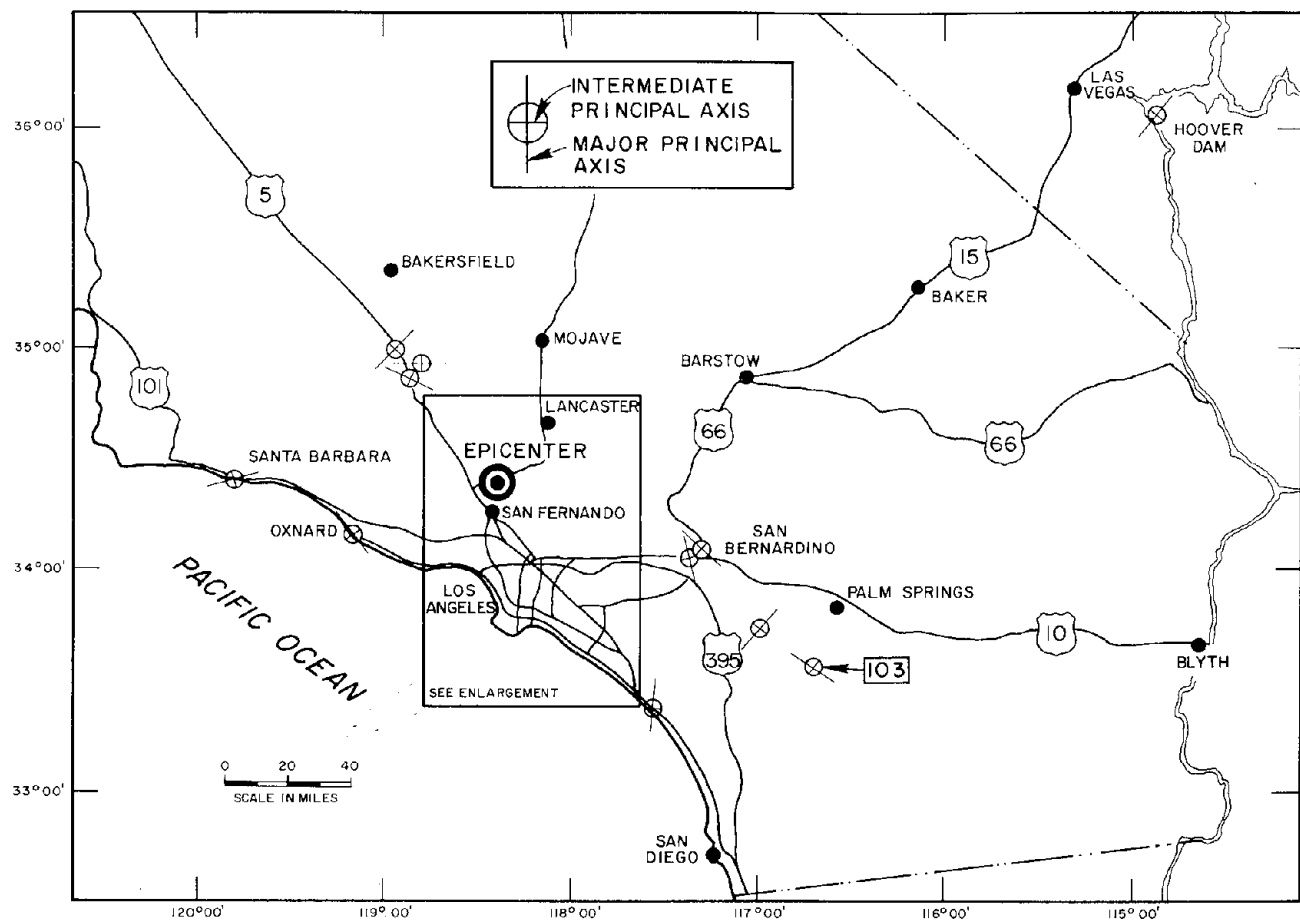


Fig. 7 Directions of major and intermediate principal axes of stations in central and southern California.

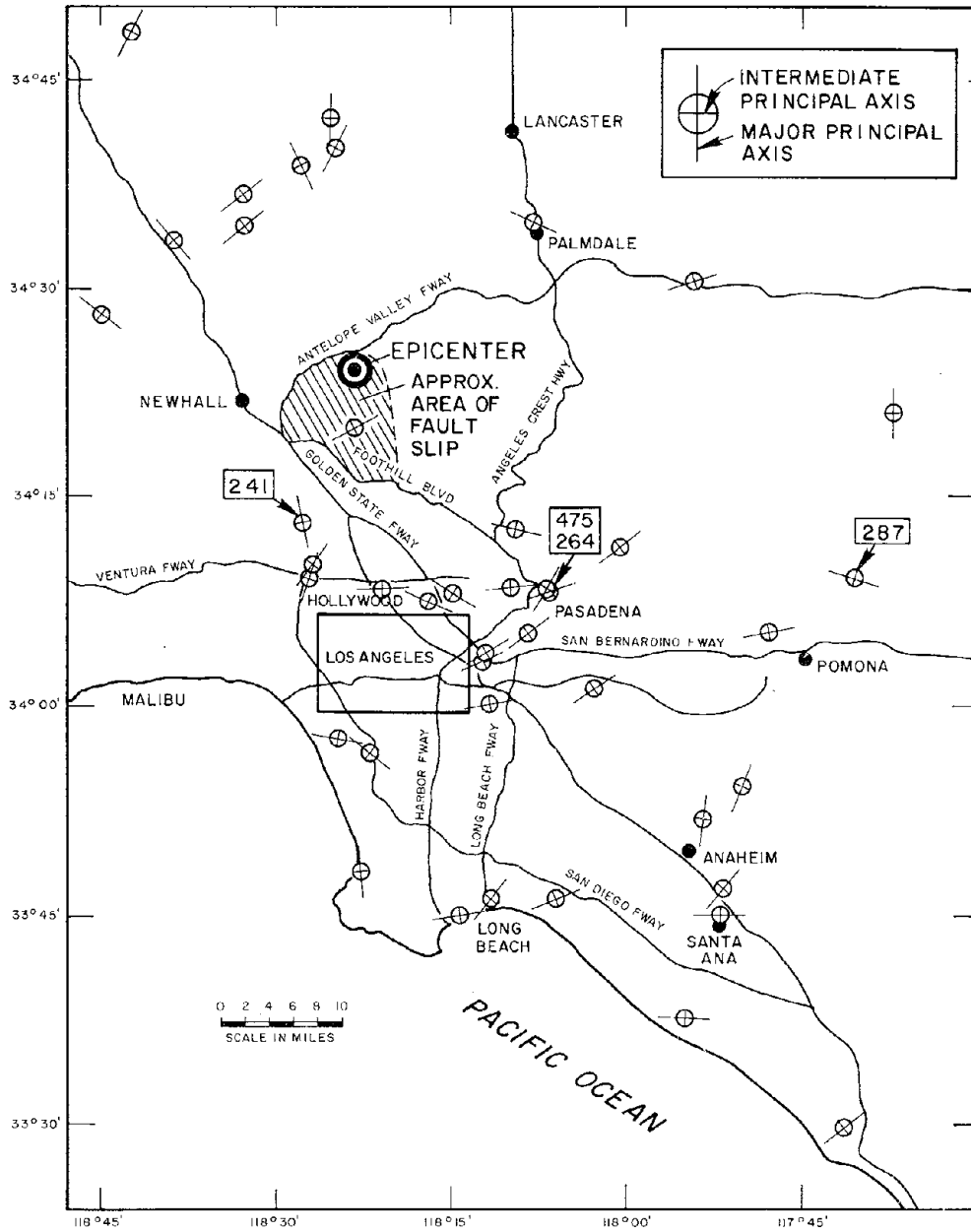


Fig. 8 Directions of major and intermediate principal axes of stations in the extended Los Angeles area.

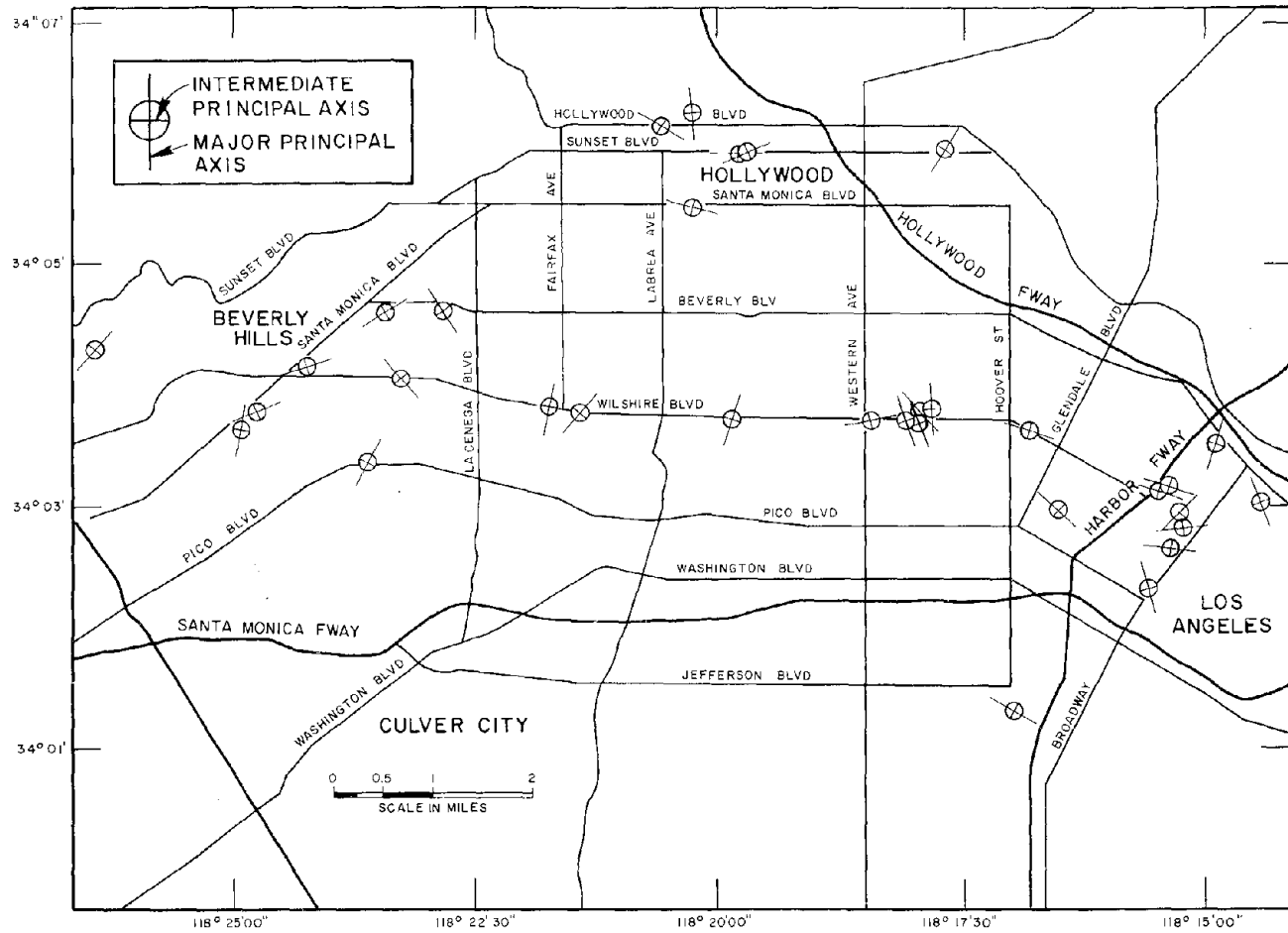


Fig. 9 Directions of major and intermediate principal axes of stations in central Los Angeles.

4 INELASTIC CYCLIC BEHAVIOR OF REINFORCED CONCRETE FLEXURAL MEMBERS

by

J. Penzien*, V. Bertero[†], B. Atalay⁺⁺

SYNOPSIS

Presented is a brief summary of the findings obtained in four series of tests on doubly reinforced concrete members. These tests were designed to obtain basic information on the members' force-deformation and failure characteristics under large-deformation reversed cyclic loading conditions. Specifically, the four series of tests were carried out to study (1) the flexural hysteretic behavior of critical regions under pseudo-static conditions, (2) the effect of rate of loading on the flexural hysteretic behavior, (3) the effect of shear on the flexural hysteretic behavior, and (4) the effect of axial force on the flexural hysteretic behavior.

I. INTRODUCTION

The general philosophy of earthquake resistant design has been well established in the United States, namely, (1) to prevent any type of damage under minor earthquake conditions, (2) to allow only minor damage under moderate earthquake conditions, and (3) to avoid total damage or complete failure under severe earthquake conditions. Except for very important structures which must remain functional under extreme earthquake conditions, economic considerations demand that the large seismic energy inputs to a building be absorbed through controlled inelastic deformations.

To achieve a large energy absorption capacity (often described using the term "ductility"), the potential sources of brittle structural failure must be eliminated. It is necessary, therefore, to prevent premature crushing and shear of the concrete, sudden cracking of the concrete causing simultaneous fracturing of the steel (as in the case of members with extremely low reinforcement ratios), sudden loss of bond and anchorage, and crushing and/or splitting of the concrete cover accompanied by local buckling of the main reinforcement. Although some of these potential sources of failure are automatically controlled by satisfying present code provisions [1,2], others continue to cause serious problems. Among the latter, local shear and anchorage failures are the most troublesome.

Present shear and bond seismic code provisions are based on experimental results obtained under pseudo-static monotonic loading conditions. It has been observed, however, that the basic behavior of shear and bond can be quite different under reversed cyclic conditions similar to those produced by severe earthquakes. In this case, members and frames undergo

* Professor of Structural Engineering, University of California, Berkeley

† Professor of Civil Engineering, University of California, Berkeley

++ Research Assistant, University of California, Berkeley

appreciable degradations of stiffness and strength; thus, greatly reducing their energy absorption capacities per cycle of deformation.

Considering a reinforced concrete frame as shown in Fig. 1, localized inelastic deformations occur at certain overstressed regions designated as critical regions. These critical regions can be classified according to the internal force components controlling their behavior as follows: (1) Moment - These regions have moment as the only important force component. They are usually located in the girders of the top stories of a building as indicated by regions Nos. 1, 2, and 3 in Fig. 1; however, they may also occur in the columns of the upper stories of a frame building. Region No. 1 can experience reversals of loading due to the vertical accelerations of ground motions. (2) Moment with High Shear - These regions, having high shear and moment, are located at the ends of short girders located in the lower stories of medium or high rise buildings; see regions Nos. 2 and 3 in Fig. 1 (3) Moment with High Shear and Axial Force - These regions have relatively high axial forces as well as moment and high shear and are usually located at the ends of columns as indicated by regions Nos. 4, 5, 6 and 7 in Fig. 1. (4) Axial Force and Shear - These regions are located within joints as indicated by regions Nos. 2 and 8 in Fig. 1.

In view of the above types of critical regions, four series of tests were conducted on doubly reinforced concrete members to study (1) the flexural hysteretic behavior of critical regions under pseudo-static conditions, (2) the effect of rate of loading on the flexural hysteretic behavior, (3) the effect of shear on the flexural hysteretic behavior, and (4) the effect of axial force on the flexural hysteretic behavior. In the following sections of this paper, these tests are briefly described and selected test data are presented and interpreted.

II. FLEXURAL HYSTERETIC BEHAVIOR UNDER PSEUDO-STATIC CONDITIONS [3]

A. OBJECTIVES

Results obtained in a series of tests on reinforced concrete frames carried out at the University of California, Berkeley, since 1959 as well as detailed analyses of results obtained by other investigators [4, 5, 6] indicate that the behavior of reinforced concrete flexural members under reversed cyclic conditions, similar to those expected in the members of buildings undergoing strong earthquake excitations, is quite different from the behavior represented by certain mathematical models often adopted for analytical studies, e.g. the elasto-perfectly plastic model. As pointed out previously, available data show there is significant degradation of stiffness and energy absorption per cycle as oscillatory inelastic deformation continues.

Analytical methods for predicting such deterioration were suggested by Bertero and Bresler some years ago [4]; however, the validity of these methods could not be verified at that time due to lack of experimental evidence. It was decided therefore to conduct the four series of tests described herein starting with quasi-static tests of critical regions under flexure. A detailed description of this particular test series follows immediately.

B. TEST FRAME AND LOADING SYSTEM

A schematic view of the test frame and loading system used in this test series is shown in Fig. 2. The test specimen is simply supported with concentrated quasi-static loads being applied at the third-points by a double acting jack. This jack can operate under either load or displacement control.

C. TEST SPECIMENS

The type of test specimen used in this series of tests is shown in Fig. 3. It consists of a 13'-2" long beam having a 9"x15" cross-section with two No. 7 bars in the bottom and two No. 7 bars in the top. The reinforcement bars consisted of deformed bars of intermediate grade steel conforming to ASTM designation A15 (grade 40). The concrete mix was designed to have a compressive strength of 4000 psi in 28 days.

As a result of the symmetrical loading condition, the central 4 ft. region of each specimen was subjected to pure flexure. In this region, the web reinforcement consisted of No. 2 welded ties having 6 in. spacings. In each 4 ft. end region, which was subjected to constant shear and linear variation of moment, the web reinforcement consisted of No. 3 bars having similar 6 in. spacings. It should be noted that this spacing does not satisfy either the ACI or UBC code provisions for ductile moment resisting frames. These provisions call for a maximum spacing of $d/4$ in regions where inelastic deformations are expected to occur. Also, it should be noted that the percentage (ρ) of main reinforcing steel equals 0.9; therefore, the specimen is obviously under-reinforced.

D. SEQUENCE OF LOADING

Since the inelastic behavior of a specimen is loading (or deformation) path-dependent, the selection of a proper loading and/or deformation sequence is of primary importance. Because one of the main objectives of the first series of tests was to obtain data regarding the main parameters controlling degradations in the critical regions, a different loading sequence was used for each specimen. Figure 4 illustrates the loading sequence used in testing specimen No. 4. The results of this test will be discussed subsequently.

E. RESULTS OF TESTS

In spite of the fact the spacings of ties used at the critical regions did not satisfy the existing code provisions for ductile moment-resisting frames, the ductility factors and energy absorption capacities developed by each test specimen reached values in excess of those required of such members under extreme earthquake conditions. The photograph in Fig. 5 illustrates the very high ductility achieved during the testing of one specimen. Further evidence of this fact is provided in Fig. 6 by the hysteretic load-deflection relation for specimen No. 4 when subjected to the loading sequence shown in Fig. 4.

In discussing and evaluating the results of this test series, it should be recognized that inelastic deformations occurred in two different types of regions (1) the complete central region subjected to pure flexure, and (2) the end regions immediately adjacent to the third-point loads where maximum

bending occurs with shear. The maximum value of shear attained in the end regions produced a maximum nominal unit shear stress, v_u , of about $2.6 \sqrt{f'_c}$.

From an analysis of the moment-strain, moment-average curvature, and moment-deflection curves, it was clear that when the critical regions were subjected to repeated loadings without reversals at approximately the same peak values of loads, the flexural stiffnesses were affected very little, although there was some accumulation of permanent strains, curvatures, and deformations. On the other hand, as soon as reversals of loading were introduced, even if below the maximum load level required to induce yielding, there was an observed reduction in the initial stiffness with each successive cycle. This reduction increased with magnitude of load reversal.

After the first yielding of the beam in each of the two loading directions, the ultimate moment capacity did not increase over many cycles of loading in spite of the fact the maximum deformation was increasing with successive cycles. The main reason for the occurrence of increasing maximum deformation with successive cycles was that, due to bond deterioration adjacent to cracked sections, yielding of the tensile reinforcement under constant stress occurred over longer and longer segments of the bars at the locations of the cracked sections.

Only when the main reinforcement was strained into its strain hardening range was an increase in moment resistance detected. From the moment-deflection curve shown in Fig. 6, it can be seen that after the first yielding of the steel, the deflection increased more than three times (from 0.4" to 1.4") before any significant increase was noted in the ultimate moment resistance. However, due to strain hardening of the steel, the beam was able to resist a load P equal to 20 kips when deflected upwards to a maximum value of about 8.4 inches (cycle 43), i.e. about 21 times the deflection at first yielding. This stage was reached without any sign of physical failure (fracture) or drop in the beam's resistance. Furthermore, when this maximum load of 20 kips was reached there was no visible crushing of the concrete which might at first be surprising because results of tests using monotonically increasing loads indicate that crushing of the concrete should have occurred at a lower load level. This apparent contradiction is associated with yielding of the bottom steel and closing of cracks in the concrete. During load reversals, the cracks which earlier developed at the bottom of the beam would not close until considerable moment had been applied to the section. Therefore, the upper concrete started to strain under compression late in the cycle; consequently, the maximum strain induced for a given load had to be smaller than the corresponding strain which would have been induced had the concrete gone into compression immediately upon application of the load. Thus, it can be concluded that the application of load reversals to doubly-reinforced concrete regions which induces yielding in the top as well as the bottom steel results in greater strength and ductility of the region. If beam No. 4 had been loaded upwards monotonically, a very sharp fall in resistance would have been observed at a load P of about 15.8 kips due to crushing of the top concrete. The actual failure (i.e. sharp drop in internal resistance) of beam No. 4 under reversed cyclic conditions occurred as a consequence of bond deterioration and splitting of concrete along the top longitudinal reinforcing bars which permitted buckling of these bars under downward loading in cycle 43.

It should be noted that when beam No. 4 was loaded up to its maximum value of 20 kips, the stress in the top steel was estimated to be near its ultimate strength value of 83 ksi; therefore, from the point of view of strength, this beam performed in an ideal manner.

E. CONCLUDING REMARKS

From an evaluation of the results obtained in this series of tests, it has been concluded that members of this type perform as follows:

1. No significant deterioration occurs at the critical regions when subjected to repeated moments acting in the same direction and having peak values at the working service level.
2. When subjected to repeated moments under complete reversal conditions, the instantaneous stiffness of critical regions is reduced with each successive cycle provided the peak moment or corresponding deformation continues to increase gradually with each successive cycle. On the other hand, the ultimate strength, curvature, ductility factor, and energy absorption are increased with this type of loading.
3. The behavior of the critical regions under reversed cyclic loading beyond initial yielding is controlled by the mechanical characteristics of the steel. Changes in these characteristics result from bond deterioration which takes place between the main cracks as the reversed moments increase in number and in magnitude. To analytically predict such behavior would require knowledge of the actual longitudinal strain distributions in the steel and complete knowledge of the stress-strain relations under histories of deformation similar to those in the critical regions of the member. The Bauschinger effect also becomes an important factor influencing deterioration of stiffness.
4. In spite of the fact the size and spacing of ties (No. 3 bars at 6" c-c) used in the critical regions did not satisfy the existing recommendations for ductile moment-resisting space frames, the ductility factors and energy absorption capacity developed by each specimen exceeded those values normally required in seismic resistant design. Therefore, the present code requirement that tie spacings in the critical regions satisfy $s \leq d/4$ could be relaxed when the nominal shear stress $v_u \text{ max.} \leq 2.6 \sqrt{f'_c}$.

III. EFFECT OF RATE OF LOADING ON FLEXURAL HYSTERETIC BEHAVIOR [7]

A. OBJECTIVES

It has been recognized for many years that the behavior of materials under dynamic loading differs from their behavior under quasi-static loading [8]. The stress-strain relationship can be altered by an increase in rate of strain and this increase can modify the mode of failure leading to increased probability of fracture. In spite of these unknown effects, most structural designs are based on test results obtained from quasi-static experiments.

Although some investigations have been conducted on model structures using harmonic and simulated earthquake excitations, with time factors introduced to speed up the scaled excitations, no significant attempt had been made to isolate the rate of loading effects in reinforced concrete structures under seismic conditions. While in some cases the rate of loading had been referred to qualitatively to explain certain discrepancies between analytical predictions and measured responses, these discrepancies were sufficiently small so that the rate of loading was assumed to have a small effect on load-deformation characteristics.

At the beginning of the general investigation reported herein, uncertainties existed as to the actual effect of rate of loading on reinforced concrete structures; therefore, it was decided to study the hysteretic behavior of the different critical regions previously defined using two different rates of straining (loading). First, tests would be conducted under quasi-static conditions and, secondly, similar tests would be conducted under a much higher rate of straining corresponding to realistic rates experienced by similar members in buildings when subjected to high intensity earthquake excitations. Consequently, those tests previously described for quasi-static conditions were repeated using a high rate of loading designed to represent realistic earthquake conditions.

B. TESTING FRAME AND DYNAMIC LOADING SYSTEM

The testing frame and dynamic loading system used for this test series is shown in Fig. 7. This system is basically similar to that used for the quasi-static tests except the loading system consisted of two independently controlled hydraulic actuators operating in parallel. Each actuator was controlled by a closed-loop feedback system which allowed either load or displacement control. In these tests, a command signal representing displacement was fed simultaneously to both actuators from a low frequency function generator. The highest displacement velocity permitted by the system was 10 in/sec. Investigation of the effects of displacement reversals was carried out using sinusoidal displacement functions.

C. TEST SPECIMENS

The type of specimen selected for this series of tests was identical to that used in the quasi-static test series, i.e. the specimen shown in Fig. 3. Also, the concrete was of a similar mix and the reinforcing steel was the same grade. Stress-strain relationships were obtained for the steel under tension using strain rates of 50, 5,000, and 50,000 μ in/in/sec. The main effect of the higher strain rates was to increase the yield strength. The maximum increase observed under 50,000 μ in/in/sec. was 28 percent. Concrete cylinders were also tested under similar rates of strain. The effects of the higher strain rates was to increase the stiffness and compressive strength of this material. The compressive strength showed an increase of about 20 percent going from the 50 to the 50,000 μ in/in/sec. strain rate.

D. SEQUENCE OF LOADING

The sequence of loading was selected specifically to evaluate strain rate effects rather than to simulate response to any realistic dynamic

excitation. Two actuator displacement velocities were used, namely, 0.1 and 10 in/sec. Pairs of beams were subjected to similar displacement histories using first one velocity and then changing to the other; however, the order of these velocities were interchanged from one displacement history to the other. Each beam was forced downward to a specified displacement and then back to its original undeformed position at one velocity. This cycle was repeated until the beam's behavior stabilized. The same cycles were then repeated but at the second velocity. Immediately following this second series of cycles the original displacement rate was again imposed. Finally, full reversals of displacements were applied using both velocity rates.

E. RESULTS OF TESTS

For the purpose of this paper, it is sufficient to describe the results of only two tests in this series. Beam 1 was loaded under full reversal conditions to amplitudes of ± 5 inches at the displacement rate of 0.1 in/sec. Beam 2 was loaded similarly except at the displacement rate of 10 in/sec. The force-displacement relationships for these two tests over the first loading cycle are shown in Fig. 8a where the differences caused by changing the strain rate can be observed. Figure 8b shows the complete load-displacement history for Beam 1.

Results of these tests indicate that because of the increased stiffness of concrete at high strain rates the dynamic secant stiffness at first yielding was typically about 10 percent higher for the 10 in/sec displacement rate over the 0.1 in/sec. (quasi-static) rate; see Fig. 8a. Regarding the effects of increased rate of straining on the strengths at different limiting states of behavior, it was observed that (1) the cracking strength was increased about 25 percent, (2) the initial yielding strengths in the positive and negative directions of the first cycle were about 22 percent greater than the corresponding values under quasi-static conditions, and (3) the ultimate strengths were not noticeably affected.

While the mode of failure was not affected by strain rate, the deformation ductility factors were slightly smaller at the higher strain rate. The main reason for this decrease in observed ductility factor was that the yield deformation was increased by the higher strain rate. The overall energy absorption capacity was little affected by rate of loading even though there was a slight increase in energy absorption for the higher strain rate during the first cycle of deformation.

F. CONCLUDING REMARKS

The principal effect which an increase in strain rate has on the hysteretic behavior of flexural critical regions is to increase the moment capacity at first yielding of the reinforcement. Although it may be conservative to neglect this effect for regions under pure flexure (or flexure and small shear), it could possibly not be so for regions under high shear and/or high axial force.

IV. EFFECT OF SHEAR ON FLEXURAL HYSTERETIC BEHAVIOR [9]

A. OBJECTIVES

Stiff flexural members with short spans are frequently used in reinforced concrete frame construction. For example, in low-rise buildings, the columns have relatively low axial loads but may have fairly high moments due to frame action caused by dead and live loads including seismic loads. Also in the case of medium and high rise buildings it may be decided to increase the stiffness and strength of the girders to control both lateral drift and lateral resistance. Should this be done, it could lead to flexural members having shear span to depth ratios lower than desirable.

Upon completion of the two series of tests previously described, it was noted that the amount of data available to indicate the effect of shear on flexural hysteretic behavior was very limited [8]. Because of this scarcity of data and because of indications that the presence of shear could have a degrading effect on flexural stiffness, strength, and ductility, it was decided to carry out a third series of tests having the following objectives (1) to study the effect of shear on the hysteretic behavior of flexural regions such as regions Nos. 2 and 3 shown in Fig. 1, (2) to investigate the effect of rate of loading on the hysteretic behavior of flexure regions having high shear, and (3) to study how the hysteretic behavior of flexure regions having high shear are affected by amount of web reinforcement.

B. TESTING FRAME AND DYNAMIC LOADING SYSTEM

The frame and dynamic loading system used for this series of tests was essentially the same as that described previously for the second series (Fig. 7), except that only one hydraulic actuator was used; see Fig. 9.

C. TEST SPECIMENS

Ten of the twelve specimens tested in this series had a 9" x 15" cross section and were reinforced longitudinally with four No. 7 bars ($\rho = 1.03\%$) as shown in Fig. 10. The theoretical flexural capacity of this section is about 750 kip inches. The lengths of the side spans of the specimen (indicated by "a" in Fig. 10) were varied resulting in shear span to depth ratios a/d in the range 5.10 to 2.31. The web reinforcement consisted of No. 3 bars having uniform spacings (s) of 3.25 inches (which satisfies the ACI and UBC provision $s = d/4$) and 6 inches.

The main reinforcement steel was grade 40 having actual yield strength that varied from 50.1 to 52.4 ksi and having maximum tensile strengths of about 80 ksi. The concrete mix was designed for a 28 day compressive strength equal to 4000 psi. The actual compressive strength at time of testing ranged from 4060 psi to 4750 psi.

D. LOADING SEQUENCE

The specimens were cyclicly loaded with full reversals using a prescribed triangularly shaped displacement time-history. The amplitude of

displacement was increased after every four cycles. The 12 specimens tested were classified into 6 groups each having 2 identical specimens. One specimen in each group was tested using a displacement velocity of 0.1 in/sec. while the other was tested using a displacement velocity of 6 in/sec.

E. RESULTS OF TESTS

Only typical results will be presented herein. The photograph in Fig. 11 shows a specimen with $a/d = 2.31$ after having been tested. The crack pattern demonstrates that failure in this case was due to combined flexure and shear. The hysteretic load-deflection diagrams obtained from tests on a pair of specimens having $a/d = 3.70$ and $s = 3.25$ are shown in Figs. 12a and 12b representing displacement velocities of 0.1 in/sec and 6 in/sec, respectively. A comparison of these results indicates an appreciable increase in resistance during the first cycle of loading due to the increase in loading rate. No significant increase is noted for the subsequent cycles of loading. The load-deflection diagram given in Fig. 13 is for a similar specimen except that the a/d ratio was 2.31; therefore, comparing these results with those shown in Fig. 12a indicates the influence of higher shear on the hysteretic behavior of flexure critical regions. Notice that the presence of high shear produces a "pinched" shape to the hysteresis loops; thus, causing a reduction in energy absorption capacity.

F. CONCLUDING REMARKS

From the results of this series of tests, it has been observed that members of this type demonstrate the following characteristic behavior.

1. Increasing rate of loading has no significant effect on the hysteretic force-deflection relation except during the first cycle into the inelastic range when an increase in yield strength by as much as 20 percent can be realized. Although this increase in yield strength produces a corresponding increase in shear at the critical region, it is not detrimental because at first yielding the cracks which develop are small and consequently aggregate interlocking is still very effective in resisting shear. Therefore, it can be concluded that effect of rate of loading on the influence of shear on the flexural behavior of critical regions can be ignored provided $v_u \leq 3.75 \sqrt{f'_c}$. This implies that future studies of these regions under similar conditions can be carried out using results from quasi-static tests.
2. Decreasing the shear span to depth ratio causes a deterioration in the initial loading stiffness with successive cycles (pinching effect); consequently, causing a degradation of energy absorption. Eventhough the maximum nominal shear stress developed was $3.75 \sqrt{f'_c}$, which is well below $10 \sqrt{f'_c}$ allowed by codes, the hysteretic loop areas were less than 65 and 55 percent of the elasto-plastic Ramberg-Osgood and the Clough stiffness degrading loops, respectively. Increasing shear on the critical section causes a corresponding increase in degradation of ultimate strength with repetitive cycles having the same amplitudes. Obviously, shear effects should be included in mathematical modelling of critical regions.

3. For flexural critical regions where $v_{u \max} \leq 2.25 \sqrt{f'_c}$, it appears that the present code requirement on tie spacing $s \leq c d/4$ can be relaxed
4. It should be noted that in this series of tests the moments on both sides of the column stub were of the same sign; whereas, in a concrete frame under seismic conditions, these two moments have opposite signs. If bond deterioration through the joint allows an interaction from one side of the column to the other, the behavior of the flexure critical regions could be altered. Therefore, caution should be used when applying the results reported herein.

V. EFFECT OF AXIAL FORCE ON FLEXURAL HYSTERETIC BEHAVIOR [10]

A. OBJECTIVES

As pointed out previously, critical flexural regions often occur in concrete frames where axial forces are present, e.g. critical regions Nos. 4, 5, 6, and 7 in Fig. 1. Since the three previously described series of tests were performed with no axial force, it was decided to conduct a fourth series of tests in which axial force would be the important variable. Specifically, it was decided to apply a constant axial force to each specimen while it was subjected to cyclic flexure conditions. To cover the practical range of interest, three levels of axial load were selected, namely, 25, 50, and 75 percent of that level corresponding to the balanced point load N_b . These three levels are indicated on the axial force-moment interaction relation shown in Fig. 14 by points A, B, and C, respectively. The shaded region in this figure therefore represents the axial force-moment range of interest.

B. TEST SPECIMEN AND LOADING SYSTEM

The test specimen, representing that portion of column between adjacent inflection points above and below a floor level, is shown in Fig. 15 where it is attached to the loading system. The axial force is applied by a 200 kip hydraulic actuator controlled electronically so that the prescribed force remains constant throughout the test. A second hydraulic actuator (70 kips capacity) applies loading to the girder stub under displacement control conditions. A passive load cell is installed to measure the column shear at one end. The distance between the end load points (inflection points) is 12 feet.

C. REINFORCEMENT DETAILS OF TEST SPECIMEN

The dimensions and reinforcement details of the 12 specimens tested in this series are shown in Fig. 16. They were all 11 ft. long having a 12" x 12" cross-section. The main reinforcing steel consisted of 4 No. 7 bars (total $\rho = 1.67\%$) and the stirrups were No. 3 bars. Stirrup spacings were 3" in the center 5'-3" region and 5" in the two end regions for the type A specimen. Similar stirrups were used for the type B specimen except that 5" spacings were used over the entire length. Additional reinforcement was, of course, placed in the girder stub.

Material properties were held constant throughout the test series and controlled tests were conducted to determine their stress-strain relations. The reinforcement steel was of intermediate grade conforming to ASTM designation A15. Mean values for yield stress, yield strain, and Young's modulus were 53.0 ksi, 0.00190 and 27,400 ksi, respectively. The concrete mix was designed to achieve an ultimate stress of 4,000 psi in 28 days. Mean values for ultimate stress at test day, strain at ultimate stress, and tangent modulus were 4,450 psi, 0.0028, and 3,200 ksi, respectively.

D. SEQUENCE OF LOADING

After each specimen was placed in the test set-up, the constant axial load was applied and the specimen was subjected to a series of small amplitude (less than 0.2"), constant velocity cycles of lateral displacement for purposes of system check-out and determination of elastic characteristics.

Following this initial series, each specimen was subjected to successive sets of nominally 4 cycles of loading under full reversal conditions at fixed amplitudes and constant velocities. These particular sets (Displacement Set 1, Table 1) were carried out at 5 different displacement amplitudes, namely, 0.4", 0.8", 1.2", 1.6", and 2.0" in that order. This full series of 20 cycles (4 x 5) in Set 1 were applied to specimens 1-9 and 12. Specimen 10 was subjected to only 3 cycles at the 2.0" displacement amplitude; thus, the total number of cycles in Set 1 was 19. Due to an error in control settings, the fixed displacement amplitudes in Set 1 for specimen 11 were 0.6", 1.2", 1.8", and 2.4", in that order. Therefore, this specimen experienced a total of only 16 cycles in Set 1. The constant velocity used for each specimen in Set 1 is shown in Table 1.

Specimens 1-8 were subjected to further cycles of loading following Set 1 as indicated in Table 1. This second series of cycles (Displacement Set 2) were also applied in successive sets of nominally 4 cycles of loading under full reversal conditions at fixed amplitudes and constant velocities. These sets were carried out at 5 different displacement amplitudes, namely 0.8", 1.6", 2.4", 3.2", and 4.0" in that order. The constant velocities used for Set 2 are shown in Table 1.

All cycles in both series (Sets 1 and 2) were carried out for each specimen in the sequences indicated above until it had suffered major damage and loss of resistance. Therefore, as shown in Table 1, only three specimens (Nos. 5, 9, and 12) could withstand the full sequence of prescribed lateral displacements.

E. RESULTS OF TESTS

A summary of test results for all 12 specimens is given in Table 1. These results include (1) maximum lateral displacement (2) yield strength, (3) yield displacement, (4) elastic stiffness, (5) displacement ductility, (6) inclined-cracking shear, (7) yield moment, (8) yield curvature, (9) concrete strain causing spalling of cover, and (10) lateral displacement when spalling of cover occurs. Comparing the results for specimens Nos. 9-12 (180^k axial load) with the corresponding results for specimens Nos. 1-4 (60^k axial load) shows that increasing the axial load has significant influences as follows: (1) decreases the maximum lateral displacement,

(2) increases the yield strength, (3) increases the yield displacement, (4) increases the initial elastic stiffness, (5) decreases the displacement ductility, (6) increases the inclined cracking shear, (7) increases the yield moment, (8) increases the yield curvature, and (9) decreases the lateral displacement at first spalling of the concrete cover. Comparing the results for specimens 1 and 2, 5 and 6, 9 and 10 with the corresponding results for specimens 3 and 4, 7 and 8, and 11 and 12, respectively, indicates that rate of loading had no significant effect on the hysteretic force-deflection behavior. Comparing the results for specimens 1,3,5,7,9, and 11 with the corresponding results for specimens 2,4,6,8,10, and 12 indicates little influence of decreasing stirrup spacings from 5" to 3". This lack of influence is undoubtedly due to the relatively large shear span to depth ratio used for these tests.

Hysteretic force-displacement loops are shown in Figs. 17 and 18 for specimens 3 and 9, respectively. The large influence of axial load on the general hysteretic behavior of critical regions is quite apparent when comparing these two cases. The rapid degradation of strength with repeated cycles of loading as caused by the increased axial load is most noticeable. These specimens had 3" spacing of ties in the critical regions. Figure 19 shows the force-displacement hysteretic loops obtained for specimen 10 which had 5" spacing of ties in the critical regions. Comparing these hysteretic loops with those obtained for specimen 9, Fig. 18, indicates that the effect of increasing the tie spacing from 3" to 5" is minimal except that it does increase somewhat the degradation of strength with cycles of deformation.

Figure 20 shows three sets of interaction relationships, namely, axial force vs. yield moment, axial force vs. shear capacity of concrete, and axial force vs. curvature in the critical region at certain strain conditions.

Figure 20a, axial force vs yield moment, shows the experimental values obtained from all 12 tests and presents two theoretical curves. The values for the experimental moments were calculated from the test loads (including the PA effect) which were applied at the instant yielding of the main reinforcing steel started. Strain gages were mounted on the steel to assist in detecting this start of yielding. The shear force represented on the upper abscissa scale of Fig. 20a is simply that shear corresponding to the yield moment represented on the lower abscissa scale. The theoretical curve labeled $\epsilon_s = \epsilon_y$ was obtained using elementary beam theory, i.e. assuming a linear normal strain distribution over the entire cross-section, applying statics, and using the actual stress-strain properties of the steel and concrete obtained from material tests. The theoretical curve labeled $\epsilon_c = 0.004$ was obtained in a similar manner except that the maximum concrete strain was assigned the value 0.004. In this case, the corresponding strain in the main reinforcing steel was slightly above the yield value. It can be observed that the latter curve fits the experimental data somewhat better than the first mentioned curve.

Figure 20b, axial force vs shear capacity of concrete, also shows the experimental values obtained from tests along with two theoretical curves. The values for the experimental shear capacity correspond to those values measured at the instant when shear cracks developed across the section causing a transfer of shear from the concrete to the stirrups. Note that

two experimental values of shear capacity are shown for most specimens. One of these values corresponds to loading in the positive direction while the other corresponds to loading in the negative direction. Because of symmetry conditions, these two values should probably be averaged to establish the mean experimental shear capacity. The straight line theoretical curve shown in Fig. 20b was obtained by the formula listed which was originally suggested by Olesen, et. al. [11], and the second theoretical curve was obtained using Eq. 11.4, ACI Sec. 71 [1]. The straight line relation seems to fit the experimental data better for lower axial loads while the ACI relation seems to fit better for the higher axial loads. The increase in shear force capacity with increasing axial load is appreciable.

Figure 20c shows the interaction relation between axial load and curvature in the critical region at certain strain conditions. The two experimental points shown per specimen represent those values of curvature measured when the main reinforcing steel started to yield and at that stage just prior to a significant drop in strength. The three theoretical relations shown were obtained using elementary beam theory, i.e. linear strain distribution, statics, and the actual stress strain relations of the steel and concrete obtained from material tests. The prescribed strain conditions for these curves were $\epsilon_s = \epsilon_y$, $\epsilon_c = 0.004$, and $\epsilon_c = 0.010$. The first of these conditions, as expected gives good agreement with the experimental data representing start of yielding of the steel and the third strain condition gives fair agreement with the experimental data representing ultimate load capacity. Also shown in Fig. 20c is the theoretical ultimate curvature ductility (see upper abscissa scale) for condition $\epsilon_c = 0.010$. Note the very large decreases in ultimate curvature ductility with increasing axial load.

The general behavior of the specimens in this series of tests was that with progressively increasing lateral displacement amplitudes inclined shear cracks formed, the main reinforcement yielded in tension, concrete cover spalled from the bars, lateral reinforcement yielded, and, at the initiation of failure, either the main reinforcement buckled or the core concrete failed in compression. Specimens 1-4 failed by progressive opening of flexural cracks which means that axial load (60 kips) had little effect on their behavior. Specimens 5-8 (120 kips axial load) failed by buckling of the main reinforcing bars at large lateral displacement amplitudes, and specimens 9-12 (180 kips axial load) failed when the strains in the confined concrete core reached values around 0.010. In the latter case, the compressive strains in the longitudinal reinforcing steel accumulated due to the high axial load. For those specimens having axial loads of 120 and 180 kips, the lateral reinforcement yielded at lateral displacement amplitudes of 3.4" and 1.9", respectively. Decreasing the stirrup spacing from 5" to 3" forced a greater spreading of the inelastic regions. At ultimate load capacity, deflections due to shear deformations constituted about 5% of the total for specimen 3 ($s = 3"$) while they constituted about 8% of the total for specimen 4 ($s = 5"$).

F. CLOSING REMARKS

The effects of axial force on the overall performance of flexure critical regions should be recognized as it can significantly affect their stiffness, strength, ductility, and degradation properties.

VI. FINAL STATEMENT

The four series of tests reported herein were conducted to obtain basic information on the performance and failure characteristics of doubly reinforced concrete members under realistic earthquake conditions. Hopefully, this information will permit the realistic development of mathematical models representing such behavior. These element models can then serve as sub-elements in global models used to predict the overall behavior of prototype structures.

VII. ACKNOWLEDGEMENT

The authors wish to acknowledge the active participation of B. Bresler, M. Celebi, H. Liao, S. Mahin, and D. Rea in conducting the four series of tests described herein. They also acknowledge with sincere thanks and appreciation the financial support provided through a series of grants by the National Science Foundation.

VIII. BIBLIOGRAPHY

- [1] "Building Code Requirements for Reinforced Concrete (ACI 318-71)," American Concrete Institute, 1971.
- [2] "Uniform Building Code," 1973 Edition, Vol. I, International Conference of Building Officials, 1973.
- [3] Bertero, V. V., Bresler, B., and Liao, H., "Stiffness Degradation of Reinforced Concrete Structures Subjected to Reversed Actions," EERC 69-12, Earthquake Engineering Research Center, University of California, Berkeley, 1969.
- [4] Bertero, V. V., and Bresler, B., "Seismic Behavior of Reinforced Concrete Framed Structures," Proceedings of the Fourth World Conference on Earthquake Engineering, Santiago, Chile, Vol. I, 1969.
- [5] Unemura, H., and Aoyama, H., "Evaluation of Inelastic Seismic Deflection of Reinforced Concrete Frames Based on the Tests of Members," Proceedings of the Fourth World Conference on Earthquake Engineering, Santiago, Chile, Vol. I, 1969.
- [6] Aoyama, H., "Restoring Force Characteristics Under Reversal of Loading of Reinforced Concrete Members and Structures," A Review of Japanese Research, Report of the U.S.-Japan Seminar on "Basic Research in Concrete as Related to Behavior of Structures in Earthquakes," Tokyo, 1967.
- [7] Mahin, S., Bertero, V. V., Rea, D., and Atalay, B., "Rate of Loading Effects on Uncracked and Repaired Reinforced Concrete Members," EERC 72-9, Earthquake Engineering Research Center, University of California, Berkeley, 1972.
- [8] Bertero, V. V., "Resistance and Ultimate Deformability of Structures Acted on by Well Defined Repeated Loads," International Association for Bridge and Structural Engineering, Lisbon, Portugal, 1973.

- [9] Celebi, M., and Penzien, J., "Experimental Investigation into the Seismic Behavior of Critical Regions of Reinforced Concrete Components as Influenced by Moment and Shear," EERC 73-4, Earthquake Engineering Research Center, University of California, Berkeley, 1973.
- [10] Atalay, B., and Penzien, J., "The Seismic Behavior of Critical Regions of Reinforced Concrete Components as Influenced by Moment, Shear, and Axial Force," EERC 75-19, Earthquake Engineering Research Center, University of California, Berkeley, 1975.
- [11] Olesen, S. O., Sozen, M. A., and Seiss, C. P., "Investigation of Prestressed Reinforced Concrete for Highway Bridges; Part IV: Strength in Shear of Beams With Web Reinforcement," Engineering Experimental Station, Bulletin 493, University of Illinois, 1967.

Table 1

Test parameters and test results for 12 specimens

① SPECIMEN NO.	TEST PARAMETERS						TEST RESULTS										
	② AXIAL LOAD, KIPS	③ LATERAL REINF'T SPACING, IN.	④ DISPLT SET 1 (*)		⑤ DISPLT SET 2 (*)		⑧ MAX. LATERAL DISPLT, IN.	⑨ YIELD STRENGTH, KIPS	⑩ YIELD DISPLT, IN.	⑪ ELASTIC STIFFNESS, KIPS/IN.	⑫ DISPLT DUCTILITY	⑬ INCLINED CRACKING SHEAR, KIPS	⑭ YIELD MOMENT, KIP-IN.	⑮ YIELD CURVATURE, RAD/IN.	⑯ CONCRETE STRAIN	⑰ LATERAL DISPLT, IN.	
④	⑤	⑥	⑦	⑧	⑨	⑩											⑪
1	60	3	20	18	0.2	0.4	4.0	26.7	0.71	66.1	5.70	10.4	923.	0.00029	NOT AVAILABLE		
2	60	5	20	16	0.2	0.4	3.2	26.7	0.67	63.3	4.75	9.3	878.	0.00030	0.0059	3.2	
3	60	3	20	16	2.	4.	3.2	26.3	0.66	68.9	4.85	13.4	906.	0.00029	0.0057	3.2	
4	60	5	20	17½	2.	4.	4.0	27.5	0.75	63.7	5.33	11.2	924.	0.00027	0.0052	2.4	
5	120	3	20	20	0.2	0.4	4.0	32.7	0.89	73.9	4.50	15.0	1185.	0.00030	0.0055	2.0	
6	120	5	20	14½	0.2	0.4	3.2	33.0	0.93	62.5	3.46	14.3	1198.	0.00046	0.0062	2.4	
7	120	3	20	15½	2.	1.	3.2	30.5	0.97	77.2	3.28	15.4	1124.	0.00037	NOT AVAILABLE		
8	120	5	20	12½	2.	1.	3.2	31.1	0.89	77.9	3.60	15.5	1132.	0.00036	0.0061	2.4	
9	180	3	20	—	0.2	—	2.0	34.0	0.95	83.1	2.11	16.7	1291.	0.00063	0.0048	1.2	
10	180	5	19	—	0.2	—	2.0	36.7	0.95	81.3	2.12	17.5	1380.	0.00051	0.0058	1.6	
11	180	3	16	—	1.	—	2.4	35.9	0.92	85.1	2.60	17.3	1349.	0.00045	0.0050	1.2	
12	180	5	20	—	1.	—	2.0	35.0	0.97	87.5	2.07	17.7	1330.	0.00052	0.0064	1.2	

(*) DISPLT SET 1: 4 CYCLES AT LATERAL DISPLT AMPLITUDES OF 0.4", 0.8", 1.2", 1.6" AND 2.0" (EXCEPT SPECIMEN 11)
 DISPLT SET 2: 4 CYCLES AT LATERAL DISPLT AMPLITUDES OF 0.8", 1.6", 2.4", 3.2" AND 4.0"

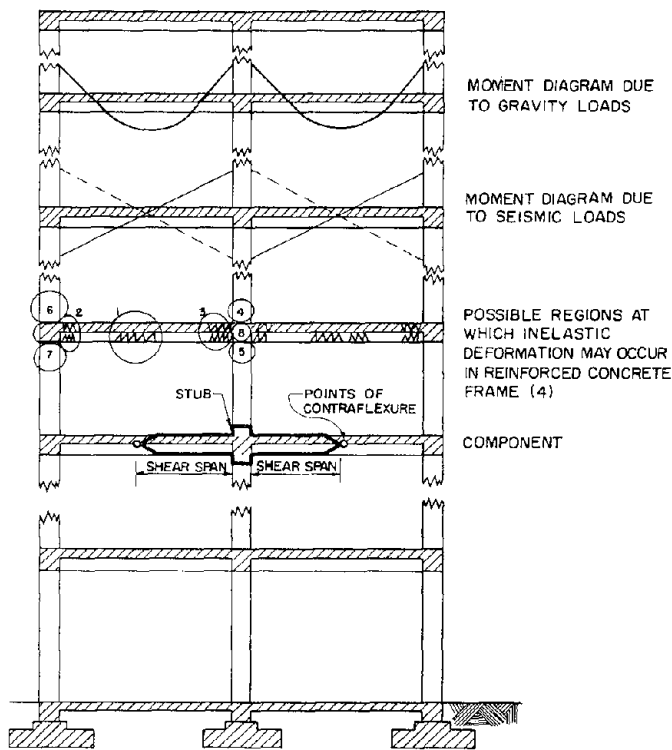


Fig. 1 An interior component in a reinforced concrete frame.

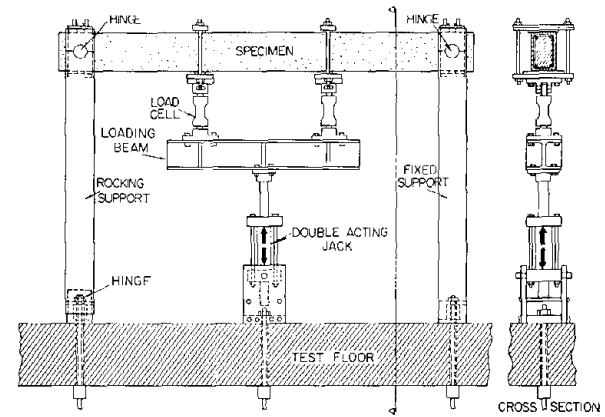


Fig. 2 Testing frame and quasi-static loading system

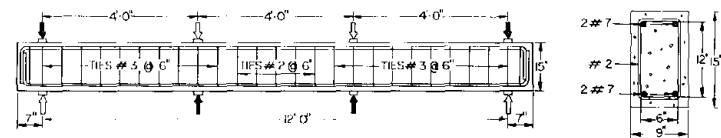


Fig. 3 Loading and reinforcement details of test specimen

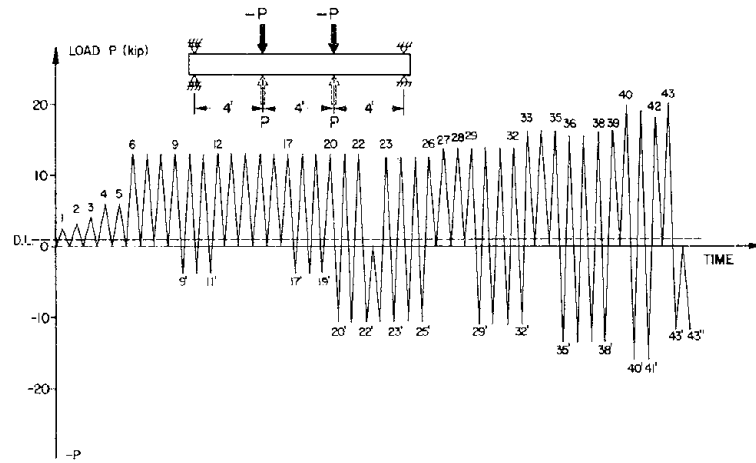


Fig. 4 History of loading - Beam No. 4

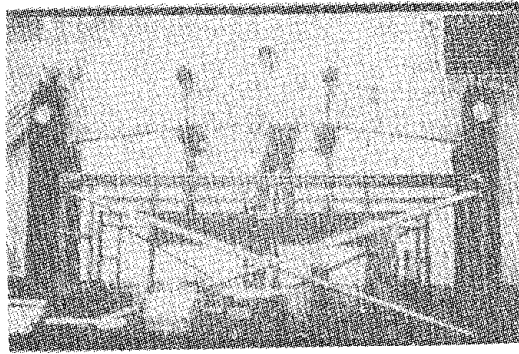


Fig. 5 Test specimen subjected to high curvature

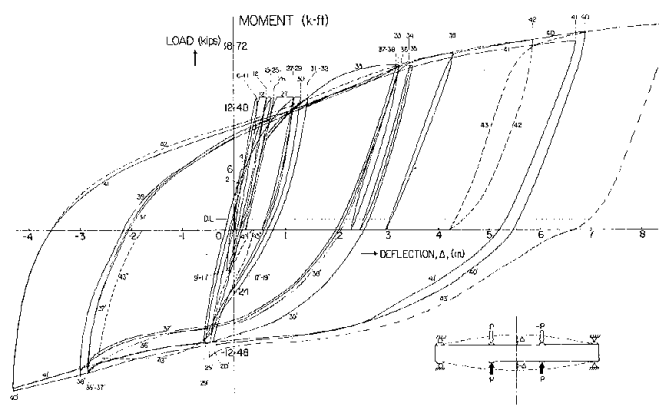


Fig. 6 Load - deflection diagram - Beam No. 4

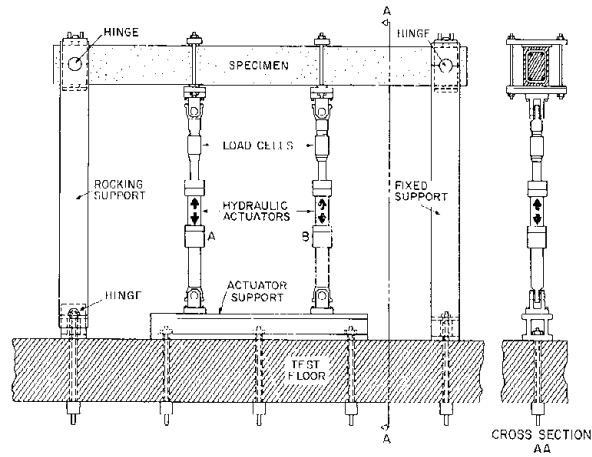


Fig. 7 Testing frame and dynamic loading system

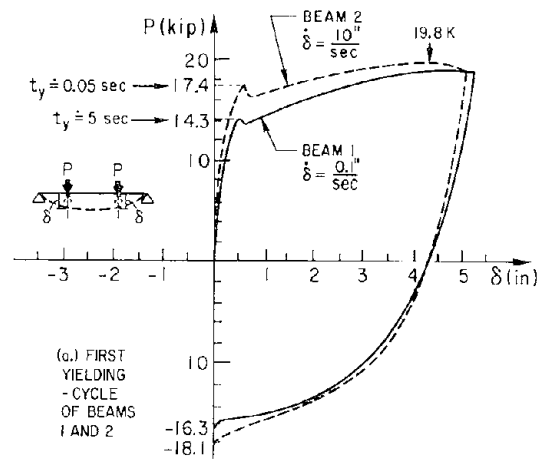


Fig. 8a Influence of deformation rate on load-deflection relation - First cycle

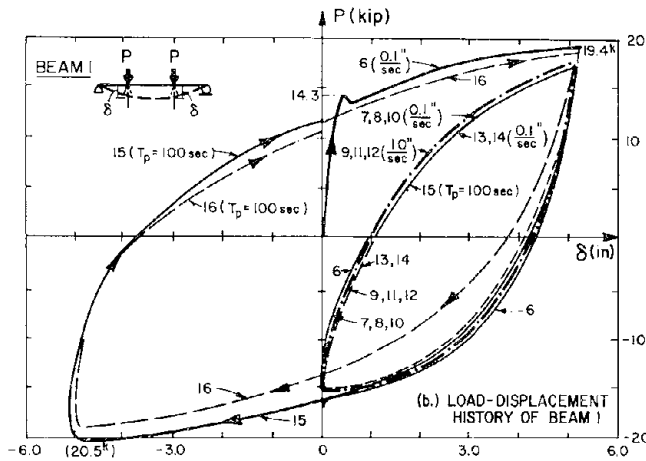


Fig. 8b Influence of deformation rate on load-deflection relation - Repeated cycles

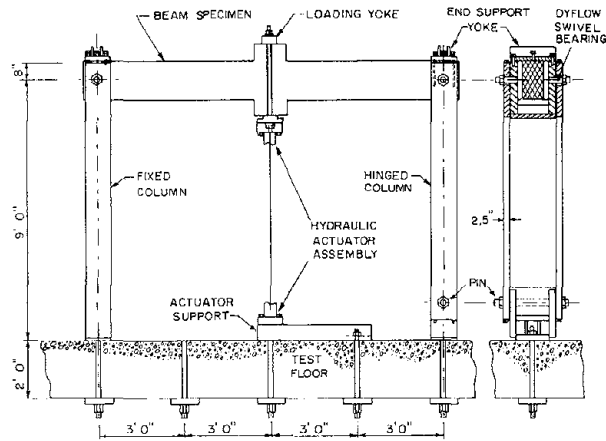


Fig. 9 Testing frame and dynamic loading system

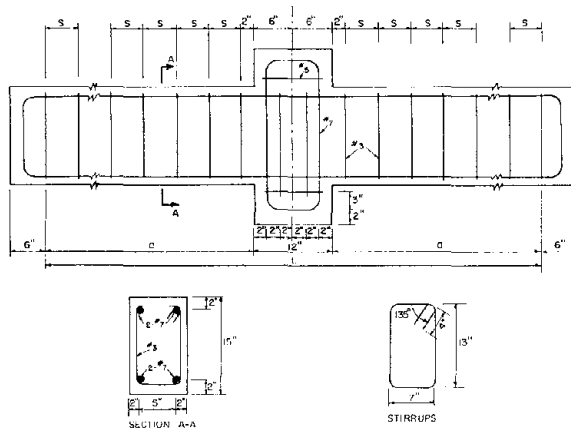


Fig. 10 Reinforcement details of test specimen.

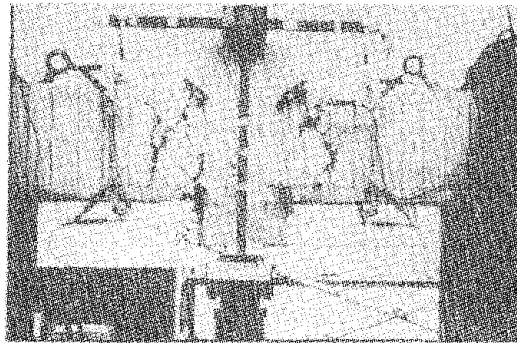


Fig. 11 Damaged test specimen with low shear span to depth ratio

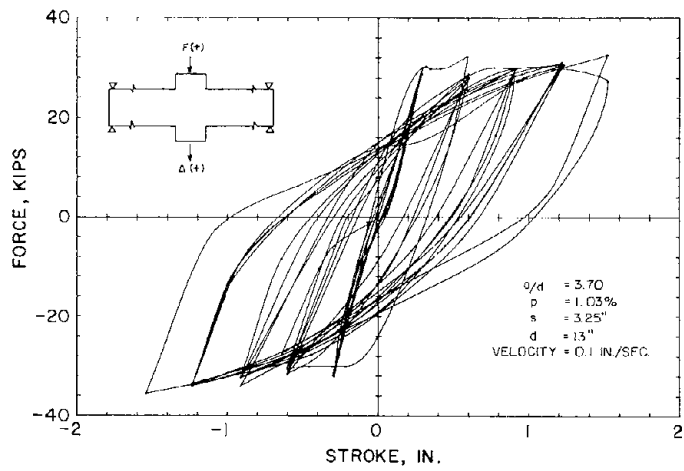


Fig. 12a Hysteretic behavior - Specimen No. 10

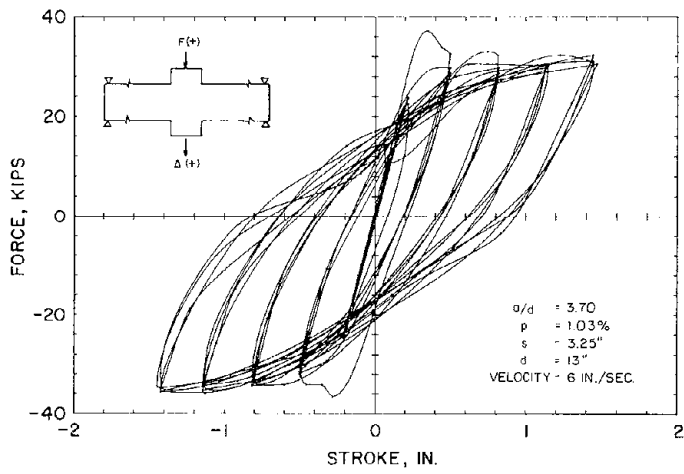


Fig. 12b Hysteretic behavior - Specimen No. 9

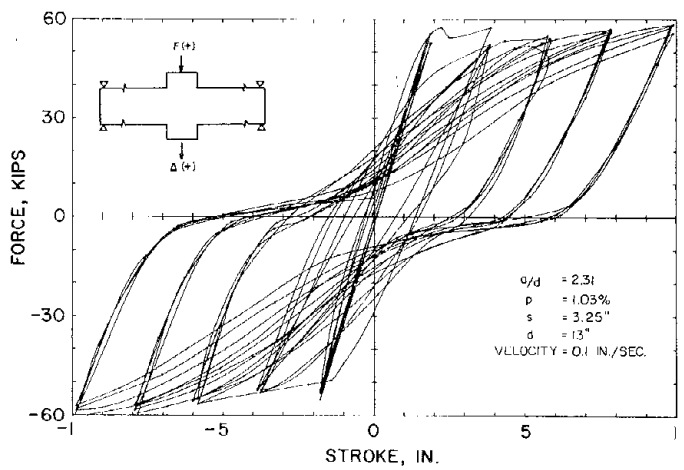


Fig. 13 Hysteretic behavior - Specimen No. 12

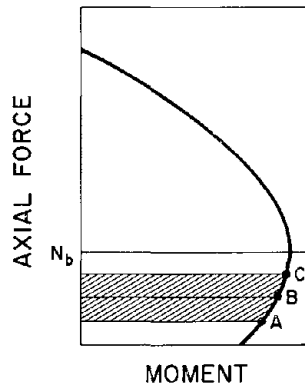


Fig. 14 Axial load - moment interaction diagram showing levels of axial forces investigated.

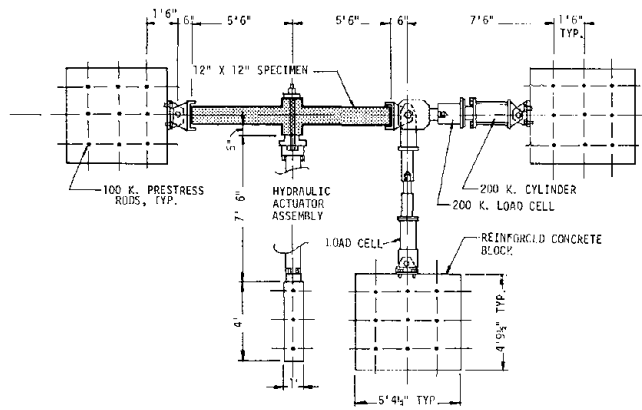


Fig. 15 Test specimen and loading system

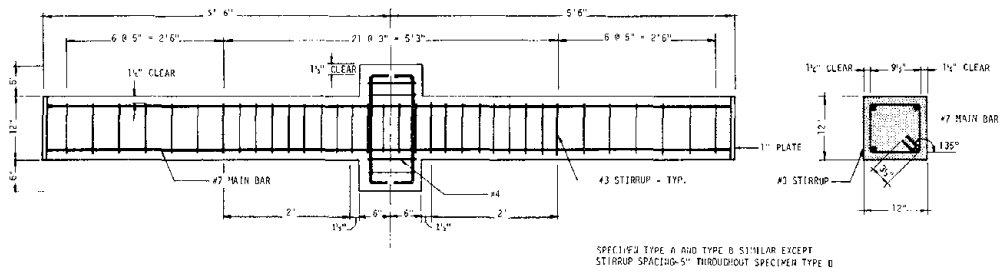


Fig. 16 Reinforcement details of the specimen

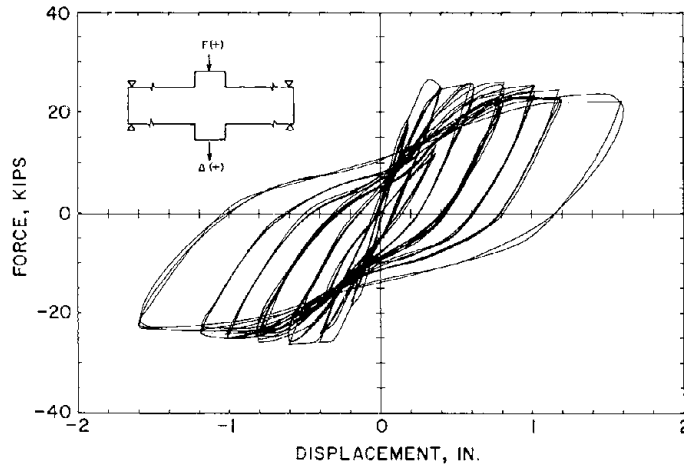


Fig. 17 Hysteretic behavior - Specimen No. 3,
Axial load = 60^k , Lateral reinforcement
spacing = 3 inches.

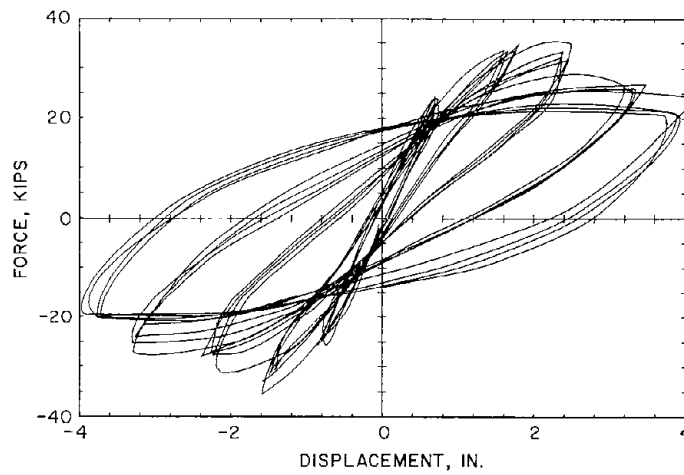


Fig. 18 Hysteretic behavior - Specimen No. 9
Axial load = 180^k , Lateral reinforcement
spacing = 3 inches.

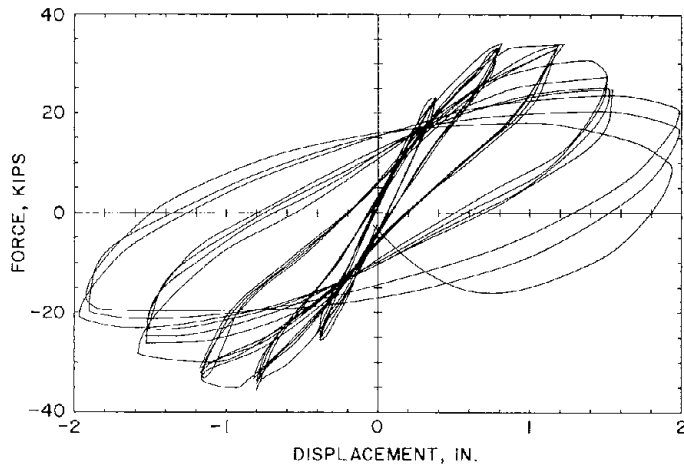


Fig. 19 Hysteretic behavior - Specimen No. 10
Axial load = 180^k , Lateral reinforcement
spacing = 5 inches.

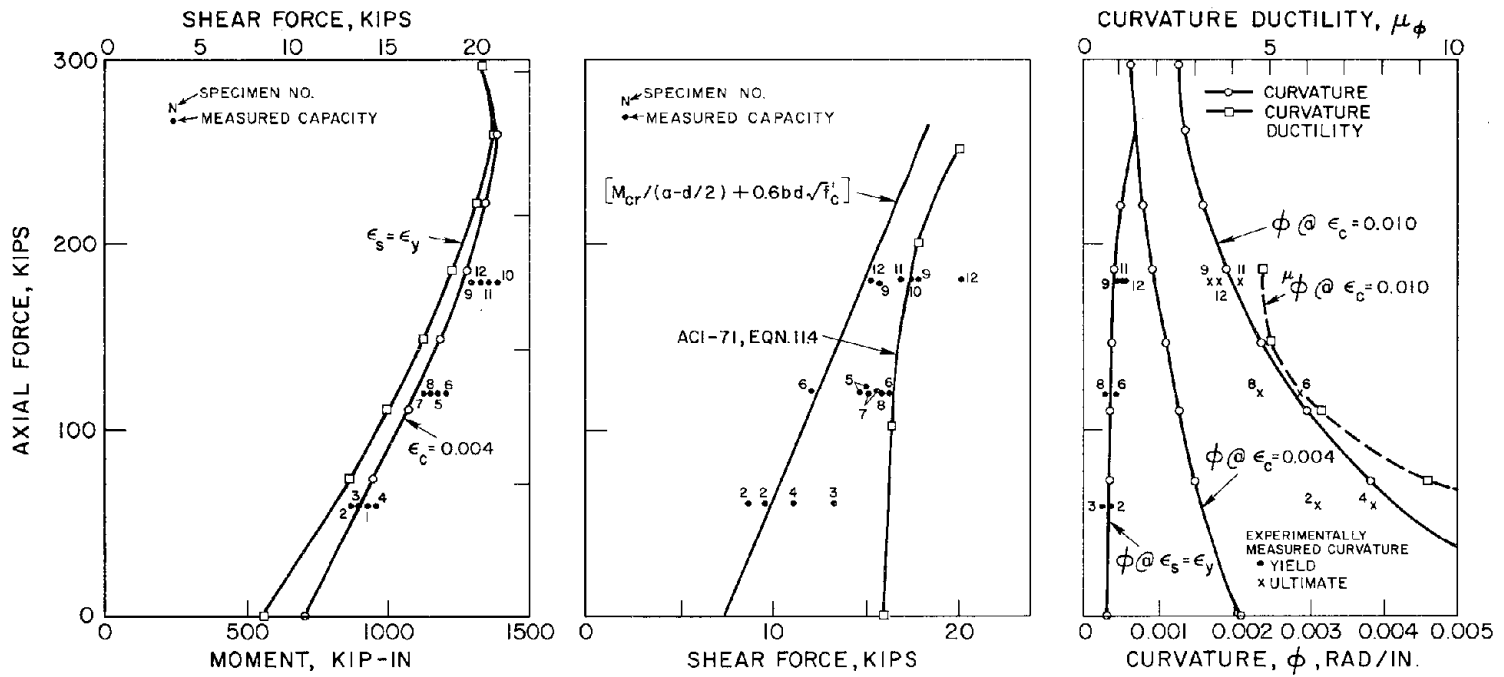


Fig. 20 Axial force vs. moment, shear force, and curvature interaction diagrams

by

Vitelmo V. Bertero*, Egor P. Popov* and Tsan-Yuan Wang[†]

SYNOPSIS

This paper reviews the research carried out at Berkeley on hysteretic behavior of structural components of ductile moment-resisting frames and frame-wall systems under high shear. The first part of the paper summarizes and evaluates the main results of experiments conducted on relatively short girders and girder-column subassemblages, and discusses their implications regarding the aseismic design of ductile moment-resisting frames. The second part considers results obtained in the tests on wall models of the first three stories of a 10-story dual frame-wall structural system, to evaluate present code provisions for the aseismic design of such systems.

I. INTRODUCTION

In designing a building located in regions where severe earthquake shaking is expected, economic considerations usually require that large seismic energy input to the building be absorbed and dissipated through large but controllable inelastic deformations of its structure. These deformations, however, should be limited to values which would avoid inducing severe damage to either structural and nonstructural elements or contents of the building which could jeopardize the lives of occupants and the safety of neighboring buildings.

The structural systems of low-rise buildings in seismic areas are often designed with ductile moment-resisting space frames. As the building becomes increasingly slender, however, it is necessary to increase the lateral stiffness of the frame. This is more effectively achieved by increasing the bending stiffness of the girders rather than that of the columns. Since an increase in bending stiffness is usually accompanied by an increase in the girders' shear, care should be taken to see that this increase does not exceed certain limits and thereby subject the potential flexural critical regions of the girders to shears which are higher than those desired.

Although data available on the behavior of critical regions subjected to reversals of combined flexural and high shear are very limited, a comparison between these results and those obtained under monotonic loadings, indicates that as the shear increases, stiffness and strength deteriorate with the increasing number of load reversals. At the same time, a considerable reduction in ductility takes place (1). Recent investigations in this area carried out at Berkeley (2-7) shed some light on reasons for the observed deteriorations and for the reduction in ductility. The reliability of present code provisions for aseismic design must now be evaluated in the light of these new data.

* Professors of Civil Engineering, University of California, Berkeley.

† Research Assistant, University of California, Berkeley.

As the height of the building increases (say, above 10 stories), its lateral stiffness may be more efficiently improved by adding some structural walls (viz., shear walls) to the moment-resisting frame, rather than by increasing the stiffness of girders and columns. The rationality of present code procedures of seismic analysis and design of this combined structural system is unclear. The code seismic design philosophy for shear walls appears to be inconsistent with that for ductile moment-resisting frames, which is not surprising since reliable data on hysteretic behavior of wall and frame-wall structural systems are very limited. Further analytical and experimental research is therefore needed.

OBJECTIVES AND SCOPE - Results on the hysteretic behavior of flexural critical regions of girders subjected to high shear, girder-column subassemblages, and wall subassemblages, under earthquake-like excitations, were recently obtained at Berkeley. The main objective of this paper is to analyze the implications of these results on aseismic design of ductile moment-resisting frame and frame-wall structural systems.

For the purposes of discussion, the analysis of hysteretic behavior has been divided into two parts. The first part analyzes the results obtained in tests of several full-sized short cantilevers using different types of web reinforcement, and those of 1/2 scale girder-column subassemblages. Implications of these results on aseismic design of ductile moment-resisting frames are then evaluated. The second part discusses the problems and the research conducted on hysteretic behavior of structural components, and analyzes results obtained in tests of two 1/3 scale models of the first three stories of a wall corresponding to a 10-story building. The significance of these results on present methods for the aseismic design of dual frame-wall structural systems are then discussed.

II. HYSTERETIC BEHAVIOR OF FLEXURAL CRITICAL REGIONS WITH HIGH SHEAR

GENERAL - To study in detail the effect of high shear reversals on the flexural behavior of critical regions, a series of experimental and analytical investigations have been carried out (2-7). In order to analyze the significance of the results obtained with regard to present code provisions related to the design of ductile moment-resisting frames, only the results obtained in four series of experiments conducted on seven similar specimens are briefly presented and evaluated. These series of experiments can be considered as complementary to the third series of experiments described in the previous paper presented by Penzien, et. al. (7).

DETAILS OF TEST SPECIMENS

Type of Specimen: Each of the seven test specimens consisted of a short cantilever beam, shown in Fig. 1, and had the same overall dimensions: a 78 in. length and a 15 x 29 in. rectangular cross-section. The shear span-to-effective depth ratio was 3.1. As illustrated in Fig. 1, the cantilever beam framed into a heavily reinforced concrete column-stub which in turn was attached to a steel reaction box prestressed to the tie down slab of the laboratory.

Main Reinforcement: In each beam, this was provided by six well-anchored

#9 bars at both the top and the bottom. These bars were welded at their ends to special plates, Fig. 1(a), to eliminate any danger of anchorage failure and to minimize the amount of slippage along their embedment lengths.

Web Reinforcement: This was the main variable under study. In the first series of specimens, single closed stirrup-ties were used consisting of #3 bars at 4.5 in. spacing in Beam 35, and #4 bars at 6 in. and 3 in. spacing in Beams 46 and 43, respectively (2). Whereas the web reinforcement of Beam 35 conformed to the general ACI (318-63) Code requirements, the ties of Beams 46 and 43 were designed to resist the total shear. Furthermore, in Beam 43, they were designed to resist the shear corresponding to the maximum possible moment which the beam could resist. In the second series of specimens, Beams 33 and 33M, narrower pairs of partially overlapping #3 stirrup-ties at 3 in. spacing, Fig. 1(b), were used to offer the interior top longitudinal bars better support against buckling than the single #4 tie used in Beam 43. Furthermore, in Beam 33, two #4 longitudinal bars and transverse supplementary #2 and #3 cross-sties were added to improve basketing of the concrete.

The third series of experiments was carried out on Beam 35I, Fig. 1(c). The main shear reinforcement consisted of eight #6 inclined bracing bars which were designed to resist the shear force corresponding to the maximum flexural capacity, (estimated on the basis of the maximum tensile strength of the main reinforcement bars), and to prevent the shear movement along vertical flexural cracks which were observed in the two previous series of tests. These bars were assembled into a rigid cage by closely spaced ties forming two 45° struts with very well confined cores which minimized the danger of bar buckling. Similar struts have been successfully used for very short span beams by Paulay (8). Results show that these inclined struts virtually eliminate the degrading effects of high shear. Their use in the field, however, may be economically infeasible; consequently, the simpler reinforcing scheme shown in Fig. 1(d), was used in the design of the specimen (Beam 33L) for the fourth series of tests. The four interior #9 main reinforcement bars of Beam 33L were bent 45° at 6 in. from the column face in an attempt to force the initial flexural yielding at a section 18 in. from this face, and at the same time to use these four bars to resist shear at this new critical region. The main reason for attempting to force the initial flexural yielding away from the column face was to determine the possibility of decreasing the significant slippage of the main bars along their anchorage in the column-stub that was observed in the test of the first three series of experiments. Whereas double, partially overlapping #3 stirrup-ties spaced at 3 in. were used in Zones I and III of the beam, single ties were used in Zone II where four main bars were bent. Transverse supplementary #3 cross-ties were added at mid-depth.

MECHANICAL CHARACTERISTICS OF MATERIALS - The compressive strength of the concrete at time of testing varied between 3.9 to 5.8 ksi. Grade 60 steel was used throughout the experiments. With the exception of one specimen in which the yielding strength of main reinforcement was 60, in all other specimens this strength exceeded 67 ksi.

EXPERIMENTAL SET-UP AND TEST PROCEDURE - Each specimen was tested in a horizontal position. Most of the specimens were subjected to repeated full reversals of shear forces and deformations of gradually increasing intensity

up to failure. A few specimens were initially subjected to a large, closed hysteretic cycle, i.e. they were tested under monotonic loading up to a certain selected maximum displacement ductility ratio.

EXPERIMENTAL RESULTS - The main results obtained from the four series of tests are summarized in Table 1. For a more detailed discussion of these results see Ref. 6.

First Series: After considerable flexural yielding, failures in the first three beams were of predominantly shear type. Beam 35, Fig. 2(a), and Beam 46, performed poorly. A dramatic improvement in hysteretic behavior was achieved by increasing the amount of web reinforcement and decreasing the spacing of the stirrups as done with Beam 43, Fig. 2(b). A displacement ductility ratio of about 6.2 was achieved before any significant drop in strength took place. From this point of view, the web reinforcement used in Beam 43 could be considered satisfactory. Closer analysis of the hysteretic behavior, however, shows that considerable reduction in energy dissipation per cycle started after the first loading to a ductility ratio, μ , of 4.

Second Series: The web reinforcement of Beam 33 was designed to eliminate the following observed weaknesses of Beam 43: (1) considerable lateral swelling in the critical region of the beam, (which extended about 25 in. from column face) and produced early spalling of the concrete cover; and (2) failure of the single ties to provide adequate lateral support to the interior bars of the main reinforcement, thereby resulting in the early buckling of these bars. The hysteretic behavior of Beam 33 is shown in Fig. 3. Although the strength of this beam was slightly greater than that of Beam 43, and there was some improvement in the total amount of energy absorbed and dissipated with respect to Beam 43, the overall improvement was not a major one. Comparing the results obtained in the tests of Beam 33 with those of test 33ME on Beam 33M, it was concluded that the addition of the extra longitudinal bars at mid-depth and supplementary cross-ties yielded no significant improvement on the observed stiffness degradation induced by the reversals of high shear.

Third Series: Although the use of closely spaced vertical ties considerably improved the ductility and energy absorption and dissipation capacities of the specimens, the stiffness continued to degrade at or before a ductility of 4 was reached, even in the case of ties at 3 in. intervals. This occurred because the diagonal tension cracks produced by the shear not only cross similar cracks resulting from the reversals of the shear, but also intersect and combine with the vertical flexural cracks as well. After reversals of loads inducing flexural yielding, one or two nearly vertical cracks, interrupted by diagonal cracks, remained open at zero load throughout the cross section of the beam. At these cracks, the initial shear was resisted by the dowel action of the main bars and by the deteriorating aggregate interlocking taking place around the numerous blocks into which the originally "continuous" concrete had been cracked. Dowel action, however, is an inefficient way of resisting shear because it enhances the longitudinal splitting of concrete. This splitting not only induces bond deterioration, but also accelerates the buckling of the main reinforcing bars and, thereby, the failure of the beam which finally occurs by sliding shear along one of these nearly vertical cracks. This mode of failure has been classified by Paulay as "Sliding Shear Failure" (8). Because it occurs

after considerable flexural yielding of the main reinforcement, its mechanism is designated herein as a "Flexure-Shear Mechanism". From the very nature of this type of degrading shear resistance mechanism, little improvement can be gained by adding vertical ties.

Beam 35I was designed for the purpose of investigating the effectiveness of using heavy diagonal bars as web reinforcement to prevent sliding shear failure. Its hysteretic behavior, shown in Fig. 4, consisted of remarkably stable, spindle-type loops, even near failure which occurred at a $\mu = 6.4$. The first significant degradation in stiffness was observed during the third cycle at a peak deformation of about 4.2 in. ($\mu = 5.2$). The hysteretic loops of Beam 35I resemble those obtained in the test on compact structural steel beams. Comparison of hysteretic loops at the same peak displacements for Beams 35I and 33, Fig. 5, illustrates the improvement achieved by using inclined bars, rather than vertical ties alone. The inelastic rotation that occurred in the critical region when Beam 35I reached its maximum tip deflection (LP 93 in. Fig. 4), corresponded to an equivalent plastic hinge rotation of 0.035 rad., it was nearly twice this value (0.067 rad) during the full load reversal (LP 91 to LP 93). This plastic hinge rotation capacity is close to that available in equivalent compact structural steel regions. This is the most that can be expected. The contribution of the different sources of deformation to the tip deflection and its variation with increasing ductility ratios for Beam 35I is compared with that of Beam 33 in Fig. 6. From this comparison it is clear that for all ductilities, the shear deformation in Beam 35I was smaller than that for Beam 33.

Fourth Series: Significant rigid body rotations of the whole cantilever were observed in previous tests. These rotations were caused by the slippage of the main bars along their embedment lengths in the column-stub despite that the main bars were welded to steel plates, which were cast with the column-stub and rigidly attached to the reaction frame, Fig. 1(a). Figure 6 shows that for Beam 35I, the contribution of this slippage to the tip deflection ($\delta_{\text{FIXED END}}$) amounted to more than 25%. Thus it is clear that slippage of these bars can be one of the controlling parameters in the overall stiffness degradation observed in real structures. This slippage was a result of the degradation of bond with repeated reversals of inelastic straining. The main reinforcement of Beam 33L, Fig. 1(d), was detailed in an attempt to decrease the slippage of the bars.

Beam 33L was subjected to two tests, Fig. 7. During the first test (33L), the beam was monotonically loaded up to a tip displacement of 4.8 in. ($\mu = 6$), without any drop in shear resistance, which reached a maximum of 160 kip. After unloading, the beam was loaded in the opposite sense up to a displacement of -4.0 in. offering a shear resistance of 163 kip. From Fig. 8(a) it is clear that the deformations due to shear distortion and slippage of the bars were smaller than those in previous beams. After its repair by epoxy injection, Beam 33L was loaded under repeated reversals of increasing shear up to failure (Test 33LR). This occurred after inducing a tip displacement of 6.5 in. without any significant drop in strength (152 kip vs a maximum of 158 kip at 4.5 in.). Although Beam 33LR had initially been subjected to an extreme cycle of shear reversal, its hysteretic behavior was very similar to that of Beam 35I. Comparison of hysteretic loops corresponding to a peak deflection of about 4.2 in. for these two beams, Fig. 9, confirms this similarity. The results presented in Fig. 8 clearly indicate that the slippage of the bars ($\delta_{\text{FIXED END}}$) in Beam 33LR was 30% less than that of Beam 35I. The

maximum plastic hinge rotation attained for Beam 33LR was 0.072 rad., and it developed along a length which was practically twice that observed in Beam 35I.

HYSTERETIC BEHAVIOR OF BEAM-COLUMN SUBASSEMBLAGES - In the tests of the cantilever beams considerable increase in tip deflection has been observed, as a consequence of pull-out of the main bars. This pull-out increases with severity of the loading and number of reversals. In practical cases where the main bars cannot be anchored mechanically by welding, (as done in the beams tested) the observed bond deterioration can lead to severe anchorage problems at the column joints. The severity of these problems can be assessed by analyzing results obtained in a series of experiments that are being conducted at Berkeley on hysteretic behavior of beam-column subassemblages (5,9). Four half scale models of an interior beam-column subassemblage of the third floor frame in a 20-story ductile moment-resisting concrete building, have been tested to date. Figure 10 shows the specimen tested and a brief discussion of the major results obtained follows.

The effect of repeated load reversals is illustrated in Fig. 11 where the hysteretic curves obtained from tests conducted on one of the specimens, BC3, is compared with the behavior of BC4 which was subjected to a monotonically increased load up to a lateral displacement ductility of 5. Comparing the results for these two specimens shows that repeated cycles of full deformation reversals of increasing amplitude induced a rapid degradation in the subassemblage stiffness. This degradation is clearly illustrated in Fig. 12, where the initial loading parts of the hysteretic loops of Fig. 11 have been shifted horizontally to a common origin. Since the amount of nominal shear stress developed in the beams was small (on the order of $3\sqrt{f'_c}$), the observed degradation was not the results of shear reversals in the beams. The main reason for this degradation was the slippage (bond failure) of the beams' main reinforcing bars along a large part of the column width as a consequence of their simultaneous pull-out (at one face) and push-in (at the other face of the column joint).

Under a monotonically increasing lateral load, a ductility ratio, μ , of 5 was attained without any decrease in strength of the specimen; whereas under repeated reversals of increasing deformation, a considerable drop in lateral resistance was observed after a $\mu = 2.5$. Drastic pinching of the hysteretic loops after a $\mu = 2.5$, clearly points out the significance of the bond deterioration induced by repeated reversal deformations.

ASEISMIC DESIGN IMPLICATIONS OF OBSERVED HYSTERETIC BEHAVIOR - Present American code provisions for the aseismic design of ductile moment-resisting space frames are based largely on results obtained in experiments carried out under monotonically increased loading. The adequacy of such provisions is questionable in the light of building damage observed in recent severe earthquakes. This is particularly true in the case of members subjected to high shears and in the case of anchorage of reinforcing bars subjected to strain reversals in the inelastic range. Penzien et. al. (7) have concluded that the present code requiring tie spacing in the critical region to satisfy $s \leq d/4$ could be relaxed when $v_{u\max} \leq 2.6\sqrt{f'_c}$. The investigation just reviewed proved that when the $v_{u\max}$ reaches values higher than $3.5\sqrt{f'_c}$, more stringent code provisions must be formulated. The results obtained to date on effects of high shear and on bond deterioration permit the following

series of observations and recommendations to be made regarding the aseismic design of moment-resisting space frames.

(1) In moment-resisting space frame systems, short span bays leading to the use of girders with low shear span-to-depth ratios (≤ 3) and high percentages of main reinforcing steel, should be avoided. The combined actions of reversals of high bending moments and corresponding shear that can be developed in the critical regions of these girders will result in significant degradations unless costly web reinforcements are used.

(2) If the use of short span girders is unavoidable, it is recommended that the flexural design of these girders be done in such a way that their maximum bending strength does not require the development of maximum average nominal shear stresses beyond $3.5\sqrt{f'_c}$ (psi). This can be achieved by the use of wide girders with a low percentage of reinforcing steel having low yielding strength, and a large plastic plateau with a small strain-hardening modulus of elasticity. Web reinforcements should be designed to resist the total shear, and the minimum practical spacing of ties should be used. If it is not possible to keep the nominal shear stress below $3.5\sqrt{f'_c}$ (psi), special web reinforcements beyond those required by present code provisions should be used. Some improvements can be achieved by placing extra longitudinal reinforcements near the faces of the girder web at mid-depth and supporting these bars and the vertical legs of the vertical ties with supplementary cross-ties. The most efficient web reinforcement tested, however, was obtained by adding inclined 45° crossing bent bars. Effective plastic hinge rotations up to 0.035 rad. (0.067 rad. during a full load reversal) have been achieved using inclined crossing bars. The maximum nominal shear stress should in no instance exceed $6\sqrt{f'_c}$ (psi) when a large number of reversals at a $\mu \geq 4$ is expected.

(3) When end critical regions of girders can be subjected to numerous cycles of reversals at large displacement ductilities, a drastic and early drop in strength, and especially in stiffness, can occur due to the slippage of the beams' main bars throughout the column at interior joints. Although such degradations are inevitable under present methods of design, they can be minimized and delayed by: (a) designing girders with a low percentage of main reinforcement; (b) using the same, or nearly the same positive and negative reinforcements at the girder ends; (c) using a beam-reinforcing steel with low yielding strength, and a large plastic plateau with a low strain-hardening modulus of elasticity; (d) selecting numerous small-diameter bars, rather than few large-diameter bars; and (e) using the deepest possible column to increase the length of anchorage of the beams' main reinforcing bars.

(4) To minimize the problems created by the slippage of the beams' main bars through the interior joint, to improve the response of the anchorage of these bars in the exterior joint, and to facilitate special web reinforcement against the combined effect of high shear with bending moment, the beams' main reinforcement should be designed and detailed to force plastic hinges to form away from the column faces. One disadvantage in locating the plastic hinges away from the ends of the girders is that the amount of inelastic rotation required to attain a certain selected displacement ductility would be greater than that for the plastic hinges forming at the column faces. One way of attaining this greater required rotation would be by detailing the reinforcement to

force the inelastic deformation to spread over a longer region. By using numerous small-diameter bars, rather than few large-diameter bars, the bending of a sufficient number of bars could be tailored to create the greater required length for the plastic hinge.

(5) A mathematical model for the behavior of flexural critical regions has been formulated (4). There is now an urgent need to develop a nonlinear dynamic computer program based on a mechanical model that includes not only the change in geometry and the observed monotonically pseudo-static inelasticity of the materials, but also, the degradation in stiffness caused by cyclic loading reversals as a consequence of: (a) higher shear, (b) bond degradation, (c) pull-out of bars due to the failure of anchorage at the exterior beam-column joint, and (d) slippage of the bars along the column at the interior joint.

Only through the use of such computer programs can dynamic analyses of the response of realistic structural models to different possible ground motions lead to a better understanding of the ramifications of the above sources of nonlinearities on the aseismic design of moment-resisting space frames. Such programs would enable determining the inelastic deformation demands at different critical regions of such frames. According to preliminary studies using existing programs (1) rotations in girders of ductile frames can reach large values, although the number of full reversals is generally not very large. From this point of view some of the specimens were overtested. On the other hand, these preliminary studies have shown that the critical regions of shear wall coupling girders can be subjected to a very large number of severe reversals in the inelastic range.

III. HYSTERETIC BEHAVIOR OF STRUCTURAL WALL COMPONENTS

The design and behavior of structural wall components depends upon the relation between the internal forces controlling their "elastic" and, particularly, "initial yielding" and "inelastic" behaviors. If bending controls behavior, these components can be classified as "flexural walls"; if shear controls behavior, they can be classified as "shear walls." This classification is usually made on the basis of the geometric proportions of the wall, particularly on the height (H) - width (B) ratio. Short walls [say, $H/B < 1/2$, according to Fintel (11); $H/B < 1$, according to Paulay (12)], are usually controlled by shear; slender walls [say, $H/B > 2$], by flexure. Because behavior depends upon the loading condition, and is also very sensitive to the amount, type and detailing of reinforcement, caution should be used when classifying walls according to geometric proportions alone. From the point of view of loading, it might be better to use the shear span (a) - depth (d) ratio, a/d rather than H/B alone.

As the H/B or a/d increases, the wall becomes increasingly slender and, consequently, more difficult to distinguish between a slender wall and a column. Perhaps one way of distinguishing them is by applying Section 2626 (f)1 of the UBC which requires the ratio of minimum to maximum column thickness to be not less than 0.4. Generally, however, the compressive stresses due to axial forces acting at the critical region of a wall are considerably less than those which develop in the column substituted by the wall.

In building construction, the structural wall is generally used in combination with the moment-resisting frame. The interaction between the wall and frame, particularly regarding the hysteretic behavior of buildings under earthquake-like conditions, is not very well-understood at present. The lack of understanding concerning this interaction and the sensitivity of inelastic behavior to the wall geometry, and to the amount, type and detailing of reinforcement, are the main reasons for the disagreement among researchers and professional engineers regarding the way that walls should be designed. This disagreement is manifested in significantly different requirements for the design and analysis of structural walls specified by different American codes. This is illustrated by Table 2 which compares the design forces for a shear wall of a 12-story building (13), calculated according to ACI and UBC code provisions. The code provisions. The code design philosophy for walls is neither very clear nor consistent with that used for designing the components of ductile moment-resisting frames.

The main concern of aseismic design is to achieve a ductile hysteretic behavior. Thus, walls should be designed so that its hysteretic behavior (particularly its mechanism of failure) is controlled by flexure. In the case where geometric proportions dictate that shear control behavior (e.g., squat walls), the wall should be designed to absorb all the earthquake energy input in its "elastic range" and to prevent large openings of cracks (diagonal and flexural). Present code provisions do not distinguish between "shear (or squat) walls" and "flexural (or slender) walls."

As illustrated in Table 2, Section 2627(a) of the 1973 UBC requires that a value of $2.8E$ be used in calculating shear stresses in shear walls of buildings without a 100% moment-resisting space frame. Section 3A of the 1974 Lateral Force Requirements of the SEAOC recommends that a value of $2.0E$ be used in calculating shear and diagonal tension in buildings other than those complying with the requirements for buildings with $K = 0.67$. According to the 1967 SEAOC Commentary, the doubling of the value of E is recommended so that the design stress level for shear in concrete is reduced to one-half that normally required. This is done to provide a greater range of elastic response in any given dynamic input prior to possible nonductile shear failures. Although it is convenient to have a greater safety factor against nonductile shear failures, it is not believed that merely doubling the value of E is the best way of achieving this (14). The actual shear stress developed during response to an extreme earthquake ground shaking not only depends on the distribution of the code static equivalent lateral forces, but also on: 1. the flexural capacity that has been built in the structure, 2. the actual distribution of inertial forces (or story shears) throughout the height of the building, and 3. the interaction between frame and wall components.

From the above discussion, it can be concluded that a slender flexural wall can be effectively achieved by designing it against the maximum shear that can be developed according to the actual flexural capacity (as affected by the axial force) of the critical region and considering the critical moment-shear ratio that can exist at such a region. Even if the maximum shear can be estimated with sufficient engineering accuracy, there still remains the problem of designing against it.

In the case of squat walls, it is generally economically infeasible to design against a shear corresponding to the flexural capacity of the wall; therefore, it seems logical to base the code requirements on a specific maximum nominal ultimate unit shear stress. This unit stress, however, should correspond to the maximum possible shear force that can be developed at the section. Consequently, this shear should be estimated from forces obtained from linear elastic design response spectra corresponding to the maximum credible ground shaking; computing the shear by merely increasing the present code specified lateral earthquake force by 2 is insufficient. It has been demonstrated, and is widely recognized, that present code design forces for relatively rigid structures can be at least three times smaller than those expected in a linear elastic response, even if high damping is assumed.

It is believed that the misunderstanding and disagreement regarding actual hysteretic behavior of structural walls under earthquake-like conditions is a direct consequence of the lack of reliable data in this area. Up until 1970, most of the experimental results that were available regarding the behavior of wall elements were obtained from tests of one- or two-story reinforced concrete walls or infilled reinforced concrete frames which were subjected to simplified loading conditions. Although some of these studies investigated the seismic behavior of wall components in medium-rise buildings, the loading conditions under which most of the tests were conducted, Fig. 13, did not simulate the real effects of earthquake excitations; rather, they simulated excitations that could have developed in wall systems used for shelters against nuclear weapons. The strength and deformational behavior of the walls tested were controlled by shear; hence, they have been designated accordingly as "shear walls."

The inaccurate simulation of loading conditions used in most of the previous experimental investigations on the seismic behavior of wall systems is believed to be the result of a lack of integrated experimental and analytical studies. Therefore it is not surprising that present methods of predicting the mechanical behavior of wall systems are of a very approximate nature, and there is an urgent need for improving them. This need has led to the initiation in 1971 of the following investigation.

OBJECTIVES AND SCOPE - The ultimate objective of the investigation started in 1971 is to develop practical methods for the aseismic design of combined frame-wall structural systems. To achieve this objective, the real mechanical behavior of wall systems subjected to earthquake-like excitations is investigated by integrated analytical and experimental studies.

The analytical studies have two main objectives. The first objective is to use available analytical techniques for studying the forces acting on different subassemblages of frame-wall systems subjected to time history earthquake ground motions, and to thereby plan a rational program of experimental studies. Analytical and experimental responses are then compared to assess the reliability of these available analytical tools. The second objective is to develop new and more efficient computer programs for the analysis of multistory frame-wall structural systems.

The main objective of the experimental studies is to obtain reliable data regarding the linear and nonlinear behavior of frame-wall structural systems. To achieve this objective, the research program covers the following: 1. a review of available data regarding the behavior of different wall systems subjected to earthquake-like excitations, 2. the design of

buildings with frame-wall systems and analysis of their seismic response using available methods, 3. experimental studies of wall and frame-wall subassemblages of such buildings, 4. the use of experimental data to improve the formulation of mathematical models for such systems, and 5. design implications of the results obtained and the formulation of practical methods for the preliminary aseismic design of such systems.

In this paper, only the experimental studies that have been carried up to the present will be discussed and the main results presented. Seismic design implications of the observed behavior will be offered based on analysis of the presented results.

SELECTION, DESIGN AND CONSTRUCTION OF TESTING FACILITY - After comparing the advantages and disadvantages of using the earthquake simulator facility available at the Earthquake Engineering Research Center with those of using a pseudo-static facility capable of simulating the significant deformation histories expected in the dynamic response of a structure during severe earthquake shaking, the latter facility was selected (15).

Testing of full or large scale models of the entire building was not possible due to the lack of a testing facility necessary for conducting such experiments and the limited budget available for constructing a new one. Therefore, it was decided to test significant subassemblages of the structural system. To predict the in-plane seismic behavior of frame-wall systems, it is necessary to have information regarding the variation of the lateral shear-displacement relationship for each story, as illustrated in Fig. 14. In order to correctly simulate the actual boundary conditions of the story under study, it was decided to test subassemblages of at least three stories, Fig. 15. To design the testing facility, two buildings, 10- and 20-stories, 61 x 180 ft., each, in plan, were designed using present UBC seismic provisions. The 10-story building, shown in Fig. 16 was redesigned using, in one case, the seismic forces resulting from the application of a smooth design response spectrum, and in another case, the Structural Standards of the Architectural Institute of Japan (16). A comparison of all these designs reveals significant differences between the present American and Japanese design philosophies of shear wall systems. Analyses of the response of the designed building to different severe earthquakes permitted estimating the relative intensity of the forces that can be expected to act on the bottom three story subassemblages. Capacity studies of these prototype assemblies were used to design the testing facility as well as to select the larger scale models which could be tested. These studies resulted in the selection of 1/3 scale models (15).

The principal feature of this facility is its ability to simulate, in a pseudo-static manner, the dynamic loading conditions which could be induced in subassemblages of buildings during earthquake ground shaking. Assuming that the wall alone could resist most of the lateral inertial forces, it is clear from Fig. 17(c), that it would be necessary to apply not only lateral forces [$S_3(t)$, $H_2(t)$ and $H_1(t)$] but also, forces which would simulate the effect of overturning moments (OVM_3) and gravity loads existing in the prototype above the top floor of the subassemblage. This is required because the principle of superposition is not applicable in studying inelastic behavior. Therefore, to simulate the actual inelastic behavior of this subassemblage when it forms part of the whole wall, the synchronized shear,

overturning, and axial forces must be applied simultaneously. Because of the difficulty of introducing the actual distribution pattern of these forces and moments, Fig. 17(b), they must be replaced by concentrated resultant forces, as illustrated in Fig. 17(c). To avoid the effect of local disturbances caused by the application of these equivalent concentrated forces and that of the alteration of the actual boundary conditions, it is necessary to employ at least two, preferably three, stories in modeling the prototype subassemblages corresponding to one selected story.

In the facility built at Berkeley, the walls are tested in a horizontal position, as shown in Fig. 18. Specimens from 1/4 to 1/2 scale of the prototype can be accommodated.

As shown in the plan of Fig. 18(a) and the photo of Figs. 18(b), the testing facility consists of a series of reaction reinforced concrete blocks and a steel reaction box. All these reaction fixtures are anchored by means of prestressed rods to the laboratory tie down slab, and serve to support the specimen and hydraulic actuators (jacks) necessary for simulating the excitations to be applied to the specimen. Two 500 kip actuators were arranged to apply axial forces to the columns of the specimen, simulating both the static gravity effects plus the dynamic alternating forces resulting from the seismic overturning moments. A 460 kip actuator was provided to apply the shear force required for simulating the total seismic shear acting on the upper story. Two small 50 kip actuators can be used to apply inertial forces acting in the two lower floors. All these lateral actuators can be electronically coupled with those connected axially to the columns so that the applied shears and overturning moments would act in phase.

To obtain the necessary information for studying the hysteretic behavior of the models, the specimens are extensively instrumented. Figure 18(b) illustrates part of the data acquisition system. The lateral displacement at each floor level and at intermediate heights of the first story are automatically plotted against the lateral shear force applied at the top of the specimen. This is achieved through the use of X-Y-Y recorders. The variations of the other applied forces, the relative shear deformation of each story, the average curvatures through different cross-sections of the wall, some axial deformations along the edges of the walls and columns, and strains of some of the reinforcing bars located in the expected critical regions of columns and walls, are also plotted directly against the applied shear force through the use of X-Y-Y recorders. Numerous strain gages placed on reinforcing bars, and clip gages used in measuring the relative deformation along 6 in. to 12 in. base lengths, are read at selected stages of the test directly through a low-speed data acquisition system whose heart is a NOVA minicomputer.

The progress of crack formation in the specimens is carefully observed and recorded. In addition, photogrammetric pictures made at the critical stages of the experiment provide a unique qualitative record of the behavior of the wall at the selected loadings, as well as highly accurate information on the movement of the cracked mosaic of the wall.

FABRICATION OF SPECIMENS AND MECHANICAL CHARACTERISTICS OF MATERIALS (17)
Two specimens, 1/3 scale models of the bottom three stories of the wall component of the 10-story frame-wall system shown in Fig. 16, were subjected to a series of tests. As illustrated in Fig. 19, the specimens consisted of

a 4 in. thick wall framed by two 10 in. square columns. The total width of the specimen was 7'-10" and the total height, 13'-7". The wall was reinforced with two layers of horizontal and vertical reinforcement (#2 at 3 in. spacing). The columns were spirally reinforced with 8 #6 main bars having a 0.21 in. diameter spiral.

To simulate the construction work in the field, the specimens were casted story by story in its vertical position, illustrated by the photos of Fig. 20. The two specimens were casted simultaneously. The main mechanical characteristics of the materials are summarized in Table 3. This table shows that the actual yielding strengths of the reinforcing bars were considerably higher than those specified. Furthermore, the actual strengths developed in these bars could even reach values considerably higher than their measured yielding strengths, due to earlier strain-hardening, especially in the #6 bars.

PREDICTION OF EXPECTED STRENGTH OF SPECIMENS (17) - Based on the actual mechanical characteristics of the materials, the possible flexural and shear strengths of the specimen under different axial forces were evaluated. Figure 21 compares the moment-axial force interaction curve so obtained with that resulting from applying the 1971 ACI Code. This figure also compares the most probable expected flexural and shear strengths with those corresponding to the design. The significance of the observed difference will be discussed later.

LOADING CONDITIONS - The prototype was designed for critical load combinations of gravity (dead and live) and seismic loads as specified by the 1973 UBC. Although these loads could be easily simulated in the testing of the specimens, rather than apply them, it was decided to investigate the behavior of this code designed wall under the most critical load combination which could be developed in the case of an extreme earthquake ground shaking. Rational selection of the actual probable critical combination requires integrated experimental and analytical studies (18) because it varies depending upon the main parameters under study. Table 4 illustrates the differences in the loading conditions that were derived for the wall model of the prototype of Fig. 16 using different methods for evaluating the seismic forces. The considerable discrepancies among the resulting shear span values point out not only the difficulties in selecting the critical combination of inertial forces but also, the need for carefully interpreting results obtained in experimental investigations in terms of the actual seismic behavior of structures.

To determine the adequacy of present code specifications for avoiding brittle shear failures, specimens were tested under the load combination corresponding to the last case presented in Table 4. This loading combination was selected because of all the cases analyzed, it resulted in the most critical shear force at the first story.

Although the two axial forces necessary to simulate the effects of gravity forces were applied first (by means of column actuators), and they were the same for the two specimens, the effects of seismic forces were introduced following a different loading pattern in each of the two specimens tested. In the first specimen, the lateral force and the change in column axial forces (needed to reproduce the corresponding change in overturning moment) were monotonically increased until a reduction in the lateral

resistance could be observed. The second specimen was subjected to a history of lateral shear and corresponding overturning moment that induced gradually increasing cycles of full reversal lateral displacement with at least 3 cycles at each displacement amplitude, Fig. 22. This loading program is considered to be the worst condition for shear resistance deterioration.

TEST RESULTS - Only the main results obtained will be presented and discussed herein. For a more detailed discussion, see Ref. 17.

Wall 1: The lateral force vs. displacement diagram is shown in Fig. 23. Except for a series of repeated reversals of load at the working load level (simulating the effect of extreme winds or minor earthquake shaking), it was planned to monotonically load the first specimen up to incipient failure. Just after yielding ($\delta_{3R} \doteq 1.0$ in., Fig. 23), however, there were some difficulties in the automatic control system and the specimen was unloaded. The specimen was then monotonically reloaded up to a $\delta_{3R} \doteq 2.7$ in. At this stage, there occurred some movement in the concrete reaction blocks; it was therefore decided to unload the specimen and reload it in the opposite sense up to a displacement reversal great enough to ensure that after unloading it became in equilibrium at a position close to that of the original, i.e. zero lateral displacement. After improving the anchorage restraint of the reaction blocks, the specimen was subjected to a series of cycles of full displacement reversals in the working load range. Considerable initial stiffness deterioration was observed. It was then monotonically loaded up to the point where a significant reduction in strength due to crushing of the concrete in the wall, was observed (LP 158 in., Fig. 23, with a $\delta_{3R} \doteq 4.25$ in.). At this point, the specimen was unloaded to avoid collapse. After unloading, a few cycles of full reversals at working load level were applied, resulting in very stable hysteretic loops. The specimen was then loaded in the opposite sense up to a $\delta_{3R} \doteq -1.9$ in., and then unloaded. This loading reversal induced considerable further damage to the specimen, as can be seen from the unstable hysteretic behavior in the working load range that resulted when the specimen was finally subjected to loading cycles in this range. The photos of Fig. 24 illustrate the damages induced at the first story of this specimen at different stages of the test. Regarding the overall behavior of this wall, the following main observations can be made:

(1) The envelope from LP 0 to LP 158 of Fig. 23 can be considered as representing the behavior of the wall under a monotonically increasing load because the unexpected unloadings and deformation reversals introduced were not severe enough to significantly alter such behavior.

(2) The overall behavior up to near crushing of the wall was essentially that expected from a ductile flexural member.

(3) The observed experimental yielding strength of the specimen, i.e. when overall stiffness became close to zero as that for LP 80, was $P_T = 215$ kip. ($M = 37,000$ kip-in.) This load was about 17% higher than that estimated for the first yielding ($V = 184$ kip). This estimation was based on the actual mechanical characteristics of the materials but assuming that yielding was reached after all the tension column steel had yielded. Compared with the ACI Code's ultimate load value ($V = 196$ kip) predicted on the basis of specified material properties and $\phi = 1$, the observed value is seen to be about 10% higher.

(4) The nominal unit shear stress corresponding to the observed yielding load has been evaluated as $v_y = 692 \text{ psi} = 9.5\sqrt{f'_c}$. This observed nominal shear stress is nearly twice the value ($5\sqrt{f'_c}$) expected according to the code design forces.

(5) After flexural yielding at the first story, the contribution of the shear deformation to the total lateral displacement of the first story began to increase considerably, as shown in Fig. 25. Considering that the shear was constant throughout the height of the specimen, comparison of the $V-\delta_1$ and $V-\delta_2$ clearly points out the importance of the interaction between flexural yielding and shear occurring at the first story.

(6) At first yielding, diagonal tension cracks existed throughout the height of the specimen wall. These diagonal cracks were uniformly and closely spaced at about 3 in. and inclined at approximately 45° (see Fig. 24). Although the width of these cracks was small in the second and third stories, some of the first story cracks opened up considerably at this stage of loading.

(7) Crushing of concrete began at the bottom part of the compressive edge column at a ductility displacement of about 3 (LP 88) at a load of about 235 kip. The crushing of the concrete column cover, however, did not affect the lateral load carrying capacity of the specimen and it was possible to increase lateral load to a value of 248 kip (LP 157-158). At this level, crushing of concrete was observed at the lower left corner of the first story wall. As soon as the concrete of the wall began to spall, the reinforcing bars in this spalling region buckled and the load resistance decreased.

(8) At the maximum load of 248 kip, the nominal unit shear stress was $11.3\sqrt{f'_c}$, i.e. more than 2.2 times the value expected according to the code seismic design forces.

(9) The maximum displacement ductility factor was 6.1 which corresponded to a total (tip) maximum displacement of 4.25 in. The contribution of the different sources of deformation to this total displacement can be seen in Fig. 26. Contribution of the shear deformation amounted to 35%. The maximum first story displacement was 1.74 in. which corresponded to a $\mu \pm 7.2$. The contribution of the shear deformation to this first story displacement was 71%.

(10) The maximum story drift indices at working load, yielding and maximum resistance were 0.002, 0.008 and 0.036, respectively. All of these occurred at the top story. The first story drift at maximum resistance was similar to that obtained at the top story.

(11) The maximum inelastic rotation was 0.02 rad. This inelastic rotation was due to yielding of the tensile column steel which extended for a length of about 60 in., i.e. close to $4/5$ the effective specimen depth.

Wall 2: As illustrated in Fig. 22, this specimen was tested under repeated reversals of lateral load and of the corresponding overturning moment, where the peak value of the load and/or deformations was gradually increased after 3 or 4 cycles at the same value. The hysteretic behavior of the specimen under this kind of excitation (perhaps the most critical one

that can be expected regarding shear), is illustrated by the hysteretic loops shown in Fig. 27. By examining these loops and other data obtained from these tests, and comparing them with the envelope obtained from the test of Wall 1, it becomes clear that behavior under monotonically increasing loads is affected by repeated reversals of lateral loads as follows:

- (1) The yielding strength was unaffected.
- (2) One cycle of reversal at the yielding strength level induced considerable degradation in initial stiffness. After three cycles at yielding ($\mu = 1$), the natural frequency of vibration dropped from 39.5 (before testing) to 18.5 hertz. This could occur only due to a reduction in stiffness of more than 4.5 times.
- (3) Each time the absolute value of the peak deformation of a hysteretic loop was increased, there was a degradation in the initial stiffness and energy dissipated during the following cycle as compared with the value in the previous cycle.
- (4) The ultimate strength was minimally affected (245 kip vs. 248 kip).
- (5) Whereas the tip displacement ductility factor, μ , was reduced by about 35% (from 6.1 to 4.2), μ for the first story was reduced by 27% (from 7.2 to 5.3).
- (6) Although the mechanism of failure was not significantly affected, crushing of the concrete at the wall corner and the buckling of the wall reinforcing were accelerated by the repeated cycles of deformation reversals. No crushing of concrete at the column cover was observed until the wall concrete crushed. The entire column cover split after the crushing of the wall concrete due to dowel action. (The column was subjected to dowel action in the band wherein this wall concrete had crushed and the wall reinforcing bars had buckled.) During the reversal after the lower left corner of the wall crushed (LP 129), the concrete in the right lower corner also started to crush (LP 133). During the next cycle of reversals, the concrete crushed and spalled all along a band extending horizontally through the wall about 10 in. from the footing (Fig. 28). At this stage, practically all the shear was resisted by dowel action offered by the confined core of the edge columns, which began acting as short columns of a frame, Fig. 29.
- (7) The repetition of cycles of full reversals led to a concentration of deformation at the first story. This can be seen by comparing Figs. 27 and 23.
- (8) The contribution of the shear deformation to lateral displacement was increased by the effect of deformation reversals, as can be seen by comparing Figs. 30 and 31 with Figs. 25 and 26.
- (9) Although the tests on the two specimens were stopped after a considerable decrease in lateral resistance was observed, both specimens were capable of resisting the effect of gravity loads, since the edge columns did not fail.

According to the above observations, the repeated full reversals

of deformations not only soften the wall but also significantly reduce its ductility. Free vibration tests, carried out on Wall 2 after testing with deformation reversals, indicate that the natural frequency was reduced to 8.5 hertz. This means that after crushing of the wall, the stiffness was about 22 times less than that of the virgin specimen. This is not surprising since after the termination of the series of tests just reported, the initial structural wall system was converted to a system with a soft moment-resisting first story having very short columns (see Fig. 29).

Damping: Several free vibration tests were carried out on Wall 2 to determine the effect of progressive damage on the dynamic characteristics of this type of structural system component. The main results are summarized in Table 5. Analysis of these data reveals the following:

(1) Small amplitude tests such as the so-called "Ambient Dynamic Tests," resulted in a somewhat greater natural frequency and considerably lower values of critical coefficients of damping than did large amplitude free vibration tests. Caution should therefore be taken when applying results obtained from ambient dynamic measurements taken at extremely low level signals.

(2) The damping coefficient increased from 2.7% to 9.1% after the specimen was subjected to reversals between peaks equal to or less than its yielding strength. This increase was due to large amounts of friction that took place along the numerous diagonal tension cracks developed in the walls along the entire height of the specimen.

(3) The damping coefficient corresponding to the stage of maximum resistance (after the apparent failure of the wall) was 39% less than that at yield level (5.6 % vs. 9.1%). This, at first sight, surprising result of decreased damping with increased damage can be explained by the fact that the damage introduced converted the initial wall system into a system with a soft partial first story moment-resisting frame (Fig. 29). During the vibration test, after failure of the first story wall, all the deformation occurred along the first story band where the wall concrete had crushed and spalled. Therefore, no great amount of energy was dissipated along the diagonal tension cracks that were distributed throughout the rest of the wall.

CONCLUDING REMARKS - From the results obtained in this series of tests, it can be concluded that it is possible to design structural wall components capable of developing large ductilities even when subjected to reversals inducing nominal unit shear stresses up to $11\sqrt{f'_c}$. Although the total lateral displacement ductility was reduced due to reversal, from 6.1 to 4.2 (7.2 to 5.3 for the first story), it is still considered large enough to permit the development of energy absorption and energy dissipation capacities exceeding even those that would be demanded in the case of very severe earthquake shaking. Furthermore, even at this large ductility, the confined core of the columns remained sound and capable of resisting both the effects of axial forces imposed by the gravity load, and of lateral loads in the working load range.

SEISMIC DESIGN IMPLICATIONS OF OBTAINED HYSTERETIC BEHAVIOR - In spite

of the limited amount of data obtained, these data, together with the studies carried out in planning and conducting this research, enable the following observations regarding the design of frame-wall structural systems to be formulated. These observations, however, should be considered as tentative and subject to modification as more data become available.

(1) Present code design specifications (regarding design forces, load factors, and design and detailing of critical regions) can lead to a wall design which considerably underestimates the amount of shear that can actually be developed. For design purposes, walls should be classified in at least two groups, flexural walls and shear walls. The design of flexural walls against shear should be based on the maximum shear that can be developed according to the flexural capacity of the critical region, and the largest shear/bending moment ratio that can be developed in the critical region according to the expected dynamic response of the entire building to severe earthquake ground motions of different dynamic characteristics.

(2) The main effects of repeated cycles of full deformation reversals with high shear on flexural walls, when compared with behavior under monotonically increased loads, are very similar to those observed in the case of beams: (a) large degradation in initial stiffness which increases as the peak deformation (amplitude) of the reversal cycle is increased, and (b) a reduction in the displacement ductility. It would appear, however, that flexural walls of the type used in this investigation (i.e. with spirally reinforced edge columns) can more successfully resist higher shear reversals without large detrimental effects than beams. Reasons for their superior behavior are suggested in the following discussion of the mechanism of failure.

(3) The mechanism of failure of the wall tested appears superficially to be different from that observed in beams. For the beam, failure usually occurred due to buckling of the main reinforcing bars; for the wall, failure was triggered by crushing of the concrete in the wall. This crushing appears to be a consequence of shear rather than flexural compression. Final failure of the wall specimen occurred by the fracture of the column reinforcing spiral. A more detailed analysis of these failures indicates that final failure for both components is actually the consequence of the same type of behavior: dowel action. The difference observed is a result of the difference in the effectiveness of these dowel actions. In the case of beams, dowel action depends on the main reinforcing bars alone and how they are laterally restrained (spacing of ties). On the other hand, dowel action in the walls tested was resisted by the whole confined core of the edge columns because of the closely spaced spiral. The column main reinforcing bars could not have buckled until the failure of the reinforcing spiral.

(4) In designing or analyzing a wall structural system in its "elastic range," i.e. up to its yielding strength, it is possible to assume larger damping than is presently assumed for this type of structural system. Note that this refers to the damping developed by the bare structural wall component itself. The damping for the response of the entire building can be affected by other sources of energy dissipation and these should also be considered.

(5) The significant degradation in stiffness as well as the type of

incipient failure that has been observed, throw some serious doubts on the present code design philosophy of so-called "dual bracing structural systems" (those having a UBC design for a $K = 0.80$). Most of the observed degradation in stiffness is due to the damage that occurs at the first story which is a consequence of the flexural and shear interaction after yielding along the critical region. As a result of this concentration of deformation, the wall component behaves like a system with a soft first story (Fig. 29). Because the behavior of the complete frame-wall system is usually controlled by the behavior of the wall component, the frame system will also be forced to behave as a moment-resisting frame with a soft first story (Fig. 32), rather than a ductile moment-resisting as assumed and required by the UBC.

ACKNOWLEDGEMENTS

The authors are grateful for the financial assistance provided by the National Science Foundation under Grant No. AEN 73-07732 A02, Sub-project Nos. 0-21987 and 0-21997. They also wish to acknowledge the active participation of Dr. T. Endo in the study of the wall components, and of H. Krawinkler, B. Lotz and graduate students R. Alamo, D. Clyde, M. Quint, S. Ma, J. Ragsdale, D. Soleimani, J. Vallenias and S. Viwathanatepa in conducting the experiments. The editorial assistance of L. Tsai is much appreciated.

REFERENCES

1. Bertero, V. V., "Experimental Studies Concerning Reinforced, Prestressed Concrete Structures and Their Elements," Introd. Report of the IABSE Symposium on Resistance and Ultimate Deformability of Structures Acted on by Well Defined Repeated Loads, Lisbon, 1973, pp. 67-100.
2. Popov, E. P., Bertero, V. V., and Krawinkler, H., "Cyclic Behavior of Three Reinforced Concrete Flexural Members with High Shear," Earthquake Engineering Research Center Report No. EERC 72-5, University of California, Berkeley, October 1972, 78 pp.
3. Bertero, V. V., Popov, E. P., and Wang, T-Y., "Hysteretic Behavior of Reinforced Concrete Flexural Members with Special Web Reinforcement," Earthquake Engineering Research Center Report No. 74-9, University of California, Berkeley, August 1974, 126 pp.
4. Ma, M. S., "Experimental and Analytical Studies of Hysteretic Behavior of Reinforced Concrete Rectangular and T-Beams," Ph.D Dissertation, University of California, Berkeley, August 1975.
5. Bertero, V. V. and Popov, E. P., "Hysteretic Behavior of Ductile Moment-Resisting Reinforced Concrete Frame Components," Earthquake Engineering Research Center Report No. EERC 75-16, University of California, Berkeley, April 1975, approx. 78 pp.
6. Bertero, V. V. and Popov, E. P., "Hysteretic Behavior of Reinforced Concrete Flexural Members with Special Web Reinforcement," Proceedings of the U. S. National Conference on Earthquake Engineering, Ann Arbor, June 1975, pp. 316-326.

7. Penzien, J., Bertero, V. V., and Atalay, B., "Inelastic Cyclic Behavior of Reinforced Concrete Flexural Members," paper presented at the Review Meeting of the U. S. - Japan Cooperative Research Program, August 1975.
8. Paulay, T. and Binney, J. R., "Diagonally Reinforced Coupling Beams of Shear Walls," ACI Special Publication 42, Detroit, 1974, pp. 579-598.
9. Popov, E. P., Bertero, V. V., and Viathanatepa, S., "Inelastic Cyclic Behavior of Reinforced Concrete Flexural Members," to be published in the Proceedings of the Fifth European Conference on Earthquake Engineering, Istanbul, Turkey, September 22-25, 1975.
10. Mahin, S. A. and Bertero, V. V., "An Evaluation of Some Methods for Predicting Seismic Behavior of Reinforced Concrete Buildings," Earthquake Engineering Research Center Report No. EERC 75-5, University of California, Berkeley, February 1975.
11. Fintel, M., "Ductile Shear Walls in Multistory Buildings," Proceedings of the 42nd Annual Convention, Structural Engineers Association of California, Coronado, California, October 4-6, 1973, pp. 39-58.
12. Paulay, T., "Design Aspects of Shear Walls for Seismic Areas," Research Report 74-11, University of Canterbury, Christchurch, New Zealand, October 1972, 29 pp.
13. "Design of Combined Frames and Shear Walls," Notes of Seminar on Simplified Design of Earthquake-Resistant Concrete Structures, San Francisco, June 2, 1973, pp. A.1 - A.59.
14. Bertero, V. V. and Collins, R. G., "Investigation of the Failures of the Olive View Stairtowers During the San Fernando Earthquake and Their Implications on Seismic Design," Earthquake Engineering Research Center Report No. 73-26, University of California, Berkeley, December 1973, 282 pp.
15. Bertero, V. V., Popov, E. P., and Endo, T., "Testing Facility for Sub-assemblages of Frame-Wall Structural Systems," Earthquake Engineering Research Center, University of California, Berkeley. Report in preparation.
16. Hatakeyama, H., "Comparative Study of Design of Shear Walls in High-Rise Buildings," CE 299 Report, Structural Engineering and Structural Mechanics Division, University of California, Berkeley, Fall 1973.
17. Wang, T-Y., Popov, E. P., and Bertero, V. V., "Hysteretic Behavior of Reinforced Concrete Framed Walls," Earthquake Engineering Research Center, University of California, Berkeley. Report in preparation.
18. Bertero, V. V., "Identification of Research Needs for Improving the Aseismic Design of Building Structures," Proceedings of the Regional Conference of the New Zealand National Society for Earthquake Engineering, Wellington, N.Z., May 1975, 56 pp.

TABLE 4. COMPARISON OF LOADING CONDITIONS FOR MODEL DERIVED FROM ANALYZING PROTOTYPE STRUCTURES USING DIFFERENT SEISMIC ANALYSIS METHODS

DESIGN CRITERIA	METHODS OF DETERMINING SEISMIC FORCES	SIMPLIFIED LOADING CONDITIONS FOR WALL SUBASSEMBLY MODEL		SHEAR SPAN $\frac{a}{l}$
		COMPUTED FORCES	ULTIMATE FORCES BASED ON ESTIMATED FLEXURE STRENGTH OF 42,000 K-IN.	
WALLS ALONE RESIST TOTAL SEISMIC LATERAL FORCES	UBC			$\frac{263}{(2.0)}$
FRAMES AND WALLS RESIST TOTAL SEISMIC LATERAL FORCES	LINEAR ELASTIC RESPONSE SPECTRUM $\ddot{u}_g = 0.33g$ and $\xi = 5\%$	FIRST MODE		$\frac{195}{(2.1)}$
		FIRST THREE MODES		$\frac{173}{(1.9)}$

TABLE 5. FREE VIBRATION TEST RESULTS

Specimen	Stage of Loading	Small Amplitude Test*		Large Amplitude Test**	
		Frequency (cps)	Damp. Ratio (%)	Frequency (cps)	Damp. Ratio (%)
SW2	Before Loading			39.5	2.7
	After three yielding cycles ($u_d = -1, 1$)	23	2.5	18.5	9.1
	After Failure	10	2.7	8.5	5.6
SW2R	Before Loading	20	2.5	16.3	6.0

* The free vibration of the specimen was initiated by hitting specimen with hand.

** The free vibration of the specimen was initiated by pulling with 10 kips lateral force and suddenly release it.

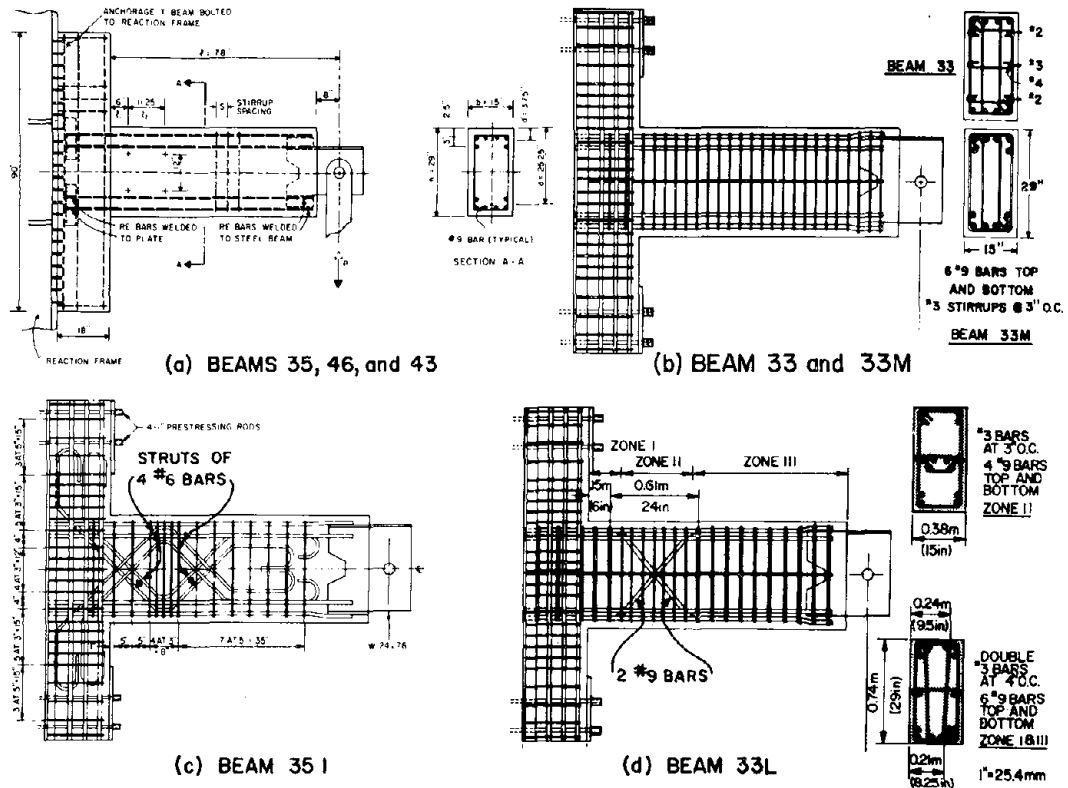


FIG. 1 DIMENSIONS AND DETAILS OF SHORT CANTILEVER BEAMS

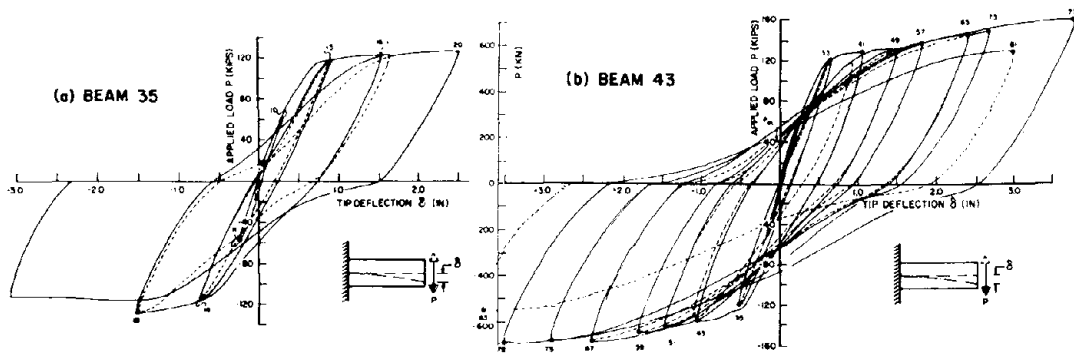


FIG. 2 LOAD DEFLECTION DIAGRAMS FOR BEAMS 35 AND 43

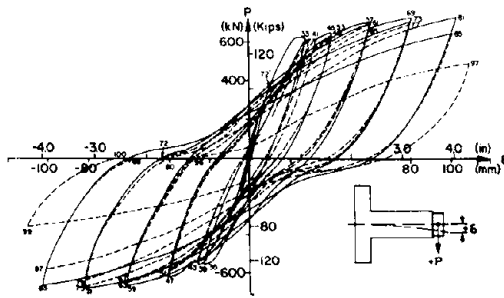


FIG. 3 LOAD-DEFLECTION DIAGRAM FOR BEAM 33

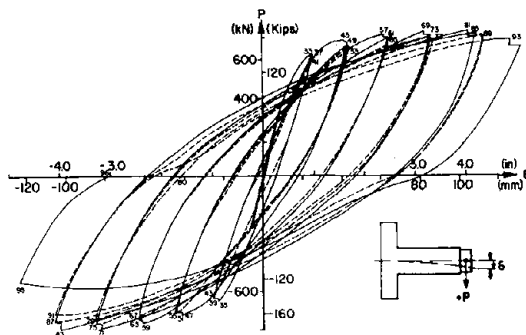


FIG. 4 LOAD-DEFLECTION DIAGRAM FOR BEAM 35 I

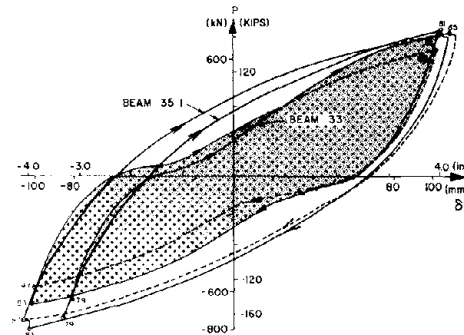


FIG. 5 COMPARISON OF HYSTERETIC LOOPS OF BEAM 35 I AND 33

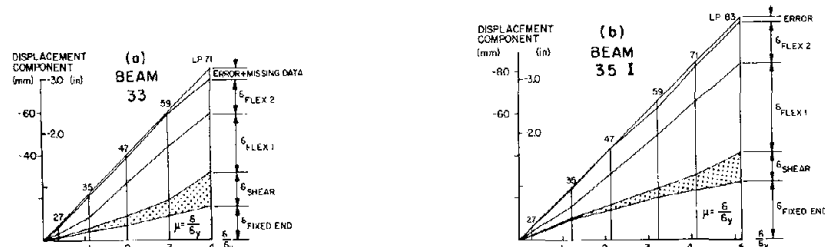


FIG. 6 BEAMS 33 AND 35 I-CONTRIBUTIONS OF DIFFERENT SOURCES OF DEFORMATION TO TIP DEFLECTION

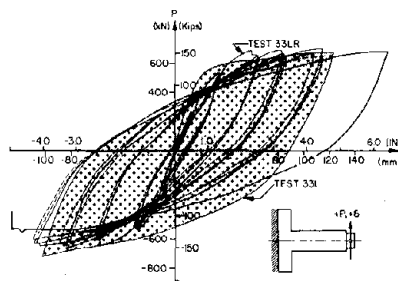


FIG. 7 BEAM 33L-COMPARISON OF HYSTERETIC LOOPS, TESTS 33L AND 33LR

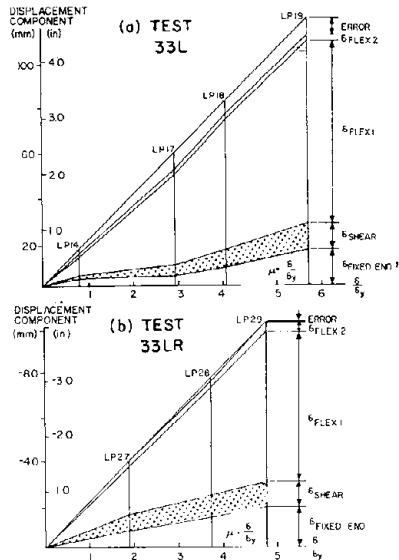


FIG. 8 BEAM 33L-CONTRIBUTION OF DIFFERENT SOURCES OF DEFORMATION TO TIP DEFLECTION

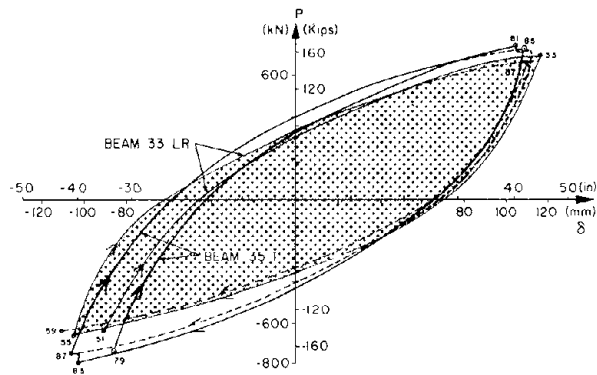


FIG. 9 COMPARISON OF HYSTERETIC LOOPS OF BEAMS 33LR AND 351

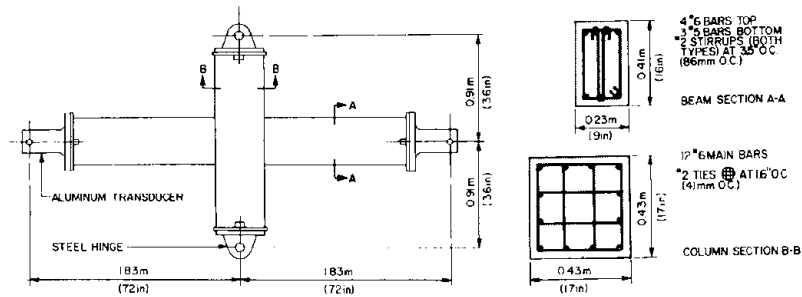


FIG. 10 DIMENSIONS AND SECTIONS OF BEAM-COLUMN SUBASSEMBLAGE

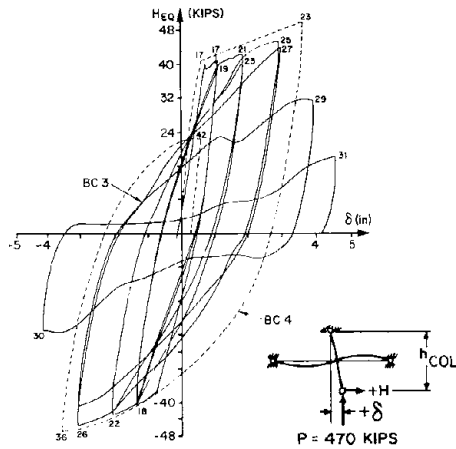


FIG. 11 SPECIMENS BC 3 AND BC4-COMPARISON OF HYSTERETIC BEHAVIOR

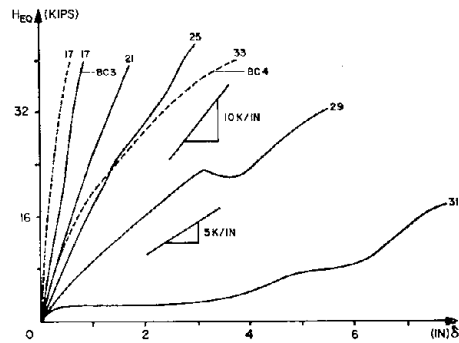


FIG. 12 COMPARISON OF H_{eq} - δ CURVES AT DIFFERENT CYCLES

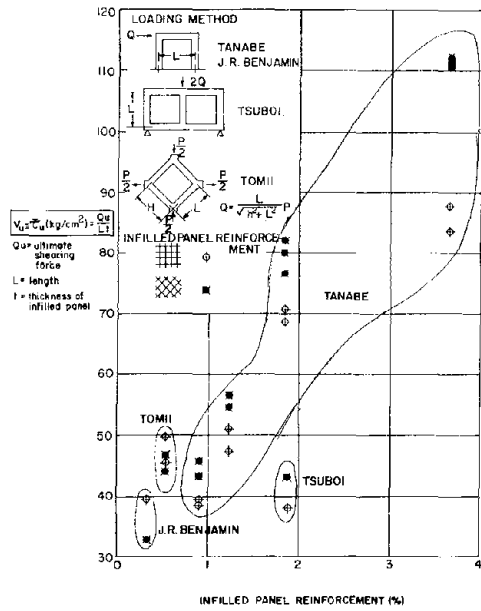


FIG. 13 EFFECTS OF LOADING METHODS AND OF TYPE AND AMOUNT OF WALL REINFORCEMENT ON v_u

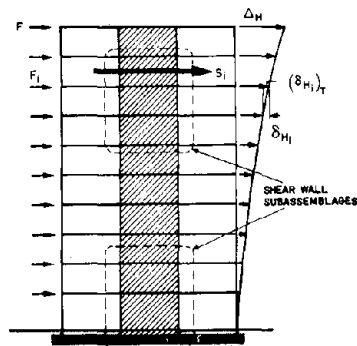


FIG. 15 WALL-FRAME STRUCTURAL SYSTEM

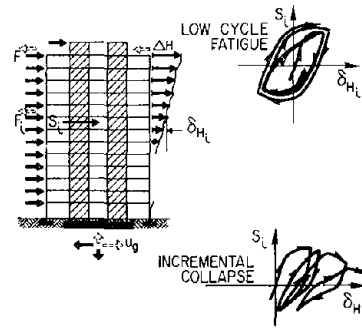
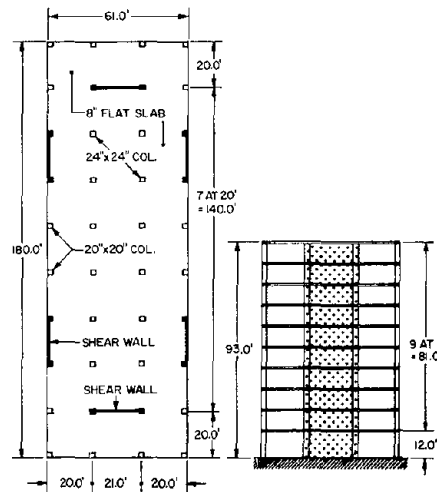


FIG. 14 STORY SHEAR-DISPLACEMENT RELATIONSHIPS



(a) TYPICAL FLOOR PLAN (b) ELEVATION
FIG. 16 PROTOTYPE BUILDING

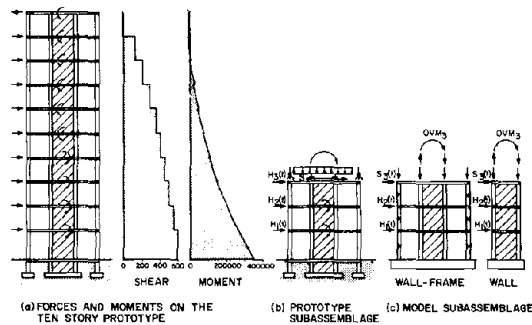


FIG. 17 COMPARISON OF ACTUAL AND SIMULATED LOADING AND SUPPORT CONDITIONS

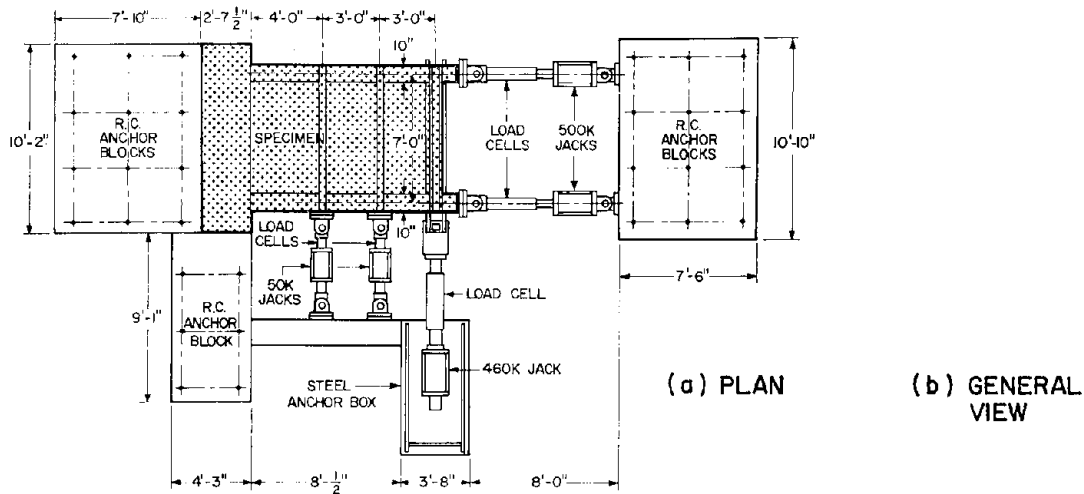


FIG. 18 PLAN AND GENERAL VIEW OF TESTING FACILITY

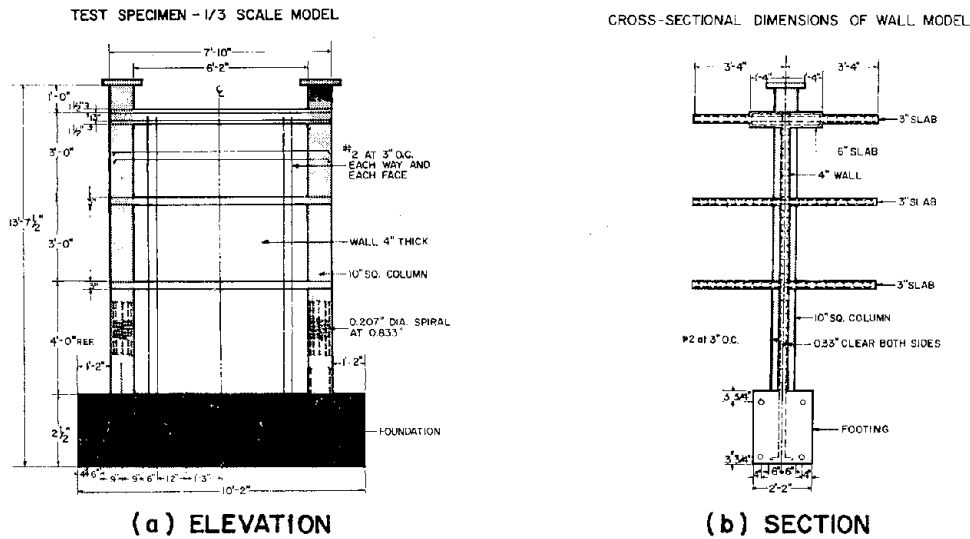
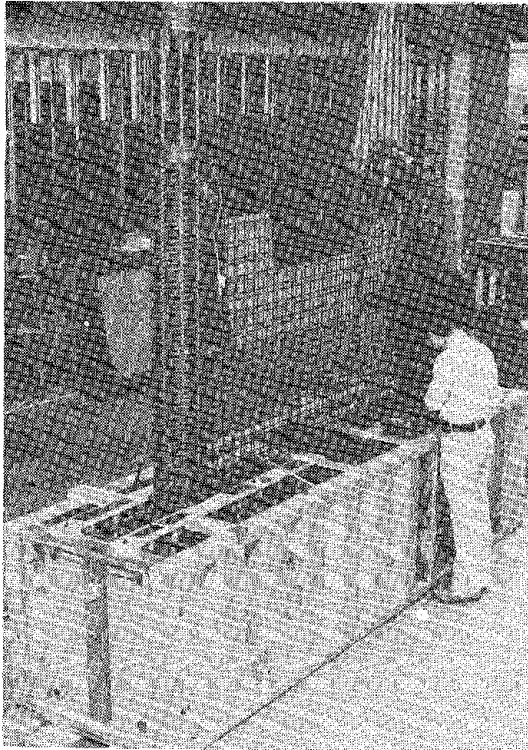
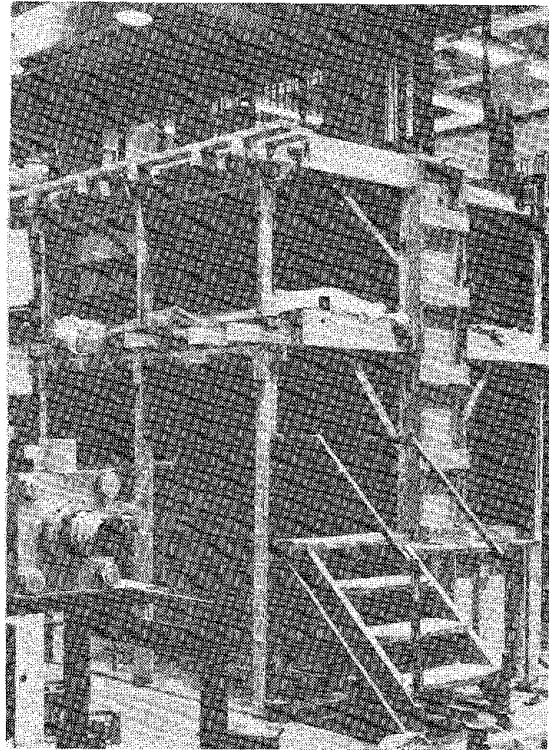


FIG. 19 DIMENSIONS AND DETAILS OF WALL SPECIMENS



(a) FORMWORK READY FOR CASTING FOUNDATION



(b) FORMWORK READY FOR CASTING 2nd STORY

FIG. 20 GENERAL VIEWS OF WALL SPECIMEN DURING CONSTRUCTION

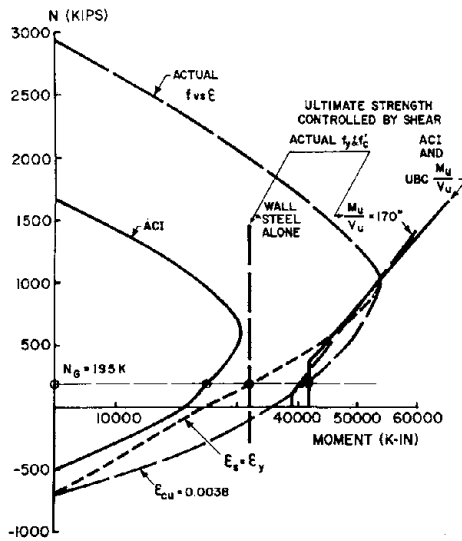


FIG. 21 MOMENT-AXIAL FORCE DIAGRAM OF WALL SPECIMEN

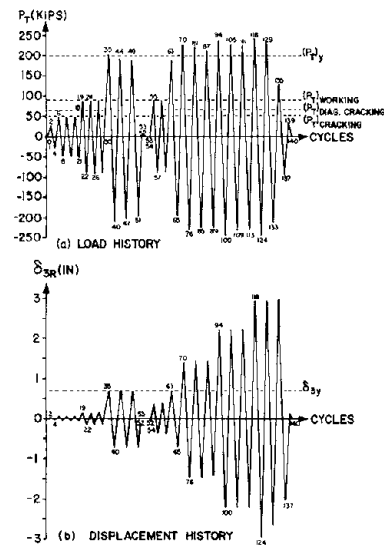


FIG. 22 LOADING PROGRAM-WALL 2

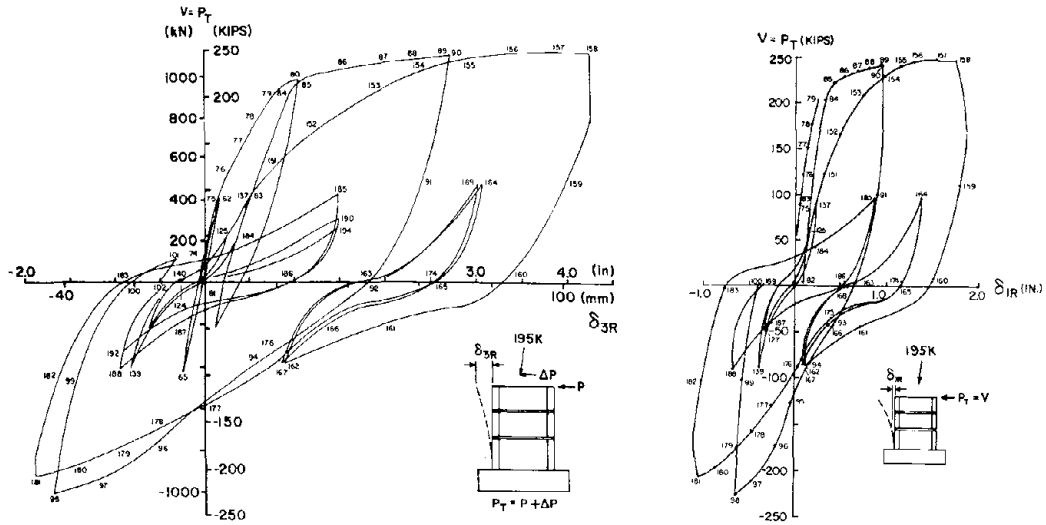
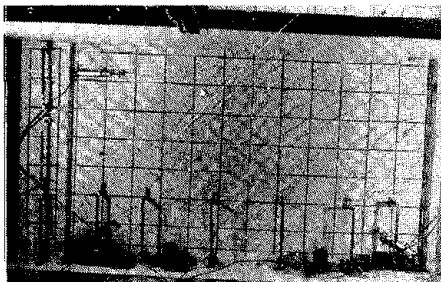
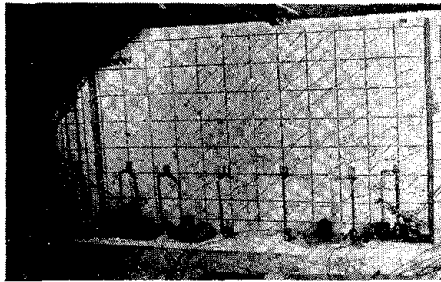


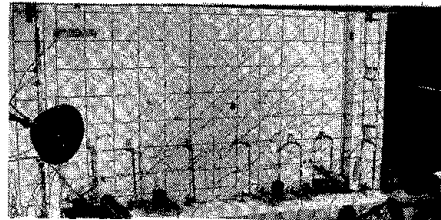
FIG. 23 TOTAL LATERAL LOAD VS. RELATIVE DISPLACEMENT DIAGRAM WALL I



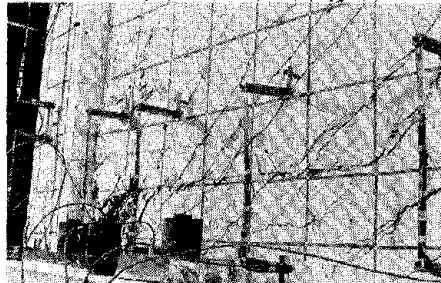
(a) AT FIRST YIELDING $\delta_{3R} = 0.76$ IN, LP 79



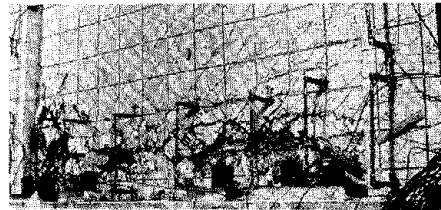
(b) AT $\delta_{3R} = 2.3$ IN ($\mu = 3$) LP 88, $P_T = 225$ K



(c) AT $\delta_{3R} = 4.25$ IN ($\mu = 6.1$) LP 158, $P_T = 248$ K



(d) CRUSHING OF CONCRETE AT LP 158



(e) AFTER $\delta_{3R} = -1.9$ IN, LP 197

FIG. 24 FIRST STORY OF WALL I. ILLUSTRATION OF DAMAGE INDUCED AT DIFFERENT STAGES OF TESTING

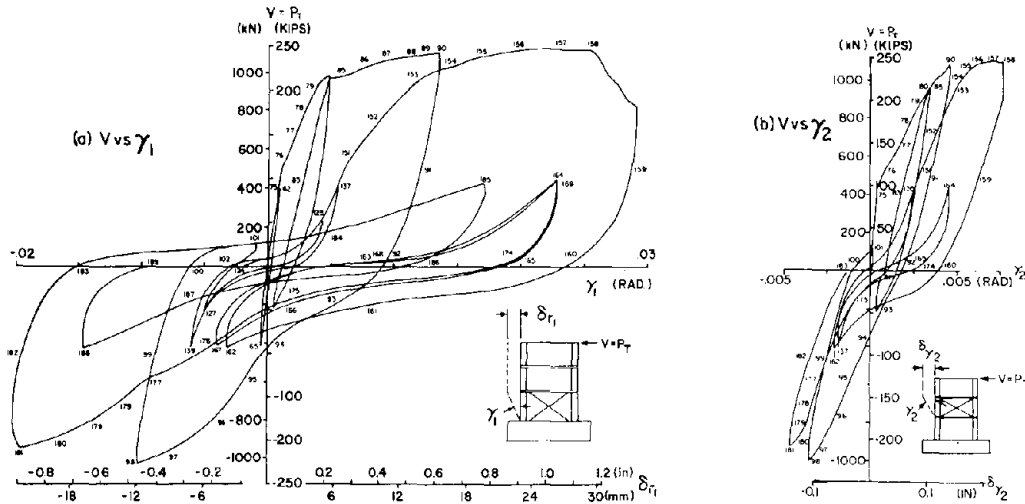


FIG. 25 SHEAR FORCE (V)-SHEAR DISTORTION (γ) DIAGRAMS, WALL 1

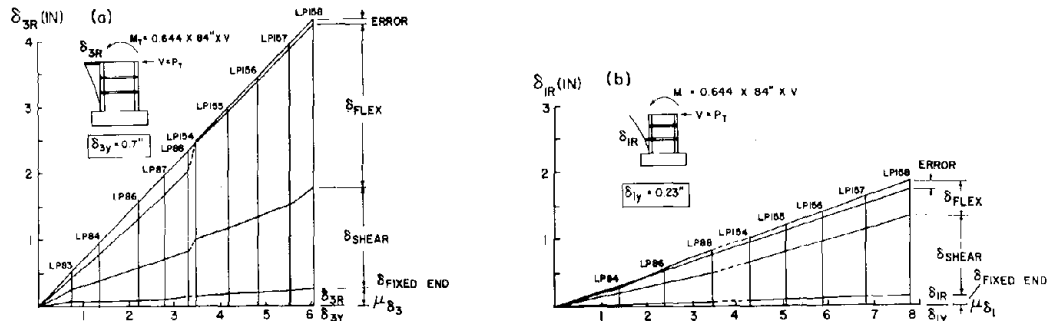
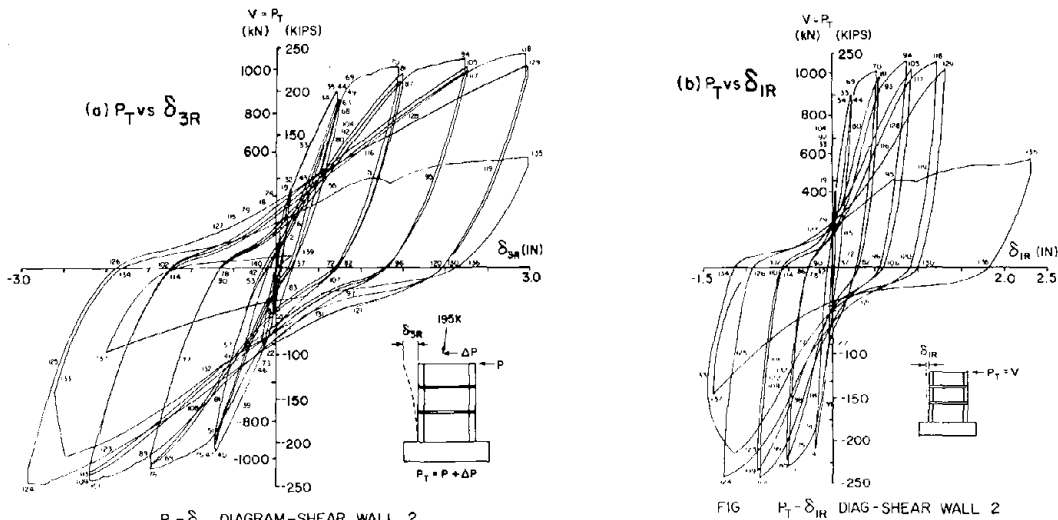


FIG. 26 VARIATION OF CONTRIBUTION OF DIFFERENT SOURCES OF DEFORMATIONS TO FLOOR DISPLACEMENT WITH INCREASING DUCTILITY, WALL 1



P₁- δ_{3R} DIAGRAM-SHEAR WALL 2

FIG P₁- δ_{IR} DIAG-SHEAR WALL 2

FIG. 27 LATERAL LOAD-LATERAL DEFLECTION DIAGRAMS, WALL 2

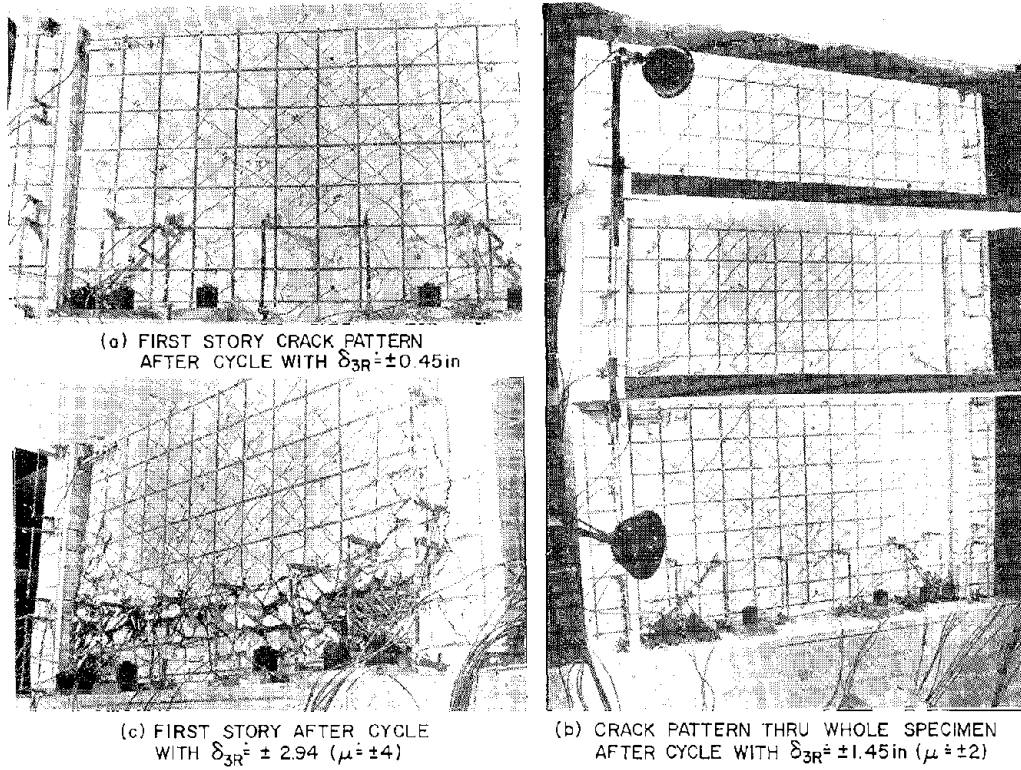


FIG. 28 FIRST STORY OF WALL 2-ILLUSTRATION OF DAMAGE INDUCED AT DIFFERENT STAGES OF TESTING

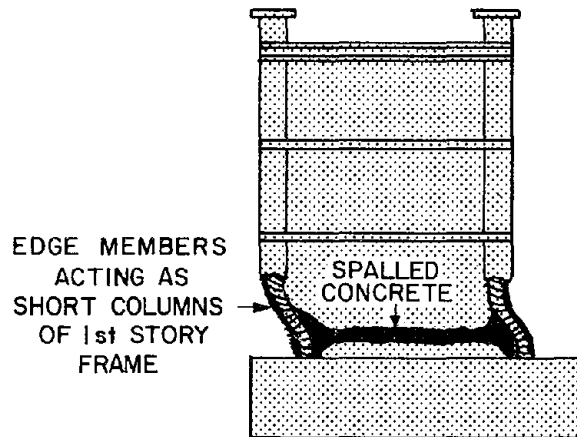


FIG. 29 MECHANISM OF FAILURE OF WALL SPECIMEN

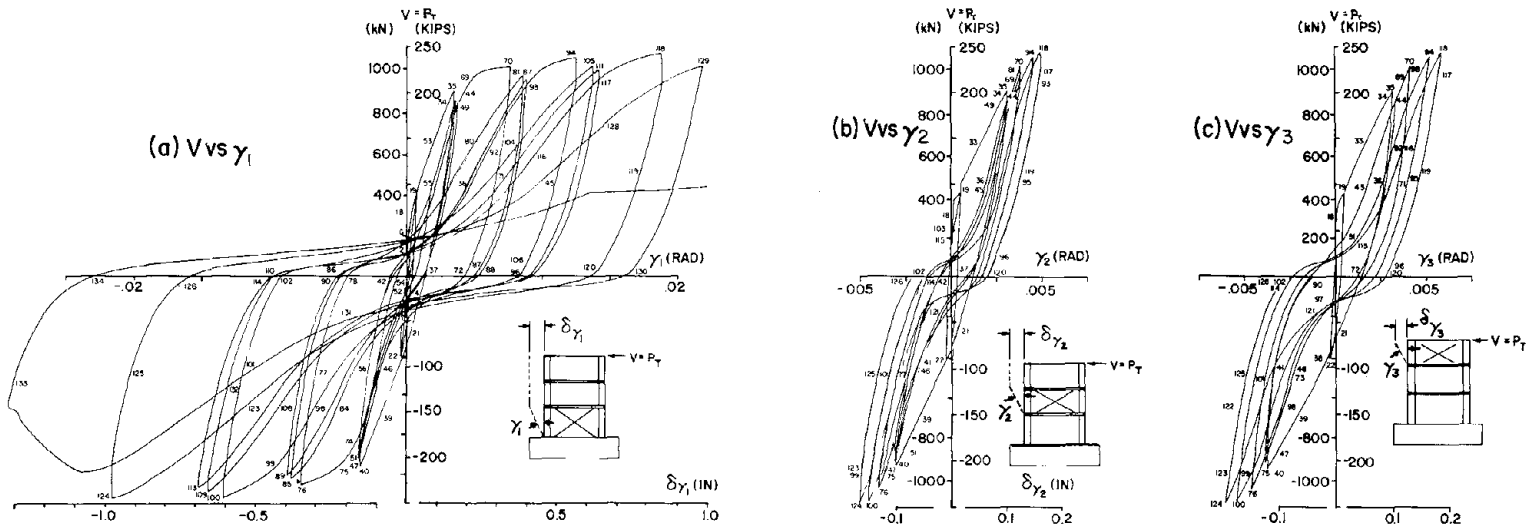


FIG. 30 SHEAR FORCE, (V)-SHEAR DISTORTION (γ) DIAGRAMS, WALL 2

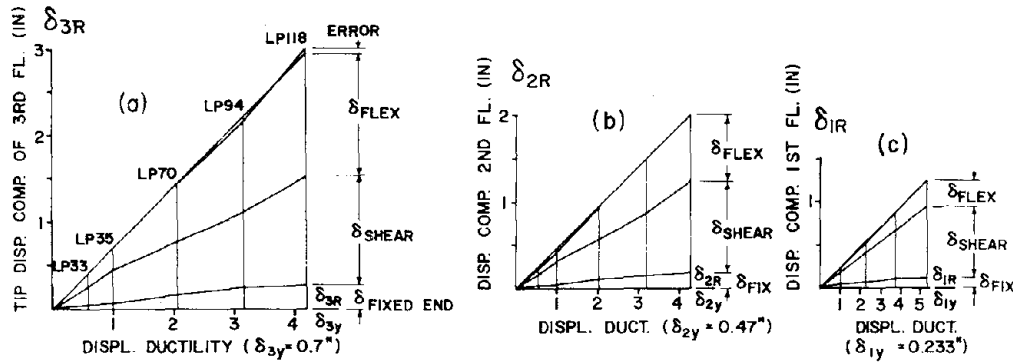


FIG. 31 VARIATION OF CONTRIBUTION OF DIFFERENT SOURCE OF DEFORMATIONS TO FLOOR DISPLACEMENT WITH INCREASING DUCTILITY, WALL 2

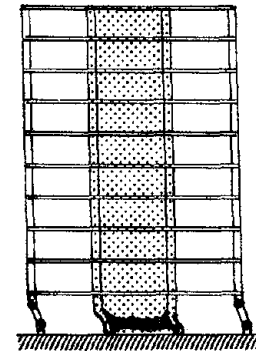


FIG. 32 COLLAPSE MECHANISM OF DUAL WALL-FRAME SYSTEM

by

Toshio Shiga^{*}, Akenori Shibata^{**} and Junichi Takahashi^{***}

ABSTRACT

The results of a laboratory investigation on the force-displacement relationship of single-story reinforced concrete shear walls are presented. Seventeen medium-size shear walls were subjected to static loads representing gravity loads and earthquake forces. The variables were the wall reinforcement ratio, the level of gravity load and the loading history. The characteristics of cyclic hysteresis loops under various types of load reversal and their envelope curves are investigated.

INTRODUCTION

In the inelastic earthquake response analyses of building structures, the force-displacement relationship is one of the important problems. Especially, in case of reinforced concrete structures, the force-displacement relationship depends on the loading history such as deflection amplitude, and a number of cyclic loading in the previous stage. Though reinforced concrete shear walls are the very important elements in building structures to resist earthquakes, experimental data on the hysteretic behavior of reinforced concrete shear walls are quite few.

To investigate these points, a series of cyclic loading tests of medium-size reinforced concrete shear walls were conducted. In this report, the effect of loading history, i.e., deflection amplitude and a number of cyclic loading, on the hysteresis loop of reinforced concrete shear walls is reported.

TEST SPECIMENS

The test specimens were designed to represent a single-story reinforced concrete shear wall. Figure 1 shows the model shear wall's configuration and reinforcing arrangements. Table 1 shows the material properties of concrete and reinforcements used for the test specimens. The reinforcement ratio of the column and beam are 4.23% and 1.69%, respectively. The shear reinforcement ratio of the column and the beam are 0.18% and 0.10% for the test specimens WB-1~8, 0.18% and 0.18% for the WB-9~17, respectively. Two kinds of test specimens, of which wall reinforcement ratios, P_w , are 0.25% and 0.50%, were tested. The wall reinforcement ratios are same in vertical and horizontal directions.

The initial stiffness of the test specimen (0.25%, wall reinforcement

* Professor, Faculty of Engineering, Tohoku University, Sendai

** Associate Professor, Faculty of Engineering, Tohoku University, Sendai

*** Assistant, Faculty of Engineering, Tohoku University, Sendai

ratio) for zero axial load calculated from the dimensions of the specimen shown in Fig. 1 with the loading conditions in Fig. 2 is as follows.

$$R = \frac{P K}{G A_w} + \frac{P h^2}{3EI} = \left\{ \frac{1}{4.75 \times 10^7} + \frac{1}{18.1 \times 10^7} \right\} P = \frac{1}{3.76 \times 10^7} P$$

where

R = translational angle at beam level	rad.
P = lateral load at beam level	ton
h = height of wall	cm
A _w = effective shear area	cm ²
E = modulus of elasticity for concrete	210t/cm ²
G = modulus of rigidity for concrete	90t/cm ²
K = shape factor of section	
I = moment of inertia	cm ⁴

which gives P/R=3.76x10⁴t. The lateral load for R=0.1x10⁻³rad. is 3.76t. The ratio of shear deflection to flexural deflection is δ_s:δ_f = 1/4.75: 1/18.1= 1:0.26. The cracking load of the wall, calculated using concrete strength F_c=160kg/cm² and shear cracking stress τ_{cr}=F_c/10, is as follows.

$$P_{cr} = \frac{A_w \tau_{cr}}{K} = \frac{496 \times 16}{1.16} = 6.84t$$

The cracking deflection calculated from the initial stiffness mentioned above, is R_{cr}=0.18x10⁻³rad. The cracking load and deflection for bending are P_{cr}=9.5t and R_{cr}=0.25x10⁻³rad., respectively.

TEST PROCEDURE

The test specimens were placed vertically in the loading rig. The concrete base block of the test specimen was firmly fastened to the rigid testing floor. The lateral load was applied at the beam level and the axial loads were vertically at the top of the columns. Oil jacks were used for loading. Figure 2 shows a schematic diagram of the loading rig.

The deflection of the test specimen was measured at the beam level with mechanical dial gauge. The lateral load applied at the beam level, was monitored using a load cell instrument with wire strain gauge. The total axial load was manually controlled to keep a constant value, even if the test specimen was made to deflect.

Table 2 shows the loading program for each test specimen. As shown in Table 2, the several different deflection amplitude and the number of loading cycles were scheduled.

The total axial loads, N, were 0t, 20t and 40t. The axial load of 20t was equal to one-third of the compressive strength of the columns, which was the sum of the strength of concrete and that of reinforcing steels.

EXPERIMENTAL RESULTS

Typical examples of the hysteresis loops are shown in Figs. 3~9.

The loading programs are as follows.

- 1) The specimen is subjected to symmetric cyclic deflection with the amplitude corresponding to the maximum load. (Fig.4, WB-1)
- 2) Similar to case 1), except that the deflection amplitude is one-half of that in case of 1). (Fig.5, WB-2)
- 3) The deflection amplitude is increased symmetrically step by step. (Fig.6, WB-3)
- 4) Similar to case 1), except that after the hysteresis loop is stabilized for the cyclic loading, the deflection amplitude is decreased symmetrically at first and then increased symmetrically to the initially experienced deflection amplitude step by step. (Fig.7, WB-12)
- 5) The deflection in the positive direction is kept constant at a large amplitude and the deflection in the negative direction is increased from zero up to the same deflection amplitude as that in the positive direction step by step. In the last step, it becomes similar to the case of the symmetric loading. (Fig.8, WB-13)
- 6) Similar to case 5), except that the amplitude in the negative direction is decreased step by step. (Fig.9, WB-14)
- 7) Random unsymmetric loading simulating earthquake response. (Fig.10, WB-17)

Figure 11 shows the virgin curves for the first cyclic loops of various amplitude levels.

From the hysteresis loops obtained by the cyclic loading with the constant symmetric deflection, the equivalent stiffness K_{eq} and the equivalent viscous damping factor h_{eq} are obtained. Relation of the K_{eq} and h_{eq} to the cyclic deflection amplitude and the number of cyclic loading are shown in Figs. 13 and 14. In these figures, the mean values of the positive and negative direction are plotted.

The K_{eq} is defined as the slope of the line connecting the peaks of the hysteresis loops. The h_{eq} is related to the ratio of the dissipated energy to potential energy. The dissipated energy is indicated by the area of the hysteresis loop.

The nominal shear stress, the deflection at both the shear cracking load and the maximum load are shown in Table 2.

DISCUSSIONS

1) When the deflection for cyclic loading is increased to a new larger level, the first hysteresis loop shows a spindle shape and closed large area. After second cyclic loading for the same deflection amplitude, the area enclosed by the loop becomes smaller and the shape becomes inverse

s-shaped as the number of cyclic is increased. The equivalent stiffness reduces mainly in the first few cycles. The loop is stabilized after several cyclic loading.

The same results are obtained for unsymmetric loading.

2) When the cyclic deflection is decreased and then increased symmetrically to the previous deflection level after the hysteresis loop is stabilized by cyclic loading at a large amplitude, the hysteresis loops show almost the same shapes as that of the hysteresis loop stabilized by the initially experienced deflection amplitude.

The same is the case for the unsymmetric loading.

3) In the case of symmetric loading in which the cyclic deflection is gradually increased, the envelope curve of the peaks of the first hysteresis loops at the initially experienced deflection is nearly consistent with the load-deflection curve of monotonically loaded specimens.

4) When the cyclic deflection in the negative direction is increased step by step keeping the deflection in the positive direction constant, the envelope curve of the peaks of the first hysteresis loop in the negative direction is similar to that obtained for symmetric loading.

5) When the load is reversed in the region beyond the shear cracking deflection or the deflection for maximum load in one direction, the hysteresis loop tends to aim at the previous maximum deflection point in the other direction. But when the deflection in one direction between the shear cracking and the deflection for maximum load and the previous maximum deflection point in the opposite direction is not beyond the shear cracking deflection, the hysteresis loop tends to go toward the shear cracking point in the opposite side. When the deflection in one direction is larger than the deflection for maximum load and the previous maximum deflection point in the opposite side is not beyond the shear cracking deflection, the hysteresis loop tends to aim at the deflection point for maximum load.

6) In case of symmetric loading with constant amplitude, the load is decreased by the cyclic loading. The ratio of the equivalent stiffness of the stabilized hysteresis loop to the first hysteresis loop is not so much influenced by the level of deflection and the loading history.

7) In case of symmetric loading, the equivalent viscous damping factor are about 0.10 for the first hysteresis loop and about 0.05 for the stabilized hysteresis loop. The value for the stabilized hysteresis loop is not so much influenced by the number of cyclic loading and the deflection amplitude.

8) At the shear cracking load, the nominal shear stress was $0.07\sim 0.17 F_c$ (average $0.10F_c$) and the deflection was $0.36\sim 0.57\times 10^{-3}$ rad. (average 0.46×10^{-3} rad.). The nominal shear stress was approximately $1/10F_c$, but the deflection was larger than the calculated value.

At the maximum load, the nominal shear stress was $0.19\sim 0.46F_c$ (average $0.31F_c$) and the deflection was $3.9\sim 7.1\times 10^{-3}$ rad. (average 5.2×10^{-3} rad.).

9) The characteristics of the hysteresis loop mentioned above are scarcely influenced by the wall reinforcement ratio and the axial load of the columns.

CONCLUSIONS

The cyclic hysteretic behavior of single-story reinforced concrete shear walls are investigated under various loading histories.

The results suggest that the force-displacement relationship of the reinforced concrete shear walls can be modeled by the combination of the envelope curve and the appropriate hysteresis loops corresponding to the deflection levels.

ACKNOWLEDGMENTS

The authors wish to thank J. Shibuya, Tohoku University, for his kind discussions.

REFERENCES

1. Shiga T., Shibata A. and Takahashi J., "Experimental Study on Dynamic Properties of Reinforced Concrete Shear Walls, Part III", Papers of the Annual Meeting, Architectural Institute of Japan, October, 1972, p. 639
2. Shiga T., Shibata A. and Takahashi J., "Experimental Study on Dynamic Properties of Reinforced Concrete Shear Walls" Fifth World Conference on Earthquake Engineering, June, 1973, No 142
3. Shiga T., Shibuya J. and Takahashi J., "Experimental Study on Dynamic Properties of Reinforced Concrete Shear Walls, Part V", Papers of the Annual Meeting, Architectural Institute of Japan, October, 1974, p. 555
4. Shiga T., Shibuya J., Takahashi J. and Kanai M., "Modeling of Restoring Force and Response of Reinforced Concrete Shear Walls, Part I and II", Papers of the Annual Meeting, Architectural Institute of Japan, October, 1974, p. 551

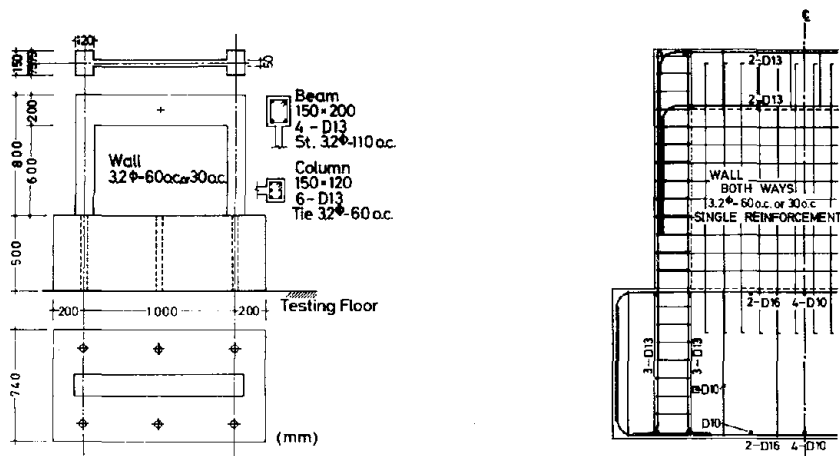


Fig. 1 Dimensions and Reinforcing Arrangements

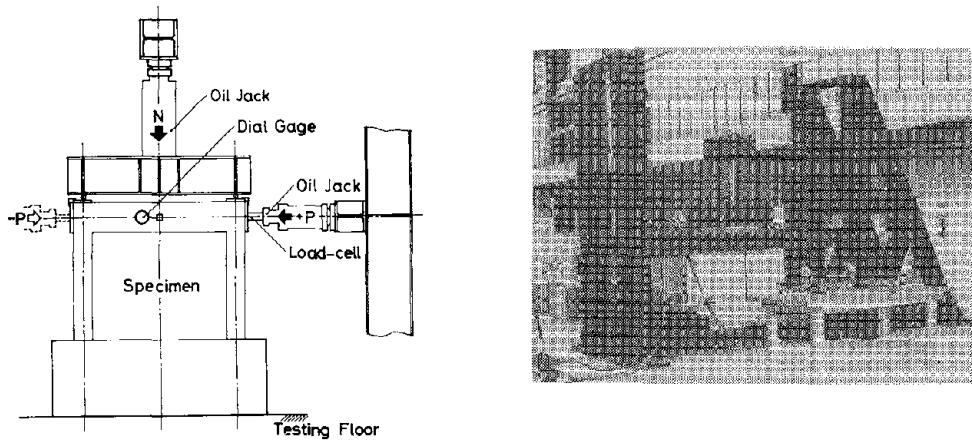


Fig. 2 Schematic Diagram and General View of Loading

Table 1 Mechanical Characteristics of Materials

Mark	Concrete Compressive Strength F_c (kg/cm ²)	Reinforcement			
		Main		Shear	
		Yield Stress (t/cm ²)	Max. Stress (t/cm ²)	Yield Stress (t/cm ²)	Max. Stress (t/cm ²)
WB-1,2	188				
3,4	164				
5,6	151	3.9	5.6	3.0	4.1
7,8	156				
9,10	173				
11,12	169				
13,14	173	3.3	5.2	5.4	5.8
15,16	119			(0.2% O.S.)	
17,18	102				

Table 2 Principal Experimental Results

Mark	Parameter			Cracking		Maximum	
	Axial Load N (t)	Wall Reinf. Ratio (%)	Reversed Deflection R ()* ($\times 10^{-3}$ rad.)	Shear Stress (kg/cm^2)	Def. R	Shear Stress (kg/cm^2)	Def. R
WB-1	0	0.25	4(30) \rightarrow 10(2)	11.3	0.36	35.7	4.00
2			2(30) \rightarrow 4(10) \rightarrow 10(10)	12.7	0.47	37.9	4.06
3			0.5(30) \rightarrow 2(10) \rightarrow 4(10) \rightarrow 10(2)	15.1	0.50	42.5	7.14
4			10(1) \rightarrow 20(one way)	11.5	0.36	46.6	7.14
5				16.9	0.53	68.8	7.14
6	0	0.50	same as WB-1	18.5	0.37	48.8	3.90
7	20			21.3	0.37	62.5	3.87
8	40			20.6	0.57	57.9	4.00
9				13.3	0.43	49.5	5.70
10	20	0.25	10(1) \rightarrow 20(one way)	11.5	0.33	48.9	5.70
11				16.5	0.43	56.8	7.70
12				21.1	0.50	68.2	7.90
13				14.7	0.50	44.2	4.00
14				15.9	0.57	41.6	4.00
15				13.9	0.50	26.6	2.00
16				11.9	0.44	27.6	2.00
17				9.5	0.43	39.6	7.43

* (): number of loading cycles

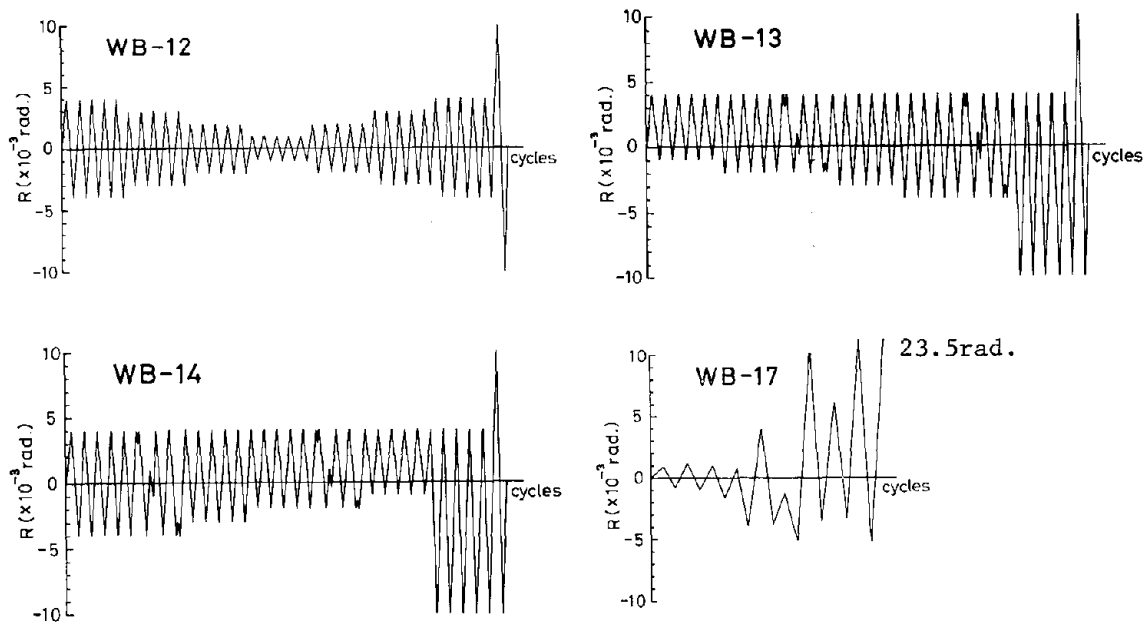


Fig. 3 Loading Programs (Displacement History)

WB-1

$P_w = 0.25\%$

$N = 0t$

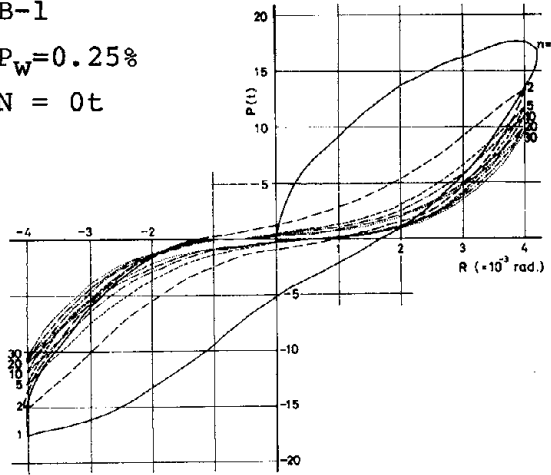


Fig. 4 P-δ Diagram for WB-1

WB-2

$P_w = 0.25\%$

$N = 0t$

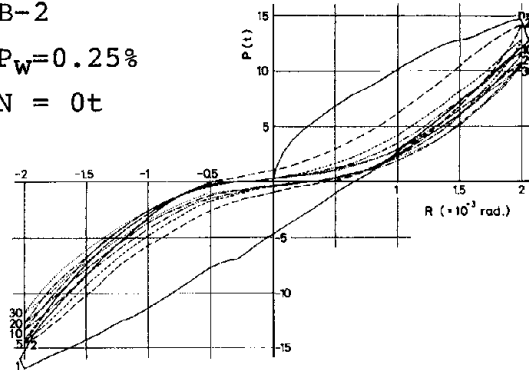


Fig. 5 P-δ Diagram for WB-2

WB-3

$P_w = 0.25\%$

$N = 0t$

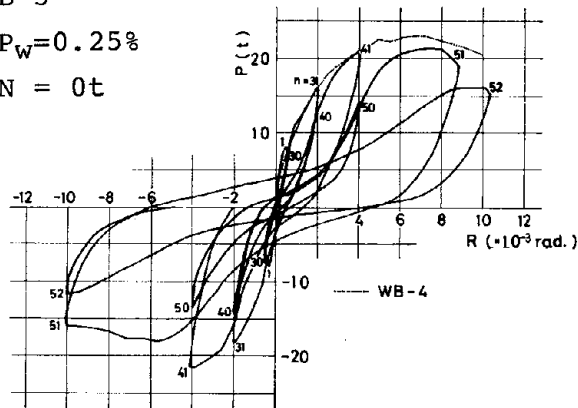


Fig. 6 P-δ Diagram for WB-3

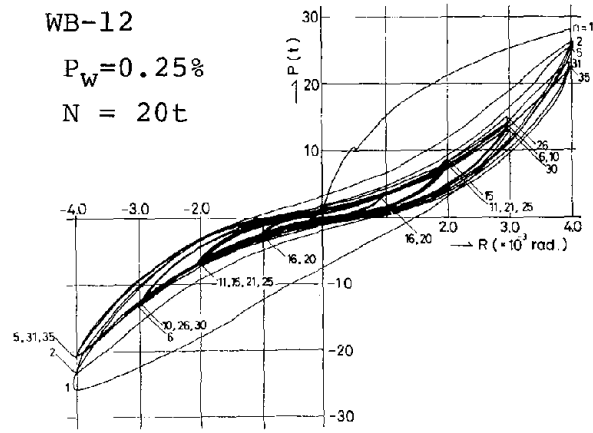


Fig. 7 P- δ Diagram for WB-12

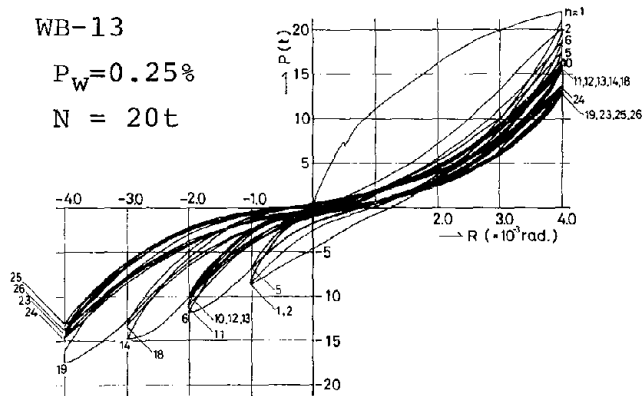


Fig. 8 P- δ Diagram for WB-13

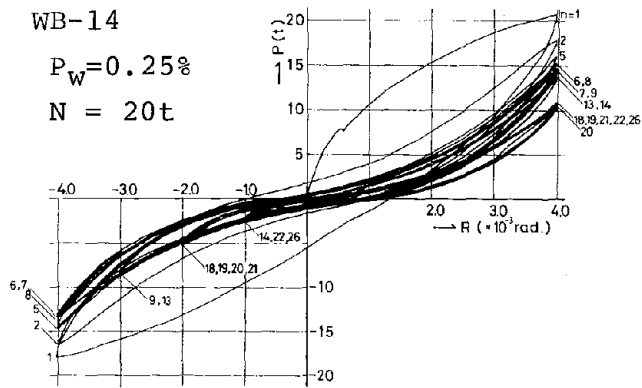
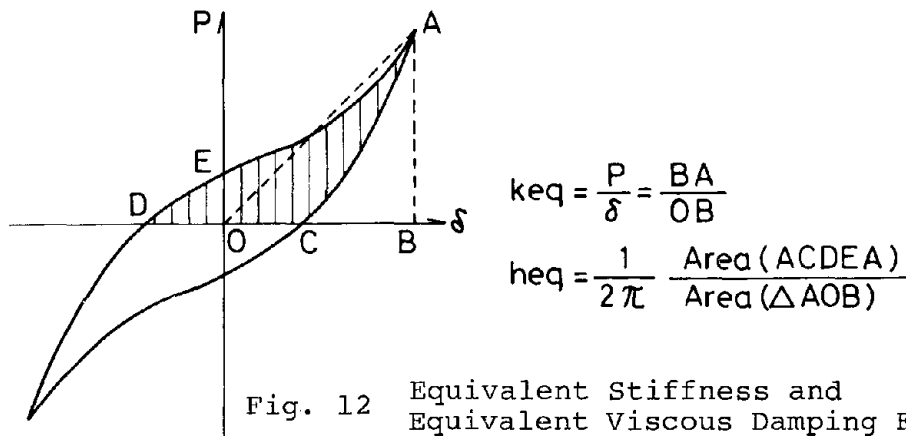
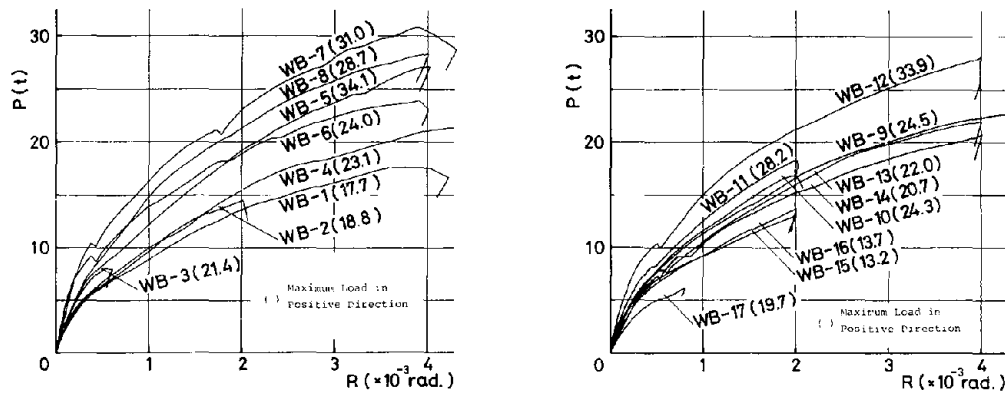
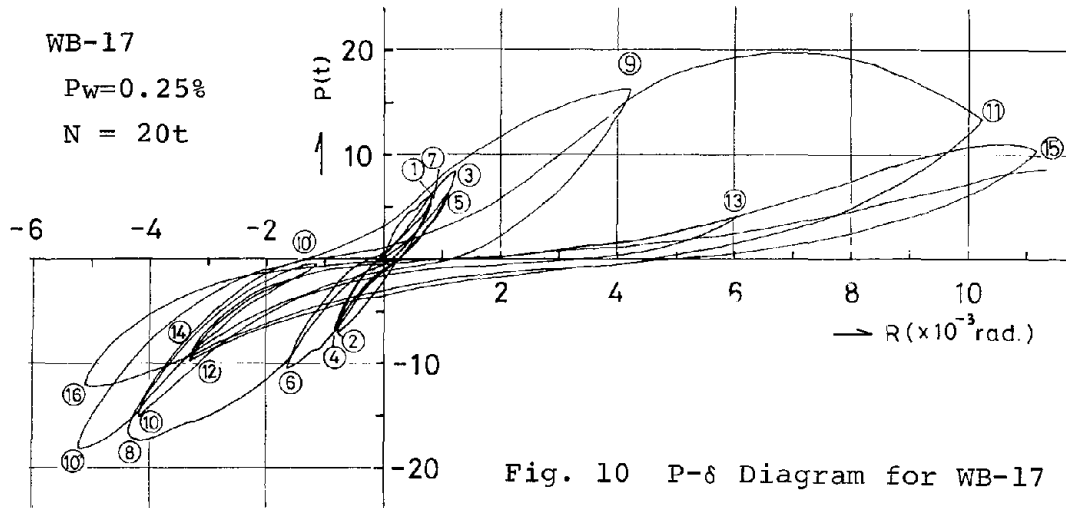


Fig. 9 P- δ Diagram for WB-14



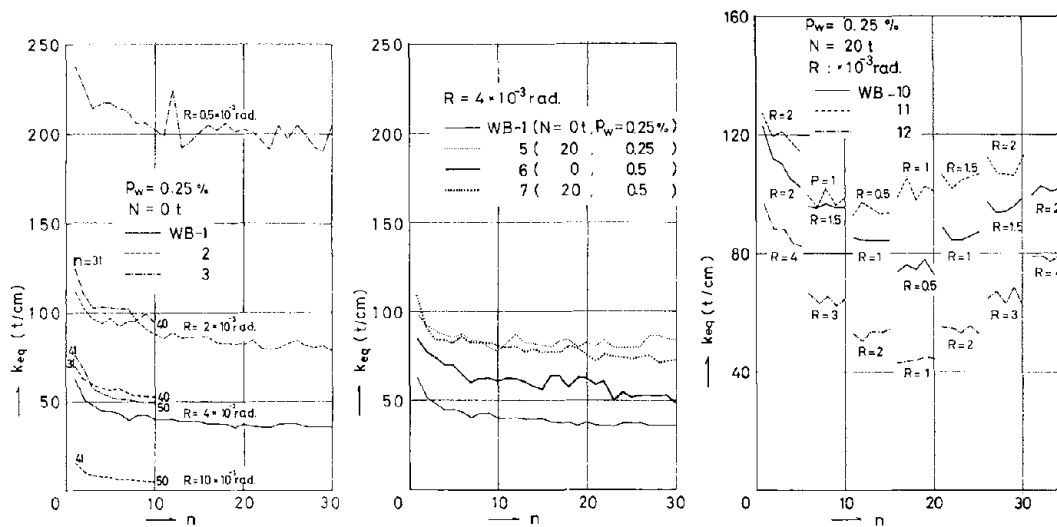


Fig. 13 Equivalent Stiffness vs Loading Cycles

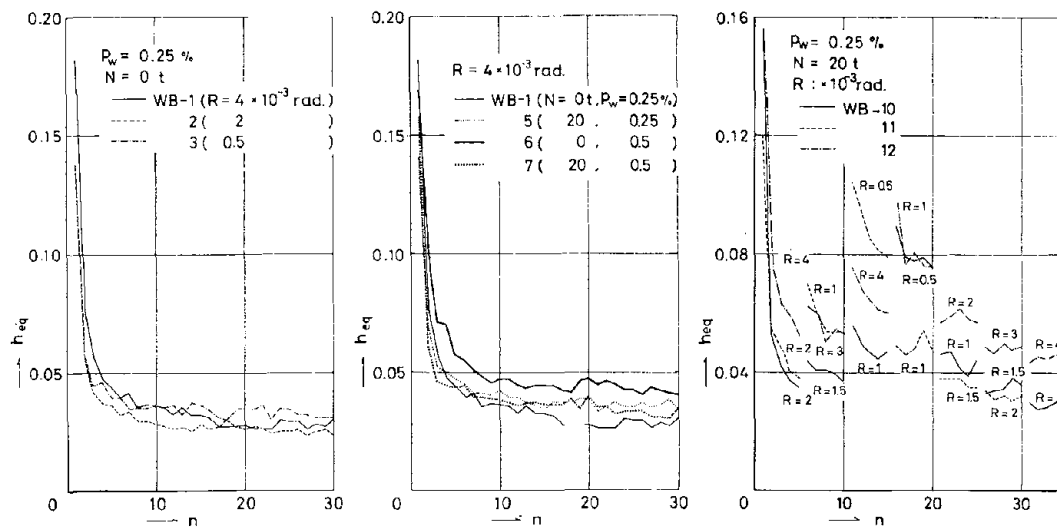


Fig. 14 Equivalent Viscous Damping Factor vs Loading Cycles

7 STRUCTURAL WALLS SUBJECTED TO SIMULATED EARTHQUAKES

by

Mete A. Sozen* and Shunsuke Otani**

SYNOPSIS

This is a progress report on recent tests at the University of Illinois, Urbana, investigating the earthquake response of multistory structural walls.

INTRODUCTION

During the past four years, four different series of physical models, incorporating structural walls, have been subjected to simulated earthquakes at the Structural Laboratory of the University of Illinois. The overall objective of all four series of tests is to study the dynamic response characteristics of reinforced concrete structural walls in order to develop conceptual models of two types: (a) elaborate theoretical models to permit detailed analysis and interpretation of the individual test results as well as to enable parametric studies for generalizing the results of the tests, (b) relatively simple theoretical models intended for analysis related to earthquake-resistant design of reinforced concrete structures.

This report provides a brief overview of the nature of the tests and some of the results.

As shown in Fig. 1, each test structure comprised at least a pair of parallel and identical elements. The uniaxial simulated earthquake motion was applied in a horizontal direction parallel to the plane of the structural elements. The number of mass concentrations along the vertical axis ranged from three to ten. Consequently, the series described below are classified as having either three stories or ten stories.

The first series of test structures had solid walls. Each wall had a thickness of one in. and a depth of 18 in., and extended in the vertical direction for three-stories of 18 in. each. Individual story masses weighed approximately 2000 lb. The series consisted of four test structures subjected to simulated earthquake motions, and two test structures subjected to static loading in order to investigate hysteresis characteristics.

*University of Illinois, Urbana, Illinois, U.S.A.

**University of Toronto, Toronto, Ontario, Canada

The second series of tests included structures similar in overall dimensions to the first series except that the walls had six perforations similar to the ones shown in Fig. 1. The number, weight, and location of the masses were the same as in the first series. Six such test structures were subjected to simulated earthquake motions and one to static loading.

The third series also included structural walls only, but the overall dimensions were different from the first two series. Each test structure consisted of two perforated walls of ten stories (Fig. 1). The masses at each story (story height = 9 in.) weighed 1000 lbs. This series included four test structures subjected to simulated earthquake motions. Static force-displacement characteristics were investigated using "coupons" of the beam-wall connections.

The fourth series was designed to investigate the interaction, under idealized conditions, of walls and frames. Of the four test structures in this series two comprised pairs of three-story frames while the other two had centrally located single solid shear walls working in parallel with the frames. Story masses were approximately 2000 lbs. The dimensions of the frames and the wall are shown in Fig. 2. The connection between the frames and the walls required that only the deflection be the same at the three floors.

The small scale reinforcement used for constructing the models ranged in yield stress from 40 to 50,000 psi. The compressive strength of the concrete was nominally 4500 psi.

All specimens were detailed to minimize the effects of distress related to bond or shear within the structural elements or at the joints. No shear failures were observed.

The base motions used in the dynamic tests were scaled versions of the NS component of the 1940 El Centro (Imperial Valley earthquake) and the N21E component of the 1952 Taft records (Kern County earthquake), as described in ref. 1. In order to excite the test structures, which have considerably shorter periods than ordinary structures, the time axis of the record was compressed by a scale of 5 or 2.5 depending on the type of the model. The value of the effective peak acceleration was varied depending on the strength of the specimen. Each test structure was usually subjected to a series of earthquake motions of increasing intensity. Wherever necessary in this paper, the intensity of the base motion is described by spectrum intensity (2) calculated for a damping factor of 20 percent of critical and over a frequency range of .04 to 1.0 sec for motions with a time scale of 2.5 and .02 to 0.5 sec for motions with a time scale of 5.

VARIATION OF FUNDAMENTAL FREQUENCY

One of the critical characteristics of the response of reinforced concrete structures to earthquake motions is the change in the effective fundamental frequency. This was readily evident in the dynamic tests of the structural-wall models. Some of the observed results in the first

three series of tests are summarized in Fig. 3. In order to provide a measure of nonlinear response, the measured fundamental frequencies, obtained from free vibration tests at low amplitudes, are plotted against the double-amplitude displacement measured at the top level of the test structure. It should be noted that a particular definition of the yield displacement, corresponding to first-mode distribution of story forces, would be approximately 0.5 in. for the solid three-story walls, 0.8 for the three-story perforated walls, and over 1.25 in. for the ten-story perforated walls. In general, the variation in the fundamental frequency was proportional inversely to the square root of the ductility attained or square root of the ratio of the maximum displacement to the yield displacement for a force distribution corresponding to the first mode.

In a given test, it was generally observed that the reduction in fundamental frequency occurred very early: the specimen responded to the excitation as a function of its stiffness characteristics as measured at the end rather than before the beginning of a particular test. This phenomenon occurred with both types of ground motion (El Centro 1940 and Taft 1952) and would be expected to occur generally unless a particular ground motion contained relatively very strong acceleration pulses toward the end of its duration.

It was a general characteristic of all test specimens that the initial measured frequency, obtained from a very-small-amplitude free-vibration test, was smaller than the frequency calculated from the geometrical and mechanical properties of the uncracked test specimen, including credible flexibilities introduced by the connection to the test platform and by the test platform.

DYNAMIC RESPONSE OF TEST STRUCTURES WITH SOLID WALLS

Figures 4a and 4c show measured records of base moment, base shear, and lateral displacement obtained during a test of one of the three-story structures with solid walls. The base motion, modeled after El Centro 1940 is shown in Fig. 4a. Its spectrum intensity, SI_{20} , was 5.2 in. The motion was strong enough to initiate yielding at the base of the wall within the first half second of the test.

As would be expected in a simple and uniform structure of this type, the critical strength criterion, the base moment, is dominated by the first mode as are the displacements. Zero crossings of the response signals indicate a fundamental frequency of approximately 4.4Hz throughout the test, as compared with the free-vibration frequency of 9.5Hz measured immediately before the test. Another significant feature is the rather abrupt reduction in response during the relatively weak periods of the ground motion, indicating the capability of the system to dissipate energy.

Figures 4b and 4d contain responses calculated using the recorded base motion and a naive model: a linear model of the test structure with

a fundamental frequency equal to that measured after the test and an arbitrary damping factor of 0.10. What is significant in the close comparison of the measured and calculated waveforms, qualitatively and quantitatively as well as throughout the duration of the strong motion, is not the desirability of the particular model, which was based on a frequency observed in the test and a damping factor obviously selected to fit, but the fact that such a simple model can reproduce the test response reasonably well in periods of strong as well as relatively weak base motion. (Naturally, the linear model does not reproduce the permanent displacement at end of test.) The comparison illustrated was typical for all test structures in this series.

RESPONSE OF TEST STRUCTURE WITH PERFORATED WALLS

The portions of the wall between perforations may be considered as connecting beams spanning between two independent structural walls. For both series two and three the strength and, in one instance, the stiffness also of the connecting beams were varied. In series two this variation was considerable. The effect of this variation on overall building response is discussed below.

Figure 5a shows the base overturning moment for three test structures of series two. (It should be noted that the scale for the top plot of base moment is not the same as those for the bottom two.) The measured base moments recorded in Fig. 7a refer to three structures and are arranged in decreasing order of connecting-beam strength. The reduction in beam strength is reflected in the maximum overturning moment reached in each test.

Figure 5b shows the top floor displacements. All structures were subjected to earthquakes of equal intensity and type. It is seen that although the beam strength and, therefore, the base moment capacity of the structure varied perceptibly, the maximum displacements of the structures were insensitive to it. From the viewpoint of drift, the structure with weak beams responded as well as the structure with stiff and strong beams.

Similar phenomena are shown for the ten-story structure in Fig. 6. Structure M1, with the stronger connecting beams, had a maximum lateral displacement comparable to that of structure D1 with the weaker beams. Both structures were subjected to virtually identical base motions.

The strength of the beams did, however, have a profound effect on the mode of failure in later test runs with more intense base motions. The test structures, of both series one and two, with the stronger connecting beams had a tendency to have more violent failures resulting from normal stresses in the walls at the base of the structure.

RESPONSE OF FRAMES COMBINED WITH WALLS

One of the interesting opportunities of earthquake simulation in the structural laboratory is testing a model structure with a series of increasingly more intense earthquake motions rather than a single strong-motion causing local or total failure. The use of this technique raises the question of whether the initial low-level motions affect the response of the test structure so as to cause extraneous effects in the event of the

major test run. In Ref. 4 it was concluded from the behavior of a series of structural models and from supporting analytical studies that, provided serious local structural failures have not taken place, such a progressive testing procedure did not affect the results of the final test run.

In order to check this conclusion, the two test structures in series four which comprised only frames were tested in two different patterns. Structure FF1 was subjected directly to a damaging motion whereas the structure FF2 was subjected to a series of three increasingly stronger earthquake motions, the last one being comparable in intensity to the single test motion for FF1.

Figure 7 compares the acceleration response histories for the two test structures. Figure 7a gives the results for the structure which was subjected directly to an intense earthquake motion. Figure 7b shows corresponding measurements for the structure which was subjected to two prior test runs of smaller intensity. (The spectrum intensities for the three consecutive motions were 4.2, 8.5, and 16.5 in.)

The acceleration-response waveforms at all three levels were virtually identical, indicating that the previous history of structure FF1 with simulated ground motions of lower intensity did not change its response for run 3 measurably from what it would have been if it had been subjected to the motion of run 3 directly.

Figures 8 and 9 show the measured base motion, accelerations, base shear, and displacements for test structure FW1 which is comparable to FF1 and FF2 except for the addition of a centrally located slender structural wall.

For the moderate base motion of run 1 (Fig. 8), the influence of the slender wall is relatively subtle but important. As illustrated in Fig. 10, the maximum displacement at a spectrum intensity of approximately six in. is reduced by one half with respect to that of the frames alone. For the extremely intense motion of run 3 (Fig. 9) the slender wall had relatively little effect because it was heavily damaged at the base at the end of run 2.

ACKNOWLEDGMENTS

The test series described in this report were supported by Grants GI-29934 and ATA 74-22962 of the National Science Foundation. The work was carried out at the Structural Laboratory of the Department of Civil Engineering at the University of Illinois under the supervision of W. C. Schnobrich, S. Otani and M. A. Sozen. The following persons executed the tests and the analysis: Series 1, L. W. Hsu; Series 2, J. M. Lybas; Series 3, D. Aristizabal; Series 4, J. Udvari. Technical supervision of the experiments and data acquisition by V. J. McDonald is gratefully acknowledged. The IBM 360/75 computer system of the University of Illinois Department of Computer Science was used for final data reduction and analyses.

REFERENCES

1. M. A. Sozen and S. Otani, "Performance of the University of Illinois Earthquake Simulator, "Proc., U. S.-Japan Seminar on Earthquake Engineering with Emphasis on the Safety of School Buildings, Sendai, Sept. 1970, pp. 278-302.
2. G. W. Housner, "Behavior of Structures during Earthquakes," Journal of the Eng. Mech. Division, ASCE, Vol. 85, No. EM4, Oct. 1959, pp. 108-129.
3. L. W. Hsu, "Behavior of Multistory Reinforced Concrete Walls During Earthquakes," doctoral thesis submitted to the Graduate College of the University of Illinois, Urbana, 1974, 262 p.
4. S. Otani and M. A. Sozen, "Behavior of Multistory Reinforced Concrete Frames During Earthquakes," Civil Engineering Structural Research Series No. 392, Univ. of Ill., Urbana, Nov. 1972, 551 p.

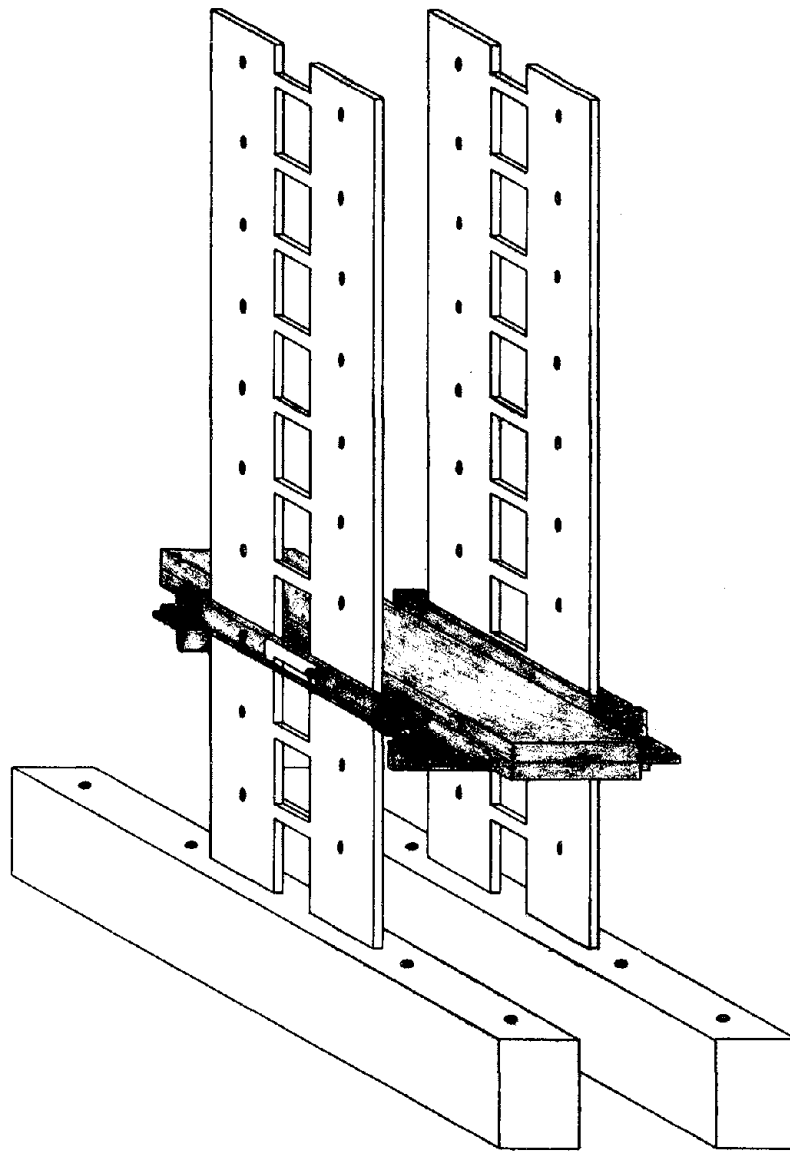


Fig. 1 Ten-Story Structural-Wall Model

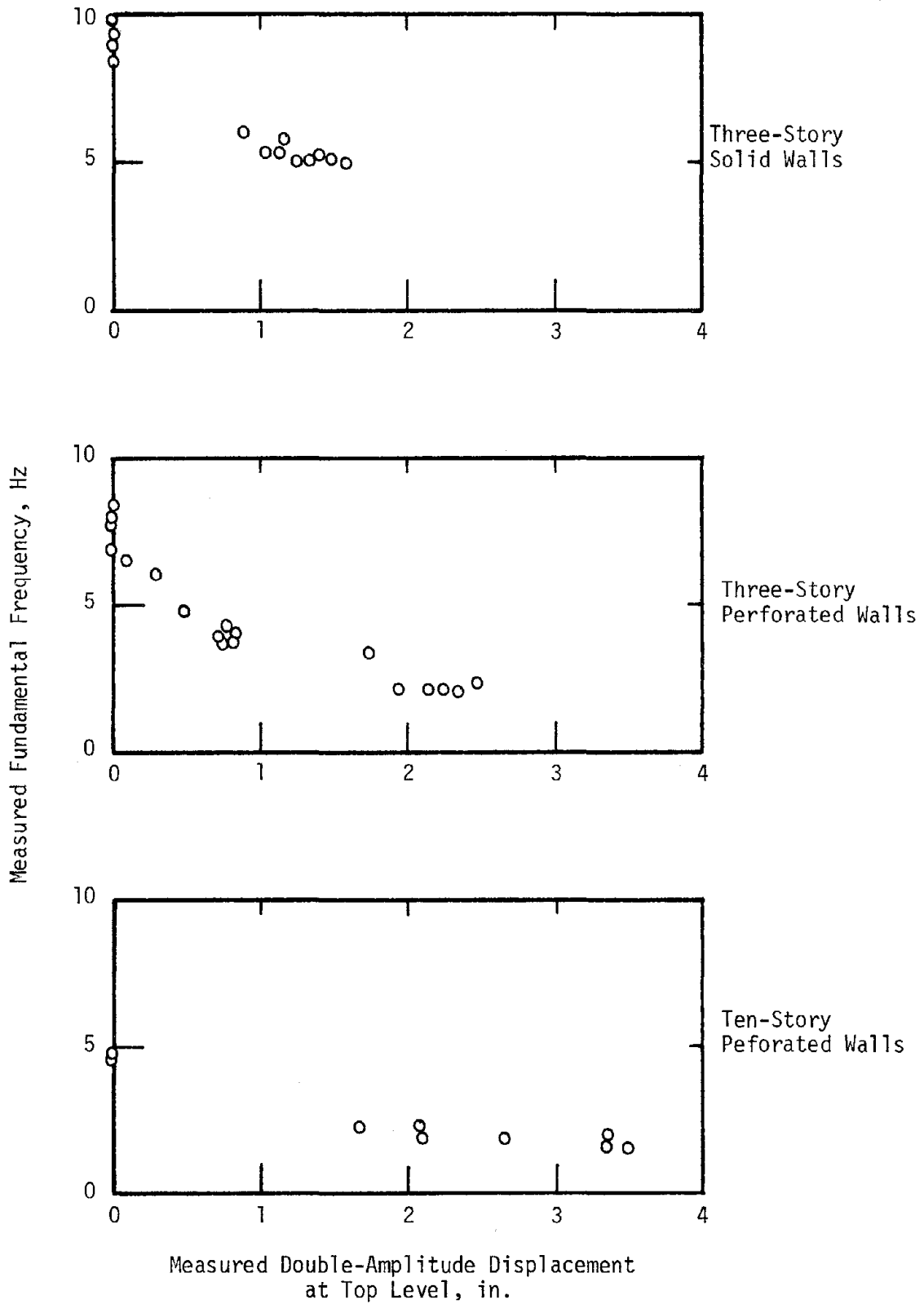
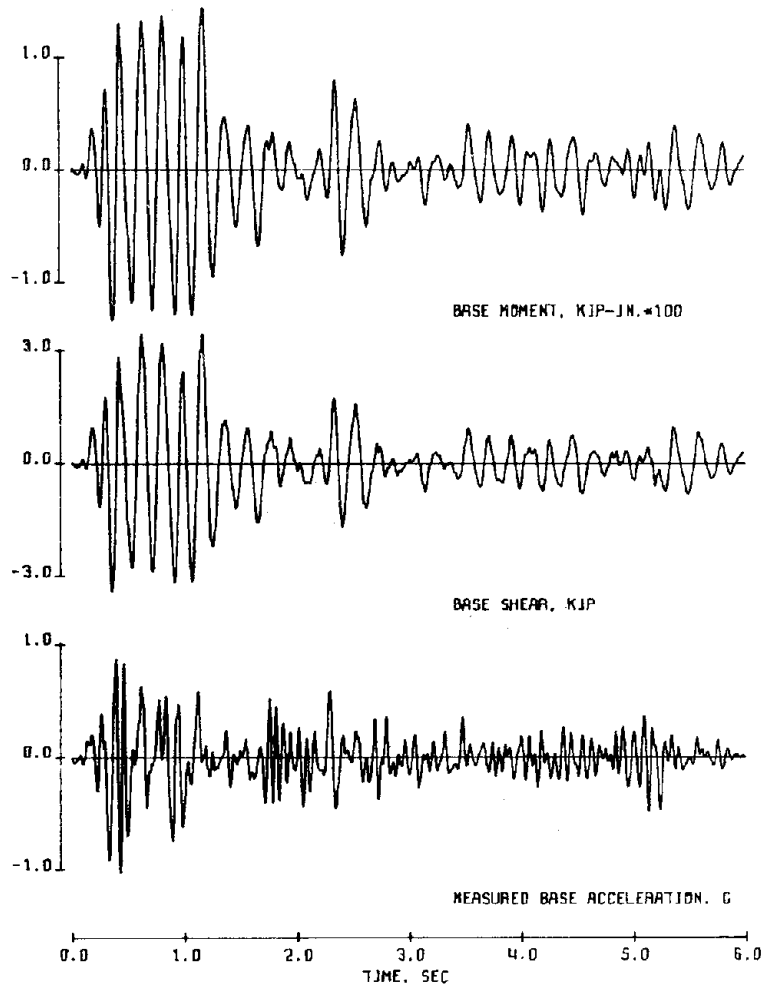
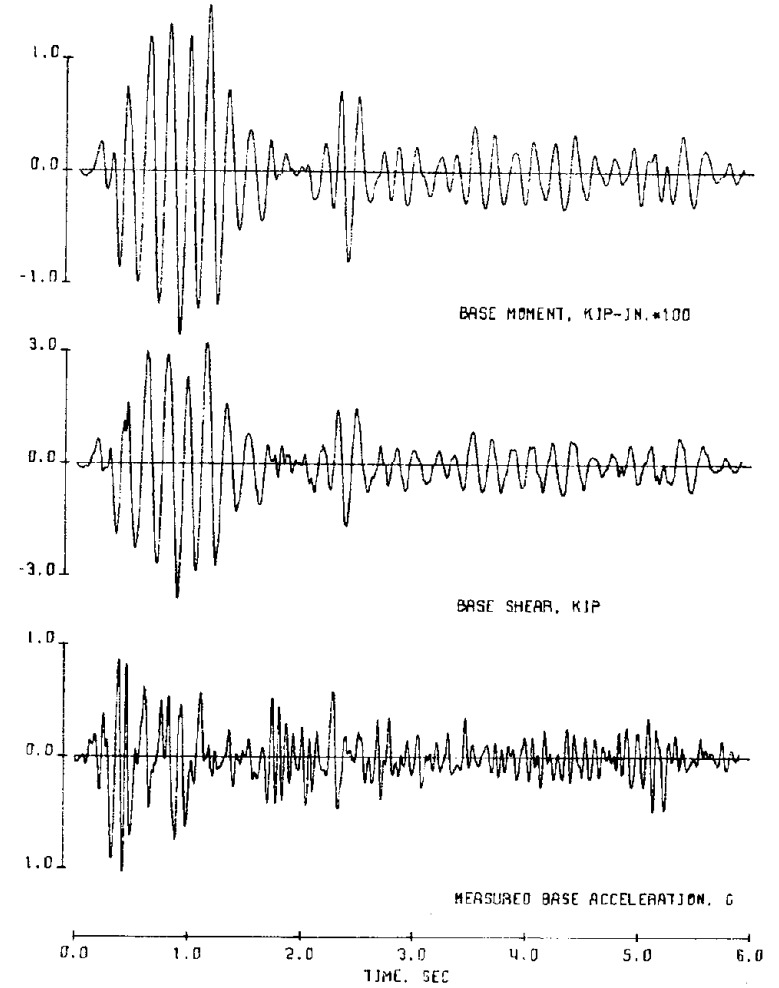


Fig. 3 Variation of Observed Fundamental Frequency



MEASURED RESPONSE, TEST D11

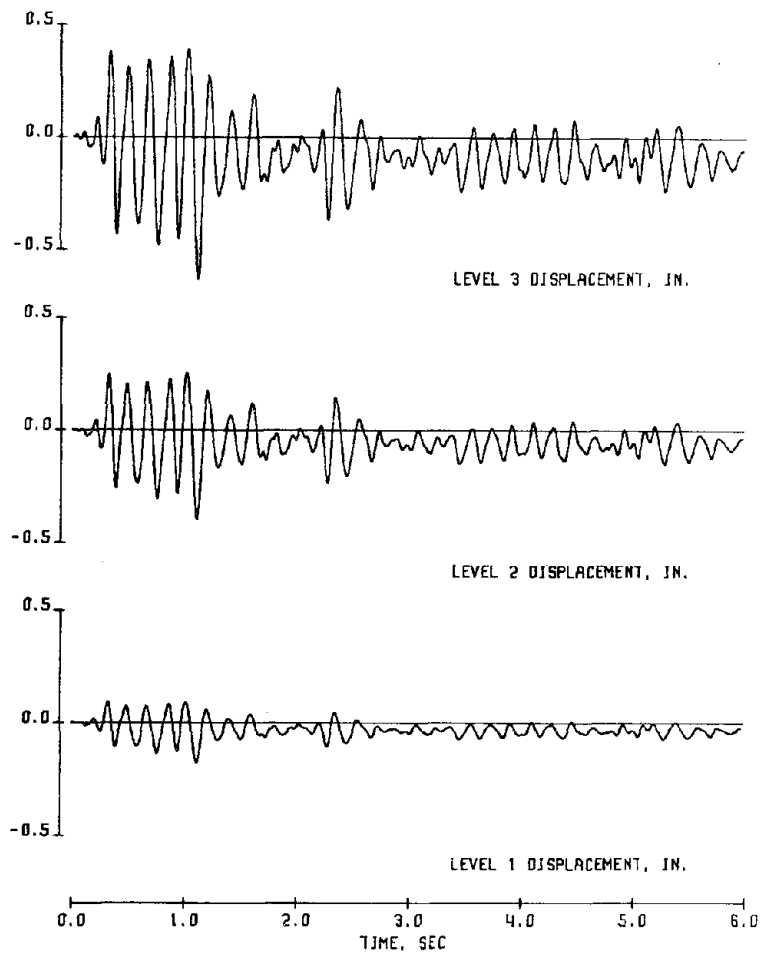
(a)



CALCULATED RESPONSE-HISTORIES FROM LINEAR MODEL,
TEST D11

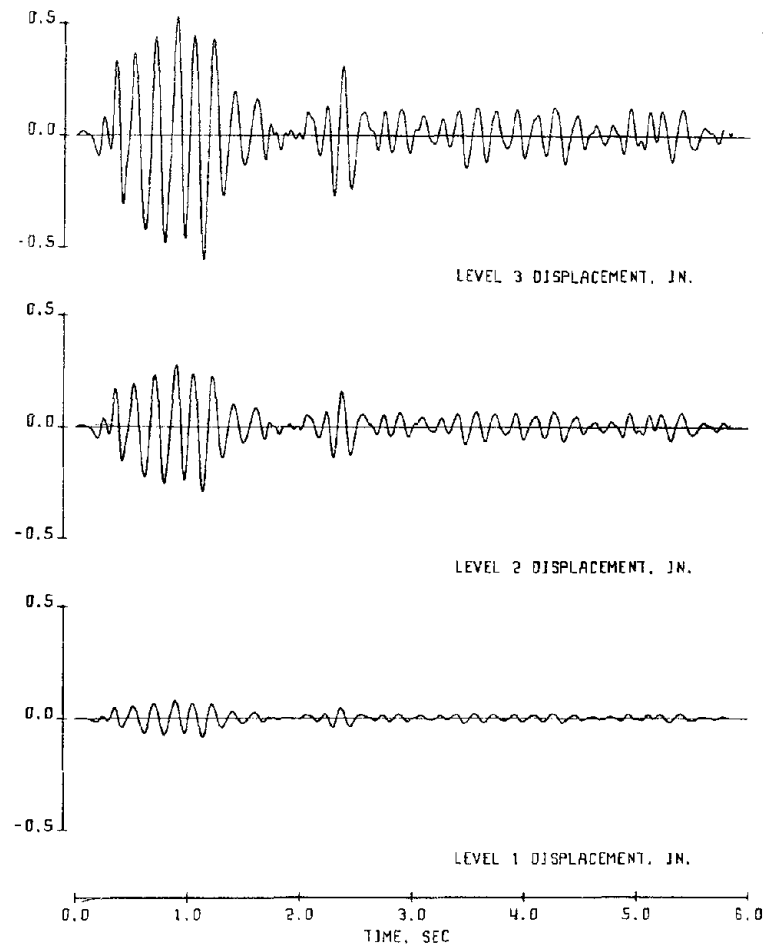
(b)

Fig. 4 Base Moment and Shear for Three-Story Solid Walls



MEASURED RESPONSE, TEST D11

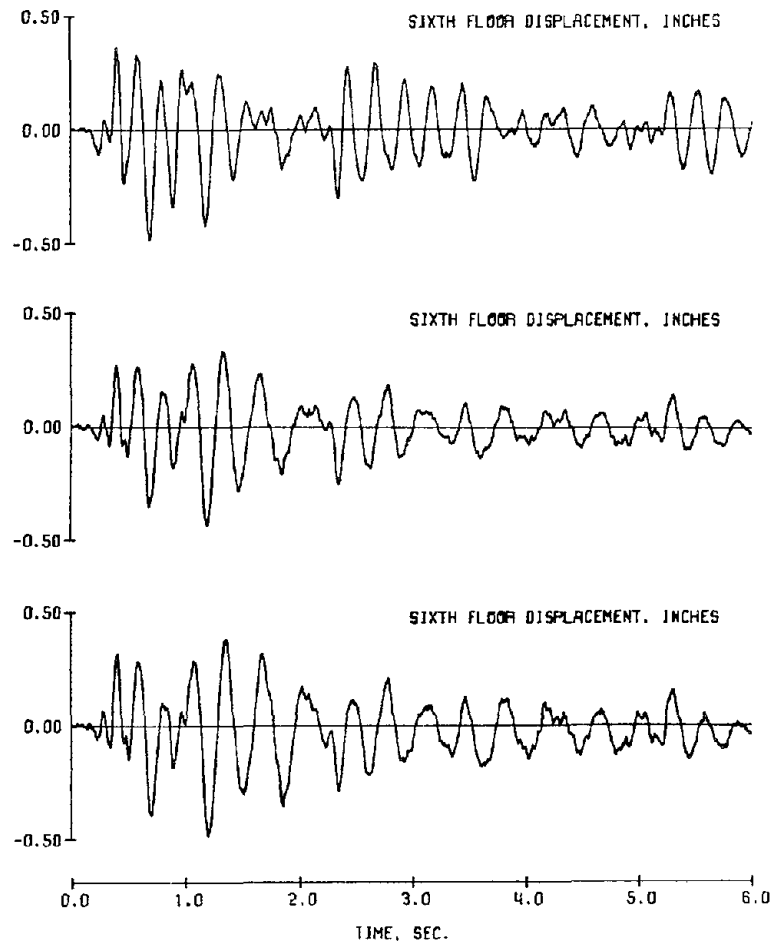
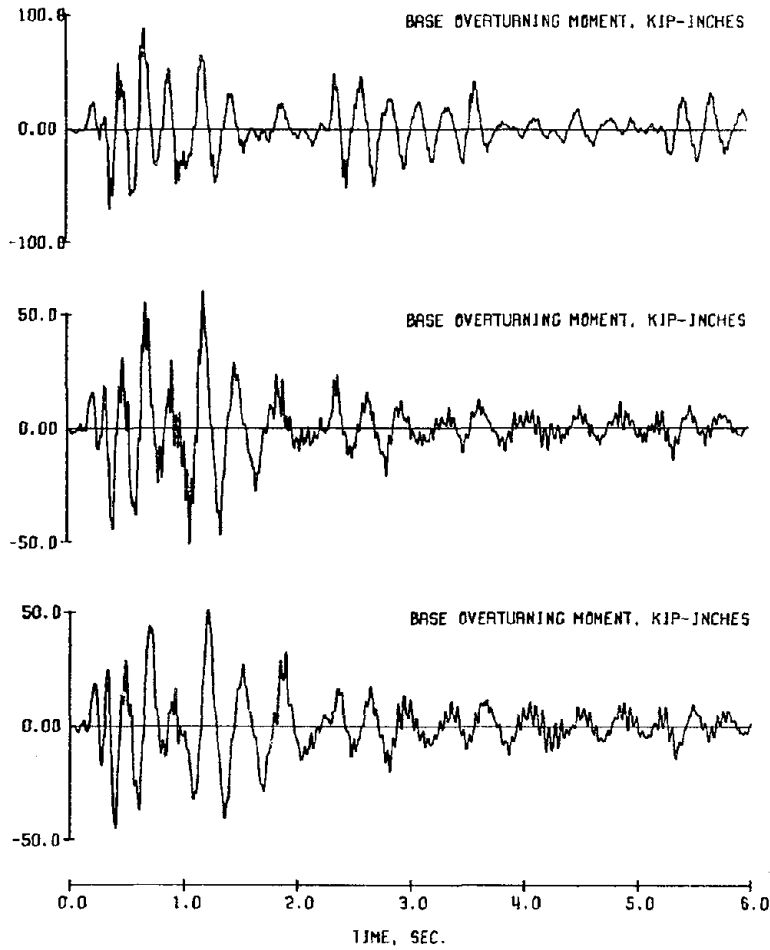
(c)



CALCULATED RESPONSE-HISTORIES FROM LINEAR MODEL, TEST D11

(d)

Fig. 4 Lateral Displacements for Three-Story Solid Walls



(a)

(b)

Fig. 5 Measured Base Moment and Displacement Responses for Perforated Three-Story Walls ("Sixth Floor" refers to the top connecting girder)

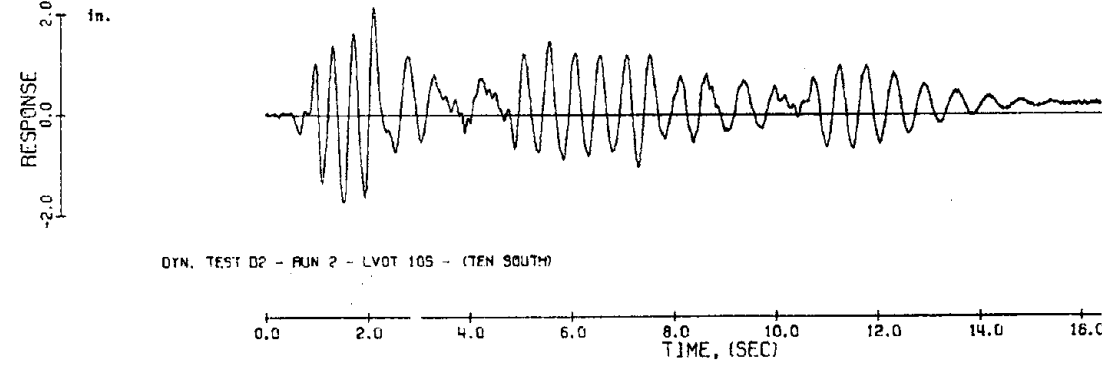
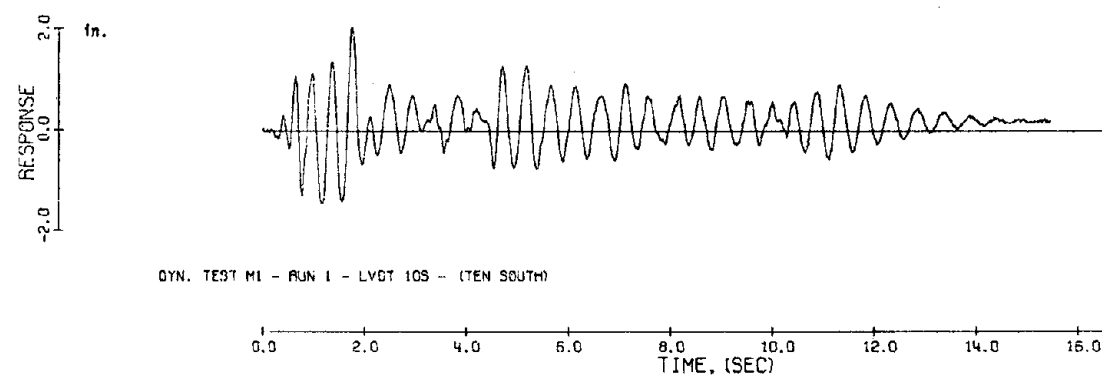
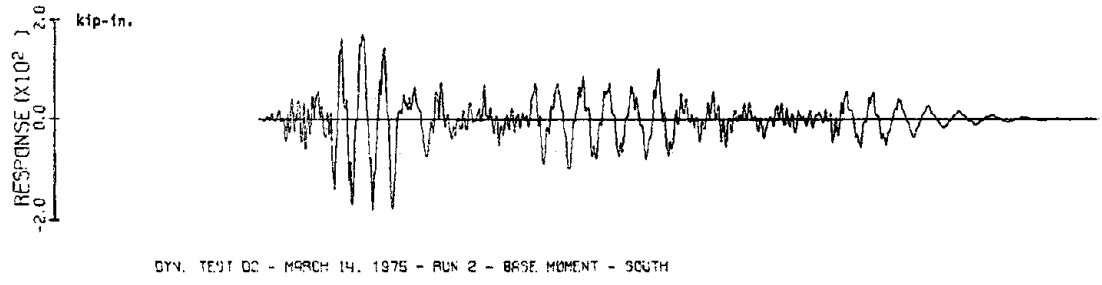
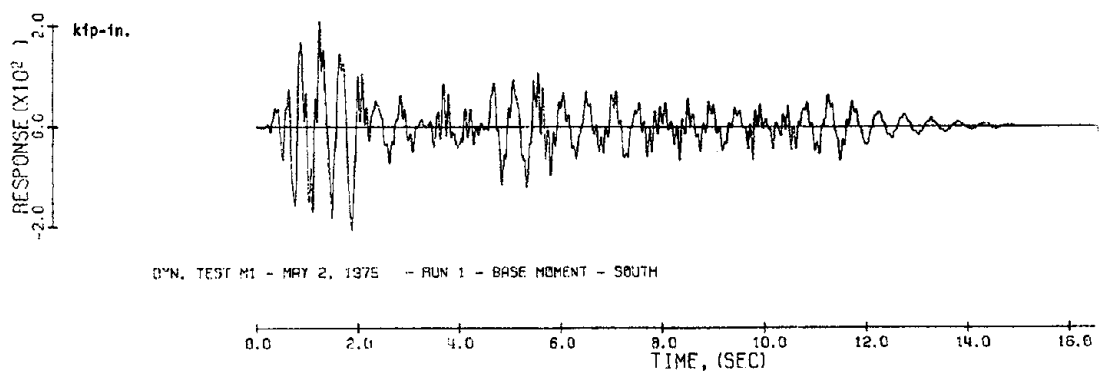
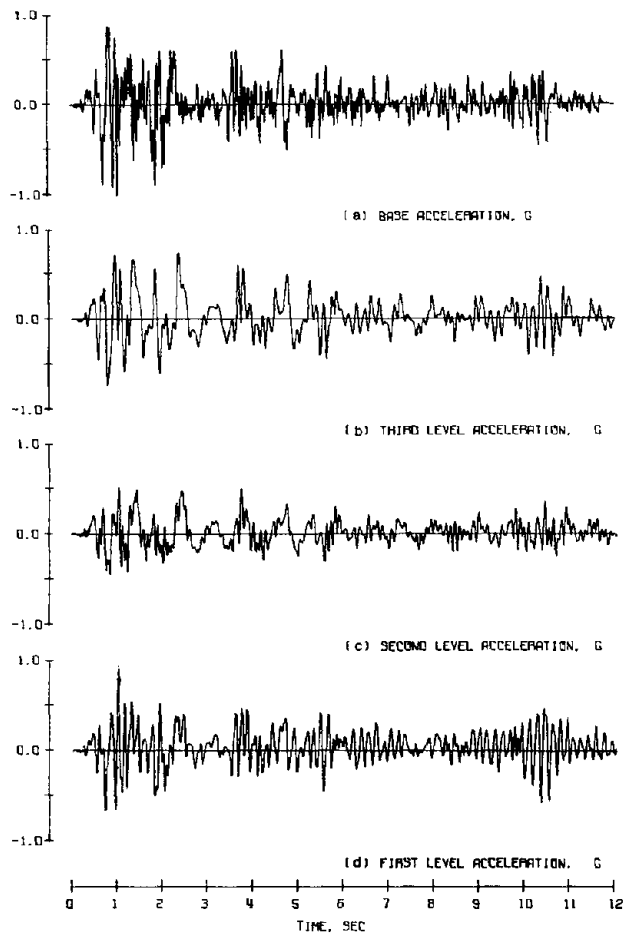
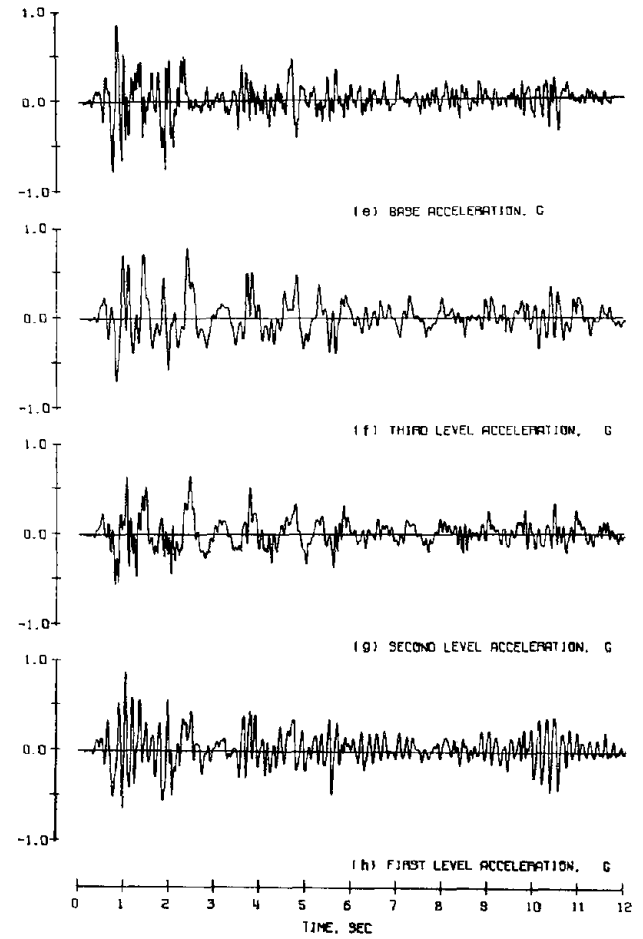


Fig. 6 Measured Base Moment and Top-Story Displacement for Ten-Story Perforated Walls



(a) Run 1, Structure FF2
Spectrum Intensity = 18.5 in.



(b) Run 3, Structure FF1
Spectrum Intensity = 16.0 in.

Fig. 7 Measured Acceleration Response of Test Frames FF1 and FF2

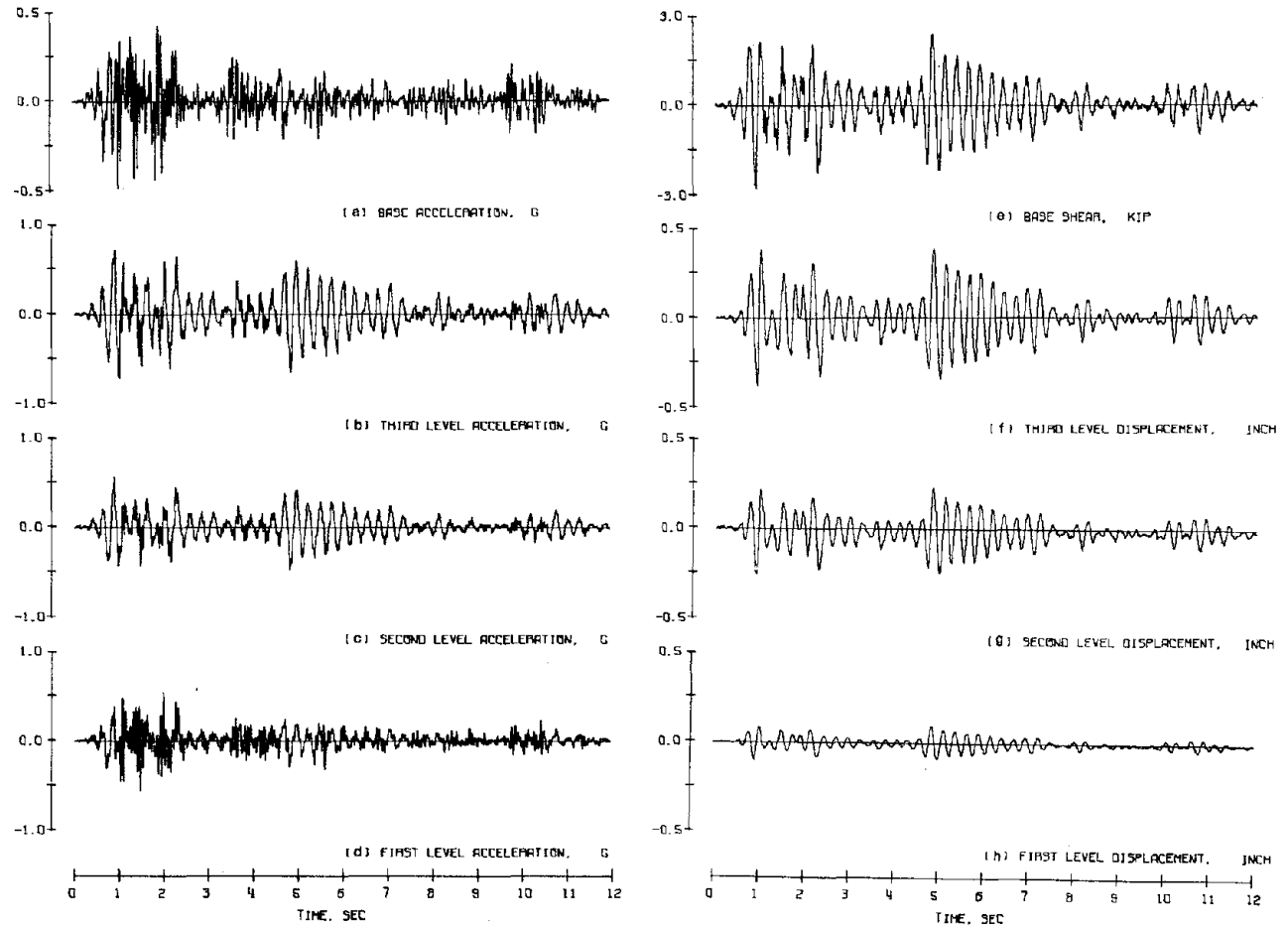


Fig. 8 Measured Response of Test Structure FWI with Combined Frames and Wall (Run 1, Spectrum Intensity = 6.2)

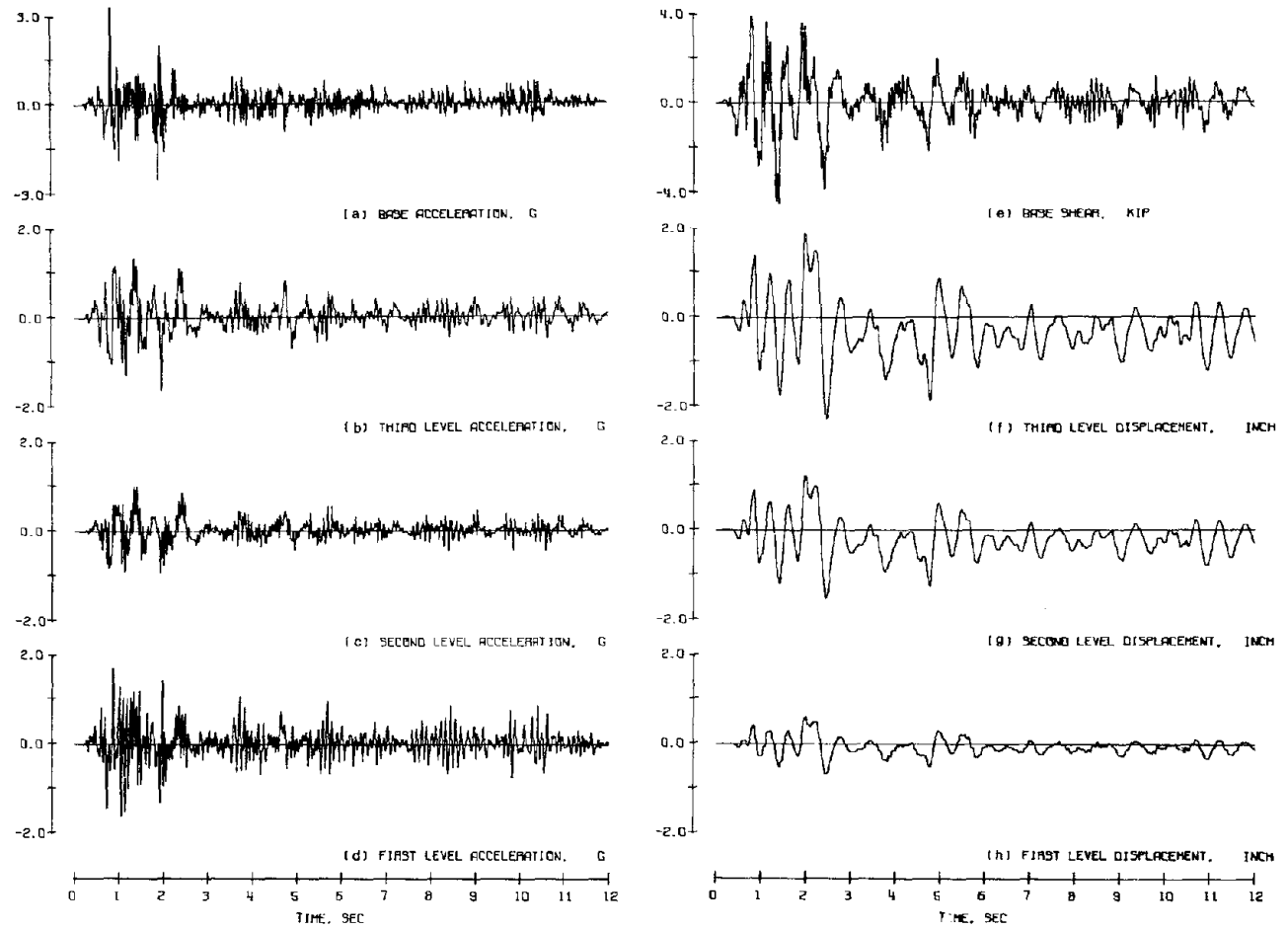


Fig. 9 Measured Response of Test Structure FWI with Combined Frames and Wall (Run 3, Spectrum Intensity = 24.0)

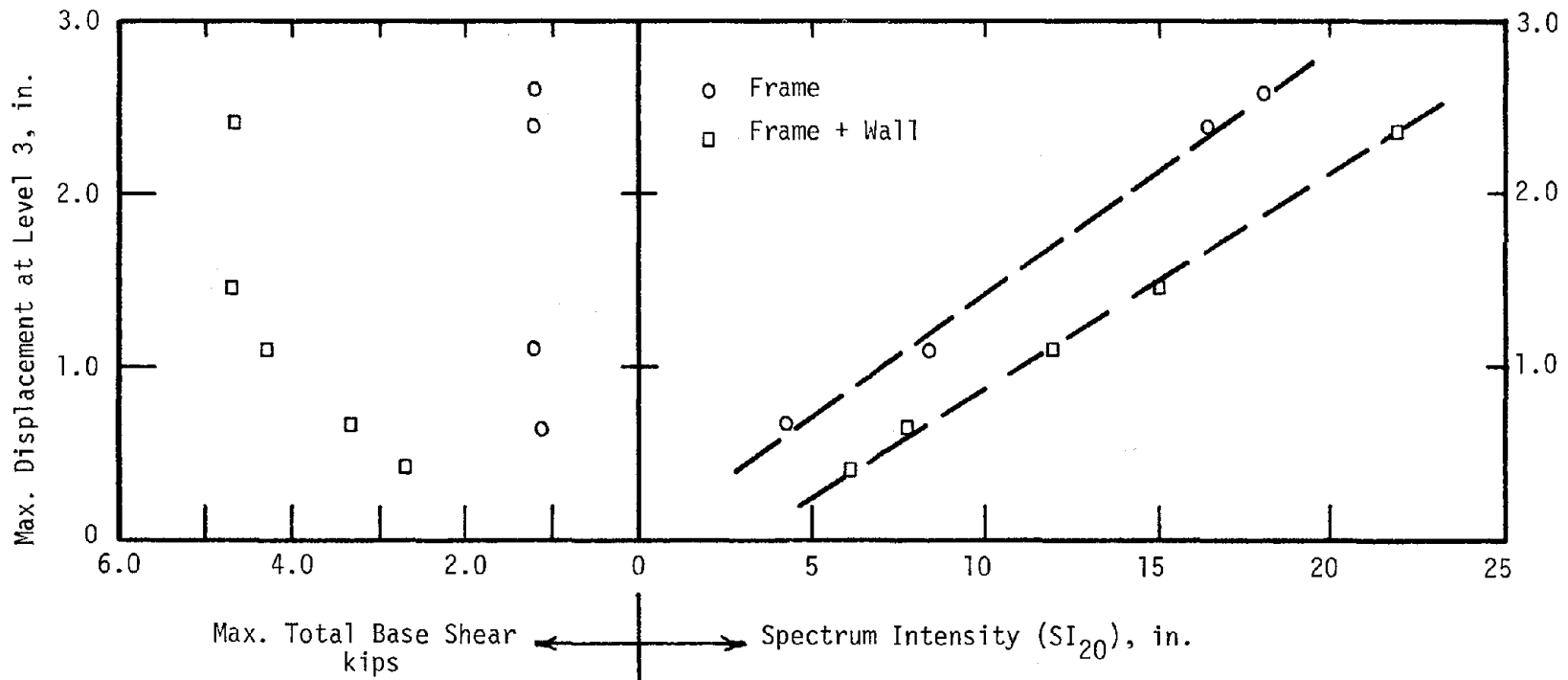


Fig. 10. Effect of Structural Wall on Lateral Displacements

by

Yutaro Omote^I and Toshikazu Takeda^{II}

SYNOPSIS

This paper is concerned with the tests and analyses of reinforced concrete chimneys subjected to strong earthquake ground motions. One objective of the investigation is to develop a realistic mathematical model for the calculation of non-linear response of reinforced concrete chimneys. In order to find a suitable model, one must first establish the moment-curvature relationship for a reinforced concrete cylinder subjected to full reversals of bending. For this purpose, four physical models of chimneys were tested on an earthquake simulator and non-linear response analyses were conducted using the sub-element method proposed in this paper. Static and dynamic test results show good agreement when compared with analytical predictions.

I INTRODUCTION

1.1 STATEMENT OF THE PROBLEM

The behavior of reinforced concrete chimneys subjected to strong base motions is not yet well defined or understood. All structures, especially reinforced concrete structures, exhibit varying amounts of non-linearity, even at the so-called small displacement stage. In order to develop a realistic model for the mathematical representation of reinforced concrete chimneys subjected to strong earthquakes, simplified models are necessary and their validity should be experimentally investigated and analyzed. This report is concerned with tests and analyses of reinforced concrete chimneys subjected to strong earthquake-like motions. The whole aspect of this study is shown in Fig. 1.1.

1.2 OBJECT AND OUTLINE OF THE EXPERIMENTAL PROGRAM

The object of this work was to establish non-linear analytical

^I Visiting Assistant Research Engineer, Earthquake Engineering Research Center, University of California, Berkeley, and Researcher, Ohbayashi-Gumi Ltd., Technical Research Institute.

^{II} Supervising Researcher, Ohbayashi-Gumi Ltd., Technical Research Institute.

methods for reinforced concrete chimneys subjected to strong earthquakes. In order to find a suitable mathematical model, three kinds of model specimen tests were conducted as follows:

Specimen Model M was a simple beam of cylindrical reinforced concrete subjected to reversal of bendings. The analysis is based on the stress-strain relationship of concrete and reinforcement, and the moment-curvature relationship between the test results and the calculated results is discussed. From these experimental and analytical results, the behavior of a reinforced concrete cylinder subjected to reversal of bending moment under constant axial load can be modeled by one of the degrading tri-linear types, as shown in Chapter 2.

Specimen Model CSF was a chimney model of reinforced concrete. CSF was used mainly for the static horizontal loading test of reversal and, in addition, for the free vibration tests during the reversal of loadings.

Specimen Models CSR-1, CSR-2, and CSR-3 were also chimneys which have the same dimensions as CSF, mentioned above. These CSR were subjected to dynamic tests by the earthquake simulator which was driven by an electro-hydraulic mechanism with servo valve. Before and after every strong random vibration test of specimens CSR-1,2,3, both free vibration tests and steady state vibration tests were conducted. The input waves were El Centro, California, 1940 NS record, Tokachi-oki, 1968 Hachinohe-harbour NS record for random tests and strong sine-wave. These experimental results for specimens CSF and CSR are discussed in Chapter 3.

The non-linear response analysis method is presented in Chapter 4, using the moment-curvature relationship of a reinforced concrete cylindrical section determined from the results of Model M. The static and dynamic test results are compared in Chapter 5 and good agreement between the analytical and the test results is obtained.

II MOMENT CURVATURE RELATIONSHIP OF A REINFORCED CONCRETE CYLINDER

2.1 INTRODUCTORY REMARKS

This chapter discusses the behavior of a reinforced concrete cylinder subjected to reversal of bending moments under constant axial load. The simple beam model test and its exact analyses were carried out, and finally the moment-curvature relationship was modeled by a degrading tri-linear hysteresis loop in order to calculate the non-linear response of reinforced concrete chimneys.

2.2 STATIC TEST UNDER REVERSAL OF BENDINGS

2.2.1 SPECIMEN AND LOADINGS

Specimen Model M was 5m in length and 80cm in outside diameter with a wall thickness of 8 cm as shown in Fig. 2.1. Both ends of the

specimen were filled with concrete, and the hollow cylindrical part in the middle was tested. The longitudinal reinforcement consisted of 12-D16 bars in the hollow cylindrical region. The percentage of reinforcement for this cross-section was $p_g = 1.31\%$. Shear reinforcement was $4\phi - @ 100$ ($p_s = 0.2\%$) at the hollow part. The average compressive strength of the concrete used was 243.7 kg/cm^2 . These material properties are listed in Table 2.1.

The reversal of bending test was conducted using the 300 ton electronically balanced testing machine. In this experiment, the number of loading cycles was eleven and the axial force was not applied.

2.2.2 THE METHOD OF ANALYSIS

The method used to calculate the moment-curvature relationship of a reinforced concrete cylinder subjected to reversal of bending under constant axial load was based on the stress-strain relationship of concrete and reinforcement. The assumptions adopted for the analysis were as follows:

1. The section for analysis consisted of many concrete segments and some steel bars as shown in Fig. 2.5(a).
2. A linear distribution of strain over the depth of section.
3. The stress-strain relationship for concrete was assumed to be as shown in Fig. 2.6(a).
4. The stress-strain relationship for a steel bar was assumed to be as shown in Fig. 2.6(b).

The calculation processes were as follows:

1. For the given curvature, a strain distribution over the section was first assumed.
2. The stress distribution over the section was determined from Figs. 2.6(a) and (b).
3. The total force and the position of the center of gravity of the concrete stress block were computed.
4. The equilibrium of the axial forces over the section was examined.
5. If the equilibrium was achieved within a given range, the moment on the section was calculated. Otherwise, another strain distribution was assumed and the same process repeated.
6. The calculation was repeated for the next specified curvature.
7. In this way, the moment-curvature hysteresis loop was calculated for the specified curvature cycles.

2.3.2 SIMULATION ANALYSIS OF SPECIMEN MODEL M

Analysis was carried out on cycles Nos. 5, 6, and 8 in Fig. 2.4; the specified curvature cycle for calculation is in Fig. 2.7. It was assumed herein that there were forty concrete segments and the stress-strain relationship of the steel was assumed to be either the R-0 type

($\alpha = 0.5$, $\gamma = 0.7$) (CASE-1) or the elasto-plastic type ($\gamma = \infty$) (CASE-2) shown in Fig. 2.6(b).

Figure 2.8 compared the primary curves from these calculated results with those of the test results, which included the primary curve of the Nos. 1, 2, 5 cycles. For the test, the initial rigidity was $EI(m) = 2060 \times 10^5$ (ton·cm) and the calculated initial rigidity was $EI(c) = 2205 \times 10^5$ (ton·cm). The measured cracking moment (M_c) was 390(ton·cm); on the other hand, the calculated result was 698(ton·cm). Although the difference between the observed and the calculated cracking moment was large, after cracking, the calculated bending moment of the section decreased for increasing curvature and then gradually increased because of the rise of steel stress. Measured first yielding moment (M_y) of the extreme edge bar at the tension side was 1040(ton·cm); on the other hand, the calculated M_y was 1255(ton·cm) in CASE-1, and was 1295(ton·cm) in CASE-2.

As for the primary curve, the test results were slightly larger than the analytical before the yielding stage, but after yielding of the bar, the test results were in between the calculated ones of CASE-1 and CASE-2.

Figure 2.9 compares the hysteresis loops for the cycles (Nos. 5, 6, and 8) with the corresponding analytical ones from CASE-1. Figure 2.9(a) shows the first cycle for yielding of the steel bars, and Fig. 2.9(b) shows the steady state cycle which has the same curvature amplitude as Fig. 2.9(a). As for the hysteresis loop, when R-0 type (CASE-1) was assumed in the stress-strain relationship of steel bars, the analytical results coincided reasonably with the test results in this example.

2.4 ANALYTICAL MODEL OF THE MOMENT-CURVATURE RELATIONSHIP

In order to calculate the non-linear response of a reinforced concrete chimney subjected to strong earthquakes, one of the degrading tri-linear type models was assumed in the moment-curvature relationship of a section, and then this model was compared with the one calculated in 2.3.

2.4.1 CRACKING STATE

The cracking moment (M_c) and the curvature ($1/\rho_c$) of the reinforced concrete cylinder were assumed to be

$$M_c = (f_r + N/A_e) \times Z_e \quad (2.1)$$

$$1/\rho_c = M_c/EI_c \quad (2.2)$$

where f_r : tension strength of concrete
 N^r : axial force
 A_e : effective section area
 Z_e : effective section modulus
 E : elastic modulus of concrete
 I_c : geometrical moment of inertia of area

2.4.2 YIELDING STATE

The yielding moment (M_y), defined as yielding of extreme edge bar on the tension side, was calculated by A. I. J. standard. The assumptions were as follows:

1. Linear distribution of strains over the depth of section
2. Linear stress-strain for compressive concrete.
3. Reinforcements over the section were assumed to be at the center of thickness.

With these assumptions, the neutral axis of the section was calculated first, then the equilibrium of the axial force was maintained and then the yield moment (M_y) around the neutral axis was calculated. Curvature at yielding stage was

$$1/\rho_y = (\epsilon_c + s_y \epsilon_s)/d \quad (2.3)$$

where ϵ_c : compressive strain of concrete at extreme fiber
 ϵ_s : tension strain of steel bars at extreme edge
 s_y : distance between the compressive extreme fiber of concrete to the center of tension steel bars at extreme edge.

2.4.3 ULTIMATE STATE

The ultimate state was defined as crushing of compressive concrete. The assumptions were as follows:

1. Linear distribution of strains over the depth of the section
2. Stress-strain relationship for steel over the section was assumed to be elasto-plastic.
3. Ultimate strain of compressive concrete was $\epsilon_{cu} = 0.4\%$ and Dr. Umemura's e-function was assumed in the stress-strain relationship of concrete.

With these assumptions, the convergence method was used in the calculation of the ultimate moment (M_u) until equilibrium of the axial force was achieved by changing the location of the neutral axis. Curvature of the ultimate stage was

$$1/\rho_u = (\epsilon_{cu} + s_y \epsilon_s)/d \quad (2.4)$$

2.4.4 HYSTERESIS LOOP

It is necessary in the response calculation for chimneys subjected to reversal of bendings to idealize the hysteresis loop for simplicity and up to now, many types of loop have been proposed for the reinforced concrete members. Here, a degrading stiffness loop was assumed as shown in Fig. 2.10.

2.4.5 COMPARISON OF IDEALIZED HYSTERESIS WITH EXACT SOLUTION

Figure 2.11(a) shows the moment-curvature relationship of the above mentioned model, both with the exact calculation presented in 2.3 and with the model test results in 2.2. Figure 2.11(b) is again a comparison between the model hysteresis and the exact solution when axial load was applied. Although this assumed model showed slightly larger energy absorption than that of the exact analysis or experimental values, because of its simplicity and similarity, it might be adequate for use for the dynamic response analysis presented later.

III STATIC AND DYNAMIC TESTS OF REINFORCED CONCRETE CHIMNEYS

3.1 INTRODUCTORY REMARKS

This chapter presents the test results of reinforced concrete model chimneys subjected to static horizontal load or strong earthquake-like base motions. Test results of the deflection, periodicity, and dampings of every damage stage of all the specimens were examined. Simulation analyses under strong earthquake-like motions are presented in Chapter 5.

3.2 MODELS AND TESTS

The model chimneys were 3m in height, 18cm at the top and 28cm at the bottom in diameter. The thickness of each specimen was 2.5cm at every height. Four steel weights were mounted on a specimen equivalent to the actual system. Figures 3.1 and 3.2 show the shape and dimension of this chimney.

Four specimens were made. Three of them, named CSR-1, CSR-2, and CSR-3 were for the dynamic tests and another one, named CSF was for the static test. Main reinforcement for bending of each specimen was $16-4\phi$ at every height, so the reinforcement ratio per gross section at the bottom was $p_q = 1.04\%$. Horizontal reinforcement for shear force was $1.6\phi - @ 40(p_s = 0.2\%)$. River sand mortar concrete in which the largest size of sand aggregate was 2.5mm was used.

The steel weight at the top was 150kg, and the other three were each 300kg, so the axial stress at the bottom was $\sigma_N = 5.75\text{kg/cm}^2$. The material properties of each specimen are listed in Table 3.1.

The test program of each specimen is listed in Table 3.2. Two kinds of test, statical reversal loading test (series S) and free vibration test were (series F) used to test specimen CSF. The reversal loading test was conducted by pulling the top steel weight in a horizontal direction (see Fig. 4.3) with a steel rod, and when the maximum displacement was attained, usually in the minus direction of each controlled loading cycle, the steel rod was cut, giving the free vibration under the first mode-like deformation of each damage stage, for the investigation of any change of the first natural period and dampings.

For every CSR specimen, there were three kinds of tests; the strong vibration test (series R), the free vibration test at very small power level (series F), and the steady state vibration test with low sine-wave input of 0.5Hz-50Hz (series S).

3.3 TEST RESULTS

Table 3.3 shows the list of test results for natural periods and damping factors of the first to the third vibration mode and also the rotation angle (max. displacement at the top/total height of chimney) at every damage stage. Figure 3.3 shows an example of crack pattern for specimen CSR-2.

3.3.1 THE FIRST VIBRATION MODE

Figure 3.4 shows the relation between the rotation angle and the ratio of the natural period measured at every damage stage (T_1) to the calculated elastic natural period (T_0) of the first mode. Figure 3.5 shows the relation between T_1/T_0 and the measured damping factors (h_1). For the first mode vibration, the following observations are drawn from these two figures.

1. In general, the static test results and the dynamic test results showed similar tendencies. After cracking of concrete, the natural period of the first mode was longer than the elastic stage. The natural period in the yield stage was about 1.5 times that in the elastic stage in these tests.
2. For the specimen CSR alone, the natural period from the free vibration test results was slightly lower than that from the steady state vibration test.
3. The damping factor for the first mode was from 2 to 4 percent in the elastic stage.
4. After cracking, damping for the first mode increased a little bit, but after yielding, it was 4 to 5 times as much as that of the elastic stage from the steady state test results.

3.3.2 THE SECOND AND THE THIRD VIBRATION MODE

The ratio of the second order elastic natural period T_2 to the first order T_1 was about $T_2 = 0.22T_1$ in this test. Figure 3.6 shows the relation between the ratio of the natural period measured at various stages (T_i , $i=1-3$) to the calculated elastic periods (T_{0i} , $i=1,-3$) for corresponding modes and the mode damping factor (h_i) measured from the resonance curve. The following conclusions may be drawn for the higher mode vibration.

1. After cracking, the first natural period increased remarkably; on the other hand, the increase of the natural period for the higher mode was slight.
2. The damping factor for the second mode was nearly equal to that of the first mode in the elastic stage, and after cracking the increase for the higher modes was not as remarkable as the increase for the first mode.

IV ANALYTICAL MODEL OF A REINFORCED CONCRETE CHIMNEY

4.1 INTRODUCTORY REMARKS

The mathematical model of a chimney for response calculations is a multi-lumped mass system. The reinforced concrete chimney is divided into idealized sub-elements between masses. The evaluation of non-linearity for a reinforced concrete chimney is presented below taking into account the moment-curvature relationship with a degrading tri-linear type of hysteresis loop. The validity of this method was verified first by both the static reversal loading test of specimen CSF and its analysis.

4.2 MATHEMATICAL MODEL AND FUNDAMENTAL EQUATION

A chimney, shown in Fig. 4.1(a) was idealized by the multi-lumped mass system shown in Fig. 4.1(b), for which both rocking and sway effects at the base were considered. When the force-deflection relationship between masses was assumed as in Fig. 4.1(c), Eq. (4.1) was obtained

$$\begin{Bmatrix} M_A \\ M_B \\ Q \end{Bmatrix}_i = 2EK_{oi} \begin{bmatrix} a & b & c \\ b & a' & c' \\ c & c' & d \end{bmatrix} \begin{Bmatrix} \Theta_A \\ \Theta_B \\ \bar{u} \end{Bmatrix}_i \quad (4.1)$$

where M_A, M_B : bending moment acting at A, B

Q : shear force between A and B

E : elastic modulus of concrete

K_o : standard unit stiffness

a, a', b : slope deflection coefficient of non-uniform member
(refer to 4.3)

$c = -(a+b)/L, c' = -(a'+b)/L, d = -(c+c')/L$

L : length between A and B

\bar{u} : relative deflection between A and B

Equation (4.1) will be written in the matrix form as follows:

$$P_i = K_i d_i \quad (4.2)$$

where K_i is the member stiffness matrix between masses. The total stiffness of the chimney can be calculated by the usual stiffness matrix method, so the horizontal force-deflection relationship can be expressed as

$$F_Q = K_T D_u \quad (4.3)$$

where F_Q : horizontal load vector

K_T : horizontal stiffness matrix of the chimney

D_u : horizontal displacement vector.

When the stiffness of some sub-elements was changed during the response calculations, the member stiffness K_1 and total stiffness K_T were changed with step by step integration.

4.3 EVALUATION OF THE INELASTIC RIGIDITY

Non-linearity for the reinforced concrete chimney was taken into account in the moment-curvature relationship of the sub-elements. That is, first the member between masses was divided into "n" sub-elements as shown in Fig. 4.2(a). When the end moments M_A and M_B acted at A and B, the moment distribution altered linearly. However, the moment of the sub-element was assumed constant with an average value as shown in Fig. 4.2(a). The bending stiffness of each sub-element became EI_j , ($j=1, \dots, n$). Let the standard rigidity in the elastic stage be EI_0 and define the rigidity coefficient of each sub-element to be $e_j = EI_j/EI_0$, then Eqs. (4.4) to (4.7) may be obtained

$$\begin{Bmatrix} M_A \\ M_B \end{Bmatrix} = \frac{6EK_0 k}{(\alpha_A' + \gamma')(\alpha_B' + \gamma') - (\alpha_{AB}' - \gamma')^2} \cdot \begin{Bmatrix} (\alpha_B' + \gamma')(\alpha_{AB}' - \gamma') - c \\ (\alpha_{AB}' - \gamma')(\alpha_A' + \gamma') - c' \end{Bmatrix} \begin{Bmatrix} \theta_A \\ \theta_B \\ R \end{Bmatrix} \quad (4.4)$$

where

$$\begin{aligned} \alpha_A' &= 3a'/(aa' - b^2) \\ \alpha_B' &= 3a/(aa' - b^2) \\ \alpha_{AB}' &= 3b/(aa' - b^2) \end{aligned} \quad (4.5)$$

$$a = \left(\sum_{i=1}^n p_j q_j^2 / e_j \right) / T$$

$$a' = \left(\sum_{j=1}^n p_j / e_j - 2 \sum p_j q_j / e_j + \sum p_j q_j^2 / e_j \right) / T$$

$$b = \left(\sum_{j=1}^n p_j q_j / e_j - \sum p_j q_j^2 / e_j \right) / T \quad (4.6)$$

$$T = 2 \left\{ \left(\sum_{j=1}^n p_j / e_j \right) \times \left(\sum p_j q_j^2 / e_j \right) - \left(\sum p_j q_j / e_j \right)^2 \right\}$$

$$c = \alpha_B' + \alpha_{AB}' \quad c' = \alpha_A' + \alpha_{AB}'$$

$$\gamma' = 6EK_0 k / \beta GA \ell \quad (4.7)$$

For the chimney, almost all the deformation was due to the bending effect and the shear deformation was slight. So when the shear effect was neglected, that is $\gamma' = 0$, parameter a , a' , b in Eq. (4.6) could be applied to Eq. (4.1) directly. The number of sub-elements of the member between masses should be as great as possible; however, five may be enough for practical use.

The validity of this method was verified first by the analysis for the static reversal loading test of specimen CSF. Figure 4.3 showed an example of relation between the horizontal load (P) and the top displacement of the chimney (Y_4), and its analysis. The calculated value (dotted line) on the curve and the damaged pattern of the chimney agreed well with the test results in this case. The method presented here may be available not only for chimneys but also for structures such as bearing wall systems whose non-linearity cannot be represented by the hinge method at the end of the members.

V SIMULATED DYNAMIC TESTS

5.1 INTRODUCTORY REMARKS

This chapter presents examples of simulation analysis of dynamic tests subjected to strong earthquake-like motions. As shown in Table 3.2, the input waves for each specimen CSR-1, CSR-2 and CSR-3 were from the El Centro 1940 NS record, Tokachi-oki 1968 Hachinohe harbour NS record and 3Hz. sine-wave; the frequency of the latter was almost equal to the resonance frequency at the yielding stage of this specimen. For every specimen the test was repeated several times, changing the input levels.

The aim of the tests with specimen CSR-1 was to observe the damage resulting from successive test runs with increasing input levels. With specimen CSR-2 it was intended that the yield stage should be reached from the elastic stage with only one strong test run. This test was to be repeated once with almost the same strong input level. Specimen CSR-3 was to be used to observe the resonance state in the yield stage. Both the experimental and the analytical response results for specimen CSR are presented in section 5.3 of this chapter.

Specifications of the shaking table were as follows:

Exitng force : 10 tons
Frequency : 0.1 - 50 Hz.
Vibration wave form ; sinusoidal, triangular, rectangular, arbitrarily
random waves
Vibration direction ; horizontal, one component
Max. amplitude ; 200 mm
Max. acceleration ; 3G in case of no load, 1G in case of full load of
10 tons
Table dimensions ; 3 x 4 x 1 m (W x L x H)
Table weight ; 5 tons
Supporting system ; roller support

5.2 ASSUMPTIONS FOR THE RESPONSE CALCULATION

The mathematical vibration equation for the response calculation was assumed to have the form Eq. (5.1), and was solved by the linear acceleration method with step by step integration.

$$[M]\{\ddot{Y}\} + [C]\{\dot{Y}\} + [K]\{Y\} = -[M]\{\ddot{y}_0\} \quad (5.1)$$

where $[M]$; mass matrix
 $[C]$; damping matrix
 $[K]$; horizontal stiffness matrix
 $\{\ddot{Y}\}, \{\dot{Y}\}, \{Y\}$; mass acceleration, velocity, displacement
vector, respectively
 $\{\ddot{y}_0\}$; base acceleration vector

The damping matrix $[C]$ in Eq. (5.1) was assumed to have the form,

$$[C] = C_e[M] + C_i[K] \quad (5.2)$$

where C_e and C_i are the so-called external and internal damping coefficients, respectively.

Figure 5.1 shows the measured base motion wave form of CSR-2, in the case of RUN-1 and Fig. 5.2 shows the acceleration response spectrum compared with the original record. In order to simulate the measured responses, the following assumptions are made:

- 1) The stiffness matrix $[K]$ in Eq. (5.2) was the same as in Eq. (5.1).
- 2) The damping factors for the first and second modes were assumed to be 2% from the experimental data.
- 3) From the damping factors h_1 and h_2 , the damping coefficients C_e and C_i were calculated and these were constant both in the elastic and inelastic stages.
- 4) Input waves for response calculations were the measured records at the base of the chimney on the earthquake simulator for each RUN.
- 5) The NEAC-2200/500 computer system of OHBAYASHI-GUMI Ltd. was used for computation and the time interval for the response was assumed to be $\Delta t = 0.001$ sec.
- 6) In the CSR-2 experiment, for example, there was a complete pause between RUN-1 and RUN-2. Accordingly, in the simulation analysis, it was assumed that after the input wave for RUN-1 finished, response accelerations and velocities of the chimney were put equal to zero, and on the other hand, the deflection, stiffness and state of hysteresis were adjusted to the initial condition for the next test RUN-2.

5.3 OBSERVED AND CALCULATED RESPONSE

The maximum response values for both the test results and the calculated for every specimen were listed in Table 5.1. Figure 5.3 shows the displacement and the acceleration wave form of the mass at the top of the chimney in case of specimen CSR-2, both for the measured and calculated. In the case of this simulation analysis for specimen CSR-2 especially, the maximum response value, vibration mode, periodicity

and wave form were in comparatively good agreement with the test results over the elastic and inelastic range.

VI SUMMARY AND CONCLUSIONS

The work presented in this report was part of the investigation of the resistance of reinforced concrete chimneys to earthquake motions. An object of the investigation was to develop a realistic model for the calculation of the response of reinforced concrete chimneys. The research included both analyses and tests of reinforced concrete hollow cylinders and chimneys.

In Chapter 2, the characteristics of the moment-curvature relationship of a reinforced concrete cylinder are discussed. In order to analyze the moment-curvature relationship of the test results, the exact solution for a section subjected to reversal of bending moment with constant axial load was determined on the basis of the stress-strain relationship of concrete and steel. The shape of the hysteresis loop for the measured and calculated resembled each other in several given cycles of the inelastic range. To calculate the dynamic response of a reinforced concrete chimney, the moment-curvature relationship was modeled with one of the tri-linear degrading hysteresis loops.

Four models of chimneys, 3m in height, were made. Three of them were for dynamic tests on the earthquake simulator. Another one was for a static test. A free vibration test and a steady state vibration test were conducted before and after every strong earthquake-like vibration test. The main characteristics of these tests with regard to the natural periods, dampings and rotation angle are summarized as follows:

- 1) In the elastic stage, measured natural periods and vibration modes were in good agreement with the calculated values.
- 2) The ratio of the second order natural period T_2 to the first order T_1 was about $T_2 = 0.22T_1$.
- 3) After cracking of the concrete, the first order natural period increased remarkably, however, the increase of natural periods for higher modes was slight.
- 4) The damping factor for the first mode was about 2 to 4 percent in the elastic stage, and for the second mode was nearly equal to that of the first mode.
- 5) After cracking, the damping factor for the first mode increased a little bit, and after yielding of the bar it was 4 to 5 times as much as that of the elastic stage. However, the increase in the damping factor for the higher modes was not so remarkable.

The mathematical model of a chimney for the response calculations was a type of multi-lumped mass system. The chimney was divided into the idealized sub-elements between masses, and non-linearity of each sub-element was taken into account in the moment-curvature relationship with degrading type hysteresis. The validity of this method was verified both by the static reversal loading tests of the chimneys and by their analyses.

Simulation analyses of test results, where external and internal damping were assumed, were conducted. In every case, a 2% damping factor was assumed for the first and the second mode. Since these analyses showed good agreement with the test results, it can be said that it is possible to predict the actual response of reinforced concrete chimneys subjected to strong earthquake motions, with adequate assumptions for the hysteresis loop and damping.

ACKNOWLEDGEMENT

This study was part of an investigation of "Dynamic Response Characteristics of Reinforced Concrete Chimneys" carried out in the Technical Research Institute of OHBAYASHI-GUMI, LTD.

The writers would like to express their thanks for the valuable advice given by Professor Hajime Umemura and Associate Professor Hiroyuki Aoyama, University of Tokyo, during this study.

BIBLIOGRAPHY

1. Y. Omote "Experimental and Analytical Study on the Non-linear Response of Reinforced Concrete Chimneys under Earthquake Motions" Doctoral Thesis, University of Tokyo 1975.3.
2. Y. Omote, T. Takeda "Theoretical and Experimental Study on the Moment-Curvature Characteristics of Reinforced Concrete Cylinders Subjected to Reversal of Bending Moment under Constant Axial Load" Report of the Technical Research Institute, Ohbayashi-Gumi Ltd., No. 10, 1975.
3. Y. Omote, T. Takeda "Non-linear Earthquake Response Study on the Reinforced Concrete Chimney"
Part - 1 Model Tests and Analyses: Trans. of A.I.J. No. 215, 1974.1.
Part - 2 Analytical Study of Some Realistic Chimneys: Trans of A.I.J. No. 227, 1975.1.
4. P. Park, D. C. Kent "Reinforced Concrete Members with Cyclic Loadings" A.S.C.E. ST 1972.6.
5. P. C. Jennings "Earthquake Response of a Yielding Structure" A.S.C.E. EM 1965.8.
6. H. Aoyama "Moment-Curvature Characteristics of Reinforced Concrete Members Subjected to Axial Load and Reversal of Bendings" A.C.I. Sp-12 1965.
7. T. Takeda et. "Reinforced Concrete Response to Simulated Earthquake" A.S.C.E. 1970.12.

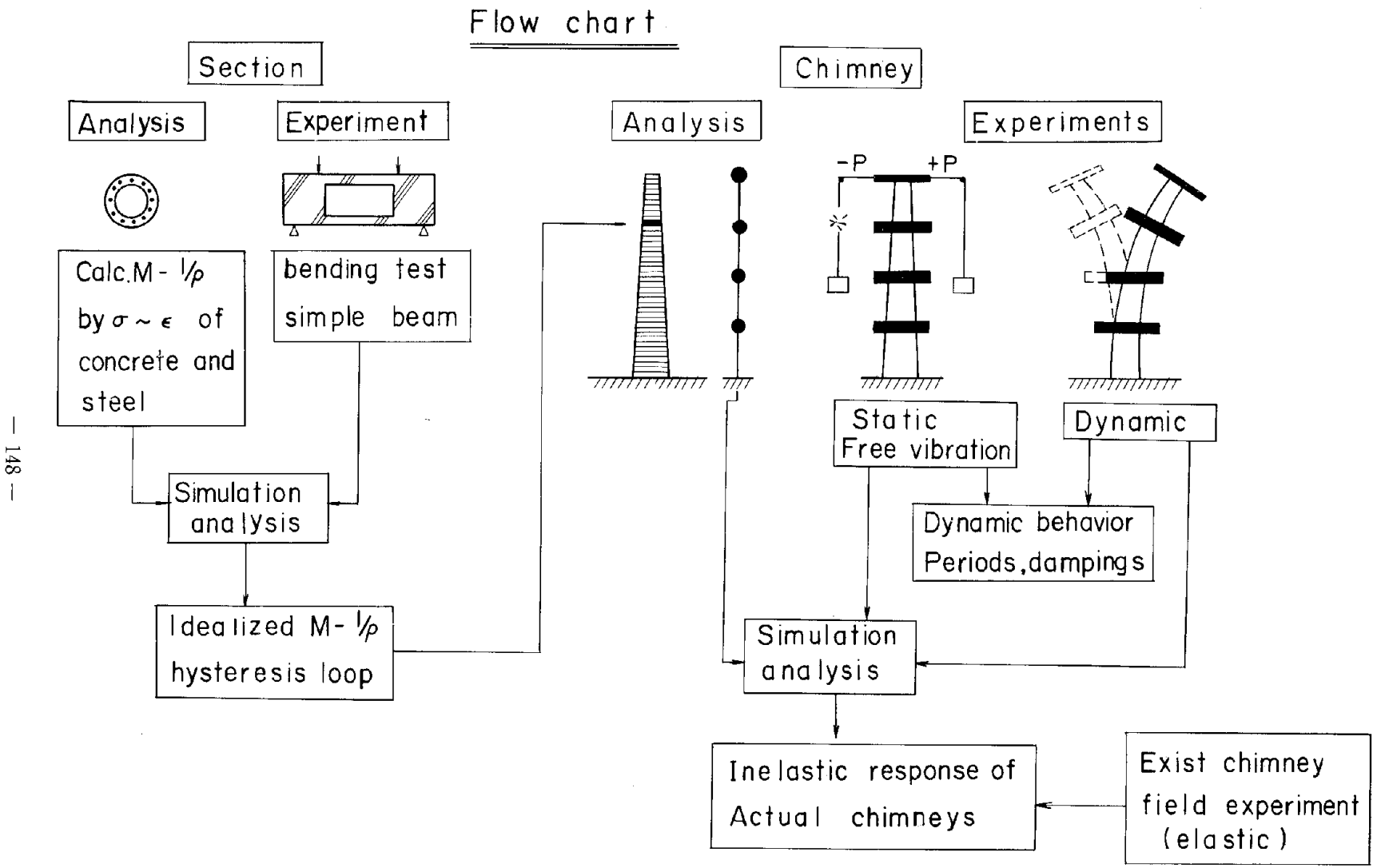


FIG. 1.1 The whole aspect of study

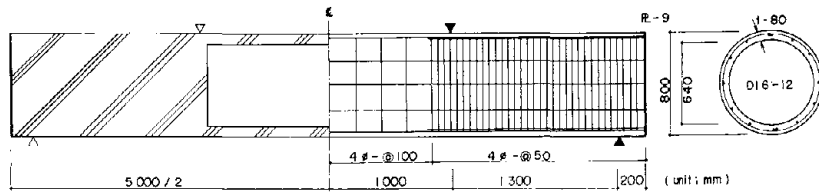


Fig.2.1 Specimen-M

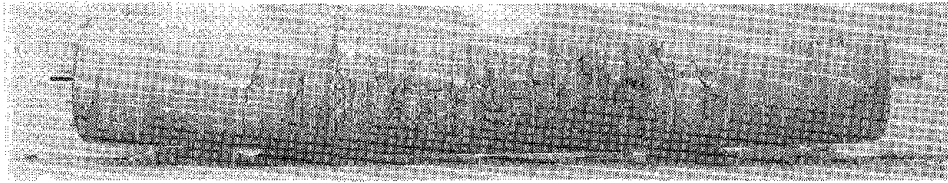


Fig.2.2 Final tested stage

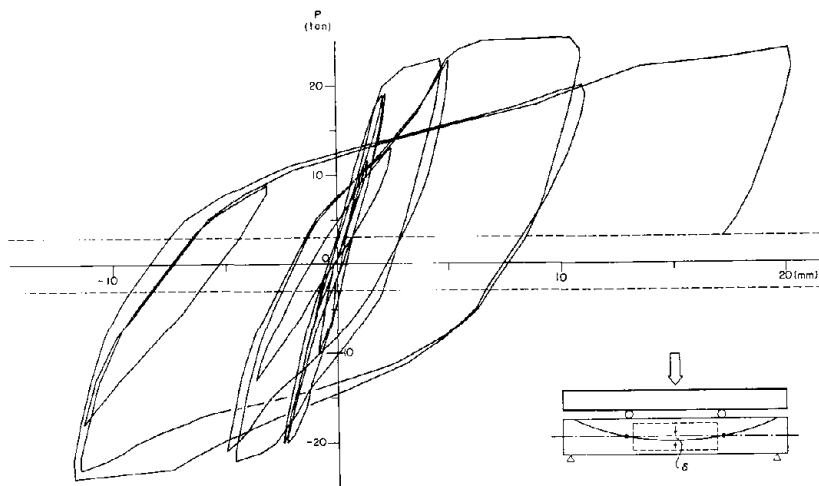


Fig.2.3 Load-Deflection relationship

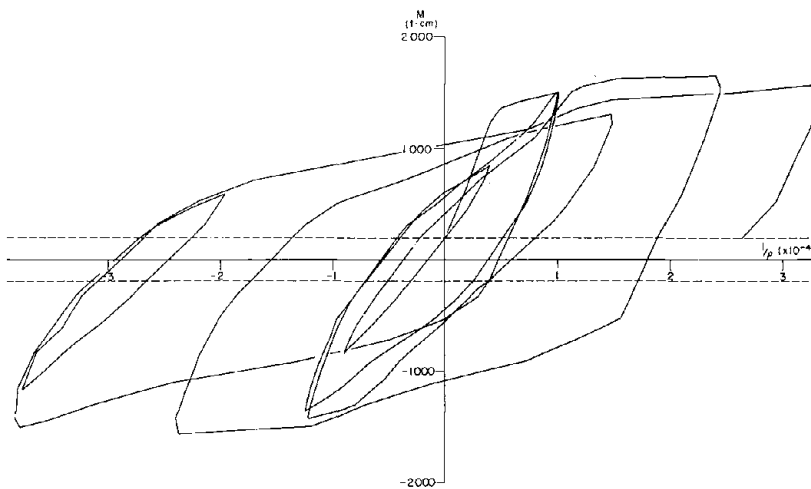


Fig.2.4 Moment-Curvature relationship (No.5-11 cycle)

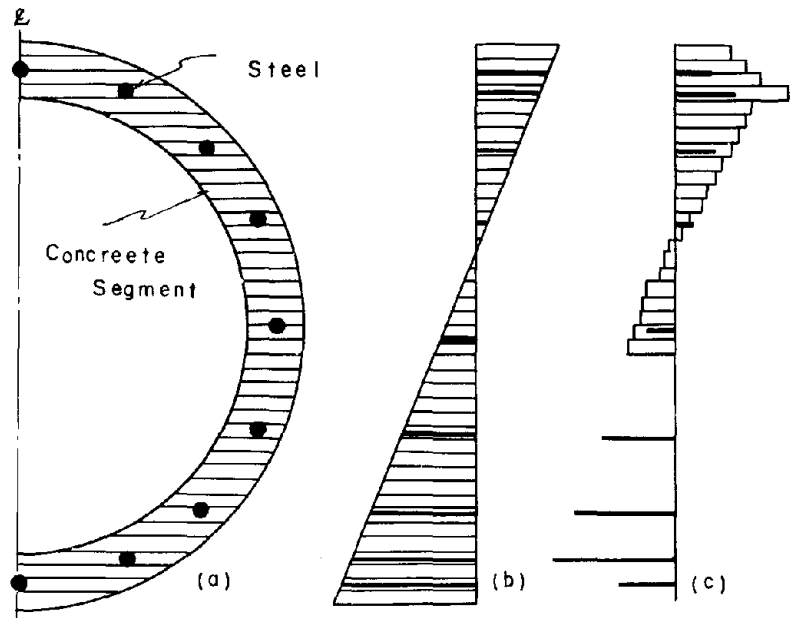


Fig.2.5 Section for analysis and stress-strain distribution

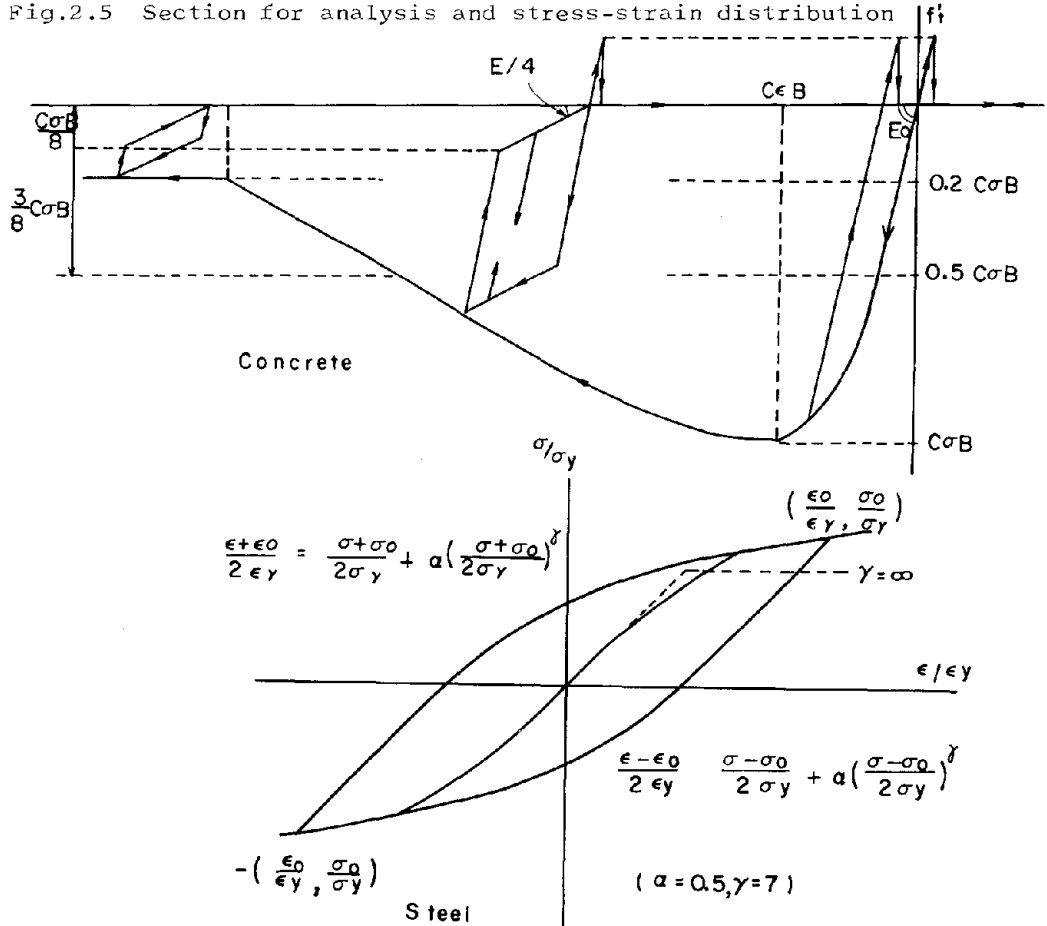


Fig.2.6 Assumed stress-strain relationship of concrete and steel

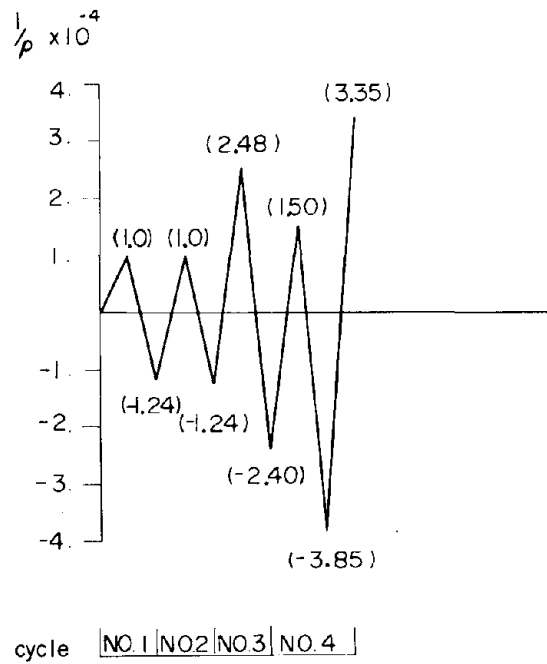


Fig.2.7 Specified curvature cycle for calculation

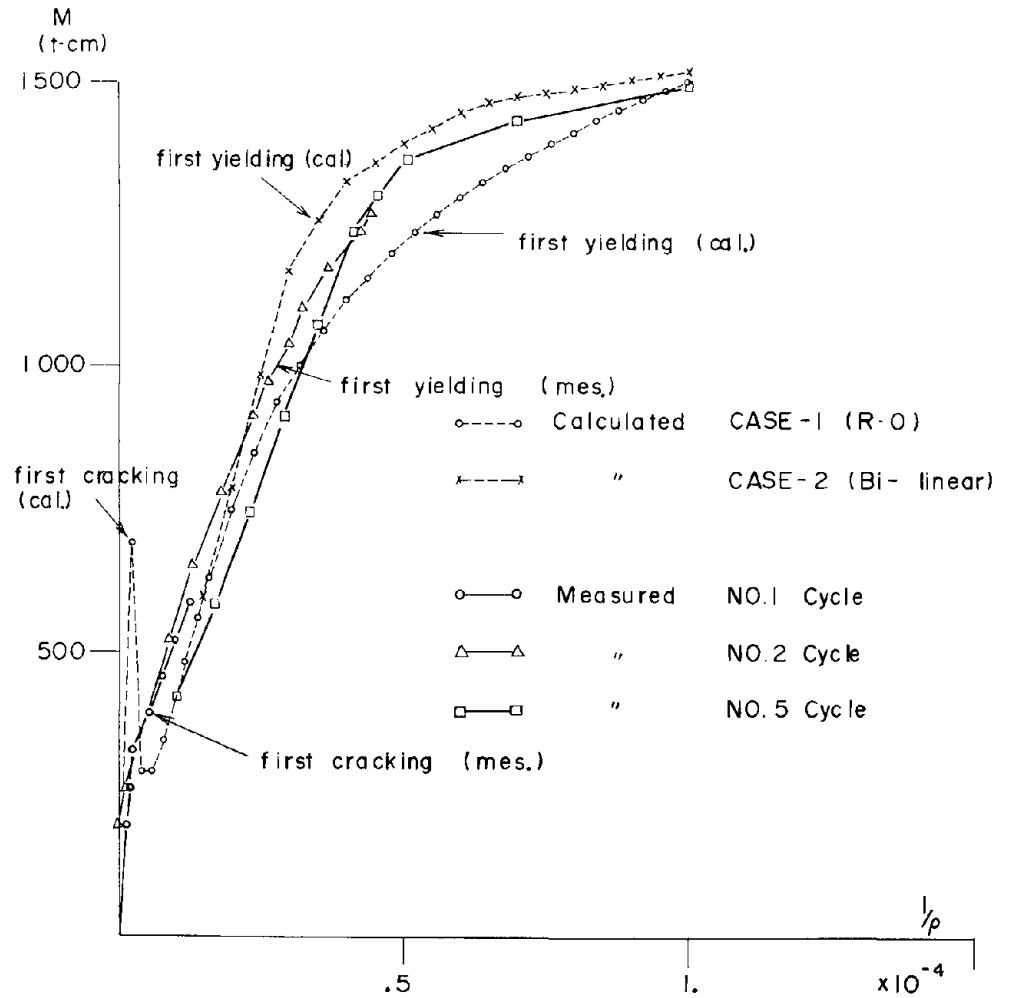
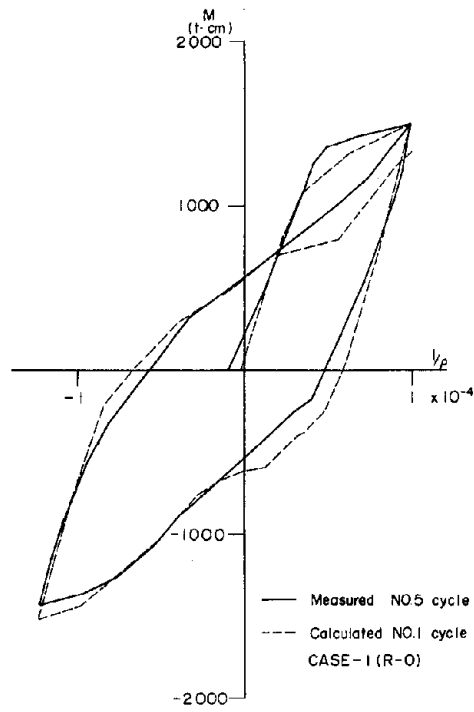
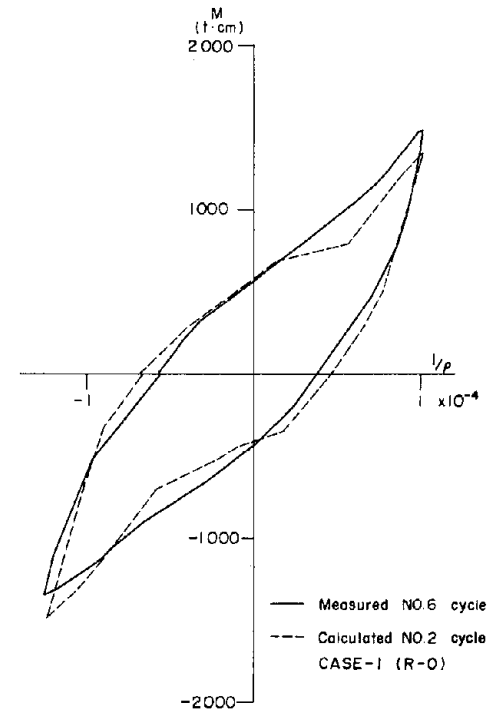


Fig.2.8 Comparison of skeleton curve



(a)



(b)

Fig.2.9 Comparison of hysteresis loop

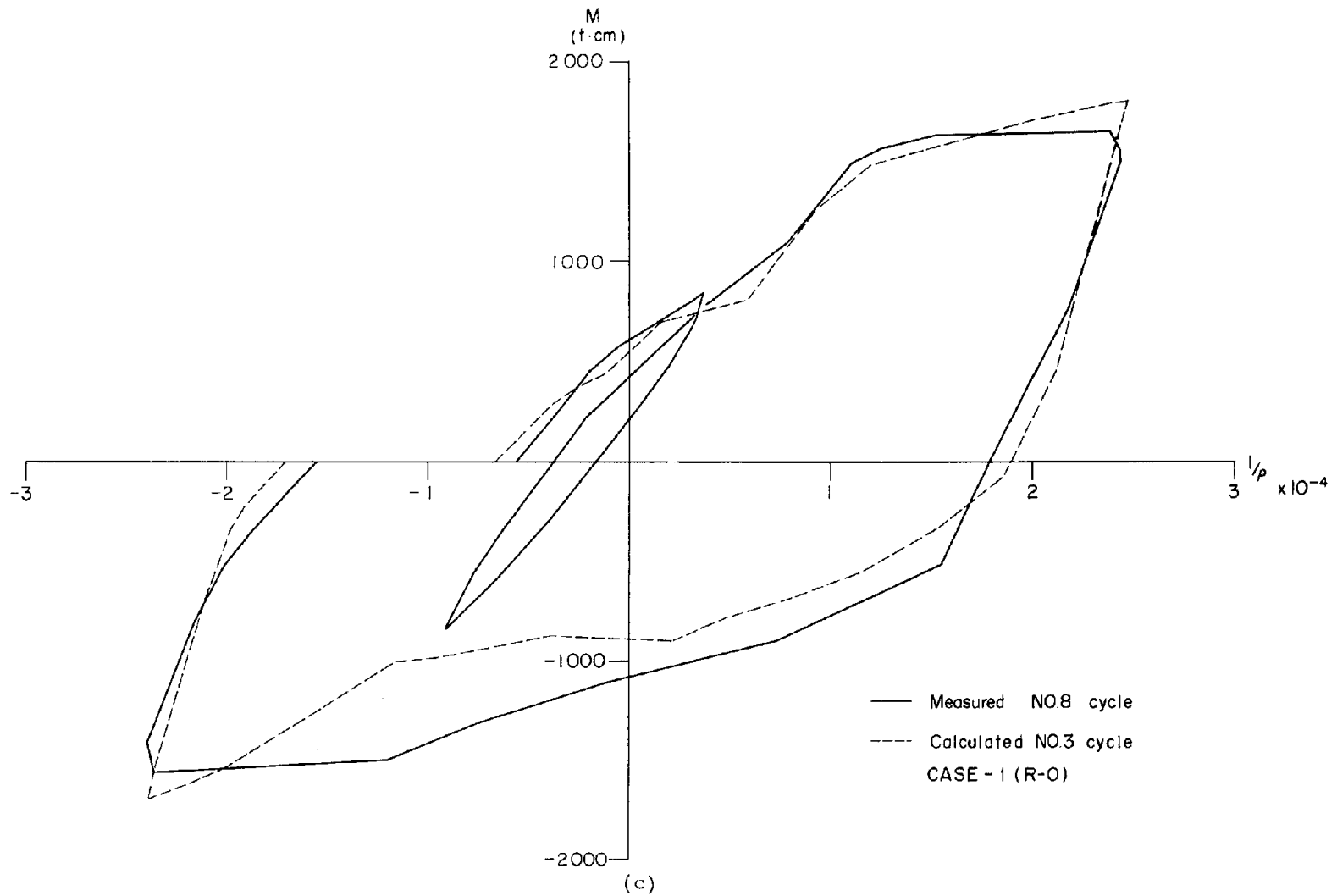


Fig.2.9 Comparison of hysteresis loop

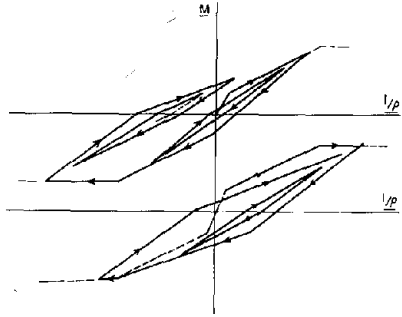


Fig.2.10 Idealized moment-curvature hysteresis loop

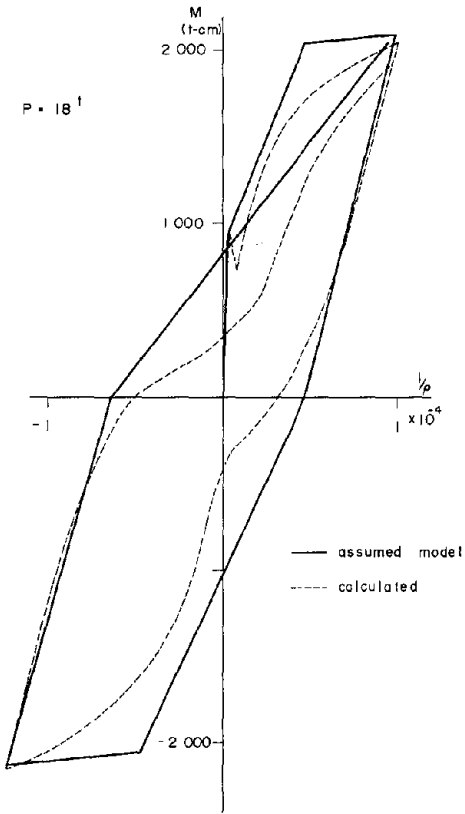
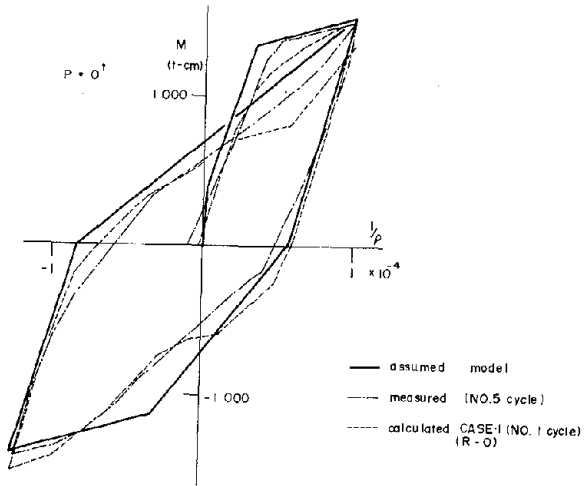


Fig.2.11 Comparison between the assumed model and the exact solution

Table 2.1 Material properties of specimen-M

Concrete	$E_c = 2.06 \times 10^5$	(kg/cm ²)
	$\sigma_{cy} = 243.7$	(")
	$\sigma_{ct} = 22.2$	(")
Steel	$E_s = 1.70 \times 10^6$	(")
	$\sigma_y = 3\ 236.$	(")
	$\sigma_{max} = 5\ 148.$	(")

Table 3.1 Material properties

Steel	Specimen	$sE (\times 10^6 \text{ kg/cm}^2)$	$s\sigma_y (\text{ Kg/cm}^2)$	$s\sigma_{max} (\text{ kg/cm}^2)$
	CSF, CSR - 1	1.75	2174.	3289.
CSR - 2,3	1.58	2715.	3707.	
Mortar	Specimen	$cE (\times 10^5 \text{ kg/cm}^2)$	$c\delta_{max} (\text{ kg/cm}^2)$	$c\delta_t (\text{ kg/cm}^2)$
	CSF	1.34	292.	16.3
	CSR - 1	1.77	259.	16.4
	CSR - 2	1.80	445.	22.4
	CSR - 3	1.90	337.	25.7

Table 3.2 Classification of tests

Specimen	Lines of experiment	Mark	Testing method
CSF	Static loading	S	Static cyclic loading of 1st. mode
	Free Vibration	F	Free Vibration tests under forced deflection by static loading
CSR	Free Vibration	F	Free vibration tests by slight power
	Steady state Vibration	S	Slight sin waves input of 0.5~5.0 HZ
	Random Vibration	R	Three specimens were tested by follow simulated earthquakes and repeated several times. changed by input-level.
CSR - 1 : E1 Centro 1940 NS (Run: R-1~R-5) CSR - 2 : Tokachioki 1968 Hachinohe Harbour (Run: R-1,2) CSR - 3 : Sin wave of 3 HZ. (Run: R-1) , 1.5 HZ (Run: R-2,3)			

Table 3.3 Experimental results of periods and dampings

CSF	mark *0	F-0				F-1	F-2	F-3				F-4	F-5							
	rotation angle					$1/526$	$1/267$	$1/48$				$1/46$	$1/29$							
	period	T1 sec	0.27			0.34	0.36	0.44				0.58	0.68							
	damping	T1/To ^{*1}	0.966			1.217	1.288	1.574				2.075	2.433							
	h1				0.031	0.040	0.051				0.059	0.071								
CSR-1	mark	F-1	Pulse	F-1'	S-1	R-1	F-2	S-2	R-2	F-3	S-3	R-3	F-4	S-4	R-4	F-5	S-5	R-5	F-6	S-6
	rotation angle					$1/53$			$1/126$			$1/62$			$1/52$			$1/40^{over}$		
	period	T1 sec	0.22	0.33	0.33		0.33	0.33		0.33	0.40		0.39	0.44		0.42	0.56		0.46	0.56
		T2			0.067			0.067			0.077			0.083			0.092			0.10
		T3			0.025			0.027			0.029			0.032			0.036			0.036
		T1/To ^{*2}	0.919	1.378	1.378			1.378	1.378	1.671		1.629	1.838		1.754	2.339		1.921	2.339	
	damping	h1	0.011	0.028	0.037		0.022	0.037		0.026	0.083		0.031	0.080		0.023	0.167		0.172	
		h2			0.033			0.053			0.063			0.058			0.091		0.075	
		h3			0.091			0.090			0.051			0.040			0.062		0.064	
	CSR-2	mark	F-1	S-1									R-1	F-2	S-2	R-2	F-3	S-3		
rotation angle												$1/72$			$1/55$					
period		T1 sec	0.235	0.238									0.43	0.526		0.44	0.588			
		T2		0.053										0.091			0.100			
		T3		—										0.029			0.037			
		T1/To ^{*3}	0.989	1.002									1.810	2.216		1.852	2.476			
damping		h1	0.021	0.034									0.048	0.097		0.054	0.103			
	h2		0.041									0.064			0.061					
	h3		—									0.050			0.067					
CSR-3	mark	F-1	S-1									R-1	F-2	S-2	R-2			R-3	F-3	S-3
	rotation angle											$1/56$			$1/56$			$1/55$		
	period	T1 sec	0.235	0.233									0.52	0.556					0.71	0.735
		T2		0.050										0.101						0.102
		T3		—										0.030						0.030
		T1/To ^{*4}	1.016	1.006									2.249	2.403					3.071	3.180
	damping	h1	0.023	0.026									0.04	0.100					0.063	0.085
	h2		0.040										0.043						0.041	
	h3		—										0.067						0.044	

*0 mark : F: Free vibration S: Steady state vibration R: Random vibration

* To : elastic natural period by calculation $\times 1 = 0.2795(\text{sec})$ $\times 2 = 0.2394(\text{sec})$ $\times 3 = 0.2376(\text{sec})$ $\times 4 = 0.2312(\text{sec})$

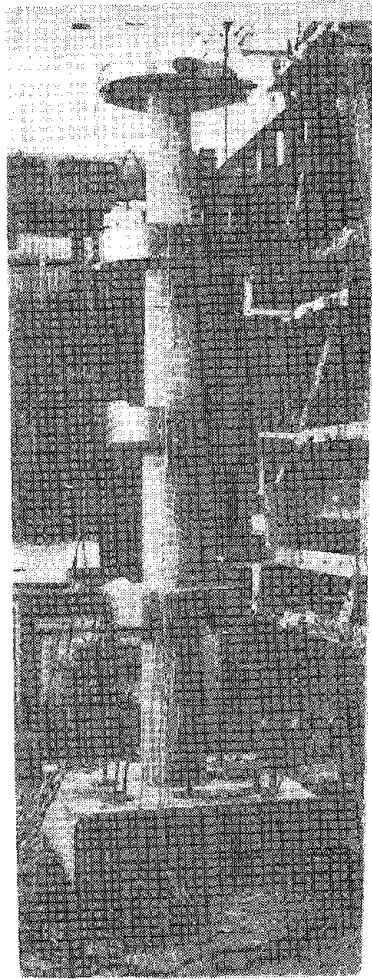


Fig.3.1 Tested chimney model

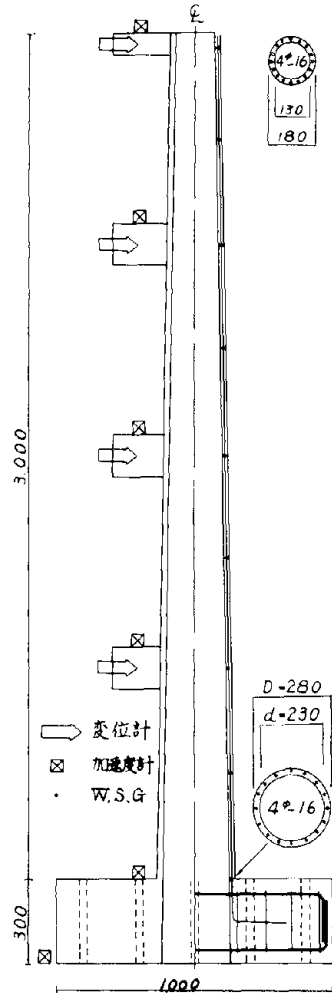


Fig.3.2 Model section

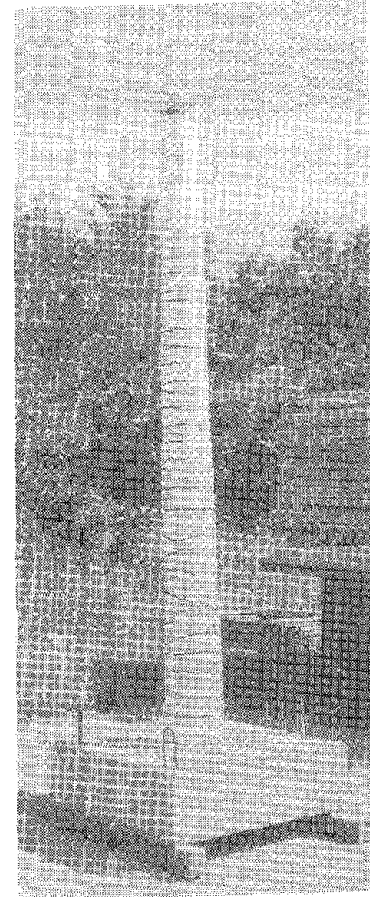


Fig.3.3 Cracked picture
in case of specimen-CSR-2

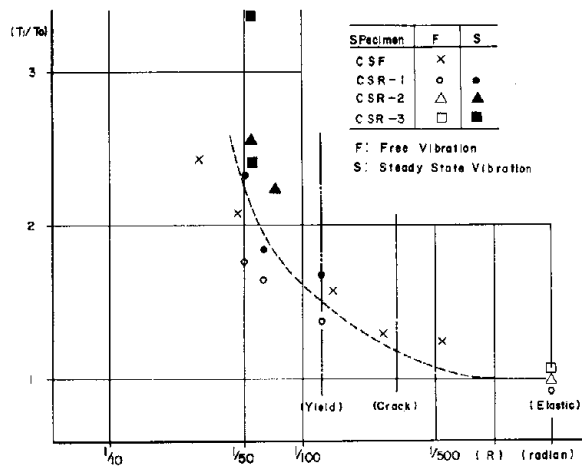


Fig.3.4 Experimental results between $R - T_1 / T_0$

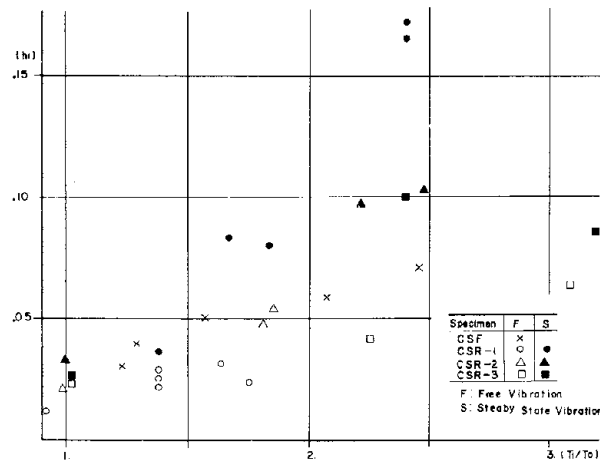


Fig.3.5 Experimental results between $T_1 / T_0 - h_1$

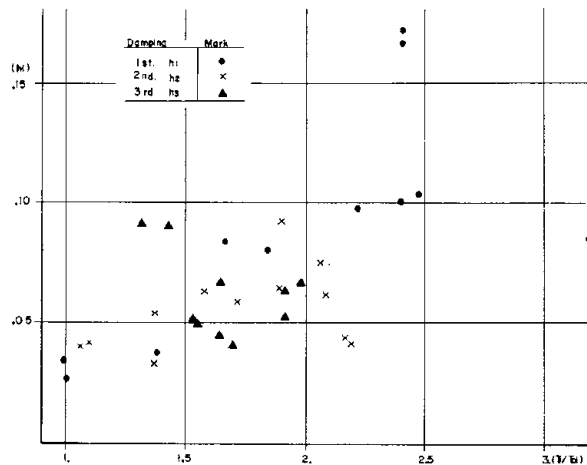


Fig.3.6 Experimental results between $T_1\lambda / T_0\lambda - h_1$

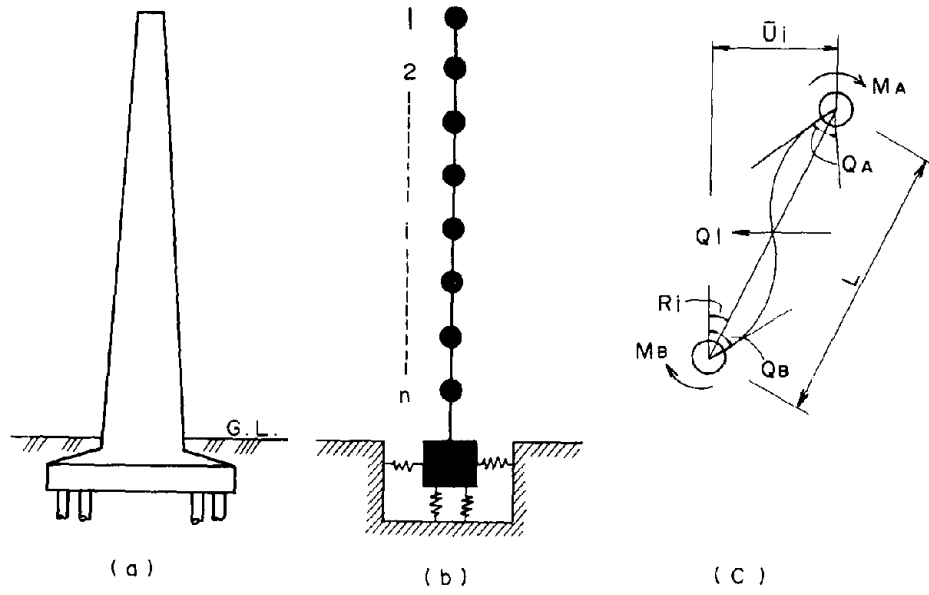


Fig.4.1 Mathematical model for response calculation

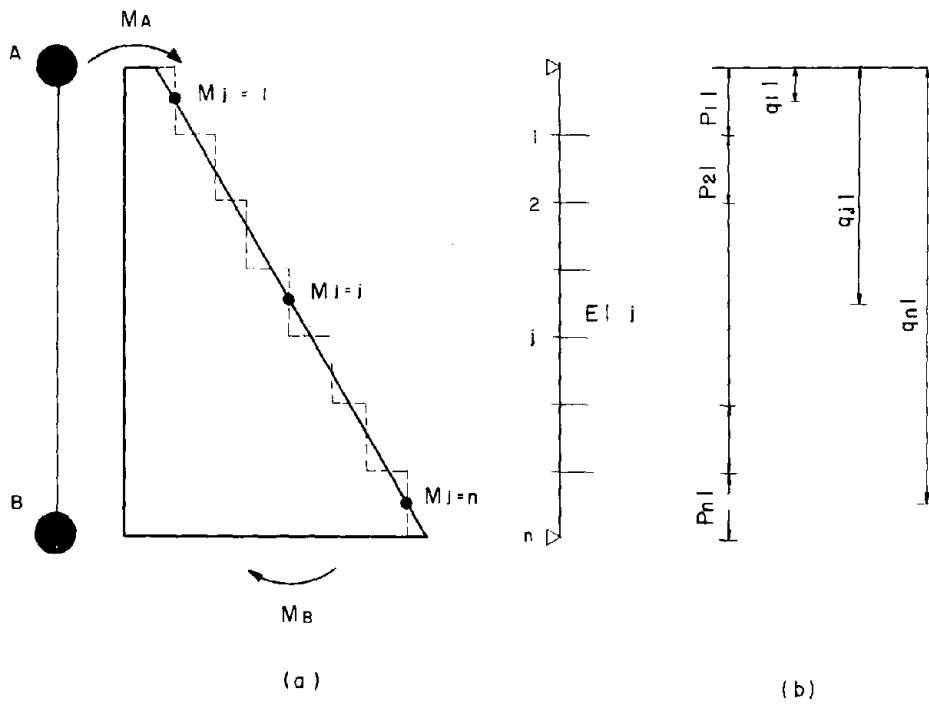


Fig.4.2 Idealized sub-element

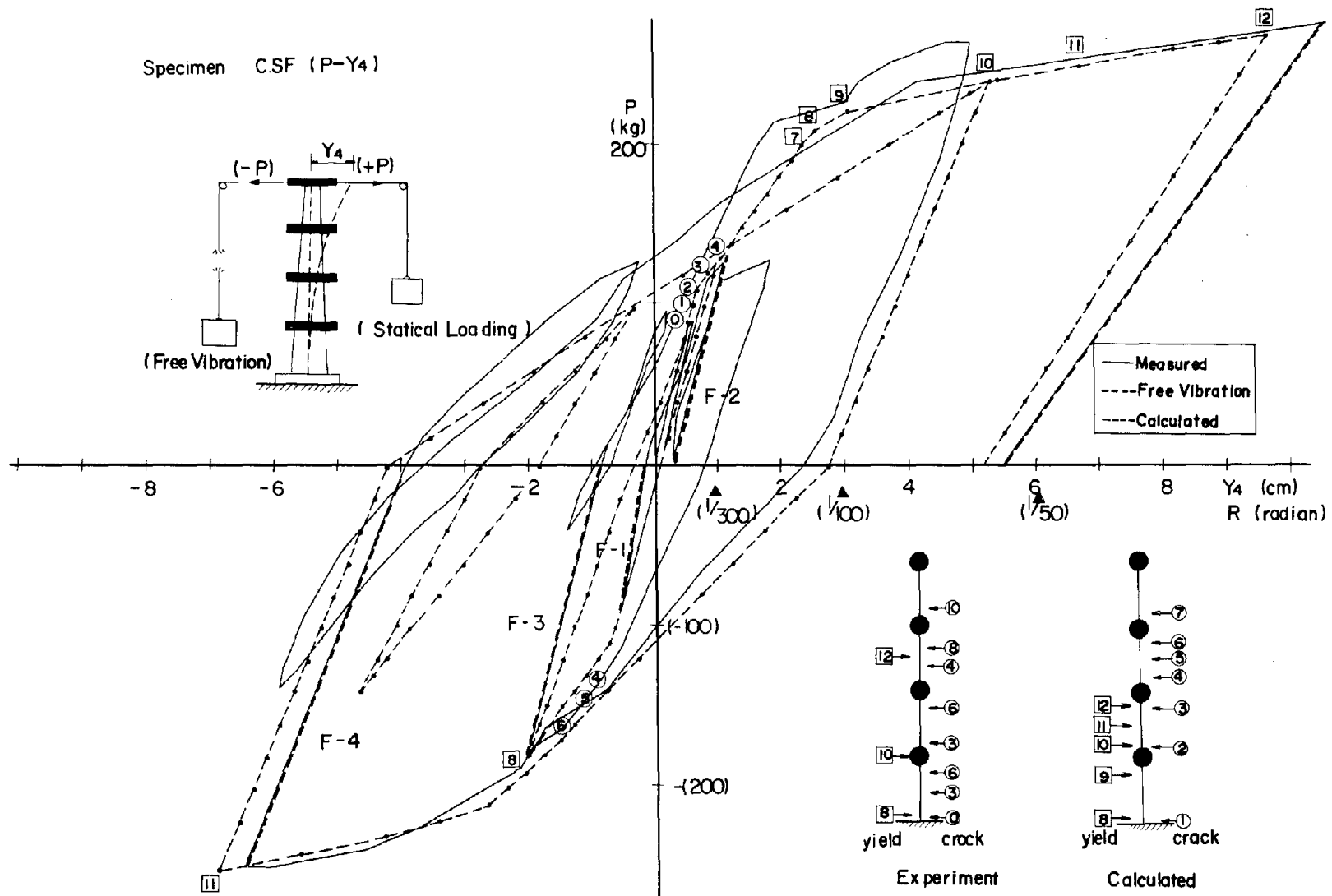


Fig.4.3 Load-deflection relationship of Specimen-CSF

Table 5.1 Maximum response value

Specimen			Run	Max. Response value of displacement (CM)				Max. Response value of acceleration (GAL.)			
				Y ₄	Y ₃	Y ₂	Y ₁	ÿ ₄	ÿ ₃	ÿ ₂	ÿ ₁
CSR-1	measured	G.-ACC. (215 GAL.)	R-2	2.375	1.250	0.840	0.258	1190.	730.	660.	410.
		(410 GAL.)	R-3	4.820	2.655	1.790	0.756	1650.	900.	820.	618.
	calculated	h ₁ = 0.02	R-2	3.619	2.542	1.489	0.541	764.	518.	455.	551.
		h ₂ = 0.02	R-3	7.147	5.032	2.965	1.071	1380.	586.	788.	639.
CSR-2	measured	G.-ACC. (823 GAL.)	R-1	4.194	3.150	1.800	0.885	1225.	731.	539.	744.
		(993 GAL.)	R-2	5.418	4.451	2.422	1.112	2177.	794.	—	—
	calculated	h ₁ = 0.02	R-1	4.532	3.145	1.822	0.634	1557.	682.	1056.	1104.
		h ₂ = 0.02	R-2	6.044	3.860	2.212	0.747	2508.	1112.	1648.	1815.
CSR-3	measured	G.-ACC. (200 GAL.)	R-1	3.048	1.868	—	—	933.	563.	—	—
	calculated	h ₁ = 0.02 h ₂ = 0.02	R-1	3.160	2.159	1.203	0.374	750.	447.	345.	258.

TOKACHI 1968 HACHINOHE HARBOUR NS

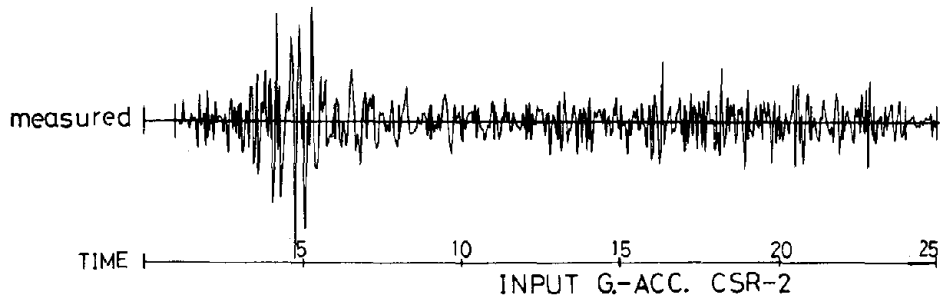


Fig.5.1 Input base acceleration (CSR-2,RUN-1)

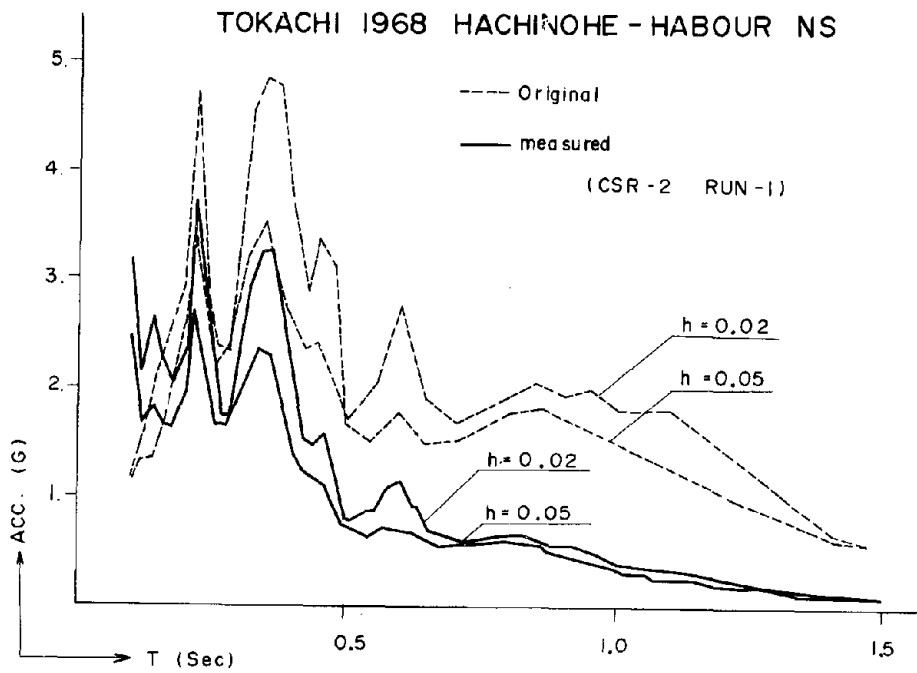


Fig.5.2 Accelation spectrum (CSR-2,RUN-1)

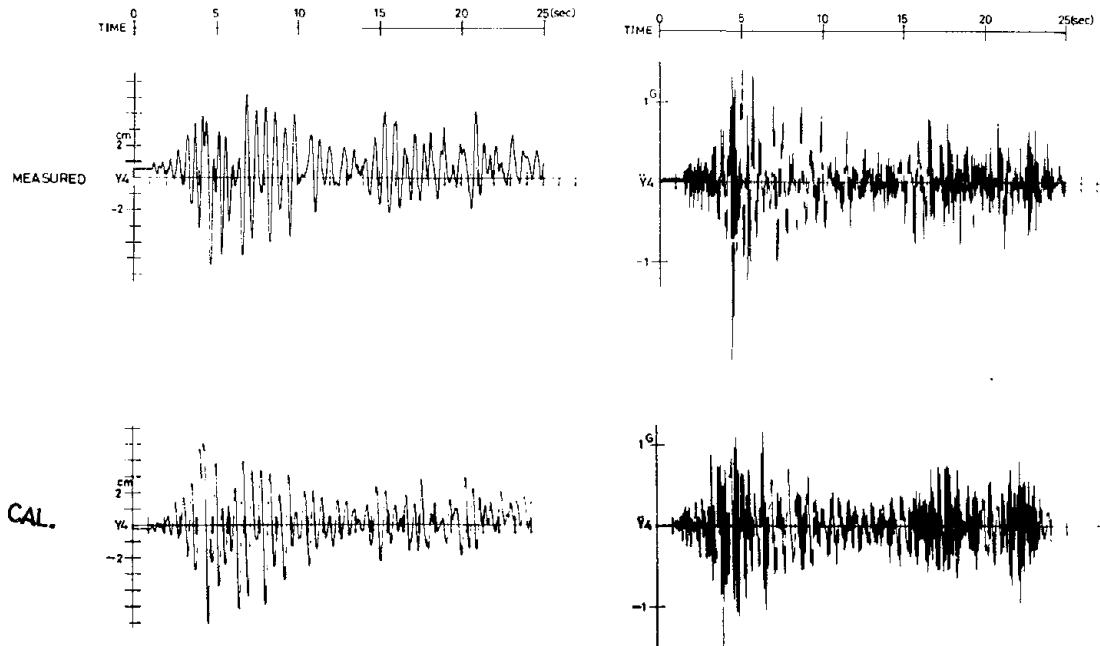
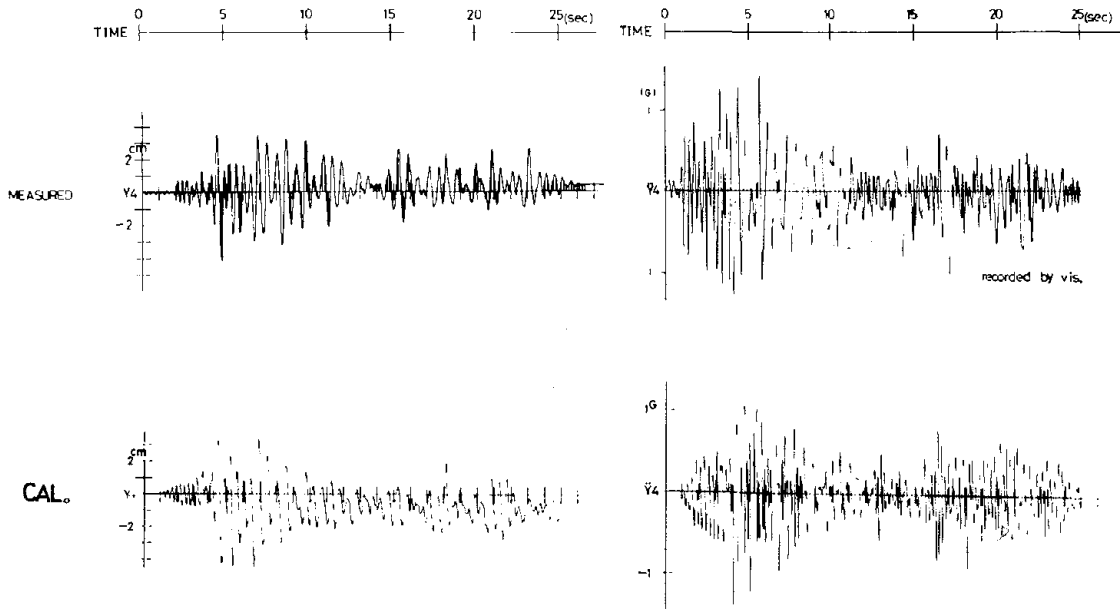


Fig.5.3 Displacement and acceleration wave form of the top mass in case of specimen-CSR-2

9 ASEISMIC MEASURES FOR REINFORCED CONCRETE STRUCTURES

(Supplement)

— IN VIEW OF DAMAGE FROM OITA EARTHQUAKE OF 1975 —

Hajime Umemura^I

INTRODUCTION

In January of 1969, the year after the Tokachioki Earthquake of 1968 had occurred, the Special Committee on Aseismic Measures for Reinforced Concrete Structures of the Architectural Institute of Japan published "Aseismic Measures for Reinforced Concrete Structures — In View of Damage from Tokachioki Earthquake of 1968 —,"¹⁾ and tentatively classified buildings which had then been designed according to the four types below,

Type I : Building of high rigidity having a large wall area

Type II : Building having walls to some extent or frame-type building of high rigidity

Type III : Pure frame building having no walls

Type IV : High-rise building

It was pointed out that Type I buildings were mostly undamaged in the earthquake, that Type II buildings if having wall ratios and wall-column ratios above certain values escaped damage, and that with Type III buildings columns were crushed or concrete failed as far inside as cores of columns. As measures to be taken to prevent such damage, it was called for that rising and hanging spandrel walls be taken into structural calculations, and that shear reinforcing bar quantities be increased arranging the bars effectively. Later, taken into consideration the experiences of the San Fernando Earthquake, the Standards for Design of Reinforced Concrete were revised in 1971 incorporating the abovementioned two measures in the standards, while quantities of hoop reinforcement for columns were greatly increased.

Subsequently, various committees aiming for establishment of new earthquake-resistant design methods were initiated in the Earthquake-Resistant Technology Division, Construction Techniques Development Council, Ministry of Construction, and comprehensive research based on a five-year plan has been carried out with much cooperation from private sectors. The final year of the five-year plan will be 1976.

Meanwhile, the Ministry of Education also commissioned the Architectural Institute of Japan to work on "Reinforced Concrete School Building Earthquake Resistance Diagnosis and Reinforcement Methods,"²⁾

I. Professor, Faculty of Engineering, University of Tokyo

and the Institute printed and published a pamphlet by that title in June 1975.

Also, in the Architectural Institute of Japan, a Joint Committee on Earthquake Loads cutting across the various sectional committees was organized in the Committee on Structural Standards and a draft was prepared on Earthquake Load Standards which is now at the stage of undergoing deliberations.

It was at such a time that the Oita Earthquake occurred on April 21, 1975, in which part of a reinforced concrete hotel building having one basement story and four stories above ground collapsed.

OUTLINE OF DAMAGE, CAUSES, AND POINTS REQUIRING ATTENTION

Outline of Damage and Causes Thereof

The earthquake is said to have had its epicenter at 33°10' north latitude and 131°25' east longitude, with the magnitude being not more than 6.4 and the focus at a depth of 20 kilometers.

The building was located at a point several kilometers from the epicenter. The foundation of the building was a raft foundation resting on the consolidated soil cement of 45-centimeter thickness, and columns were connected by tie beams of 1-meter depth built monolithically with the raft foundation.

The basement and first story was 73.5 meters by 38.8 meters while the superstructure from the second story was 60 meters by 17.2 meters. The structure above the first floor was divided by expansion joints into three blocks, A, B and C, in order from the west side (Fig. 1).

Block A consisted of 6 spans (5 spans in the second story and above), Block B of 2 spans including a staircase, and Block C of 6 spans (5 spans in the second story and above) with the first story of this block a lobby with small wall area. The second story and above were comprised of guest rooms having relatively large wall areas.

The building was designed in 1964 and completed in 1966 and thus was built before the revision of the AIJ Standards in 1971. The design seismic coefficient was 0.16. There was ample strength of concrete and workmanship was good.

The damage consisted of collapse of the first story of Block C (Fig. 2). The ultimate strength of this collapsed portion in terms of base shear coefficient was approximately 0.55 at the displacement corresponding to the failure of shear walls. At the greater displacement corresponding to the yielding of frames, it reduced to about 0.15.

Photo 1 shows the building before the earthquake. Photos 2 to 6 shows damages.

The causes of the damage which can be estimated at present are the followings:

1. The input earthquake motion, as estimated from the nonlinear response analysis, was of maximum acceleration of more than 400 gal.
2. The collapsed portion had little wall area and included two spans of short columns with this part thought to have failed first in shear followed by collapse of ordinary columns.
3. The quantities of hoops in ordinary columns were small.
4. The predominant period of the ground surface stratum was about the same as the natural period of the superstructure.
5. The vibration mode of the first story of the superstructure was larger compared with the vibration modes of other stories.
6. The axial forces at the first-story columns were larger compared with columns in general being in the order of 50 kilograms per square centimeter.

Points Requiring Attention

1. The building was constructed before revision of the AIJ Standards in 1971.
2. The building was designed with seismic coefficient of 0.16, and with the same input to the three blocks of A, B and C, Block C collapsed, Block A was severely damaged and Block B was moderately damaged.
3. It is thought Block C, at the initial stage of the earthquake, was Type II out of the four types described in the Introduction, after which it changed rapidly into Type III, a behavior which had not been considered very much in the past, and this phenomenon should be reflected in some way in regulations on earthquake load in the future.
4. The characteristics of moderate-scale, close-distance earthquake waves should be clarified and reflected in artificial earthquake waves.

It is necessary for modifications to be made at an early date in the currently-used earthquake-resistant design method taking into consideration the recent experience of the Oita Earthquake and the research carried out since the Tokachioki Earthquake. The principles would be the following.

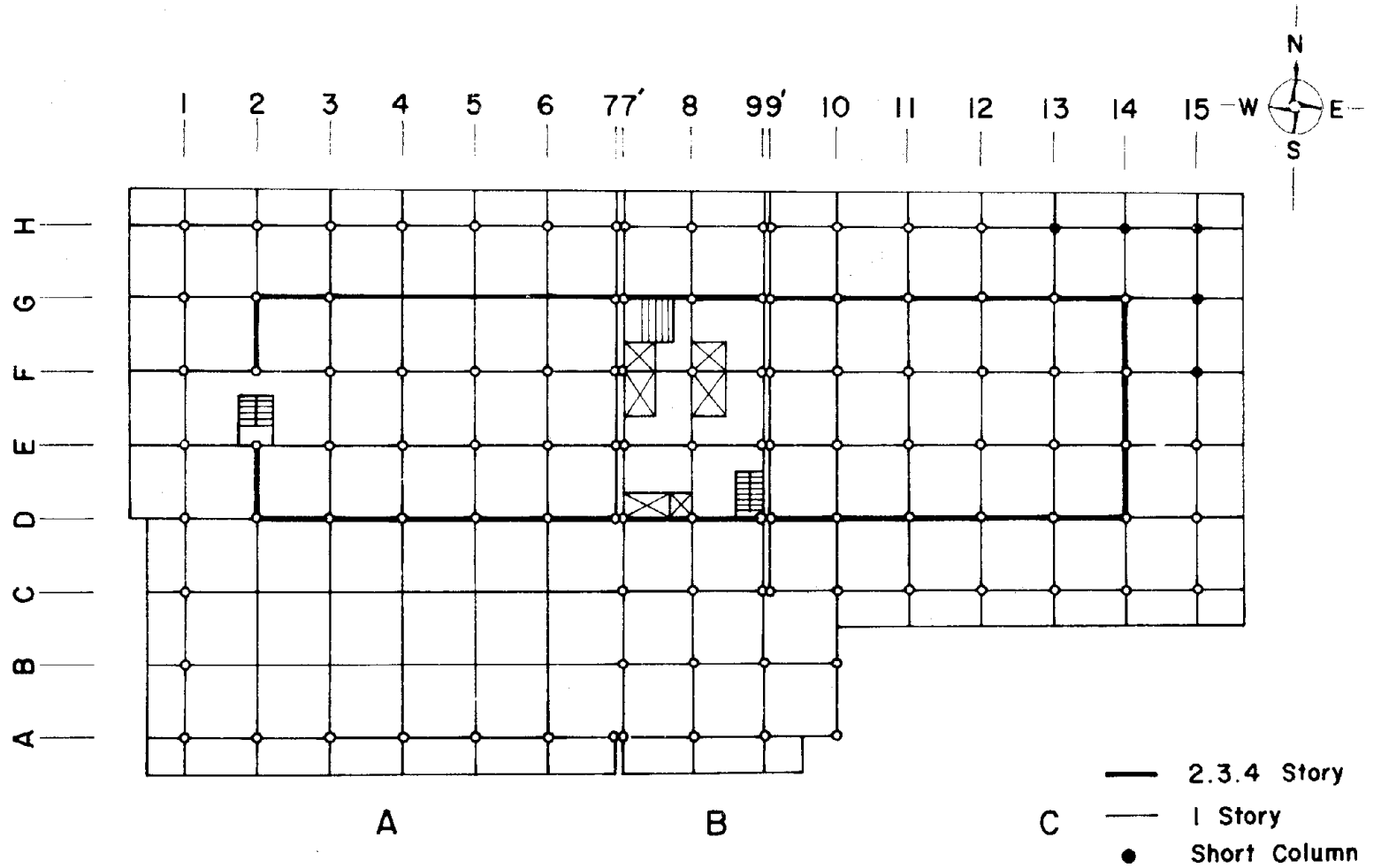
- (1) For ordinary buildings, the current seismic coefficient regulations and design calculations are to be maintained in carrying out designing.

- (2) The safety as Type I of a building designed according to (1) is to be secured from the provisions regarding wall area.
- (3) The safety of a building outside the scope of securing safety as Type I according to (2) above, is to be secured as Type II from regulations on wall-column ratios.
- (4) Buildings outside the category of safety secured as Type I or II are to be considered as being Type III, and the safeties of these buildings are to be secured by (a) and (b) of the third-stage method of determination in the "Reinforced Concrete School Building Earthquake Resistance Diagnosis and Reinforcement Methods."(Note)
- (5) Buildings which cannot be assured of safety even by (4) above, are to be made safe in accordance with the Earthquake Load Standards of the Architectural Institute of Japan.

Note: The ultimate strength of a building is calculated separating columns and walls into bending type and shearing type, determining the building to be safe if the values are higher than the standard values.

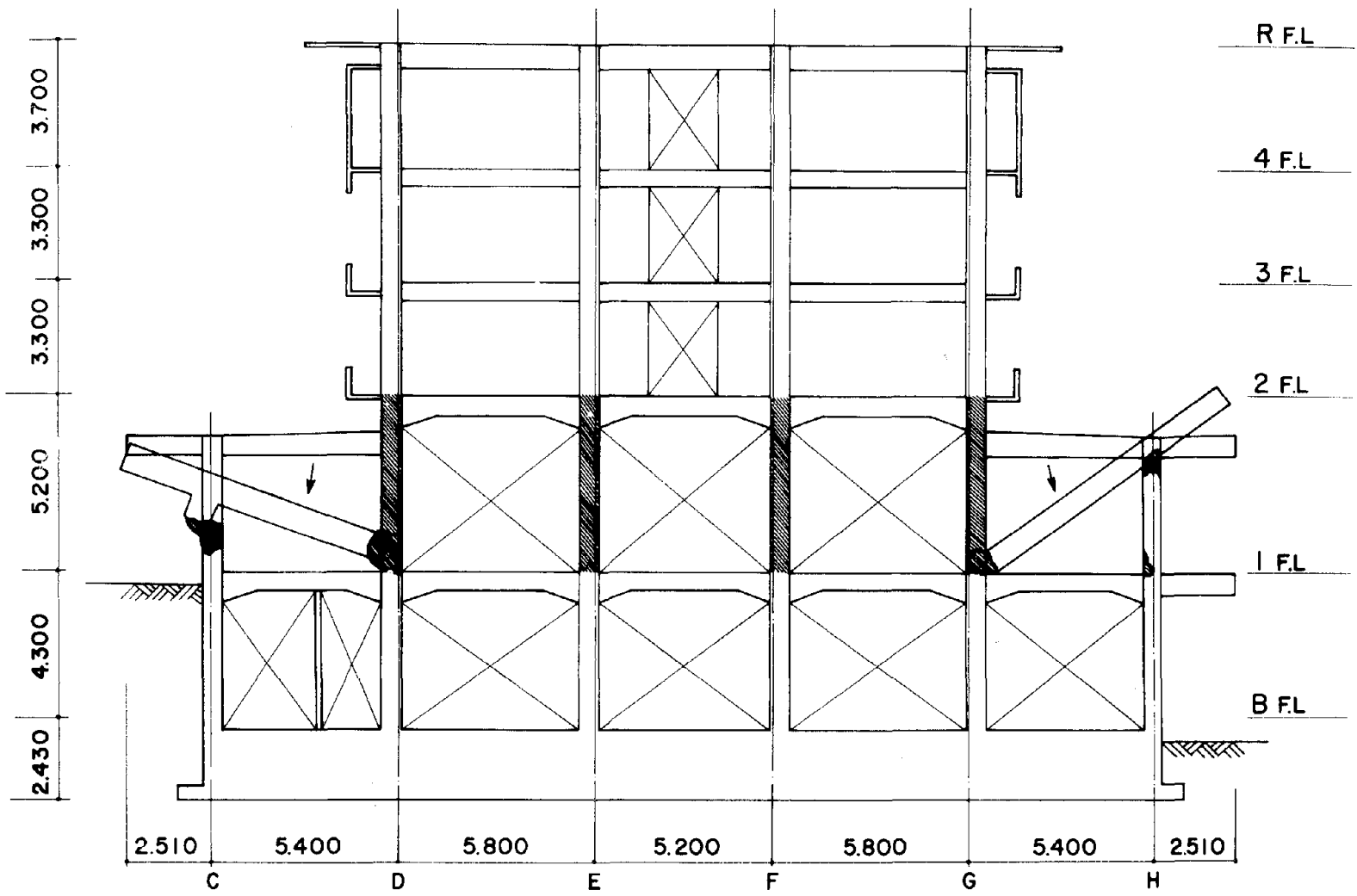
REFERENCES

- 1) Journal of Architecture and Building Science, Architectural Institute of Japan, January 1969.
- 2) M. Hiroswa, Y. Higashi, K. Ogura and S. Kokusho, "An Evaluation Method of Earthquake Resistant Properties of Existing Reinforced Concrete School Buildings," Review Meeting, U. S.-Japan Co-operative Research in Earthquake Engineering with Emphasis on the Safety of School Buildings, August 1975, Honolulu, Hawaii



Plan of the Lake - Side Hotel

Fig. 1 Plan of the Lakeside Hotel Building



Section of the Lake - Side Hotel

Fig. 2 Section of the Lakeside Hotel Building

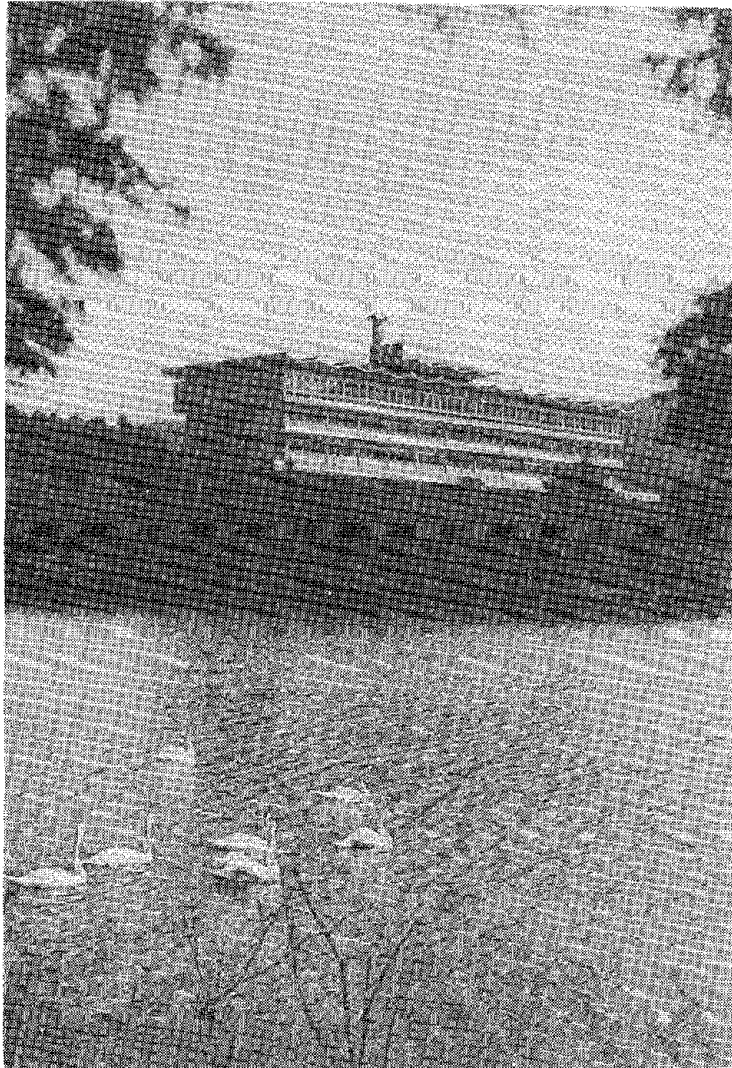


Photo 1 Lakeside Hotel before the April 21, 1975, Earthquake

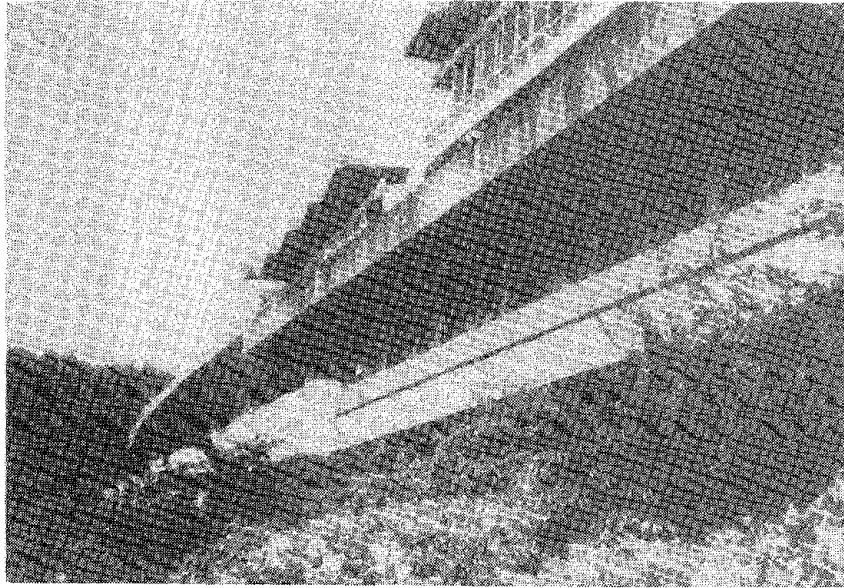


Photo 2 Damage Seen from the North Side

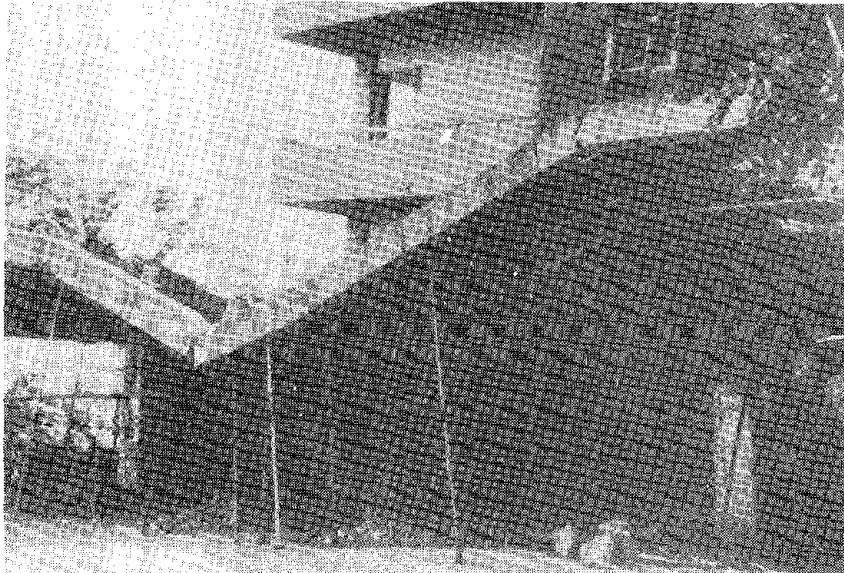


Photo 3 Damage Seen from the East Side

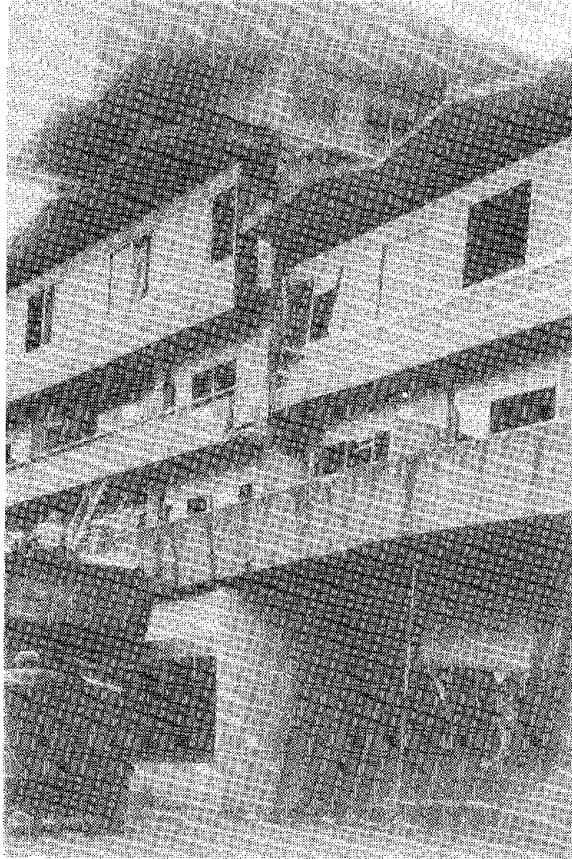


Photo 4 Damage Seen from the South Side

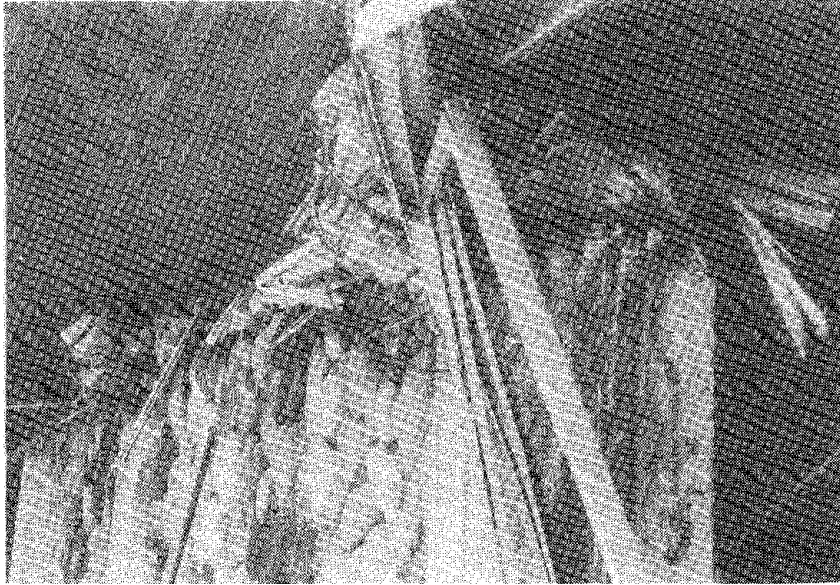


Photo 5 Failure of Short Column in the First Story
(North Side)

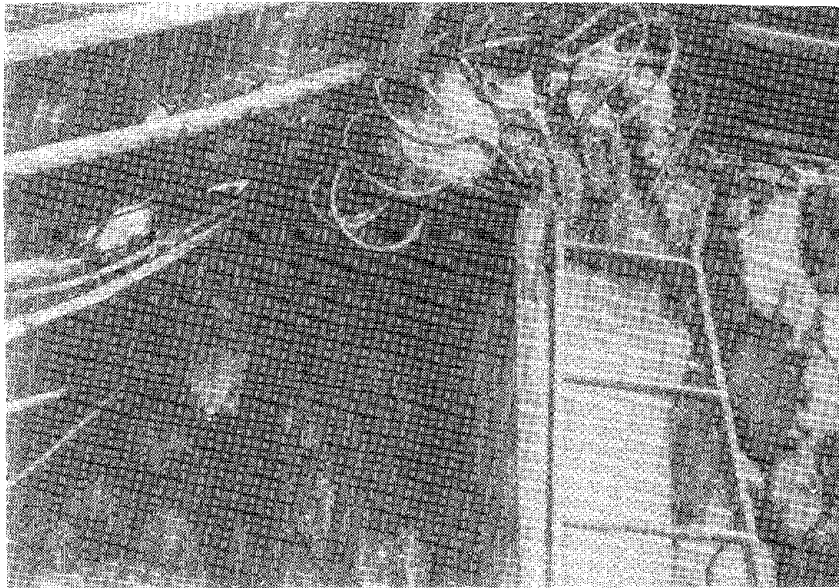


Photo 6 Failure of Short Column in the First Story
(East Side)

OF EXISTING REINFORCED CONCRETE SCHOOL BUILDINGS

by

Masaya Hirose^I, Yoichi Higashi^{II},
 Koichiro Ogura^{III} and Seiji Kokusho^{IV}

SYNOPSIS

This paper presents an evaluation method of earthquake resistant properties of the existing reinforced concrete school buildings. First of all, the lateral resistance of building is evaluated by a simple calculation. If the lateral strength is not sufficient to the expected response force excited during a strong earthquake, the building shall be investigated whether its columns will fail by the shear force or not, and the building with columns of mode of shear failure shall be investigated in further details. The building, which is found un-safe against a future strong earthquake, shall be strengthened by an appropriate method.

INTRODUCTION

In Tohoku and Hokkaido districts of Japan, several reinforced concrete school buildings, designed in accordance with the existing regulations, suffered serious damages due to the 1968 Tokachi-oki Earthquake. In order to prevent the existing reinforced concrete buildings from such serious damages due to a strong earthquake, studies have been made on the evaluation methods of the earthquake resistant properties.

Since 1972, studies have been carried out by the 5th Committee for School Buildings, Architectural Institute of Japan^V, in compliance with the request of the Ministry of Education, Japanese Government. This paper is an abstract of the report¹⁾ of the 5th Committee. One of

-
- I : Chief Research Member, Building Research Institute, Ministry of Construction, Japanese Government
 II : Professor, Department of Architecture, Faculty of Engineering, Tokyo Metropolitan University
 III: Professor, Department of Architecture, Faculty of Engineering, Meiji University
 IV : Professor, Department of Architecture and Building Engineering, Faculty of Engineering, Tokyo Institute of Technology
 V : Chairman : Y. Higashi
 Secretary : S. Kokusho
 Members : H. Aoyama, H. Endoh, M. Fukuhara, M. Hirose,
 T. Kameda, T. Katoh, M. Kitahara, T. Minami,
 T. Mukai, M. Murakami, M. Nakao, K. Oami,
 K. Ogura, M. Ohkubo, K. Osada, Y. Ohsawa and
 A. Yoshida

the most practical and simple evaluation methods of earthquake resistant properties of the existing reinforced concrete school buildings, whose properties are fixed by the strength of columns and shear walls, is described in this paper.

In order to evaluate the earthquake resistant properties of the existing buildings, an investigation of the structural drawings shall be made in regards to such structural defects as deformations, cracks, etc., and to check the possibility of such ground failures as landslide, collapse of precipice and soil liquefaction. The investigation of the lateral resistance of the building shall be made by the following steps. If the building is evaluated un-safe by the 1st step, the investigation of the next step is required, successfully.

1st step: The investigation of the horizontal sectional area of shear walls on each floor.

2nd step: The investigation of the approximate strengths of the shear walls and the columns on each floor against the horizontal force.

3rd step: The investigation of the strengths of the shear walls and the columns on each floor against the horizontal force, taking account of the fracture mode and ductility of the members.

4th step: The investigation of the 1st and 2nd steps taking account of the predominant period of the ground.

The results of the investigation of the existing reinforced concrete school buildings by this evaluation method are described in this paper with respect to the damages due to the 1968 Tokachi-oki Earthquake.

NOTATIONS

- A_c : sum of sectional area of column on the floor (cm^2)
- A_{w1} : sum of sectional area of shear wall with columns at both ends in each of lengthwise and widthwise directions on the floor (cm^2)
- A_{w2} : sum of sectional area of shear wall without columns at both ends in each of lengthwise and widthwise directions on the floor (cm^2)
- a_s : sectional area of reinforcement in shear wall (cm^2)
- a_t : sum of sectional area of tensile reinforcement in column (cm^2)
- a_w : sectional area of a group of shear reinforcement in column (cm^2)
- b : width of column in the considering direction (cm^2)

D : depth of column in the considering direction (cm^2)
 F_c : compressive strength of concrete (kg/cm^2)
 H : height of precipice (m)
 H_i : height of shear wall from the floor to the top of the building (cm)
 h_o : clear height of column between horizontal members adjoined at top and bottom of the column, considering the effects of the spandrel walls (cm)
 I_o : standard lateral seismic force coefficient
 l : distance of centers of columns at both ends of the shear wall; if the shear wall has opening, the length of opening shall be subtracted from the above mentioned distance (cm)
 l_w : depth of column with wing wall including the length of the wing wall (cm)
 M_u : ultimate bending moment ($\text{kg}\cdot\text{cm}$)
 M_w : ultimate bending moment of shear wall ($\text{kg}\cdot\text{cm}$)
 N : axial force of column (kg)
 n : number of floors from the top to the investigated floor
 p_s : reinforcement ratio of wall ($=a_s/ts$) (%)
 p_t : tensile reinforcement ratio of column ($=a_t/bD$) (%)
 p_w : shear reinforcement ratio of column ($=a_w/bs$) (%)
 Q : shear capacity of the floor (kg)
 Q_1 : shear capacity of column considering the bending failure (kg)
 Q_2 : shear capacity of column considering the shear failure (kg)
 ΣQ_c : sum of shear capacity of columns on the floor (kg)
 ΣQ_w : sum of shear capacity of walls on the floor (kg)
 Q_{w1} : shear capacity of wall considering the bending failure (kg)
 Q_{w2} : shear capacity of wall considering the shear failure (kg)
 R_c : reduction factor determined by the structural defects
 R_e : factor of earthquake force determined by the unbalanced lateral stiffness

- R_h : ratio of clear height to the depth of column ($=h_o/D$)
 R_{h_o} : same as the above
 S_B : shear resistant force coefficient of the floor
 s : spacing of shear reinforcement in the column or the wall (cm)
 T_G : predominant period of the ground (sec)
 t : thickness of the wall (cm)
 W : total weight of the building above the investigated floor (kg)
 α : correction factor of the shear resistance
 β : factor for the estimation of shear stress
 σ_o : mean compressive stress of column (N/bD) (kg/cm^2)
 σ_y : yield strength of the longitudinal reinforcement of column (kg/cm^2)
 σ_{wy} : yield strength of the shear reinforcement of column (kg/cm^2)

INVESTIGATION OF BUILDING SITE

Investigations of landslides and liquefaction of the ground shall be made in the cases of following conditions:

(1) The relative location between the buildings and precipices is as shown in Fig. 1, the cracks or movements are found at the retaining walls of the precipices, and the angle of inclination of the natural slopes to horizontal plane is not less than 30 deg. in fill-up ground or not less than 45 deg. in cut-off ground.

(2) The ground conditions are the reclamation of sandy soil and high ground-water level, and the building is supported by sand having not more than 5 in the N-values, or by end bearing piles or friction piles in the sand ground having not more than 10 in the N-values by the standard penetration test.

EVALUATION METHOD OF SEISMIC SAFETY OF BUILDING

(1) Scope

This method shall not be applied to the buildings damaged seriously due to unequal settlement of foundations or due to fire.

(2) Method of application

In case of a monolithic building having irregular plan, this

method shall be applied to the divided parts of rectangular plan.

The evaluation shall be made in each of the widthwise and lengthwise directions at each floor. In the case that the plans, elevations and arrangement of shear walls are almost same at each floor, this method will be applied to the lowest floor only.

(3) Materials for evaluation

a) Ground conditions

In case of the following conditions, the value of standard lateral seismic force coefficient, I_0 , is 1.

- i. a building on the different ground conditions
- ii. a building on the fill-up ground
- iii. the height of precipice, which is at distance within 5 times the height of the building, is not less than the height of the building
- iv. cracks due to the unequal settlements found in the building on the soft deposits
- v. an extended building supported by combinational use of different types of foundations

b) Predominant period of the ground

- i. In case of no datum by actual measurements, the value of I_0 is 1.
- ii. In the case that the predominant period of the ground is actually measured and the ground conditions do not conform to a), the value of I_0 is $(1.25 - 0.5T_G)$, but not less than 1.0.

c) Compressive strength of concrete

- i. It is advisable to use the actually measured concrete strength, if possible.
- ii. In case of no datum by actual measurements, the concrete strength used in the structural design shall be used.
- iii. In the case that the concrete strength used in structural design is not available, it will be assumed 180 kg/cm^2 taking the actual circumstances in Japan into consideration.

d) Yield strength of reinforcement

The yield strength of reinforcement shall be the specified yield strength in Japanese Industrial Standard (JIS) G 3112. In case of Grade SR24, however, the yield strength will be 3000 kg/cm^2 taking the

the actual circumstances in Japan into consideration.

(4) 1st step of evaluation method^{3,4)}

In the case that the shear wall length rate in each of the lengthwise and widthwise directions on the floor is not less than $2n$ cm/m² and not less than 4 cm/m², the building is evaluated to be safe. n means the number counted from the top to the investigated floor.

The shear wall length rate is defined as the value of the sum of the horizontal clear length (cm) of reinforced concrete walls surrounded by rigid frame members divided by the floor area (m²), in each of lengthwise and widthwise directions. That is the clear length of shear wall excluding the column size in one direction per unit floor area. If the thickness of the shear wall, t , is more than 15 cm, the length of the wall will be multiplied by $t/15$.

When the building can not be evaluated to be safe by the 1st step investigation, the next step of investigation shall be required.

(5) 2nd step of evaluation method

In the case that the shear resistant force coefficient of the floor, S_B , given by Eq. (1) is not less than I_0 , the building is evaluated to be safe.

$$S_B = \frac{Q}{W} \cdot \alpha \quad (1)$$

$$Q = \Sigma Q_c + \Sigma Q_w = \left\{ 5 \left(1 + \frac{A_c}{A_c + A_{w1} + A_{w2}} \right) A_c \right\} + (30 A_{w1} + 20 A_{w2}) \quad (2)$$

W is the total weight of the building above the investigated floor. It will be calculated as 1200 kg per unit floor area for the normal concrete and 1000 kg per unit floor area for the lightweight concrete, on each floor, taking the actual circumstances in Japan into consideration.

$$\alpha = \frac{R_c}{R_e} \quad \text{and} \quad 0.7 \leq \alpha \leq 1.0 \quad (3)$$

R_c is 1.0 in case of no water leakage without remarkable cracks on the wall, and 0.7 in case of water leakage with remarkable shear cracks on the wall.

R_e is 1.0 in the case that the building has columns of considerably different stiffness on the same floor, and 0.8 in the case that the distribution of lateral stiffness is uniform in elevations and plans.

When the building can not be evaluated to be safe by the 2nd step investigation, the next step of investigation shall be required.

(6) 3rd step of evaluation method^{5,6,7,8)}

a) A method

i. Shear resistance of a story

In accordance with the shear resistant force coefficient, S_B^1 , given by Eq. (4), the seismic safety of the building shall be evaluated as follows:

$$S_B^1 = \frac{Q}{W} \cdot \alpha \quad (4)$$

$$Q = \Sigma Q_c + \Sigma Q_w \quad (5)$$

Q_c shall be the smaller of Q_1 and Q_2 .

$$Q_1 = \frac{2 M_u}{h_o} \quad (6)$$

In case of $N \leq 0.4 bD \cdot F_c$, where N is axial force of column,

$$M_u = 0.8 a_t \cdot \sigma_y \cdot D + 0.5 N \cdot D \left(1 - \frac{N}{b \cdot D \cdot F_c} \right) \quad (7)$$

In case of $N > 0.4 bD \cdot F_c$,

$$M_u = 0.8 a_t \cdot \sigma_y \cdot D + 0.12 b \cdot D^2 \cdot F_c \quad (8)$$

When the columns have wing walls as shown in Fig. 2, M_u shall be calculated as follows, instead of Eqs. (7) and (8).

In case of $N \leq \{ 0.5 m (0.9 + n') - 13 p_t \} bD \cdot F_c$, where m and n' are given by Eq. (9) and Fig. 2, respectively,

$$m = \left(1 - \frac{D}{I_w} \right) \frac{t}{D} - \frac{D}{I_w} \quad (9)$$

$$\begin{aligned}
M_u &= (0.9 + n') a_t \cdot \sigma_y \cdot D \\
&+ 0.5 N \cdot D \left\{ 1 + 2 n' - \frac{N}{m \cdot b \cdot D \cdot F_c} \right. \\
&\left. \left(\frac{a_t \cdot \sigma_y}{N} + 1 \right)^2 \right\} \quad (10)
\end{aligned}$$

In case of $N > \{ 0.5 m (0.9 + n') - 13 p_t \} bD \cdot F_c$, M_u shall be given by substituting $\{ 0.5 m (0.9 + n') - 13 p_t \} bD \cdot F_c$ into N in Eq. (10).

$$\begin{aligned}
Q_2 &= \left\{ \frac{0.043 (F_c + 180)}{0.56 R_{h_0} + 0.12} + 2.7 \sqrt{3000 p_w} + 0.1 \frac{N}{b \cdot D} \right\} \\
&\cdot 0.8 b \cdot D \quad (11)
\end{aligned}$$

When columns have wing walls as shown in Fig. 2, Q_2 shall be the larger of the values given by Eqs. (12) and (13).

$$\begin{aligned}
Q_2 &= \left\{ \frac{0.043 (F_c + 180)}{0.56 R_{h_0} + 0.12} + 2.7 \sqrt{3000 p_w} + 0.1 \frac{N}{b \cdot D} \right\} \\
&\cdot 0.8 b \cdot D + 3000 p_s \cdot t (l_w - D) \quad (12)
\end{aligned}$$

$$Q_2 = \left(\frac{F_c}{6} + 3000 p_s \right) t \cdot l_w \quad (13)$$

Q_w shall be the smaller of Q_{w1} and Q_{w2} . Because Q_w includes the shear capacities of columns adjoined to shear wall, the shear capacities of those columns shall not be included in Q_c .

$$Q_{w1} = \frac{M_w}{0.5 H_i} \quad (14)$$

$$Q_{w2} = \left(\frac{F_c}{6} + 3000 p_s \right) t \cdot l \quad (15)$$

ii. Evaluation

In case of $S'_B \geq I_o$, the building is evaluated to be safe.

In case of $1.0 I_o > S_B' \geq 0.6 I_o$, the building is evaluated to be safe, if Q_2 of typical columns is larger than Q_1 .

In case of $0.6 I_o > S_B' \geq 0.45 I_o$ and of $S_B' \geq 0.3$, the building is evaluated to be safe, if the shear reinforcement ratio of columns is given by Eq. (16).

$$p_w \geq \frac{\left(\frac{Q_1}{\beta \cdot b \cdot D} \right) - \left(\frac{F_c}{20} \right)}{1200} + 0.002 \quad (16)$$

When $h_o \geq 3 D$, β may be 2, and when $h_o < 3 D$, β may be 1.5.

In case of $0.45 I_o > S_B' \geq 0.3 I_o$, and of $S_B' \geq 0.25$, the building is evaluated to be safe, if the shear reinforcement ratio of columns is given by Eq. (17) and not less than 0.2 %, and if the spacing of shear reinforcement is not larger than 8 times the diameter of longitudinal reinforcement.

$$p_w \geq \frac{\left(\frac{Q_1}{\beta \cdot b \cdot D} \right) - \left(\frac{F_c}{20} \right)}{1200} + 0.002 \quad (17)$$

When $h_o \geq 3 D$, β may be 1, and when $h_o < 3 D$, β may be 0.75.

b) B method

In the old buildings, it is very difficult to find the structural drawings and specifications. Therefore, B method will be used instead of A method taking the old circumstances in Japan into consideration.

Q_w , α and W shall be calculated by the method in the 2nd step. In columns, the following values will be assumed; $p_t = 0.6 \%$, $p_w = 0.159 \%$, $\sigma_o = 20 \text{ kg/cm}^2$ and $F_c = 210 \text{ kg/cm}^2$.

Evaluation method of seismic safety is as follows.

- i. to calculate $R_h = h_o/D$ in typical columns
- ii. to obtain the smaller value, $\bar{\tau}_i$, of $\bar{\tau}_1$ and $\bar{\tau}_2$ by R_h and two curves in Fig. 3
- iii. to calculate $\Sigma Q_c'$ by Eq. (18)

$$\Sigma Q_c' = \Sigma (\bar{\tau}_i \cdot b \cdot D) \quad (18)$$

iv. to calculate S_B'' by substituting the above mentioned values into Eq. (1)

v. to evaluate as follows:

In case of $S_B'' \geq 1.0 I_0$, the building is evaluated to be safe.

In case of $1.0 I_0 > S_B'' \geq 0.6 I_0$, the building is evaluated to be safe, if $\bar{\tau}_i$ is determined by $\bar{\tau}_1$.

When the building can not be evaluated to be safe, $\bar{\tau}_2'$ shall be obtained by Fig. 4 and by actually measured shear reinforcement ratio, p_{wa} . By using this $\bar{\tau}_2'$ instead of $\bar{\tau}_2$, the evaluation of seismic safety of the building shall be made.

When the building can not be evaluated to be safe by using this corrected $\bar{\tau}_2'$, the building is evaluated to be safe, if p_{wa} is larger than p_{wr} obtained from Fig. 5 by using Q calculated from the smaller of $\bar{\tau}_1$ and $\bar{\tau}_2'$.

c) C method

This is the evaluation method obtained by modifying N method taking in consideration of the results given by B method and actual behavior of the damages to buildings due to the 1968 Tokachi-oki Earthquake.

The shear resistant force coefficient of the floor, S_B''' , is obtained by the coefficients of bending failure type columns, S_{B1} , of shear failure type columns, S_{B2} , and of shear walls, S_{B3} , as follows.

$$S_{B1} = \frac{\Sigma (A_{c1} \cdot \bar{\tau}_1)}{W} \quad (19)$$

$$S_{B2} = \frac{\Sigma (A_{c2} \cdot \bar{\tau}_2)}{W} \quad (20)$$

$$S_{B3} = \frac{(30 \Sigma A_{w1} + 20 \Sigma A_{w2})}{W} \quad (21)$$

A_{c1} is the sectional area of column whose R_h is not less than 3.3, A_{c2} is the sectional area of column whose R_h is less than 3.3, $\bar{\tau}_1$ is $\bar{\tau}_1$ of column, whose R_h is not less than 3.3, obtained by Fig.3, and $\bar{\tau}_2$ is $\bar{\tau}_2$ of column, whose R_h is less than 3.3, obtained by Fig. 3.

$$S_B''' = \frac{S_{B1}}{S_{B1} + S_{B2} + S_{B3}} + S_{B2} + S_{B3} \quad (22)$$

Evaluation method of seismic safety is as follows.

- i. In case of $S_B''' \geq 1$, the building is evaluated to have sufficient seismic resistance.
- ii. In case of $1 > S_B''' \geq 0.6$, the building is evaluated to have considerable seismic resistance.
- iii. In case of $0.6 > S_B''' \geq 0.4$, the building is evaluated to be poor in seismic resistance. The building is required to be investigated precisely.
- iv. In case of $0.4 > S_B'''$, the building is evaluated to be dangerous in seismic resistance. The building must be investigated precisely.

When the building can not be evaluated to be safe by the 3rd step investigation, the next step of investigation shall be required.

(7) 4th step of evaluation method

The building shall be evaluated again in accordance with the 3rd step investigation using the predominant period of the ground and the concrete strength actually measured.

When the building can not be evaluated to be safe by the 4th step investigation, another minute and precise investigation must be required.

APPLICATION TO EXISTING BUILDING

In order to investigate the adaptability of the evaluation method, the investigations of 14 reinforced concrete school buildings, those were damaged due to the 1968 Tokachi-oki Earthquake^{VI}, are carried out by the 5th Committee for School Buildings of the Architectural Institute of Japan. The investigations are made by all of the prescribed evaluation methods. From those, the comparison between the results by the C method of the 3rd step and the degree of damages are shown in Fig. 6.

It is found that the degree of damages is medium or serious in case of less than 0.6 in S_B''' , and slight or no in case of not less than 0.6 in S_B''' . Therefore, it may safely be said that the grade of evaluation by the C method of the 3rd step is appropriate.

CONCLUSIONS

We have found one of the most practical and simple evaluation methods of earthquake resistant properties of the existing reinforced concrete school buildings, whose properties are fixed by the strength

VI : The maximum ground accelerations recorded by the strong motion accelerograph in the Hachinohe Port, are 225 gals in the NS component, 183 gals in the EW component and 114 gals in the UD component.

of columns and shear walls. In the case that the earthquake resistant properties of the buildings are fixed by the strength of beams, it needs to take the special notice for the evaluation of capacities of columns into consideration.

The C method of the 3rd step is very easy for practical use. nevertheless, the grades of evaluation by this method correspond to the degrees of damages due to the 1968 Tokachi-oki Earthquake. In this method, however, the ductilities of members are not considered. Therefore, it is desirable to use A or B method of the 3rd step in order to evaluate the seismic safety taking in consideration of the ductilities of members.

This kind of evaluation method is required to be elaborated further in order to evaluate more accurately.

ACKNOWLEDGEMENT

The evaluation method of the earthquake resistant properties of existing reinforced concrete school buildings described in this paper, is the results investigated by the members of the 5th Committee for School Buildings of the Architectural Institute of Japan sponsored by the Ministry of Education, Japanese Government. The authors wish to acknowledge gratefully for these contributions.

REFERENCES

- 1) Architectural Institute of Japan, " The evaluation method of the earthquake resistant properties and the strengthening method of reinforced concrete school buildings " 1975
- 2) T. Miki, T. Homma and M. Hiroswawa, " Evaluation of earthquake resistant properties and strengthening of existing buildings " Fifth World Conference on Earthquake Engineering, 1973
- 3) K. Nakagawa, I. Kamei and S. Kokusho, " Relationship between wall rate and damage due to earthquake in reinforced concrete building " Transaction of AIJ, No. 60, 1958
- 4) T. Shiga, A. Shibata and T. Takahashi, " Damages due to earthquake and wall ratios in reinforced concrete buildings " Report of Tohoku Branch of AIJ, 1968
- 5) Architectural Institute of Japan, " AIJ Standard for Structural Calculation of Reinforced Concrete Structures " 1975
- 6) M. Ohkubo, " Study of elasto-plastic behavior of reinforced concrete beams with spandrel walls " Transaction of AIJ, No.207, 1973
- 7) T. Arakawa, " Allowable shear stress and shear reinforcing method in reinforced concrete beams " Concrete Journal, Vol. 8, No. 7, 1970
- 8) M. Hiroswawa and T. Gotō, " Strength and ductility of reinforced concrete members subjected to axial force " Report of AIJ, 1971

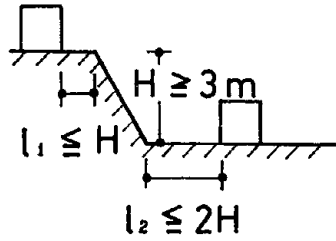


Fig. 1 Relative location between building and precipice

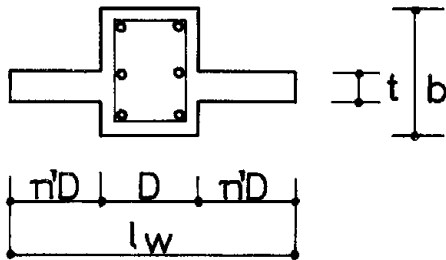


Fig. 2 Notation of column having wing wall

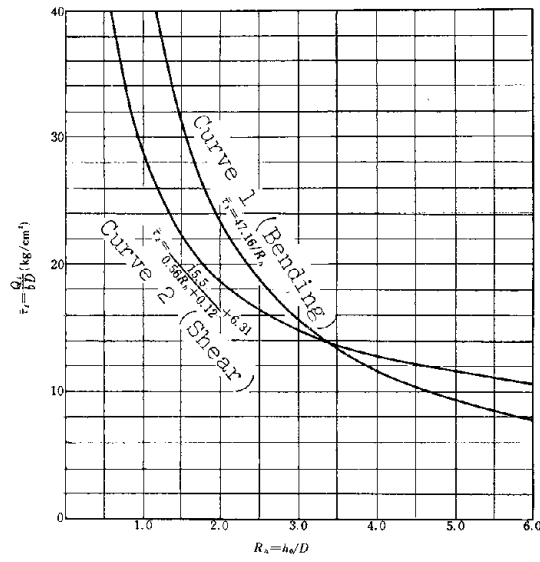


Fig. 3 Calculation diagram of $\bar{\tau}_1$ and $\bar{\tau}_2$ in B method of 3rd step

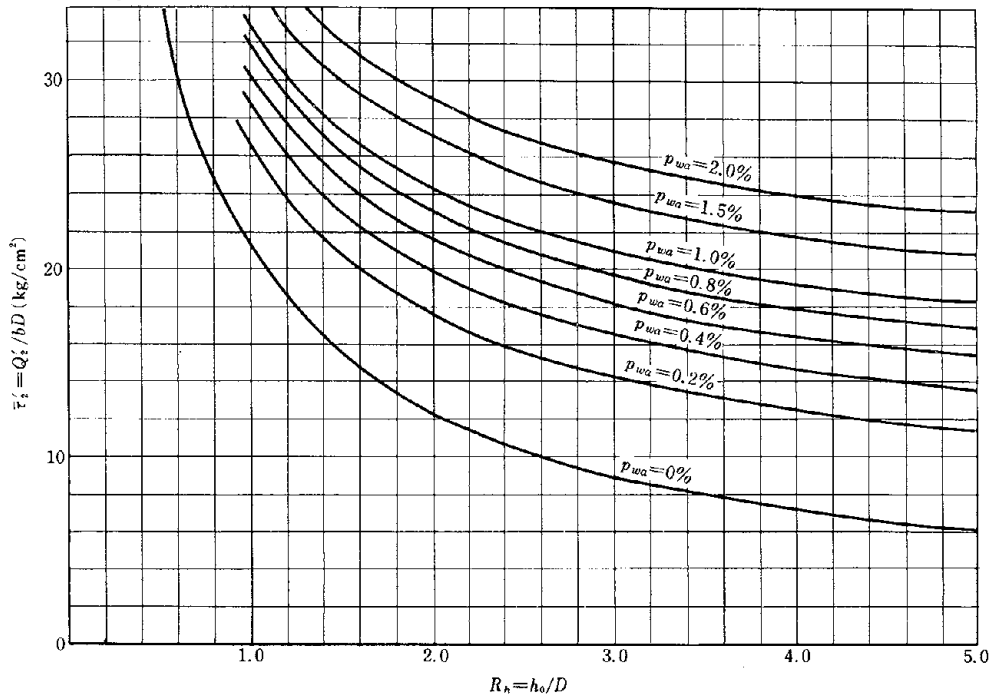


Fig. 4 Calculation diagram of $\bar{\tau}_1'$ in B method of 3rd step

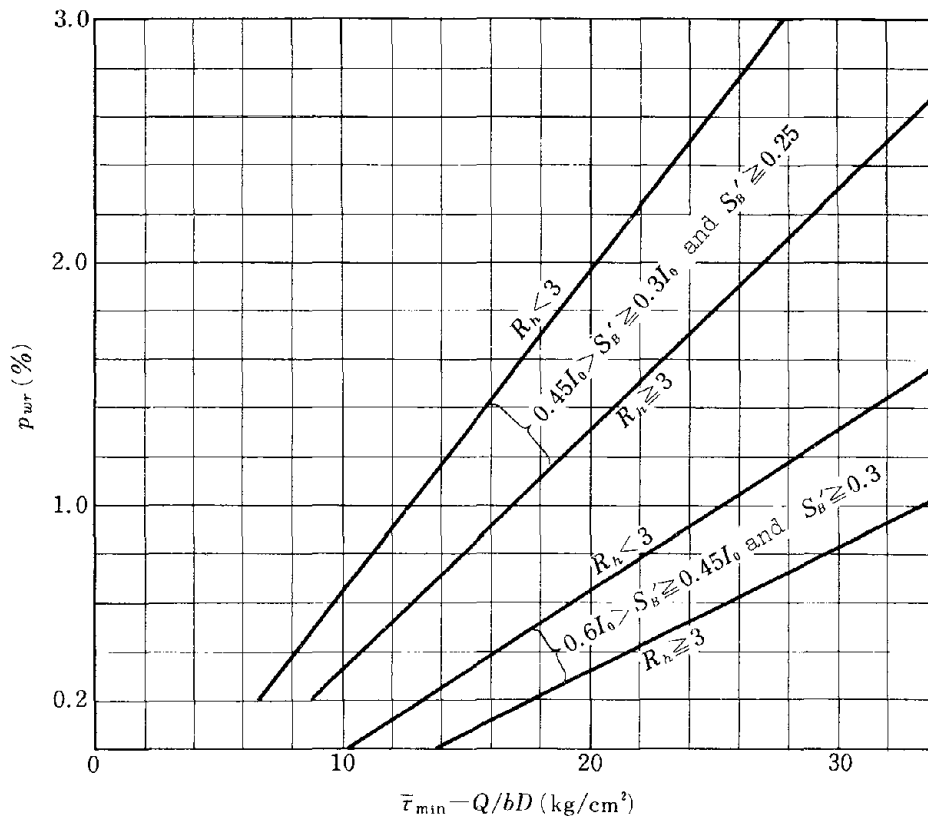


Fig. 5 Calculation diagram of p_{wr} in B method of 3rd step

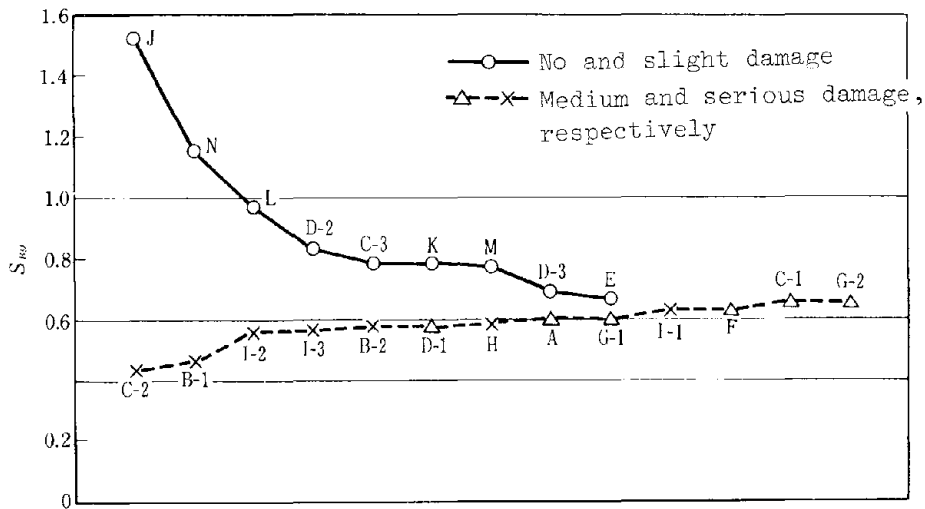


Fig. 6 Comparison between results by C method of 3rd step and degree of damages due to 1968 Tokachi-oki Earthquake

Note: Symbol marks show the investigated building. Abscissa has no special meaning.

Boris Bresler^{I)}, Tsuneo Okada^{II)}, and David Zisling^{III)}

SYNOPSIS

Methods for assessing the seismic safety of structures are discussed, and procedures for establishing priorities for evaluating and abating hazards are indicated. Field evaluation, code compliance evaluation, and maximum tolerable earthquake intensity evaluation are summarized, and results of a pilot study to identify possible hazards and levels of seismic resistance in several reinforced concrete frame buildings are reported.

1. INTRODUCTION

1.1 Need for Evaluation - The need for assessing the residual safety of buildings damaged in the event of a major earthquake is obvious. Immediate inspection of post-earthquake damage, under emergency conditions, is required to determine the condition of structures, the feasibility of occupying structures and resuming ordinary life processes of the community at an early date, and to determine which structures pose life or health hazards to the public and must therefore be demolished.

The need for evaluating potential seismic hazards in existing buildings is less obvious, but just as essential in regions of seismic activity. Most existing buildings were built before adequate seismic design standards were developed or accepted and these buildings may require some modification or strengthening to minimize the risk of injury or loss of life. If the same seismic performance criteria were used for existing buildings as are used for new buildings^{IV}, then clearly the same levels of earthquake resistance must be developed in both old and new buildings. Even if the acceptable level of damage in existing buildings were greater than that for new buildings, existing buildings must be evaluated in order to determine which structures could be expected to sustain damage exceeding this level during an earthquake.

I Professor, Department of Civil Engineering, University of California, Berkeley, California, U.S.A.

II Associate Professor, Institute of Industrial Science, University of Tokyo, Tokyo, Japan.

III Research Assistant, Department of Civil Engineering, University of California, Berkeley, California, U.S.A.

IV Buildings should: (1) resist minor earthquakes without damage, (2) resist moderate earthquakes without structural damage, although some nonstructural damage may be allowed, and (3) resist major (severe) earthquakes without collapse, although some local structural damage may be allowed. Special public buildings should remain operational during and after the earthquake.

Also, special hazards to the public may exist due to unsafe portions of buildings (usually nonstructural) such as ornaments, parapets, and accessways (stairs, elevators), which must be corrected. There are other conditions under which evaluation of existing buildings is essential. For example, structures damaged by nonseismic causes (e.g. fires, foundation distress, aging deterioration, corrosion, etc.) may have considerably less residual earthquake resistance than that provided in the original structure. Buildings which have undergone structural modification due to change in occupancy or for other reasons must also be evaluated in the modified state.

1.2 Evaluation Process - The process for evaluating the seismic safety (degree of hazard) of existing buildings in a given city requires the following two stages:

- (1) Legal requirements must be established for reviewing seismic as well as other hazards in existing buildings and a judicial and administrative process instituted for carrying out this review.
- (2) In order to evaluate the degree of hazard in the large inventory of existing buildings in a reasonable time and at a reasonable cost, a systematic procedure for establishing priorities for review of classes of buildings and a methodology for evaluating hazards in individual buildings must be established. In some cases, review of design documents and a site inspection may be sufficient to determine the approximate degree of hazard in a given building. In other cases, more refined analytical evaluation may be required.

1.3 Priority Categories - Life safety and continuity of indispensable services are the bases for establishing priority categories. The following categories can be identified:

- (1) Facilities which must remain operational during and after a severe earthquake.
- (2) Essential institutions providing important social services which should continue to operate with minimal disruption.
- (3) Buildings in which damage would result in high risk to life safety and concomitant disaster.

Other priority categories may be established on the basis of vulnerability associated with location (local seismicity), design standards of safety such as code requirements, workmanship, materials of construction, age, and possible deterioration. For example, the following categories may be identified:

- (1) Buildings in high seismicity zones which were built prior to enforcement of the first effective seismic design provisions.
- (2) Buildings in high seismicity zones which were built under old seismic design provisions, but which are constructed of

unreinforced masonry, nonductile moment-resisting concrete frames, buildings with heavy precast concrete curtain walls or structural elements, and buildings of unusual construction or configuration.

2. EVALUATION METHODS

2.1 General - Various methods for evaluating hazards in classes of buildings and individual buildings, ranging from field evaluations which may require only a few man-hours to field-testing and sophisticated analyses which require thousands of man-hours, are available. Some of these methods are briefly reviewed here, and the results of a pilot study to identify possible hazards and levels of seismic resistance in several reinforced concrete frame buildings are reported.

2.2 Field Evaluation - Field evaluation methods rate a building rapidly and approximately as either "Good," "Fair" or "Poor" for a specified earthquake intensity. Review of design documents (drawings, calculations) and a site inspection should be sufficient for an appropriate rating. When plans and specifications for an existing structure are not available, field measurements, materials testing, and other means of identifying the construction scheme and the quality of materials and workmanship should be used. Basically, field evaluations determine whether or not a more detailed analysis of a building is necessary to assess its safety.

Several schemes for field evaluations have been proposed recently [1, 2, 3, 4]. Each of these schemes rates structures using a numerical or qualitative scale to evaluate a number of essential elements and characteristics of the buildings. The rating is then compared to a minimum composite score in order to classify the building.

The NBS field evaluation method (FEM) will be summarized here as representative of such methods. The first step in this method is to assemble information pertinent to determining the probable seismic performance of a structure. These data from an examination of plans and an on-site inspection are summarized in a standardized Data Collection Form. The geographic location of the building is assigned an expected Modified Mercalli Intensity (MMI), and the building is rated, as follows:

- (1) Structural system general rating: (GR) is based on the type of structural system and construction materials. The rating scale is from 1 to 4, with steel and ductile moment-resisting frames rated 1, and unreinforced masonry or unsheathed wood frames rated 4.
- (2) Structural system vertical elements rating: (SR₁) is based on the quantity of resisting elements, symmetry of arrangement, and present condition. Each of these factors is rated on a scale from 1 to 4, and the composite score value of SR₁ is as follows:

$$SR_1 = \frac{1}{6}(Q + S) + \frac{2}{3} PC \quad (1)$$

where Q is the quantity rating, S is the symmetry rating, and PC is the present condition rating.

- (3) Structural system horizontal elements rating: (SR_2) is based on the worst case (largest grade on a scale from 1 to 4) of roof and floor rigidities (R), chord adequacy (C), and connections and anchorage (A), as follows:

$$SR_2 = \text{largest value of A, C, or R on scale from 1 to 4.} \quad (2)$$

- (4) Nonstructural systems are graded on a qualitative scale: Good (A), Fair (B), Poor (C), and Unknown (X). The principal items rated are:

- a. corridor and stair enclosure walls (with regard to earthquake performance and life hazard),
- b. interior partitions other than corridor and stair enclosures,
- c. exterior curtain walls,
- d. interior and exterior appendages, ornamentation,
- e. ceiling and light fixtures,
- f. glass breakage,
- g. special hazards (gas connection, hazardous contents).

The overall composite rating: (CR) for the structural system is determined as follows:

$$CR = \frac{1}{3}[GR + 2(SR_m)]/ILF \quad (3)$$

where SR_m is the larger value of SR_1 and SR_2 , and ILF is the intensity level factor based on MMI varying from 1 to 4 as shown in Table 1. The structural system is then classified "Good" to "Very Poor," depending on the value of CR, as in Table 2.

The NBS field evaluation method has been used to evaluate a typical school building in California, resulting in a rating of "Good" for this building for MMI of IX. Results of other approximate methods of evaluating this building indicated that the risk of damage in a severe earthquake would be relatively high, and that more precise evaluations would be desirable.

While the NBS method is simple to apply, the results obtained by this method appear to be questionable. The algebraic formulations for SR_1 and CR appear to be entirely arbitrary. The contribution of PC rating₁ is given a $\frac{2}{3}$ weight, whereas the other contributions are weighted at only $\frac{1}{6}$ each. The present condition factor is given excessive weight, particularly for relatively new buildings, and the quantity (Q) of resisting elements is given too little weight. Furthermore, the strength of the building is not adequately accounted for.

2.3 Capacity Ratio - A possible measure of the seismic structural safety of an existing building is obtained by comparing its calculated

earthquake resistance capacity to the design requirement for a similar new building. For this purpose, the structural system (geometry, materials, detailing) must be identified as completely as possible using design documents, site inspections, and testing. Then, using appropriate analytical techniques (the same as those used in designing new buildings), the value of required earthquake resistance, Q_{REQ} , must be determined on the basis of the element which is critical in resisting seismic effects. The available earthquake capacity, Q_{CAP} , for the same element must be determined using the criteria for evaluating capacity specified for designing new buildings. In the process of evaluating Q_{REQ} and Q_{CAP} , various modes of potential damage or failure must be considered and the critical element (or elements) must be identified. A measure of the earthquake safety of an existing building, relative to that of a new building, is defined by the capacity (or resistance) ratio R:

$$R = \frac{Q_{CAP}}{Q_{REQ}} \quad (4)$$

Depending on the desired level of performance, i.e. damage control or collapse control, the definitions of Q_{CAP} and Q_{REQ} may be different. In the case of damage control, these values should reflect the capacity of the weakest element in the building. In the case of collapse control, damage or failure of the weakest element may not result in collapse, as in highly indeterminate systems, and in such cases, Q_{CAP} and Q_{REQ} should be based on those critical elements which would initiate collapse in a progressive development of failure.

The capacity ratio R is an index of hazard: the lower the value of R, the greater is the hazard, potential damage, distress, and risk of collapse.

2.4 Code Compliance - When determination of Q_{REQ} and Q_{CAP} is based on the current code, this ratio may also be used as a measure of code compliance or noncompliance. The value of Q_{REQ} considers appropriate loading combinations with specified load factors, and the value of Q_{CAP} considers appropriate capacity reduction factors ϕ , as for example those given in the 1973 UBC or 1974 SEAOC. These load and capacity reduction factors may be either too high or too low for a given existing building, although their use is appropriate for designing new buildings. For buildings where previous damage or other deterioration has taken place, or for buildings where superior design and quality of workmanship has been observed, special ϕ factors should be used.

Determination of Q_{REQ} may be based on the response to the specified earthquake or on the response required to develop appropriate ductility in a flexural mode of failure. For example, using the 1974 SEAOC Recommendation for Seismic Design, the response to a specified earthquake may be expressed in terms of base shear Q_{REQ} as follows:

$$Q_{REQ} = Z I K C S W_E = C_E W_E \quad (5)$$

where

- Z - numerical coefficient related to the seismicity of a region
- I - occupancy importance coefficient, varying from 1.0 to 1.5
- K - numerical coefficient based on the dynamic response characteristics of the structure
- C - numerical coefficient representing intensity and dynamic response characteristics of the building; variations in this coefficient in the building code standards during the past 70 years are shown in Table 3 (Ref. 5). The values shown in this Table indicate that the empirical expressions for C_E change from the simplistic conservative 1927 and 1935 UBC values, to more sophisticated and less conservative 1973 UBC values. However, more conservative values of C_E were proposed by the SEAOC in 1974, thus reversing the trend to lower values of C_E during the preceding thirty years.
- S - numerical coefficient representing local site conditions, particularly site-structure interaction
- W_E - effective weight of structure and other building components contributing to earthquake forces.

When Q_{REQ} is based on the condition that an element must not fail prematurely in a brittle mode, and that potential ductility of an element is fully developed, special code requirements for shear and moment capacities are specified. Such requirements were introduced in the SEAOC Recommendations in 1967 in Sec. 2630, Concrete Ductile Moment Resisting Space Frames. Thus,

$$Q_{REQ} = \frac{M_A + M_B}{L} + \alpha_3 Q_D + \alpha_4 Q_L \quad (6)$$

where M_A and M_B are ultimate moment capacities of opposite sense at each end of the member, α_3 and α_4 are appropriate load factors (see Table 7) and subscripts D and L refer to dead and live loads, respectively.

2.5 Other Methods for Evaluating Safety - The degree of noncompliance with the current code expressed in terms of the capacity ratio R, Eq. 4, does not reflect the maximum earthquake resistance of existing buildings. This resistance may be expressed in terms of earthquake intensity, resulting in a specified degree of damage or failure.

If the maximum response of a structure, Q_{MAX} , can somehow be related to earthquake intensity and if the capacity of a structure, Q_{CAP} , is expressed in the same terms as the response, then the maximum tolerable earthquake will be such that:

$$Q_{MAX} = Q_{CAP} \quad (7)$$

Then, if a linear relationship between some measure of earthquake intensity

and response is assumed, the earthquake intensity which will produce the specified degree of damage or failure can be determined. The maximum response can be defined as:

$$Q_{MAX} = Q_{GRV} + C_Q W_E \quad (8)$$

where Q_{GRV} is the effect of gravity loads, C_Q is a coefficient representing earthquake intensity, and W_E is the effective weight of the building. Then, the maximum value of the earthquake intensity coefficient, C_Q , which would result in maximum forces within the permissible limit Q_{CAP} is:

$$C_Q = \frac{Q_{CAP} - Q_{GRV}}{W_E} \quad (9)$$

The value of Q_{GRV} should consider effects of the deformed shape of the structure and of vertical accelerations under earthquake conditions. As a first order approximation, these may be neglected, and Q_{GRV} may be calculated on the basis of undeformed static conditions for (D+L) gravity loads. In this simple formulation of C_Q , the value indicates a base shear coefficient which can be related to earthquake intensity.

A variety of other methods for evaluating the structural adequacy of existing buildings may be used. Ideally, appropriate three-dimensional, nonlinear dynamic response analyses for different types and intensities of ground motion would provide the most reliable results. These analyses must account for soil-structure interaction and for the nonlinear behavior of structural elements under dynamic loading conditions. However, mathematical modeling of this problem is extremely complex, and available techniques are highly approximate. Therefore, the most desirable and practical method for evaluating structural safety would be one combining simplicity of execution with an acceptable level of reliability. Various methods are now being developed (Refs. 6-10) and their relative advantages can be determined by correlating results obtained by these methods in evaluating the response of relatively large groups of buildings.

3. HAZARD ABATEMENT

When for a given existing building the resistance ratio R , defined by Eq. 4, is equal to or greater than unity, it may be concluded that such a building complies with the current standards for seismic design of new buildings. However, when the calculated resistance ratio R is less than 1.0, the risk of earthquake damage in this building is larger than the risk of damage in a similar new building designed according to current standards. The degree of hazard indicated by R should be related to various risks, such as overall risk of life safety (e.g. life loss per 10^6 population per year), risk of life safety in buildings with high density occupancy, mix of the buildings in the community, risk of social and economic losses from interruption of services or use of special buildings and facilities (hospitals, fire service stations, communication centers, etc.).

A variety of options are available in hazard abatement:

- (1) When hazard abatement is impossible or not economical, the building must be demolished.
- (2) When preservation of the building and its use are essential, the building must be strengthened to an acceptable level of performance (R) within the required time.
- (3) Intermediate corrective measures may include changes in use or occupancy, a reduction in the number of stories (partial demolition), or a reduction in projected lifetime (legal commitment to demolish within prescribed time limit).
- (4) Acceptable combination of 2 and 3 above.

Because data are lacking for objectively correlating R values with various risks and for defining acceptable levels of hazard, decisions regarding hazard mitigation must be made on a subjective basis. Constraints on such subjective decisions must be derived on the basis of reasonable judgment, and on studies of probabilistic models of seismic damage consequences (hazards) and cost/benefit analysis.

For example, a subjective decision to accept a low value of R (say 0.10) may be rationalized for the existing inventory of buildings. In realistic terms, this subjective decision is based on accepting the principle that the earthquake safety of existing buildings will be improved through a natural process of "survival of the fittest."

On the other hand requiring uniform performance (risk of damage) for existing old and new buildings would necessitate upgrading all existing buildings to a value of $R = 1.0$, possibly involving considerable cost. Such expenditure may or may not be economically justifiable, except when special conditions require preservation of existing old buildings with a minimum risk of damage. When the cost of strengthening a building is not justified, the structure must be demolished or the larger risk of damage accepted.

An intermediate solution may be provided by varying acceptable values of R, depending on the nature and consequences of damage in different buildings. For example, critical or essential facilities which must remain operational during and after a severe earthquake should be strengthened to achieve a value of $R = 1.0$. Sufficient hazard abatement in other structures may be achieved using lower values of R.

The difference between the acceptable capacity ratio R and unity may be called the leniency ratio λ , so that

$$\lambda = (1 - R) \quad (10)$$

Different values of λ may be indicated for different categories of buildings. For example, it may be possible to establish building categories A, B, and C, specifying that $\lambda_A = 0.2$, $\lambda_B = 0.4$, and $\lambda_C = 0.6$.

For economic and technical reasons the objectives of hazard abatement in all existing buildings cannot be accomplished in a short period of time. For different categories of buildings the permissible time for compliance with hazard abatement requirements may vary from 15 to 35 years or possibly even longer periods of time.

The leniency ratios λ and the time duration for accomplishing the objectives of hazard abatement are closely related to social and economic considerations, such as acceptable risk levels (Ref. 11), capacity of the construction industry, availability of funds and rates of interest for financing hazard abatement, and economic incentives for investing in hazard abatement. A possible schedule for strengthening or demolishing hazardous buildings is illustrated in Table 4, where three categories of buildings are chosen in such a way that for Type A ($\lambda = 0.2$) all buildings will be brought up to capacity ratio $R = 0.8$ within 15 years, and for Types B and C ($\lambda = 0.4$ and 0.6 , respectively) all buildings will be brought into compliance within 28 and 35 years, respectively. The schedule also accounts for the degree of hazard, so that buildings with lower capacity ratios R will be brought into compliance within a shorter time period (Fig. 1). For example, a building in Class B with a capacity ratio of $R = 0.2$ should be strengthened to $R = 0.6$ within 8 years or demolished. Another building in the same class but with $R = 0.4$ should be strengthened to $R = 0.6$ within 18 years.

In establishing building categories A, B, and C, the following factors may be considered: (1) use and occupancy of the building, (2) seismic zone and local site seismicity, (3) special hazards (release of toxic or combustible contents), (4) original design criteria (seismic intensity and seismic resistance, provisions considered in design), (5) original quality of materials and workmanship, and present physical condition (evidence of prior damage or deterioration).

The following classifications based only on use and occupancy may be adopted for a hazard abatement program. However, further refinements in these classifications may be introduced, considering factors other than use or occupancy.

Class A

Facilities which must remain operational during and after a severe earthquake

Hospitals	Essential Communications
Police Stations	Power Plants
Fire Stations	Water Plants

Class B

Other essential facilities

Institutions	Public Assembly
Incapacitated	Schools
Orphanages	Theaters
Nursing Homes	Shopping Centers

Institutions (cont'd.)	High-Rise Buildings
Schools	
Dentention and Correctional	
Hazardous Uses	Buildings in "Inner Fire
Industrial (production)	Districts"
Commercial (storage, service)	

Class C

All buildings other than single- or two-family dwellings.

Other approaches to hazard abatement may involve "balanced risk" of damage or "cost effective" level of abatement. In both of these approaches, the "remaining life expectancy" of the building must be known. In practice, it is extremely difficult to ascertain this life expectancy.

In addition to the technical provisions for dealing with the criteria and methods for identifying the hazards and for their removal, legal and administrative procedures for a "just, equitable, and practical method" for hazard abatement must be included in the Code.

An important factor in implementing provisions for hazard abatement in existing buildings is capital investment. Normally, investment in new buildings or in other productive ventures is more profitable than investment in hazard abatement in existing buildings. Unless appropriate economic incentives are introduced for this investment, it may be very difficult to implement the requirements for hazard abatement, except through extensive demolition of old buildings, resulting in economic injury to owners and occupants as well as in social dislocations in the community.

4. EARTHQUAKE RESISTANCE OF TYPICAL BUILDINGS - PILOT STUDY

4.1 Introduction - A pilot study of the effect of building code changes on the earthquake resistance of low-rise reinforced concrete frame buildings was carried out and is briefly summarized below. The objective of this study was to calculate values of R (Eq. 4) and C_Q (Eq. 9) for typical 3- and 4-story reinforced concrete frame buildings designed in accordance with UBC Codes during the period 1946-1973. Computer programs were developed for generating building prototypes and for determining R and C_Q values for these prototypes.

In the evaluation, it was assumed that the critical element in a building frame was the beam-column joint at the first floor level, and that either a bending or shear mode of failure in either the beam or the column could control. The criteria for evaluation were the 1973 UBC and the 1974 SEAOC Recommended Lateral Force Requirements.

The principal variables were the number of stories (3 and 4), the material characteristics ($f'_c = 3$ ksi with $f_y = 40$ ksi, and $f'_c = 5$ ksi with $f_y = 60$ ksi), and the Code criteria used for design [UBC 1946, 1956, 1963 (WSD and USD), and 1973]. By combining different variables, twenty cases were studied. The following notation is used to describe the particular

design: (Tables 5, 8, 9)

(N - number of stories) - (f'_c and f_y - concrete and steel strengths) -
(Y - years),

so that 4-5-60-1964 refers to a 4-story building with 5 ksi concrete strength, 60 ksi reinforcing steel yield strength, designed in accordance with the 1946 UBC Code. For the 1963 designs, both the working stress design (WSD) and the ultimate strength design (USD) criteria were used.

A number of characteristics were held constant in designing the typical building elements.

Bay Size:	25 ft. x 25 ft.	Floor dead load	= 100 psf
Floor System:	2-way slab	Floor live load	= 40 psf
Story Height:	12 ft.	Effective weight W_E	= 140 psf*
Beam width	= 12 inches	Column shape	square
Reinforcement ρ	= 0.0125†	Reinforcement ρ	= 0.035†
Concrete cover	= 2 inches	Concrete cover	= 2 inches
Stirrup steel f_y	= 40 ksi	Tie steel f_y	= 40 ksi

* includes weight of walls, partitions, and fixed equipment

† average value

The details of the connection are shown in Fig. 2 and are summarized in Table 5.

4.2 Frame Analysis Idealization - The response of the frame building was represented by that of an interior frame, and the ground story was considered to be the critical one. For gravity loads, it was assumed that the beams resist a maximum moment at the support $M_{GB} = (q_B L^2/11)$ and maximum shear $V_{GB} = (q_B L/2)$, where q_B is the gravity load per unit length of the beam, and L is the beam span (centerline dimensions). Under gravity loading, the column was assumed to resist axial load only, so that

$$N_{GL} = \sum_i p_i \ell_x \ell_y \quad (11)$$

where p_i is the combined dead and live load per unit area of the i^{th} story, and ℓ_x and ℓ_y define the contributing area for the column load. Possible live load reduction factors were neglected in this study.

For lateral loading, it was assumed that all inflection points were located at the midspan of the beams and at midheight of the columns. Furthermore, the overturning moment effect on axial load in the columns was neglected. Distribution of lateral loads is specified in the Code so that the column shear V_{EC} at the i^{th} story can be calculated and the column maximum bending moment M_{EC} is:

$$M_{EC} = \frac{1}{2} V_{EC} H_s \quad (12)$$

where H_s is the story height (centerline dimension).

The beam maximum moments were calculated assuming equal stiffness of the beams framing into the column, i.e. half the sum of the column moments above and below the beam level:

$$M_{EB} = \frac{1}{2} (M_{EC}^i + M_{EC}^{(i+1)}) \quad (13)$$

The beam maximum shear is then:

$$V_{EB} = (M_{EB}/0.5L) \quad (14)$$

Biaxial bending in the columns may occur when adjacent spans are not equal in both directions, or when both longitudinal and transverse earthquake components with respect to the building axes are considered. In this study, the effects of biaxial bending were neglected.

4.3 Forces Used in Design - The moments, shears, and axial forces in beam and column sections were calculated using the base shear force Q_{REQ} and the frame analysis idealization previously described. For buildings designed in accordance with WSD, a 0.75 reduction factor was used to evaluate the combined effect of gravity and earthquake, representing the permissible 0.33 increase in allowable stresses for this condition. For buildings designed in accordance with USD, appropriate load factors were used (Table 7).

The base shear force was calculated using Eq. 5 in which the coefficient C_E is specified in the appropriate Code. The values of C_E used in this study are shown in Table 6. The trend to lower values of C_E during 1946-1973 is clearly demonstrated. Also, the reversal of this trend in 1974 is shown.

General expressions for moment M , shear V , axial load N , in either beams or columns, can be written as a sum of the contributions due to dead, live, or earthquake loads with appropriate load factors. Two loading conditions were considered: gravity (G) only, and combined gravity and earthquake ($G + E$):

$$(M, V, N)_G = \alpha_1 (M, V, N)_D + \alpha_2 (M, V, N)_L \quad (15)$$

$$(M, V, N)_{G+E} = \alpha_3 (M, V, N)_D + \alpha_4 (M, V, N)_L + \alpha_5 (M, V, N)_E \quad (16)$$

where α_i are the appropriate load factors specified in the codes. These factors are summarized in Table 7.

In order to ensure a ductile mode of failure, the 1967 SEAOC Recommendation specifies that the maximum shear force for USD should not be less than:

$$V_{G+E} = 1.4(V_D) + 1.4(V_L) + \frac{M_u^A + M_u^B}{L} \quad (17)$$

where M_u^A and M_u^B are the ultimate moment capacities of opposite sense at each end of the member, and L in this case is the clear length of the member. In 1973, this requirement was further clarified by stipulating that ultimate moment capacities M_u^A and M_u^B shall be computed with ϕ equal to 1.25 rather than 0.9 to allow for possible excess yield strength over the minimum specified value of f_y .

4.4 Design of Beams and Columns - In designing beams for bending compression steel reinforcement was neglected and the reinforcement ratio ρ was taken approximately as 0.012. The beam width was taken as $b = 12$ in. for all cases, and the required depth d was calculated by equating moment resistance with maximum design moment. The beam-depth dimension was then rounded off to the nearest larger inch, and the number of bars was selected to provide the required area A_s as closely as possible using No. 8 bars. The beam was then checked for shear and shear reinforcement was provided in accordance with the relevant code requirements. In the older designs, No. 2 bars were used as stirrups, but in later designs No. 3 bars were used. In all cases, the yield strength of stirrup reinforcing steel was $f_y = 40$ ksi. The beam overall depth, tension steel reinforcement A_s , area of stirrups A_v , and their spacing s for all twenty cases are shown in Table 5.

The column design followed an iterative procedure with slightly different methods for estimating the initial column sizes for the WSD and USD conditions. In both cases, the columns were taken as square in cross-section with lateral tie reinforcement. For 18 inches or smaller columns, 8 main bars were used, and for 20 inches or larger columns, 12 main bars were used. Bar sizes varied from No. 8 to No. 11. After initial column size and steel reinforcement were selected, the adequacy of the trial column was verified by constructing an appropriate interaction diagram (Fig. 3), and checking the design N and M values for compliance with the diagram.

Lateral ties were provided to conform to the minimum tie and shear reinforcement requirements. All ties were designed using No. 3 bar size and the tie arrangement shown in Fig. 3 was used. The column side dimension, total longitudinal steel reinforcement area A_{st} , the area A_v of lateral reinforcement effective in resisting shear, and the tie spacing S_c are shown in Table 5.

4.5 Discussion of Results - The values of the capacity ratio R and of the earthquake coefficient C_Q are summarized in Tables 8 and 9. Values of R below unity indicate that the particular element in the building does not have sufficient capacity to resist the earthquake intensity in a ductile manner as required by the current code. Four modes of failure were considered: beam bending and shear, and column bending and shear. However, all modes of failure which result in $R < 1.0$ indicate a deficiency in the required level of earthquake resistance.

It can be seen that for all buildings designed prior to 1967, when

shear requirement to develop full moment capacity was introduced in the SEAOC Recommendations, column shear capacity is deficient. Capacity ratios for column shear for these old buildings vary from 0.2 to 0.5, and indicate a high degree of compliance.

The values of C_Q indicate the level of earthquake intensity which the particular existing building can resist without exceeding the capacity based on the specified code. In order to obtain a realistic estimate of the earthquake intensity coefficient C_Q , all load factors were taken as unity and all transverse steel reinforcement was assumed to resist shear, even when A_v was below the minimum value specified by the code.

Based on the capacity ratio values in Table 8, the maximum permissible time for hazard abatement was determined for building categories A, B, and C in accordance with the tentative schedule illustrated in Table 4. These values are shown in Table 10. It is interesting to note that in category C, none of the post-1946, 3-story reinforced concrete buildings need strengthening. For the 4-story buildings in this category, only pre-1963 buildings need some strengthening, and then only if their remaining service life is projected beyond 35 years (i.e., beyond the year 2010). In this case, strengthening would be required when buildings constructed in 1955 were to serve for a total of more than 55 years.

In category A, most 3- and 4-story reinforced concrete buildings would need strengthening in a relatively short period of time. Even most of the 1973 buildings would require strengthening within 12-14 years to comply with the 1974 SEAOC requirements with a leniency ratio of 0.2. In category B, a majority of the buildings in this pilot study would require strengthening within 18-28 years, i.e., when they reach a service age of 40-50 years

5. ACKNOWLEDGEMENTS

This paper was prepared for the project "Seismic Safety of Existing Buildings" at the University of California, Berkeley, sponsored by the National Science Foundation, and for the U.S.-Japan cooperative research program entitled "Earthquake Engineering with Emphasis on the Safety of School Buildings" under the joint sponsorship of the National Science Foundation and the Japan Society for Promotion of Science. The authors gratefully acknowledge the support of the National Science Foundation under Grant No. GI 38463 and the assistance of Ms. Judith Sanders in editing the paper.

REFERENCES

1. "Natural Hazards Evaluation of Existing Buildings," National Bureau of Standards Science Series No. 61, 1975.
2. "Santa Rosa Resolution 9820, A Resolution of the City of Santa Rosa Establishing Criteria for the Inspection of Buildings within the City of Santa Rosa, California," October 1971.
3. Uniform Building Code, Building Standards, "Earthquake Hazard Regulations for Rehabilitation of Existing Structures, Report of Code Changes Committee," May-June 1974.
4. Long Beach Municipal Code, Sub Division 80, "Earthquake Regulations for Rehabilitation of Existing Structures within the City," Long Beach, California, June 1971.
5. Okada, T., "History of Seismic Codes in the U.S.A.," Japan Society for Earthquake Engineering Promotion News, No. 22, 1975.
6. O'Connor, E.M., "Correcting Existing Earthquake Hazardous Buildings in the City of Long Beach, California," Proceedings of U.S. National Conference on Earthquake Engineering, Ann Arbor, Michigan, Earthquake Engineering Research Institute, 1975.
7. Freeman, S.A., Nicoletti, J.P., and Tyrrell, J.V., "Evaluation of Existing Buildings for Seismic Risk - A Case Study of Puget Sound Naval Shipyard, Bremerton, Washington," Proceedings of U.S. National Conference on Earthquake Engineering, Ann Arbor, Michigan, Earthquake Engineering Research Institute, 1975.
8. Lefter, J., and Colville, J., "Reinforcing Existing Buildings to Resist Earthquake Forces," Proceedings of U.S. National Conference on Earthquake Engineering, Ann Arbor, Michigan, Earthquake Engineering Research Institute, 1975.
9. Okada, T., and Bresler, B. "Seismic Safety of Existing Reinforced Concrete Buildings," Proceedings of Review Meeting of the U.S.-Japan Cooperative Research Program on Earthquake Engineering, Honolulu, Hawaii, 1975 (in preparation).
10. McClure, F.E., "Survey and Evaluation of Existing Buildings, Building Practices for Disaster Mitigation," National Bureau of Standards Building Science Series No. 46, 1973.
11. "Risk Acceptance and Public Policy," Proceedings of Session IV, International Systems Safety Society Symposium, Denver, Colorado, 1973.



Table 1 Relationship of ILF to MMI

MMI	VIII+	VII	VI	V-
ILF	1	2	3	4

Table 2 Rating Classification vs. Composite Score

$CR < 1.0$	$1.0 \leq CR \leq 1.4$	$1.5 \leq CR \leq 2.0$	$2.0 < CR$
Good	Fair	Poor	Very Poor

Table 4 Permissible Time for Hazard Abatement
(Time to strengthen or abolish, years)

Capacity Ratio R	Category A $\lambda = 0.2$	Category B $\lambda = 0.4$	Category C $\lambda = 0.6$
0.1	2	3	5
0.1-0.2	4	8	15
0.2-0.3	6	13	25
0.3-0.4	8	18	35
0.4-0.5	10	23	--
0.5-0.6	12	28	--
0.6-0.7	14	--	--
0.7-0.8	16	--	--

Table 5 Beam and Column Dimensions and Reinforcement Details
(See Fig. 2)

FRAME	YEAR	Beam (b = 12 in)				Column			
		H, IN	A _s , IN ²	A _v , IN ²	S _b , IN	t, IN	A _{st} , IN ²	A _v , IN ²	S _c , IN
1 3-3-40	46	32	4.8	0.10	10	22	18.7	0.44	11
	56	31	4.8	0.10	10	20	15.2	0.44	10
	63W	29	4.0	0.22	12	18	10.2	0.37	9
	63U	27	4.0	0.22	12	18	10.2	0.37	9
	73	29	4.0	0.22	6	18	10.2	0.37	3
2 3-5-60	46	32	4.8	0.10	10	18	10.2	0.37	9
	56	31	4.8	0.10	10	18	10.2	0.37	9
	63W	28	4.0	0.10	5	14	6.3	0.37	7
	63U	23	3.2	0.22	10	14	6.3	0.37	7
	73	24	3.2	0.22	5	14	6.3	0.37	4
3 4-3-40	46	35	4.8	0.10	10	24	18.7	0.44	12
	56	33	4.8	0.10	10	22	18.7	0.44	11
	63W	30	4.8	0.22	12	20	15.2	0.44	10
	63U	28	4.0	0.22	12	20	12.0	0.44	10
	73	30	4.8	0.22	5	22	15.2	0.80	4
4 4-5-60	46	34	4.8	0.10	10	20	15.2	0.44	10
	56	33	4.8	0.10	10	18	12.5	0.37	9
	63W	30	4.8	0.10	5	16	8.0	0.37	8
	63U	24	3.2	0.22	11	16	8.0	0.37	8
	73	25	4.0	0.22	4	16	8.0	0.37	3

Table 6 Base Shear Coefficients C_E

Year	Code	Number of Stories	
		3	4
1946	UCB	0.091 ⁽¹⁾	0.091 ⁽¹⁾
1956	UCB	0.080	0.072
1963	UCB	0.050	0.045
1973	UCB	0.050	0.045
1974	SEAOC	0.080	0.070 ⁽²⁾
1974	SEAOC	0.110	0.110 ⁽³⁾

(1) Base coefficient 0.080; C_E adjusted for 0.5 live load contribution to W_E ; i.e., $0.080 (160/140) = 0.091$.

(2) $S = I = 1.0$

(3) $S = 1.5, I = 1.25$

Table 7 Load Factors

Code	α_1	α_2	α_3	α_4	α_5
WSD	1.0	1.0	0.75	0.75	0.75
USD-63	1.5	1.8	1.25	1.25	1.25
USD-73	1.4	1.7	1.40	1.40	1.40

Table 8 Capacity Ratios R (Eq. 4) - 1973 UBC and 1974 SEAOC

1. Load factors and capacity reduction factors based on code
2. Shear resistance of reinforcement is neglected when

$$A_v < A_{vMIN}$$

Frame	Year	R - UBC 1973				R - SEAOC 1974 ⁽¹⁾			
		Beam		Column		Beam		Column	
		Bend'g	Shear	Bend'g	Shear	Bend'g	Shear	Bend'g	Shear
1 3-3-40	1946	1.44	0.51	3.15	0.41	0.96	0.51	1.34	0.41
	1956	1.39	0.50	2.41	0.46	0.92	0.50	1.03	0.46
	1963W	1.09	0.81	1.61	0.59	0.72	0.81	0.69	0.59
	1963U	1.00	0.77	1.61	0.60	0.66	0.77	0.69	0.60
	1973	1.09	1.02	1.61	1.12	0.72	1.02	0.69	1.12
2 3-5-60	1946	2.19	0.54	2.25	0.45	1.45	0.54	0.96	0.45
	1956	2.11	0.53	2.25	0.45	1.40	0.53	0.96	0.45
	1963W	1.59	0.81	1.23	0.71	1.05	0.81	0.52	0.71
	1963U	1.03	0.81	1.23	0.74	0.68	0.81	0.52	0.74
	1973	1.08	1.04	1.23	1.02	0.72	1.04	0.52	1.02
3 4-3-40	1946	1.46	0.53	3.07	0.36	0.87	0.53	1.19	0.36
	1956	1.36	0.52	2.78	0.37	0.81	0.52	1.08	0.37
	1963W	1.22	0.77	2.15	0.46	0.72	0.77	0.84	0.46
	1963U	0.95	0.79	1.84	0.57	0.57	0.79	0.71	0.54
	1973	1.22	1.06	2.40	1.12	0.72	1.06	0.93	1.12
4 4-5-60	1946	2.14	0.55	3.30	0.34	1.27	0.55	1.18	0.34
	1956	2.07	0.55	2.34	0.38	1.23	0.55	0.91	0.38
	1963W	1.85	0.78	1.54	0.54	1.10	0.78	0.60	0.54
	1963U	0.99	0.81	1.54	0.57	0.59	0.81	0.60	0.57
	1973	1.26	1.10	1.54	1.00	0.75	1.10	0.60	0.99

(1) In calculating C_E values, the following factors were used:

$$S = 1.5, I = 1.25.$$

Table 9 Coefficient C_Q (Eq. 9) for Maximum Tolerable Earthquake

1. Capacity reduction factors based on UBC 1973 Code.
2. Load factors = 1.0.
3. Shear resistance of reinforcement is included in all cases.

Frame	Year	C_Q			
		Beam		Column	
		Bending	Shear	Bending	Shear
1 3-3-40	1946	.19	.15	.22	.16
	1956	.18	.14	.17	.13
	1963W	.12	.18	.11	.10
	1963U	.10	.15	.11	.10
	1973	.12	.33	.11	.36
2 3-5-60	1946	.32	.24	.16	.13
	1956	.31	.22	.16	.13
	1963W	.21	.25	.09	.08
	1963U	.11	.17	.09	.08
	1973	.12	.33	.09	.22
3 4-30-40	1946	.16	.14	.20	.14
	1956	.14	.12	.18	.12
	1963W	.12	.14	.14	.10
	1963U	.08	.12	.12	.10
	1973	.12	.29	.15	.51
4 4-5-60	1946	.26	.19	.19	.12
	1956	.25	.18	.15	.10
	1963W	.21	.21	.10	.08
	1963U	.09	.13	.10	.08
	1973	.13	.31	.10	.24

Table 10 Time for Abatement of Hazard in
Different Building Categories

Hazard evaluation based on 1974
SEAOC values; see Table 8 for
R values and Table 4 for permis-
sible time for hazard abatement.

Building Category		A	B	C
Frame	Design Year	Col	Col	Col
3-3-40	1946	10	23	--
	1956	10	23	--
	1963W	12	28	--
	1963U	12	--	--
	1973	14*	--	--
3-5-60	1946	10	23	--
	1956	10	23	--
	1963W	12	28*	--
	1963U	12	28*	--
	1973	12*	28*	--
4-3-40	1946	8	18	35
	1956	8	18	35
	1963W	10	23	--
	1963U	12	28	--
	1973	--	--	--
4-5-60	1946	8	18	35
	1956	8	18	35
	1963W	12	28	--
	1963U	12	28	--
	1973	14*	--	--

*Note: Abatement not required by 1973 UBC.

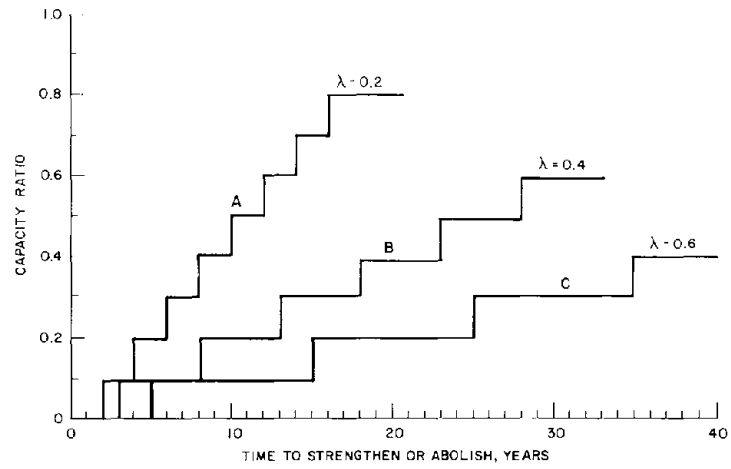


FIG. 1 PERMISSIBLE TIME FOR HAZARD ABATEMENT

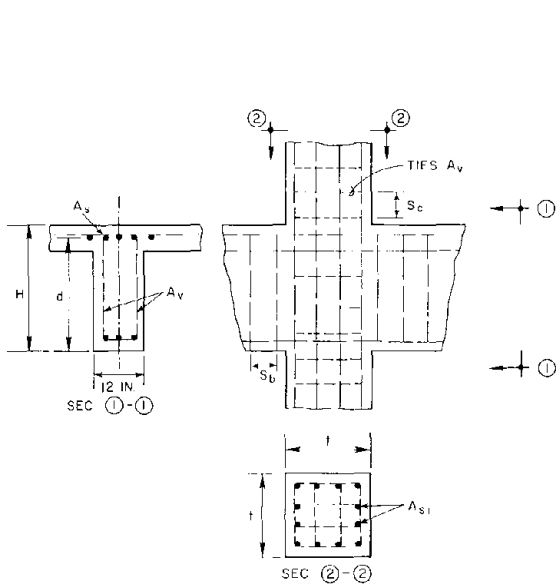


FIG. 2 TYPICAL DETAILS

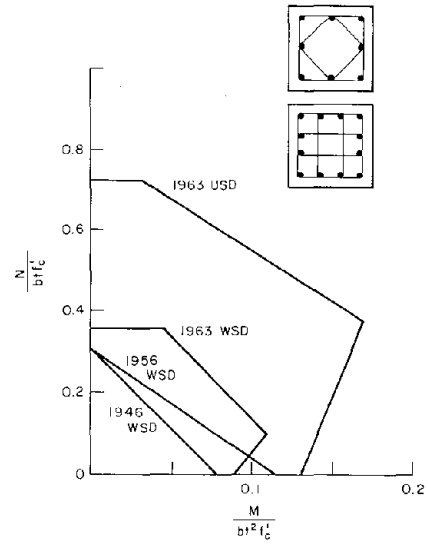


FIG. 3 TYPICAL WSD AND USD INTERACTION DIAGRAMS FOR SQUARE COLUMNS

SEISMIC SAFETY OF
EXISTING LOW-RISE REINFORCED CONCRETE BUILDINGS
- SCREENING METHOD -

by

Tsuneo Okada^{I)} and Boris Bresler^{II)}

SYNOPSIS

This paper describes a methodology for evaluating the seismic safety of low-rise reinforced concrete buildings and its application to existing school buildings. The method classifies buildings according to three types of failure mechanisms; the criteria by which buildings are judged consider nonlinear behavior in response to two levels of earthquake motion. The overall method consists of a sequence of procedures which are repeated in successive cycles using more refined idealizations of behavior in each cycle. The first cycle of the procedure is called the "First Screening" and is the cycle described in this paper.

1. GENERAL

1.1 Introduction

A methodology has been developed for evaluating the structural adequacy of existing school buildings subjected to strong earthquakes (1). In this paper, both the methodology and its application to the evaluation of existing school buildings are described. The method is based on the earthquake resistant design method for reinforced concrete buildings proposed by H. Umemura and others in 1973 (2,3). However, as the method was initially developed for the design of new buildings, it has been revised and adapted especially for evaluating the structural safety of existing buildings. The method described here evaluates low-rise reinforced concrete buildings, but could, with appropriate modification, be applied to medium-rise reinforced concrete buildings.

Although the methodology presented here may require elaboration in the future, the basic concept of using criteria for evaluating structural safety and accounting for types of failure mechanisms and nonlinear behavior in response to graded earthquake motions will provide a basis for developing even more reliable methods of evaluation.

I) Associate Professor, Institute of Industrial Science, University of Tokyo, Tokyo, Japan.

II) Professor, Department of Civil Engineering, University of California, Berkeley, California, U.S.A.

1.2 Screening Method

The structural safety evaluation considered in this report consists of a sequence of steps (Fig. 1), each following a procedure which will be described in Section 1.4. This procedure is repeated in successive cycles, the assumptions and details of the calculations being refined in each successive cycle when necessary for a reliable estimate of structural performance. This repetitive procedure is called "Screening," and is believed to be the fastest and the most practical method for reasonably evaluating the structural adequacy of a large number of buildings subjected to strong earthquake motions.

The first execution of the basic procedure is called the "First Screening." If a building cannot be classified as structurally safe after the first screening, a second more elaborate screening is required. The process continues until the structural adequacy (or inadequacy) of a building has been reliably estimated.

Three screening stages have been proposed in developing the methodology. In the first screening, the load-deflection characteristic of the first story or of the weakest story is approximately evaluated. This load-deflection characteristic is adopted as an analytical model and earthquake response is evaluated using linear response spectra for the strength safety evaluation and nonlinear earthquake response spectra for the ductility safety evaluation. In the second screening, the overall structural behavior of each story is estimated more precisely and a time history nonlinear response analysis is adopted. In the third screening, a nonlinear response analysis based on the nonlinearity of each member is adopted. Since the second and the third screening methods are not fully developed, this paper primarily describes the first screening.

1.3 Criteria for Evaluation of Structural Safety

The most important factors in determining structural adequacy are the criteria which define permissible damage resulting from a specified earthquake. The characteristics and intensities of future earthquakes are uncertain and the response of buildings to such earthquakes involves many unknown factors.

In attempting to account for these unknowns, two grades of earthquake ground motion and two degrees of building damage corresponding to the two ground motions were adopted as shown in Table 1(a). The decision criteria are based on the assumption that only slight structural damage which can be easily repaired is permitted for a strong earthquake, and that for a severe earthquake structural damage is permitted, but collapse is not.

1.4 Flow Diagram of Basic Procedures

A flow diagram of the procedure adopted in this report is shown in Fig. 1, which represents the procedure of the first screening; the procedure is basically the same for all screening stages, but the details of carrying out the calculations differ.

The procedure consists of the following five major steps:

- (A) Structural Modeling
- (B) Analytical Modeling (Evaluation of Structural Response under Lateral Forces)
- (C) Strength Safety Evaluation
- (D) Ductility Safety Evaluation
- (E) Synthesis Evaluation of Safety

1.4.1 Structural Modeling - Step (A)

The evaluation is begun by selecting a structural model representing the load transmission system of the building. Gravity and seismic load transmission systems and the intensity of gravity load are determined by examining drawings, design calculations, specifications, construction records, and field investigations. Since proper structural modeling is one of the most important steps in evaluating structural safety, this step should be performed with utmost care. If, however, it is difficult to choose a structural model which accurately characterizes the structural behavior of the building, several types of models representing different load transmission systems should be investigated and the adequacy of the building should be judged within the bounds of the results based on the adopted structural models.

1.4.2 Analytical Modeling (Evaluation of Structural Response under Lateral Forces) - Step (B)

The load-deformation characteristics of a structural system subjected to lateral forces in both linear and nonlinear ranges are determined in this step. Analytical models for earthquake response analysis are also chosen.

1.4.3 Strength Safety Evaluation - Step (C)

The adequacy of lateral strength is evaluated by considering the relationship between the strength of the building and the applicable decision criteria. In order to ensure that only buildings having a high degree of seismic safety are classified as "safe," the strength requirement is evaluated using a linear earthquake response analysis. If it is not clear that a building fully satisfies the criteria matrix, it is classified as "uncertain," and the next step of the evaluation must be carried out. This step in the evaluation is used primarily in the first screening, because buildings which do not pass the first screening will probably be judged "uncertain" at this step in the second screening.

1.4.4 Ductility Safety Evaluation - Step (D)

The ductility safety evaluation is performed for buildings which are classified "uncertain" in the strength safety evaluation. This evaluation must be based on a nonlinear response analysis. If the response ductility of the building is greater than the specified limit value, then the building cannot be classified "safe" and a more precise evaluation of strength and ductility (the "Second Screening") must be carried out. If, however, it is clear that the building is "unsafe," the building is so

judged at this step without requiring any further evaluation.

1.4.5 Synthesis Evaluation of Safety - Step E (E)

While the question of seismic safety can be resolved in the previous step, it is recommended that the synthesis evaluation be performed as the final step of each screening stage, in order to determine how safe, unsafe, or uncertain a building may be. This step in the evaluation should also provide a basis for reviewing the many assumptions and unknowns incorporated into the screening process. The synthesis evaluation is helpful in indicating the need for rehabilitation and strengthening in existing buildings.

2. FIRST SCREENING METHOD

The criteria for evaluating structural safety and the procedure of the first screening method are described in this section.

2.1 Decision Criteria for First Screening

For the first screening, the terms "strong" and "severe" earthquakes and "reparable" and "noncollapse" structural damage are generally defined in Table 1(a) and are more precisely defined in Table 1(b). A strong earthquake was defined as having an intensity of 0.3g (i.e., 30% of gravity) and a severe earthquake as having an intensity of 0.45g, where intensity is given in terms of normalized peak ground acceleration.

Three different types of failure mechanisms, bending, shear, and shear bending, were considered. In a bending failure, the failure mechanism of the building is governed by the bending failure of members and the failure mechanism is ductile. In a shear failure, the failure mechanism of the building is governed by the shear failure of members and is not ductile but brittle. In a shear-bending failure, shear and bending failures in individual members occur with the possibility of shear cracking, but the overall failure mechanism is governed by bending.

The decision criteria are defined by considering the two earthquake intensities and the three types of failure mechanisms discussed above (Table 1(b)). This set of criteria is called the "Criteria Matrix." The criteria are also illustrated schematically in Fig. 2, where the symbol ∇ indicates the criterion corresponding to each earthquake intensity and each type of failure mechanism.

The criteria matrix (Table 1(b)) together with the assumptions adopted in the analytical modeling define acceptable levels of damage for strong and severe earthquakes. The degree of damage acceptable in the event of a strong earthquake (0.3g) is defined to be less than that which occurred in buildings in the city of Hachinohe during the 1968 Tokachi-oki earthquake. For a severe earthquake (0.45g), a structure satisfying the criteria matrix must not collapse.

In order to improve the accuracy of the first screening, modifications of the criteria matrix should be made to account for the following:

- (1) Local seismological conditions should be considered in choosing the intensity and characteristics of earthquake ground motion used in the evaluation.
- (2) Since the ductility factors in the criteria matrix, i.e., 2.0 for an 0.3g earthquake or 4.0 for an 0.45g earthquake, are approximated for the overall ductility of buildings, these factors may be modified to account for the structural performance of a particular building. For example, if there is a sufficient amount of lateral reinforcement to ensure ductility greater than that defined by the criteria matrix, then the ductility factors of the criteria may be increased; if the axial stress in the column due to gravity load is large, the factor should be reduced.
- (3) All buildings are classified into the three major types according to failure mechanism. However, if more failure mechanisms are considered, classification may result in more reliable evaluation. For example: (a) the mechanism governed by overturning of the foundation which is included in the bending type in this paper, could be separated from the bending type, and (b) the bending type of failure could be subdivided into the beam yielding type and the column yielding type, because it is reasonable to allow higher ductility for the beam yielding than the column yielding type.
- (4) As the criteria shown in Table 1(b) were defined for the overall response of a building, the matrix should be modified if the evaluation is based on the structural performance of each frame or each member.

These considerations are important for improving the reliability of the first screening method and in developing additional screening stages. Also, seismic safety may be reasonably evaluated if these considerations are accounted for by engineers when executing the proposed first screening.

2.2 Description of First Screening Method

The overall procedure of the first screening method is described in this section:

- Step (A): Structural Modeling - The procedure for the first screening is the same as that for the general procedure described in Section 1.4.1.
- Step (B): Analytical Modeling - Shear cracking strength, ultimate shear strength, and bending strength for all stories are calculated independently and the building is classified by failure type. Failure type is usually determined by the characteristics of the first story; if failure at another story controls, modification of the method is required (1).

By comparing the shear cracking strength C_{sc1} , ultimate shear strength C_{su1} , and bending strength C_{By1} in terms of base shear coefficients, the type of failure is determined as follows:

$$C_{Byl} < C_{scl} < C_{sul} : \text{ Bending type}$$

$$C_{scl} < C_{sul} < C_{Byl} : \text{ Shear type}$$

$$C_{scl} < C_{Byl} < C_{sul} : \text{ Shear-bending type}$$

Load-deformation characteristics and the values in the decision criteria matrix also depend on the type of failure mechanism as shown in Fig. 2.

The fundamental natural period and modal participation factors are assumed either at this step or at the next step.

Step (C): Strength Safety Evaluation - The lateral strength determined at Step (B) is compared with the linear response base shear coefficients. If the building satisfies one of the following conditions, it is evaluated "safe" both for an 0.3g and an 0.45g earthquake:

$$\text{For bending type} : C_E(0.3g) \leq C_{Byl}$$

$$\text{For shear type} : C_E(0.3g) \leq C_{scl} \text{ and} \\ C_E(0.45g) \leq C_{sul}$$

$$\text{For shear-bending type: } C_E(0.3g) \leq C_{scl} \text{ and} \\ C_E(0.45g) \leq C_{Byl}$$

where

$C_E(0.3g)$ - Linear response base shear coefficient for 0.3g earthquake

$C_E(0.45g)$ - Linear response base shear coefficient for 0.45g earthquake.

In this study, a standardized response spectrum was adopted for estimating linear response.

Step (D): Ductility Safety Evaluation - The first story response displacement is calculated using modified modal participation factors and a nonlinear response displacement spectrum; the safety of the building is then evaluated using this first story response displacement. If the response displacement of the first story is less than that defined by the criteria matrix, the building is evaluated "safe." The nonlinear response spectrum used in this evaluation must correspond to the type of failure mechanism established in Step (B). Therefore, three kinds of nonlinear response spectra corresponding to the types of failure mechanisms are used to evaluate response ductility (1).

Step (E): Synthesis Evaluation of Safety - The synthesis evaluation of safety in the first screening uses a shear strength-bending strength diagram with shear cracking strength and bending strength axes (Fig. 11(a)).

2.3 Details of First Screening Method

2.3.1 Step (A): Structural Modeling

The main items for the structural modeling are as follows:

(1) Structural System: The plan of each floor, section of each frame, cross-section of each member, and detailing of all joints are investigated through drawings. The foundation system should also be investigated by examining drawings and specifications. Any modification of the original design should be carefully checked by field inspection and all available documentation.

(2) Load Intensity: The average weight per unit floor area, including all gravity dead and live loads, is either determined from design calculations or independently calculated.

(3) Load Transmission System: Both gravity and seismic load transmission systems should be considered. A rough estimate of the building's safety may be made by an experienced investigator at this step.

(4) Properties of Materials: The specified material properties should be evaluated whenever possible. Information on soil conditions is necessary for evaluating the overturning capacity of the building, and should be ascertained from drawings or soil investigation reports.

(5) Design Method: Building code provisions, especially those adopted for the original seismic design, should be checked, and any discrepancy between design calculations and the code should be noted.

(6) Other Special Structural Features: Special features which might affect the seismic safety of a structure should be investigated. Such features include asymmetry and discontinuity in plan and in elevation, and local seismicity.

2.3.2 Step (B): Analytical Modeling (Evaluation of Structural Response under Lateral Forces)

The following approximations are adopted for estimating shear cracking strength, ultimate shear strength, bending strength, fundamental natural period, and modal participation factors:

(1) Shear Cracking Strength (C_{sci}): The average shear stress method (1,2) is used. If the shear cracking capacity of a story level is assumed as a function of the total cross-sectional area of concrete, then the shear cracking capacity can be determined as some assumed shear stress times the total area of concrete.

$$Q_{sci} = \tau_{av} \times (A_{ci} + A_{wi}) \quad (1)$$

where

- Q_{sci} - shear cracking strength at i-th story
- τ_{av} - assumed average shear cracking stress
- A_{ci} - Σ column cross-sections at i-th story
- A_{wi} - Σ wall cross-sections at i-th story

Defining the column-area ratio (a_{ci}) and the wall-area ratio (a_{wi}), the shear cracking strength in terms of shear coefficient (C_{sci}) is:

$$C_{sci} = \frac{Q_{sci}}{\sum_{j=i}^n \bar{W}_j} = \frac{\tau_{av}}{w_i} \times (a_{ci} + a_{wi}) \quad (2)$$

where

- \bar{W}_j - weight of j-th story
- n - total number of stories
- $a_{ci} = \frac{A_{ci}}{\sum_{j=i}^n A_{fj}}$
- $a_{wi} = \frac{A_{wi}}{\sum_{j=i}^n A_{fj}}$
- A_{fj} - floor area of j-th story
- $w_i = \frac{\left(\sum_{j=i}^n \bar{W}_j \right)}{\left(\sum_{j=1}^n A_{fj} \right)}$ - average weight of the i-th floor level and above

If the average shear cracking stress τ_{av} is assumed, the shear cracking strength can be calculated by Eq. 2.

The average shear cracking stress is estimated by the following method:

Average shear stress when shear cracking occurs at the i-th seismic element of the j-th story is:

$$\tau_{av} = \tau_c \times \left(\frac{A_i}{\bar{A}_j} \bigg/ \frac{K_i}{\bar{K}_j} \right) \quad (3)$$

where

- τ_c - shear cracking stress which was assumed as $4\sqrt{f'_c}$
(f'_c : concrete compressive strength in psi).
- A_i - cross-sectional area of i-th element
- \bar{A}_j - Σ cross-sectional area of elements of j-th story
- K_i - lateral stiffness of i-th element
- \bar{K}_j - Σ lateral stiffness of j-th story

The term of $\left(\frac{A_i}{\bar{A}_j} / \frac{K_i}{\bar{K}_j} \right)$ in Eq. 3 is defined as the modification factor for

shear cracking stress (α_s) and is assumed as follows:

If it is assumed that all wall elements and all column elements have similar geometries then the modification factor (α_s) for shear cracking in walls is obtained by:

$$\alpha_s = \frac{A_w}{A_w + A_c} \left(1 + \frac{K_c}{K_w} \right) \quad (4)$$

where

- A_w - Σ cross-sectional area of walls
- A_c - Σ cross-sectional area of columns
- K_c - Σ stiffness of columns
- K_w - Σ stiffness of walls

The modification factor (α) can be approximately estimated by Eq. 4 by assuming the ratio $(K_c/K_w)^s$.

(2) Ultimate Shear Strength (C_{sui}): Ultimate shear strength is calculated by the following equation:

$$C_{sui} = \alpha \times C_{sci} \quad (5)$$

In the first screening, α is actually taken as 1.9. However, as this value has been derived from experimental data on shear walls surrounded by frames (2), it is recommended that the value of 1.9 be modified for walls without frames or for columns by considering shear span ratio, amount of shear reinforcement, etc.

(3) Bending Strength (C_{Byi}): Bending strength is evaluated by an approximate limit state analysis assuming that plastic hinges form at each connection of structural beams, columns, and footings.

The computer programs "HMECH" and "SWALL" have been developed for this purpose (1). The base shear coefficient for a frame consisting of beams and columns is calculated by the following method:

At each connection, one of the following failure mechanisms is assumed: beam-hinge type, column-hinge type, or tie beam-footing type (Fig. 3). The type of mechanism assumed is determined by comparing either the sum of the column moments (above and below the connection) to the sum of the beam moments (to the left and to the right of the connection) or the column moment to the sum of the tie beam moments and the footing moment. The lowest sum determines the type of failure mechanism. The average moment for the type of failure mechanism is assigned either to the column above and below the connection or to the beam left and right of the connection. The shear force is then determined:

$$Q_i = \sum_{j=1}^m \frac{T^M_{cj} + B^M_{cj}}{h_i} \quad (6)$$

and

$$C_i = \frac{Q_i}{\sum_{j=i}^n \bar{W}_j} \quad (7)$$

where

- Q_i - story shear at the i-th story
- T^M_{cj} - moment at the top of the column
- B^M_{cj} - moment at the bottom of the column
- h_i - story height of the i-th story
- m - number of columns and walls of the i-th story
- C_i - shear coefficient at the i-th story
- n - total number of stories

A shear wall with frames is modeled as an equivalent beam-column frame with rigid zones as shown in Fig. 4 and analyzed by the following method:

- (1) Inflection points of the boundary beams and the tie beams are assumed between the midspan and the adjacent column line;
- (2) Yield hinges at the end of the boundary beams are assumed to have formed;
- (3) Distribution of lateral force is assumed to be either uniform or triangular along the stories;

(4) Base shear coefficients for all possible yield hinge mechanisms are calculated using equilibrium and the minimum value is used as the base shear coefficient.

The yield moments are calculated by the following equations (2,4):

$$\text{Beam: } M_y = 0.9 A_t f_y d \quad (8)$$

where

M_y - yielding moment

A_t - area of tension steel

f_y - yield strength of tension steel

d - distance from extreme compression fiber to centroid of tension steel

$$\text{Column: } M_y = 0.8 A_t \cdot f_y \cdot D + 0.5ND \left(1 - \frac{N}{bDf'_c}\right) \quad (9)$$

If the axial load N is greater than $0.4 bDf'_c$, this equation may not be used.

where

D - depth of column

b - width of column

N - axial load (positive in compression)

f'_c - compressive strength of concrete

$$\text{Wall Surrounded by Columns: } M_y = A_g \cdot f_y \cdot L + \frac{N}{2} \cdot L \quad (10)$$

where

A_g - area of longitudinal steel in a column

L - distance from the centroids of columns surrounding the wall

N - axial load (positive in compression)

Wall without Columns: Use strain compatibility or Eq. 9.

Footing: The moment based on soil-bearing capacity is substituted for the yielding moment of the footing.

$$M_y = \frac{f_o}{2} \left(1 - \frac{f_o}{f_b}\right) BL^2 \quad (11)$$

where

- f_o - stress of foundation soil by axial load $N (= N/BL)$
- f_b - ultimate bearing stress of foundation soil
- B - width of footing slab
- L - depth of footing slab

(4) Natural period: The following equation may be adopted for approximately estimating the fundamental natural period:

$$T = (0.06 - 0.10) \times n \quad (12)$$

where

- n - total number of stories

Generally speaking, a smaller value of T results in a conservative estimation of the nonlinear response displacement, but an unconservative estimation of the nonlinear response ductility factor. Therefore, it is recommended that a smaller value of T be assumed in calculating the response ductility factor and a larger value of T be assumed in calculating the response displacement for the ductility safety evaluation.

(5) Modal Participation Factor: The modal participation factors of the first mode are adopted, since the influence of higher modes is negligible for low-rise reinforced concrete buildings. An idealized lumped mass system, such as a system with uniformly distributed story masses and stiffnesses or a system with a linear mode shape, etc., is adopted for approximately estimating modal participation factors.

2.3.3 Step (C): Strength Safety Evaluation

In order to evaluate structural adequacy quickly, strength in terms of the base shear coefficient is compared to the linear response base shear coefficient. As shown in Fig. 5, if the linear response base shear coefficient falls within the range indicated by the heavy line, the building is considered to satisfy the decision criteria shown by the symbols ∇ and \blacktriangledown , and is evaluated as "safe." Thus, as this evaluation primarily deals with strength, it is called the "Strength Safety Evaluation." Nonlinear response is indirectly considered in this step.

In calculating the linear response base shear coefficient C_E , the building is assumed to be a story level lumped mass system with n degrees of freedom (where $n =$ no. of stories). The linear elastic response of the equivalent one-mass system is determined by assuming the first mode shape and neglecting the other modes. The response base shear coefficient, C_E , is then determined by the following equation:

$$C_E = \frac{\sum_{i=1}^n (\beta u)_i \bar{W}_i}{\sum_{i=1}^n \bar{W}_i} \times \frac{S_\alpha}{g} \quad (13)$$

where

- C_E - response base shear coefficient
 $(\beta u)_i$ - modal participation factor at the i-th story
 \bar{W}_i - weight of the i-th story
 n - total number of stories
 S_α - linear response spectral acceleration

In calculating the linear response spectral acceleration S_α , it is desirable to use a response spectrum which considers foundation condition, local seismicity and other features at the site of the building. In order to simplify the evaluation, however, the following standardized spectrum by H. Umemura is adopted in this report

$$\begin{aligned} S_\alpha &= 3500 \cdot k_g \quad (\text{cm/sec}^2) \quad \text{for } T < 0.5 \text{ sec} \\ S_\alpha &= \frac{1750}{T} \cdot k_g \quad (\text{cm/sec}^2) \quad \text{for } T \geq 0.5 \text{ sec} \end{aligned} \quad (14)$$

where

- T - natural period of one-mass system in seconds
 k_g - maximum acceleration of ground motion normalized by the acceleration of gravity g .

2.3.4 Step (D): Ductility Safety Evaluation

Step (D) estimates the first story displacement using nonlinear response spectra of displacement and modified modal participation factors to idealize the nonlinear behavior of the building.

The simple method adopted here roughly evaluates ductility. If, however, the result obtained using this method is questionable, the final evaluation of safety should be deferred.

In estimating building ductility:

- 1) the type of failure (type of hysteresis loop) is determined;
- 2) the equivalent one-mass system is estimated;
- 3) the normalized response spectrum is entered with an estimated natural period and strengths of the equivalent one-mass system, and the maximum response ductility of the one-mass system (μ_0) is then estimated;
- 4) the response ductility factor at the first story of the building ($\beta \mu$) is estimated using μ_0 and the modification factor ($m \cdot f$) for the modal participation factors; and

5) the ductility safety of the building is evaluated by comparing the response ductility factor ($\beta\mu$) with the decision criteria.

(1) Nonlinear Response Spectra: Nonlinear response displacement spectra for the Taft 1952, El Centro 1940 and Hachinohe 1968 earthquakes for the three types of hysteresis loops are used in the first screening.

They are:

Origin-oriented hysteresis loop for Shear type

Degrading Tri-linear hysteresis loop for Bending type

Modified Degrading Tri-linear hysteresis loop for Shear-Bending type.

The response spectra of the origin-oriented and the degrading tri-linear type are from Reference (2). The response spectra of the modified degrading tri-linear type were calculated by Dr. M. Murakami from Reference (1) and two examples are shown in Fig. 13. The hysteresis loops are shown in Fig. 6.

(2) Equivalent One-Mass System and Modified Modal Participation Factors: A three-story shear type building is used to illustrate the procedure for assuming an equivalent one-mass system and for estimating the nonlinear response at the first story of the building (Fig. 7).

The basic assumptions for the procedure are that the first mode of vibration dominates in the linear range, and that each story reaches the critical stage simultaneously or the first story reaches the critical stage first.

The shear cracking strength of the equivalent one-mass system is:

$$k_c = C_{scl} \times \frac{\sum_{i=1}^n \bar{W}_i}{\sum_{i=1}^n (\beta u)_i \bar{W}_i} \quad (15)$$

where

k_c - cracking strength in terms of shear coefficient of the equivalent one-mass system

C_{scl} - cracking strength in terms of shear coefficient of the first story of the building

$(\beta u)_i$ - modal participation factor of i-th story

\bar{W}_i - weight of i-th story

For a low-rise building, the term, $\frac{\sum_{i=1}^n \bar{W}_i}{\sum_{i=1}^n (\beta u)_i \bar{W}_i}$ may be assumed as

1.0-1.2. The response displacement for the equivalent one-mass system obtained from the nonlinear response spectrum is modified for the ductility safety evaluation of the first story by the following method:

As shown in Fig. 7, the relationship between the displacement of the equivalent one-mass system and that of the first story of the multi-mass system is:

$$B \delta_c = (\beta u)_1 \times \delta_c \quad (16)$$

$$B \delta_{\max} = (m \cdot f) \times (\beta u)_1 \times \delta_{\max} \quad (17)$$

$$B \mu_1 = (m \cdot f) \times \mu_0 \quad (18)$$

where

- $B \delta_c$ - displacement at the first story of the building at the shear cracking stage
- δ_c - displacement of the equivalent one-mass system at the shear cracking stage
- $B \delta_{\max}$ - maximum displacement at the first story of the building
- δ_{\max} - maximum displacement of the equivalent one-mass system
- $B \mu_1$ - ductility factor at the first story of the building
- μ_0 - ductility factor of the equivalent one-mass system
- $(m \cdot f)$ - modification factor

The modification factor $(m \cdot f)$ in Eqs. 17 and 18 is assumed considering the pseudo-modal participation which depends upon the mode shape in non-linear range.

As shown in Fig. 7, if each story in Building Type A reaches the cracking stage simultaneously, the modification factor for displacement can be assumed as unity. The mode shape in the nonlinear range is assumed to be similar to the linear mode shape in this case.

In the case of Building Type B where the first story reaches the cracking stage before other stories, a modification factor should be adopted.

If it is assumed that the maximum displacement at the top of Building Type B is equal to that of Building Type A (5), the modification factor may be assumed as follows:

$$1 < (m \cdot f) < \frac{(\beta u)_{top}}{(\beta u)_1} \quad (19)$$

where

- $(\beta u)_{top}$ - modal participation factor at the top of linear system
 $(\beta u)_1$ - modal participation factor at the first story of linear system.

2.3.5 Step (E): Synthesis Evaluation of Safety

The result of the first screening is illustrated on the shear cracking strength-bending strength diagram (Fig. 11).

This diagram is prepared as follows:

(1) Classification of the Type of Failure: Two lines are drawn on the shear cracking strength-bending strength diagram as shown in Fig. 8. The solid line indicates the boundary between the bending type and the shear-bending type and the broken line indicates the boundary between the shear-bending type and the shear type. The bending strength and the shear cracking strength at the first story of the building obtained in Step (B) are plotted in this diagram.

(2) Zoning by Strength Safety Evaluation: Further zoning is possible both for an 0.3g earthquake and for an 0.45g earthquake by using the results of the strength safety evaluation (Step (C)) as shown in Fig. 9. C_E is the linear response shear coefficient at the first story from Eq. (13). The hatched zone shows that the safety of a building in this zone is uncertain at this step.

(3) Zoning by Ductility Safety Evaluation: The safety zone is enlarged by using the results of the ductility safety evaluation (Step (D)) as shown in Fig. 10. As the strength is adopted for the coordinates in Fig. 10, an appropriate conversion from displacement to strength is required to express the results of the ductility safety evaluation. For this purpose, a "Critical Strength" concept (2,3) is adopted in this report.

It has been recognized that the minimum strength which is required in order that a building's maximum response displacement be within the given ductility factor could be approximately estimated using a nonlinear response spectrum (2,6,7,8). This minimum strength is called "Critical Strength." Generally speaking, critical strength depends on nonlinear load-deformation characteristics, damping characteristics, characteristics of the ground motion, etc.

In this report, these factors have been already assumed. Critical strength can be estimated if the natural period, the mode shape of the building, and the modification factor ($m \cdot f$) for the mode shape in the non-linear range are evaluated.

For example, for a bending type building in an 0.3g earthquake, the maximum allowable ductility factor of an equivalent one-mass system is:

$$\mu_o = 2.0/(m \cdot f) \quad (20)$$

From the nonlinear response spectrum for the degrading tri-linear system, the minimum yield strength of the one-mass system (k_{cr}) for preventing larger displacements than the ductility factor of μ_o is obtained as follows:

$$k_{cr} = \alpha_o \cdot k_g \quad (21)$$

The minimum yield strength of the first story is:

$$C_{cr} = \frac{\sum_{i=1}^n (\beta u)_i \bar{W}_i}{\sum_{i=1}^n \bar{W}_i} \times \alpha_o \times k_g \quad (22)$$

Similar considerations are possible for shear-bending and shear type buildings. However, since the critical strength of a shear-bending type building in an 0.45g earthquake depends on the ratio of bending strength and shear cracking strength, one critical strength which suffices for a number of buildings of this type cannot be defined. The boundary is, thus, neither parallel to the ordinate nor to the abscissa in Fig. 10, but is a curve beginning at point-1 and terminating at point-2 as shown in Fig. 10. In order to facilitate calculation and to keep the evaluation conservative, the line 1-2-3 was adopted instead of the curve 1-2 (Fig. 10).

In Fig. 10, $C_{cr}(0.3g)$ and $C_{cr}(0.45g)$ indicate the critical strengths for the 0.3g and 0.45g earthquakes. \bar{C}_{cr} is the critical shear strength for the 0.45g earthquake.

Diagrams for the 0.3g and 0.45g earthquakes are shown together in Fig. 11(a) which is divided into nine zones. The characteristics of each zone are shown in Fig. 11(b). By plotting the results obtained by the first screening in a diagram such as Fig. 11(a), the synthesis evaluation of safety, including the ranking of safety, can be easily carried out.

The buildings belonging to Zones A, B, C, and D are evaluated "safe" in the Strength Safety Evaluation and are ranked as I. The buildings of Zone E are evaluated as "safe" in the Ductility Safety Evaluation and are ranked as II.

Because the buildings in Zones F and G satisfy either the criteria for an 0.3g or an 0.45g earthquake but not both, they are ranked as III. However, since they are located at the boundary between safety and unsafety, it is recommended that they be more precisely evaluated in further screenings.

The buildings in Zones H and I receive the worst ranking of IV. These buildings can be classified as "unsafe" in the first screening.

3. APPLICATION OF FIRST SCREENING TO EXISTING BUILDINGS

The method described above was applied to two school buildings in California; in this paper, these buildings will be identified as "School Building A" and "School Building B." The method was also applied to damaged and undamaged buildings located in the city of Hachinohe which was affected by the 1968 Tokachi-oki Earthquake.

3.1 School Building A

3.1.1 Step (A): Structural Modeling

(1) Structural System: School Building A, constructed in 1965, is a three-story reinforced concrete building consisting of core walls, precast concrete columns, and lift-slabs with post-tensioning. On the second and third floors there are exterior walls of precast concrete panels. The plan of the structural system is shown in Fig. 12.

(a) Foundation - Ground soil consists of "sandy silty clay." The allowable bearing capacities adopted in the original design were 3000 lb. per sq. ft. for the vertical load of (dead load + 1/4 x live load) and 4500 lb. per sq. ft. for (dead load + live load).

(b) First Floor - The first floor slab is a 4 in. concrete slab, directly supported on the ground soil. First floor vertical elements consist of precast concrete columns 16 in. x 16 in. with 4 No. 9 bars for exterior columns and 18 in x 18 in. with 6 or 8 No. 9 bars for interior columns, core walls 9 in. thick, shear walls 10 in. thick, and brick veneer exterior walls. Since the brick veneer exterior walls are located at the columns' midspans and terminate at the ceiling, they are not considered to be structural elements.

(c) Second and Third Floors - The structural elements of the second and third floors are the same as those of the first floor with the exception of the reinforcement used for the interior columns and exterior walls. The floor slabs are concrete lift-slabs, 8-1/2 in. thick with post-tensioning. The slab is connected to columns by steel shear collars and shear bars inserted into the columns. The anchorage bars are placed at the connection between the slab and the concrete wall. The exterior wall was not considered to be a structural element in the original design. However, it is expected that the exterior wall acts as a structural element during an earthquake because lateral stiffness may be fairly great.

(d) Roof - The roof consists of roofing, vermiculite, and a post-tensioned concrete slab 8-1/2 in. thick.

(2) Load Intensity: The average dead weight of the building per unit floor area including beam, column, wall, and other dead load was calculated as 156 psf.

(3) Load Transmission System:

(a) The gravity load of the floor system is transmitted to the foundation primarily by the columns, although part of the gravity load can be

transmitted through the interior walls. The exterior wall panels may also transmit some part of the gravity load.

(b) Seismic load is primarily transmitted through the core walls to the stairs and elevators and the walls in the F- and J-frames. These are called "core wall," "elevator wall," and "FJ-wall," respectively in this paper. As there was a construction joint at the middle of the floor slab, the floor system of the building was considered to consist of two separate parts in the original design. But since the joint was filled by concrete after fabrication, the floor system was considered to be continuous in evaluating lateral force response. The exterior wall panels at the second and third floors were not considered to be structural elements in the original design, but can carry fairly large portions of lateral force.

(4) Material Properties: Material properties specified in the original design were as follows:

- concrete - 5000 psi compressive strength for precast concrete columns
4000 psi lightweight aggregate concrete for slabs and walls
- steel - A432 (Grade 60) for longitudinal reinforcement of columns
A15 (Grade 40) for other reinforcement

(5) Structural Design: The structural design of Building A was based on Title 19 and Title 21 of the California Administrative Code and the ACI Building Code (318-63). The adopted lateral shear coefficient was 0.092 for the first story, 0.109 for the second story, and 0.133 for the third story.

(6) Special Structural Features: In order to evaluate the behavior of this building in response to lateral forces, the following special features were considered:

(a) The stiffnesses of the slab-column connection and the slab-wall connection are uncertain; these values may significantly affect the lateral force capacity of the columns and walls.

(b) The strength of the slab, which could behave as an equivalent beam in the overall response to lateral forces, is uncertain.

(c) The stiffness and strength of the exterior precast concrete panels at the second and third stories are also uncertain.

In order to accommodate the range of values represented by these uncertainties, the following two structural models were adopted:

Model A: Lateral forces were assumed to be carried only by the core walls, elevator walls, and F-J walls.

Model B: Some part of the lateral force was assumed to be carried by the columns as well as the walls considered in Model A.

3.1.2 Step (B): Analytical Modeling

(1) Shear Cracking Strength: Shear cracking strength was evaluated using Eqs. 2 and 3. The wall ratio, column ratio, and wall-column ratio are shown in Table 2. Shear cracking strengths in terms of shear coefficients are shown in Table 3. In calculating shear cracking strength, the following values were assumed:

$w = 172$ psf including live load of 22.5 psf for the second and the third floors and 5 psf for the roof

$\tau_c = 280$ psi (20 kg/cm²) ($4\sqrt{f'_c}$, $f'_c = 5000$ psi)

$\tau_{av} = \tau_c = 280$ psi for Model A

$= 0.7 \tau_c = 196$ psi for Model B

In estimating τ_{av} for Model B, the modification factor α_s was calculated by Eq. 4 using the wall ratio and column ratio in Table 2 and assuming K_c/K_w to be 0.25.

Because it was predicted that shear cracking strength was greater than bending strength for Model B, it was not necessary to calculate ultimate shear strength.

(2) Bending Strength: Bending strengths in terms of shear coefficients are shown in Table 3. The computer programs HMECH and SWALL (1) were used in calculating the bending strength of frames and walls with boundary beams, respectively, based on the method described in Section 2.3.

The following assumptions were adopted in the calculation:

Yield strength of reinforcement: 60,000 psi for Grade 60 and 40,000 psi for Grade 40

Concrete compressive strength: 5000 psi for precast concrete columns and 4000 psi for walls

Ultimate bearing capacity of ground soil: A value twice the allowable bearing capacity of 4500 psf adopted in the original design was assumed

Bending capacity of equivalent beam for lift-slab: A value greater than the bending capacity of the columns in Model B was assumed.

(3) Estimation of Failure Type: In order to determine the failure type for the building, shear strength was compared to bending strength. For both Model A and Model B, the failure type was "Bending" as shown in Table 3.

In the case of Model A, the rotation of the footings of the shear wall, which is included in the "Bending Type" in this report, may govern the failure mechanism. In the case of Model B, the yielding of the columns as well as the rotation capacity of the shear wall may contribute to the failure mechanism. For buildings with such failure mechanisms, evaluations can be made for the first story.

(4) Fundamental Natural Period: A value of 0.3 sec. was assumed for the analysis using an approximation from Eq. 12.

(5) Modal Participation Factors: Assuming the uniform distribution of mass and stiffness, the modal participation factors were estimated as follows:

$$(\beta u)_3 = 1.22, (\beta u)_2 = 0.98, (\beta u)_1 = 0.54$$

3.1.3 Step (C): Strength Safety Evaluation

The linear base shear coefficient C_E was calculated using Eqs. 13 and 14.

$$\text{For } 0.3g \text{ earthquake: } C_E(0.3g) = 0.99$$

$$\text{For } 0.45g \text{ earthquake: } C_E(0.45g) = 1.48$$

After comparing the strength of the building shown in Table 3 with the linear response base shear coefficients, it was judged that the safety of the building could not be evaluated at this step.

3.1.4 Step (D): Ductility Safety Evaluation

The nonlinear response spectra for the degrading tri-linear loop shown in Fig. 13 were used for the ductility safety evaluation.

(1) The strength of the equivalent one-mass system was calculated using Eq. 15 by substituting C_{By1} for C_{scl} . The term $(\sum_{i=1}^n \bar{W}_i / \sum_{i=1}^n (\beta u)_i \bar{W}_i)$ was assumed to be 1.1 (Table 4).

(2) Nonlinear responses of the equivalent one-mass systems are shown in Tables 5(a) and 5(b). They were calculated by the following method:

The X-direction of Model A for an 0.3g earthquake (Taft) is chosen as an example for explaining the method. Assuming a natural period of 0.3 seconds, the response displacement for a 1.0g earthquake was estimated as more than 12 inches (30 cm) (Fig. 13). The displacement of 30 cm was obtained from the curve for k_y/k_g of 0.5.

The ductility factor was obtained by the following equation:

$$\mu = \frac{S_D \cdot k_g}{\frac{g}{4\pi^2} \cdot T_2^2 \cdot k_y} \quad (23)$$

where

S_D - response displacement for 1.0g earthquake

T_2 - natural period for yielding stiffness

Substituting 30 cm for S_D , 0.37 for k_y/k_g , and $\sqrt{2} T_1 (\sqrt{2} \times 0.3)$ for T_2 , a ductility factor of 9 was obtained.

(3) The nonlinear responses of the building are shown in Table 6. They were obtained using the method described in Section 2.3.4, incorporating the response of the equivalent one-mass system. The modification factor (m.f) was assumed to be 1.0. This assumption is probably reasonable for Model A because the failure mechanism is governed by the rotation of the wall footing. However, this value is slightly unconservative for Model B because the failure mechanism in that case is a combination of the footing rotation and column yielding types. As shown in Table 6, the displacements of Model A are much greater than those allowed by the criteria, both for the 0.3g and 0.45g earthquakes. The displacements of Model B satisfy the criteria for all cases but that of the 0.45g earthquake of the 1968 Hachinohe EW type.

3.1.5 Synthesis Evaluation of Safety

The structural characteristics of the building are shown in Fig. 14. The critical strengths C_{cr} and \bar{C}_{cr} were calculated using Eq. 22. From the response spectra for degrading tri-linear loop, the values of α_0 for C_{cr} were assumed to be 1.5 for an 0.3g earthquake and 1.0 for an 0.45g earthquake. For \bar{C}_{cr} , α_0 was assumed to be 1.5 for an 0.45g earthquake from the response spectra for an origin-oriented loop.

The results of the safety evaluation described above suggest the following:

(1) If Model A represents the building, the extremely large displacement beyond the displacement capacity may occur in both the 0.3g and 0.45g earthquakes. The building is thus evaluated to be "unsafe."

(2) If Model B represents the building, the building may be "safe" in an earthquake of the Taft 1952 type or the El Centro 1940 type, but "uncertain" in an earthquake of the Hachinohe 1968 type.

For Model B, it was assumed that the bending moment of the column transferred fully to the slab through the joint, while the moment transmission through the joint was neglected for Model A. Considering the detailing of the joint, the real behavior of the building may be supposed to lie between that of Model A and Model B, but closer to Model A.

The final decision as to the safety of the building at the end of the

first screening was that it was "uncertain," but close to "unsafe."

3.2 School Building B

School Building B, constructed in 1964, is a two-story reinforced concrete structure with a partial basement, consisting of beams, columns, joist slabs, and tilt-up concrete walls as shown in Fig. 15.

The gravity load of the floor system is transmitted primarily through the beams in the Y-direction and the columns to the foundation. Some part of the gravity load may be carried by the walls. The seismic load is transmitted through the columns and the walls. However, the lateral force transmission capacity of the walls in the X-direction is uncertain because the stiffness of the joint between the wall and the slab is not known. A base shear coefficient of 0.133 was adopted for the original seismic design.

Concrete with compressive strengths of 2500, 3000, and 2000 psi was used for the frames, walls, and footings, respectively. A15 steel (Grade 40) was used as reinforcement.

Since the stiffness of the joint between the slab and the wall in the X-direction (walls in lines 2 and 5 in Fig. 15) was not known, two structural models were adopted for the X-direction. In one model, Model XA, the walls mentioned above were not considered to be seismic elements, and in the other, Model XB, the contribution of such walls to the lateral force capacity was fully considered. The fundamental natural period was assumed as 0.2 sec. for the Y-direction and for Model-XA, and as 0.16 sec. for Model-XB.

The response displacement and ductility factor of the building are shown in Table 7 and the characteristics of the building are shown in Fig. 16. The failure mechanism in the Y-direction is estimated as "Bending Type" and the building is evaluated as "safe."

The safety of the X-direction strongly depends on the behavior of the exterior precast concrete tilt-up walls in lines 2 and 5. If the stiffness and strength of the joint between the slab and the wall were enough to transfer shear force, then the failure type in the X-direction would be "Shear Type" and the building would be evaluated as "safe." If, however, the stiffness and strength of the joint were insufficient, a large displacement would be predicted and the building might be judged "unsafe." More investigation of the detailing of the joint is required.

As far as can be determined from the drawings, it would not be difficult to increase the stiffness and strength of the building even if structural performance at the joint were evaluated to be inadequate.

3.3 Buildings in the City of Hachinohe in the 1968 Tokachi-oki Earthquake

The characteristics of the reinforced concrete low-rise buildings in the city of Hachinohe during the 1968 Tokachi-oki Earthquake are shown in Fig. 17.

The major assumptions adopted in the evaluation were:

Average weight of the buildings: 1 t/m^2 (205 psf)

Average shear cracking stress: $\tau_{av} = 10 \text{ kg/cm}^2$ (140 psi)

In estimating C_{cr} using Eq. 22, the term:

$$\frac{\sum_{i=1}^n (\beta u)_i \bar{w}_i}{\sum_{i=1}^n \bar{w}_i} \times \alpha_0$$

was assumed to be 1.5 for an 0.3g earthquake and 1.0 for an 0.45g earthquake.

It should be noted that the proposed first screening method can evaluate buildings damaged in an earthquake.

ACKNOWLEDGEMENTS

This paper was prepared for the project "Seismic Safety of Existing School Buildings" at the University of California, Berkeley, sponsored by the National Science Foundation, and for the US-Japan cooperative research program entitled "Earthquake Engineering with Emphasis on the Safety of School Buildings" under the joint sponsorship of the National Science Foundation and Japan Society for Promotion of Science.

The authors are grateful to Professors H. Umemura, University of Tokyo, and Joseph Penzien, University of California at Berkeley, the coordinators of the US-Japan cooperative research program.

The authors also wish to express their appreciation to Mr. John F. Meehan, Supervising Structural Engineer, California Office of Architecture and Construction, Sacramento, who gave them the opportunity to examine drawings of the existing school buildings discussed in this paper; to Dr. M. Murakami who advised and helped them in preparing this paper; to Mr. David Zisling who helped to collect the data for the examples; and to Ms. Judith Sanders for her kind advice and assistance in preparing this report.

REFERENCES

1. Okada, T., and Bresler, B., "Strength and Ductility Evaluation of Existing Low-Rise Reinforced Concrete Buildings," University of California, Berkeley, Earthquake Engineering Research Center, (Draft Report), Oct. 1974.
2. Umemura, H., et. al., "Earthquake Resistant Design of Reinforced Concrete Buildings, Accounting for the Dynamic Effects of Earthquakes," published by Giho-do, Tokyo, Japan, 1973, (in Japanese).

3. Okada, T., "A Proposal for the Principle of Preliminary Earthquake Resistant Design of Reinforced Concrete Buildings," paper submitted for presentation at the U.S.-Japan Seminar on Earthquake Engineering with Emphasis on the Safety of Reinforced Concrete Structures, Berkeley, California, U.S.A., September 1973.
4. Architectural Institute of Japan, "Building Code and Commentary for Reinforced Concrete Structures," 1971 (in Japanese).
5. Umemura, H., "Earthquake Resistant Design of Structures - From Wooden Frame to High-Rise," published by Kozai-kurabu, Tokyo, Japan, 1972.
6. Penzien, J., "Dynamic Response of Elastic-Plastic Frames," Proc. of ASCE, July, 1960.
7. Osawa, Y., and Shibata, A., "Earthquake Response of One-Mass Systems," Transactions of the Architectural Institute of Japan, No. 69, Oct. 1961 (in Japanese).
8. Blume, J.A., et. al., "Design of Multistory Reinforced Concrete Buildings for Earthquake Motions," Portland Cement Association, 1961.

TABLE 1 CRITERIA MATRIX FOR JUDGING EARTHQUAKE SAFETY OF REINFORCED CONCRETE BUILDINGS

(a) General Criteria

Grade of Earthquake	Strong Earthquake	Severe Earthquake
Grade of Safety	Reparable Damage	Noncollapse

(b) Criteria for First Screening Stage

Failure Mechanism	0.3g Earthquake	0.45g Earthquake
Bending Type (Ductile)	Ductility Factor (μ) ¹⁾ is less than 2.0	Ductility factor (μ) is less than 4.0
Shear Type (Brittle)	Shear cracking stage	Before shear failure stage ²⁾
Shear-Bending Type	Shear cracking stage	Yielding stage ³⁾

- 1) ductility factor = maximum displacement/yield displacement.
- 2) shear deformation at this stage is considered to be one half of the ultimate deformation capacity ($v_{ult} = 4 \times 10^{-3}$ radian).
- 3) displacement at this stage is considered to correspond approximately to a ductility factor of 2.0 for the bending type.

TABLE 2 WALL RATIO, COLUMN RATIO, AND WALL-COLUMN RATIO OF SCHOOL BUILDING A

	Story	Wall Ratio a_w (in ² /ft ²)	Column Ratio a_c	Wall-Column $a_{wc} = a_w + a_c$
x-direction	3	0.60	0.49	1.09
	2	0.30	0.24	0.54
	1	0.20	0.16	0.36
y-direction	3	0.38	0.49	0.87
	2	0.21	0.24	0.45
	1	0.21	0.16	0.37

TABLE 3 STRENGTH IN TERMS OF SHEAR COEFFICIENTS OF SCHOOL BUILDING A

x-Direction

	Model A		Model B	
	Shear* C_{sci}	Bending C_{Byi}	Shear* C_{sci}	Bending C_{Byi}
3	1.0	0.18	1.26	0.55
2	0.52	0.13	0.63	0.34
1	0.33	0.10	0.41	0.27

*Shear cracking strength

y-Direction

	Model A		Model B	
	Shear* C_{sci}	Bending C_{Byi}	Shear* C_{sci}	Bending C_{Byi}
3	0.62	0.30	0.99	0.62
2	0.34	0.22	0.52	0.40
1	0.34	0.17	0.42	0.32

*Shear cracking strength

TABLE 4 STRENGTH OF EQUIVALENT ONE-MASS SYSTEM FOR SCHOOL BUILDING A

Earthquake k_g		Model A			Model B		
		Strength		k_y/k_g	Strength		k_y/k_g
		Building E_{Cy}	One-Mass k_y		Building E_{Cy}	One-Mass k_y	
0.3	x	0.10	0.11	0.37	0.27	0.30	1.00
	y	0.17	0.19	0.63	0.32	0.35	1.17
.045	x	0.10	0.11	0.24	0.27	0.30	0.67
	y	0.17	0.19	0.42	0.32	0.35	0.78

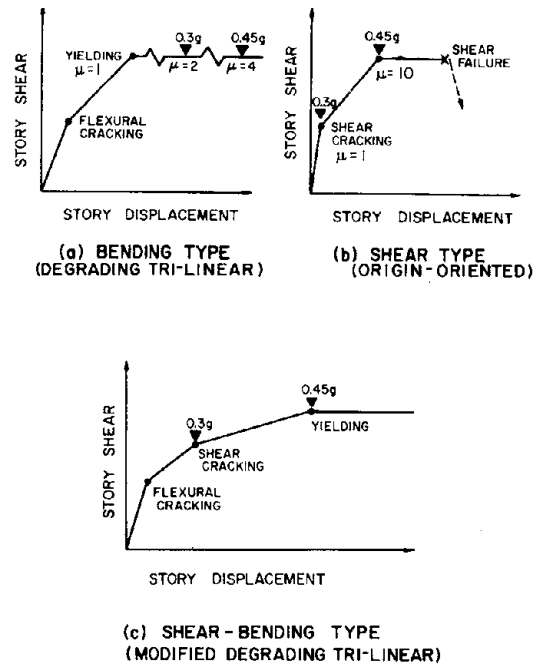


FIG. 2 DECISION CRITERIA AND TYPE OF FAILURE FOR FIRST SCREENING

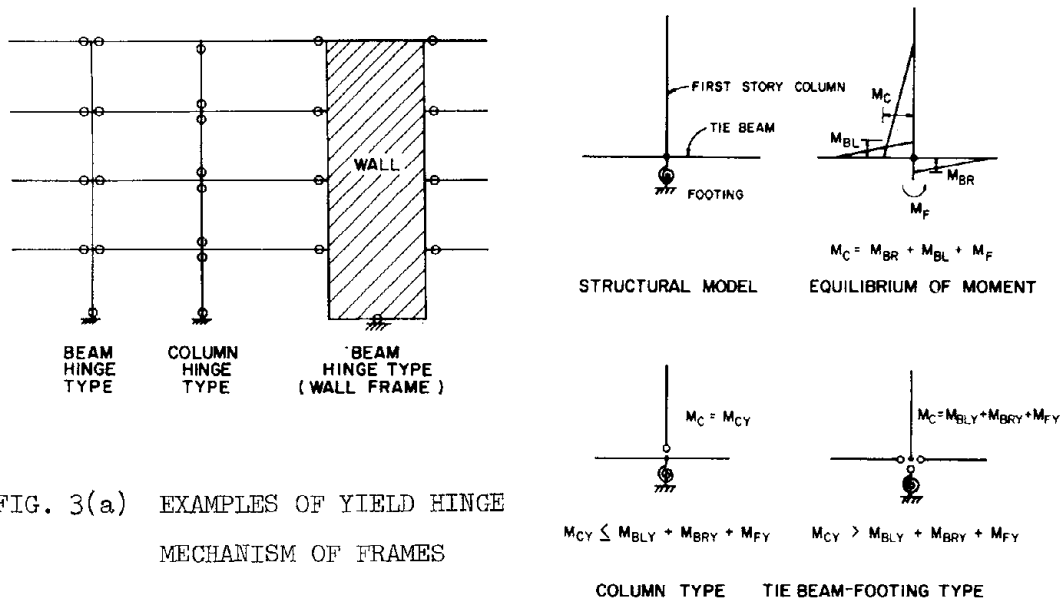


FIG. 3(a) EXAMPLES OF YIELD HINGE MECHANISM OF FRAMES

FIG. 3(b) YIELD HINGE MECHANISM AT FOOTING LEVEL

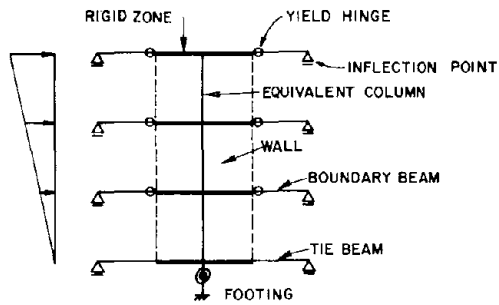
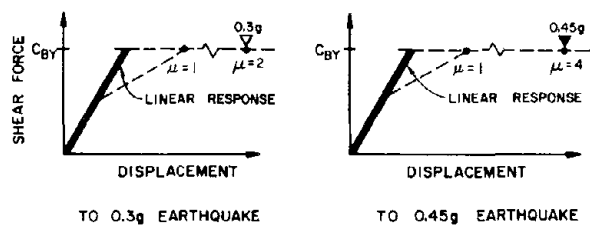
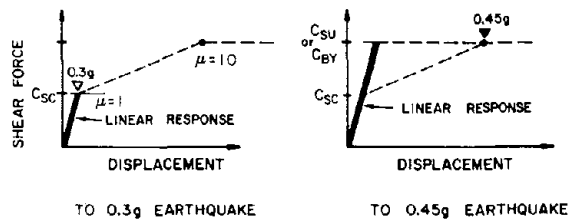


FIG. 4 EQUIVALENT FRAME FOR SHEAR WALL WITH BOUNDARY BEAMS



(a) BENDING TYPE OF BUILDING



(b) SHEAR TYPE OR SHEAR-BENDING TYPE OF BUILDING

FIG. 5 STRENGTH SAFETY EVALUATION

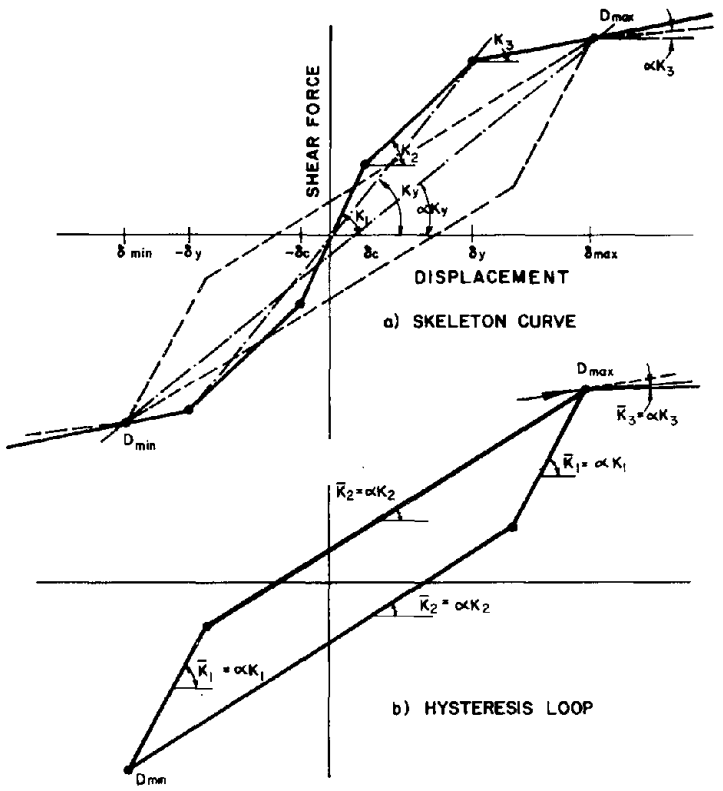


FIG. 6(a) DEGRADING TRI-LINEAR TYPE

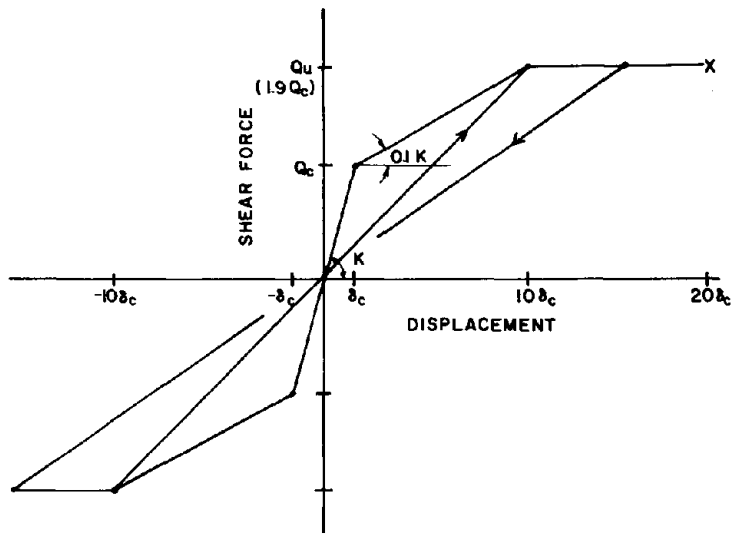
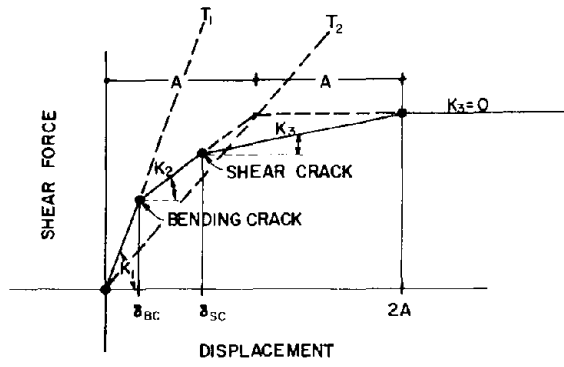


FIG. 6(b) ORIGIN-ORIENTED TYPE



DUCTILITY FACTOR (μ) = MAXIMUM DISPLACEMENT / δ_{SC}

FIG. 6(c) MODIFIED DEGRADING TRI-LINEAR TYPE

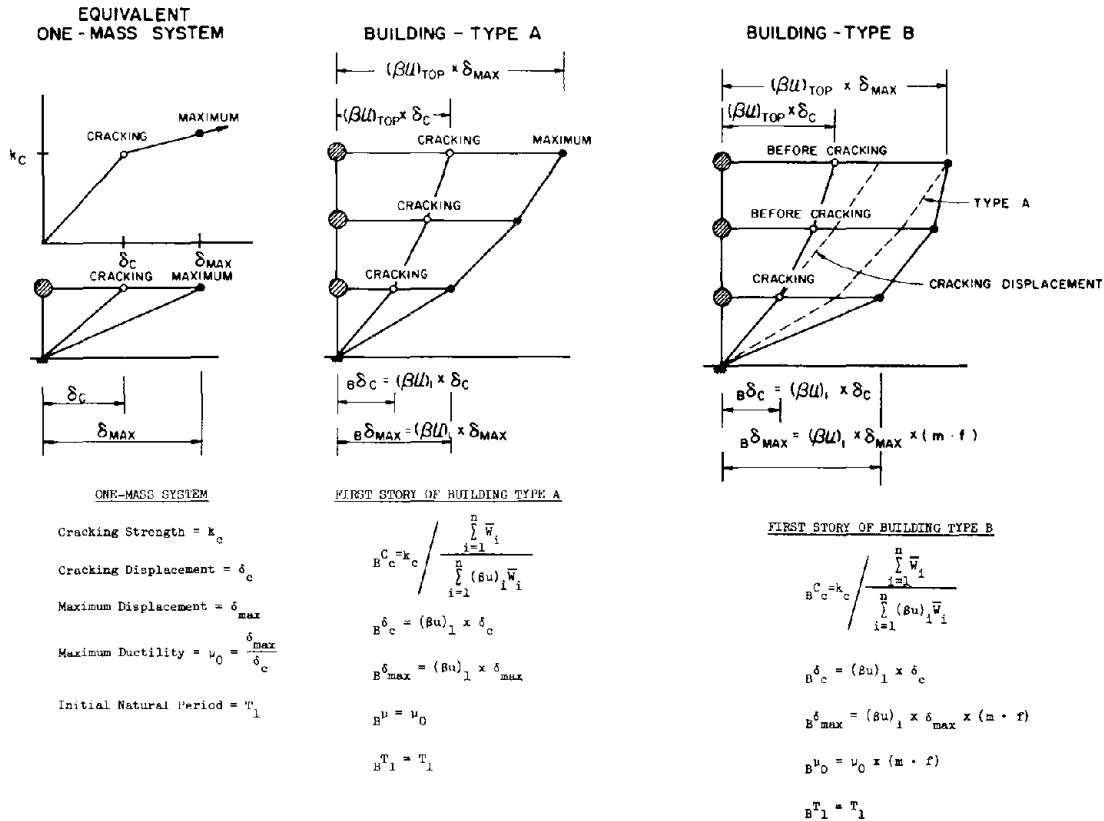


FIG. 7 CONVERSION OF STRENGTH AND DISPLACEMENT

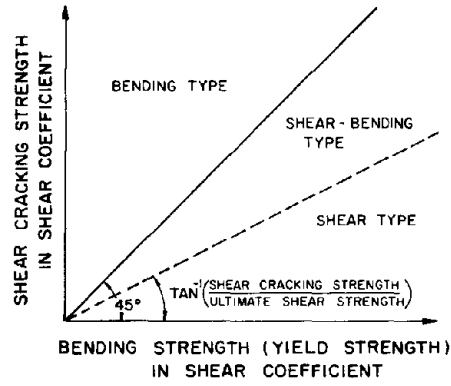


FIG. 8 CLASSIFICATION OF TYPE OF FAILURE - STEP B

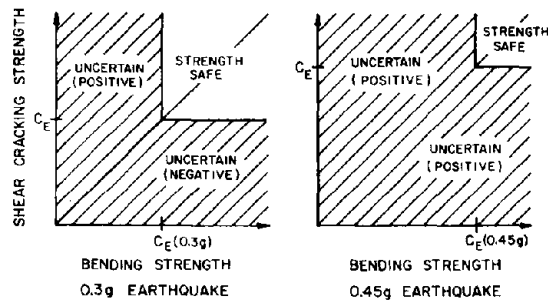


FIG. 9 STRENGTH SAFETY EVALUATION - STEP C

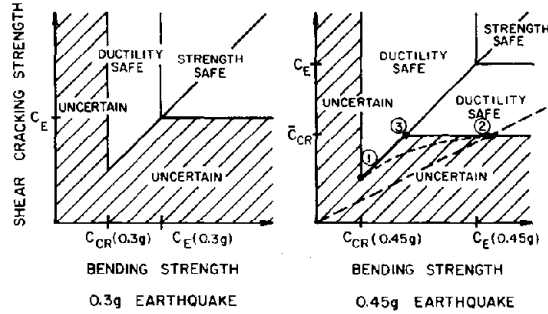
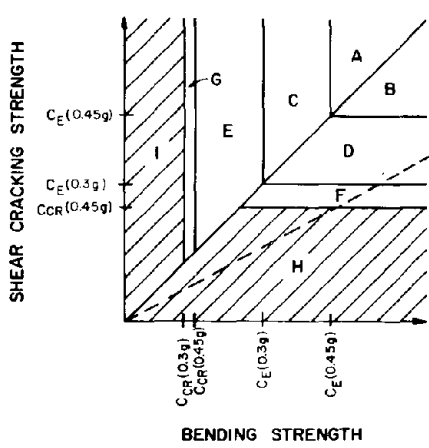


FIG. 10 DUCTILITY SAFETY EVALUATION - STEP D



a) SHEAR CRACKING STRENGTH - BENDING STRENGTH DIAGRAM

Zone	Type	0.3g Earthquake		0.45g Earthquake		Ranking
		Strength	Ductility	Strength	Ductility	
A	Bending	Safe	Safe	Safe	Safe	I
B	Shear or Shear-Bending	Safe	Safe	Safe	Safe	
C	Bending	Safe	Safe	Uncertain	Safe	
D	Shear or Shear-Bending	Safe	Safe	Uncertain	Safe	
E	Bending	Uncertain	Safe	--	Safe	II
F	Shear or Shear-Bending	Uncertain	Uncertain	--	Safe	III
G	Bending	--	Safe	--	Uncertain	
H	Shear or Shear-Bending	--	--	--	Uncertain	IV
I	Bending	--	--	--	Uncertain	

b) RANKING OF SAFETY

FIG. 11 SYNTHESIS EVALUATION OF SAFETY - STEP E

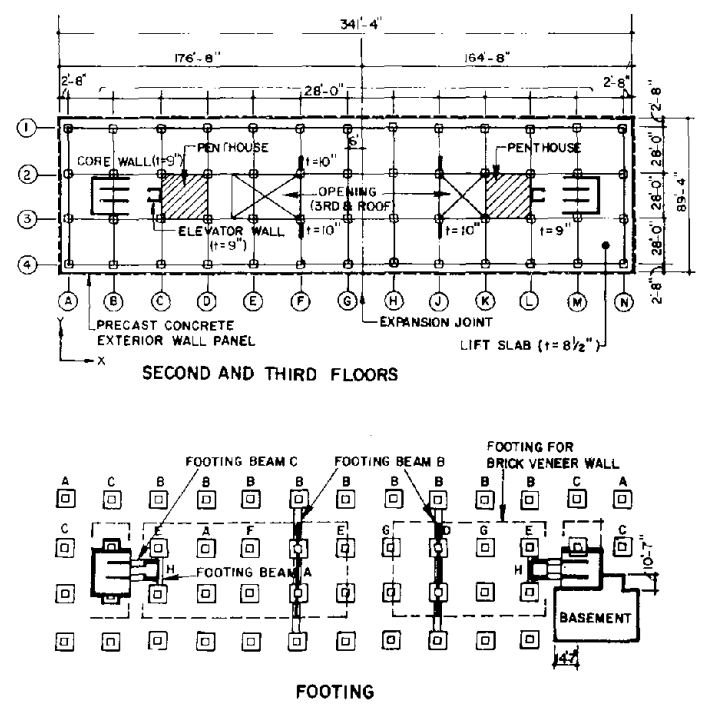


FIG. 12 PLAN OF SCHOOL BUILDING A

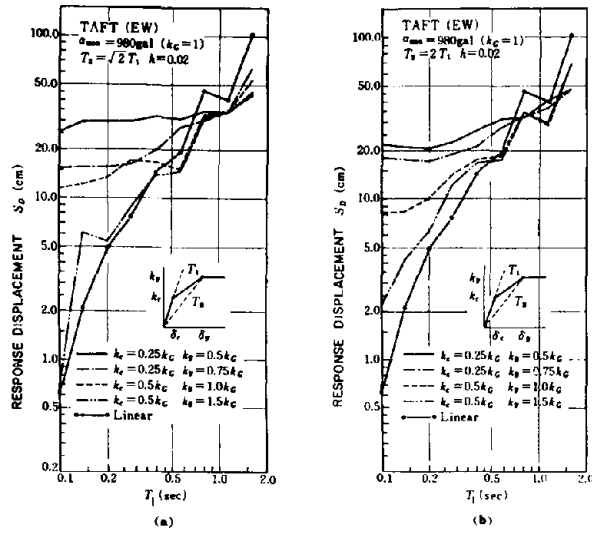


FIG. 13 RESPONSE SPECTRA FOR DEGRADING TRI-LINEAR TYPE
(AFTER REFERENCE 2)

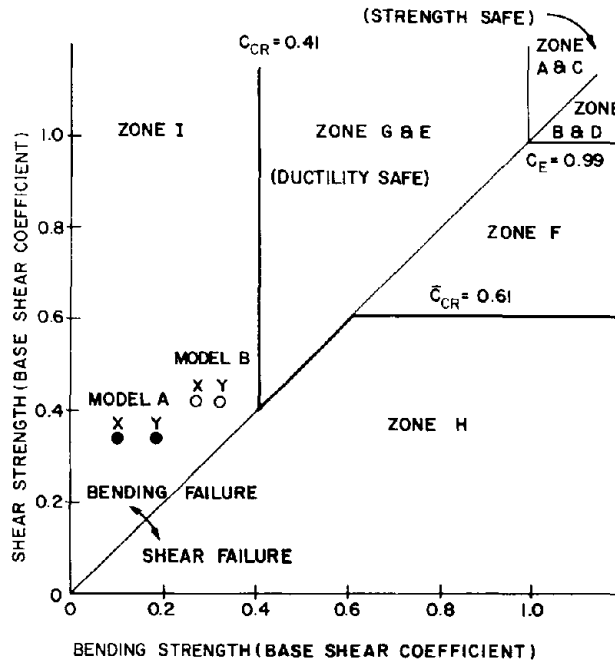


FIG. 14 SYNTHESIS EVALUATION OF SAFETY OF SCHOOL BUILDING A

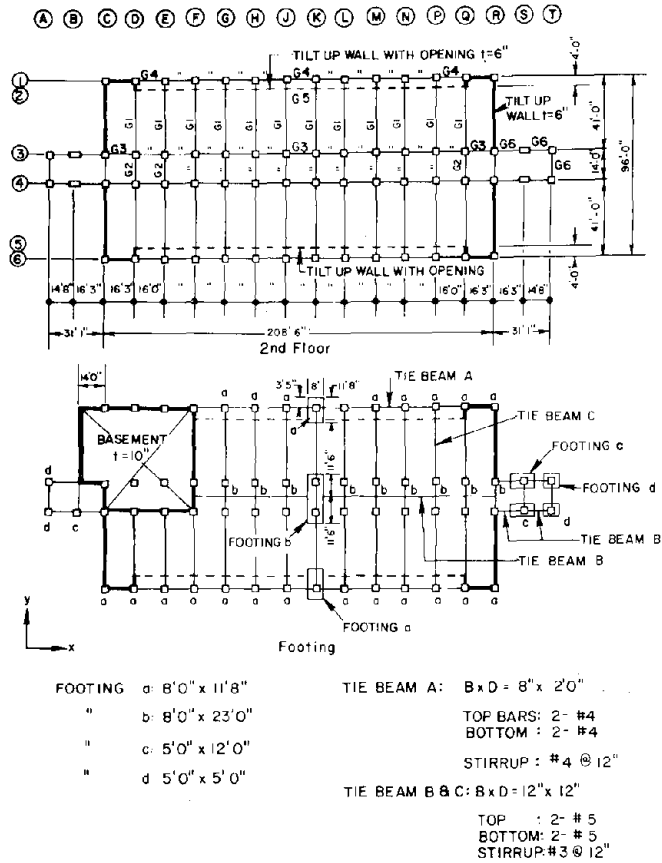


FIG. 15 PLAN OF SCHOOL BUILDING B

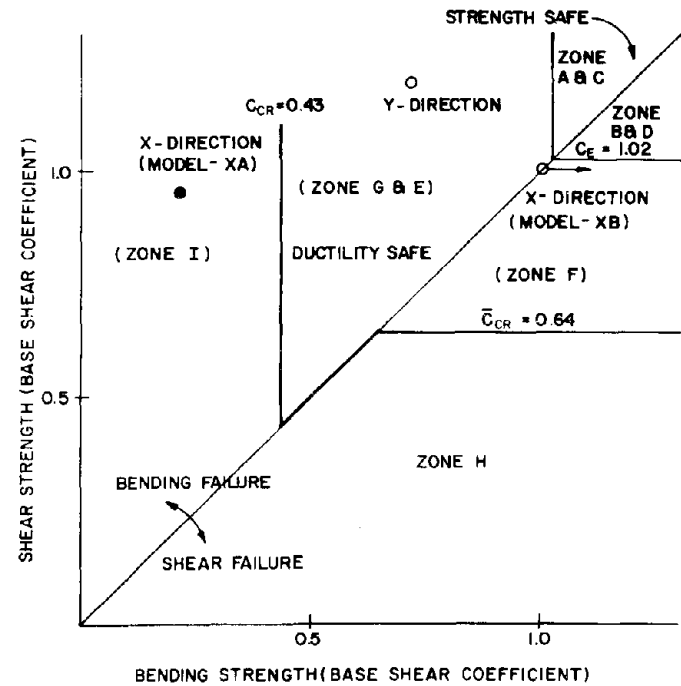
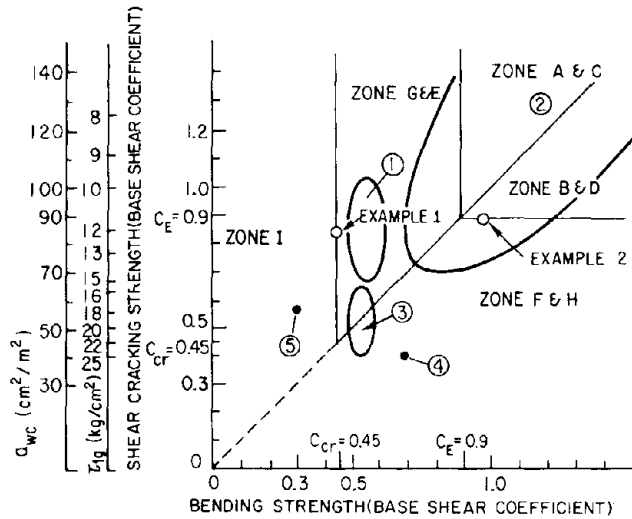


FIG. 16 SYNTHESIS EVALUATION OF SAFETY OF SCHOOL BUILDING B



- ① SCHOOL BUILDINGS OF TYPE C, NO DAMAGE
- ② MANY SHEAR WALLS, NO DAMAGE
- ③ MEDIUM DAMAGE
- ④ HACHINOHE TECHNICAL HIGH SCHOOL, SEVERE DAMAGE
- ⑤ HACHINOHE LIBRARY, SEVERE DAMAGE

EXAMPLES 1 & 2 ARE DISCUSSED IN REFERENCE 2

FIG. 17 CHARACTERISTICS OF BUILDINGS IN 1968
TOKACHI-OKI EARTHQUAKE
(AFTER REFERENCE 3)

13 NONLINEAR RESPONSE SPECTRA FOR PROBABILISTIC SEISMIC
 DESIGN OF REINFORCED CONCRETE STRUCTURES

by

Masaya Murakami* and Joseph Penzien†

SYNOPSIS

In the investigation reported herein, twenty each of five different types of artificial earthquake accelerograms were generated for computing nonlinear response spectra of five structural models representing reinforced concrete buildings. To serve as a basis for probabilistic design, mean values and standard deviations of ductility factors were determined for each model having a range of prescribed strength values and having a range of natural periods. Adopting the standard design philosophy, i.e. only minor damage is acceptable under moderate earthquake conditions and total damage or complete failure should be avoided under severe earthquake conditions, required strength levels were investigated for each model. Selected results obtained in the overall investigation are presented and interpreted in terms of prototype behavior.

I. INTRODUCTION

The general philosophy of seismic resistant design in most countries of the world, including Japan and the United States, is that only minor damage is acceptable in buildings subjected to moderate earthquake conditions and that total damage or complete failure should be prevented under severe earthquake conditions. This philosophy serves as the basic criterion for assessing the potential seismic performance of existing buildings and for defining design criteria for new buildings.

Usually, the above philosophy is applied to performance assessments and to design in a deterministic manner. In this case, seismic response analyses are carried out for fixed mathematical models using fully prescribed ground motion excitations. It should be realized however that many uncertainties exist in this method. The highly variable characteristics of ground motions, even for a given site, is the major cause of these uncertainties. However, other causes also exist such as the variability of structural properties. For this reason, nondeterministic methods which formally recognize uncertainties and which predict response in probabilistic terms should be encouraged. Meanwhile every effort should be made to reduce the uncertainties through experimental and analytical research and through improved design and construction methods.

* Visiting Assistant Research Engineer, University of California, Berkeley and Associate Professor of Architectural Engineering, Chiba University, Japan.

† Professor of Structural Engineering, University of California, Berkeley

To carry out nondeterministic seismic analyses, an appropriate stochastic model must be established for the expected ground motions. If sufficient strong ground motion data were available this model could be obtained by direct statistical analyses. However, due to the limited data available, one is forced to hypothesize model forms and to use the existing data primarily in checking the appropriateness of these forms. The particular model used in this investigation is essentially nonstationary filtered white noise as commonly used by many investigators [1, 2]. While this model is admittedly not perfect, it does reflect the main statistical features of real ground motions; therefore, its use in seismic response analyses leads to more realistic predictions than does a single fully prescribed accelerogram.

Since it was the intent of this investigation to concentrate on low-rise reinforced concrete buildings, two basic single degree of freedom structural models were selected for dynamic analysis purposes, namely, the so called "Origin-Oriented Model" and the "Trilinear Stiffness Degrading Model" [3]. These models were selected to represent structures which fail primarily in shear and flexure, respectively. Various strength values were prescribed for these models and their initial stiffnesses were varied to produce a wide range of fundamental periods.

Mean values and standard deviations of ductility factor were generated using the five different classes of earthquake accelerograms for each structural model having a prescribed period and assigned strength values. These statistical quantities can be used as the basis for probabilistic design.

Accepting the basic philosophy of design previously mentioned, namely that only minor damage is acceptable under moderate earthquake conditions and that total damage or complete failure should be avoided under severe conditions, Umemura has proposed a basic criterion for seismic design which has been adopted herein [3]. This criterion has been used in probabilistic terms to establish appropriate strength levels for each model consistent with the basic design philosophy.

II. GENERATION OF ARTIFICIAL EARTHQUAKE ACCELEROGRAMS

A. STOCHASTIC MODELS

Two basic types of nonstationary processes are commonly used to represent earthquake ground motions, namely, nonstationary filtered white noise and filtered shot noise [1, 4, 5]. Shinozuka and Sato suggest that under similar conditions both types lead to essentially the same response characteristics of linear systems [6].

In the present investigation, five specific types (Types A, B, B₀₂, C, and D) of artificial accelerograms were generated using the second of the above mentioned basic types. A digital computer program (PSEQGN) developed by Ruiz was used for this purpose. This program follows a procedure consisting of five phases, (1) stationary wave forms are generated having a constant power spectral density function (white noise) of intensity

S_o over a wide range of frequencies starting at zero frequency, (2) non-stationary shot noise is next obtained by multiplying each stationary wave form by a prescribed time intensity function, (3) each of the resulting wave forms of shot noise is then passed through a second-order filter which amplifies the frequency content in the neighborhood of a characteristic frequency and attenuates the higher frequencies, (4) next each of these filtered wave forms is passed through a second second-order filter which eliminates the very low frequency content, and finally (5) a baseline correction is applied to the double filtered accelerograms in accordance with the procedure of Berg and Housner [7]. Both second-order filterings are accomplished digitally by solving numerically the second-order differential equations relating filter outputs to their corresponding inputs [8]. These solutions are obtained numerically by the standard linear acceleration method using constant integration time intervals of 0.01 seconds. By this procedure, final accelerograms are obtained in digitized form with each having similar 0.01 second time intervals.

B. TIME INTENSITY FUNCTIONS

Five classes of earthquake accelerograms (Types A, B, B_{02} , C and D) were generated using four different time intensity functions as shown in Fig. 1. These intensity functions are the same as those used previously by Jennings, et al [2]. Note that accelerograms of Types B and B_{02} were generated using the same intensity function. All four intensity functions consist of three phases (1) a parabolic build-up phase, (2) a constant intensity phase, and (3) an exponential decay phase. The total durations of these particular functions are 120, 50, 12 and 10 seconds, respectively; however, since the ends of the decay phase do not affect maximum response of damped structural systems, they were cut off at 75, 30, 10 and 5 seconds for Types A, B, C and D, respectively.

C. HIGH FREQUENCY FILTER CHARACTERISTICS

As previously stated, the nonstationary shot noise wave forms were obtained by multiplying each stationary wave form having a power spectral intensity S_o by a prescribed time intensity function.

The high frequency filtering procedure was then used to shape the frequency content of the shot noise wave forms using the transfer function (complex frequency response function [8])

$$H_1(i\omega) = \frac{[1+(4\xi_o^2-1)(\omega/\omega_o)^2] - 2i\xi_o(\omega/\omega_o)^3}{[1-(\omega/\omega_o)^2]^2 + 4\xi_o^2(\omega/\omega_o)^2} \quad (1)$$

This transfer function, previously suggested by Kanai and Tajimi for this purpose [9,10], is usually written in the more familiar form

$$|H_1(i\omega)|^2 = \frac{1 + 4\xi_o^2(\omega/\omega_o)^2}{[1 - (\omega/\omega_o)^2]^2 + 4\xi_o^2(\omega/\omega_o)^2} \quad (2)$$

Jennings, Ruiz, and other investigators have also used this same transfer function.

Parameters ω_0 and ξ_0 appearing in the above filter function may be thought of as some characteristic ground frequency and damping ratio, respectively. Kanai has suggested 15.6 rad/sec for ω_0 and 0.6 for ξ_0 as representative values for firm soil conditions. The frequency transfer function in the form of Eq. 2 is plotted in Fig. 2a for $\xi_0 = 0.6$. These same values of ω_0 and ξ_0 were used in the present investigation for four of the five classes of accelerograms, namely, Types A, B, C, and D. Accelerograms of Type B₀₂ used the same value for ω_0 , i.e. 15.6 rad/sec., but a different value for ξ_0 , namely, 0.2. This damping value was selected for Type B₀₂ accelerograms to study the influence of a relatively narrow band excitation on structural response.

D. LOW FREQUENCY FILTER CHARACTERISTICS

The low frequency filter used in this investigation had the transfer function [2,8]

$$H_2(i\omega) = \frac{(\omega/\omega_f)^2 [1 - (\omega/\omega_f)^2] - 2i\xi_f (\omega/\omega_f)^3}{[1 - (\omega/\omega_f)^2]^2 + 4\xi_f^2 (\omega/\omega_f)^2} \quad (3)$$

or

$$|H_2(i\omega)|^2 = \frac{(\omega/\omega_f)^4}{[1 - (\omega/\omega_f)^2]^2 + 4\xi_f^2 (\omega/\omega_f)^2} \quad (4)$$

where ω_f and ξ_f are the characteristic frequency and characteristic damping ratio, respectively, for the filter. The damping ratio term ξ_f was assigned the numerical value $1/\sqrt{2}$ which reduces Eq. (4) to

$$|H_2(i\omega)|^2 = \frac{(\omega/\omega_f)^4}{1 + (\omega/\omega_f)^4} \quad (5)$$

Introducing the period ratio T/T_f , where $T = 2\pi/\omega$ and $T_f = 2\pi/\omega_f$, Eq.(5) becomes

$$|H_2(iT)|^2 = \frac{1}{1 + (T/T_f)^4} \quad (6)$$

In this investigation, T_f equals 7 and 2 seconds for Types A, B and B₀₂ and for Types C and D, respectively. The square root of the function given by Eq. (6) is shown in Fig. 2b.

E. DISCUSSION ON ARTIFICIAL ACCELEROGRAMS

The constant power spectral intensity S_0 , used in generating the stationary wave forms, was assigned the value $0.8952 \text{ ft}^2/\text{sec}^3$. Using a family of 20 Type B accelerograms, this intensity resulted in a mean peak acceleration of $0.300g$ with a standard deviation of $0.032g$. Increasing the number of accelerograms to 40 gave a mean peak acceleration of $0.308g$ and a standard deviation of $0.037g$. Following the method of Gumbel [11], it is estimated that for an infinite number of similar accelerograms, the mean peak acceleration would be $0.309g$ and the standard deviation would be $0.041g$. Therefore, in view of this mean peak acceleration and the time intensity function used, the Type B accelerograms closely represent that class of motions containing the N-S component of acceleration recorded during the 1940 El Centro, California, earthquake [2,4].

Table 1 lists the mean values and standard deviations for the peak accelerations in all 5 classes of accelerograms, i.e. for Types A, B, C, D, and B_{02} . In obtaining these results, S_0 was assigned the same value $0.8952 \text{ ft}^2/\text{sec}^3$ in each case. Notice that the mean peak acceleration decreases as the duration of the constant intensity phase in the motion decreases. This observation is, of course, consistent with the theory of extreme values. Notice also that the standard deviations are relatively small in each case.

Following the suggestion of Jennings, et. al. [2], the Type A accelerograms are intended to represent the upper bound ground motions expected in the vicinity of the causative fault during an earthquake having a Richter Magnitude 8 or greater. Type B accelerograms are intended to represent the motions close to the fault in a Magnitude 7 earthquake, such as the 1940 El Centro, California, earthquake and the 1952 Taft, California, earthquake. The Type C accelerograms are intended to represent the ground motions in the epicentral region of a Magnitude 5.5 shock, such as occurred during the 1957 San Francisco earthquake, and the Type D accelerograms are intended to represent the motions present in the immediate vicinity of the fault of a 4.5 to 5.5 Magnitude earthquake having a small focal depth, such as the 1966 Parkfield, California, earthquake. If the artificial accelerograms generated as Types A, B, C, and D are indeed to be representative of these conditions, then each class of motions should be normalized by the appropriate factors to raise the mean peak acceleration levels from $0.332g$, $0.309g$, $0.244g$, and $0.189g$, respectively, to approximately $0.45g$, $0.33g$, $0.10g$, and $0.50g$.

Since the extreme values of response for all 5 structural models used in this investigation were measured in terms of ductility factors, the above mentioned normalization of accelerograms is not required. These ductility factors are controlled by a structural model strength to ground motion intensity ratio; i.e. $p_s/m\bar{v}_g$ where p_s is the significant structural strength parameter, m is the mass of the single degree of freedom system, and \bar{v}_g is the mean peak acceleration. Allowing this ratio to vary over a prescribed range of values is equivalent to allowing p_s and/or \bar{v}_g to vary independently over restricted ranges.

Further, it should be recognized that the structural response data generated for ground motions of Types A, B, C, D, and B_{02} can be interpreted in terms of structural response to other classes of motions. For example,

suppose one wished to interpret these response data for similar classes of earthquake motions but for a change in the characteristic ground frequency ω_0 to reflect a change in soil conditions. This interpretation can be accomplished by considering a change in the time scale of the accelerograms; thus, forcing corresponding changes in the time intensity functions, the value of T_f , the value of ω_0 , and the mean peak acceleration. Since the value of S_0 representing the new classes of accelerograms is to remain unchanged, the mean peak accelerations of the new motions will be changed exactly in proportion to the square root of the ratio of the original time interval to the new time interval. Specifically, suppose the time interval is considered to be changed from 0.01 sec. to 0.005 sec. for the Type A accelerograms. In this case, the total duration (as represented by OC, Fig. 1) is reduced from 75 sec. to 37.5 sec., ω_0 is increased from 15.6 rad/sec. to 31.2 rad/sec., T_f is reduced from 7 sec. to 3.5 sec., and the mean peak acceleration is increased from 0.33g to 0.46g ($\sqrt{2} \cdot 0.33 = 0.46$).

III. STRUCTURAL SPRING MODELS

A. BASIC PARAMETERS OF MODELS

The single degree of freedom system shown in Fig. 3a was used as the basic form for all structural models investigated. This model has a linear viscous dashpot but a nonlinear hysteretic spring. The restoring spring force is therefore some prescribed nonlinear function $F(v)$ of the relative displacement $v(t)$. The principal quantities used to characterize this function are p_c , p_y , v_c , and v_y as shown in Fig. 3b. Loads p_c and p_y represent the spring restoring forces corresponding to the concrete cracking strength and the ultimate strength, respectively. Displacements v_c and v_y are the corresponding relative displacements.

B. ORIGIN-ORIENTED HYSTERETIC MODEL

One of the five structural models used in this investigation was the so-called "Origin-Oriented" hysteretic model proposed by Umemura, et. al. [3]. This model is shown in Fig. 4 where it is characterized by p_{sc} , p_{sy} , v_{sc} , and v_{sy} which represent the concrete shear cracking strength, the ultimate shear strength, the relative displacement produced by p_{sc} , and the relative displacement produced by p_{sy} , respectively. Application of this model is restricted to those structural types where the nonlinear deformations and failure characteristics are controlled primarily by shear.

This model is defined such that the hysteretic behavior takes place with increasing relative displacements greater than v_{sc} or decreasing displacements less than $-v_{sc}$. Reduction of loads from values greater than p_{sc} or less than $-p_{sc}$ follow linear paths always directed through the origin, e.g. paths A'O and A''O in Fig. 4. Oscillatory motions can, of course, take place along the linear paths such as A'OA' and A''OA'' (with a constant damping ratio ξ_1) without developing hysteretic loops provided the maximum displacements do not exceed the maximum displacement previously developed. The particular model plotted in Fig. 4 is for the case where $p_{sy} = 1.9 p_{sc}$, $v_{sy} = 10.0 v_{sc}$, $k_2 = 0.1 k_1$, and $k_3 = 0.19 k_1$.

C. TRILINEAR STIFFNESS DEGRADING HYSTERETIC MODEL

Four of the five structural models used in this investigation were the so-called "Trilinear Stiffness Degrading" hysteretic model [3]. This model is shown in Fig. 5 where it is characterized by p_{Bc} , p_{By} , v_{Bc} , and v_{By} which represent the load at which the concrete cracks due to flexure, the load at which the main reinforcing steel starts yielding due to flexure, the relative displacement produced by p_{Bc} , and the relative displacement produced by p_{By} , respectively. Application of this model is restricted to those structural types where the nonlinear deformations and failure characteristics are primarily controlled by flexure.

The trilinear model is defined such that linear elastic behavior (without hysteretic loops) always takes place for oscillatory displacements where the corresponding oscillator loads are in the range $-p_{Bc} < p < p_{Bc}$; however, hysteretic behavior occurs with every cycle of deformation which has load levels above p_{Bc} or below $-p_{Bc}$. During that period of time between the initiation of loading and that instant at which the relative displacement first increases above v_{By} or decreases below $-v_{By}$, the trilinear model behaves exactly like the standard bilinear hysteretic model having stiffnesses k_1 and k_2 (QPOAB; Fig. 5a). However, as soon as the relative displacement increases above v_{By} or decreases below $-v_{By}$, a new bilinear hysteretic relation controls the response. For example, suppose the relative displacement for the first time increases above v_{By} to level v_{max} as represented by C in Fig. 5a. Upon decreasing the displacement from this level, the corresponding load decreases along path CD which has a slope equal to αk_1 , where

$$\alpha = \frac{2 v_{By}}{v_{max} + v_{By}} \quad (7)$$

As soon as the load drops by the amount $2p_{Bc}$ reaching point D in Fig. 5a, any further drop in load will follow the continuing path shown having a slope αk_2 . It should be noted that point D is located at load level p_{Bc} in Fig. 5a but only because the particular trilinear model represented in that figure is for $p_{By}/p_{Bc} = 3.0$. If this ratio had been assigned a different numerical value, the load level at point D would be different from p_{Bc} .

The new bilinear hysteretic model controlling the continuing motion is shown in Fig. 5b. Note that the origin of the skelton curve is shifted from point O, the origin of the original bilinear hysteretic model, to point O'. This point is the intersection point of line QC and the abscissa axis in Fig. 5a; therefore OO' is equal to BC/2. The stiffnesses of the new bilinear model are αk_1 , and αk_2 .

If during the period of response controlled by the second bilinear model (Fig. 5b) the relative displacement should increase beyond v_{max} ($v_{max} = v_{By}$) as represented by point B' to a new level as represented by C', the continuing response would be controlled by a third bilinear hysteretic model whose characteristics could be obtained in exactly the same manner as the characteristics of the second model. Also, if yielding

of the trilinear model had taken place at load level $-p_{By}$ rather than load level p_{By} , the new bilinear model controlling the continuing motion would be obtained by a similar procedure.

One characteristic feature of the trilinear stiffness degrading model worth noting is that when subjected to full-reversal cyclic displacements at a constant amplitude the bilinear hysteretic loops are perfectly stable, i.e. each loop retraces the preceding one. The energy absorbed during each successive cycle must therefore be equal. Using a period $T_2 = 2\pi \sqrt{m/k_y}$, where k_y is an average stiffness as shown in Fig. 6, one can calculate the equivalent damping ratio ξ for a linear viscously-damped single degree system which represents the same energy absorption per cycle of oscillation. This damping ratio is shown in Fig. 6 for each of four different bilinear models.

IV. SELECTION OF MODEL PARAMETERS

A. ORIGIN-ORIENTED HYSTERETIC SPRING MODEL

As previously defined, the origin-oriented hysteretic model shown in Fig. 4 is completely characterized by any four of the seven parameters k_1 , k_2 , k_3 , p_{sc} , p_{sy} , v_{sc} , v_{sy} . Based on experimental data [3], it has been determined that

$$p_{sy} \doteq 1.9 p_{sc} \quad (8)$$

$$v_{sy} \doteq 10 v_{sc} \quad (9)$$

which reduces the number of independent parameters to two. It is most meaningful to let one of these two parameters be a stiffness parameter and the other be a strength parameter. For this purpose, it is convenient to use period $T_1 = 2\pi \sqrt{m/k_1}$ and the concrete cracking force p_{sc} . As shown later, p_{sc} is normalized by the force $m\bar{v}_g$, where \bar{v}_g is the mean peak ground acceleration.

B. TRILINEAR STIFFNESS DEGRADING HYSTERETIC SPRING MODEL

The general trilinear stiffness degrading hysteretic model shown in Fig. 5 is completely characterized by any four of the seven parameters k_1 , k_2 , k_y , p_{Bc} , p_{By} , v_{Bc} , v_{By} . Four specific models, which were previously studied by other investigators [3], were selected for this investigation,

$$\begin{aligned} 1. \quad k_y &= 2k_1 ; p_{By} = 3p_{Bc} \\ 2. \quad k_y &= 2k_1 ; p_{By} = 2p_{Bc} \\ 3. \quad k_y &= 4k_1 ; p_{By} = 3p_{Bc} \\ 4. \quad k_y &= 4k_1 ; p_{By} = 2p_{Bc} \end{aligned} \quad (10)$$

These four models were chosen because k_y and p_{By} are often found in the ranges $2k_1 < k_y < 4k_1$ and $2p_{Bc} < p_{By} < 3p_{Bc}$, respectively, for reinforced concrete members. For frame structures, these ranges are not so well defined so that engineering judgment must be relied upon in assigning values consistent with their overall nonlinear behaviors.

Having assigned numerical values to the ratios k_y/k_1 and p_{By}/p_{Bc} , only two independent model parameters remain. In this case it is most convenient to select a stiffness parameter measured in terms of $T_1 = 2\pi \sqrt{m/k_1}$ and a strength parameter measured in terms of p_{By} . Again, the strength parameter selected (p_{By}) is normalized by the force $m \ddot{v}_g$.

C. VISCOUS DAMPING MODEL

As shown in Fig. 3a, the single degree of freedom model used in this investigation included a linear viscous dashpot having a variable coefficient c . The amount of viscous damping used with both the origin-oriented shear model and the trilinear stiffness degrading flexure model was controlled by using a stiffness proportional dashpot coefficient with the proportionality constant set by prescribing the initial damping ratio.

V. DYNAMIC RESPONSE ANALYSIS

The complete time history of dynamic response was generated for the single degree of freedom system using the five different structural models subjected separately to the twenty artificially generated earthquake ground motions. The equation of motion governing this response is the well known relation

$$m \ddot{v}(t) + c(t)\dot{v}(t) + F(v) = -m \ddot{v}_g(t) \quad (11)$$

where $F(v)$ is the nonlinear spring force defined by the hysteretic model being considered; i.e. the spring force defined by either Fig. 4 or Fig. 5. Dividing through by $m \ddot{v}_g$ (a constant) gives

$$\left[\frac{1}{\ddot{v}_g} \right] \ddot{v}(t) + \left[\frac{c(t)}{m \ddot{v}_g} \right] \dot{v}(t) + \frac{F(v)}{m \ddot{v}_g} = - \frac{\ddot{v}_g(t)}{\ddot{v}_g} \quad (12)$$

Note that the third term on the left hand side of this equation is the same force-displacement relation defined by the hysteretic model but with the force normalized (as previously mentioned) by the constant $m \ddot{v}_g$. Knowing the numerical values assigned to constants \ddot{v}_g , ξ_1 , and T_1 , as well as the prescribed value of $p_{sc}/m \ddot{v}_g$ (or $p_{By}/m \ddot{v}_g$), one can solve Eq. (12) for the complete time history of response $v(t)$. This solution is obtained numerically using the standard "linear acceleration" method. The time interval Δt generally used in the integration was shortened to a subdivided value $\Delta t'$ during short periods of time in which the model stiffness changed value. The numerical values of Δt and $\Delta t'$ used for four different ranges of period T_1 , are shown in Table 2.

The response quantity of primary interest is the ductility factor μ which is defined as $v(t)_{\max}/v_{sc}$ for the origin-oriented model and as $v(t)_{\max}/v_{By}$ for the trilinear stiffness degrading model. This factor was obtained for each of the five structural models when subjected separately to each of the 20 ground motions generated for Types A, B, C, D, and B₀₂. The damping ratio ξ_1 was assigned the value 0.05 for the origin-oriented model and 0.02 for the trilinear stiffness degrading model. Since the ductility factor was desired for a range of stiffnesses, period T_1 was assigned 10 different numerical values as given by

$$T_1 = 0.1(2)^{n/2} \quad (n = 0,1,2,\dots,9) \quad (13)$$

Using the origin-oriented model, ductility factors were obtained for a range of values of $p_{sc}/m \bar{v}_{go}$, namely 0.50, 0.75, 1.00, 1.25, 1.50, 1.75, 2.00, 2.25, 2.50, and 3.00. Using the trilinear stiffness degrading model, these values were obtained for $p_{By}/m \bar{v}_{go}$ equal to 0.50, 0.75, 1.00, 1.125, 1.25, 1.50, and 1.75.

VI. DUCTILITY RESPONSE SPECTRA

A. LINEAR ELASTIC MODEL

To characterize the five classes of earthquake motions (Types A, B, C, D, and B₀₂) in most familiar terms, all 20 accelerograms of each type were separately used as the excitation applied to a linear, viscously damped ($\xi = 0.05$) single degree of freedom system. Mean absolute acceleration response ratios α as defined by

$$\alpha = \frac{\bar{\ddot{v}}^t(t)_{\max}}{\bar{v}_{go}} \quad (14)$$

, where $\bar{\ddot{v}}^t(t)_{\max}$ is the mean value of 20 maximum absolute accelerations [$\ddot{v}^t(t)_{\max}$] and where \bar{v}_{go} is the peak mean value of ground accelerations, were determined for each excitation over a range of periods T . The coefficients of variation (ratio of standard deviation to mean value) of $\ddot{v}^t(t)_{\max}$ were also determined for the 20 accelerograms in each type of excitation.

The results of the analyses for all five classes of earthquake are shown in Fig. 9 where the mean absolute acceleration response ratios α and the coefficients of variation of $\ddot{v}^t(t)_{\max}$ are plotted as functions of period T . As would be expected, the values of α for the five classes of earthquakes are widely separated at the long period end of the abscissa scale but converge together towards the low period end of the scale. As the period goes to zero, α must of course, approach unity. It is seen in Fig. 9 (excluding Type B₀₂) that α increases with duration of the earthquake excitation. The very high peak shown in the function of α for Type B₀₂ is caused by the narrow band excitation in the ground motion in the neighborhood of $T = 0.4$ sec.

The coefficients of variation of $\ddot{v}^t(t)_{\max}$ decrease with duration of excitation and increase generally with period T . It should be recognized

that as T approaches zero the coefficients of variation of $\ddot{v}^t(t)_{\max}$ approach the corresponding coefficients of variation of $\ddot{v}_{go}^t(t)_{\max}$, as given in Table 1.

B. ORIGIN-ORIENTED SHEAR MODEL

Mean ductility factors $\bar{\mu}$ and their corresponding coefficients of variation were generated for the origin-oriented shear model using the 20 response time histories for each class of earthquake ground motions. Values, as obtained over the period range $0.1 < T_1 < 1.6 \sqrt{Z}$ and over the normalized load range $0.50 < \beta_s < 3.00$ (where β_s is defined as the ratio $p_c/m \ddot{v}_{go}$), are shown in Figs. 10a-10e. For each type of earthquake, these ductility factors generally increase with decreasing period and the spread of ductility factors over the full strength range increases with decreasing period. Also the ductility factors for a fixed period increases with decreasing structural strength.

The trends of the coefficients of variation with period are similar to those previously described for mean ductility factor, particularly regarding strength level and strength variation. It is most significant to note that the coefficients of variation are low when the response is essentially elastic ($\mu < 1$) but they can become very large with increasing inelastic deformations.

When interpreting the results in Figs. 10a-10e, it should be noted that the strength ratio $\beta_s \equiv p_c/m \ddot{v}_{go}$ can be expressed in the form

$$\beta_s = (p_c/W)/(\ddot{v}_{go}/g) \quad (15)$$

where W is the weight of the single degree of freedom mass and g is the acceleration of gravity. Therefore, this parameter can be considered as the ratio of base shear to coefficient of mean peak ground acceleration.

If for any particular case one wishes to determine the mean maximum relative displacement $\bar{v}(t)_{\max}$, this can be accomplished by using the appropriate mean ductility factor $\bar{\mu}$ taken from Figs. 10a-10e. By definition of ductility factor, one can state

$$\bar{v}(t)_{\max} = v_c \bar{\mu} = (p_c/k_1) \bar{\mu} \quad (16)$$

Making use of the definition of β_s given above, this equation can be written in the form

$$\bar{v}(t)_{\max} = \frac{m}{k_1} \beta_s \bar{\mu} \ddot{v}_{go} \quad (17)$$

or

$$\bar{v}(t)_{\max} = T_1^2 \beta_s \bar{\mu} \left[\frac{g}{4\pi^2} \right] \left[\frac{\ddot{v}_{go}}{g} \right] \quad (18)$$

Equation (18) is the most convenient form for calculating $\bar{v}(t)_{\max}$.

C. TRILINEAR STIFFNESS DEGRADING FLEXURE MODEL

Mean ductility factors and their corresponding coefficients of variation were generated for the four trilinear stiffness degrading flexure models using the 20 response time-histories for each class of earthquake ground motions. Values, as obtained over the period range $0.1 < T_1 < 1.6 \sqrt{2}$ and over the normalized load range $0.50 < \beta_f < 1.75$ (where β_f is defined as the ratio $p_y/m \ddot{v}_{g0}$), are shown in Figs. 11a-11d, 12a-12d, 13a-13d, 14a-14d, and 15a-15d for earthquake types A, B, C, D, and B_{02} , respectively.

The general trends of these results are very similar to those previously described for the origin-oriented shear model. It is worth pointing out again that the coefficients of variation of maximum response are relatively low for cases of essentially elastic behavior but can become very large for cases involving inelastic deformations.

As in the case of the origin-oriented model, mean maximum response can be calculated using the relation

$$\bar{v}(t)_{\max} = T_2^2 \beta_f \bar{u} \left[\frac{g}{4\pi^2} \right] \left[\frac{\bar{v}_{g0}}{g} \right] \quad (19)$$

VII. USE OF DUCTILITY RESPONSE SPECTRA FOR PROBABILISTIC SEISMIC DESIGN

A. SELECTION OF REQUIRED DUCTILITY LEVELS

It is implied in the basic philosophy of design previously stated that economical considerations do not permit the design of structures for zero risk of damage in high seismic regions. To minimize total costs (initial costs, repair costs after earthquakes, etc.), damage is often permitted to limited degrees under moderate to severe earthquake conditions. It should be understood that permitting some damage to occur in a well designed structure has the beneficial effect of limiting damage to that same structure. This is due to the fact that the energy absorption associated with damage is effective in limiting the maximum levels of oscillatory motion in the structure. Therefore, a good seismic resistant structure should be designed for high energy absorption capacity assuming it will experience controlled damage under severe to moderate earthquake conditions. In terms of the hysteretic structural models presented herein, this concept means that the ductility factor should be limited to certain values consistent with the basic design philosophy.

Assume for the moment that one prescribes two numerical values of ductility factor for a given structural model. The smaller value was chosen to be consistent with light damage under moderate earthquake conditions and the larger value was chosen to be consistent with heavy damage (but not complete failure) under severe conditions. Two questions come to mind (1) "What is the probability of these ductility factors being exceeded during a single earthquake of Types A, B, C, D, or B_{02} ?" and (2) "What ductility factors are required, consistent with the design philosophy?". To answer these questions, one must establish the appropriate probability density or distribution functions.

Previous investigations have shown that the probability distribution function for extreme value of structural response for a single earthquake follows closely the Gumbel Type I distribution [1,4]

$$P(\mu) = \exp \{- \exp [- \alpha (\mu - u)]\} \quad (20)$$

where μ is the maximum response measured in terms of ductility factor, and α and u are parameters which depend on the average and standard deviation of μ . If only 20 sample values of μ are available as in this investigation, α and u can be obtained using the relations [11]

$$\alpha = 1.063/\sigma_{\mu} \quad (21)$$

and

$$u = \bar{\mu} - 0.493 \sigma_{\mu} \quad (22)$$

where $\bar{\mu}$ and σ_{μ} are the mean and standard deviation of the 20 sample values of μ . Using these equations and expressing the standard deviation of μ in terms of its coefficient of variation ($\sigma_{\mu} = c \bar{\mu}$), Eq. (20) can be written in the nondimensional form

$$P(q) = \exp \{- \exp [- \frac{1.063}{c} (q - 1 + 0.493c)]\} \quad (23)$$

where

$$q = (\mu/\bar{\mu}) \quad (24)$$

This probability distribution function is plotted in Fig. 7 over a range of values of c , i.e. over the range $0 < c < 1.5$. Since the probability distribution function is defined such that

$$P(x) \equiv \text{Probability } [\mu < x] \quad (25)$$

, the probability exceedance function is given by

$$Q(x) \equiv \text{Probability } [\mu > x] = 1 - P(x) \quad (26)$$

The first question previously raised, namely, "What is the probability of these ductility factors being exceeded during a single earthquake of Types A, B, C, D, or B_{02} ?", can be easily answered using Eq. (26), Fig. 7 and the data provided in Figs. 10a-15d. The second question raised, i.e. "What ductility factors are required consistent with the design philosophy?", is more difficult to answer. Before attempting to answer this question, one must realize that the basic design criteria cannot be met in absolute terms, i.e. with 100% confidence. This complication is due to the scatter of coefficient of variation of ductility factor present for each family of earthquake excitations. The best one can do is reduce the probability of exceedance associated with each of the two ductility factors to an acceptable level. Deciding on an acceptable level is complex as it involves economic, social, and political considerations.

Suppose for example, it was decided that a 15 percent probability of exceedance was acceptable, i.e. $Q(\mu) = 0.15$ and $P(\mu) = 0.85$. Using Fig. 7

and the data provided in Figs. 10a-15d, one can easily establish that ductility factor μ_{85} associated with $P(\mu) = 0.85$. This has been done for two trilinear stiffness degrading models subjected to Type A ground motions giving the results shown in Fig. 8.

B. SELECTION OF REQUIRED STRENGTH LEVELS

To establish the required strength levels of the various structural models for each class of earthquake motions, one must first prescribe basic criteria consistent with the basic design philosophy. In the following discussion, it will be assumed that a 15 percent probability of exceedance ($Q = 0.15$, $P = 0.85$) is an acceptable risk level. Further, it will be assumed that moderate and severe earthquake conditions are represented by 0.30g and 0.45g, respectively, for the mean peak acceleration of ground motions. Finally, the two ductility factors, consistent with light and heavy (but controlled) damage, are chosen as 2 and 10 for the origin-oriented shear model and 2 and 4 for the trilinear stiffness degrading model. The values of peak accelerations and ductility factors selected above follow the suggestions of Umemura, et al. [3].

Using data such as shown in Fig. 8 for each structural model and for each type of earthquake motions, i.e. using curves of μ_{85} vs. T_1 , one can easily obtain the required strength ratios ($\beta = p/m \bar{v}_{g0}$) for discrete values of T_1 . Linear interpolation between the curves (μ_{85} vs. T_1) for a fixed value of T_1 can be used for this evaluation. The resulting required strength ratios can then be plotted as functions of period T_1 as shown in Fig. 16. The three sets of curves in the upper left hand corner of this figure are for the origin-oriented shear model while the remaining sets of curves are for the trilinear stiffness degrading flexure model. Two of the three sets of curves for the origin oriented model are for μ_{85} equal to 2 and 10 consistent with the established design criteria. The third set is for μ_{95} (5% probability of exceedance) equal to 10.

Four sets of curves are shown in Fig. 16 for the trilinear stiffness degrading model for each of three values of ductility factor, i.e. for μ_{85} equal to 2, 4, and 8. The first two of these (2 and 4) correspond with those values chosen to meet the basic design criteria. Therefore, the third group for μ_{85} equal to 8 have no particular practical value but are of interest in showing the influence of high ductility on the required load level. One characteristic feature of all sets of curves shown in Fig. 16 is that the four curves representing earthquake Types A, B, C, and D are quite close together in each case showing that the influence of duration of ground motions is not large. Results for earthquake Type B₀₂ are not shown in Fig. 16, but as would be expected, these results do show a high tendency to peak at $T_1 \leq 0.4$ seconds which corresponds with the predominant period in the narrow band excitation.

When judging which of the two prescribed ductility factors control a particular design, one should be careful not to base the decision on a direct comparison of the required strength ratios as shown in Fig. 16 since these ratios have different normalization factors. For example, consider a shear model with $T_1 = 0.4$ sec. Using the light damage criteria, i.e. $\bar{v}_{g0} = 0.30$ g and $\mu_{85} = 2$, gives $\beta = 2.2$ and $p_c = 0.66$ mg. Using the heavy damage criteria, i.e. $\bar{v}_{g0} = 0.45$ g and $\mu_{85} = 10$, gives $\beta = 0.8$ and $p_c = 0.36$ mg.

Note that for these two different levels of damage, the resulting values for β have a different ratio to each other than do the two values for p_c . Obviously in this case, the light damage criteria requiring $p_c = 0.66$ mg control the design. Let us consider a second example of the origin-oriented model with $T_1 = 0.15$ sec. In this case the light damage criteria give $\beta = 1.7$ and $p_c = 0.51$ mg and the heavy damage criteria give $\beta = 1.3$ and $p_c = 0.58$ mg. For this particular structural model, the heavy damage criteria requiring $p_c = 0.58$ mg control the design. Making similar comparisons for the various trilinear stiffness degrading models represented in Fig. 16, one finds that the heavy damage criteria ($\bar{v}_g = 0.45g$ and $\mu_{85} = 4$) always control the design.

When using the results in Fig. 16 in accordance with the above example calculations, one should remember that they are based on the ground motion parameters $\omega_0 = 15.6$ rad/sec ($T_0 = 0.4$ sec) and $\xi_0 = 0.6$ which represent firm ground conditions. If one should have quite different ground conditions, these parameters should be adjusted appropriately. These adjustments shift the level of the predominant frequencies in the ground motions and also change the mean intensity level \bar{v}_{g0} . With considerable experience and using engineering judgement, certain modifications to the data in Fig. 16 can be made to reflect these new conditions.

One very significant feature to notice in Fig. 16 is that generally for all structural models represented, the required strength ratios for $T_1 > 0.2$ sec vary in a linear manner with negative slopes along the log scale for T_1 . Converting to a linear scale, the required strength ratios would vary in inverse proportion to the square root of T_1 , i.e. $\beta \sim (T_1)^{-1/2}$ for $T_1 > 0.2$ sec.

VIII. CONCLUDING STATEMENT

The response ductility factors and coefficients of variation presented herein provide the necessary data for carrying out probabilistic seismic resistant designs consistent with basic design criteria and the statistical nature of earthquake ground motions.

IX. ACKNOWLEDGEMENT

The authors express their sincere thanks and appreciation to the National Science Foundation for its financial support of this investigation under grant NSF GI 38463.

X. BIBLIOGRAPHY

- [1] Ruiz, P., and Penzien, J., "Probabilistic Study of the Behavior of Structures during Earthquakes," Earthquake Engineering Research Center, No. EERC 69-3, University of California, Berkeley, California, March, 1969.
- [2] Jennings, P. C., Housner, G. W., and Tsai, N. C., "Simulated Earthquake Motions", Earthquake Engineering Research Laboratory, California Institute of Technology, Pasadena, California, April, 1968.

- [3] Umemura, H., et. al., "Earthquake Resistant Design of Reinforced Concrete Buildings, Accounting for the Dynamic Effects of Earthquake," Giho-do, Tokyo, Japan, 1973, (in Japanese).
- [4] Penzien, J., and Liu, S-C., "Nondeterministic Analysis of Nonlinear Structures Subjected to Earthquake Excitations," Proceedings of the 4th World Conference on Earthquake Engineering, Santiago, Chile, January, 1969.
- [5] Amin, M., and Ang, A. H. S., "A Nonstationary Stochastic Model for Strong-Motion Earthquakes," Structure Research Series 306, University of Illinois, Urbana, Illinois, April, 1966.
- [6] Shinozuka, M., and Sato, Y., "Simulation of Nonstationary Random Process," Proceedings, ASCE, Vol. 93, EMI, February, 1967.
- [7] Berg, G. V., and Housner, G. W., "Integrated Velocity and Displacement of Strong Earthquake Ground Motion," Bulletin of the Seismological Society of America, Vol. 51, No. 2, April, 1961.
- [8] Clough, R. W., and Penzien, J., "Dynamics of Structures," McGraw Hill, 1975.
- [9] Kanai, K., "Semi-Empirical Formula for Seismic Characteristics of the Ground," Bulletin of Earthquake Research Institute, University of Tokyo, Japan, Vol. 35, June, 1967.
- [10] Tajimi, H., "A Statistical Method of Determining the Maximum Response of a Building Structure during an Earthquake," Proceedings of the 2nd World Conference on Earthquake Engineering, Tokyo, Japan, Vol. II, July, 1960.
- [11] Gumbel, E. J., and Carlson, P. G., "Extreme Values in Aeronautics," Journal of the Aeronautical Sciences, 21, No. 6, June, 1954.

TABLE 1

Mean Values and Standard Deviations of Peak Ground Accelerations

Type of Earthquake	Statistical Quantity	Number of Earthquakes		
		20	40	Infinity
A	Mean	0.327	0.331	0.332
	Std. Deviation	0.023	0.036	0.040
B	Mean	0.300	0.308	0.309
	Std. Deviation	0.032	0.037	0.041
C	Mean	0.240	0.243	0.244
	Std. Deviation	0.022	0.035	0.039
D	Mean	0.191	0.188	0.189
	Std. Deviation	0.041	0.039	0.044
B ₀₂	Mean	0.346	0.336	0.337
	Std. Deviation	0.048	0.049	0.055

TABLE 2

Standard Time Interval and Subdivided Time Interval

Interval Type	Natural Period T_1 , sec.			
	0.1 and 0.14	0.2-0.4	0.57-1.13	1.6 and 2.26
Standard	0.005	0.01	0.01	0.01
Subdivided	0.000625	0.00125	0.0025	0.005

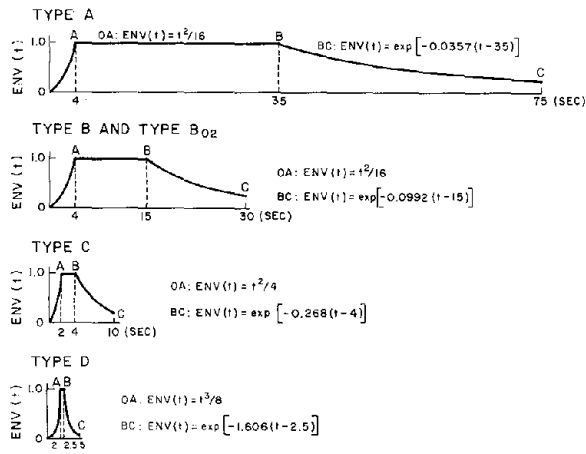
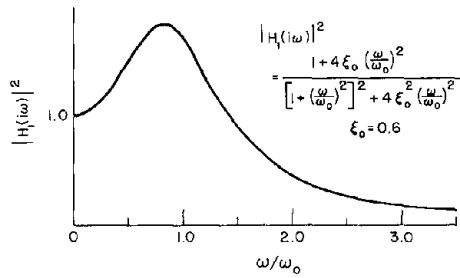
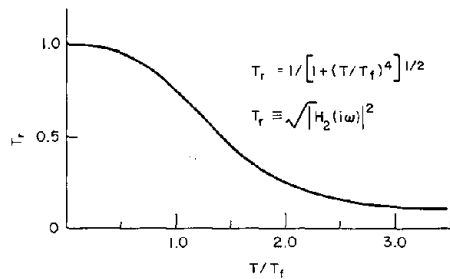


Fig. 1 Time intensity functions

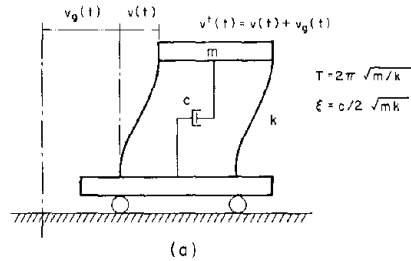


(a)

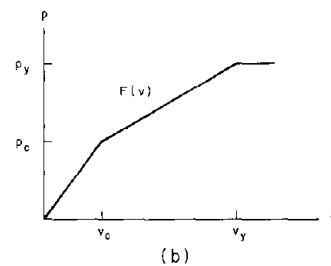


(b)

Fig. 2 Filter transfer functions



(a)



(b)

Fig. 3 Single degree of freedom model with force-displacement relationship

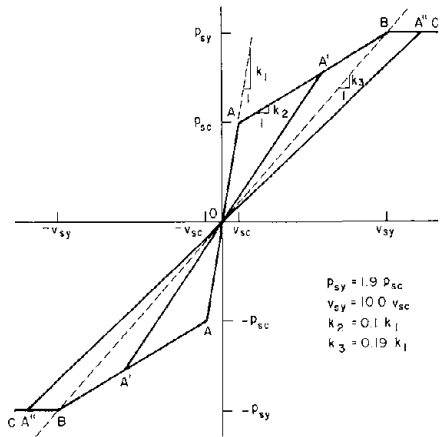


Fig. 4 Origin-oriented hysteretic model

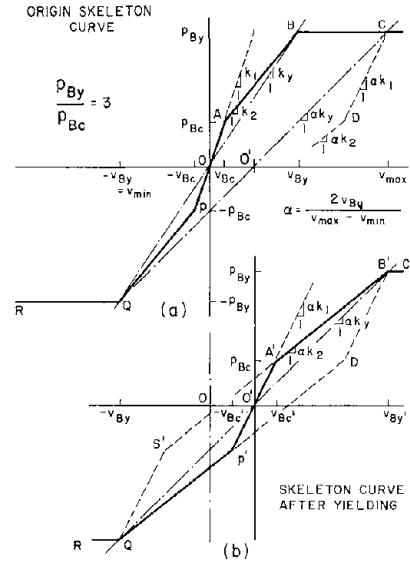


Fig. 5 Tri-linear hysteretic model

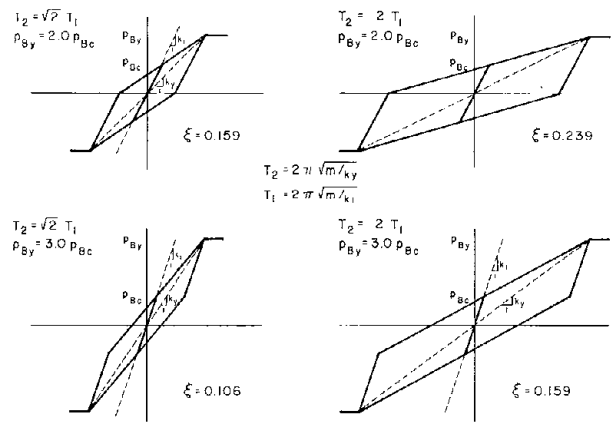


Fig. 6 Stable bilinear hysteretic loop for trilinear stiffness degrading model

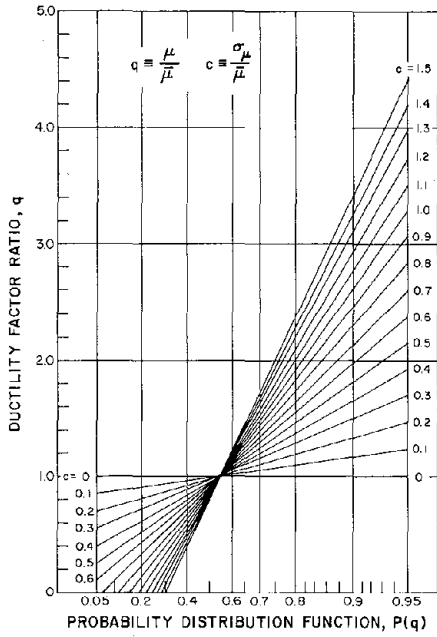


Fig. 7 Probability distribution functions for ductility factor ratios on Gumbel plots.

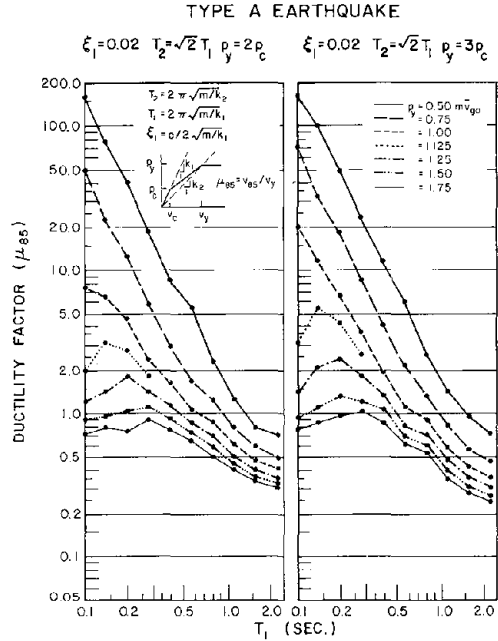


Fig. 8 Response ductility factors for 85% level on probability distribution functions

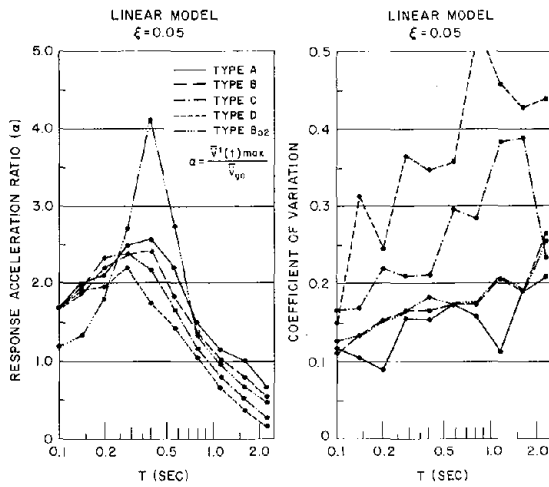


Fig. 9 Response acceleration ratios for linear model

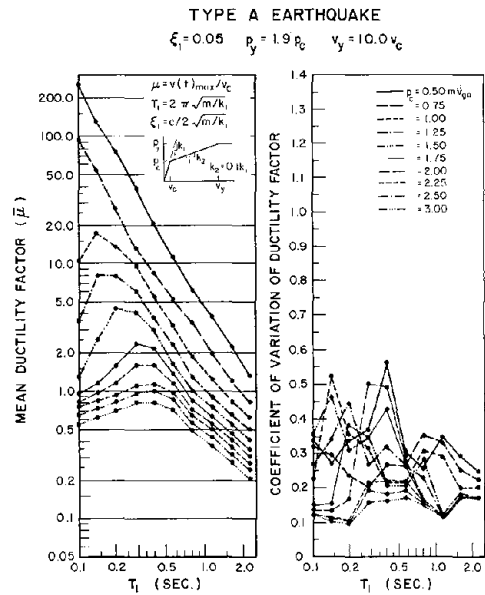


Fig. 10a Mean ductility factors and corresponding coefficients of variation for origin-oriented model having different strength levels

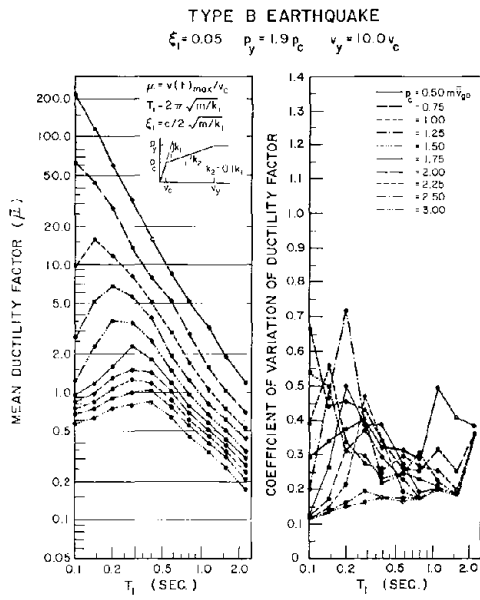


Fig. 10b Mean ductility factors and corresponding coefficients of variation for origin-oriented model having different strength ratios.

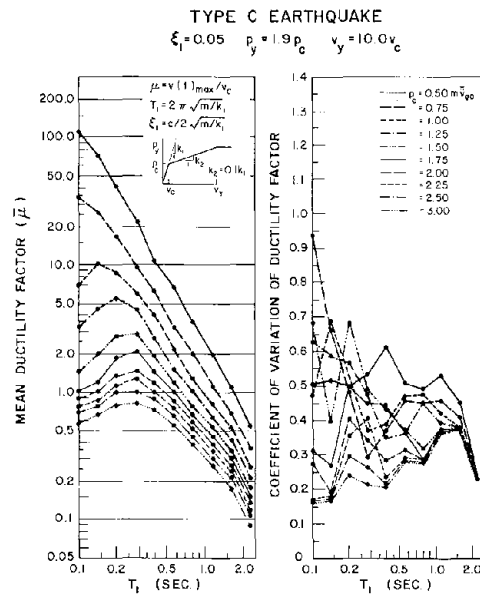


Fig. 10c Mean ductility factors and corresponding coefficients of variation for origin-oriented model having different strength ratios.

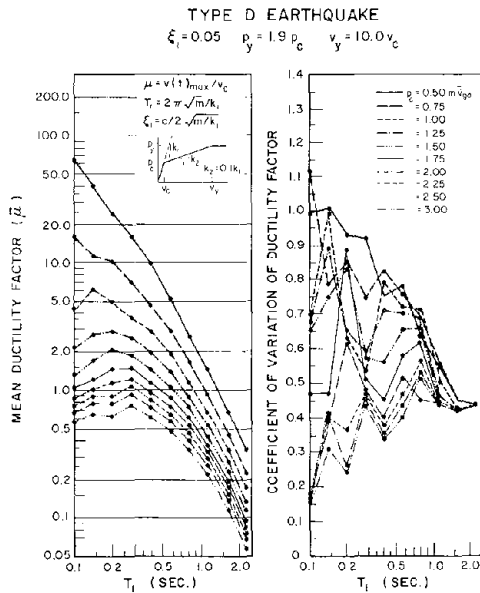


Fig. 10d Mean ductility factors and corresponding coefficients of variation for origin-oriented model having different strength ratios.

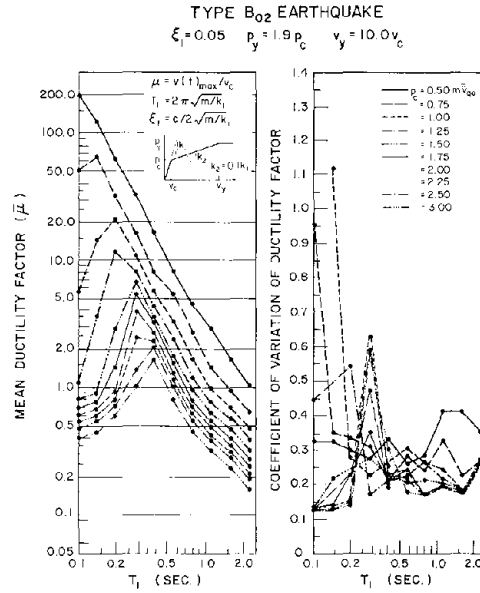


Fig. 10e Mean ductility factors and corresponding coefficients of variation for origin-oriented model having different strength levels

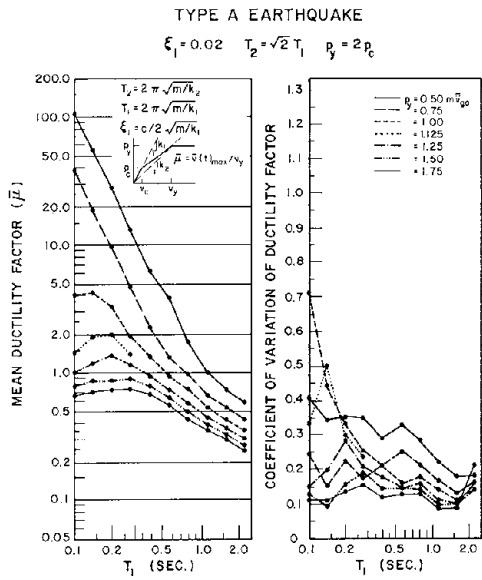


Fig. 11a Mean ductility factors and corresponding coefficients of variation for trilinear stiffness degrading model having different strength levels.

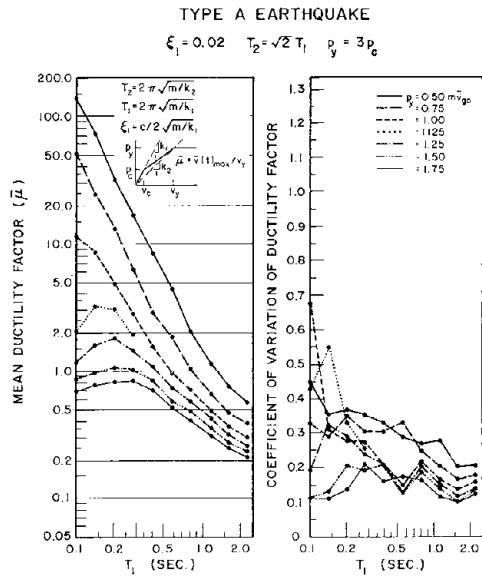


Fig. 11b Mean ductility factors and corresponding coefficients of variation for trilinear stiffness degrading model having different strength levels.

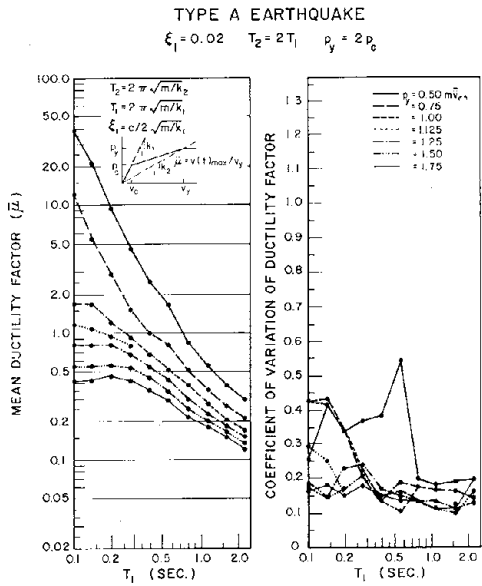


Fig. 11c Mean ductility factors and corresponding coefficients of variation for trilinear stiffness degrading model having different strength levels.

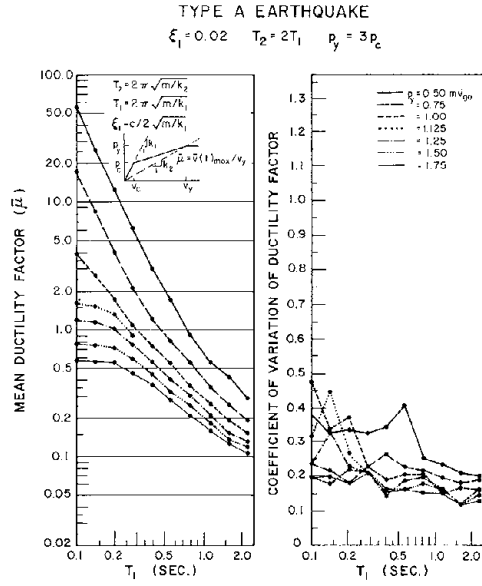


Fig. 11d Mean ductility factors and corresponding coefficients of variation for trilinear stiffness degrading model having different strength levels.

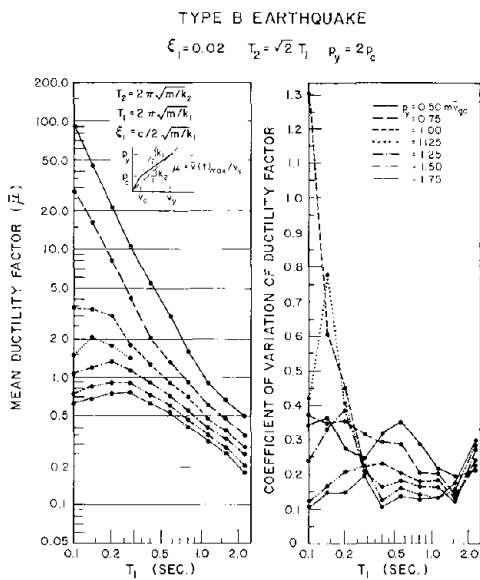


Fig. 12a Mean ductility factors and corresponding coefficients of variation for trilinear stiffness degrading model having different strength levels.

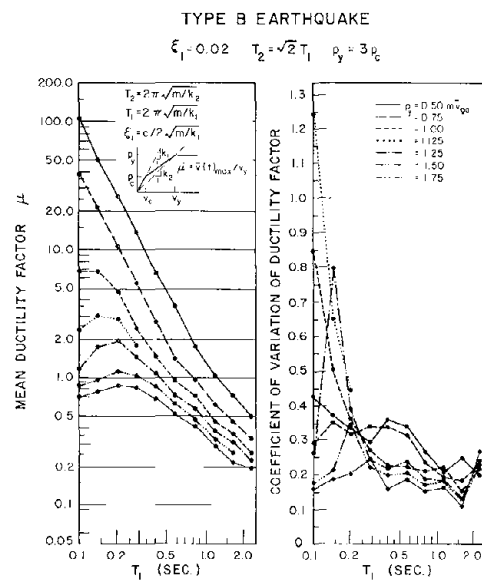


Fig. 12b Mean ductility factors and corresponding coefficients of variation for trilinear stiffness degrading model having different strength levels.

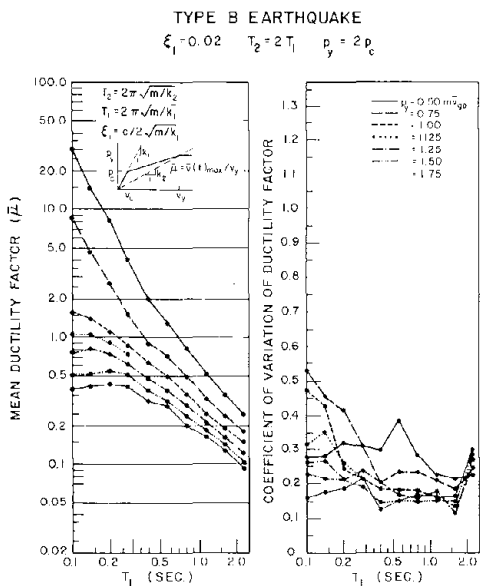


Fig. 12c Mean ductility factors and corresponding coefficients of variation for trilinear stiffness degrading model having different strength levels.

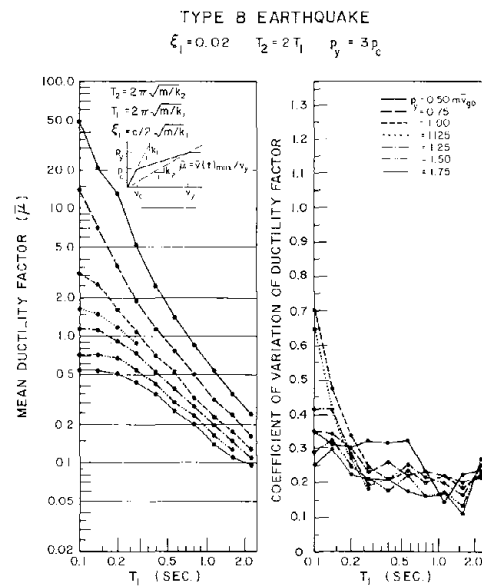


Fig. 12d Mean ductility factors and corresponding coefficients of variation for trilinear stiffness degrading model having different strength levels.

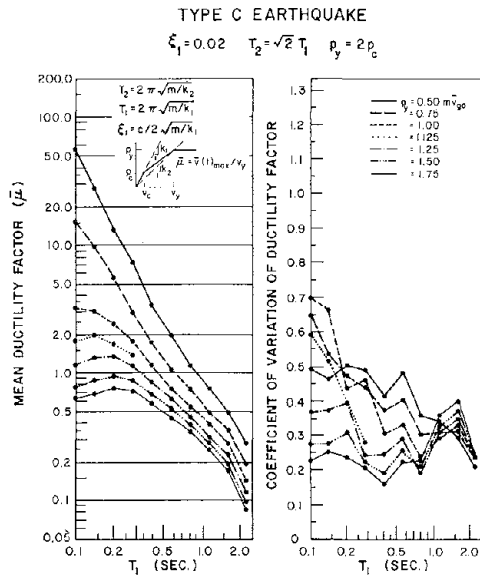


Fig. 13a Mean ductility factors and corresponding coefficients of variation for trilinear stiffness degrading model having different strength levels.

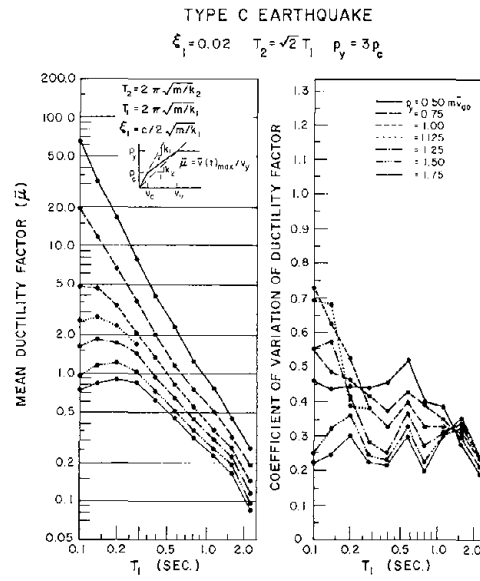


Fig. 13b Mean ductility factors and corresponding coefficients of variation for trilinear stiffness degrading model having different strength levels.

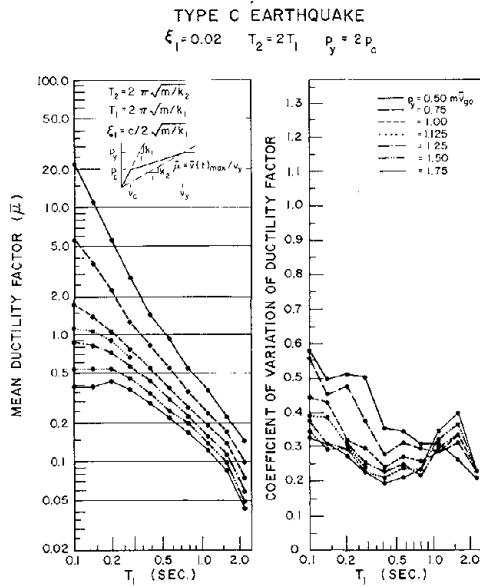


Fig. 13c Mean ductility factors and corresponding coefficients of variation for trilinear stiffness degrading model having different strength levels.

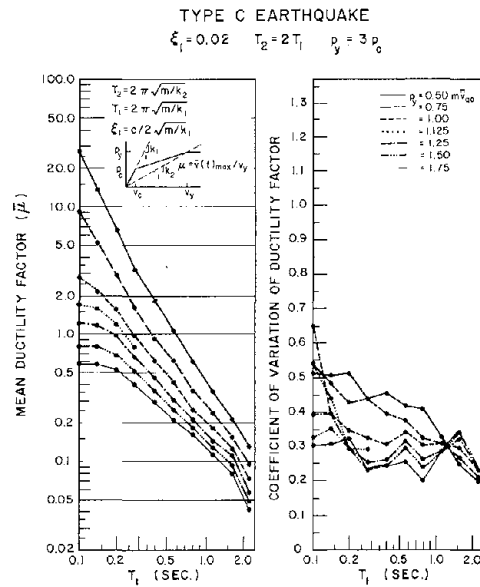


Fig. 13d Mean ductility factors and corresponding coefficients of variation for trilinear stiffness degrading model having different strength levels.

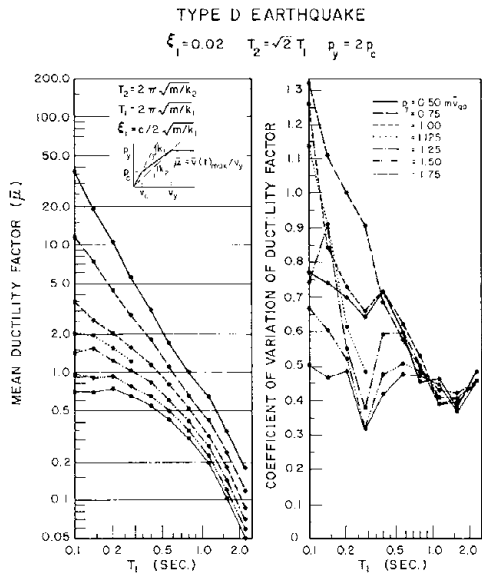


Fig. 14a Mean ductility factors and corresponding coefficients of variation for trilinear stiffness degrading model having different strength levels.

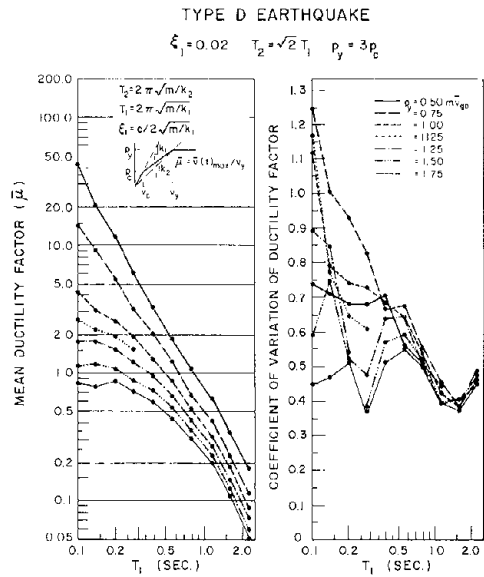


Fig. 14b Mean ductility factors and corresponding coefficients of variation for trilinear stiffness degrading model having different strength levels.

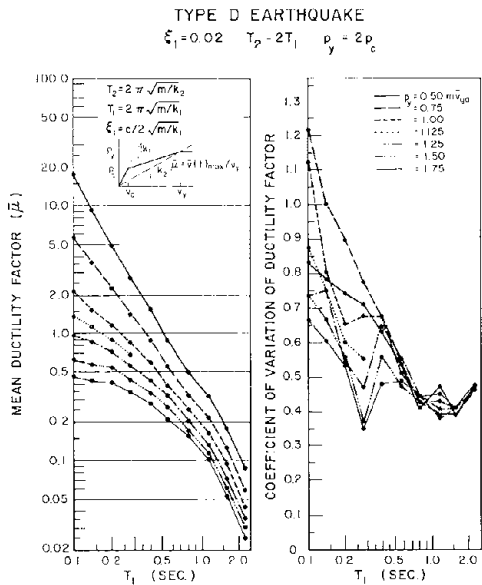


Fig. 14c Mean ductility factors and corresponding coefficients of variation for trilinear stiffness degrading model having different strength levels.

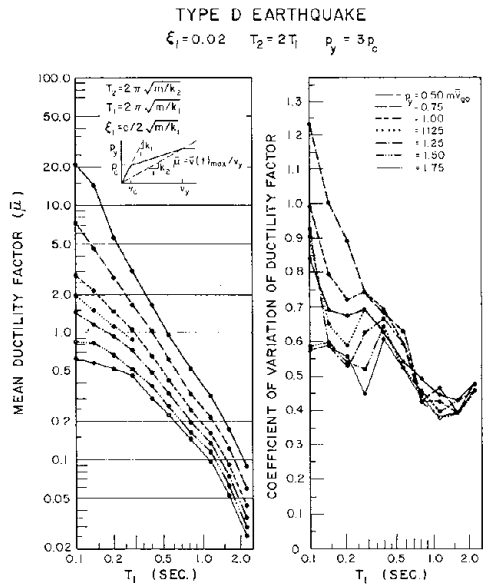


Fig. 14d Mean ductility factors and corresponding coefficients of variation for trilinear stiffness degrading model having different strength levels.

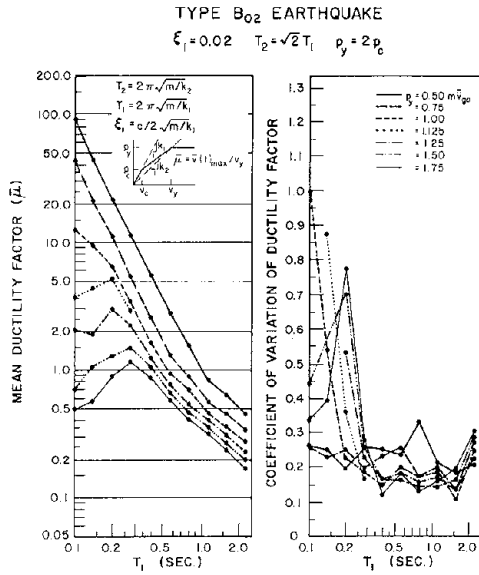


Fig. 15a Mean ductility factors and corresponding coefficients of variation for trilinear stiffness degrading model having different strength levels.

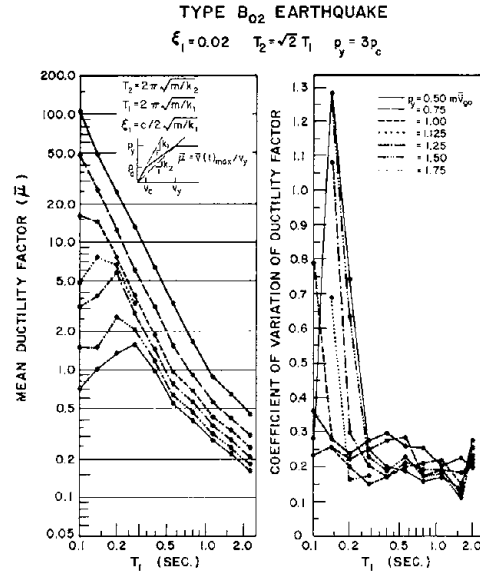


Fig. 15b Mean ductility factors and corresponding coefficients of variation for trilinear stiffness degrading model having different strength levels.

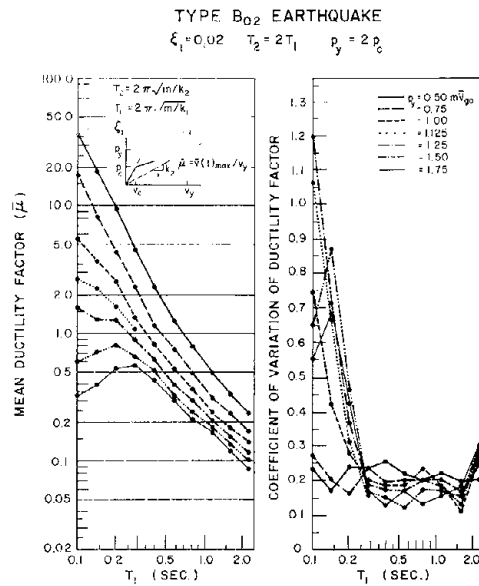


Fig. 15c Mean ductility factors and corresponding coefficients of variation for trilinear stiffness degrading model having different strength levels.

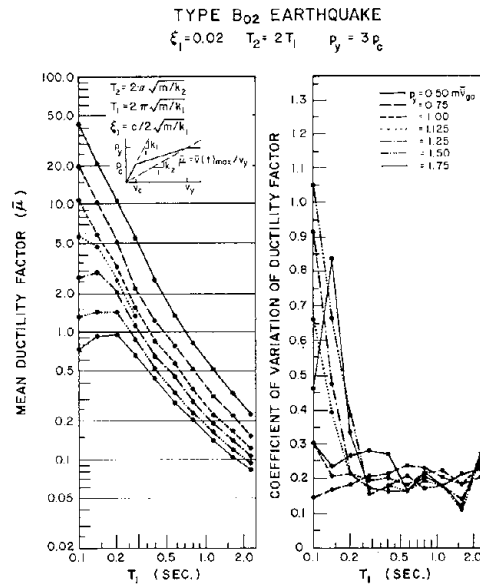


Fig. 15d Mean ductility factors and corresponding coefficients of variation for trilinear stiffness degrading model having different strength levels.

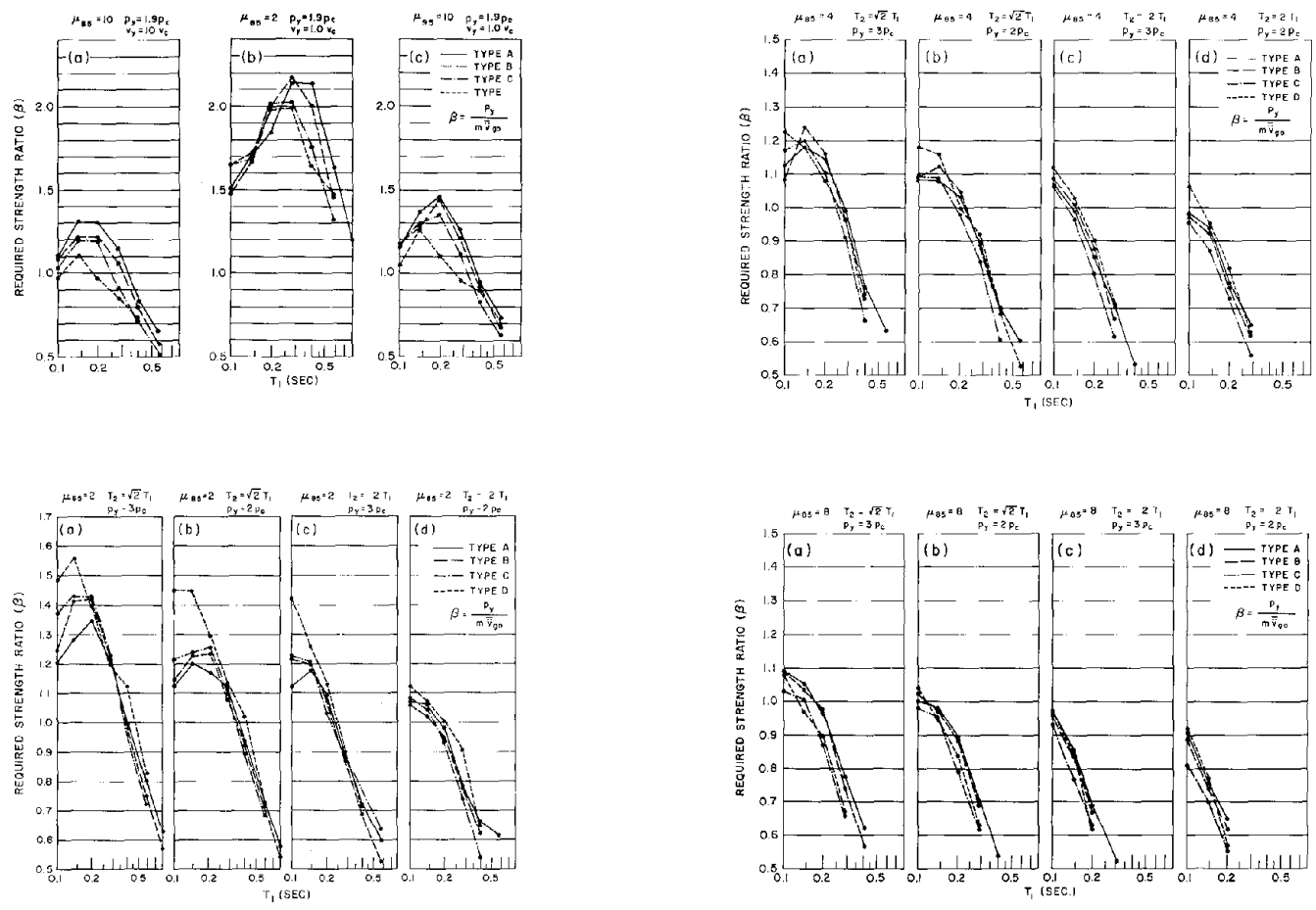


Fig. 16 Required strength ratios for origin-oriented model and four types of trilinear stiffness degrading models having three different levels of ductility at the 85% probability distribution level.

USE OF LINEAR MODELS IN DESIGN TO REFLECT
THE EFFECT OF NONLINEAR RESPONSE

By Akenori Shibata* and Mete A. Sozen**

SYNOPSIS

A method to determine design forces for earthquake resistant design of reinforced concrete structures is described. The method, which recognizes energy dissipation in the nonlinear range of response, utilizes linear models and response spectra. The paper contains discussions of (1) equivalent linear earthquake response of single-degree-of-freedom hysteretic systems, (2) description of the substitute structure method, and (3) a design example using the method.

INTRODUCTION

The objectives of this report are (a) to discuss the relationship between nonlinear and equivalent linear response of SDF systems to provide background for the use of equivalent linear models in seismic design, (b) to introduce the substitute structure method, a design procedure for multi-story frames to reflect the effect of nonlinear response while using linear response models for analysis, and (c) to describe a specific design example in which a three story reinforced concrete frame is designed with the proposed method and its performance to earthquake motions is evaluated.

SDF SYSTEMS

It has been recognized that the maximum inelastic response of hysteretic yielding systems can be satisfactorily determined using equivalent linear models with reduced stiffness and increased damping determined as a function of attained maximum displacements or damage ratios. Various approaches to the linear representation of nonlinear response are discussed in References 1 - 3 and 6 - 13.

Calculated Responses of Nonlinear and Equivalent Linear Models

Maximum responses of nonlinear and equivalent linear SDF systems are compared in order to describe the basis for the use of equivalent linear models in the seismic design of reinforced concrete structures.

An equivalent linear model to simulate the maximum inelastic response of hysteretic system is described by Eq. 1 and 2. It is assumed that the stiffness of the "prototype" reduces and the damping increases with increase in inelastic deformation.

$$T_e = \sqrt{\mu} \cdot T \quad \text{----- (1)}$$

where T_e = equivalent period, T = period based on average stiffness at yield corresponding closely to cracked-section stiffness in reinforced concrete,

* Associate Professor, Faculty of Engineering, Tohoku University, Sendai

** Professor of Civil Engineering, University of Illinois, Urbana

μ = damage ratio = k/k_e , k = stiffness at yield, k_e = equivalent stiffness.

$$\beta_e = 0.2 (1 - 1/\sqrt{\mu}) + 0.02 \quad \text{----- (2)}$$

where β_e = equivalent damping factor. Ductility factor $\mu' = \delta_{\max}/\delta_Y$ may be used in stead of μ in Eq. 2.

Eq. 2 is based on the analysis of substitute damping defined in Eq. 3.

$$\beta_s = - \int_0^{t_L} \ddot{y} \cdot \dot{x} dt / 2 \omega_e \int_0^{t_L} \dot{x}^2 dt \quad \text{----- (3)}$$

where \ddot{y} = ground acceleration, \dot{x} = velocity response, ω_e = equivalent frequency = $\sqrt{k_e/m}$, t_L = response duration, β_s = substitute damping factor.

Substitute damping factors have been evaluated either from the results of dynamic tests of reinforced concrete frames (Ref. 1 and 2) or nonlinear response histories of reducing stiffness models representing reinforced concrete elements. Fig. 2 shows the relation between substitute damping factors and ductility factors (corresponding closely to damage ratios) calculated from inelastic response results discussed in the following. It is seen that β_s could be approximately represented by the type of curves in the figure. Eq. 2 corresponds to the curve for $\gamma = 1/5$ in Fig. 2.

Inelastic responses of SDF systems with reducing stiffness hysteresis relation shown in Fig. 1 are calculated for various yield levels with step-by-step integration method using El Centro 1940 NS 0.31G and Taft 1952 N21E 0.18G ground-motion records. The assumed force-displacement relation in Fig. 1 is a simple and reasonably good representation of the hysteresis properties of reinforced concrete frames. Effect of tensile strength of concrete is not considered here. The stiffness k in the nonlinear range is assumed to be five percent of k , the stiffness before yield. A damping factor of 0.02 is used for response in the linear range. (Ref. 15)

Calculated maximum responses of nonlinear and equivalent linear systems are compared graphically in Fig. 3 and 4. The correlation is good. It should be noted that the stiffness as well as damping of the equivalent linear system is based on the maximum displacement calculated for the nonlinear system. Maximum responses of equivalent linear systems are obtained from linear response spectra.

General Trends for Nonlinear Maximum Response

It has been shown in Ref. 5 that there are three approximate rules for correlating elastic response of linear systems having initial periods and inelastic response of yielding systems for earthquake motions.

- 1) Displacement is preserved for systems with relatively long periods.
- 2) Energy is preserved for systems with short periods.
- 3) Force is preserved for systems with very short periods.

The above trends for nonlinear maximum response to earthquake motions may be interpreted in terms of the equivalent linear models and the spectrum shape of earthquake.

The calculated maximum displacements of equivalent linear systems for the idealized response spectra shown in Fig. 5 with $A_{\max} = 0.3G$ are presented in Fig. 6.

The smoothed response spectra in Fig. 5 were selected to reflect response spectra for six acceleration records, i.e., two components of El Centro 1940, Taft 1952 and Managua 1972 whose maximum accelerations were all scaled to the same values (Ref. 3). The spectral acceleration S_A for a damping factor of 0.02 is related to the maximum ground acceleration A_{\max} and period T as shown below.

$$S_A = \begin{cases} \text{Max} (25T \cdot A_{\max}, A_{\max}) & \text{for } T \leq 0.15\text{sec} \\ 3.75 \cdot A_{\max} & 0.15 < T \leq 0.4\text{sec} \\ 1.5 \cdot A_{\max} / T & T > 0.4\text{sec} \end{cases} \quad \text{-----(4)}$$

The smoothed spectra have increasing spectral acceleration with period up to 0.15sec, constant spectral acceleration between 0.15sec and 0.4sec and constant spectral velocity for periods greater than 0.4sec.

The effect of damping on spectral response is quite important in the equivalent linear response analysis. Though it takes very scattered values in actual response, it is assumed to be expressed by Eq. 5 in relation to the values for the damping factor of 0.02.

$$S_A(\beta) / S_A(0.02) = \beta / (6 + 100\beta) \quad \text{-----(5)}$$

where $S_A(0.02)$ and $S_A(\beta)$ are the spectral accelerations for the damping factor of 0.02 and β , respectively.

Each plot in Fig. 6 refers to a SDF system with a certain period, which defines the initial slope of "k". Displacement response for equivalent linear systems for various damage ratios k/k_p are indicated by the solid curve on each plot. Eq. 4 is entered to pick the response acceleration at $\beta = 0.02$ corresponding to the equivalent period by Eq. 1. This value is modified using Eq. 2 and Eq. 5. The resulting displacement may be interpreted in terms of a definition of ductility by connecting this point on the force-displacement plot back to the line representing linear response by a straight line with the positive slope k_p (assumed to be 0.05).

The solid curve in Fig. 6 suggest, in conformity with Ref. 5, that in the nearly constant acceleration range of response ($T = 0.1$ and 0.3sec) energy tends to be constant whereas in the nearly constant velocity range of response ($T = 0.5$ and 1.0sec) displacement tends to be constant. This agreement is significant only in that it demonstrates a behavioral model, explicitly related to the shape of the response spectrum and the energy-dissipating characteristics of the material (reinforced concrete), which leads to the same approximate rules for the interrelationship between linear (initial) and nonlinear response in SDF systems as those obtained from over-all observation of a series of calculated response.

Application to Design

In analyzing the equivalent linear response of a nonlinear structure of which strength is given in advance, the final damage ratio is found iteratively so that the assumed damage ratio matches the damage ratio calculated from the estimated maximum displacement and specified force-displacement relation. On the other hand, if the damage ratio is initially assumed, the estimated maximum displacement together with the assumed damage ratio determines the approximate strength required to produce the assumed damage ratio. This provides a procedure for determination of design forces for given allowable damage ratios.

THE SUBSTITUTE STRUCTURE METHOD

A method is proposed to determine design forces for earthquake resistant design of MDF reinforced concrete structures taking account of inelastic response using the concept of equivalent linear response. Its objective is to establish the minimum strength the components must have so that a tolerable response displacement is not likely to be exceeded. The specific advantages are: (1) use of linear models for dynamic analysis, (2) choice in setting limits of tolerable inelastic response in different elements of the structure, and (3) deliberate consideration of displacements in the design process.

The method is applied to structures satisfying the following:

1. The system can be analyzed in one vertical plane.
2. No abrupt changes in geometry or mass in the height of the system.
3. Columns, beams and walls (represented as columns) may be designed with different limits of inelastic response, but the limits should be the same for all beams in a given bay and all columns in a given axis.
4. All structural elements and joints are reinforced to avoid significant strength decay as a result of repeated reversals of the anticipated inelastic displacements.
5. Nonstructural components do not interfere with structural response.

Schematic description of the design procedure is given in the following. (See Ref. 3 and 14 for detail.)

Smoothed Response Spectra

The method requires a set of smoothed response spectra corresponding to the expected intensity and characteristics of anticipated earthquakes at the building site. The idealized response spectra in Fig. 5 are used tentatively for design in this paper. The effect of damping on spectral response is also assumed as in Eq. 5.

Description of the Method

The main operations of the method are divided into three steps.

1. Based on tolerable limits of inelastic response, determine the

- stiffness of the substitute-frame members.
2. Calculate modal frequencies and smeared damping factors for the substitute structure.
 3. Determine design forces from the modal analysis of the substitute frame using linear response spectra.

It is assumed that preliminary member sizes of the actual frame are known from gravity-load and functional requirements, precedent, or a previous trial.

The Substitute Structure. The flexural stiffnesses of substitute-frame elements are related to those of actual-frame elements in accordance with Eq. 6.

$$(EI)_{s_i} = (EI)_{a_i} / \mu_i \quad \text{----- (6)}$$

where $(EI)_{s_i}$ and $(EI)_{a_i}$ are cross-sectional flexural stiffnesses of the element i in the substitute and actual frames, respectively, and μ_i is the selected tolerable damage ratio for element i .

$(EI)_{a_i}$ is calculated using the fully cracked section and represents the member stiffness when the member end moments reach the yield points under the moment pattern considered. $(EI)_{s_i}$ and $(EI)_{a_i}$ are illustrated in Fig. 6. The damage ratio is comparable but not exactly the same as the ductility factor based on the ratio of maximum to yield rotation. Quantitatively, damage ratio and ductility factor are identical only for elasto-plastic response. It must be emphasized that a damage ratio of, say, six requires a large ratio of ductility based on curvature or strain in members with moment gradients.

Modal Frequencies and Damping Factors. Periods or frequencies, modal shapes and modal forces are calculated from the undamped substitute structure. Modal damping factors for the substitute structure (smeared damping factor) are estimated by taking the weighted average of member substitute damping factors assuming that each element contributes to the modal damping factor in proportion to its relative flexural strain energy associated with the modal shape.

$$\beta_m = \sum_i \frac{P_i}{\sum_i P_i} \cdot \beta_{s_i} \quad \text{----- (7)}$$

$$P_i = \frac{L_i}{6(EI)_{s_i}} \cdot (M_{A_i}^2 + M_{B_i}^2 - M_{A_i} \cdot M_{B_i}) \quad \text{----- (8)}$$

where β_m is the smeared modal damping factor for mode m , β_{s_i} is the substitute damping factor for element i calculated from Eq. 2, L_i is the length of frame element i , $(EI)_{s_i}$ is the assumed stiffness of substitute-frame element i , M_{A_i} and M_{B_i} are the moments at ends of substitute-frame element i for mode m , and P_i is the flexural strain energy in element i for mode m .

Design Forces. Design forces in individual elements are based on the root-sum-square combination amplified by a factor given in terms of the base shear.

$$F_i = F_{i, r_{ss}} \cdot \frac{V_{r_{ss}} + V_{abs}}{2 V_{r_{ss}}} \quad \text{----- (9)}$$

where F_i is the design force in element i , $F_{i, r_{ss}}$ is the root-sum-square of the modal forces for element i , $V_{r_{ss}}$ is the base shear based on RSS of modal base shears, and V_{abs} is the maximum value for absolute sum of any two of the modal shears.

To reduce risk of excessive inelastic action in the columns in case of weak-beam strong-column combinations, the design moments for column from Eq. 9 are amplified by a factor of 1.2.

Rationalization of the Method

The "tests" of frames "designed" with the method were conducted in Ref. 3. Two to ten story frames with rigid beams and three to ten story frames with flexible beams were tested. The tests were analytical. Design forces for a series of frames were determined. Then, inelastic responses of these frames, with members having flexural yield capacities determined by the design process, were calculated against various ground motions having similar response spectra to the design spectra using the inelastic response analysis program SAKE (Ref. 4). The detailed discussion of the results is given in Ref. 3. It is considered that the test results were satisfactory.

Design of a Three Story Frame

To illustrate the method, a three-story three-bay model frame was designed using the substitute structure method. The model frame was taken from the three story building which appears in the design example of AIJ (Architectural Institute of Japan) Standard for Structural Calculation of Reinforced Concrete Structures.

The Model Frame. The plan of the example building is shown in Fig. 8. An interior frame in the transverse direction is chosen as the representative model frame (Fig. 9). As six frames in the transverse direction have almost the same lateral stiffness, 1/6 of the total floor weight of the building is assigned to each floor of the model frame. The bottom of the first story column is assumed to be fixed, though it is pin-supported with footing beam (40*100cm) in the original building. Member dimensions, floor weights and story heights of the model frame are shown below. Haunches in beams were neglected in stiffness calculation.

Story	Beam	Column	Weight	Height
3	30 × 55 cm	50 × 50 cm	70 ton	338 cm
2	30 × 60	55 × 55	75	343
1	35 × 65	60 × 60	82	375

Substitute Frame. Initial uncracked stiffnesses are calculated from the gross concrete sections with Young's modulus of concrete of 210 ton/cm**2. For beams, cross-sectional stiffnesses of rectangular section are multiplied by a factor of 2.0 to take account of the effect of slab to increase the sectional stiffness.

Stiffnesses at yield point (cracked section) are assumed to be 1/3 of initial uncracked stiffness for beams and 1/2 for columns. Allowable damage ratio is six for beams and one for columns.

Periods for uncracked, cracked and substitute frames and smeared modal damping factors for substitute frame are shown below.

Mode	Period			Smeared Modal Damping
	Uncracked	Cracked	Substitute	Substitute
1	0.39 sec	0.60 sec	1.00 sec	0.091
2	0.14	0.21	0.27	0.054
3	0.08	0.12	0.12	0.028

Modal moments for 1.0G spectral acceleration are shown in Fig. 10 for substitute frame.

Design Seismic Forces. The smoothed response spectra in Fig. 5 with maximum effective ground acceleration A_{max} of 0.3G are used as the design spectra. The damping effect of Eq. 5 is assumed. The maximum ground acceleration of 0.3G in Eq. 4 corresponds to the constant spectral velocity of 70 cm/sec which is similar to the value for El Centro 1940 NS.

Modal spectral accelerations and modal base shears are obtained as follows for the substitute frame.

Mode	Modal Acceleration	Modal Base Shear ($\frac{\text{Base Shear}}{\text{Total Weight}}$)
1	0.24G	42 ton (0.19)
2	0.79G	32 (0.14)
3	0.84G	10 (0.04)

RSS and ABSOLUTE SUM (two modes) base shears, V_{rss} and V_{abs} , are 54 ton (0.24) and 74 ton (0.33) respectively and the factor of $(V_{abs} + V_{rss})/2V_{rss}$ is 1.19. Seismic moments obtained with Eq. 9 are shown in Fig. 11.

Column moments are multiplied by a column-overdesign factor of 1.2 in the substitute structure method. Fig. 12 shows the larger of the two end moments in Fig. 11 with column moments amplified by 1.2.

Design Story Displacements. Relative story displacements (RSS*1.19) are calculated as follows.

Story	Relative Story Displ.	Rel. Story Displ./Story Height
3	3.95 cm	0.012
2	3.63	0.011
1	2.12	0.006

It is considered that the story deflection of the order of 1/100 of story height during earthquakes could be tolerated provided the details for nonstructural elements are properly designed.

Response of Designed Frame to Ground Motions. Response histories of the designed frames to four ground motions were calculated by an inelastic dynamic analysis program, SAKE(Ref. 8). Ground motions used were El Centro

1940 NS, EW and Taft 1952 N21E, S69E, with the maximum accelerations normalized to 0.3G. The yield moments at both ends of each members were set at the design moments shown in Fig. 12. The initial stiffnesses were determined from the cracked sectional stiffnesses. The assumed hysteresis relation was the same as that for SDF analysis. Stiffness beyond yield was taken as five percent of initial stiffness. Viscous damping proportional to stiffness amounting to a damping factor of 0.02 for the first mode was used.

Results of inelastic dynamic analysis are shown in Fig. 13. Beam damage ratios range from 2 to 7 in contrast with the target value of 6. Column damage ratios are 0.6 to 1.0, all within the elastic range. In view of the wide variations in earthquake effects, the results are considered positive.

CONCLUSIONS

From the observation that the maximum nonlinear structural response to earthquakes can be simulated reasonably by appropriate linear-response models, a procedure was developed to determine design forces using linear response spectra but taking account of inelastic energy dissipation by using an analytical model with stiffness and damping characteristics depending on the permissible degree of nonlinear action.

The method can be used to determine earthquake design-force requirements for individual elements of a reinforced concrete structure given a design response spectrum and explicit decisions about tolerable inelastic response, with the option of different limits of inelastic response in different structural elements. Design forces in a three story frame were determined by the proposed method and the inelastic responses for earthquake motions were examined.

ACKNOWLEDGMENTS

The work in this report was carried out in the course of the U. S. - Japan Cooperative Research Program, "Earthquake Engineering with Emphasis on the Safety of School Buildings" under the auspices of Japan Society for Promotion of Science and U. S. National Science Foundation. (Grant G129934) The IBM 360/75 computer system at the University of Illinois and the NEAC 2200 computer system at Tohoku University were used for computation. The authors are indebted to Professor S. Otani, University of Toronto, for his critical thoughts and for use of computer programs SAKE and SUSHI. Cooperation of Haluk Cecen, University of Illinois, in preparing the response data is gratefully acknowledged.

REFERENCES

1. Gulkan, P. and Sozen, M.A., "Response and Energy Dissipation of Reinforced Concrete Frames Subjected to Strong Base Motions," Civil Engineering Studies, Structural Research Series No.377, University of Illinois, Urbana, May 1971
2. Gulkan, P. and Sozen, M.A., "Inelastic Response of Reinforced Concrete Structures to Earthquake Motions," ACI Journal, Dec. 1974, pp. 604-610

3. Shibata, A. and Sozen, M.A., "The Substitute-Structure Method for Earthquake-Resistant Design of Reinforced Concrete Frames," Civil Engineering Studies, Structural Research Series No.412, University of Illinois, Urbana, Oct. 1974
4. Otani, S., "SAKE, A Computer Program for Inelastic Response of R/C Frames to Earthquakes," Civil Engineering Studies, Structural Research Series No.413, University of Illinois, Urbana, Nov. 1974
5. Newmark, N.M., "Current Trends in the Seismic Analysis and Design of High-Rise Structures," Chapter 16 of "Earthquake Engineering" edited by Wiegel, R.L., Prentice Hall, 1970
6. Caughey, T.K., "Sinusoidal Excitation of a System with Bilinear Hysteresis," Journal of Applied Mechanics, ASME, Vol.27, No.4, Dec.1960, pp. 640-643
7. Caughey, T.K., "Random Excitation of a System with Bilinear Hysteresis," Journal of Applied Mechanics, ASME, Vol.27, No.4, Dec. 1960, pp. 649-652
8. Hudson, D.E., "Equivalent Viscous Friction for Hysteretic Systems with Earthquake-Like Excitations," Proceedings, Third World Conference on Earthquake Engineering, New Zealand, 1965, pp. II 185-202
9. Idris, I.M. and Seed, H.B., "Seismic Response of Horizontal Soil Layers," Journal of the Soil Mechanics and Foundation Division, ASCE, Vol. 94, No. SM4, July 1968, pp. 1003-1031
10. Jennings, P.C., "Equivalent Viscous Damping for Yielding Structures," Journal of the Engineering Mechanics Division, ASCE, Vol. 94, No. EM1, Feb. 1968, pp. 103-116
11. Newmark, N.M. and Rosenblueth, E., "Fundamentals of Earthquake Engineering," Prentice Hall, 1971
12. Tajimi, H. and Ishimaru, T., "Ductility Factor Control Method (in Japanese)," Transactions of Architectural Institute of Japan, No.214, Dec. 1973, pp. 17-28
13. Shibata, A., "Equivalent Linear Response of Hysteretic Systems for Earthquake Motions (in Japanese)," The Architectural Reports of the Tohoku University, No.16, March 1975, pp. 27-39
14. Shibata, A. and Sozen, M.A., "Substitute Structure Method for Seismic Design in R/C," To be published in the Journal of Structural Division, ASCE
15. Takeda, T., Sozen, M.A. and Nielsen, N.N., "Reinforced Concrete Response to Simulated Earthquakes," Journal of the Structural Division, ASCE, Vol. 96, No. ST12, Dec. 1970, pp. 2557-2573

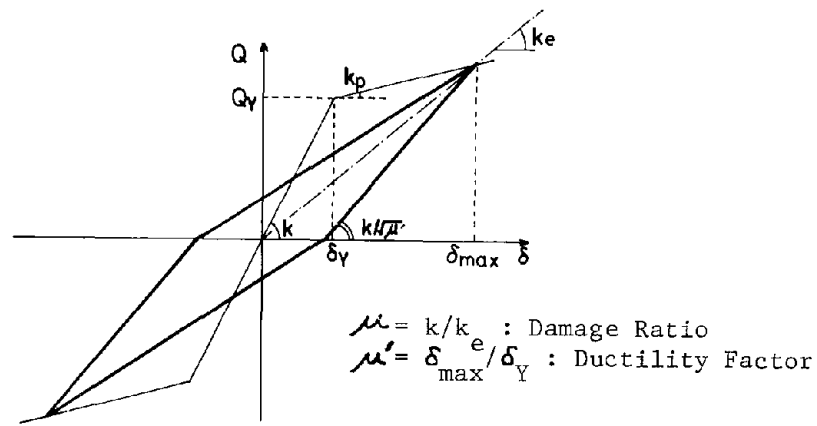


Fig. 1 Reducing Stiffness Force-Displacement Relation

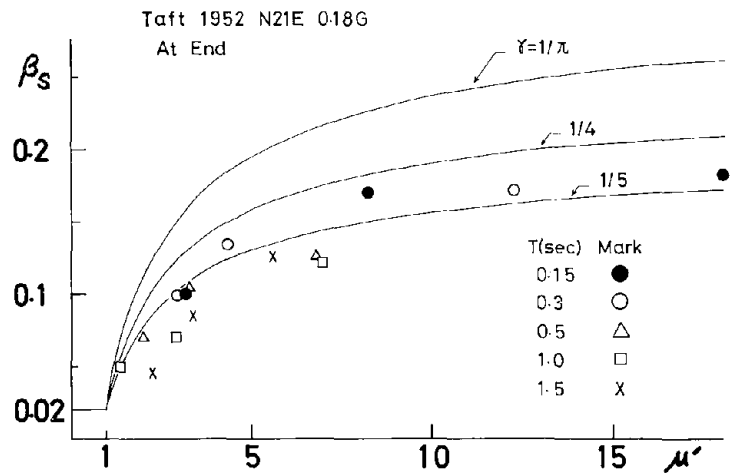
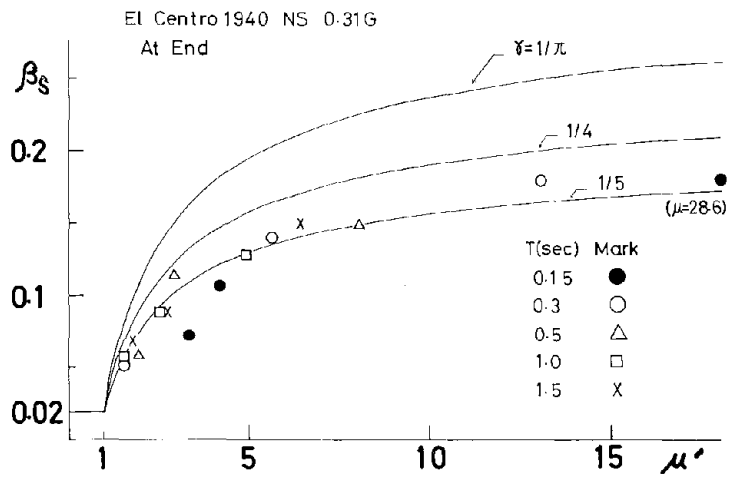


Fig. 2 Relation between Substitute Damping Factor and Ductility Factor

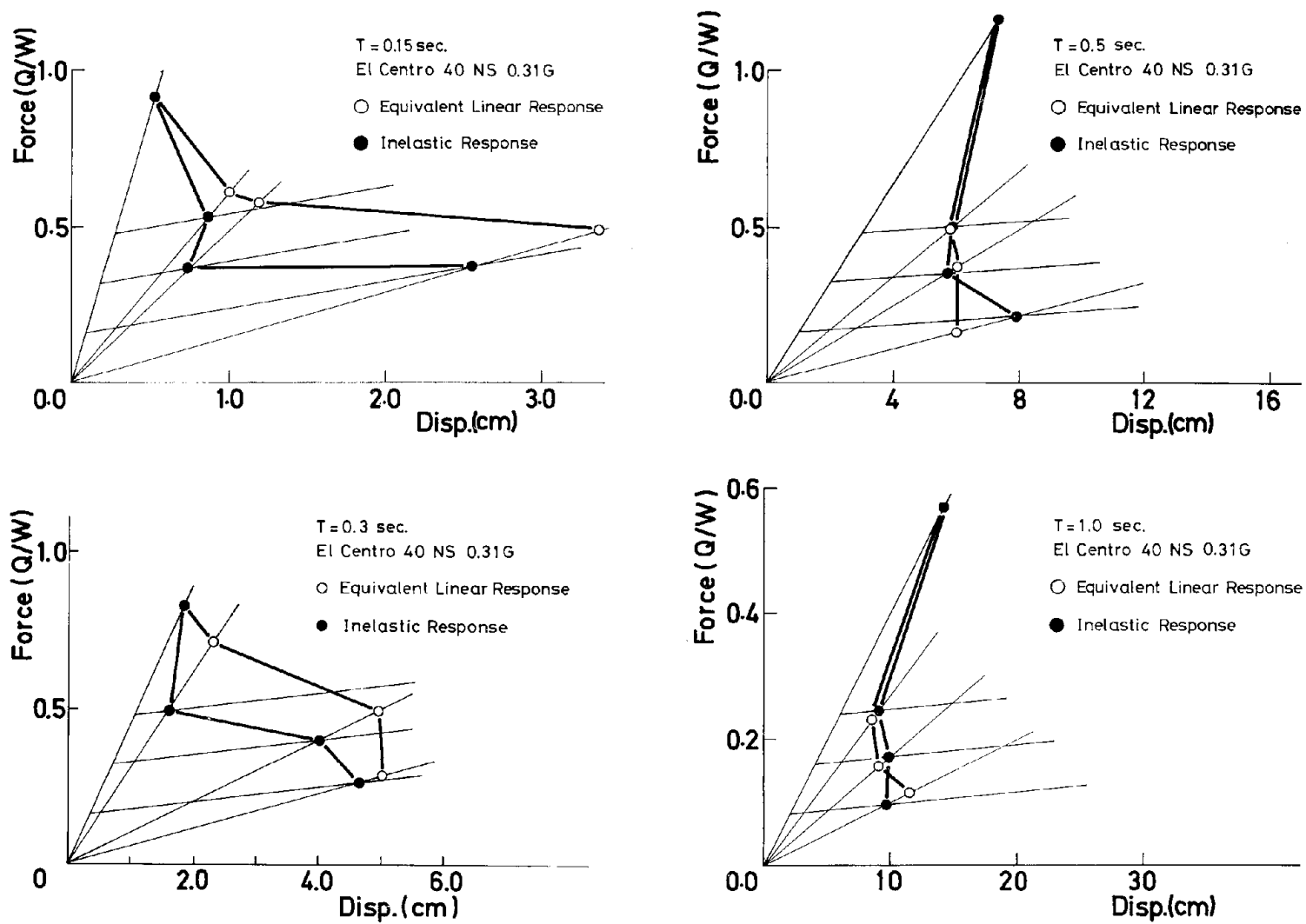


Fig. 3 Relation between Maximum Inelastic Displacement and Yield Force
 El Centro 1940 NS 0.31G (μ' is used in Eq. 2)

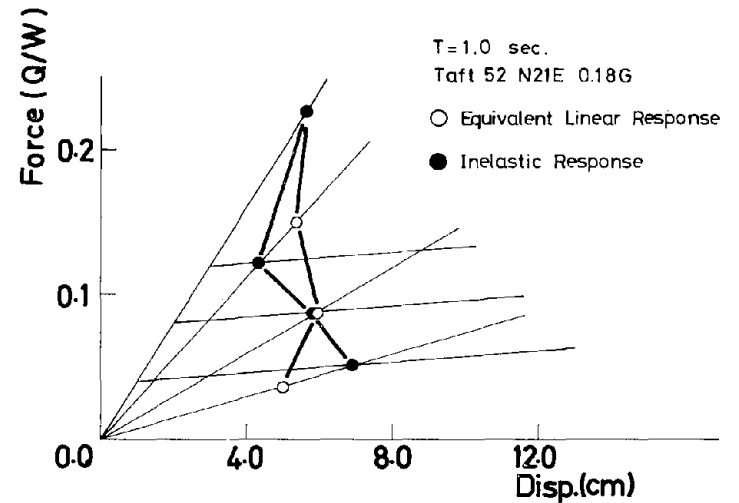
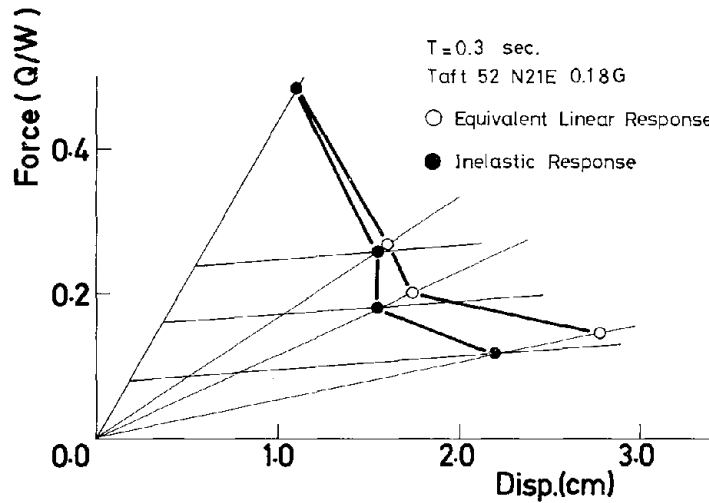
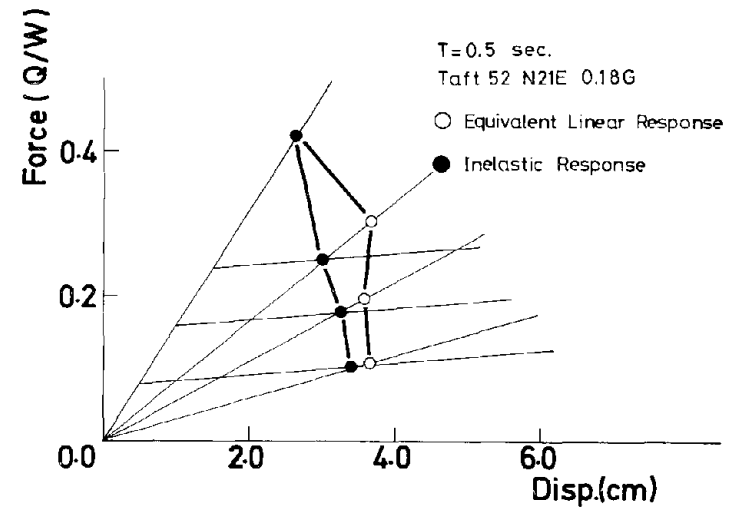
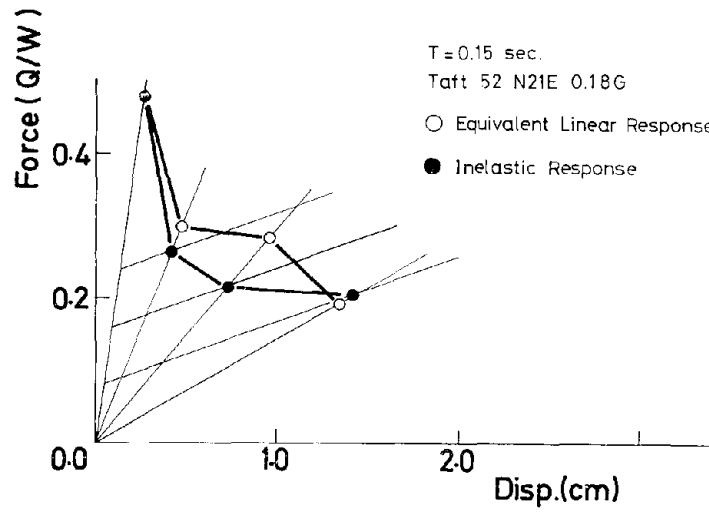


Fig. 4 Relation between Maximum Inelastic Displacement and Yield Force
 Taft 1952 N21E 0.18G (μ is used in Eq. 2)

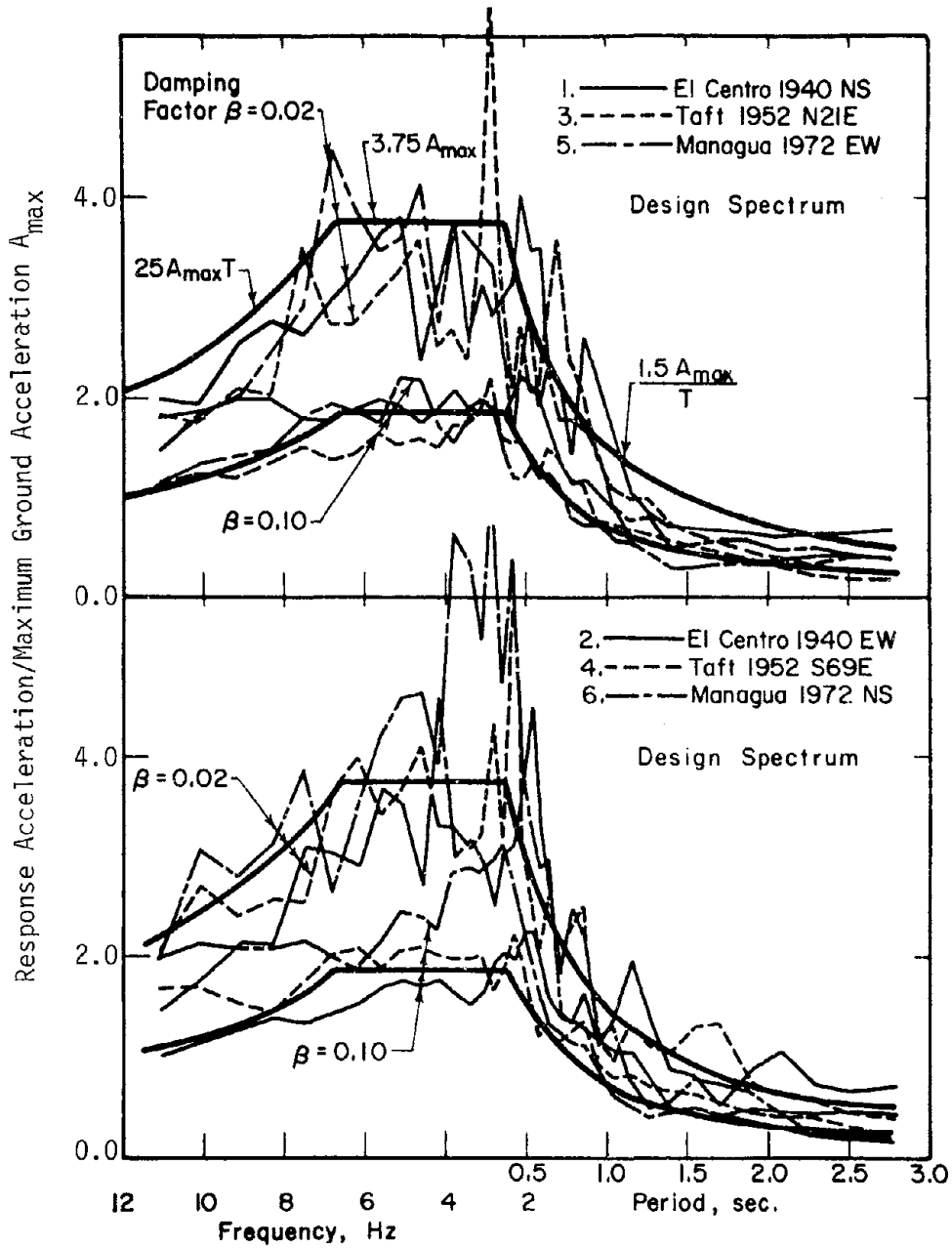


Fig. 5 Smoothed Response Spectra

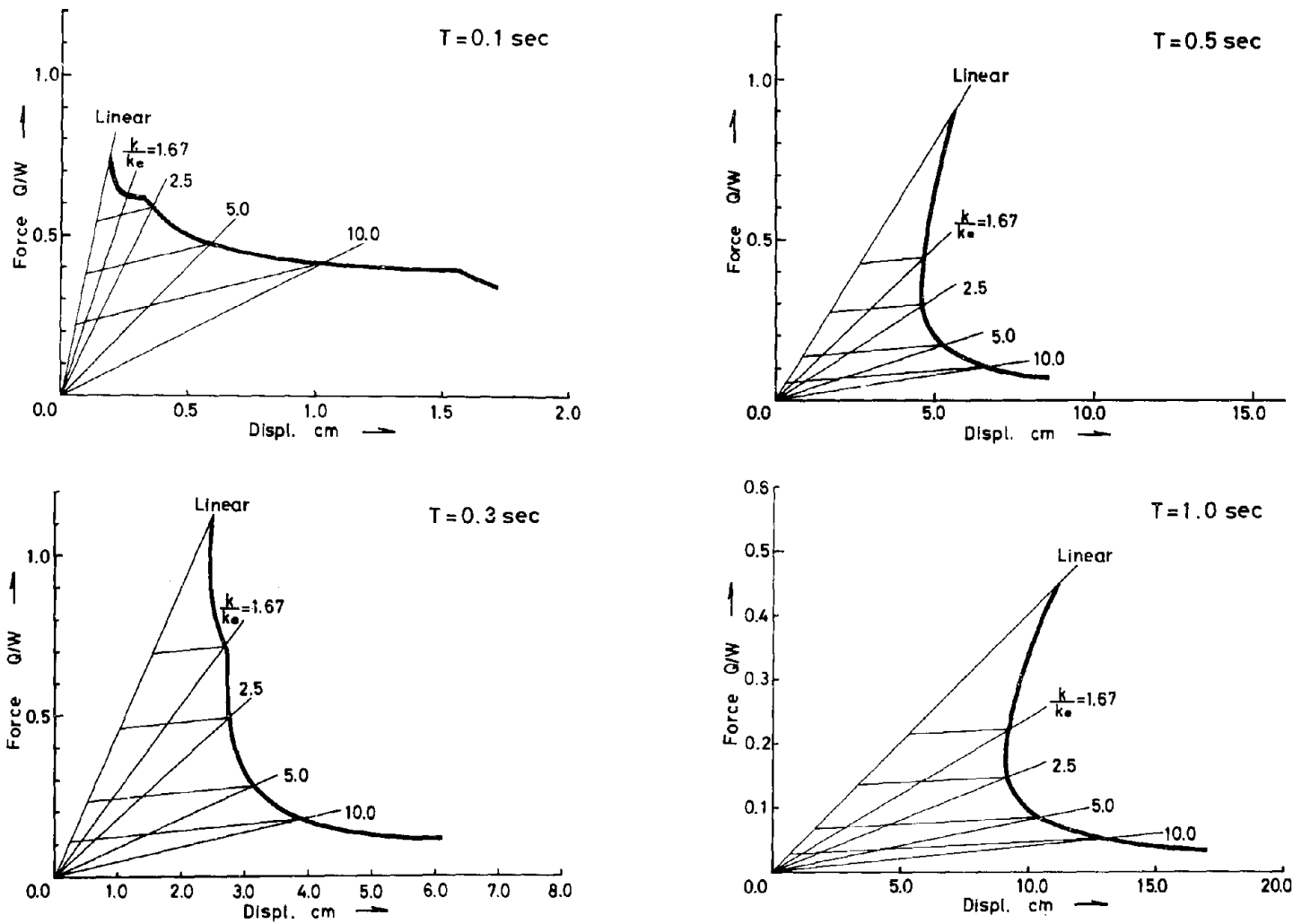


Fig. 6 Relation between Maximum Inelastic Displacement and Yield Force Calculated from Equivalent Linear Models and Smoothed Spectrum ($A_{max} = 0.3G$)

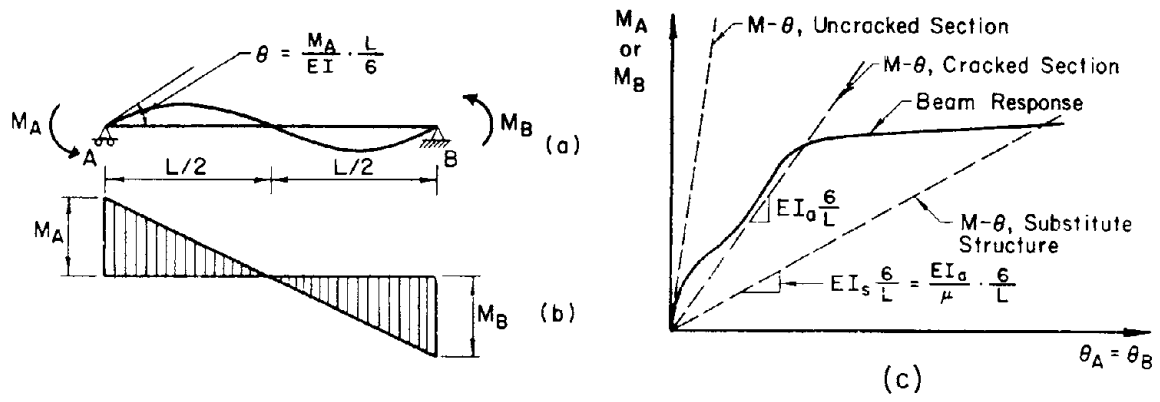


Fig. 7 Interpretation of Damage Ratio

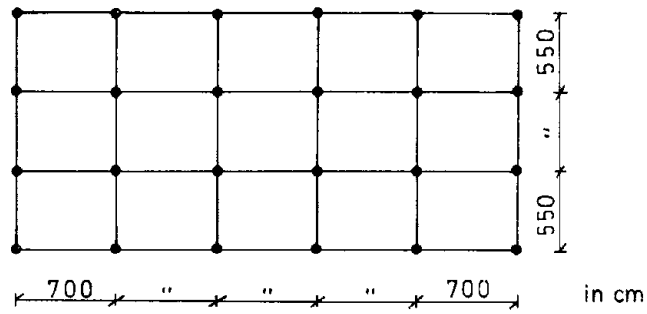


Fig. 8 Plan of the Example Building

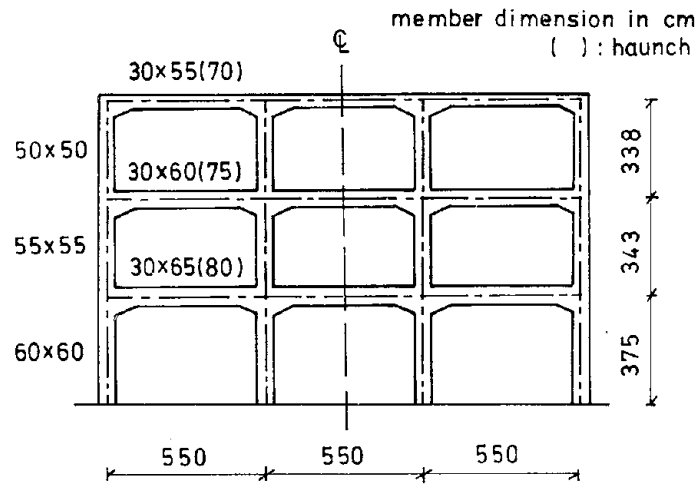


Fig. 9 Model Frame

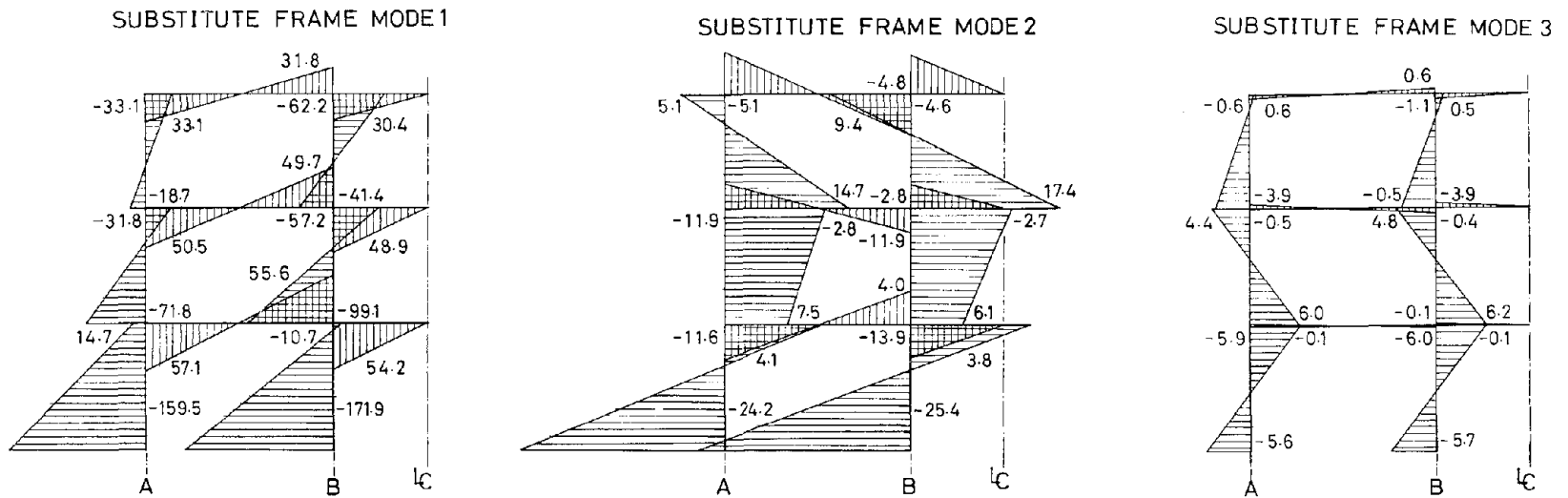


Fig. 10 Modal Moments of Substitute Frame for Spectral Acceleration of 1.0G

289

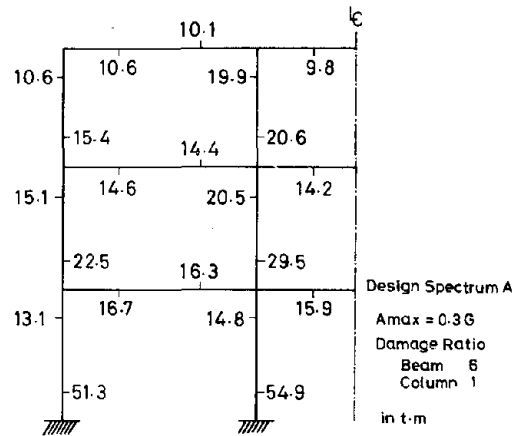


Fig. 11 Seismic Moments obtained by Substitute Structure Method

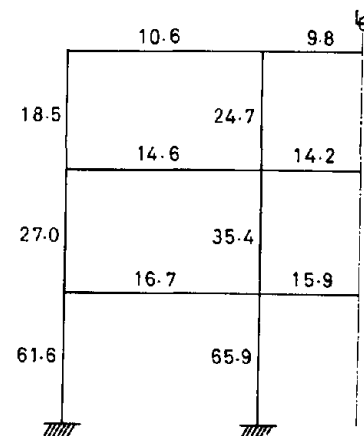


Fig. 12 The Larger of Two End Moments with Column Moments *1.2

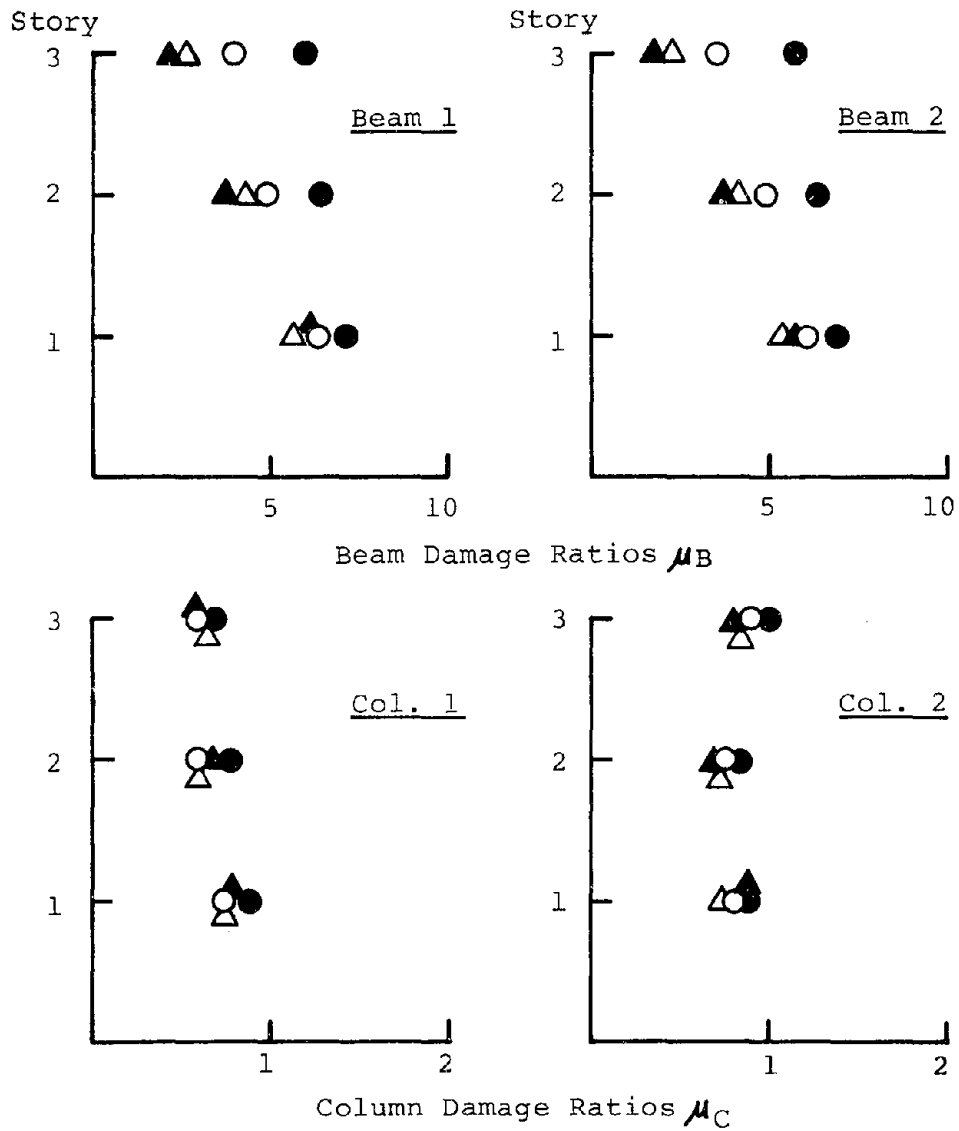
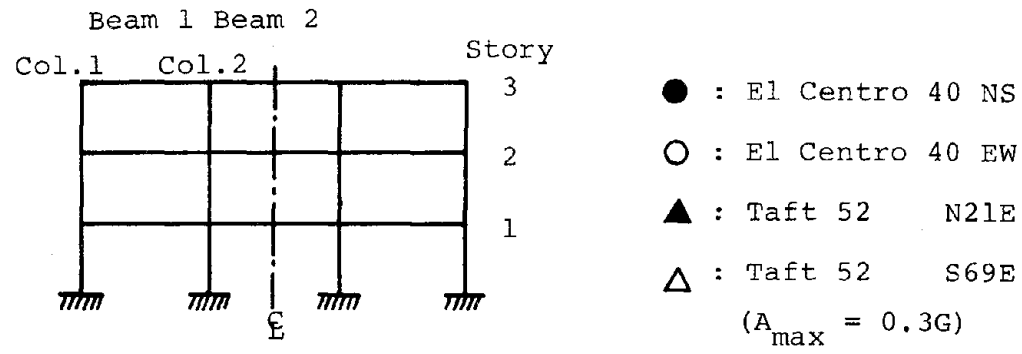


Fig. 13 Maximum Damage Ratio Response in Members

SIMPLE NONLINEAR MODELS FOR THE SEISMIC RESPONSE
OF REINFORCED CONCRETE BUILDINGS

by

Hiroyuki Aoyama¹

SYNOPSIS

Shear model, frequently used to simplify inelastic response analysis, is shown to be improper for weak girder type frames because it ignores the story interaction by the columns. A new model, called SB model, is proposed which improves the shear model by adding bending springs to represent the story interaction. A procedure is proposed to determine parameters for the SB model by which the degree of story interaction is automatically evaluated. The SB model includes shear model as a special case. It was shown that the response analysis using SB model is satisfactorily accurate for frames with wide variety of structural characteristics.

INTRODUCTION

Response analysis for earthquake motions in the inelastic range is needed in order to evaluate the seismic safety of low-rise reinforced concrete buildings. Such necessity arises in various instances. When a building suffers a structural collapse or severe damage due to a destructive earthquake, analysis is usually required to demonstrate how, and possibly why, the damage has progressed. In this case the complication in the method of analysis is no problem; it is required that the analysis must reflect all the available knowledge pertinent to the dynamic behavior of the structure. On the other hand, seismic safety of existing buildings are sometimes questioned. Seismic safety of projected buildings may also be investigated as a part of structural design. In such instances, simpler methods of analysis are usually preferred as long as the simplification does not impair the essential feature of the dynamic response.

A number of methods are available for the purpose of inelastic response analysis, although they differ in the basic approach to idealize the hysteretic behavior and in the degree of sophistication in the formulation and solution techniques. A method developed at the University of Tokyo^{1),2),3)} is one of the most generalized method to analyze a planar frame based on the

1. Assoc. Prof., Dept. of Architecture, Univ. of Tokyo

inelastic property of members. The basic feature of this method is empirical in the sense that most of the inelastic characteristics of members are evaluated by a set of empirical equations, but the mathematical treatment is quite general and rigorous.

This method, hereafter called the "rigorous analysis," has been successfully applied to several building frames, and the mechanical characteristics of typical frames were studied. Following conclusions may be derived from these analytical studies.^{2),3)}

(1) Actual building frames have wide variety in the mode of mechanism. Typical frames with ordinary floor girders would fail in the girder-hinge collapse mechanism as in Fig. 1 (a), while exterior frames with deep spandrel girders would fail in the column-hinge collapse mechanism as in Fig. 1 (b). However, there are many frames which fail in the mixture of above two modes as in Fig. 1 (c). In many instances, moreover, modes of mechanism under static loading and dynamic excitation are different, and it would vary according to the distribution of lateral forces or types of excitation.

(2) Rigorous analysis requires enormous amount of computer memory and time. For the purpose of earthquake resistant design or evaluation of earthquake resistance of existing buildings, it is desirable to have some simplified method of analysis.

SHEAR MODEL

For the purpose of simplified response analysis, the so-called shear model (Fig. 2) has been used most frequently. In fact for the practical design of frame buildings, shear model is almost exclusively used when the inelastic response analysis is required. A shear model of the building has number of freedom equal to the number of stories. This visual similarity makes the determination of parameters for shear model relatively easy. In addition, shear model reduces the computational effort tremendously.

General trend of the hysteretic behavior of reinforced concrete frames failing in flexure of members can be idealized by the degrading trilinear model.⁴⁾ In case of shear model made out of reinforced concrete frame (Fig. 3), four parameters should be determined in each story: elastic stiffness, cracking story shear, yield story shear, and one parameter to determine the yield point (slope after cracking, yield point secant stiffness, or yield displacement). There are several alternative methods to determine these parameters.^{2),3)}

The first method, hereinafter called shear model-1, was developed mainly for hand calculation. The elastic story stiffness is determined by the D-method.^{5),6)} The cracking story shear is determined as the average of story shears at which each of the critical sections relevant to that story (top and bottom of the columns and girder ends connecting into the top and bottoms of the columns) reaches cracking moment according to the elastic analysis. The yield story shear is evaluated from the column top and bottom moments at which either columns or girders produce yield hinges: that is, for weak-column type frames, the yield moment of column is taken at both ends

of the column, and for weak-girder type frames, the sum of yield moments of girders are transferred to column ends according to the elastic stiffnesses of columns above and below. The yield point is determined by specifying the secant yield stiffness of the story, which is determined by the D-method using reduced stiffness prescribed by the distribution of moment at the yielding.

The second method, hereinafter called shear model-2, was developed chiefly to overcome the deficiency of the shear model-1 of the inappropriate evaluation of yield story shear for weak-girder type frames. The evaluation of elastic story stiffness is same as the shear model-1. The cracking and yield story shear is calculated by the limit analysis technique, using cracking and yield moment at each critical section, respectively, for a specified distribution of lateral loads (in most cases, invented triangular distribution). The yield point is determined by specifying the tangent stiffness after cracking, calculated by the D-method using tangent stiffnesses of the members after cracking (elastic stiffness for members not reaching to cracking stage at the yielding of the frame).

There are third and fourth methods available which employs static inelastic frame analysis based on the inelastic member properties. This, however, requires extensive computer analysis just in order to establish a shear model, and as such, somewhat contradictory for the purpose of simplification. These methods were investigated in order to see if the sophistication in the modeling technique would improve the behavior of shear models.

Shear models thus established were excited by the same earthquake motions as used in the rigorous analysis. Comparison of the results led to the following conclusions.

(1) The accuracy of the shear model is not improved by the sophistication in the modeling technique.

(2) Shear models give acceptable response results if the prototype frame is of weak-column type. On the other hand, shear models made out of prototype frame of weak-girder type may lead to significantly different result. Typically, a story in the shear model with weaker yield strength will produce much larger response displacement than obtained from the rigorous analysis.

These conclusions clearly pointed out that shear models, although frequently used in the practice, are appropriate simplification only if the prototype structure is weak-column type. For actual building frames having so much wide variety in the mode of mechanism, a new method is necessary which would incorporate interaction between stories for a frame of weak-girder type. For this purpose, a model shown in Fig. 4 was invented.

It is a model of a frame structure consisting of conventional shear springs connecting masses, and in addition, springs representing story interaction of adjacent stories (to be called bending springs) are inserted. Considering that the parameters for shear models are determined assuming, implicitly, that frame deforms into a uniform story displacement, bending springs are intended to represent additional stiffness and strength of the frame when it undergoes a deformation different from the uniform deformation.

Since the model has both shear and bending springs, it will be called SB model hereafter.

SIMPLIFIED MODEL CONSIDERING STORY INTERACTION (SB MODEL)

Fig. 5 shows an n-story SB model having n-masses (m_1 to m_n), n-shear spring (K_{S1} to K_{Sn}), and (n-1) bending springs (K_{B1} to K_{Bn-1}). Bending spring K_{Bi} is supported by a massless bar of length l_i (arbitrary length) at a point dividing the bar to the lengths $a_i l_i$ and $b_i l_i$ where $a_i + b_i = 1$. It is postulated that bending springs should not carry any force, hence the model should reduce to a shear model, under the specified mode of deformation. This mode is called the standard mode, and may be taken as the elastic fundamental mode of vibration, or simply the inverted triangular mode. This condition is achieved by determining the ratios a_i and b_i as

$$a_i/b_i = u_{i+1}/u_i \quad (i=1 \sim n-1) \quad (1)$$

where u_i is the story displacement of i-th story under the standard mode.

The story shear in i-th story Q_i may be expressed by the forces in shear spring Q_{Si} and bending spring Q_{Bi} as follows,

$$\begin{aligned} Q_1 &= Q_{S1} + b_1 Q_{B1} \\ Q_i &= Q_{Si} - a_{i-1} Q_{Bi-1} + b_i Q_{Bi} \quad (i=2 \sim n-1) \\ Q_n &= Q_{Sn} - a_{n-1} Q_{Bn-1} \end{aligned} \quad (2)$$

where Q_{Si} is taken positive for clockwise shear force in the shear spring, and Q_{Bi} is taken positive if the bending spring is given a force directing to the right from the mass.

The story displacement in the i-th story δ_i and the deformations of shear spring δ_{Si} and bending spring δ_{Bi} are related as follows.

$$\begin{aligned} \delta_{Si} &= \delta_i \quad (i=1 \sim n) \\ \delta_{Bi} &= b_i \delta_i - a_i \delta_{i+1} \quad (i=1 \sim n-1) \end{aligned} \quad (3)$$

Where δ_{Si} is taken positive for clockwise story deformation, and δ_{Bi} is taken positive if the displacement of the mass relative to the bar is directing to the right.

The story shear vs. story displacement of the model is expressed as follows.

$$\begin{Bmatrix} Q_1 \\ Q_2 \\ \dots \\ \dots \\ Q_{n-1} \\ Q_n \end{Bmatrix} = \begin{bmatrix} K_{S1} + b_1^2 K_{B1}, & -a_1 b_1 K_{B1} & & & & \\ -a_1 b_1 K_{B1}, & K_{S2} + a_1^2 K_{B1} + b_2^2 K_{B2}, & -a_2 b_2 K_{B2} & & & \\ \dots & \dots & \dots & \dots & \dots & \\ \dots & \dots & \dots & \dots & \dots & \\ -a_{n-2} b_{n-2} K_{Bn-2}, & K_{Sn-1} + a_{n-2}^2 K_{Bn-2} + b_{n-1}^2 K_{Bn-1}, & -a_{n-1} b_{n-1} K_{Bn-1} & & & \\ & -a_{n-1} b_{n-1} K_{Bn-1}, & K_{Sn} + a_{n-1}^2 K_{Bn-1} & & & \end{bmatrix} \begin{Bmatrix} \delta_1 \\ \delta_2 \\ \dots \\ \dots \\ \delta_{n-1} \\ \delta_n \end{Bmatrix} \quad (4)$$

In case of inelastic analysis, eq. (4) holds for the increments. As seen in eq. (4), the stiffness matrix of SB model is tri-diagonal, as compared to a diagonal matrix of shear model. If δ_i in eq. (4) is proportional to the standard mode u_i , one can easily see that K_B terms in eq. (4) cancel out, leaving only the diagonal matrix of K_{Si} . This means that the SB model reduces to shear model if the mode of deformation matches the standard mode. Bending springs act only when the mode of deformation deviates from the standard mode.

PHYSICAL MEANING OF BENDING SPRING

(a) Stiffness of Bending Spring

Unless girders are infinitely strong, story shear of a frame depends not only on the relative displacement of that story but also on the relative displacement of adjacent stories. Typically, take an infinite uniform frame as shown in Fig. 6 (a) where k_c and k_g are stiffness ratios of column and girder, respectively.

$$k_c = \frac{I_c}{hK_0}, \quad k_g = \frac{I_g}{lK_0} \quad (5)$$

The corresponding SB model is also uniform as shown in Fig. 6 (b), in which $K_{Si} = K_S$, $K_{Bi} = K_B$, $h_i = h$, $l_i = 2h$, $a_i = b_i = 0.5$.

Suppose that both the prototype frame and the model deforms with a uniform story displacement angle R as in Fig. 6 (c), which is the standard mode in this case. The column stiffness of the prototype frame may be written as follows.

$$\frac{Q}{\delta} = \frac{1}{\frac{1}{k_c} + \frac{1}{k_g}} \left[\frac{12EK_0}{h^2} \right] = ak_c \left[\frac{12EK_0}{h^2} \right] \quad (6)$$

Where $a = \frac{\bar{k}}{2+\bar{k}}$, $\bar{k} = \frac{\sum k_g}{2k_c}$ (D method notation).^{5),6)} The bending springs of SB model does not carry force under the standard mode. Hence the sum of column stiffness of the prototype frame gives the stiffness of shear spring.

$$K_S = \sum \frac{Q}{\delta} = \sum ak_c \left[\frac{12EK_0}{h^2} \right] \quad (7)$$

Then, suppose that both the prototype frame and the model deforms with an alternate story displacement angle R as in Fig. 6 (d). Because of symmetry the rotation at girder ends must be zero. Hence no bending moments will be induced in the girders, and the column stiffness is expressed as follows.

$$\frac{Q}{\delta} = k_c \left[\frac{12EK_0}{h^2} \right] \quad (8)$$

The SB model under this deformation configuration carries the story shear by both shear and bending springs, and the story stiffness is given, from eq. (4), by $K_S + K_B$. Hence we obtain

$$K_S + K_B = \Sigma k_c \left[\frac{12EK_0}{h^2} \right] \quad (9)$$

and

$$K_B = \Sigma (1-a) k_c \left[\frac{12EK_0}{h^2} \right] \quad (10)$$

Thus we see that the stiffness of the bending spring represents the increase of story stiffness as the deformation configuration changes from the uniform mode as assumed in the D-method to another mode where the joints do not rotate. In other words it compensates for the loss of story stiffness due to girder flexibility under the uniform mode.

(b) Strength of Bending Spring

Let us assume that column yield moment M_{cy} and girder yield moment M_{gy} are uniform throughout the frame, and the frame forms a girder-hinge collapse mechanism as shown in Fig. 6 (e) under a uniform mode ($M_{cy} > M_{gy}$). Then the column shear at the formation of collapse mechanism can be expressed as

$$Q_y = 2M_{gy}/h \quad (11)$$

The bending spring of SB model does not carry force under this mode. Hence the strength of shear spring of SB model is expressed by the sum of column shear in eq. (11).

$$Q_{SY} = \Sigma 2M_{gy}/h \quad (12)$$

On the other hand, under the alternate mode as shown in Fig. 6 (f), girders of prototype frame do not carry moments, and the frame inevitably forms a column-hinge collapse mechanism. The column shear at collapse is

$$Q_y = 2M_{cy}/h \quad (13)$$

The SB model under this mode carries the story shear by both shear and bending springs, and when both springs yield, the story shear is given from eq. (2) by $Q_{SY} + Q_{BY}$. Hence we obtain

$$Q_{SY} + Q_{BY} = \Sigma 2M_{cy}/h \quad (14)$$

and

$$Q_{BY} = \Sigma 2(M_{cy} - M_{gy})/h \quad (15)$$

Thus we see that the strength of the bending spring represents the increase of story shear as the deformation configuration changes from the one corresponding to girder-hinge mechanism to another one corresponding to column-hinge mechanism. In other words it represents the reserve strength of strong columns in the weak-girder type frames.

For a frame which forms a column-hinge collapse mechanism even in case of uniform mode, that is, for a weak-column frame, above consideration will lead to equal shear in eqs. (12) and (14), and Q_{BY} equals to zero. Such a frame does not have any reserve strength to be represented by bending spring.

(c) Hysteresis of Bending Spring

The force-deformation relation of bending spring may be obtained quite similarly to above. Calculate story shear vs. story displacement relations for both uniform mode and alternate mode, and subtract the story shear of the former from the latter. Fig. 7 shows a very simple example of above operation using uniform frame as appeared in Fig. 6.

Fig. 7 (a) and (b) shows assumed force-deformation relation of girder and column in terms of story shear and story displacement. For the uniform mode, Fig. 7 (c) is obtained by adding the deformation axis of Fig. 7 (a) and (b), which gives the force carried by the shear spring. For the alternate mode, Fig. 7 (d), identical in the primary curve to Fig. 7 (b), gives the sum of forces carried by both springs. When the force in Fig. 7 (c) is subtracted from Fig. 7 (d), we obtain Fig. 7 (e), which is the force carried by the bending spring.

As seen in Fig. 7 (e), the force-deformation relation of bending spring is rather complicated. Because of the smaller yield displacement in Fig. 7 (d) as compared to that in Fig. 7 (c), it shows maximum and negative slope before reaching yield point mentioned in the previous section. Fig. 8 shows another example of hysteresis of bending spring computed for actual frame by the same method as mentioned above. Although it is only for primary loading, it shows the same trend.

The behavior of bending spring is thus not so simple, but for all practical purposes, it would be sufficient to idealize it into an elasto-plastic hysteresis defined by the stiffness of eq. (10) and strength of eq. (15). The so-called shear model fails to represent the story interaction in the inelastic range of beam failure type frame. Hence it would be most pertinent for the SB model to represent the reserve strength expressed by eq. (15). This consideration led to the adoption of the abovementioned elasto-plastic hysteresis. Accordingly, a column failure type frame is idealized into a shear model without having bending spring at all, even in the elastic range.

PROCEDURE TO DETERMINE PARAMETERS FOR SB MODEL

Following is a procedure recommended for establishing an SB model mainly by hand calculations.

(i) The elastic stiffness of shear springs K_{Si} are determined by D-method,⁶⁾ considering, where necessary, the effect of rigid zones at the connections and shear deformation of members.

(ii) The inelastic parameters of shear springs, that is, cracking shear force Q_{SCi} , yield shear force Q_{SYi} , yield displacement δ_{SYi} , are determined according either to the shear model-1 or shear model-2, as mentioned before. Shear springs follow degrading trilinear hysteresis rule.

(iii) Take the inverted triangular mode as the standard mode, and determine the span ratio of massless bars for bending spring, a_i , b_i from eq. (1). u_i in eq. (1) can now be taken as the story height of i -th story.

(iv) To determine the elastic stiffness of bending springs K_{Bi} , following procedure is taken. For intermediate stories, obtain the difference of stiffness as determined from eq. (9) and K_{Si} from (i) above, and denote them by ΔK_i ($i=2\sim n-1$). For the top story, or the bottom story of frames with footing beams, the stiffness corresponding to eq. (9) is determined from the D-method equation for one story frame with fixed base shown in Fig. 9, and the difference to the stiffness from (i) above is denoted as ΔK_n or ΔK_1 . Assuming that these ΔK_i correspond to the difference between standard mode and alternate mode where the sign of story displacement in the standard mode changes alternately (strictly speaking some joint rotation will be induced in the above-mentioned alternate mode which is neglected here), substitute

$$\delta_{i+1} = -(b_i/a_i)\delta_i \quad (i=1\sim n-1) \quad (16)$$

into eq. (4), and we obtain

$$\begin{aligned} 2b_1^2 K_{B1} &= \Delta K_1 \\ 2a_{i-1}^2 K_{Bi-1} + 2b_i^2 K_{Bi} &= \Delta K_i \quad (i=2\sim n-1) \\ 2a_{n-1}^2 K_{Bn-1} &= \Delta K_n \end{aligned} \quad (17)$$

from which K_{Bi} are determined by the least square method.

(v) To determine the yield strength of bending springs Q_{BYi} , following procedure is taken. For intermediate stories, obtain the difference of yield shear force as determined from eq. (14) and Q_{SYi} from (ii) above, and denote them by ΔQ_i ($i=2\sim n-1$). For the top story, or the bottom story of frames with footing beams, the yield shear force corresponding to eq. (14) is determined as the single story frame with fixed base shown in Fig. 10, and the difference to the yield shear force from (ii) above is denoted as ΔQ_n or ΔQ_1 . Assuming that these ΔQ_i correspond to the difference between standard and alternate modes, we obtain from eq. (2),

$$\begin{aligned} b_1 Q_{BY1} &= \Delta Q_1 \\ a_{i-1} Q_{BYi-1} + b_i Q_{BYi} &= \Delta Q_i \quad (i=2\sim n-1) \\ a_{n-1} Q_{BYn-1} &= \Delta Q_n \end{aligned} \quad (18)$$

from which Q_{BYi} are determined by the least square method. When a non-positive value of Q_{BYi} is obtained for a story, let $K_{Bi} = Q_{BYi} = 0$ for that story. Bending springs follow elasto-plastic hysteresis rule.

EXAMPLE OF NUMERICAL ANALYSIS

For the purpose of demonstrating the validity and limitation of the proposed SB model, three examples will be shown here. These are the analysis of three-story reinforced concrete buildings with shear walls, which are the structural design examples contained in the Commentary to the Architectural Institute of Japan Structural Standards. The first case is the longitudinal direction of the design example No.1 (hereinafter called No.1-L), the second, the transverse direction of the same building (No.1-T), and the third, the longitudinal direction of the design example No.2 (No.2-L). For these building frames, the rigorous and shear model analyses have

been reported.³⁾ Fig. 11 shows the floor plan (common to examples 1 and 2). Fig. 12 and 13 show the frame elevation in the longitudinal direction of each example building. The frame elevation in the transverse direction of both buildings is similar to Fig. 12.

The failure modes of these buildings are as follows. No.1-L fails under girder-hinge type mode in the first and second story and column-hinge type in the top story. But the story interaction between the first and second stories is not so significant. No.1-T fails under girder-hinge type mode in all three stories, and the story interaction is quite large. No.2-L consists of two parallel frames, one of which, the exterior frame, is column-hinge type because of heavy wall girders, and the other, similar to the frame in No.1-L. The story interaction is least in this case.

Table 1 summarizes the parameters for simplified models, and elastic periods of vibration including those by rigorous analysis. Two shear models (shear model-1 and -2 explained above), and two SB models (SB-1 and -2 corresponding to two shear models) were analyzed for each of three cases. Four parameters describing the shear spring characteristics in Table 1, K_S , Q_{SC} , Q_{SY} , and δ_{SY} , dictate also the parameters of shear models. With two parameters for bending spring, K_B and Q_{BY} , the SB models are completely described. In order to determine these parameters for bending spring, inverted triangular mode was used as the standard mode. Other modes, such as rigorous fundamental mode or shear model fundamental mode, were also used for some cases but the result did not show any significant difference. Moreover, in some cases the hysteresis of bending spring was assumed to be degrading trilinear, but the resulted model showed quite similar response. Hence these are not included in this paper.

Looking at Table 1, it is noticed that the yield forces of shear spring, Q_{SY} , in shear model-1 and -2 differ in a consistent way. Q_{SY} in the top and bottom stories are greater, and Q_{SY} in the intermediate story is smaller, in the shear model-1. The trend is most pronounced in case of No.1-T, which fails in girder-hinge type mode, and least in case of No.2-L, which is almost a weak-column type frame. These differences make the yield forces of bending spring, Q_{BY} , different between SB-1 and SB-2 models, but in general, values of Q_{BY} are large in case of No.1-T and small in case of No.2-L.

Fundamental periods of shear models in Table 1 are longer than those by rigorous analysis, because of the error involved in the determination of elastic shear stiffness, K_S , by D-method. Higher mode periods of shear models are even longer, as commonly experienced by the use of shear models. As to SB models, the fundamental period is almost same as that for shear models. But the accuracy of higher mode periods is greatly improved.

The simplified models were subjected to various earthquake excitations for which the rigorous analysis have already been made. Shown below is one case where NS component of Hachinohe Harbor record, Tokachioki Earthquake, 1968, expanded to maximum acceleration of 500 gal. Dynamic response analysis was executed by Newmark's β -method with internal damping having retardation time of 0.005 sec.

Table 2 and Fig. 14 show the maximum response story displacements. For No.1-L building, shear models evaluate the first story displacement much

greater than the rigorous analysis, while the third story displacement much smaller. SB models evaluate the response closer to the rigorous model. Because of the inaccurate evaluation of fundamental period in the simplified models (due to the use of D-method), response of simplified models are generally greater than the rigorous analysis.

Response of No.1-T building is interesting. Shear model-1 responds in the second story much greater than the rigorous model, while shear model-2 responds greater in the first story. Thus the response of shear model is quite unstable depending on a slight variation in the determination of yield story shear. SB models evaluate reasonably close response to rigorous analysis in both cases. Simplified models generally produce greater response because of the inaccurate fundamental period as in No.1-L.

Response of No.2-L was, as expected, satisfactorily approximated by the shear models, and SB models also produce similar results. It can be seen, hence, that SB models, evaluated according to the procedure in this paper, show satisfactory behavior regardless of the type of prototype structure, within the limitation in the accuracy of elastic stiffness inherent to the use of D-method. It appears that shear model-2, and hence SB-2, would be a more appropriate procedure to determine shear spring parameters.

CONCLUSION

In order to overcome computational complexity of rigorous response analysis for low-rise reinforced concrete buildings in the inelastic range, the so-called shear models are frequently used for practical purposes. But it has been pointed out that the accuracy in such simplified analysis would be greatly impaired by the presence of story interaction in case the prototype frame structure fails into a girder-hinge collapse mechanism. The proposed SB model is an attempt to improve shear models in such a way that the story interaction in the inelastic range would be incorporated as needed by the characteristics of the frame. The procedure to determine model parameters is as simple as that for the shear model. It is expected that the SB model can be easily handled by those who are already familiar with shear models.

REFERENCES

1. H. Umemura, H. Aoyama and H. Takizawa, "Analysis of the Behavior of R.C. Structures During Strong Earthquakes Based on Empirical Estimation of Inelastic Restoring Force Characteristics of Members," Proc. 5-WCEE, Rome, Italy, June, 1973.
2. H. Takizawa, "Strong Motion Response Analysis of R.C. Buildings," Concrete Journal, Jap. Nat. Council on Concrete, Vol. 11, No.2, Feb. 1973.
3. H. Takizawa, "Non-linear Models for Simulating the Dynamic Damaging Process of Low-rise Reinforced Concrete Buildings During Severe Earthquakes," a paper submitted for publication in Int. Jour. of Earthquake Engrg. and Str. Dynamics.
4. Y. Fukada, "Study on the Restoring Force Characteristics of R.C. Buildings," Proc. Kanto Dist. Symp., Arch. Inst. Japan, No.40, Nov. 1969.
5. K. Muto, "Seismic Analysis of Reinforced Concrete Buildings," Proc. 1-WCEE, Berkeley, Calif., June, 1956.
6. K. Muto, "Aseismic Design Analysis of Buildings," Maruzen, Tokyo, 1974, 361 pp.

Table 1 Model Parameters

Building		No. 1-Longitudinal			No. 1-Transverse			No. 2-Longitudinal		
Story (mode for T)		1	2	3	1	2	3	1	2	3
Weight (t)		51.6	48.1	44.5	103.2	96.2	88.9	46.2	45.8	39.8
Rigorous T (sec)		0.419	0.142	0.077	0.449	0.149	0.079	0.313	0.104	0.059
SB-1	K_S (t/cm)	54.4	43.7	32.5	100.5	74.5	55.0	99.0	79.1	69.2
	Q_{SC} (t)	20.6	15.7	10.4	35.3	21.7	17.3	20.6	16.8	12.5
	Q_{SY} (t)	39.4	29.6	21.5	67.4	36.3	31.4	54.5	44.5	32.2
	δ_{SY} (cm)	2.88	3.38	2.55	2.80	2.32	2.32	2.09	2.19	1.52
	K_B (t/cm)	61.5	-		137.3	72.1		150.7	-	
	Q_{BY} (t)	12.2	-		48.3	17.1		4.3	-	
	T (sec)	0.448	0.171	0.098	0.475	0.165	0.091	0.317	0.113	0.065
(S-1)	T (sec)	0.448	0.178	0.121	0.477	0.191	0.130	0.314	0.120	0.085
SB-2	K_S (t/cm)	54.4	43.7	32.5	100.5	74.5	55.0	99.0	79.1	69.2
	Q_{SC} (t)	22.5	18.4	10.4	32.0	26.6	16.0	21.7	18.1	10.8
	Q_{SY} (t)	38.8	32.3	19.4	58.2	48.5	29.1	54.1	45.1	27.0
	δ_{SY} (cm)	4.52	3.81	3.21	3.50	3.95	3.66	2.35	2.17	1.65
	K_B (t/cm)	61.5	32.1		137.3	72.1		150.7	58.7	
	Q_{BY} (t)	9.6	0.5		49.9	11.0		0.7	6.5	
	T (sec)	0.448	0.154	0.090	0.475	0.165	0.091	0.317	0.105	0.060
(S-2)	T (sec)	0.448	0.178	0.121	0.477	0.191	0.130	0.314	0.120	0.085

Table 2 Maximum Response Story Displacement (cm)

Building	No. 1-Longitudinal			No. 2-Transverse			No. 2-Longitudinal		
Story	1	2	3	1	2	3	1	2	3
Rigorous Model	4.35	4.47	2.48	4.17	4.92	5.16	5.07	2.26	0.68
Shear Model-1	7.75	4.20	1.81	5.79	8.36	1.03	4.21	1.98	0.95
Shear Model-2	7.48	4.15	1.88	8.15	4.11	2.60	5.27	1.79	0.96
SB Model-1	6.03	5.75	2.29	5.56	5.30	4.82	3.76	2.19	0.92
SB Model-2	5.53	4.33	3.07	4.81	5.68	4.19	5.41	1.56	1.30

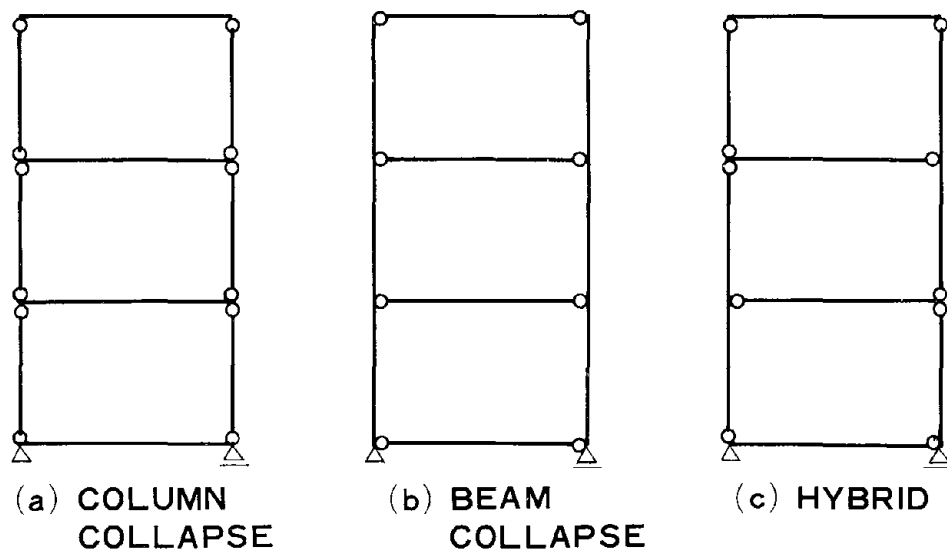


Fig. 1 Various Mode of Mechanism of Frames

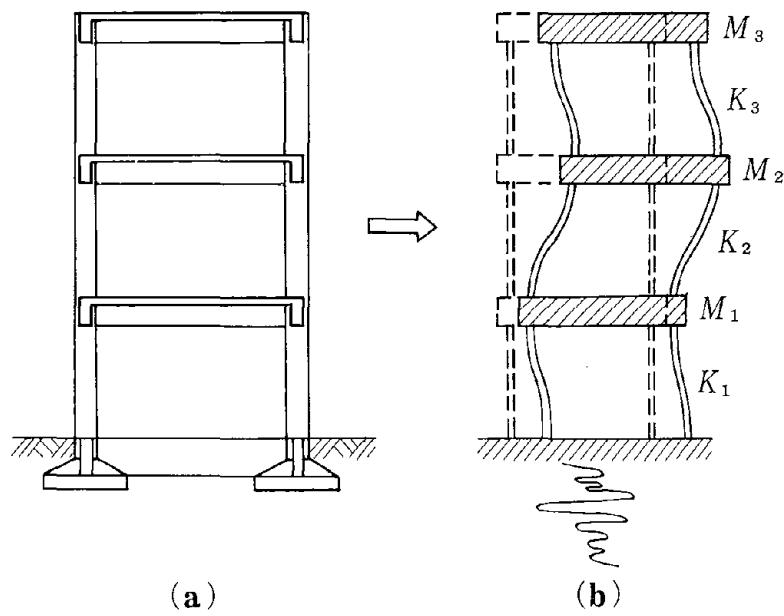


Fig. 2 Shear Model

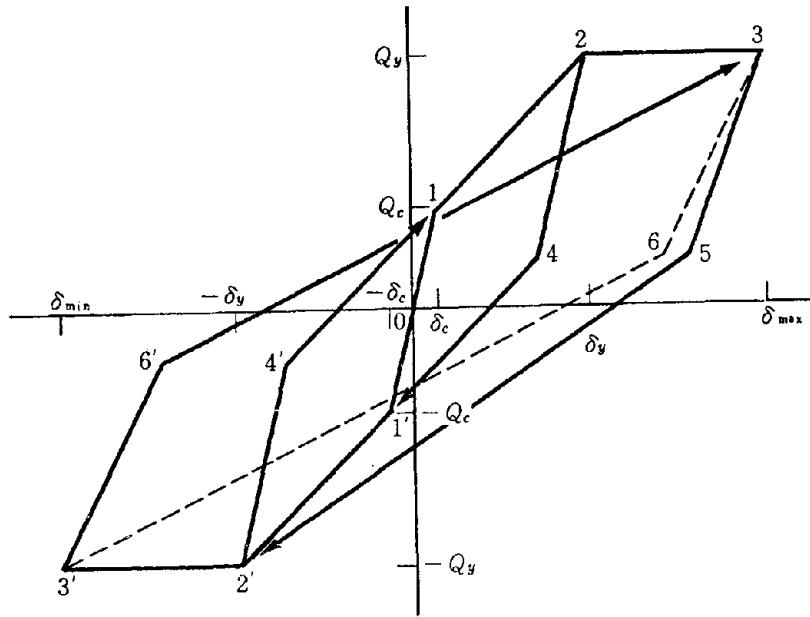


Fig. 3 Degrading Trilinear Model of Hysteresis

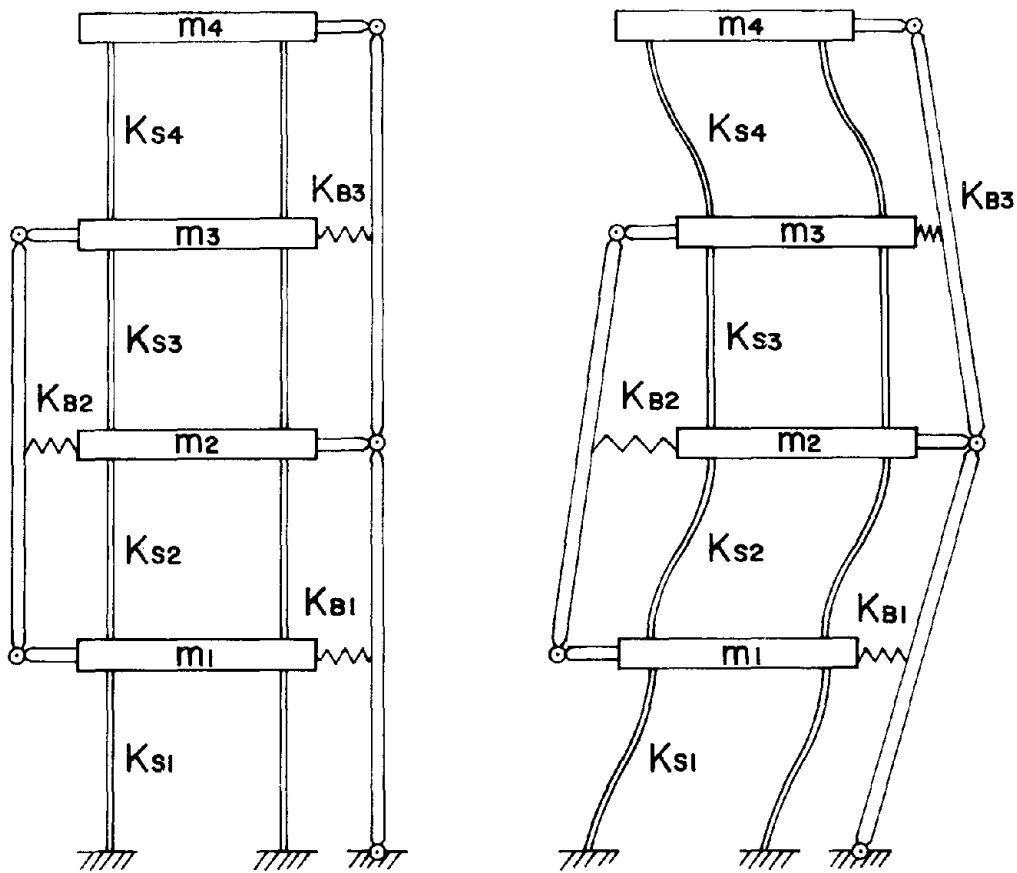


Fig. 4 A Model Considering Story Interaction

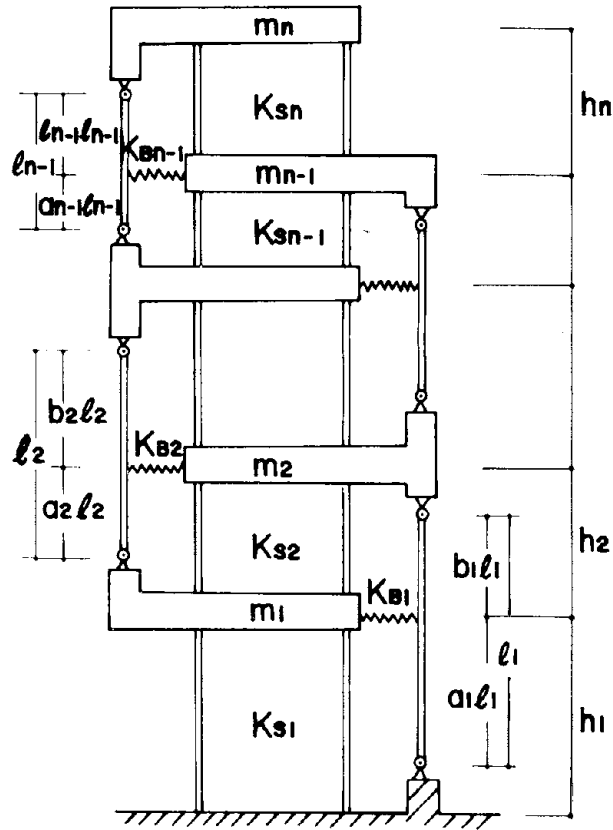


Fig. 5 SB Model

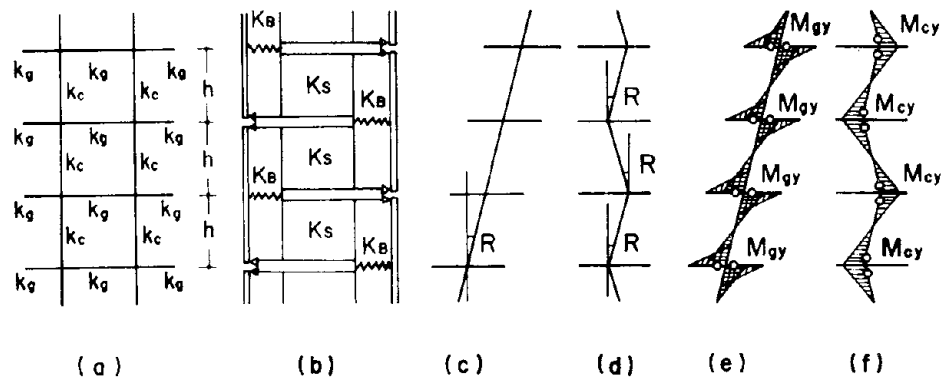


Fig. 6 Uniform Frame and Its SB Model

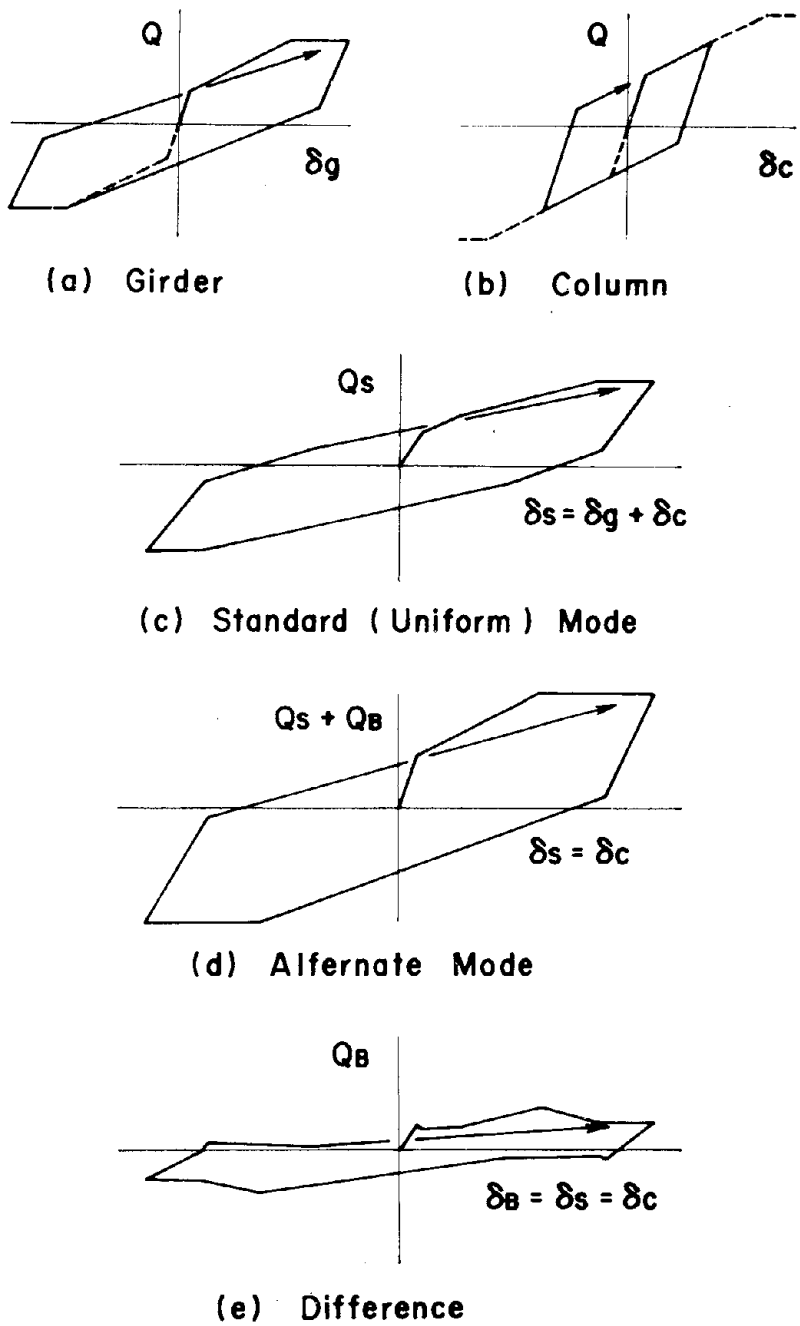


Fig. 7 Hysteresis of Shear and Bending Springs

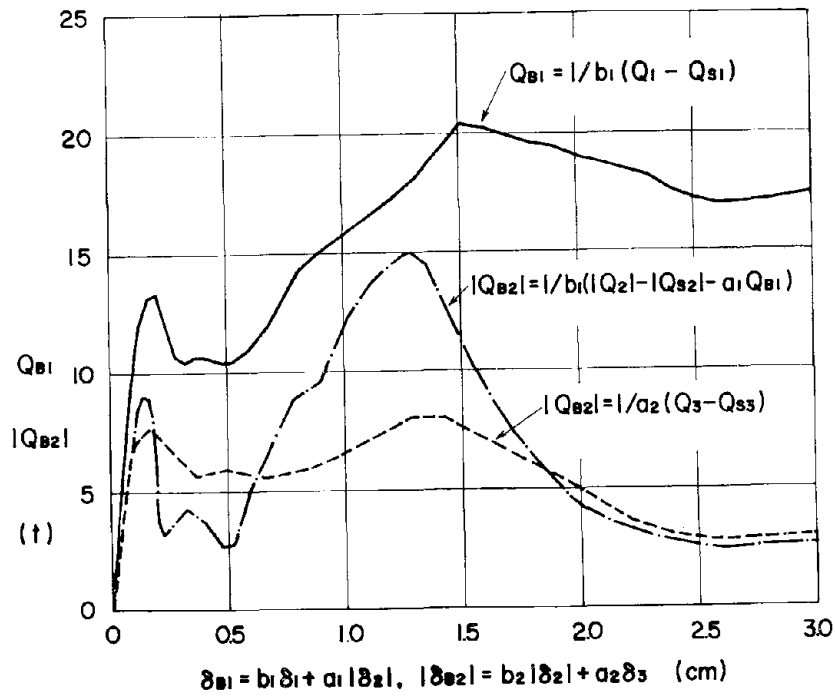


Fig. 8 Hysteresis of Bending Spring by Analysis

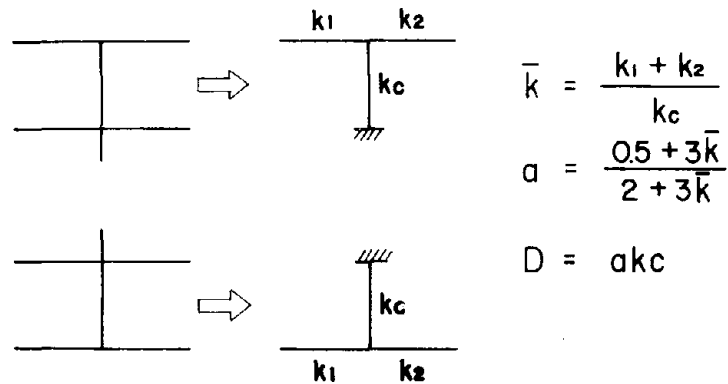


Fig. 9 Stiffness in Top and Bottom Stories

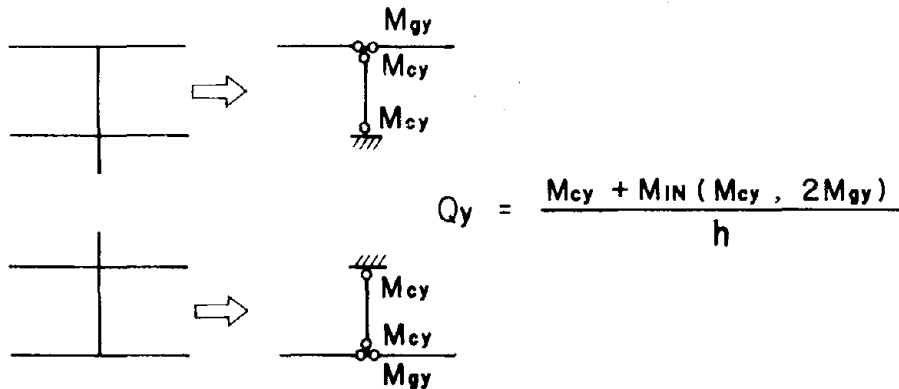


Fig. 10 Yield Shear Force in Top and Bottom Stories

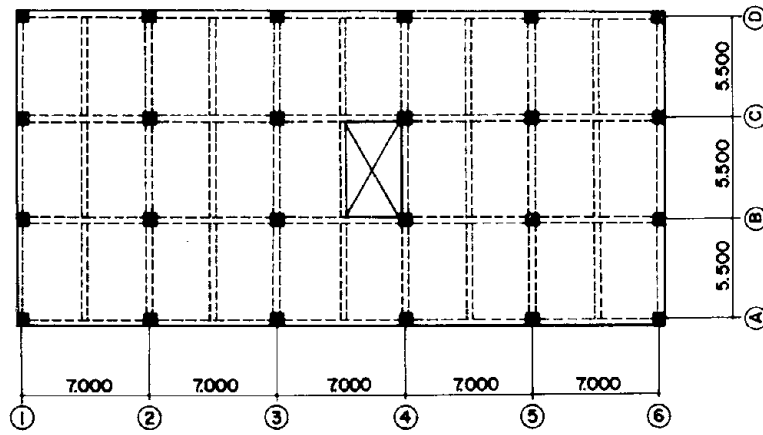


Fig. 11 Plan of the Buildings (Design Example No. 1 and No. 2)

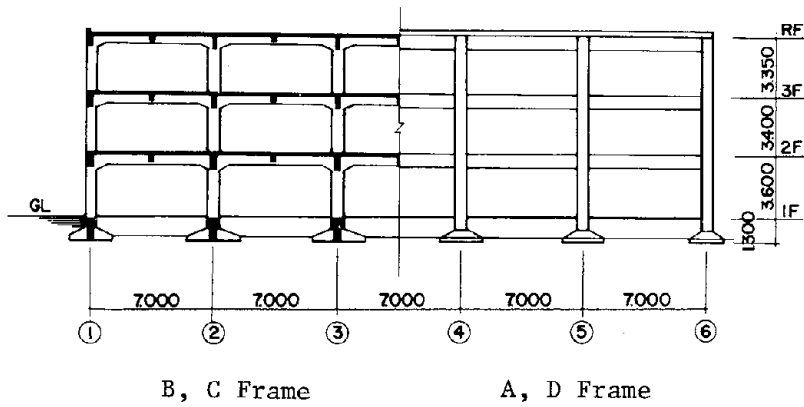


Fig. 12 Frame Elevation of Design Example No. 1

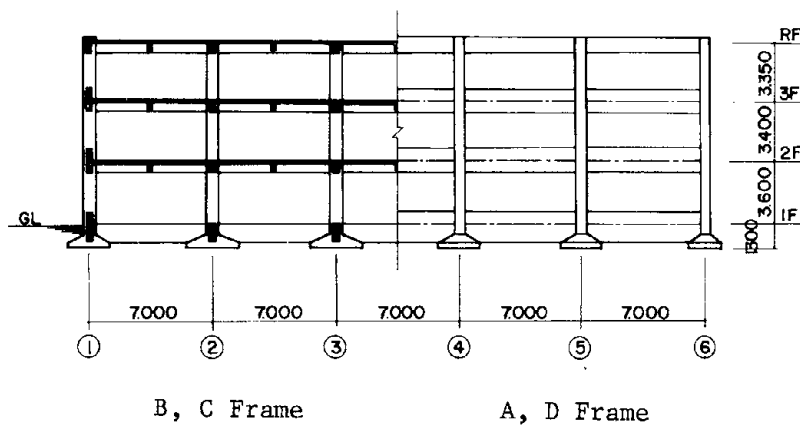


Fig. 13 Frame Elevation of Design Example No. 2

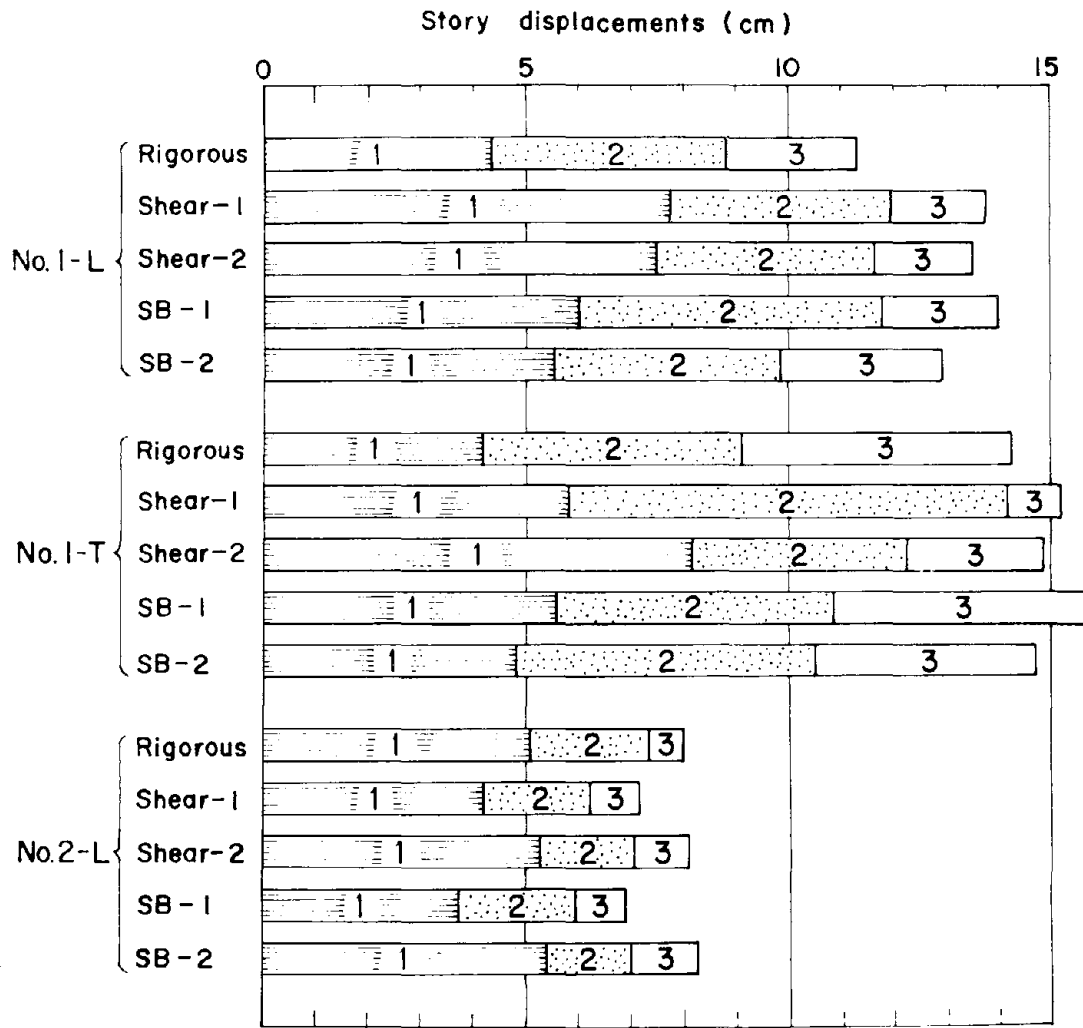


Fig. 14 Maximum Response Story Displacements

by

Takao Nishikawa⁽ⁱ⁾, Martin E. Batts⁽ⁱⁱ⁾, and Robert D. Hanson⁽ⁱⁱⁱ⁾

INTRODUCTION

Practising engineers and researchers require a more economical method of nonlinear dynamic analysis. A conventional nonlinear member by member program is costly. Some researchers have used the lumped mass pure shear beam to model the structure since it significantly reduces the number of calculations. This model has been reported (10) to be appropriate for weak column-strong girder types of structures in which yielding of the column ends occurs prior to that of the girder ends. However, for weak girder-strong column structures, this model is not always suitable due to its lack of stiffness interaction between the story levels. One method to adjust this has been given (11).

The characteristics method partially accounts for stiffness interaction but does not include the flexural behavior of the structure. The structure is treated as a continuous shear beam with distributed mass coupled in two ways with a lumped mass bending beam. The resulting hyperbolic partial differential equations for the shear beam are solved by the method of characteristics. The results of the characteristics method solution for two different structures will be compared with the results of a member by member nonlinear analysis using DRAIN-2D (5) and a special purpose computer program (2).

BASIC EQUATIONS

The basic equations of the characteristics method ((6)-(9)) for one-dimensional shear wave transmission mode as shown in Figure 1 are as follows

$$\begin{aligned} C^+ : Q_P - Q_S - \rho A v_s \cdot (V_P - V_S) + \frac{(\mu A)}{\Delta z} (V_C - V_B) &= 0 \\ C^- : Q_P - Q_R + \rho A v_s \cdot (V_P - V_R) + \frac{(\mu A)}{\Delta z} (V_A - V_C) &= 0 \end{aligned} \quad (1)$$

where the C^+ equation is for an upward traveling wave and C^- is for a downward traveling wave, Q the shear force, V = particle velocity, Δz = floor height, ρA the distributed mass per height and μA the pseudo-viscosity.

The shear wave velocity in Equation 1 v_s is defined as

(i) Assistant, Fac. of Tech., Tokyo Metropolitan University
(ii) Grad. Student, Dept. of Civil Engineering, University of Michigan
(iii) Professor of Civil Engineering, University of Michigan

$$v_s = \sqrt{\frac{GA}{\rho A} + \frac{\mu A}{\rho A \Delta t}} \quad (2)$$

in which GA = shear stiffness/unit height and Δt = time interval.

In the case of inelastic response analysis the shear force-story shear strain could be defined by the Ramberg-Osgood function

$$\gamma = \frac{Q}{G_o A} \left[1 + \left| \frac{Q}{Q_y} \right|^{R-1} \right] \quad (3)$$

for shear increasing from zero, and by

$$\gamma - \gamma_1 = \frac{Q - Q_1}{G_o A} \left[1 + \left| \frac{Q - Q_1}{2Q_y} \right|^{R-1} \right] \quad (4)$$

when unloading from (Q_1, γ_1) where Q_y represents the yield shear force and $G_o A$ is the initial stiffness.

Stability of the characteristics technique requires that $v_s \cdot \Delta t \leq \Delta z$ in each layer. This means the C^+ and C^- lines (or points R and S) lie within the space A to B, Figure 2. The shearing force and particle velocity are assumed to vary linearly within the intervals AC (C^-) and BC (C^+). The values at points R and S (needed because GA has different values during different time steps) are evaluated by linear interpolation in the intervals. The story shear stiffness is based on the average shear force in the story.

PARALLEL MODEL

In modeling the entire structure for motion in one plane two methods of coupling the shear and bending are possible. These are designated as parallel and series models using a simple spring analogy. The parallel model assumes the shear and bending lateral displacements are equal as would occur in a building with moment frames and shear wall frames connected by rigid floor diaphragms. The series model assumes the total displacement is the sum of shear and bending lateral displacement as in an individual frame. The parallel model is considered first.

The dynamic equation of motion at floor i using the notation U and L representing above and below the floor respectively, is

$$Q_i^U - Q_i^L = P_i = m_i \ddot{Y}_i + \sum_{j=1}^N K_{b_{ij}} (Y_j - Y_{N+1}) \quad (5)$$

where m_i = lumped mass at floor i , K_b = bending beam lateral stiffness, N = number of floors and Y = absolute lateral displacement (see Figure 3). Using the linear acceleration method Equation 5 becomes

$$\{P\} = \{e\} + [E]\{V\} \quad (6)$$

where (using a preceding subscript o to represent a value at the previous time step)

$$e_i = m_i \left(-\ddot{y}_o - \frac{2}{\Delta t} \dot{v}_o \right) + \sum_{j=1}^N K_{b_{ij}} \dot{y}_j + \frac{\Delta t}{2} \sum_{j=1}^N K_{b_{ij}} v_j - \sum_{j=1}^N K_{b_{ij}} \dot{y}_{N+1}$$

$$E_{ii} = \frac{\Delta t}{2} K_{b_{ii}} + \frac{2}{\Delta t} m_i \quad ; \quad E_{ij} = \frac{\Delta t}{2} K_{b_{ij}} \quad , \quad i \neq j .$$

Combining Equation 1 with the left-hand portion of Equation 5 gives

$$\{V\} = [f] - [F]\{P\} \quad (7)$$

where $f_i = \frac{1}{(\rho A v_s)_i + (\rho A v_s)_{i-1}} \left[(\rho A v_s)_{i-1} \cdot \dot{v}_{i-1} + (\rho A v_s)_i \cdot \dot{v}_{i+1} + \right.$

$$\left. \frac{\mu A}{\Delta z}_i \cdot (v_i - v_{i+1}) - \frac{\mu A}{\Delta z}_{i-1} \cdot (v_{i-1} - v_i) + Q_{i-1}^L - Q_{i+1}^U \right]$$

$$f_1 = \dot{v}_2 - \frac{Q_2^U}{(\rho A v_s)_1} + \frac{1}{(\rho A v_s)_1} \cdot \frac{\mu A}{\Delta z}_1 \cdot (v_1 - v_2)$$

and [F] is a diagonal matrix where

$$F_{ii} = \frac{1}{(\rho A v_s)_{i-1} + (\rho A v_s)_i}$$

$$F_{11} = \frac{1}{(\rho A v_s)_1} .$$

Solving Equation 6 and 7 for {V} by eliminating {P} we get

$$\{V\} = [I + [F][E]]^{-1} \left\{ \{f\} - [F]\{e\} \right\} \quad (8)$$

where the right hand side is known from the previous time step's information. The results from Equation 8 are inserted into the characteristics equation to determine Q^L and Q^U .

DETERMINATION OF STRUCTURAL PARAMETERS

The parameters are determined on the basis of the average story shear force.

Shear stiffness, GA

The shear stiffness is defined by the relation

$$Q_i \text{ avg} = (GA)_i \cdot \gamma_i, \text{ avg} \quad (9)$$

In the simple spring mass system

$$Q_i = K_i \cdot \delta_i \quad (10)$$

Where δ_i is defined as story relative displacement and is equal to

$$\delta_i = \Delta z_i \gamma_i, \text{ av} \quad (11)$$

Equation 9, 10 and 11 give the relationship between the shear stiffness and the simple shear spring stiffness to be

$$(GA)_i = K_i \cdot \Delta z_i \quad (12)$$

Viscosity

Several methods for selecting the viscosity term can be considered. The first approach attempts to equate the viscosity of the distributed mass system to the viscous damping of the conventional lumped mass system. The distributed mass could be adjusted to provide convenient Δz values. The total mass of the structure is maintained by appropriately adjusting the corresponding lumped masses.

The dynamic shear force-strain relation for the distributed mass system is

$$Q = GA\gamma + \mu A \frac{\partial \gamma}{\partial t} \approx GA\gamma + \mu A \frac{d\gamma}{dt} \quad (13)$$

when $\frac{\partial \gamma}{\partial z} \approx 0$. For the lumped mass system the corresponding relation is

$$Q = K\delta + C \frac{d\delta}{dt} \quad (14)$$

Comparing Equation 13 and 14

$$\mu A \frac{d\gamma}{dt} = C \frac{d\delta}{dt} = C \cdot \Delta z \frac{d\gamma}{dt}; \mu A = C \cdot \Delta z \quad (15)$$

Using mass and stiffness proportional damping (Rayleigh damping)

$$[C] = a_0 [m] + a_1 [K]$$

and assuming equal damping in the first two modes ($\beta_1 = \beta_2 = \beta$) and shear beam type frequency spacing ($w_2 = 3 \cdot w_1$) the fraction of critical damping can be obtained using orthogonality of modes (1). This damping can be expressed as

$$\beta_n = \frac{a_o}{2w_n} + \frac{a_1 w_n}{2} \quad \text{and in matrix form}$$

$$\begin{Bmatrix} \beta_1 \\ \beta_2 \end{Bmatrix} = \frac{1}{2} \begin{bmatrix} \frac{1}{w_1} & w_1 \\ \frac{1}{w_2} & w_2 \end{bmatrix} \begin{Bmatrix} a_o \\ a_1 \end{Bmatrix} \quad \text{Solving for the coefficients}$$

$$\begin{Bmatrix} a_o \\ a_1 \end{Bmatrix} = \frac{2w_1 w_2}{w_2^2 - w_1^2} \begin{bmatrix} w_2 - \frac{1}{w_2} \\ -w_1 \quad \frac{1}{w_1} \end{bmatrix} \begin{Bmatrix} \beta \\ \beta \end{Bmatrix} = \begin{Bmatrix} \frac{3}{2} \beta w_1 \\ \frac{1}{2} \frac{\beta}{w_1} \end{Bmatrix}$$

gives the damping matrix $[C] = \frac{3}{2} \beta w_1 [m] + \frac{\beta}{2w_1} [K]$ (16)

This value is used for the bending portion of the damping. Similarly, the damping term for the distributed mass system (shear portion) can be defined as:

$$\mu A_i = \frac{3}{2} \beta w_1 \rho_i A \Delta z_i^2 + \frac{\beta}{2w_1} G A_i \quad (17)$$

The second method for determining the viscosity is to select a value for the distributed mass ρA and adjust the viscosity according to Equation 2. Both methods were tried for the parallel model studies and no differences were seen. This is probably due to the fact that with large nonlinearities, the energy dissipated by damping is relatively ineffective.

The third method for determining viscosity, which is preferred for small nonlinearities, is to select the desired values for distributed mass and viscosity with the requirement that $\Delta z \geq v_s \Delta t$. The resulting shear wave velocity results interpolation in the $\Delta z - \Delta t$ frame similar to the condition for nonlinearities.

Mass per Height, ρA

The structure has a real distributed mass ρA in the interior and exterior walls. However, if Equation 2 is to be satisfied, then

$$\rho A = \Delta t \left(\Delta t + \frac{\mu A}{G_o A} \right) \frac{G_o A}{\Delta z} \quad (18)$$

The effect of varying the distributed mass has not been fully studied. Since the total mass of the structure must be maintained

$$\sum W + g \sum \rho A \Delta z = \text{total building weight} \quad (19)$$

in which W is the weight lumped at each floor.

Time Interval, Δt

The time interval Δt should be equal throughout the calculations and it is convenient to be the same as the input accelerogram. The characteristics method requires that

$$v_s \Delta t \leq \Delta z$$

for a stable numerical solution. The physical interpretation of this requirement is that the C^+ and C^- lines in Figure 2 lie between the space A to B. Using Equation 2 it can be seen that Δt is limited by

$$\Delta t \leq - \frac{\mu A}{2GA} + \sqrt{\left(\frac{\mu A}{2GA}\right)^2 + \frac{\rho A \Delta z^2}{GA}}$$

Structural Example and Response Results

The structure selected to illustrate the parallel model is a 6-story steel moment frame shown in Fig. 4 with sizes given in Table 1. The earthquake response of the structure was calculated by three methods: the characteristics method, the conventional lumped mass method, and a bilinear member by member method (DRAIN 2D) described in reference 5.

Because the framing was appropriate, the model was considered to be a pure shear model without the coupling effect of a bending beam. The equivalent interstory shear stiffnesses are calculated based on the assumption of primarily first mode response.

With the first mode $\{\phi^1\}$ and fundamental frequency w given, the equivalent shear stiffness is

$$K_{ei} = Q_i / \delta_i$$

where

$$Q_i = \sum_{i=1}^N (M_i \phi_i^1 w^2) \quad \text{and} \quad \delta_i = \phi_i^1 - \phi_{i-1}^1$$

are based on first mode displacements. Floor masses and equivalent shear stiffnesses are summarized in Table 2.

The earthquake accelerogram used for the response computation was a simulated earthquake motion Type A1, generated by P.C. Jennings, G.W. Housner, and N.C. Tsai (4). This earthquake was intended to simulate severe ground shaking in the vicinity of the causative fault with a peak acceleration about 0.38 g. The first 20 sec. of the record was used to compare the results to the analysis of DRAIN-2D.

In the following discussion of results, the conventional lumped mass shear model is denoted LMS, the distributed mass model (characteristics model) DMS, and the DRAIN-2D model DRA. Elastic response results for DMS and LMS with 5% critical damping showed good correlation as was expected. The time histories of the roof displacement relative to the ground are shown in Figure 5. The differences in peak values may be caused by the effects of damping on the higher modes. The intended use and the potential savings of the characteristics method though, lie in inelastic response.

For the inelastic response of LMS and DMS, the hysteretic relation between shear force and story displacement is assumed to be a Ramberg-Osgood function as described by Equations 3 and 4 with the sharpness coefficient R of 7. In the DRA analysis, an elasto-plastic relation was used. Viscous damping was taken as zero for these inelastic response studies.

The story yield shear force, Q_y , was calculated by the following simplified procedure. Each girder-column joint is judged to be weak-girder or weak-column by comparing the sum of the yield moments of the girders to that of the columns. The weak girder is transformed to a pseudo weak column by distributing the sum of the girder yield moments to the columns. Using these yield moments, the yield story shear force is obtained by summing the column yield shear forces for all columns in the story. The structure modeled here was a weak-girder type.

The maximum response of story shear forces, overturning moment, relative story displacements and floor displacements obtained in 20 seconds of the earthquake record are summarized in Fig. 6, 7, 8 and 9 respectively. Shear forces of the DMS model are the values at midheight of each story and overturning moments are based on those midheight forces. The results show good agreement except for the relative displacement of the second floor of the LMS model.

Since this is a weak-girder structure the conventional shear model (LMS) may not be accurate because the story shear force and relative story displacement have a one to one correspondence while the actual story shear is a function of girder yielding which is a function of not just one story displacement but several. In the DMS model the story shear forces are dependent upon motion of 3 adjacent stories as seen in Equation 1. This is the reason the DMS more accurately predicts the DRA results.

The time histories of the second floor displacement are shown in

Fig. 10 for the first 20 sec. of DMS and DRA and the time histories for the first 37 sec. of DMS and LMS are shown in Figures 11a and 11b. The apparent residual displacement of LMS is about 3 inches while that of DMS is about 0.5 inches. This highlights the importance of story stiffness interaction since the residual drift are expected to be nearly zero.

The computation costs of LMS and DMS were about 20% of the DRA method using one frame of a quarter of the building.

SERIES MODEL

The series model and the parallel model are different. For the series model there is only one set of forces which cause bending and shear displacement; the total displacement is the sum of these two displacements. For the parallel model there is only one set of displacements caused by independent forces on the bending and shear portions of the model; the total force is the sum of these two forces. For the series model

$$\{Y^t\} = \{y^b\} + \{Y^{sh}\} \quad (21)$$

and

$$[K^t] \{Y^t\} = [K^b] \{y^b\} = [K^{sh}] \{Y^{sh}\}, \quad (22)$$

Using the shear part stiffness force in the dynamic equation of motion yields

$$m_i \ddot{Y}_i^t + \sum_j^N C_{ij}^b \dot{y}_i^b + (Q_i^L - Q_i^U) = 0. \quad (23)$$

For both the series and parallel model there are two damping terms possible: bending related and shear related. In this paper the bending related damping C_{ij}^b are taken to be zero. In the series solution there are two displacements we are solving for. The second equation necessary for solution is of the form of Equation 22.

$$Q_i - Q_{i-1} = \sum_j^N K_{ij}^b y_j^b \quad (24)$$

where Q_i is the average shear force in story i ,

$$Q_i = \frac{Q_i^L + Q_{i+1}^U}{2}.$$

Using Equation 1 and assuming linear acceleration Equation 23 reduces to

$$(m_i \circ Y_i^t + \frac{2m_i}{\Delta t} \circ V_i^t) - \frac{2m_i}{\Delta t} V_i^t = Q_i^L - Q_i^U = (TP_i - TM_i) + (v_s \rho A_i + v_s \rho A_{i-1}) V_i^{sh}$$

or

$$\{A4\} - \frac{2}{\Delta t} [m] \{V^t\} = \{A5\} + [A6] \{V^{sh}\} \quad (25)$$

where TP_i and TM_i are information from the previous time step in Equation 1

$$TM_i = \circ Q_{i+1}^U + v_s \rho A_i \circ V_{i+1}^{sh} - \left(\frac{\mu A}{2\Delta z}\right)_i \left(\circ V_{i-1}^{sh} - \circ V_{i+1}^{sh}\right)$$

$$TP_i = \circ Q_{i-1}^L - v_s \rho A_i \circ V_{i-1}^{sh} - \left(\frac{\mu A}{2\Delta z}\right)_{i-1} \left(\circ V_{i-1}^{sh} - \circ V_{i-1}^{sh}\right)$$

Rearranging Equation 24,

$$Q_i - Q_{i-1} = 1/2 \left\{ (TP_i + TM_i - TP_{i-1} - TM_{i-1}) - (v_s \rho A)_{i-1} V_{i-1}^{sh} \right. \\ \left. + ((v_s \rho A)_{i-1} + (v_s \rho A)_i) V_i^{sh} + (v_s \rho A)_i V_{i+1}^{sh} \right\} = \sum_j^N K_{ij}^b y_j^b$$

or,

$$2 [K^b] \{y^b\} = \{A1\} + [A2] \{V^{sh}\} \quad (26)$$

Again using linear acceleration Equation 26 reduces to

$$\left[1/2 [K^b]^{-1} [A2] + \frac{\Delta t}{2} [I] \right] \{V^{sh}\} = \left\{ \circ y^b + \frac{\Delta t}{2} \circ v^b \right\} - 1/2 [K^b]^{-1} \{A1\} \\ + \frac{\Delta t}{2} \{V^t\} \quad (27)$$

or

$$[A2]' \{V^{sh}\} = \{A3\}' + \frac{\Delta t}{2} [V^t]$$

Solving Equations 25 and 27 for V^t yields

$$\{V^t\} = \left[\frac{2}{\Delta t} [A2]' [A6]^{-1} [m] + \frac{\Delta t}{2} [I] \right]^{-1} \left\{ [A2]' [A6]^{-1} \{A4\} - \{A5\} - \{A3\}' \right\} \quad (28)$$

where

$$\{V^t\} = \{V^{sh}\} + \{v^b\}. \quad (29)$$

Equations 27, 28 and 29 represent the characteristics method solution for the series model.

The series model is used for buildings where the total displacement can be taken as the sum of the bending and shear displacement.

Structural Response

The structure selected to illustrate the series model was the staggered truss framing system whose dynamic response was studied by Gupta (2) and subsequently by Hanson and Berg (3). The framing system is illustrated in Fig. 12 and the structure selected was Gupta's (2) 20 story structure. The shear stiffness can be deduced from the truss member properties because there appears to be little stiffness interaction between floors. The bending stiffness can be calculated from the full column areas since there are only exterior rows of columns. Table 3 summarizes the most significant structural data. The trusses are designed so the interior-chord-members yield first and as such exhibit a marked yield story shear force. In order to be compared with Gupta's results, 1.5 times El Centro 1940 N-S component accelerogram and 5% critical damping was used. Gupta used 5% strain hardening elasto-plastic moment-rotation relations. It was found that a Ramberg-Osgood sharpness coefficient of 7 most closely matches this. The structure was modeled as a 5 story building for the characteristics solution.

The results for maximum response of story shear, overturning moment, relative story displacement and floor displacement are shown in Figures 13, 14, 15 and 16 respectively. The characteristics method results show good agreement with Gupta's results.

The top floor displacement time history is shown in Figure 17. The period characteristics match closely and the peaks are fairly close.

The cost of the characteristics solution was \$1.85 versus \$87.60 for Gupta's results; but the characteristic method results were for a 5 level representation of the building. Ongoing studies indicate that for stability of solution for the series model the time step should be a function of the lowest bending beam period so that as the number of levels increases the time step greatly decreases, increasing the cost.

For this structure, the inelastic activity was small, thereby making the energy dissipated by damping important. Therefore, the viscosity was chosen to be close to the desired value rather than arbitrarily set to satisfy Equation 2. Thus, the shears and velocities were interpolated between the layers as previously described. These results matched Gupta's results more closely than the arbitrary damping approach.

CONCLUSION

The weak-girder type structure has been recommended for earthquake resistant design rather than the weak-column type in order to prevent concentration of damage which could lead to collapse. However, the con-

ventional lumped mass shear model does not accurately model the weak-girder type. The characteristics method has been shown to accurately represent this weak-girder type of structure at a significant cost savings. Much work still needs to be done in the areas of establishing the appropriate parameters such as the proportion of lumped and distributed mass, the effect of the bending beam on the time step (stability of solution), the appropriate shear and bending stiffness and the yield story shear. Also, practising engineers have preferred to deal in member data in addition to story data such as story shears, and story ductilities. So a method to translate the story data to inelastic member data is desirable.

For the purposes of practical design the proposed method appears to be accurate, convenient and economical.

ACKNOWLEDGMENT

The present paper is based upon research sponsored in part by the National Science Foundation within Grant Nos. GI39123, FJ7009 and AEN74-00930. The first project supported the senior author as a Visiting Research Associate at The University of Michigan during 1974/75. The results presented herein are those of the authors and do not necessarily reflect the views of NSF.

APPENDIX I - REFERENCES

1. Clough, R. and Penzien, J., Dynamics of Structures, McGraw Hill, New York, 1975.
2. Gupta, Raj Pal, "Seismic Behavior of Staggered Truss Framing System," Ph.D. Thesis, Department of Civil Engineering, The University of Michigan, Ann Arbor, Michigan, September, 1971, (University Microfilms Access No. 72-14882).
3. Hanson, R.D., and Berg, G.V., "Aseismic Design of Staggered Truss Buildings," Journal of the Structural Division, ASCE, Vol. 100, No. ST1 January 1974, pp. 175-193.
4. Jennings, P.C., Housner, G.W., and Tsai, N.C., "Simulated Earthquake Motions for Design Purpose," Proceedings, 4th World Conference on Earthquake Engineering, Vol. I, Al Santiago, Chile, Jan., 1969, pp. 146-160.
5. Kanaan, A.E., and Powell, G.H., "General Purpose Computer Program for Inelastic Dynamic Response of Plane Structures," Report No. EERC 73-6, University of California, Berkeley, California, April 1973.
6. Papadakis, Constantine N., "Soil Transients by Characteristics Method," Ph.D. Thesis, Department of Civil Engineering, The University of Michigan, Ann Arbor, Michigan, November, 1973, (University Microfilms Access No. 74-15823).
7. Streeter, V.L., and Wylie, E.B., Hydraulic Transients, McGraw-Hill Book Company, New York, 1967.
8. Streeter, V.L., and Wylie, E.B., "Two and Three-Dimensional Transients," Trans. ASME, Jour. of Basic Engineering, Vol. 90, Series D, No. 4, Dec. 1968, pp. 501-510.
9. Streeter, V.L., Wylie, E.B., and Richart, F.E., Jr., "Soil Motion Computations by Characteristics Method," Journal of the Geotechnical Engineering Division, ASCE, Vol. 100, No. GT3, Proc. Paper 10410, March, 1974, pp. 247-263.
10. Umemura, H., Aoyama, H., and Takizawa, H., "Analysis of the Behavior of Reinforced Concrete Structures During Strong Earthquakes Based on Empirical Estimation of Inelastic Restoring Force Characteristics of Members," Proceedings, Fifth World Conference on Earthquake Engineering, Vol. 1, Rome, Italy, June, 1973, pp. 2201-2210.
11. Umemura, H., Aoyama, H., and Mukai, Y., "Strong Earthquake Response Analysis of Reinforced Concrete Frames," Proceedings, Architectural Institute of Japan, Oct., 1973, pp. 793-794.

Note: References 2 and 3 are combined in, "Seismic behavior of Staggered Truss Framing System," Steel Research for Construction, Bulletin No. 26, American Iron and Steel Institute, April 1974.

APPENDIX II - NOTATION

C^+ , C^-	= equation for wave propagation
G_oA , GA	= shear stiffness
K_{ij} , K_i	= story stiffness
K_{ei}	= equivalent story stiffness
P_i	= lateral force
Q_i	= average story shear
Q_i^u	= shear force above floor i
Q_i^L	= shear force below floor i
Q_y	= yield story shear force
R	= Ramberg-Osgood sharpness coefficient
V^{sh}	= shear model velocity (absolute)
v^b	= bending model velocity (relative)
V^t	= total velocity (absolute)
W	= corresponding lumped floor weight
Y	= absolute floor displacement
ΔZ	= story height
a_o , a_1	= damping constants
C_{ij}	= damping coefficient
m_i	= floor lumped masses
Δt	= time increment for integration
v_s	= shear wave velocity
w_i	= natural frequency
y	= floor displacement relative to ground
β	= percentage of critical damping
γ	= story rotation
δ	= relative story displacement
μA	= pseudo-viscosity
ρA	= distributed mass per unit height

Table 1. Member sizes for 6 story example structure
(See Figure 4 for member location in doubly symmetric structure.)

Frame Line		A	B	C
Beams	R	W16x26	W18x40	W18x40
	6	W18x40	W21x55	W21x55
	5	W21x44	W21x62	W21x62
	4	W21x44	W21x62	W21x62
	3	W21x49	W24x61	W24x61
	2	W21x55	W24x61	W24x61
Exterior Columns				
	R-5	W14x61	W14x87	W14x87
	R-3	W14x84	W14x111	W14x111
	R-1	W14x103	W14x142	W14x142
Interior Columns				
	R-5	W14x74	W14x78	W14x74
	5-3	W14x95	W14x111	W14x103
	3-1	W14x119	W14x167	W14x158

Table 2. Mass and Stiffness of Equivalent Shear Model

Floor	Weight kips	Mass, Kips·Sec ² /in	Stiffness Kips/in
R	252	0.654	109.53
6	325	0.843	156.78
5	325	0.843	186.90
4	325	0.843	201.26
3	325	0.843	240.38
2	328	0.850	276.37

Table 3. Staggered Truss Framing System

Floor weight = 226 kips Shear stiffness: Floors 1-10 2260 kips/in
Floors 11-20 2460 kips/in.

	Column Sizes	Truss Chord Members
R-19	W14x30	11-20 W10x45
18-17	W14x48	1-10 W10x54
16-15	W14x68	
14-13	W14x84	
12-11	W14x103	
10-9	W14x119	
8-7	W14x136	
6-5	W14x158	
4-3	W14x176	
2-1	W14x193	

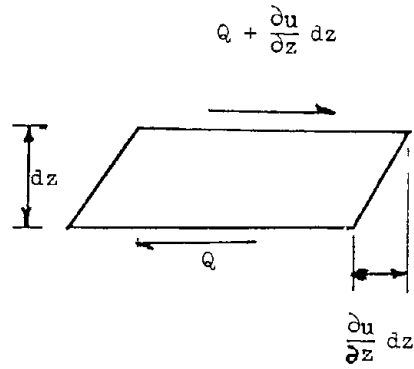
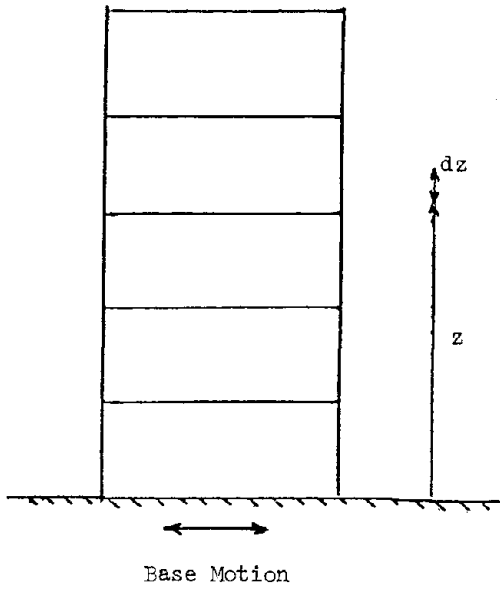


Fig. 1. One Dimensional Shear Wave Transmission Model

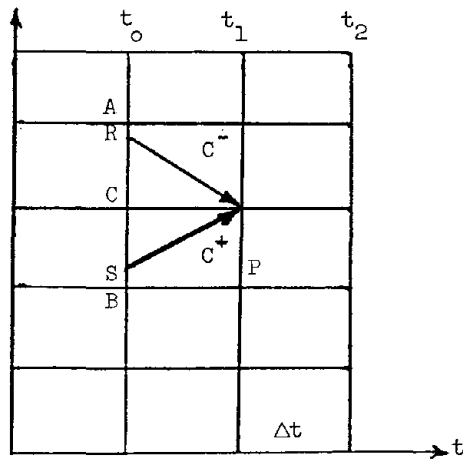


Fig. 2. $\Delta z-\Delta t$ Diagram

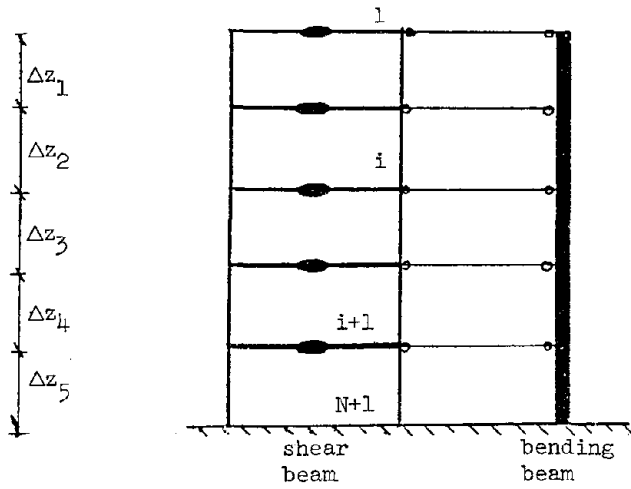
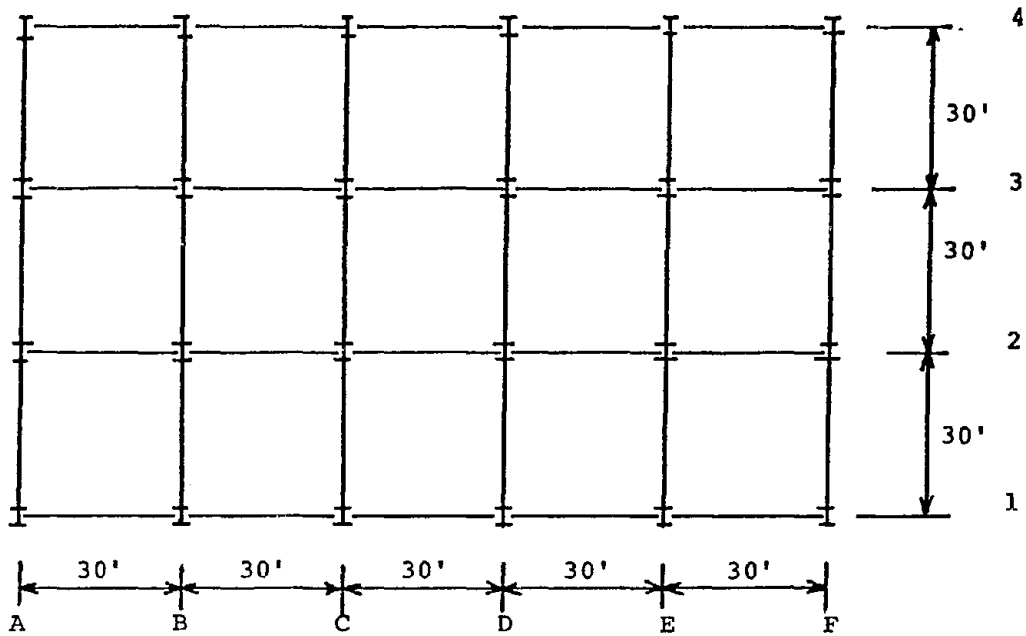
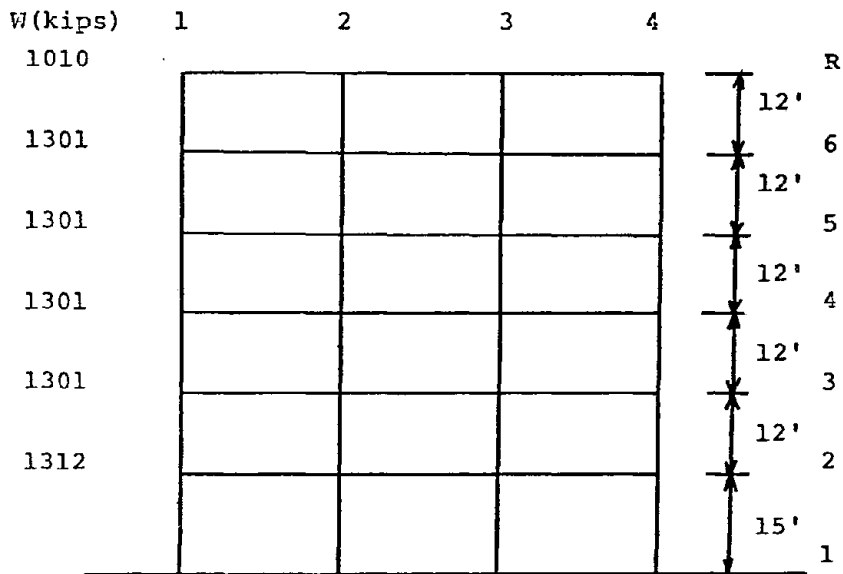


Fig. 3. Parallel Model



(a) Plan of example structure.



(b) Typical frame in X-direction

Figure 4 Example Moment Frame Structure Details

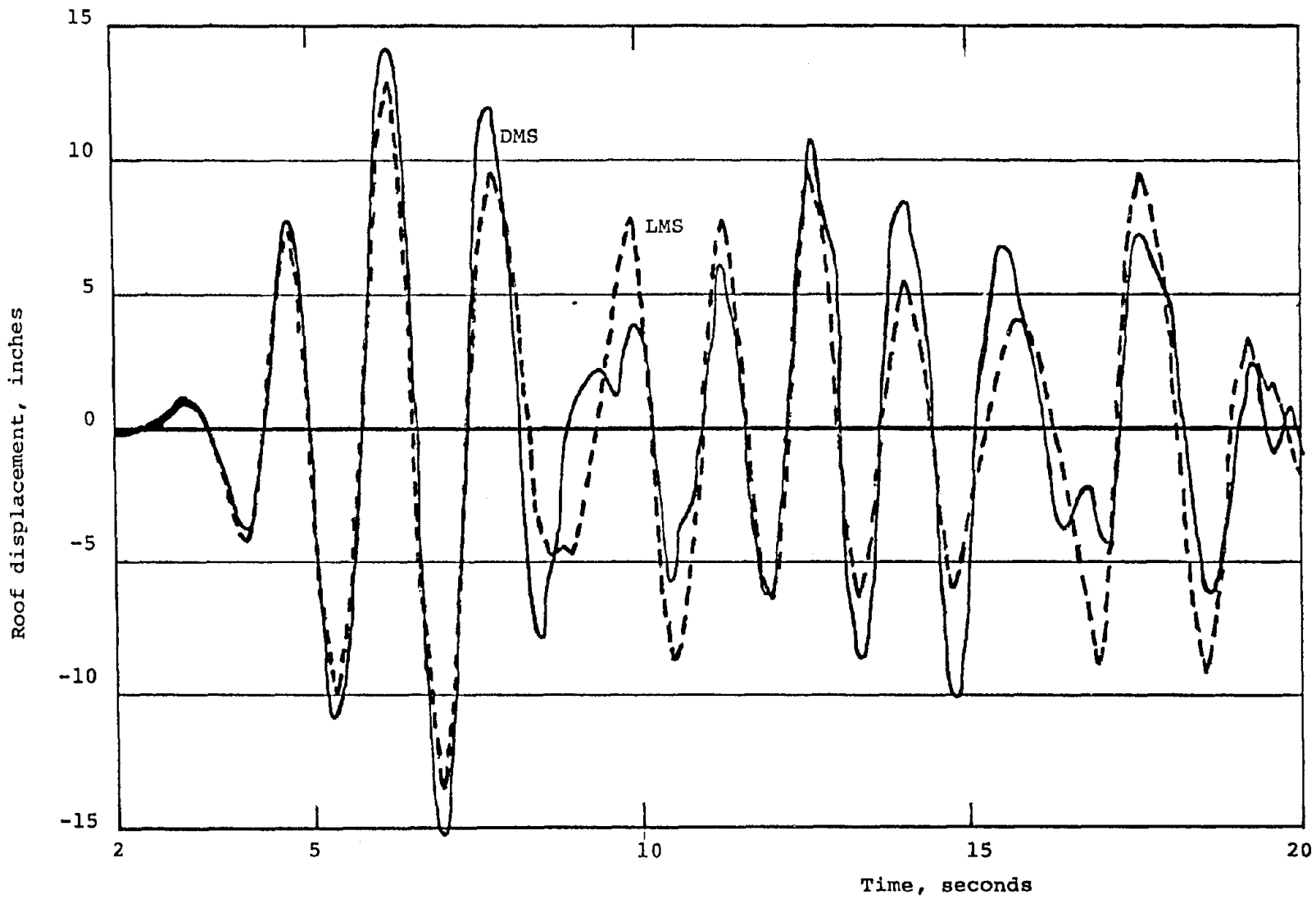


Figure 5 Elastic Displacement of the Roof Relative to the Base Computed by DMS and LMS

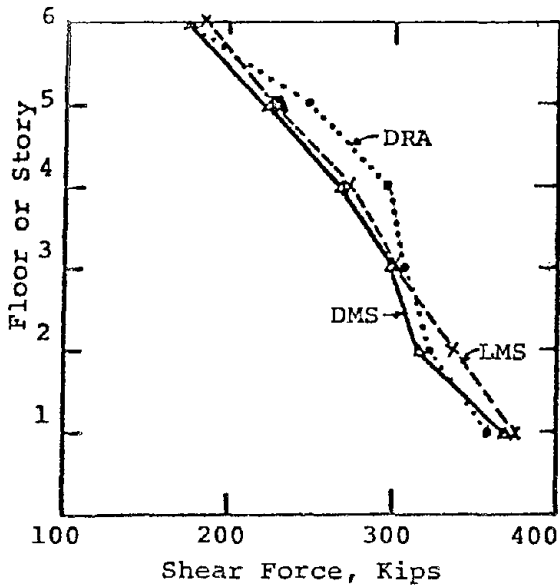


Figure 6 Maximum Story Shear Force

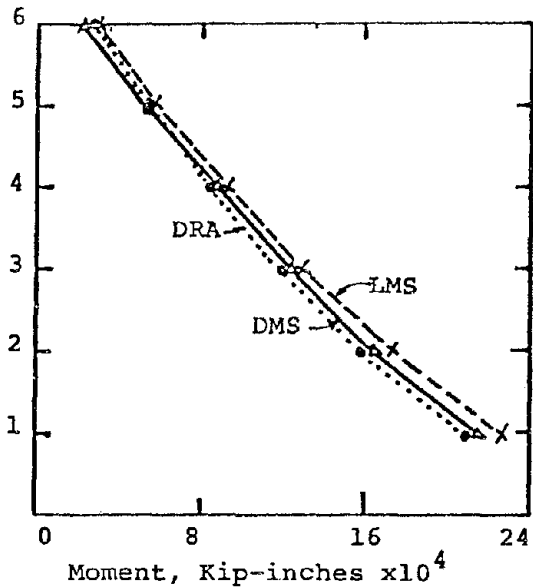


Figure 7 Maximum Overturning Moment

DMS = Distributed Mass System, LMS = Lumped Mass System, DRA = Drain-2D Solution - Maximum values recorded during the first 20 seconds of A1 earthquake.

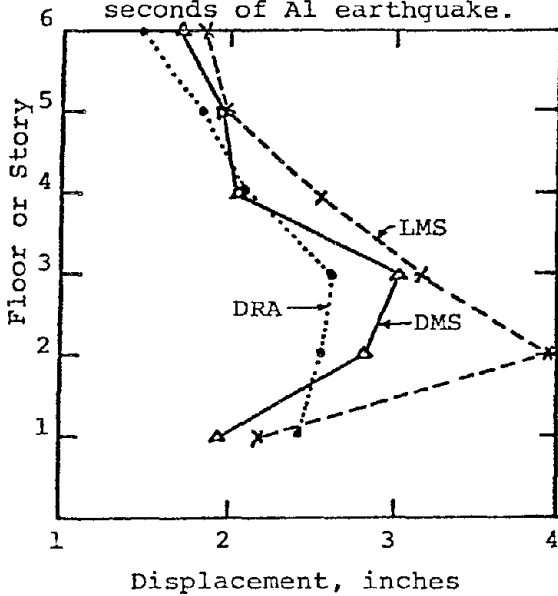


Figure 8 Maximum Relative Floor Displacement

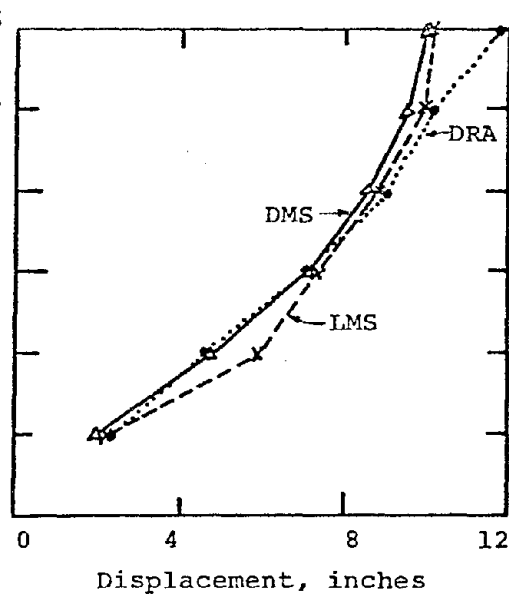


Figure 9 Maximum Floor Displacement Relative to the Base

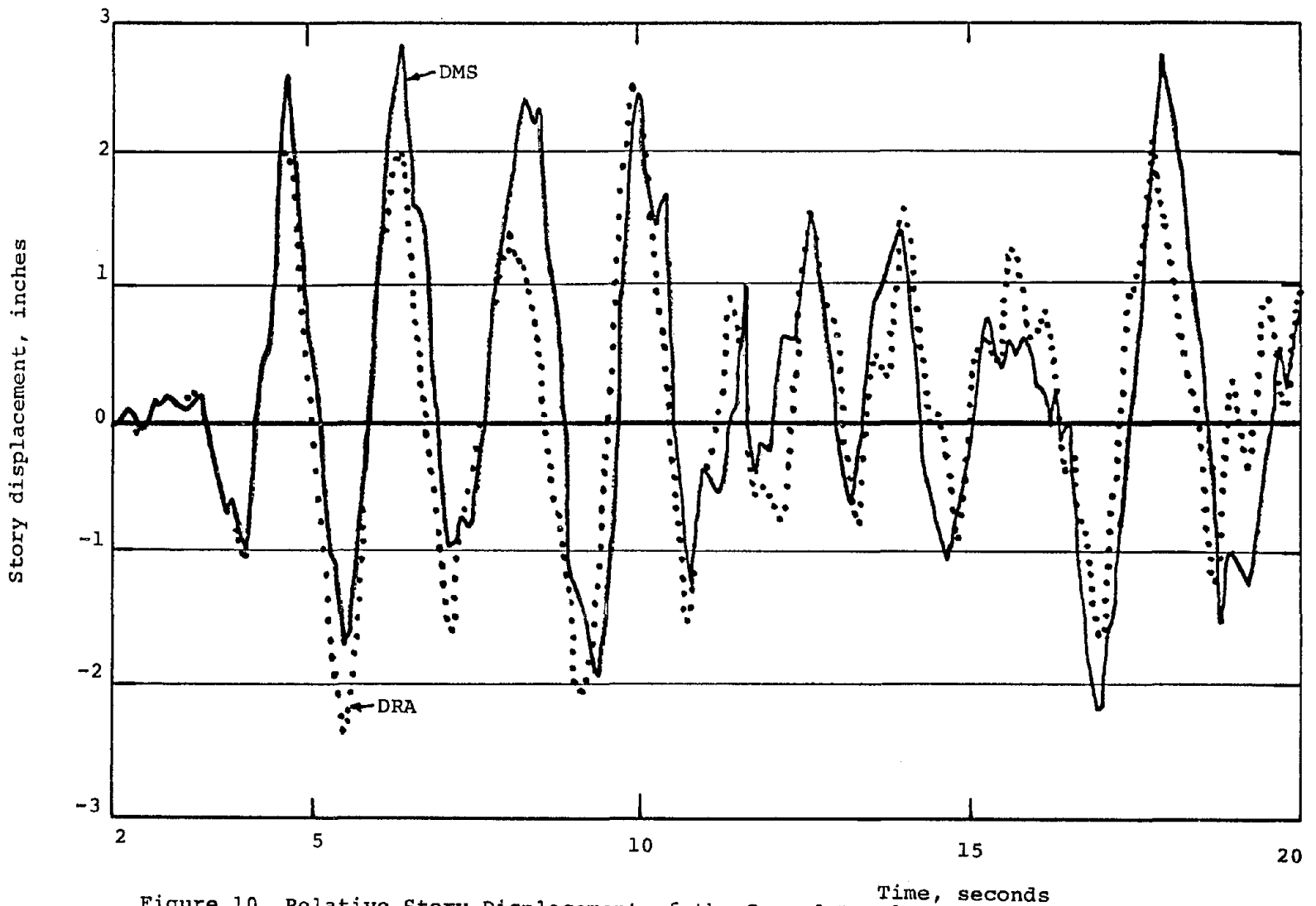


Figure 10 Relative Story Displacement of the Second Level Determined by Inelastic DMS and DRA

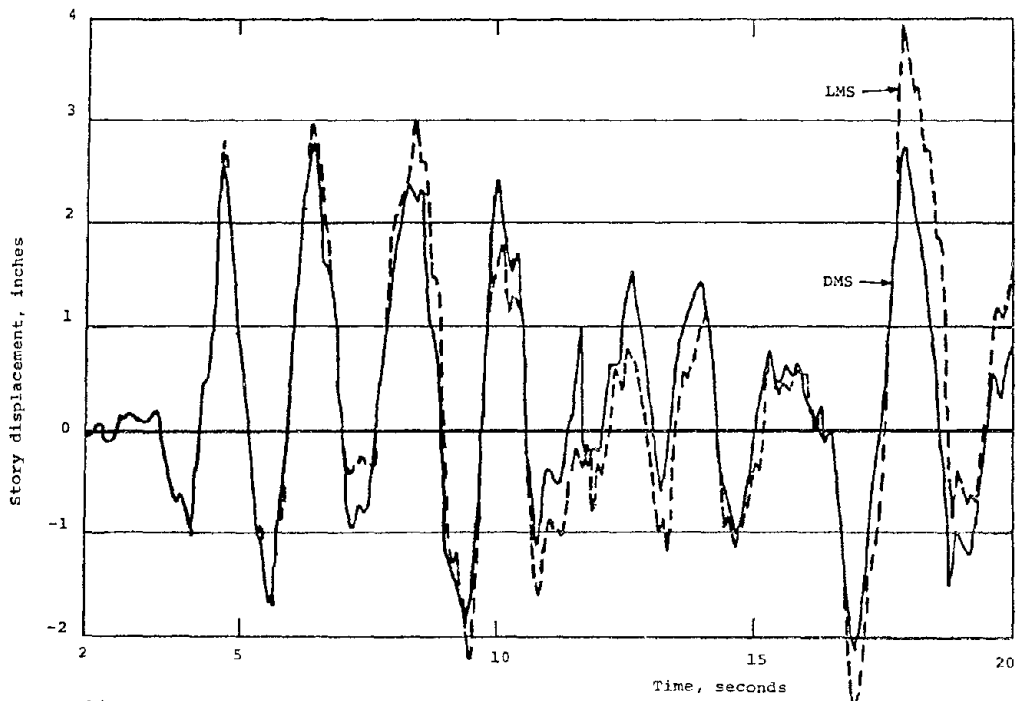


Figure 11(a) Relative Story Displacement of the Second Level Determined by Inelastic DMS and LMS

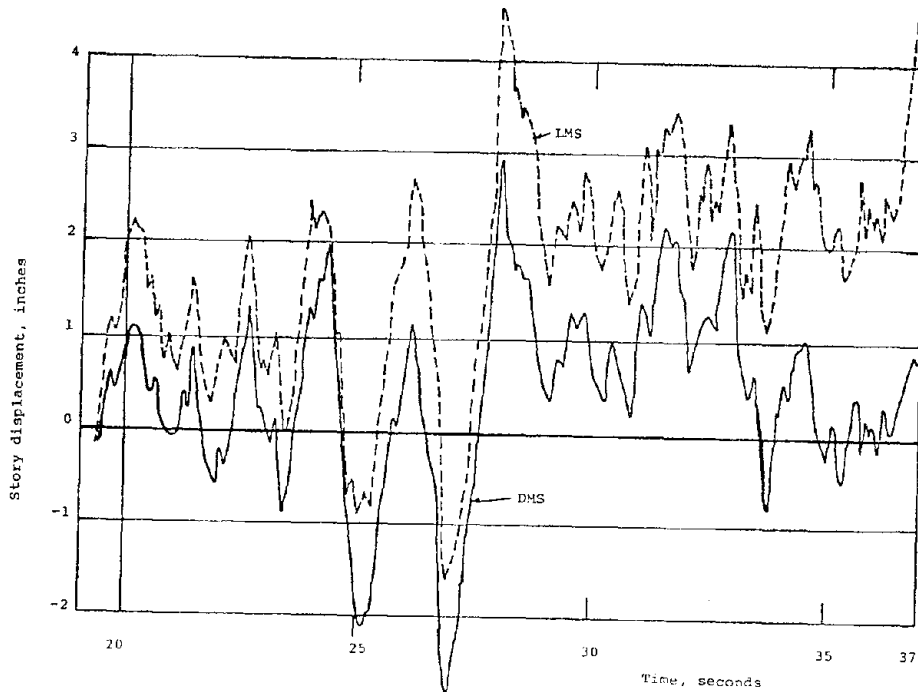


Figure 11(b) Relative Story Displacement of the Second Level Determined by Inelastic DMS and LMS

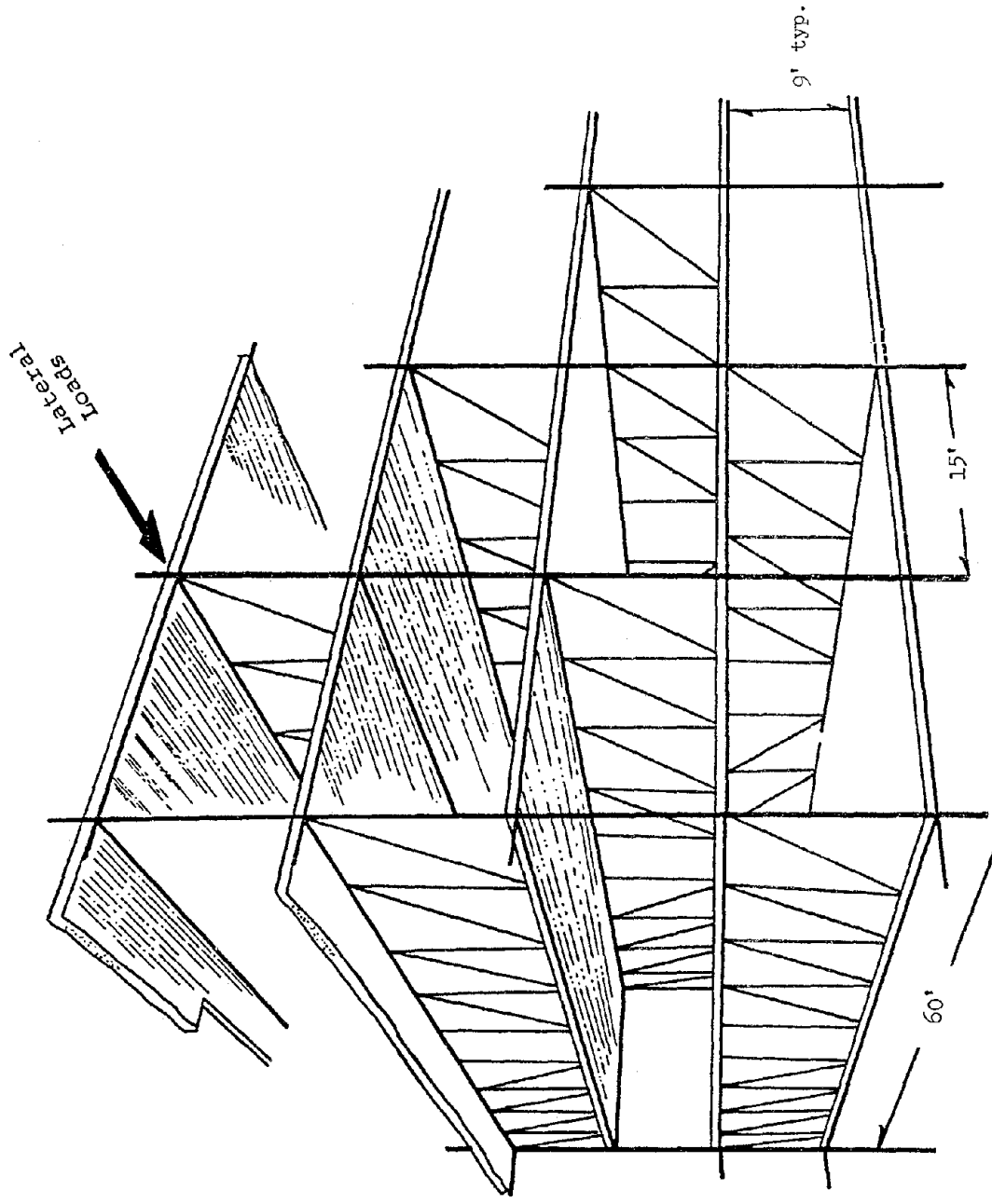


Figure 12. - Staggered Truss Framing System

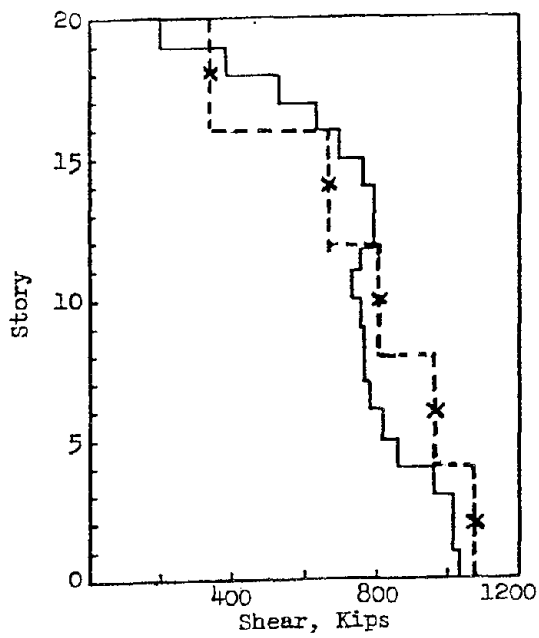


Fig. 13. Maximum Story Shear

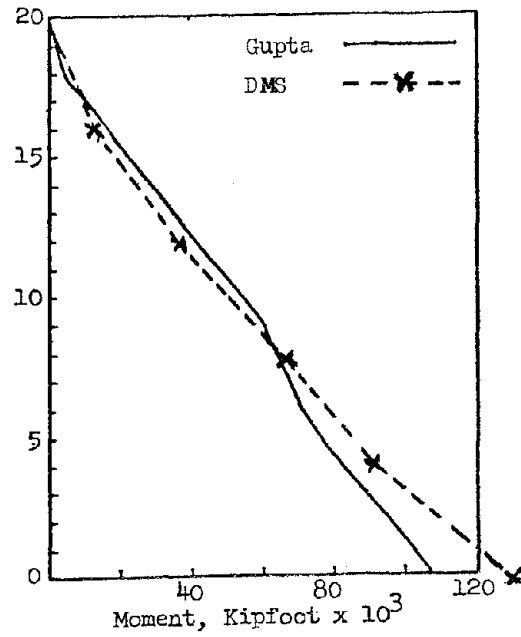


Fig. 14. Maximum Overturning Moment

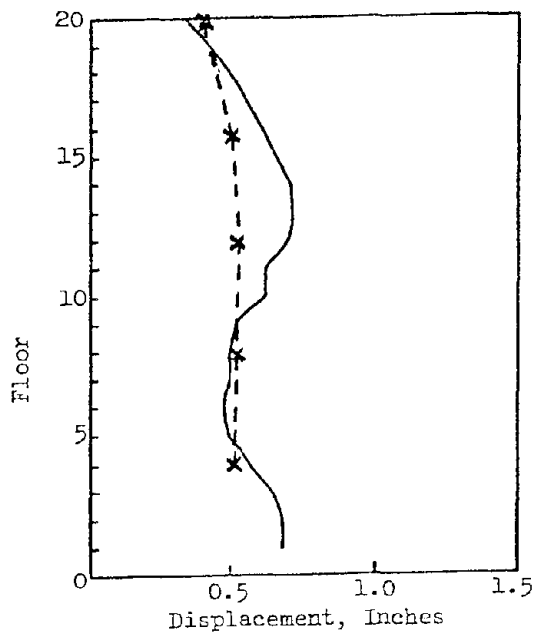


Fig. 15. Maximum Relative Story Displacement

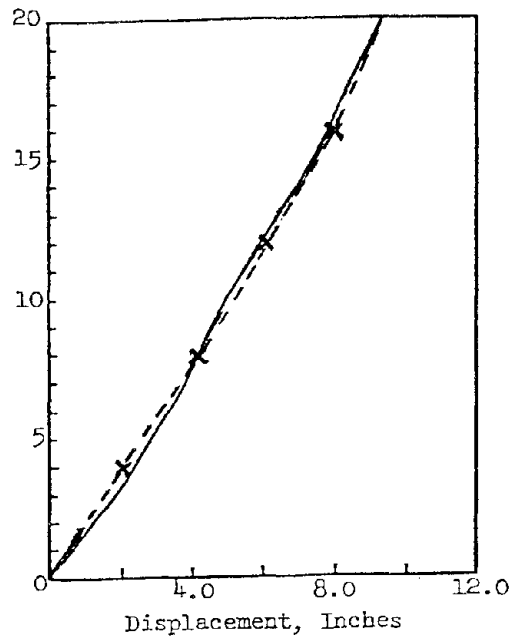


Fig. 16. Maximum Floor Displacement

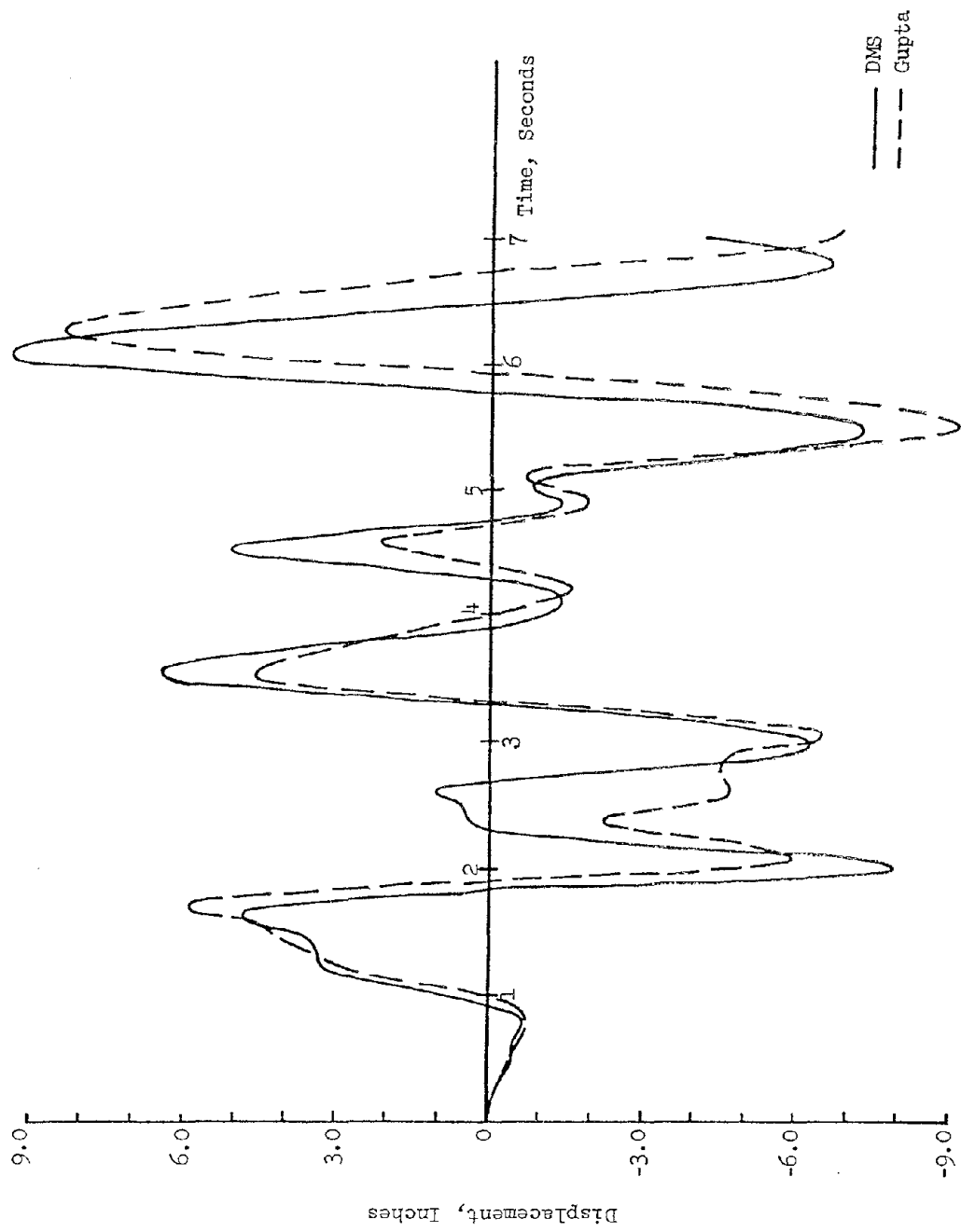


Figure 17. Top Floor Displacement

THE STRENGTHENING METHODS OF
EXISTING REINFORCED CONCRETE BUILDINGS

by

Yōichi Higashi^I and Seiji Kokusho^{II}

SYNOPSIS

In order to investigate the effects of the strengthening methods, several tests were made as follows:

- 1) Strengthening by the solid walls poured in place under a certain pressure within the existing frames
- 2) Strengthening by adding reinforced concrete or precast concrete wing walls at the sides of the existing columns, or precast concrete panels within the existing frames
- 3) Strengthening the existing columns with welded wire fabrics and mortar

The results of these tests are described in this paper.

INTRODUCTION

For the existing reinforced concrete buildings, which are evaluated to be un-safe against strong earthquakes, proper strengthening is required. Therefore, the strengthening method of existing reinforced concrete buildings have been studied.

In case of strengthening a building, the following methods are considered:

- (1) to increase the strength of the building
- (2) to increase the ductility of the building
- (3) combination of (1) and (2)

In order to achieve these purposes, the following experimental tests have been carried out:

- (A) strengthening by the solid walls poured in place under a certain pressure within the existing frames
- (B) strengthening by adding reinforced concrete or precast concrete wing walls at the sides of the existing columns, and the precast concrete panels within the existing frames
- (C) strengthening the existing columns by welded wire fabrics and mortar

I : Professor, Department of Architecture, Faculty of Engineering, Tokyo Metropolitan University

II : Professor, Department of Architecture and Building Engineering, Faculty of Engineering, Tokyo Institute of Technology

Experimental tests of (A) were carried out in the laboratory of Tokyo Institute of Technology under co-operation of Taisei Corporation. Experimental tests of (B) and (C) were carried out in the laboratories of Tokyo Metropolitan University and of Tokyo Institute of Technology, respectively, as the investigations¹⁾ of the 5th Committee^{III} for School Buildings of the Architectural Institute of Japan, in compliance with the requests of the Ministry of Education and of the Ministry of Construction, Japanese Government.

As the results, the effects of the strengthening methods are found to be remarkable, and the prospects of the strengthening methods are found.

EXPERIMENTAL TEST A

(1) Test specimens

Test specimens are two as shown in Figs. 1 through 3. One, OW, is a monolithic shear wall with rigid frame. The other, PWC, is a rigid frame strengthened by a monolithic shear wall poured under pressure of about 0.3 kg/cm^2 , in place within the frame.

The thicknesses of wall in both test specimens are 7.5 cm. In case of PWC, the perimeter of the wall is jointed by the shear keys of concrete, whose height, length and width are 1 cm, 4 cm and 7.5 cm, respectively, to the frame. The wall reinforcements of both test specimens are not anchored to the surrounding frames.

The compressive strength of concrete except for the wall part of PWC is 354 kg/cm^2 . The compressive strength of concrete poured by pressure into the wall part of PWC is 320 kg/cm^2 .

The yield strengths of round bars of 6 mm and 9 mm in diameter, and of deformed bars of 13 mm in nominal diameter, are 2560 kg/cm^2 , 3270 kg/cm^2 and 4030 kg/cm^2 , respectively.

(2) Test procedure

The testing facility is shown in Fig. 4. Both test specimens are tested by alternately reversal loading, and the horizontal relative displacements between the top beams and the basement are measured.

(3) Results of test

Figs. 5 and 6 show the relationship between the lateral forces

III: Chairman : Y. Higashi
Secretary : S. Kokusho
Members : H. Aoyama, H. Endoh, M. Fukuhara, M. Hirose, M. Hirose,
T. Kameda, T. Katoh, M. Kitahara, T. Minami,
T. Mukai, M. Murakami, M. Nakao, K. Oami,
K. Ogura, M. Ohkubo, K. Osada, Y. Ohsawa, and
A. Yoshida

and the relative rotation angles of members. Fig. 7 shows the envelope curves of load-deflection curves shown in Figs. 5 and 6.

The initial rigidity of PWC is about 0.85 times that of OW.

The maximum strengths of both test specimens are almost same and about 3.5 times the strength of the frame only.

In case of PWC, the shear keys between wall and frame fractured due to the shear at the rotation angle of about 1/100 rad.

The lateral force capacity of OW at the rotation angle of over 1/100 rad. is almost same as the maximum strength. On the other hand, the lateral force capacity of PWC at the same rotation angle is about 0.8 times the maximum strength.

OW fractured due to bending crush. On the other hand, PWC fractured due to punching shear at the top of the column after shear failure of shear keys.

(4) Conclusions

The results from these tests are summarized as follows:

a) The effect of the strengthening method is remarkable against the maximum strength. The maximum strength of the strengthened frame is almost same as the monolithic shear wall.

b) The effects of the strengthening method is considerable on the initial rigidity and the lateral force capacity under large deflections.

c) The mode of fracture between two test specimens are different. Therefore, in order to find accurate mechanism of fracture in the frame strengthened by shear wall and the effects of this kind of strengthening methods, the investigations must be further carried out.

EXPERIMENTAL TEST B

(1) Test specimens

Test specimens consist of the following four types as shown in Table 1.

a) Specimens of type AC are strengthened by the reinforced concrete wing walls poured in place at the sides of the existing columns as shown in Figs. 8 and 14. The thickness of the wing wall is 70 mm.

b) Specimens of type PW are strengthened by the precast reinforced concrete wing walls at the sides of the existing columns as shown in Figs. 9 and 14. The thickness of the precast wing wall is 40 mm.

c) Specimens of type PA are strengthened by adjoining the precast reinforced concrete wing walls at the sides of the existing columns with steel anchor pieces as shown in Figs. 10, 12 and 15. The thickness of the precast wing wall is 40 mm.

d) Specimens of type PCW are strengthened by adjoining the precast reinforced concrete panels at the inside of the existing frames with steel anchor pieces as shown in Figs. 11, 12 and 17. The thickness of the precast panel is 40 mm.

The compressive strengths of concrete for types AC and PW are about 230 kg/cm^2 in the existing parts and in the precast parts, and 300 kg/cm^2 in the parts poured in place. The compressive strengths of concrete for types PA and PCW are about 245 kg/cm^2 and 415 kg/cm^2 , in the existing and precast parts and in the parts poured in place, respectively.

The yield strengths of reinforcement of 9 mm and 4 mm in diameter for types AC and PW, are about 3865 kg/cm^2 and 2290 kg/cm^2 , respectively. The yield strengths of reinforcement of 9 mm and 4 mm in diameter for types PA and PCW, are about 3755 kg/cm^2 and 3615 kg/cm^2 , respectively.

(2) Test procedure

The axial force and antisymmetric bending moment are loaded by means of special loading system in the test of types AC, PW and PA as shown in Fig. 13. The horizontal loads are applied to type PCW as shown in Fig. 16. All test specimens are tested by alternately reversal loading, and the horizontal relative displacements between top and bottom beams are measured.

(3) Results of test

Fig. 18 shows the envelope curves of the relationships between the lateral force and the relative rotation angle of members in the tests of types AC, PW and PA. The relative rotation angle of members, R , means the horizontally relative deflections between top and bottom beams divided by clear height of the column.

Table 2 shows the ratios of maximum experimental strengths after strengthening to the calculated strengths before strengthening.

From these results, it is found that the above mentioned ratios of increase in the maximum strength are around 2, and that the effects of precast reinforced concrete wing walls are remarkable in the increase of ductilities due to the effect of the steel angles surrounding the precast concrete walls.

Fig. 19 shows the envelope curves of the relationships between the lateral force and the relative rotation angle of frames, R , in type PCW. Table 2 shows the ratios of maximum experimental strengths after strengthening to the calculated strengths before strengthening.

From the results, it is found that the above mentioned ratios

of increase in the maximum strengths are around 4, and that the increase of ductilities in PCWC and PCWH is remarkable in comparison to the monolithic shear walls, RCW.

(4) Conclusions

The results from these tests are summarized as follows:

a) Such rigidities and strengths of the existing columns strengthened with the reinforced concrete or precast concrete wing walls by welding the wall reinforcements to the hoops of columns and by pouring concrete or mortar, are almost same as those of monolithic columns and wing walls.

b) In case of the columns strengthened with the precast concrete wing walls jointed to the existing columns by steel anchor pieces and mortar grouting, the rigidities and strengths do not increase sufficiently. However, the strength reductions due to alternately reversal loading are little, and the deformation capacities increase.

c) In case of the frames strengthened with precast concrete panels within the frame, the rigidities are not increased much, but the strengths and the deformation capacities are increased.

d) In order to find accurate effects of this kind of strengthening methods, the investigations must be further carried out.

EXPERIMENTAL TEST C²⁾

(1) Test specimens

Test specimens consist of the existing columns and the columns strengthened by the welded wire fabrics and the mortar poured in place. The width, B , over-all depth, D , longitudinal reinforcement ratio, p_t , and shear reinforcement ratio, p_w , of the existing columns are 25 cm, 25 cm, 0.61 %, and 0.07 %, respectively. Test specimens have various shear span length, a , thickness of mortar, t , mean axial compressive stress, N/BD , and diameter, ϕ , and spacing, $@$, of the welded wire fabrics, as shown in Table 3 and in Figs. 20 and 21.

The compressive strengths of concrete are about 210 kg/cm². The compressive strengths of mortar are about 340 kg/cm². The yield strengths of longitudinal reinforcement, hoop and welded wire fabric are about 4000 kg/cm², 3810 kg/cm² and 5000 kg/cm², respectively.

(2) Test procedure

The testing facility³⁾ is shown in Fig. 22. All test specimens are tested by alternately reversal loading, and the horizontal relative displacements between top and bottom stubs are measured.

(3) Results of test

Figs. 23 through 28 show the examples of the relationships between the lateral forces and the relative deflections.

In case of the un-strengthened columns, the brittle fractures occur under a few cycles of alternately reversal loading. On the other hand, in case of the strengthened columns by the welded wire fabrics and by the mortar with gaps at both ends of the columns, the ductilities after bending yield are increased remarkably.

(4) Conclusions

The results from these tests are summarized as follows:

a) In case of the columns strengthened by the welded wire fabrics and by the mortar with gaps at both ends of the columns, the theoretical bending strengths of the existing columns are guaranteed and the deformation capacities are increased remarkably.

b) Due to the scale effects, the relationships between the effects and the amounts of strengthening on the strengths and the deformation capacities are not found accurately.

c) The investigations of this kind of strengthening methods must be further carried out in order to find the degree of the effects accurately.

CONCLUSIONS

The effects on the strengths and deformation capacities of the various kinds of strengthening methods are obtained by the experimental tests. As the results, it is found that the effects are remarkable, and that these strengthening methods are effective.

Due to the limited number of tests, the investigations of this kind of strengthening methods must be further carried out in order to find the degree of the effects accurately. Further research and development are hopefully waited.

ACKNOWLEDGEMENTS

The investigations of the strengthening methods of existing reinforced concrete buildings described in this paper, are carried out by the members of the 5th Committee for School Buildings of the Architectural Institute of Japan sponsored by the Ministry of Education and the Ministry of Construction, Japanese Government, and by Mr. S. Hayashi and others of Tokyo Institute of Technology under co-operations of Taisei Corporation. The authors wish to acknowledge gratefully for these contributions.

REFERENCES

1) Architectural Institute of Japan, " The evaluation method of the earthquake resistant properties and the strengthening method of reinforced concrete school buildings " 1975

2) S. Kokusho and M. Fukuhara, " Experimental studies on the strengthening methods of existing reinforced concrete columns " Report of Kantō Branch of AIJ, 1975

3) M. Hirosawa, M. Ozaki and M. Wakabayashi, " Experimental study on large models of reinforced concrete columns " Fifth World Conference on Earthquake Engineering, 1973

4) T. Miki, T. Homma and M. Hirosawa, " Evaluation of earthquake resistant properties and strengthening of existing building " Fifth World Conference on Earthquake Engineering, 1973

5) T. Sasaki, A. Hattori and others, " Experimental studies on the strengthening methods of existing reinforced concrete columns " Report of AIJ, 1972

Table 1. Kinds of test specimens in experimental test B

Type	No.	h_0/D	$\frac{(l_w - D)}{2}$	t/b	Column		Wall	Note
					$p_c(\%)$	$p_w(\%)$	$p_{wk}(\%)$	
AC	A-1	4	$0.5D$	0.47	0.56	0.21	0.45	
	B-1	2	D	"	0.85	0.56	1.20	
PW	A-2	4	$0.5D$	0.27	0.56	0.21	0.79	
	B-2	2	D	"	0.85	0.56	1.05	
PA	CW4H0	4	$1.87D$	"	0.56	0.21	0.31	1) & 3)
	CW4H1	4	"	"	"	"	"	1) & 4)
	CW4H2	4	"	"	"	"	"	1) & 5)
	CW4C1	4	"	"	"	"	"	2) & 4)
	CW2H1	2	"	"	"	"	"	1) & 6)
	CW2C1	2	"	"	"	"	"	2) & 4)
PCW	RCW	6.67	$l_w = 100 \text{ cm}$	"	"	"	"	7)
	PCWH	"	$l_w = 103 \text{ cm}$	"	"	"	"	1)
	PCWC	"	"	"	"	"	"	2)

- Note: 1) mechanical anchor (cf. Fig. 12)
 2) chemical anchor (cf. Fig. 12)
 3) without steel anchor pieces in vertical joints
 4) 10 cm spacing of steel anchor pieces in vertical joints
 5) 5 cm spacing of steel anchor pieces in vertical joints
 6) 10 cm spacing of steel anchor pieces in vertical joints; wing walls adjoined to column without eccentricity
 7) monolithic wall

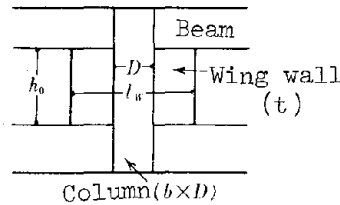


Table 2. Ratios of maximum experimental strength of specimens after strengthening to calculated strength of specimens before strengthening in experimental test B

Type (number of specimens)	Bending strength	Shear strength	Note
AC (2)	2.14	2.58	cf. Table 1
PW (2)	1.56	2.09	
PA (6)	1.73 ~ 2.09	1.32 ~ 1.43	
PCW (3)	3.81 ~ 4.16	4.47	

Table 3. Kinds of test specimens in experimental test C

No	Symbol	a/D	Mortar t (cm)	N/BD (kg/cm ²)	B'xD' / BxD	Welded wire fabric	P _w ' (%)	P _w '' (%)
1	0.61-1.0-26.3(0)*	1.0		26.3				0.07
2	0.61-1.0-26.3(1)6	1.0	6	26.3	2.19	8φ-50 @ double	1.14	1.69
3	0.61-1.0-26.3(0.5)6	1.0	6	26.3	2.19	8φ-50 @ single	0.59	0.88
4	0.61-1.5-26.3(0)*	1.5		26.3				0.07
5	0.61-1.5-26.3(1)6	1.5	6	26.3	2.19	8φ-50 @ single	0.59	0.88
6	0.61-1.5-26.3(0.5)6	1.5	6	26.3	2.19	6φ-50 @ single	0.35	0.52
7	0.61-1.5-26.3(0.5)3	1.5	3	26.3	1.64	6φ-50 @ single	0.41	0.52
8	0.61-1.5-52.5(0)*	1.5		52.5				0.07
9	0.61-1.5-52.5(1)6	1.5	6	52.5	2.19	8φ-50 @ double	1.14	1.69
10	0.61-2.0-26.3(0)*	2.0		26.3				0.07
11	0.61-2.0-26.3(0.5)6	2.0	6	26.3	2.19	4φ-50 @ single	0.18	0.27
12	0.61-2.0-26.3(0.5)3	2.0	3	26.3	1.64	4φ-50 @ single	0.21	0.27
13	0.61-2.0-52.5(0)*	2.0		52.5				0.07
14	0.61-2.0-52.5(1)6	2.0	6	52.5	2.19	8φ-50 @ single	0.59	0.88

Note: *: existing column
a/D: shear span ratio of existing column
t: thickness of mortar
B'xD': sectional area of column including strengthening mortar
P_w': shear reinforcement ratio including welded wire fabric in section after strengthening
P_w'': shear reinforcement ratio including welded wire fabric in section before strengthening

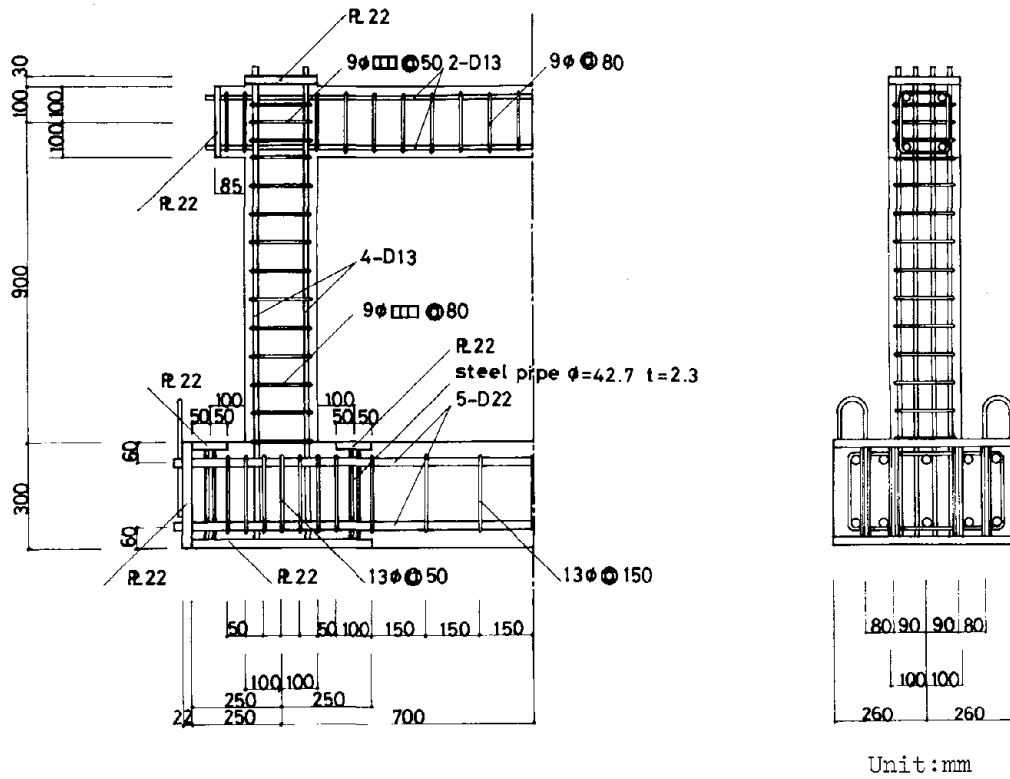


Fig. 1 Reinforcing bar arrangement of frame in experimental test A

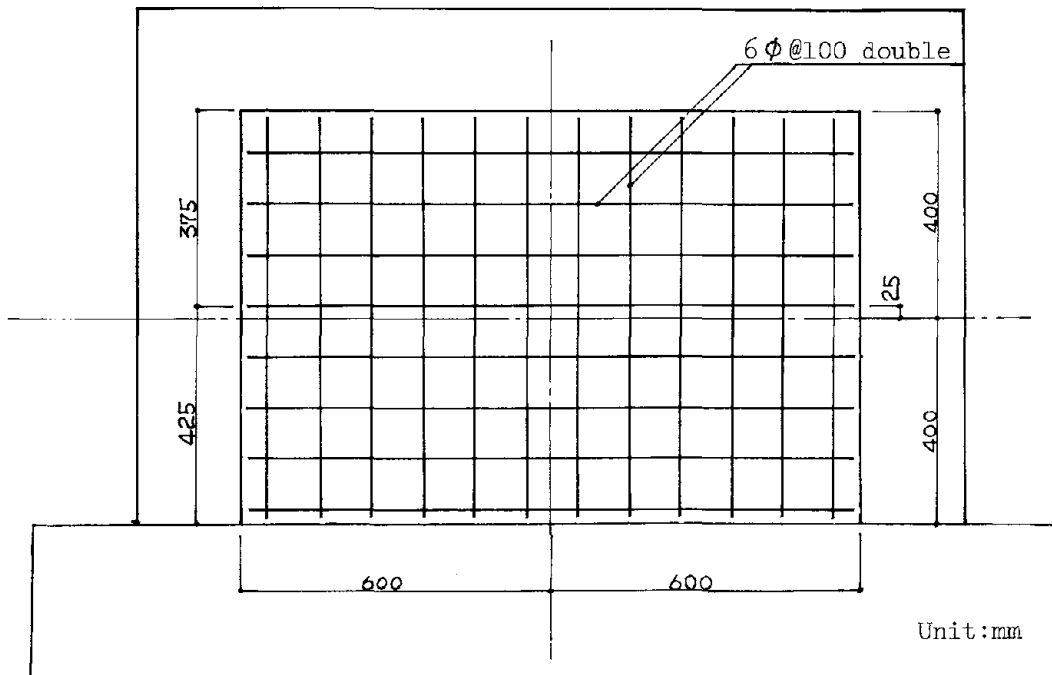


Fig. 2 Reinforcing bar arrangement of wall in experimental test A

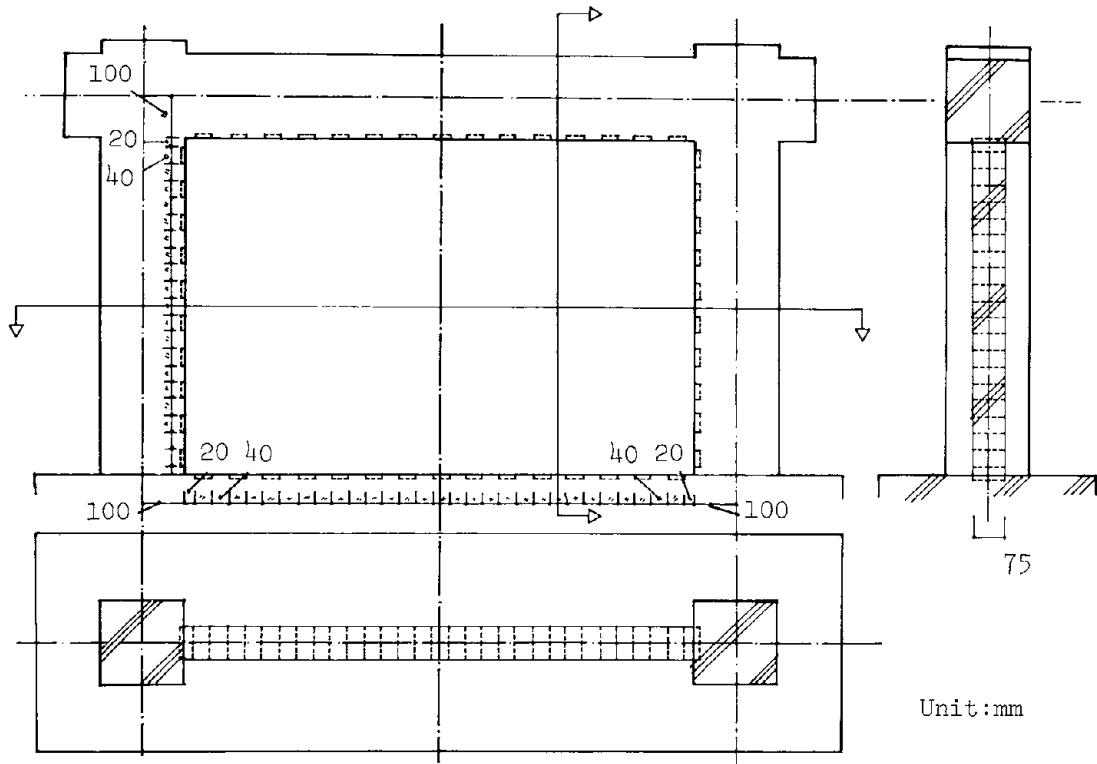


Fig. 3 Arrangement of shear key in experimental test A

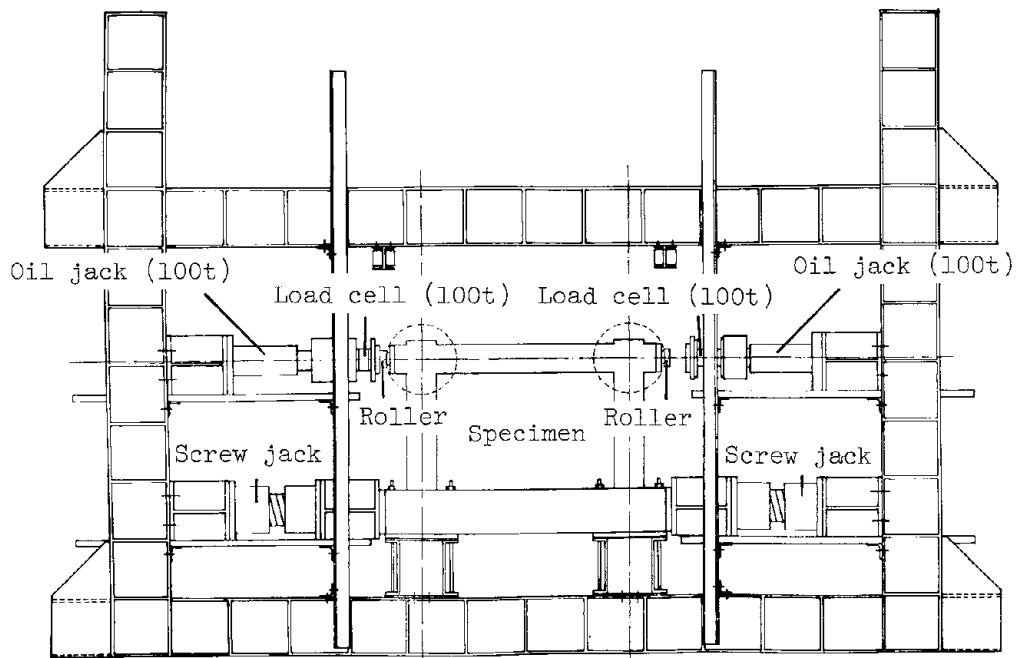


Fig. 4 Testing facility in experimental test A

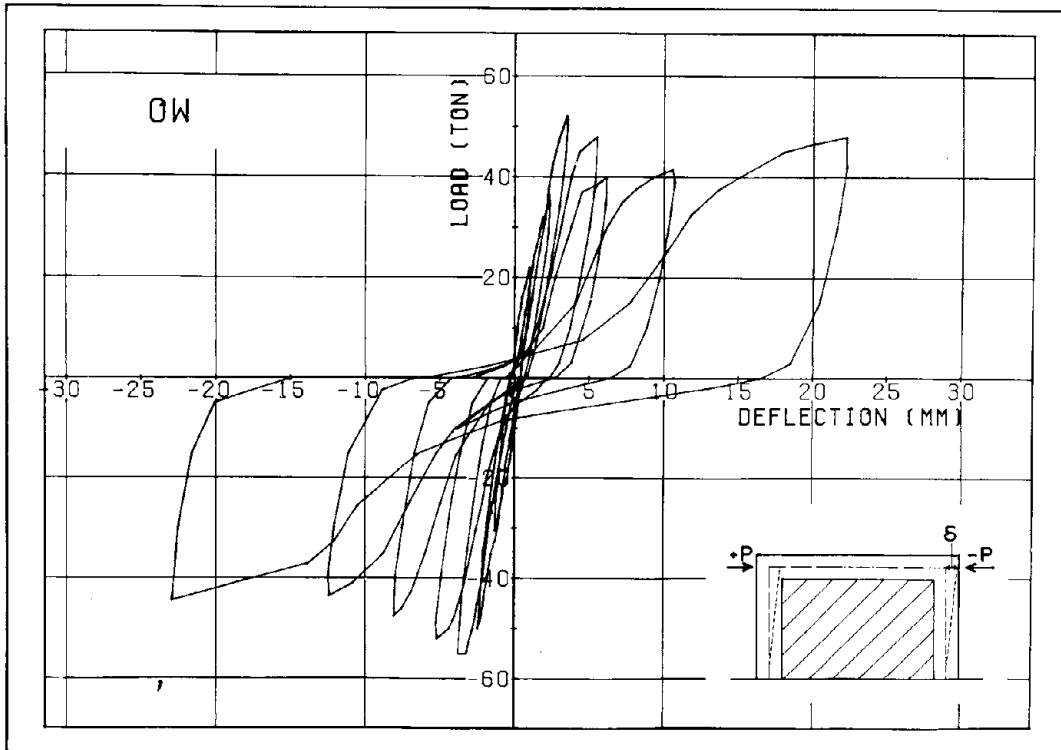


Fig. 5 Load-deflection curves of OW in experimental test A

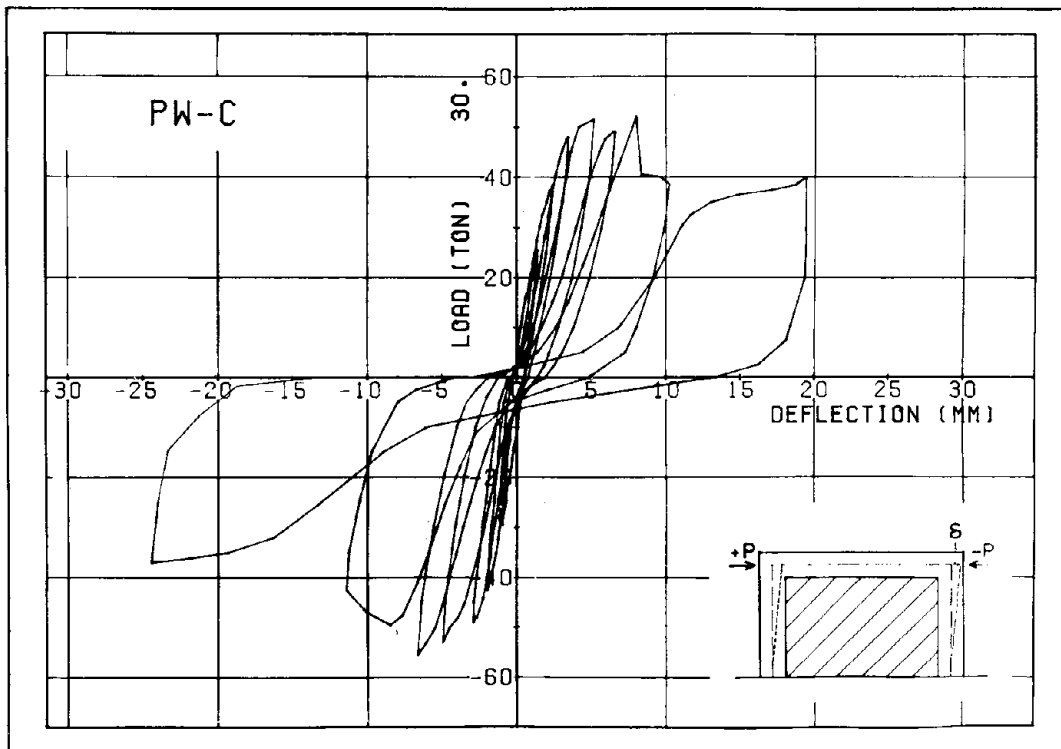


Fig. 6 Load-deflection curves of PWC in experimental test A

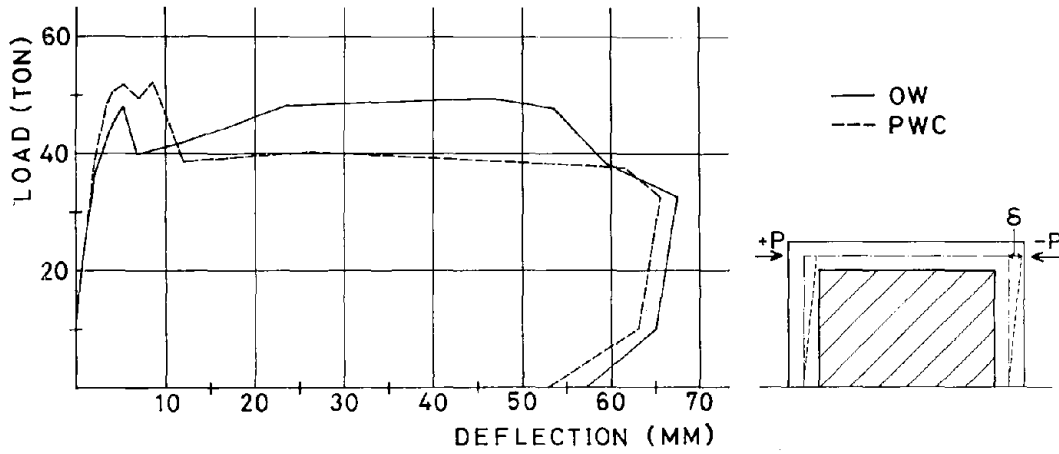


Fig. 7 Envelope curves of relationship between load and deflection of OW and PWC in experimental test A

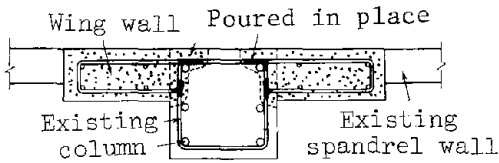


Fig. 8 Type AC in experimental test B

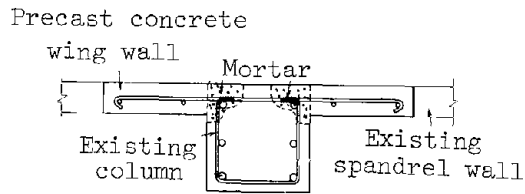


Fig. 9 Type PW in experimental test B

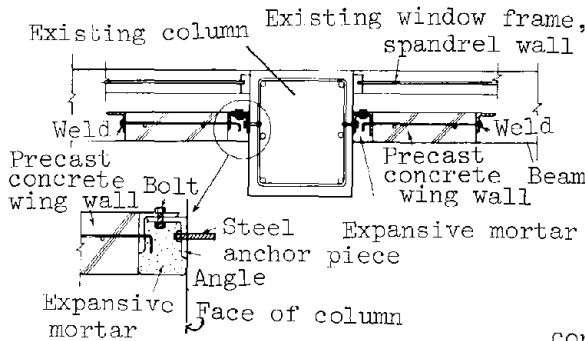


Fig. 10 Type PA in experimental test B

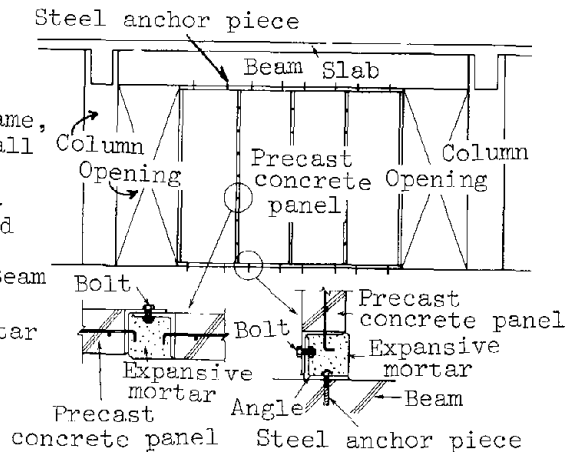


Fig. 11 Type PCW in experimental test B

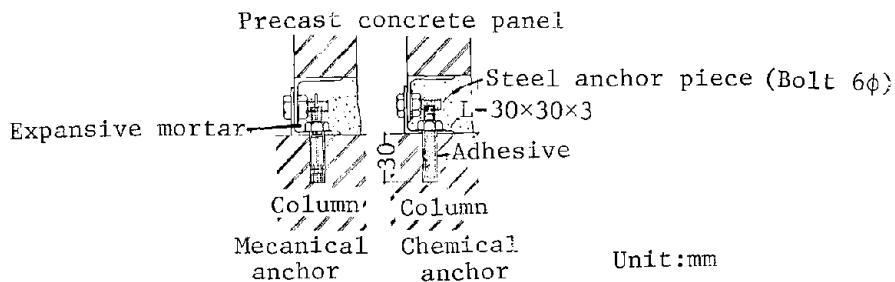


Fig. 12 Detail of mechanical anchor and chemical anchor

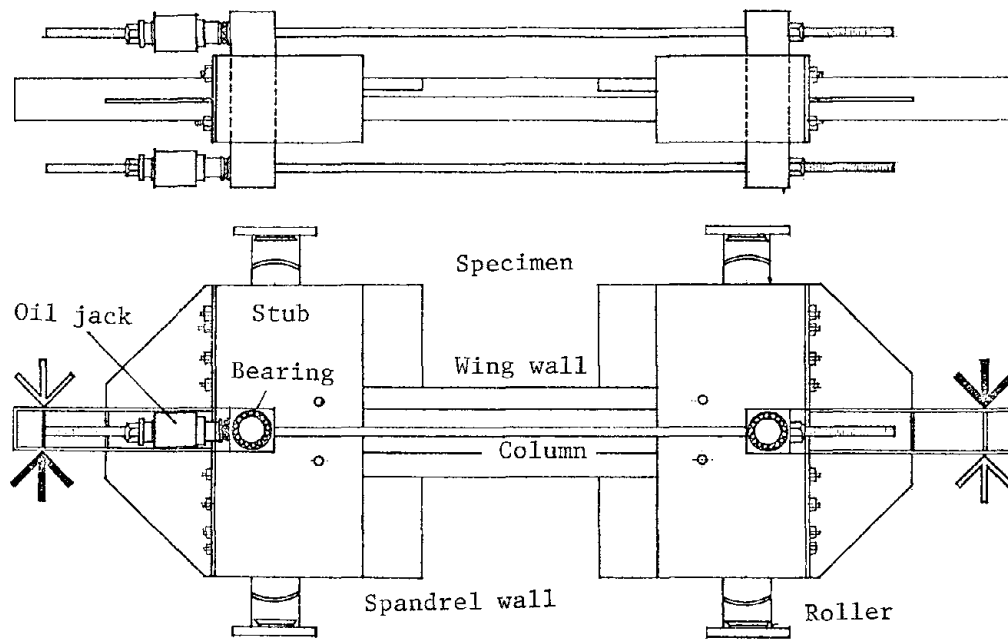


Fig. 13 Testing facility in types AC, PW and PA of experimental test B

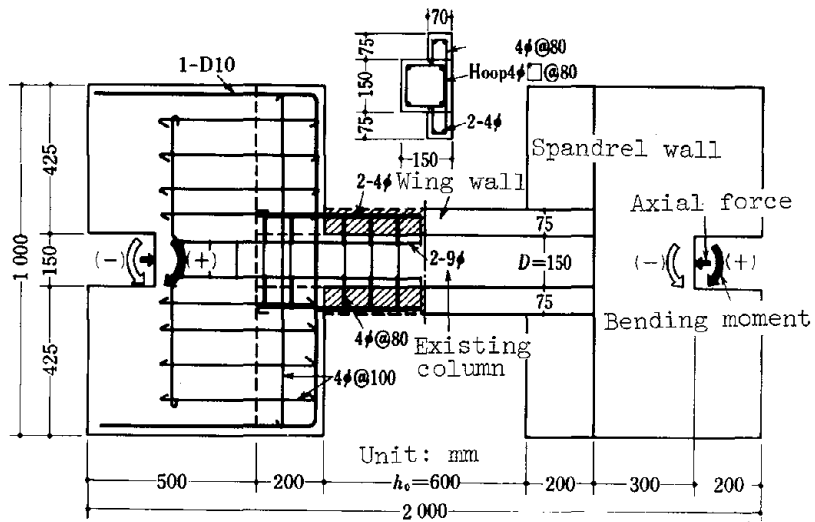


Fig. 14 Specimen AC(A-1) in experimental test B

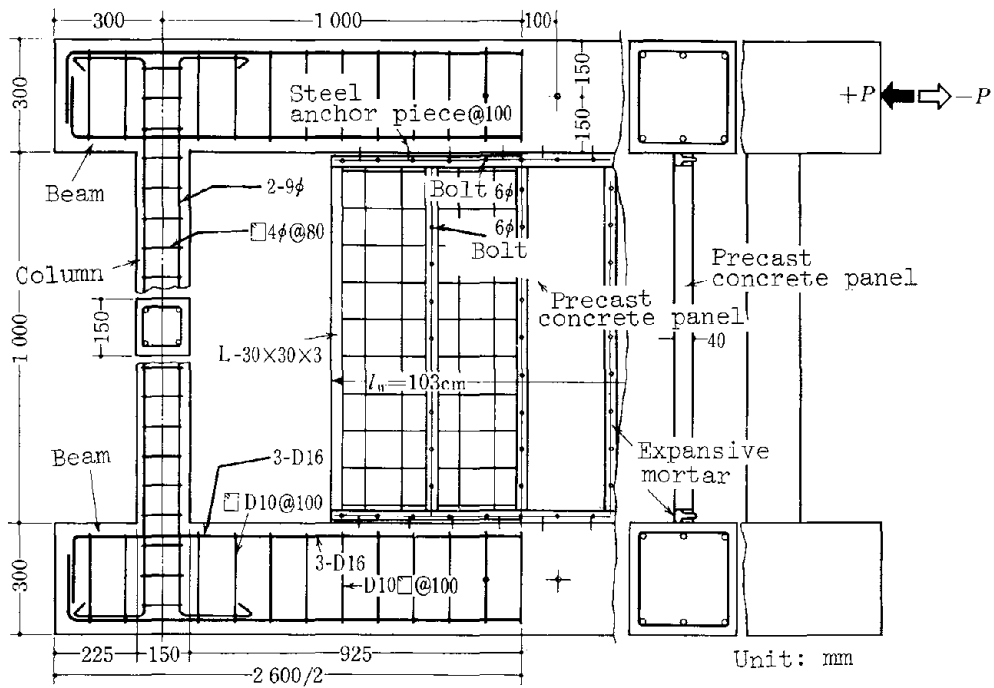


Fig. 17 Specimen PCW(PCWH) in experimental test B

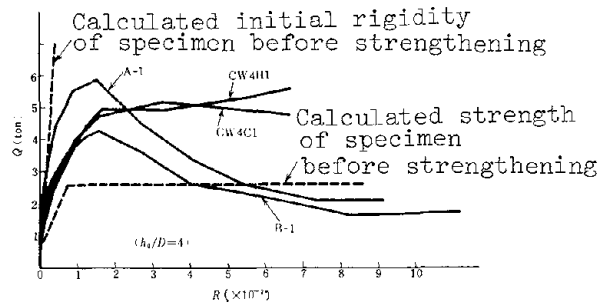


Fig. 18 Envelope curves of relationship between lateral force and relative rotation angle of member in types AC, PW and PA of experimental test B

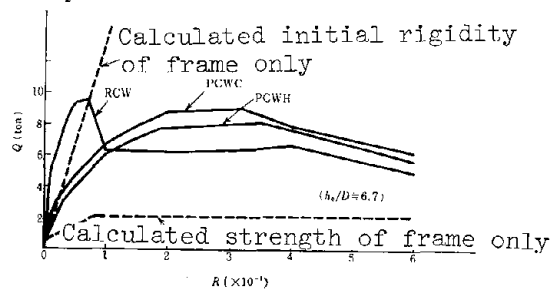


Fig. 19 Envelope curves of relationship between lateral force and relative rotation angle of member in type PCW of experimental test B

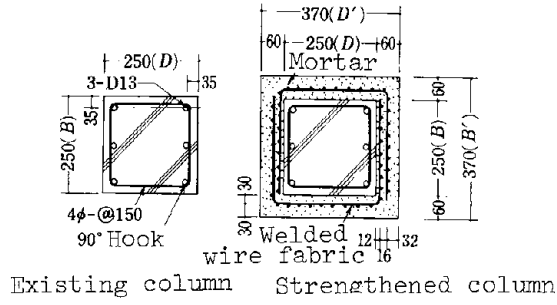


Fig. 20 Examples of section of test specimens Unit:mm
in experimental test C

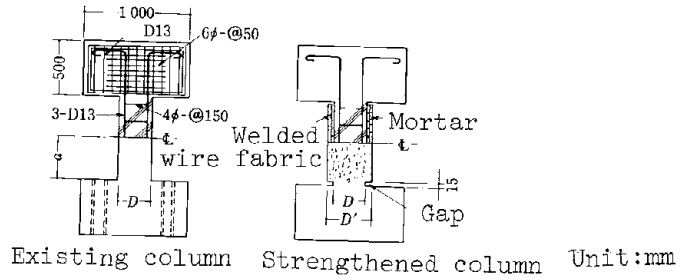


Fig. 21 Examples of test specimens in experimental
test C

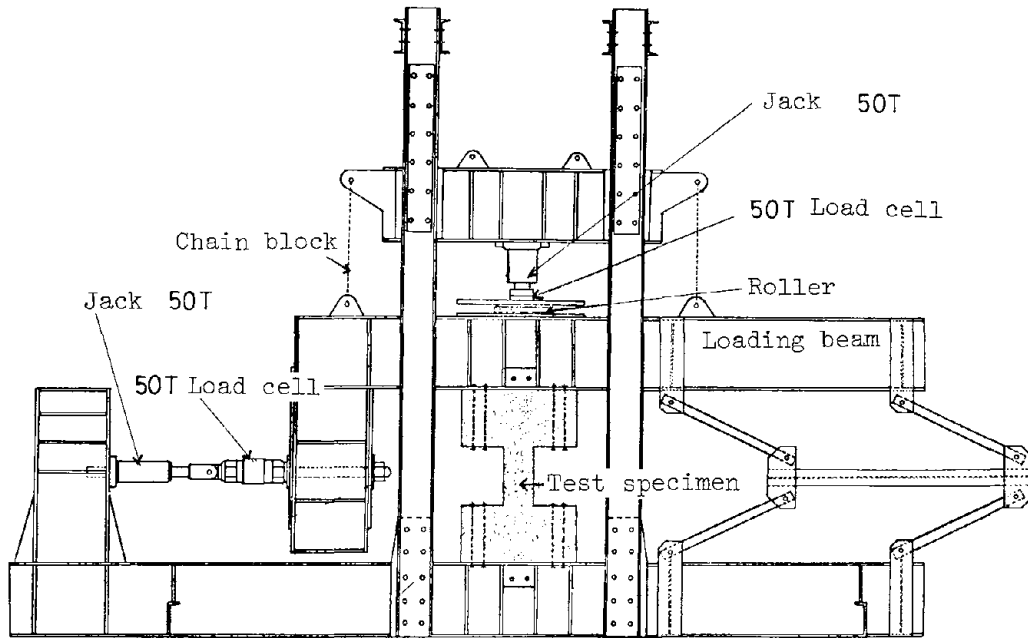


Fig. 22 Testing facility in experimental test C

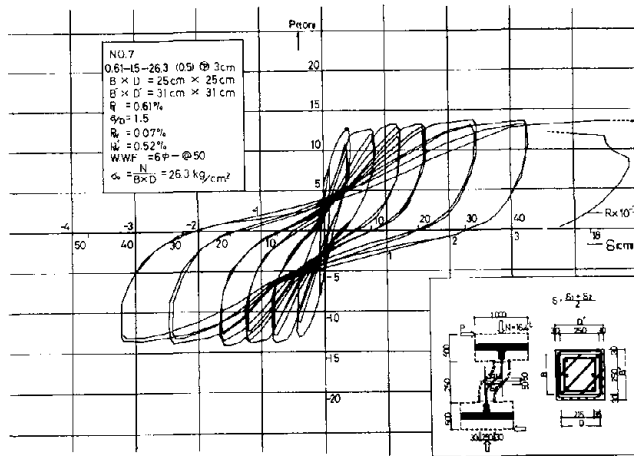


Fig. 26 Relationships between lateral force and relative deflection (No. 7) in experimental test C

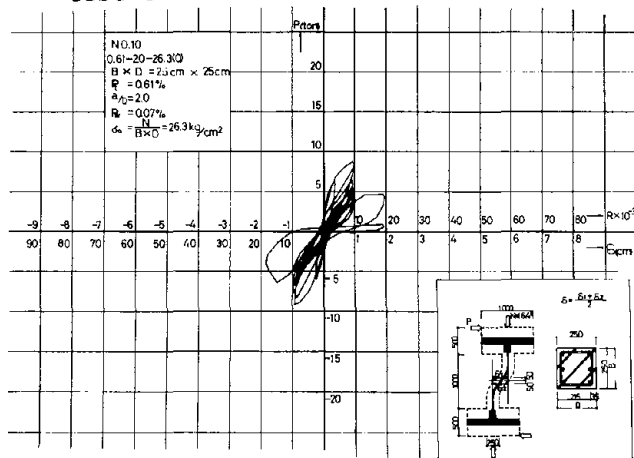


Fig. 27 Relationships between lateral force and relative deflection (NO. 10) in experimental test C

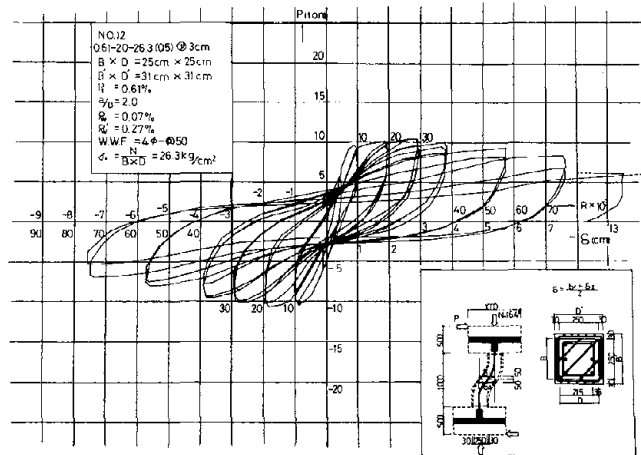


Fig. 28 Relationships between lateral force and relative deflection (No. 12) in experimental test C

AN EXPERIMENTAL STUDY ON EARTHQUAKE RESISTANT STRENGTHENING WORK FOR EXISTING REINFORCED CONCRETE BUILDINGS

by

Tetsuya Sasaki ^(I), Atsusi Hattori ^(II), Naoharu Mori ^(II),
Kohichi Nonaka ^(II) and Tatsuo Suenaga ^(II).

Synopsis

The object of this investigation is to present a practical method for strengthening the existing reinforced concrete buildings with inadequate earthquake resistance. The method investigated herein is to cover an existing concrete column by a thin steel plate and to grout the clearance between the column and the steel plate with non-shrink mortar.

The test was performed by applying repeated alternate distortions to the column specimen, simulating the effects of earthquakes. This paper deals with existing columns, thickness of steel plate, shear-deflection behavior, shear-axial length behavior and failure mode of the column specimens.

1. OBJECT

Damages resulting from the Tokachi-Oki Earthquake of 1968 demonstrated that some of reinforced concrete buildings designed by former code do not have adequate earthquake resistance. According to the authorities' survey, there exist considerable number of reinforced concrete buildings with poor earthquake resistance in Tokyo City, which are thought to become one of the causes of earthquake disaster.

The object of this investigation is to present a practical strengthening method for these weak buildings.

2. STRENGTHENING METHOD

There would be various methods for the strengthening of weak buildings, as mentioned as follows:

- 1) adding shear walls or bracings to the existing frame,
- 2) adding a new earthquake resisting frame to the existing frame—double frame.
- 3) Strengthening the existing column itself by means of reinforcing

(I) Senior Research Engineer, Kajima Institute of Construction Technology

(II) Research Engineer, Kajima Institute of Construction Technology

the surface of the column.

While methods 1) and 2) mean "strength proof" strengthenings which make the weak buildings stronger, method 3) means "ductility proof" strengthening which prevents the column from brittle shear failure and gives adequate rotation capacity at the column ends. Method 3) was only dealt with in this investigation.

Three strengthening details were decided as shown in Fig.1 so that they meet as much as possible the clients' needs for the architectural design and planning of existing building, strengthening period and various troublesome businesses before and after the strengthening work. These methods are to cover existing old column by a thin steel plate and to fill the clearance between the column and steel plate with non-shrink mortar. These strengthening works are easy to practise and estimated not to cost so much.

The shapes of cover plate in horizontal section may be designed in box or circular shell, and sometimes in band when needed to strengthen a column in spandrel walls. They are called as Box, Pipe and Band type respectively.

3. TYPICAL EXISTING COLUMNS EVER DAMAGED DURING EARTHQUAKES

The damages which reinforced concrete buildings suffered from the Tokachi-Oki Earthquake and San Fernando Earthquake might be superficially classified into two types as follows;

1) Open columns (long columns) which stand on the "pirot'i floor" or on the floor with small area of shear walls were damaged at the top and the bottom and much swayed.

2) Short shear span columns such as columns with spandrel were failed in shear.

Long column and short column, therefore, were adopted as the original columns. The characteristic values of the original columns such as sectional size, length, reinforcement, designed shear stress, designed normal stress and etc. were determined as the ordinary values of the already constructed reinforced concrete buildings' columns, as shown in Fig.2.

4. ESTIMATION OF THE THICKNESS OF STEEL PLATE ,

How many thickness of steel plate shall be needed so that the strengthened column may be saved from the failure in shear and have sufficient ductility. The authors roughly estimated the thickness of steel plate under the following consideration. In these estimations, the existing shear reinforcement and the increment of moment capacity of column due

to the strengthening work were neglected.

(1) Estimation by A. I. J. Structural Standards (1971)

The required shear reinforcement of the column under the designed shear stress $\tau_D = 12.5 \text{ kg/cm}^2$ is calculated from the following formula (1).

$$p_w = \frac{1.5 \tau_D - f_s}{0.5 w f_t} + 0.002 \dots \dots \dots (1)$$

$$= \frac{1.5 \times 12.5 - \frac{210}{20}}{1200} + 0.002 = 0.89\%$$

This shear reinforcement corresponds to the strengthening steel plate of 2.5 mm thickness.

On the other hand, the required shear reinforcement under the shear in the case when the top and the bottom of column come to yielding in bending is calculated from the following formulas (2) to (4).

$$M_u = 0.8 a_t \sigma_y D + 0.5 ND \left(1 - \frac{N}{bDFc} \right) \dots \dots \dots (2)$$

$$= 6,520 \text{ t} \cdot \text{cm}$$

$$Q_u = \frac{2M_u}{h} \dots \dots \dots (3)$$

$$= 52.1 \text{ t}$$

$$p_w = \frac{Q_u/bj - f_s}{0.5 w f_t} + 0.002 \dots \dots \dots (4)$$

$$= 1.16\%$$

This reinforcement corresponds to the steel plate of 3.2 mm thickness.

Notations in formulas (1) to (4) are as follows;

p_w : shear reinforcement ratio

τ_D : designed shear stress

F_c : designed compressive strength of concrete

f_s : allowable shear stress of concrete for temporary loading

wf_t : allowable tensile stress of shear reinforcing bar for temporary loading

M_u : ultimate bending strength of the column at the ends

σ_y, a_t : allowable tensile yield stress and the sectional area of longitudinal tension reinforcement of the column at the ends, respectively

b, D, j : width, depth and effective depth of the column, respectively

N : axial force applied to the column

Q_u : shear force produced on the column in the moment yielding at the ends

(2) Estimation by the ACI-SEAOC Standards (318-71) for Ductile Moment Resisting Frame

The required shear reinforcement is calculated from the following formula (5) or (6), whichever is larger.

$$p_w = 0.3 \frac{f_c'}{f_y''} \left(\frac{A_g}{A_c} - 1 \right) \dots \dots \dots (5)$$

$$= 1.31\%$$

$$p_w = 0.12 \frac{f_c'}{f_y''} \dots \dots \dots (6)$$

$$= 1.05\%$$

where,

p_w : required shear reinforcement ratio

f_c' : designed compressive strength of concrete

f_y'' : tensile yield stress of shear reinforcing bar

A_g : gross sectional area of column

A_c : sectional area of the core of column

Based on the above mentioned calculation, 3.2 mm (standard size) was adopted as the thickness of strengthening steel plate, which corresponds to $P_w = 1.2\%$.

5. EXPERIMENT

(1) Specimens

The test consists of two series. One is a series of long columns and the other is a series of short columns. Each series contained one column without strengthening and two with various strengthening as shown in Table 1, thus six specimens were prepared. All specimens were of $1/2$ reduced scale. As shown in Fig. 3, the specimens are ++ shaped columns with beam stubs on both sides. The portions outside of the stubs which are for the loading are increased in both sectional area and reinforcements.

Strengthening works were performed according to the standard procedure of this strengthening system, that is to say, existing column was covered with steel plate and then the bottom of steel plate was shielded with cement mortar and finally non-shrink cement mortar was poured down from the clearance between the column and steel plate at the top of the column, patting steel plate several times with a small wooden hammer. The clearance was observed to have been filled consistently with the non-shrink mortar by the opening of steel plate after test.

Physical properties of steel plates, re-bars, concrete and grouted mortar used for the specimens were as shown in Table 2 to Table 4.

(2) Instrumentation and Test Procedure

The same test setup was employed for all specimens. An over all view of the testing arrangement is shown in Fig. 4. The specimen was placed horizontally in the loading frame. Lateral loads were applied by means of oil jacks as shown in Fig. 5, producing anti-symmetric moments on the test column. First, the column axial load $N (=0.25 bDF_c)$ was applied and was kept constant throughout the test. Then, the loads P were applied simultaneously to both stubs of the specimen which was supported at the ends. The stub loads were applied repeatedly and alternately into both directions as indicated by +P and -P in Fig. 5.

Dial gages and electric displacement meters were used to measure deformation of the specimen as shown in Fig. 5. Extensive measurement was taken of strains by wire strain gages at various locations, including

main re-bars, hoops and steel plate, in order to observe the outline of the state of stress and yielding.

Each specimen was tested according to the loading scheme as shown in Table 5.

6. TEST RESULT

The restoring forces at the characteristic points were summarized in Table 6. Figs 7(a) to 7(c) and Figs 8(a) to 8(c) show the shear-deflection curve for each specimen of long column series and short column series, respectively. The definition of the deflection is as shown in Fig. 6. The number at the top of loops indicates the cycle number counted from the beginning of the test. Hysteresis loops under the constant displacement were shown only for the first and last loading. The calculated ultimate bending strength shown by dashed line in Fig. 7(a) is based on the formula (2). The dashed line shown in Fig. 8(a) which means ultimate shear strength was calculated from the following formula (7).

$$Q_u = b_j \left[\frac{0.082 k_p (180 + F_c)}{a/d + 0.115} + 2.7 \sqrt{p_w \sigma_y} \right] + 0.1 N \dots \dots \dots (7)$$

$$k_p = 0.82 p_t^{0.23}$$

where,

b, j : width and effective depth of column, respectively (cm)

Q_u : ultimate shear strength (kg)

F_c : compressive strength of concrete (kg/cm^2)

N : axial force applied to the column (t)

a/d : shear span ratio

p_w : shear reinforcement ratio

σ_y : yield stress of shear reinforcing bar (kg/cm^2)

p_t : tensile reinforcement ratio (%)

From shear-deflection curves the following remarks may be derived.

- 1) Original columns were not ductile. Almost of the initial restoring

force was rapidly lost after a few repetitions. They kept their calculated ultimate strength within only the limited deformation.

2) Maximum strength of the strengthened column was 1.25 to 1.5 times as strong as the original column.

3) The restoring force of the strengthened column specimen at large displacement over maximum strength point, at the first displacement of 60×10^{-3} rad. for example, was larger than 80% the maximum strength of each specimen. In contrast, original long column specimen kept only 32% its maximum strength and original short column specimen already collapsed.

4) The effect of the strengthening was more remarkable in short column than in long columns. Pipe type was most effective among the types.

Figs. 9 shows the reduction of restoring force of the specimens at $R = 15 \times 10^{-3}$ rad. under alternately repeated distortion, which is indicated as normalized average values for positive and negative loads.

Fig.10 shows the relationship between the elongation or shortening of axial length and the displacement of specimen, plotting the values at the peak load in the first loading of each constant displacement.

Figs.11 shows the same plotting of the residual values at the complete unloading in the first and last cycles of each displacement. From these figures, it may be seen that the more the strengthening effective, the more the columns elongate and that original columns shortened at the large displacement and short original column collapsed due to axial force at the final state.

Fig.12 shows the specimens after testing. L specimen failed in bending and the covering concrete spalled off at the ends. □ - L, □ - S and ⊠ - S specimens also failed in bending at the ends. Concrete failed and strengthening steel plate buckled at the compression side, and main rebars were elongated at the tension side of the section.

○ -L specimen was little damaged. S specimen failed in shear and swelled and collapsed due to axial load.

7. CONCLUDING REMARKS

(1) Original column with small shear reinforcement had poor ductility and lost most of its initial restoring force after a few repetitions of cyclic loading. This deterioration of earthquake resistance was more conspicuous in short column than in long column.

(2) The strengthening method investigated herein, in spite of its easy work and cheap cost, proved to give remarkable effects on the improvement of the earthquake resistance of these weak columns. The effects were more remarkable in short columns than in long columns. Pipe type had the most remarkable effects among the strengthening types investigated herein.

(3) It was found that the strengthening effects were obtained by the surrounding steel plate which prevented the column concrete from spalling off and maintained the confinement. The continuity at the interface between the grouted mortar and the original column was lost during alternately repeated distortions. If the continuity between them could be obtained the strengthening effects would be improved further.

This investigation had been carried out under the leadership of Prof. Muto and Dr. Hisada to whom the authors express many thanks.

REFERENCES

- 1) Architectural Institute of Japan; Report on the investigations of damage due to 1968 Tokachi-Oki Earthquake, Dec., 1968.
- 2) Architectural Institute of Japan; A.I.J. standard for structural calculation of reinforced concrete structure revised in 1962.
- 3) Ditto, Revised in 1971.
- 4) T. Arakawa; Experimental studies on shear strength of reinforced concrete beams - Conclusions -, Trans. of A.I.J., No. 66, Oct., 1960.
- 5) Architectural Institute of Japan; A.I.J. standard for structural calculation of steel pipe concrete structure, 1967.
- 6) T. Odaka and K. Saito; Experimental studies on steel pipe light weight concrete columns, Trans. of A.I.J., No. 103.
- 7) H. Muguruma, S. Morita and K. Tomita; Fundamental study on bond between steel and concrete, Trans. A.I.J., No. 131, Jan., 1967.
- 8) P. Gulkan and M. Sozen; Response and energy dissipation of reinforced concrete frames subjected to strong base motions, Civil Eng. Studies, Structural Research Series No. 377, Univ. of Illinois, 1971.

Table 1 Test Programm & Name of Specimen

	Existing Column	Fortification Types		
		BOX	PIPE	BAND
Long Column Series	L	□ - L	○ - L	—
Short Column Series	S	□ - S	—	⊞ - S

Table 2 Physical Properties of Steel Plate and Reinforcing Bars

Test Piece		Cross Section		Yield Point (kg/mm ²)	Tensile Strength (kg/mm ²)	Elongation (%)	Notes
		Thickness or Diameter (mm)	Sectional Area (mm ²)				
Steel Plate	⊞ - 2.3	2.28	57.0	31.9	46.7	26.4	S S 41
	⊞ - 4.5	4.41	110.4	33.0	44.4	22.6	S S 41
Re-Bar	6 ϕ	5.51	23.8	-	50.9	28.4	S R 24
	19 ϕ	18.92	280.9	34.3	52.2	27.4	S R 24

Table 3 Cylinder Test of Concrete

Specimen	Compressive Strength σ_B (kg/cm ²)	Modulus of Elasticity $\times 10^5$ (kg/cm ²)	Muximum Strain ϵ_B ($\times 10^{-3}$)	Age (day)
L	224	2.06	2.49	41
○ - L □ - L	211	2.33	2.48	58
S	231	2.37	2.16	69
- S ⊞ - S	241	2.01	2.59	85

Note: Test pieces were put in the air near the specimen

Table 4 Mix Design and Cylinder Test of Grouting Mortar

Mix Design			Test Results			
Weight Proportion	W/C	Flow	Tensile Strength (kg/cm ²)	Compressive Strength (kg/cm ²)	Expansion (x10 ⁻⁴)	Age (day)
Cement : CSA : Sand						
0.89 : 0.11 : 1.00	0.45	14sec	80.0	385.0	+2.09	61

Table 5 Loading Scheme
Long Column Series

Cycle No.	1	2 - 11	12 - 21	22	23 - 27	28	29
Load Control	0.7Q _y	Q _y *					
Displacement Control		δ _y *	2 δ _y	δ _y	4 δ _y	3 δ _y	6 δ _y

* shear and displacement at the yielding of L specimen.

Short Column Series

Cycle No.	1	2	3 - 7	8 - 12	13-17	18
Displacement Control(rad)	1/1,000	1/500	1/200	1/100	1/50	1/25

Table 6 Restoring Forces (ton)

Characteristic Points	Series Specimen	Long Columns			Short Columns		
		L	□-L	○-L	S	□-S	⊘-S
Bending Crack	Exp.	15.0	-	-	15.0		
	Cal.	9.4			15.5		
Shear Crack	Exp.	25.0	-	-	27.5		
	Cal.	15.8			18.9		
Bending Yield	Exp.	32.5	40.0	46.5			
	Cal. ¹⁾	37.1			61.2		
Shear Yield	Exp.				37.5	55.0	55.0
	Cal. ²⁾	28.0			36.7		
Maximum Strength	Exp.	33.0	41.2	50.0	40.9	60.0	59.6
Failure Mode		B. F	B. F	B. F	S. F	B. F	B. F

- Notes: 1) Based on the formula (2)
 2) Based on the formula (7)
 3) B. F and S. F mean bending failure and shear failure, respectively.

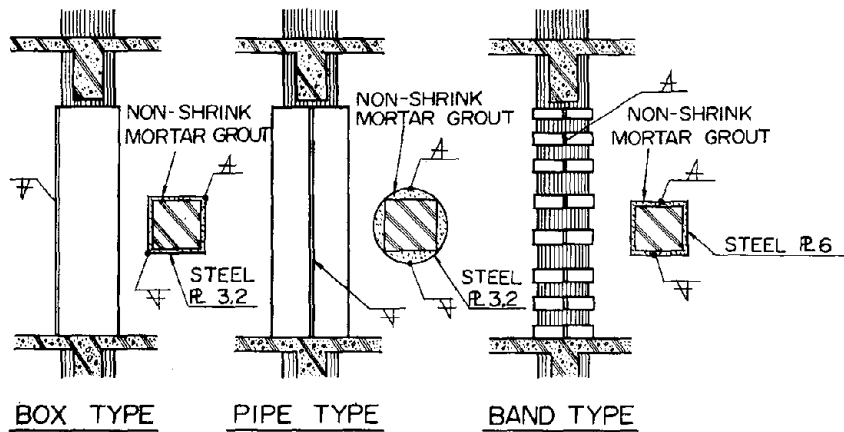


Fig. 1 Strengthening Methods

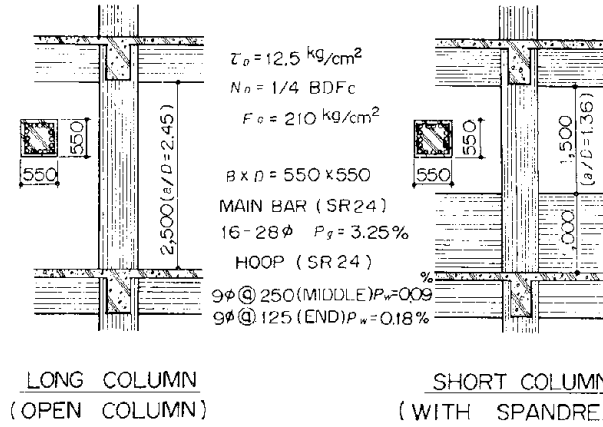


Fig. 2 Two Types of Column in a Existing Reinforced Concrete Building

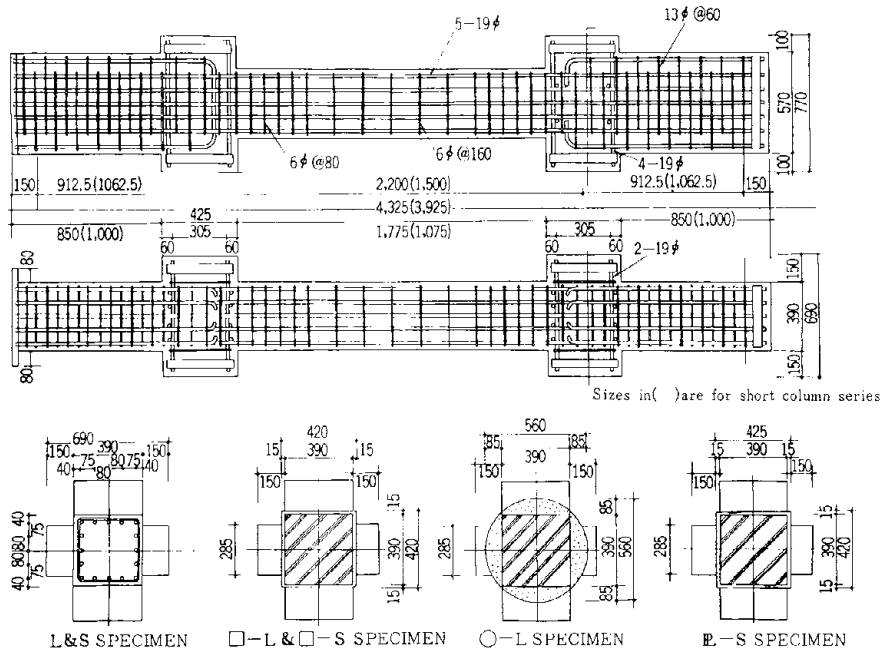


Fig. 3 Specimen Details

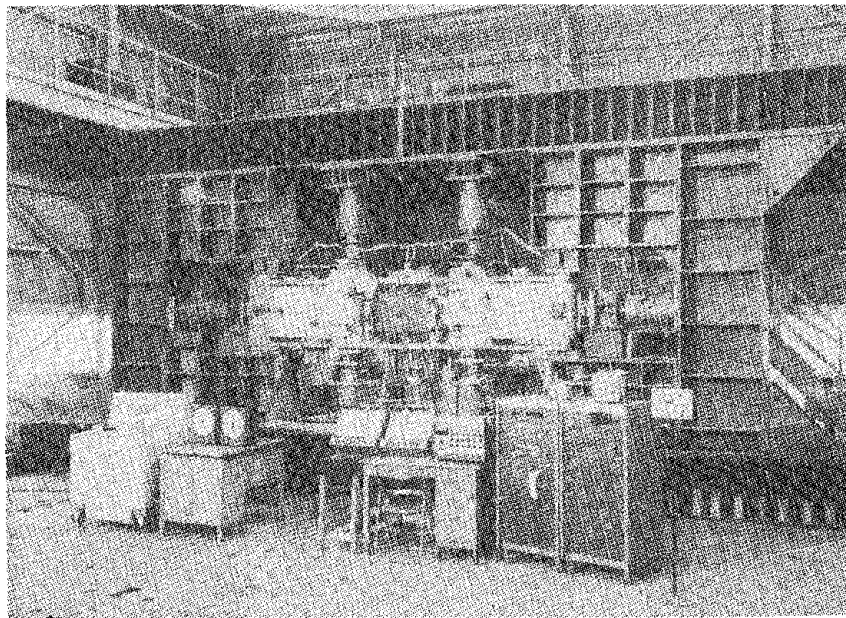


Fig. 4 Over All View of Test Arrangement

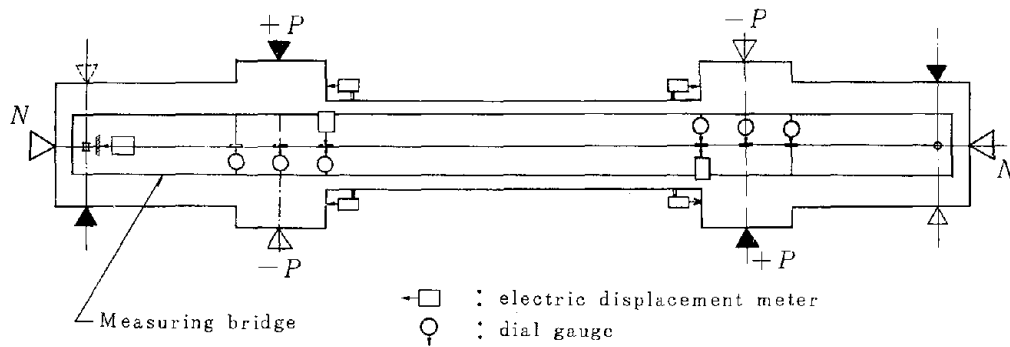


Fig. 5 Method of Loading and Measurement

$$\delta = \delta_V + \delta_R$$

$$\delta_V = \delta_{V1} + \delta_{V2}$$

$$\delta_R = h/2 (\theta_{B1} + \theta_{B2})$$

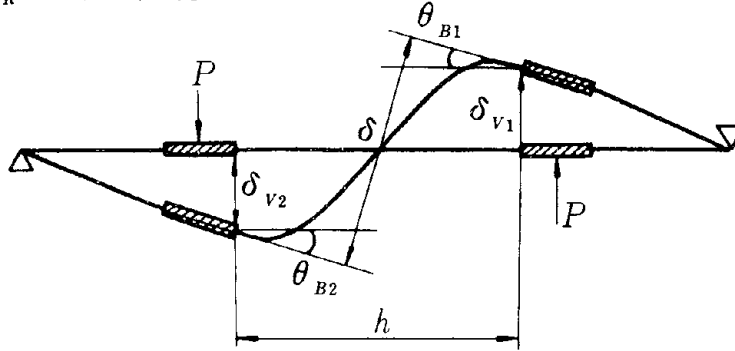


Fig. 6 Story Deflection

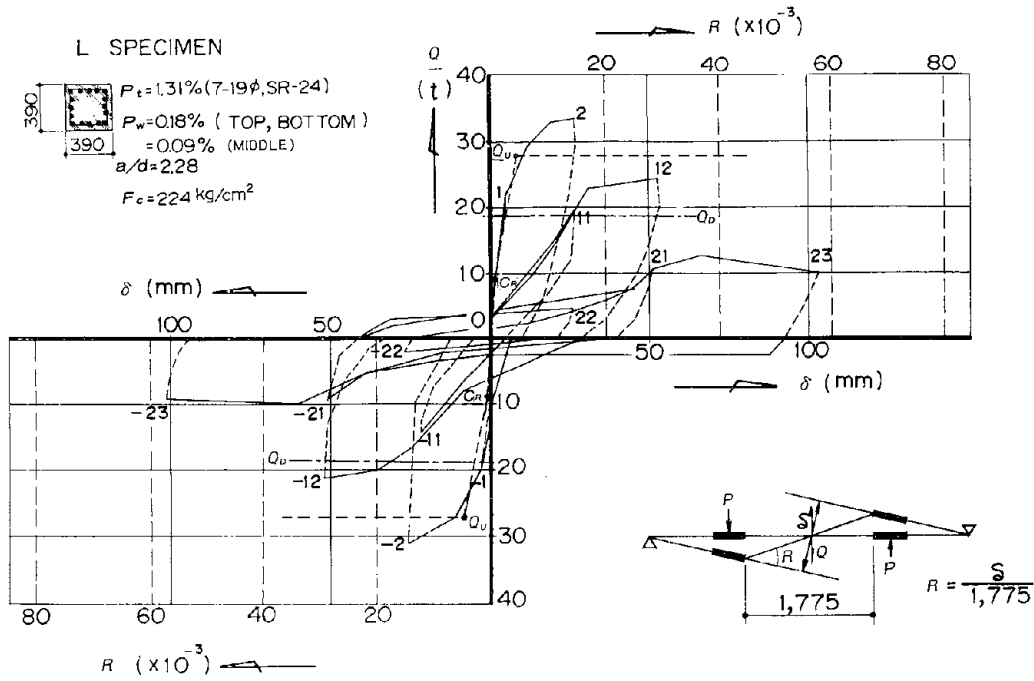


Fig. 7 (a) $Q-\delta$ Curve of L Specimen

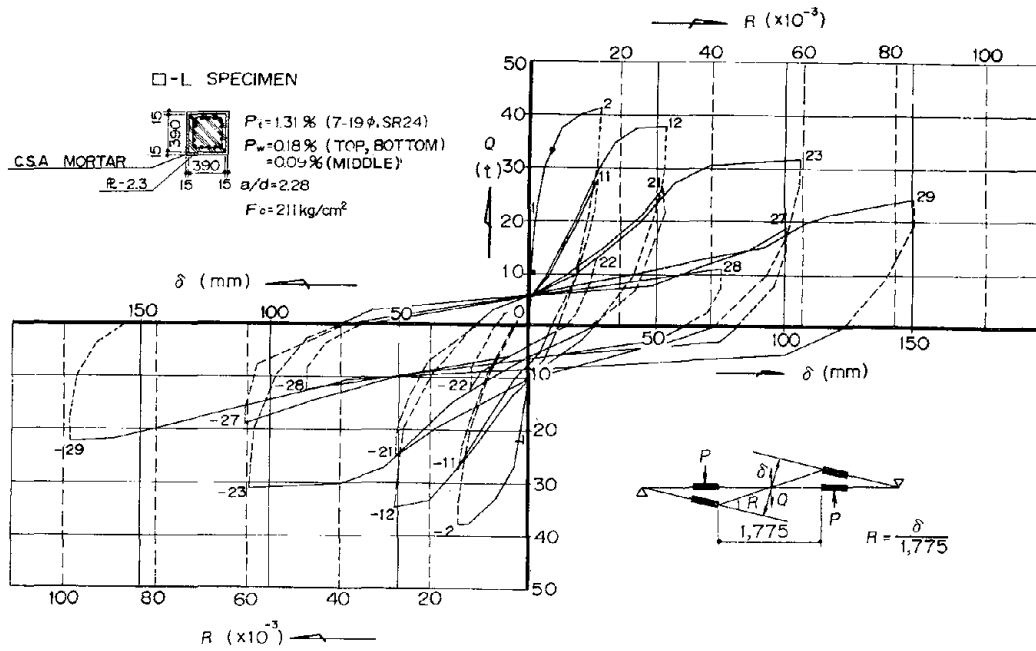


Fig. 7 (b) $Q-\delta$ Curve of □ - L Specimen

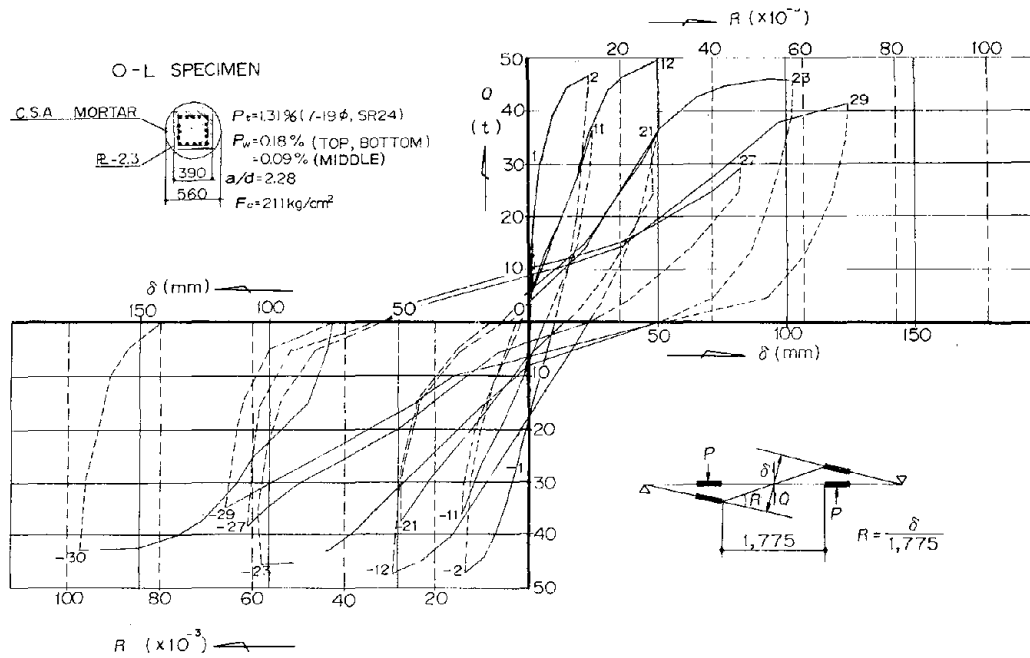


Fig. 7 (c) $Q-\delta$ Curve of ○ - L Specimen

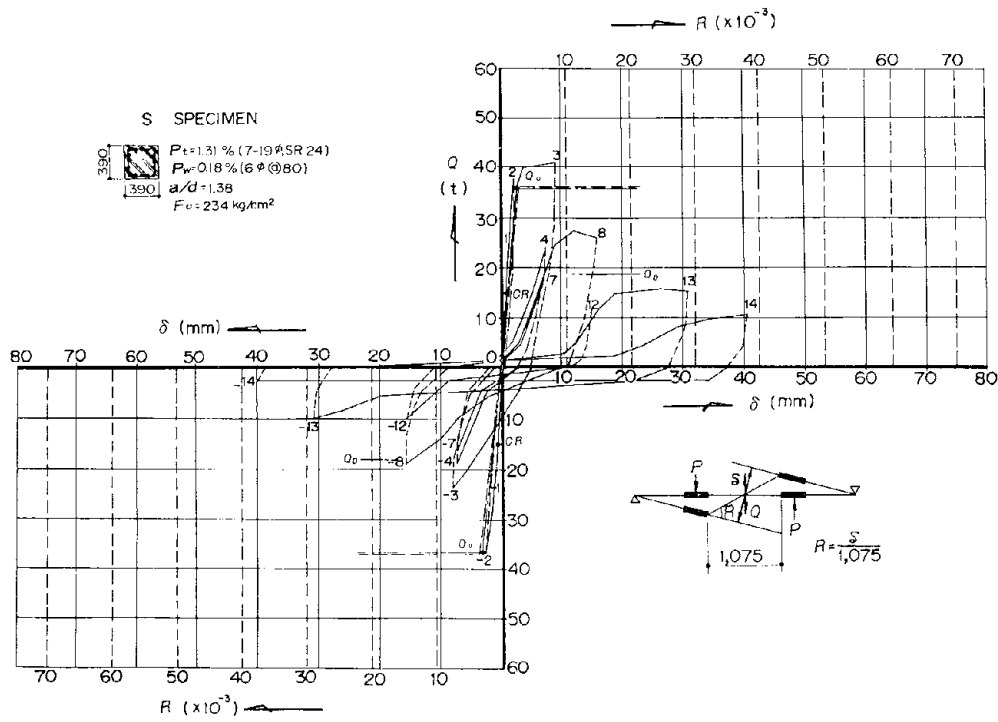


Fig. 8 (a) $Q-\delta$ Curve of S Specimen

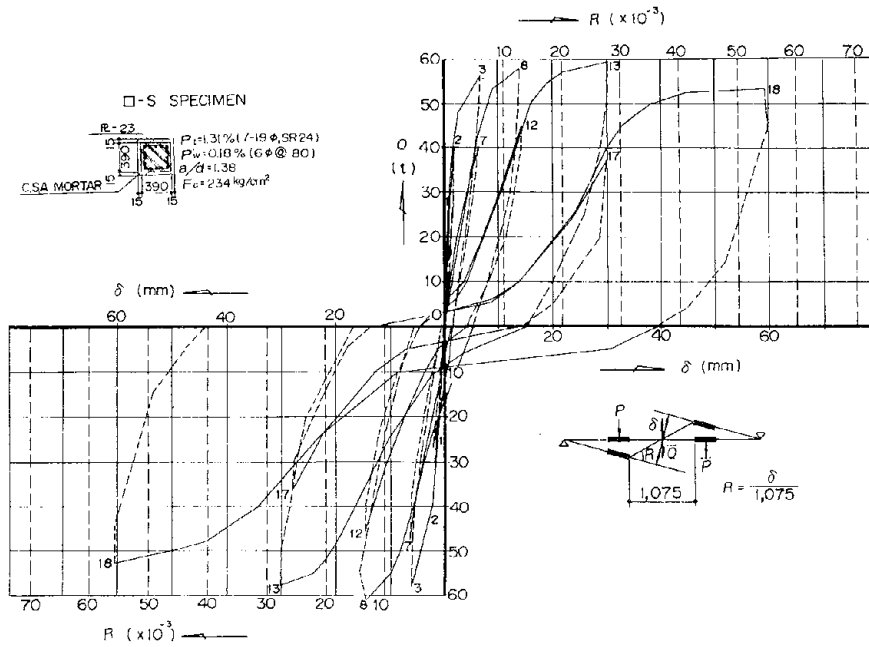


Fig. 8 (b) $Q-\delta$ Curve of □ - S Specimen

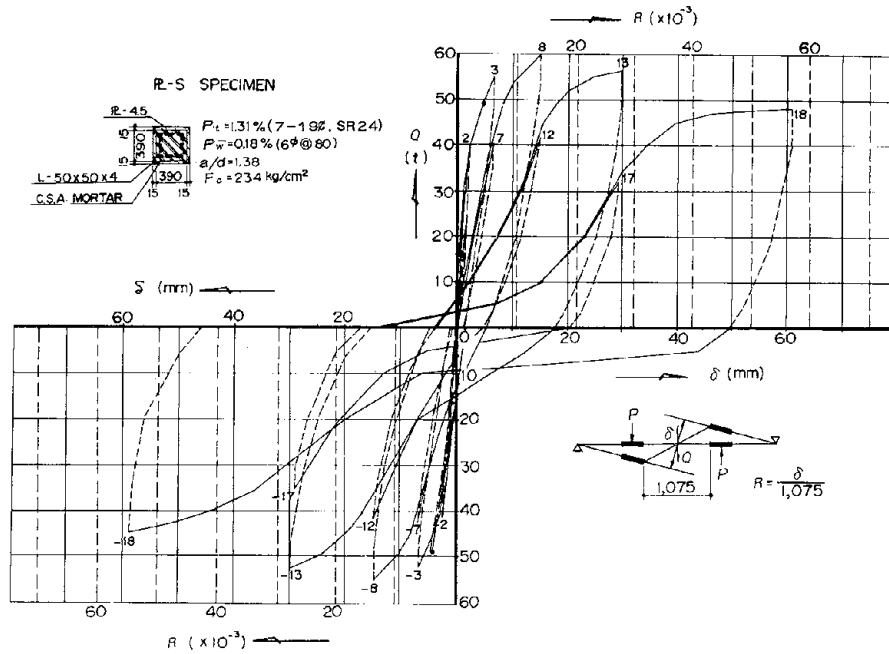


Fig. 8 (c) $Q-\delta$ Curve of R - S Specimen

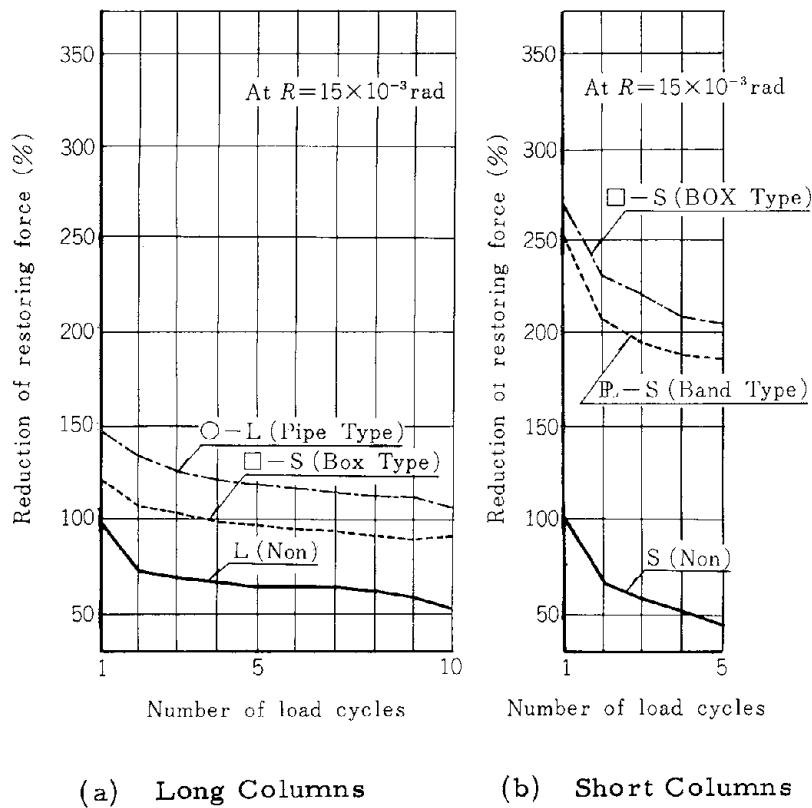


Fig. 9 Reduction of Restoring Force Under Alternately Repeated Distortion

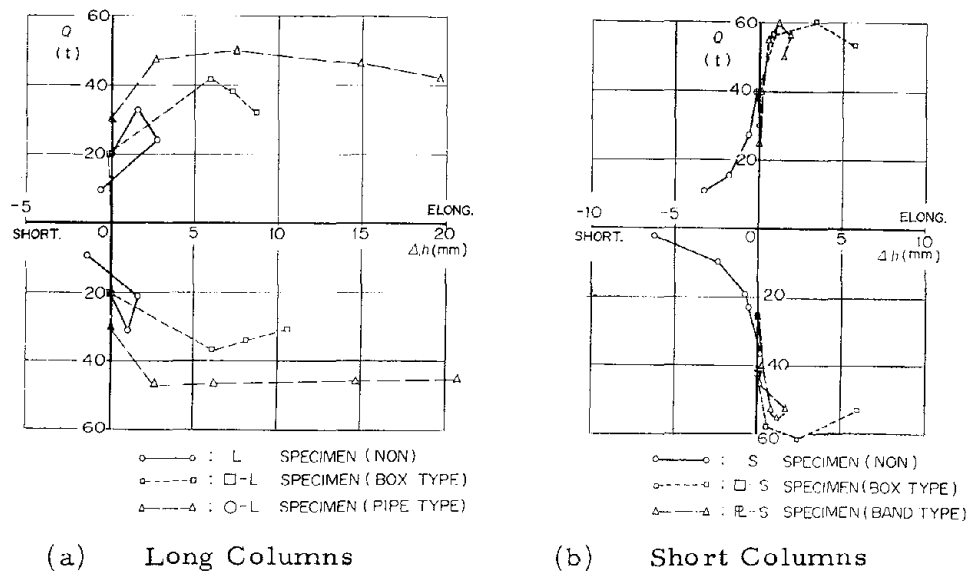


Fig. 10 Variation of Axial Length of Column

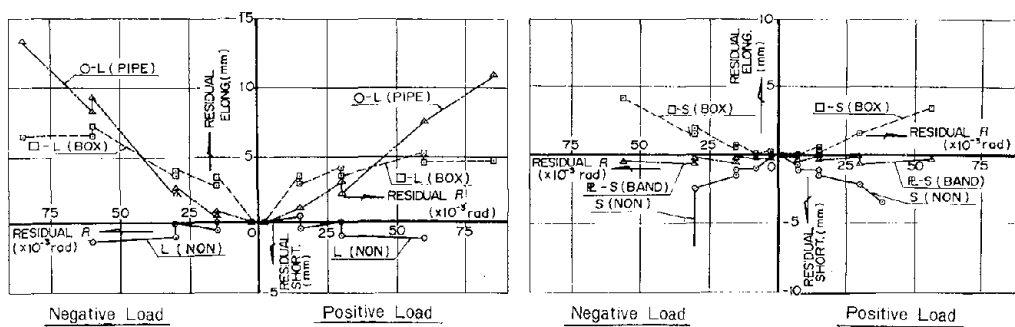
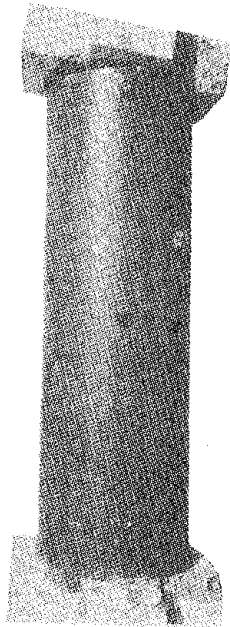
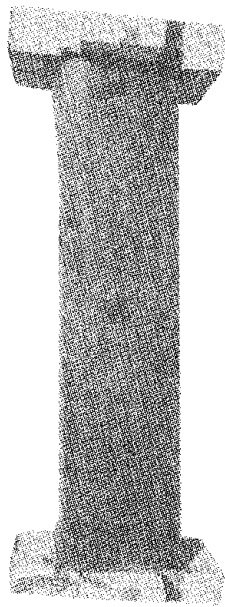


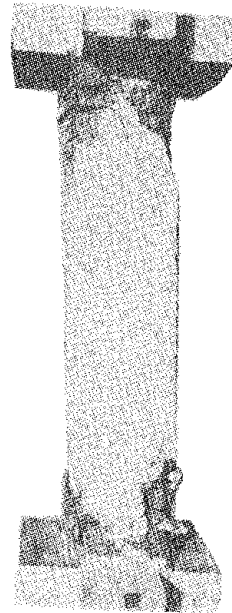
Fig. 11 Relationship Between Residual Displacement and Residual Column Length



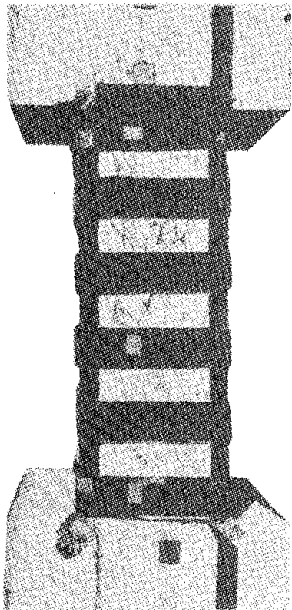
○ - L Specimen



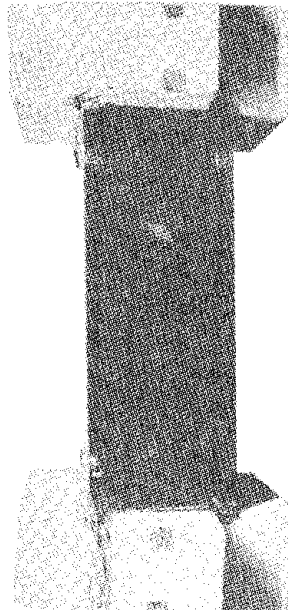
□ - L Specimen



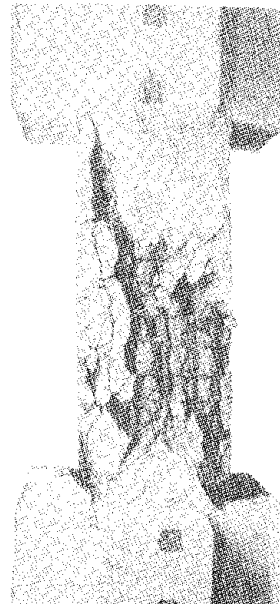
L Specimen



L - S Specimen



□ - S Specimen



S Specimen

Fig. 12 Specimens after Test

by

Duane L. N. Lee (i), James K. Wight (ii) and Robert D. Hanson (iii)

SYNOPSIS

An investigation on the effectiveness of repaired reinforced concrete exterior beam-column subassemblages is presented. The epoxy injection technique and the removal and replacement technique using different high early strength materials were used to repair the specimens. Details of the repair procedure along with the strength properties of the materials used in the repairs are given. Based on the results, it is concluded that epoxy injection, and removal and replacement methods of repair can restore structural integrity to the members.

INTRODUCTION

It is recognized as impractical, if not impossible, to design a structure which will withstand a severe earthquake without damage. Structural and nonstructural damage should be anticipated during a severe earthquake. The repair of this damage should at least restore the structure to its previous capacity to resist gravity and lateral loads and in many instances, an increase in the lateral load resistance capability would be desirable. In practice when the damaged region is repaired with higher strength material, the repair is assumed to be sufficient to carry gravity loads. However, it is not known if the capability of the structure to withstand seismic loads has been restored. It may be necessary to strengthen the structure during repair to insure sufficient lateral stiffness and strength. As the amount of earthquake produced structural damage accumulates, there will be an increasing need to understand the behavior of repaired structural members as well as to determine the effectiveness of rehabilitation schemes for a structure.

REPAIR AND BEHAVIOR

In practice structures that have survived an earthquake with only minor damage will usually be repaired by epoxy injection. More extensive damage will necessitate complete removal of the loose concrete and filling of the resulting void with material of the same or higher strength. It is desirable to use a high early strength material so that the structure can be repaired and reoccupied in the shortest possible time.

(i) Graduate Student in Civil Engineering
(ii) Assistant Professor of Civil Engineering
(iii) Professor of Civil Engineering
The University of Michigan, Ann Arbor, Michigan, USA.

EPOXY INJECTION

Technique. Epoxy injection is a technique where low viscosity epoxy is injected into cracks to restore continuity in the member and bond between the concrete and reinforcing steel. A procedure used by Sika Chemical Corporation (i) for the repairs discussed in Appendix A is as follows. Polyethylene check valve nipples in which reverse flow in the valves are permitted if the stopper in the valve is depressed were located along the crack on both sides of the specimen for cracks penetrating the entire width of the member. For narrow cracks, the nipples were spaced closer together. High viscosity epoxy was used to seal over the cracks and around the nipples to prevent escape of the injected epoxy material. After the sealant cured, a caulking gun was used to inject low viscosity epoxy into the nipple at the lowest elevation while the higher elevation valve stoppers were depressed to bleed off air and witness epoxy overflow. When overflow was evident in the nipples of next higher elevation on both sides of the specimen, the crack between the injected and overflowing nipples was assumed to be saturated with epoxy. The injection process now shifted to the overflowing nipples and the process repeated until the entire crack has been saturated. If leakage of epoxy occurs in the sealed cracks or around the base of the nipples during the injection process, a bar of soap is rubbed over the area of leakage to provide a temporary seal. If this method fails, the epoxy injection process is delayed until the sealant can be reapplied. Figure 1 shows the location of the nipples and the injection. After repairs, the sealant can be heated and scraped off to return the member to its original smooth surface.

Epoxy injection repairs made at the University of California (1),(2), (3) by Adhesive Engineering Company used a similar procedure. However, no check valve nipples were used to receive the epoxy. Instead, epoxy was injected directly into unsealed ports along the crack. Small lengths of unsealed cracks were used to witness epoxy overflow which were then rubbed with paraffin to prevent further escape of the material. This procedure is satisfactory if there is no leakage of epoxy in the paraffin sealed cracks. If leakage occurs under pressure, the penetration of epoxy into unsaturated cracks may be incomplete.

Behavior. To date the amount of research on the effectiveness of members repaired with epoxy injection is limited. Investigators at the University of California have used this technique to repair members and frames. Celebi and Penzien (2) found the epoxy injection technique to be effective in restoring a beam's stiffness, strength and energy dissipation capabilities. However, Mahin, Bertero, Atalay and Rea (1) found the stiffness and strength were restored, but the energy dissipation capabilities were reduced. Also, Mahin, et al (i), and Hidalgo and Clough (3) expressed doubt on the effectiveness of the epoxy injection technique to restore the bond between the reinforcement and concrete.

Recent tests on beam-column subassemblages described in Appendix A shows the epoxy injection technique to adequately restore structural integrity to the member. The hysteresis loops in Figs. 2a and 2b for

(i) Sika Chemical Corporation, Lundhurst, New Jersey, USA.

Specimen 1 indicate the repaired specimen has equivalent stiffness, strength, and energy dissipation capability as the original specimen. Nominal strengths of the epoxy-neat material used in the repairs are given in Table 1.

REMOVAL AND REPLACEMENT

The only effective method of repairing severely damaged structural members is to remove the damaged material and replace it with new material. The repair should satisfy the latest code requirements as suggested by Fratt (4). For the repairs made during this investigation, high early strength materials were used.

Properties of Repair Materials. Strength and stiffness properties of the materials used in the repair of beam-column subassemblages in Appendix A are tabulated in Table 1. Except for the epoxy-neat material, the test specimens were 4 in. by 8 in. (10.16 cm by 20.32 cm) cylinders that were manufactured and cured in the laboratory. Because the comparison was made against Portland Cement concrete, the rate of loading during testing was the same as that suggested by ASTM (5) for concrete. The tensile strengths were obtained from the standard splitting test. The values listed in Table 1 show that these materials have high three day compressive strengths. The tensile strengths are comparable to that of Type I Portland Cement concrete except for the epoxy materials which are significantly higher.

Stiffness properties given in Table 1 were obtained from stress-strain curves such as those shown in Fig. 3. The modulus of elasticity was obtained by taking the secant modulus up to 0.45 of the ultimate load. Fig. 3 and Table 1 indicate the epoxy materials have a lower stiffness than regular (Type I Portland Cement) concrete and have larger strains at ultimate load. The stiffness of the other non-epoxy type materials in Fig. 3 and Table 1 are comparable to regular concrete.

For cyclic loading in the inelastic range, the following are considered to be ideal mechanical properties for repair material:

- 1) Compressive strength equal or greater than adjacent regions.
- 2) Stiffness comparable to that of adjacent regions.
- 3) High ultimate strains to delay crushing.

Technique. For the investigation given in Appendix A, the procedure for the removal and replacement type of repair is as follows. Loose concrete was removed by a hammer and chisel although electric and pneumatic tools can be utilized. Buckled bars were straightened as much as possible and when required, shear reinforcement was added in the void area during repairs (Fig. 4) to satisfy the current American Concrete Institute Building Code (6) requirements for shear and confinement. The reinforcement and existing concrete surfaces were then sandblasted if epoxy was to be used to improve the bond between the new and original material. Wood forms, covered with polyethylene were erected to enclose the existing void. The polyethylene was used to protect the forms from

the epoxy although other materials may be used. If epoxy was used, it was painted on the existing surfaces before placing the new material. After placement, the new material was vibrated to eliminate voids.

The prepack method of placement was utilized when epoxy-sand mortar was used in the repair. For this procedure, the sandblasted surfaces of concrete and steel were coated with epoxy after erecting tightly fitted forms. One inch (2.54 cm) layer of aggregate was placed in the void and then saturated with low viscosity epoxy. Additional one inch layers of aggregate were placed and saturated until a total thickness of five inches (12.70 cm) was attained. A delay of several hours was taken before starting the next five inch accumulation in order to dissipate the heat generated by the chemical reaction during epoxy curing. For smaller void areas, a deeper accumulation is possible before a pause is required. This method maximizes the strength of the material by minimizing the air voids in the mortar which are created by mixing.

Behavior. Previous investigation by Lee and Hanson (7) has shown that repairing the connection with a high strength material can shift the damage from the joint into the beam and/or columns.

For the tests described in Appendix A, the removal and replacement technique was effective as shown by the hysteresis loops for Specimen 2 in Figs. 5a and 5b. The damage from both original testing and retesting occurred in the beam. A comparison of the hysteresis loops in Figs. 5a and 5b indicate the stiffness, strength, and energy dissipation capability was restored during repairs.

The repaired beams were stronger during retest due to the use of high strength materials and strain hardening of the steel during original testing. Because of the increase in strength, the damage during retest often moved into the joint and/or column which were damaged during original testing, but were not repaired. Joint used in this context implies the column at the level of the beam. In practice, the minor cracks that are too narrow to epoxy inject are usually not repaired. An example of this can be shown by the photographs in Figs. 6a and 6b and by the hysteresis loops in Figs. 7a and 7b for Specimen 6. A comparison of hysteretic behavior shows that the load and energy dissipation degrades more rapidly during retest than during the original test. The difference in hysteretic behavior is due to the change in behavior from a flexural type in the beam during original testing to a shear type in the joint during retest. Another indication of joint deterioration can also be seen by comparing the joint distortion as shown in Figs. 8a and 8b for Specimen 6.

Brittle material should be avoided in repairs. Because of its low ultimate strains, these materials will usually crush sooner during bending action and cause a sudden loss of the beam's compression zone cover, thus reducing the beam's cross-section. Also, after these materials are cracked in tension, smooth crystalline planes that offer little resistance to shear slippage during load reversals are formed.

Epoxy used as a bonding agent needs further investigation. Observation after retesting showed no traces of residual epoxy on the reinforcing

bars in the damaged area. Also for Specimen 7, where epoxy was used to bond the first lift of repair material to the second lift, the repair material separated at the construction interface after a few cycles of inelastic loading. Further examination showed the epoxy to bond only to the second lift. Therefore, it is suggested that epoxy used with different materials should be laboratory tested before field utilization.

REHABILITATION

The purpose of rehabilitation as used herein is to increase the lateral strength and stiffness of the structural system so that it is capable of safely resisting larger earthquake ground motions. There is little laboratory data available to verify the effectiveness of various rehabilitation techniques. Current experimental studies at The University of Michigan have been planned to determine the effectiveness of rehabilitation of moment frame structures with infill wall panels. The first series of tests will include (a) cast-in-place reinforced concrete wall, (b) single panel precast reinforced concrete wall, and (c) multiple panel precast reinforced concrete wall. A monolithic infill shear wall and an open moment frame provide the limiting conditions for evaluation of these three rehabilitation techniques. It is expected that this data will be available in October 1975 (8).

CONCLUSION

The behavior of repaired reinforced concrete beam-column subassemblies using the epoxy injection, and removal and replacement repair techniques was presented. Based on the results of the investigation, the following conclusions are suggested.

1. Epoxy injection, and removal and replacement repair techniques can be used to restore structural integrity to the member.
2. Repair of the beam may result in the damage moving to the joint and/or column during inelastic cyclic action.
3. Brittle materials may be less suitable for certain repair situations.
4. The effectiveness of epoxy as a bonding agent between reinforcing steel and new concrete is unknown for inelastic cyclic loading.

ACKNOWLEDGEMENT

The repair and retesting program was supported by National Science Foundation Grant GI39123. However, any opinions, findings, conclusions or recommendations expressed herein are those of the authors and do not necessarily reflect the views of NSF. The repair material and technical assistance were furnished by Messrs. Andrew Rossi and Raymond Schutz of Sika Chemical Corporation, Robert Best of Republic Steel Corporation, and William Bleecker of United States Gypsum Company.

REFERENCES

1. Mahin, S., V. Bertero, M. Atalay and D. Rea, "Rate of Loading Effects on Uncracked and Repaired Reinforced Concrete Members," Earthquake Engineering Research Center, University of California, Berkeley, California, Report No. EERC 72-9, December 1972.
2. Celebi, M. and J. Penzien, "Hysteretic Behavior of Epoxy-Repaired Reinforced Concrete Beams," Earthquake Engineering Research Center, University of California, Berkeley, California, Report No. EERC 73-5, February 1973.
3. Hidalgo, P. and R. Clough, "Earthquake Simulator Study of a Reinforced Concrete Frame," Earthquake Engineering Research Center, University of California, Berkeley, California, Report No. EERC 74-13, December 1974.
4. Fratt, J., "Structural Repair of Earthquake Damaged Buildings," Presented at the ASCE National Structural Engineering Meeting, San Francisco, California, April 1973, Preprint No. 1973.
5. American Society for Testing and Materials, 1971 Annual Book of ASTM Standards, Part 10, Philadelphia, Pennsylvania, 1971.
6. American Concrete Institute, Building Code Requirements for Reinforced Concrete (ACI 318-71), Detroit, Michigan, 1971.
7. Lee, D. and R. Hanson, "Inelastic Behavior of Repaired Beam-Column Connections," Presented at US-Japan Seminar on Earthquake Engineering, Berkeley, California, September 1973.
8. Kahn, Lawrence F., "Infilled, Reinforced Concrete Shear Walls for Aseismic Rehabilitation," Ph.D. Dissertation, University of Michigan, Ann Arbor, Michigan, (in progress).
9. Lee, Duane L.N., "Original and Repaired Reinforced Concrete Beam-Column Subassemblages Subjected to Earthquake Type Loading," Ph.D. Dissertation, University of Michigan, Ann Arbor, Michigan, (in progress).

Table 1. Strength and Stiffness Characteristics of Material Used in Repairs.
(1 ksi = 6.89 N/mm²)

Material	3-Day Compressive Strength (psi)	28-Day Compressive Strength (psi)	3-Day Tensile Strength (psi)	28-Day Tensile Strength (psi)	3-Day Modulus of Elasticity (psi)	28-Day Modulus of Elasticity (psi)
Epoxy- Neat (i)	10,400	12,000		4,900 (ii)	260,000	490,000
Epoxy-Sand Mortar (iii)	8,400	9,900	740	920	2,000,000	2,200,000
Duracal Cement Concrete (iv)	4,800	7,200	430	570	3,200,000	4,000,000
High Strength Quick Setting Concrete (v)	5,000	7,900	420	610	3,600,000	4,200,000
High Early (Type III) Concrete		7,000 (vi)				4,300,000 (vi)

(i) Data supplied by Sika Chemical Corporation, Lyndhurst, New Jersey, USA

(ii) Based on 14 days.

(iii) Sand had uniformity coefficient of 1.33 and a D₅₀ of 1.55 mm.

(iv) Produced by United States Gypsum Company, Chicago, Illinois, USA.

(v) Developed by Republic Steel Corporation, Cleveland, Ohio, USA

(vi) Based on 18 days.

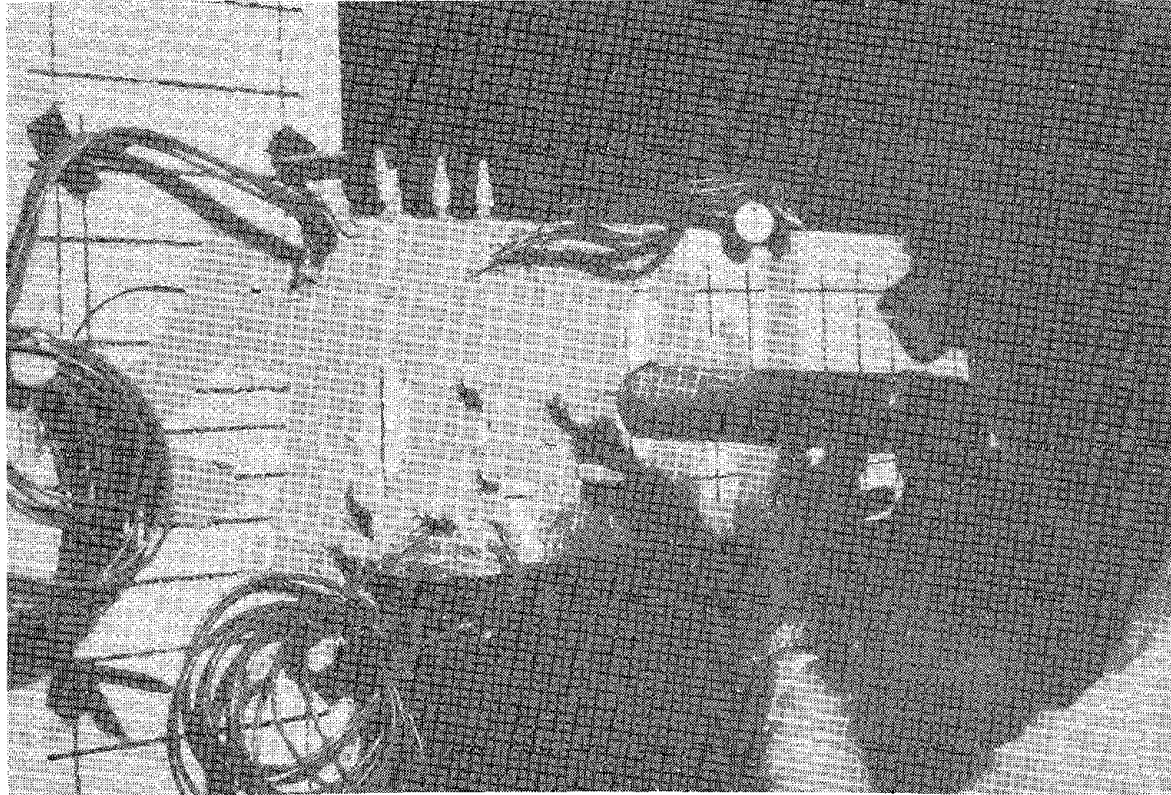


Figure 1. Epoxy injection in progress after locating the nipples and sealing the cracks.

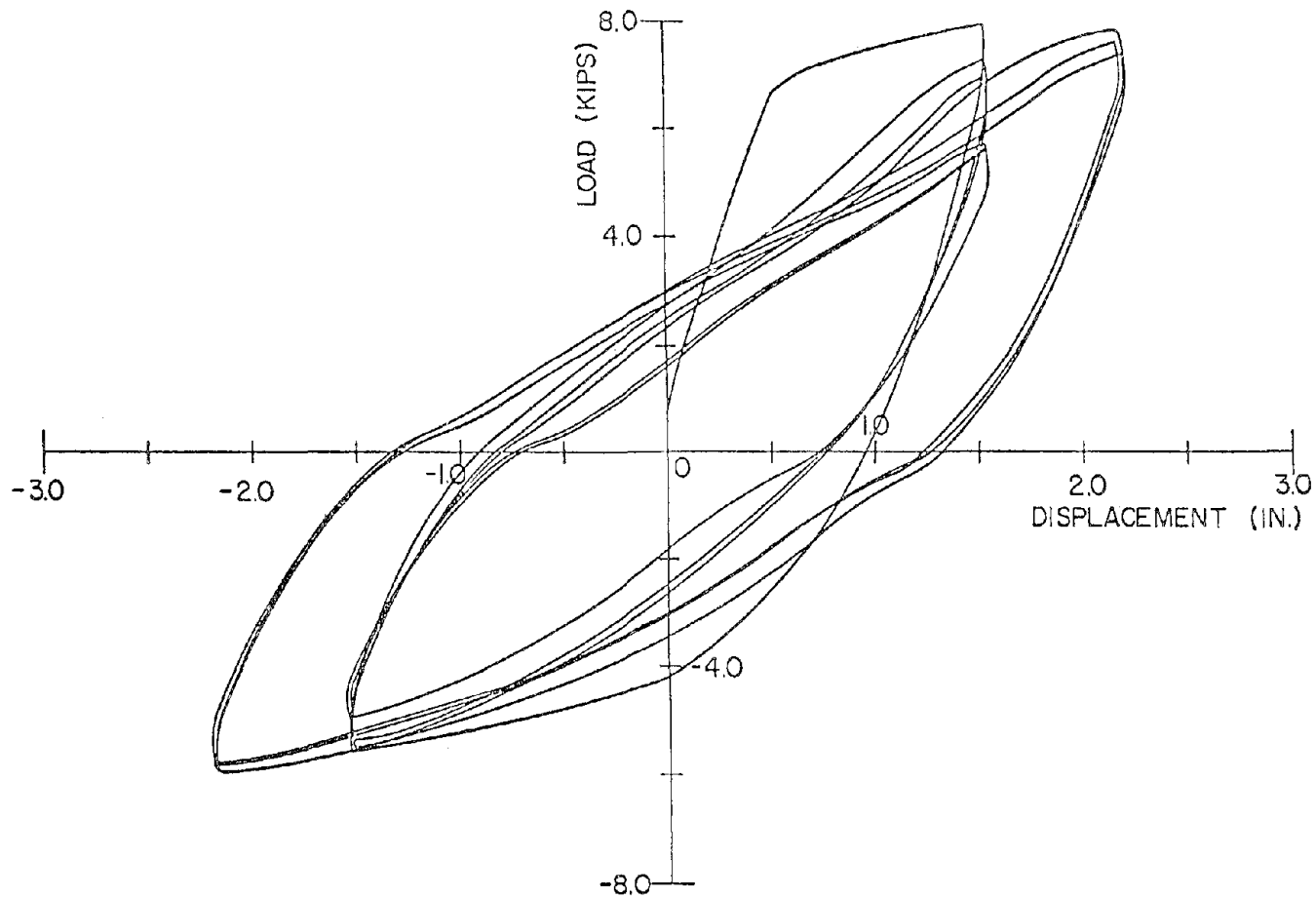


Figure 2a. Beam-tip force vs. deformation curves for original Specimen 1.
(1 kip = 4450 N and 1 in. = 2.54 cm)

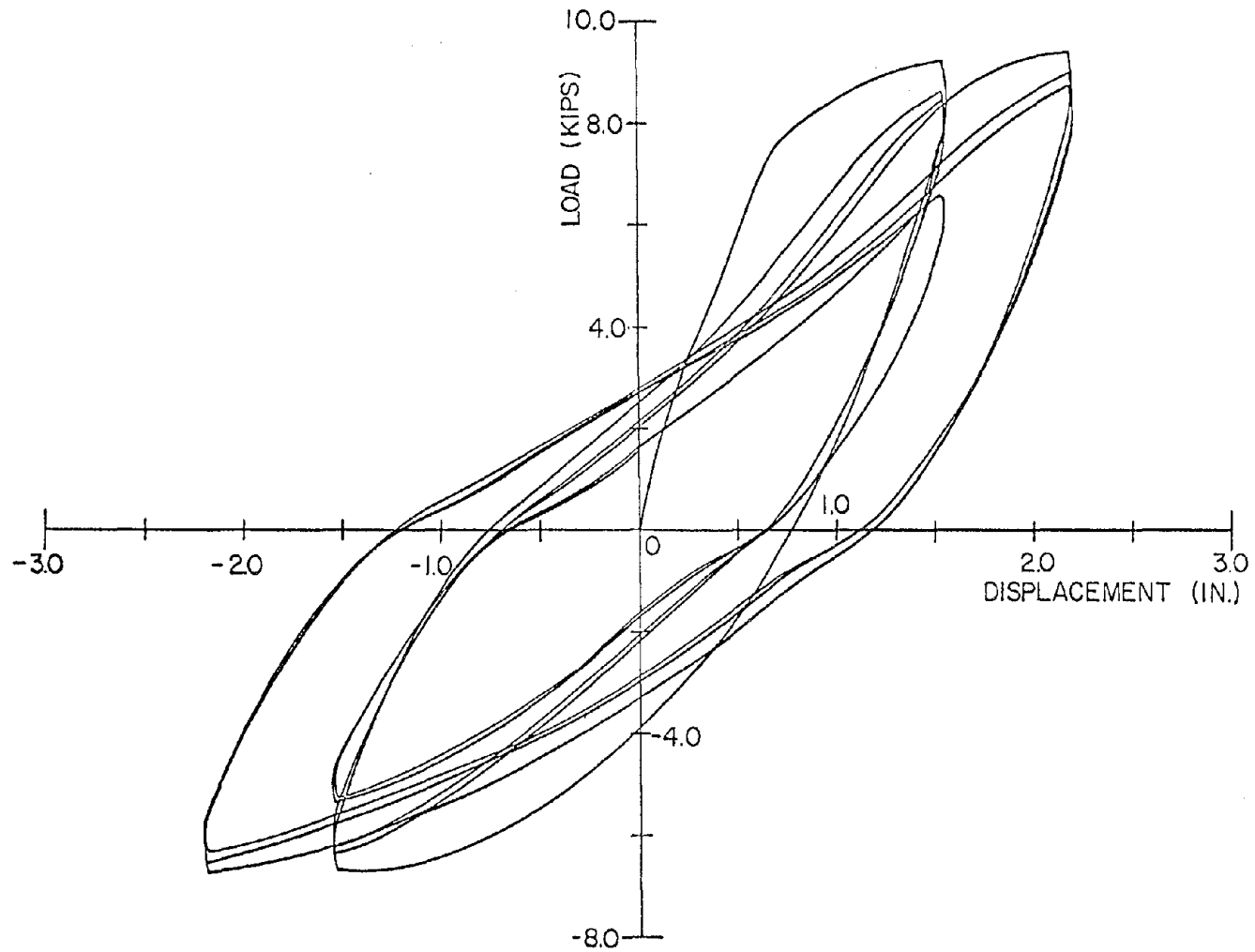


Figure 2b. Beam-tip force vs. deformation curves for repaired Specimen 1.
(1 kip = 4450 N and 1 in. = 2.54 cm)

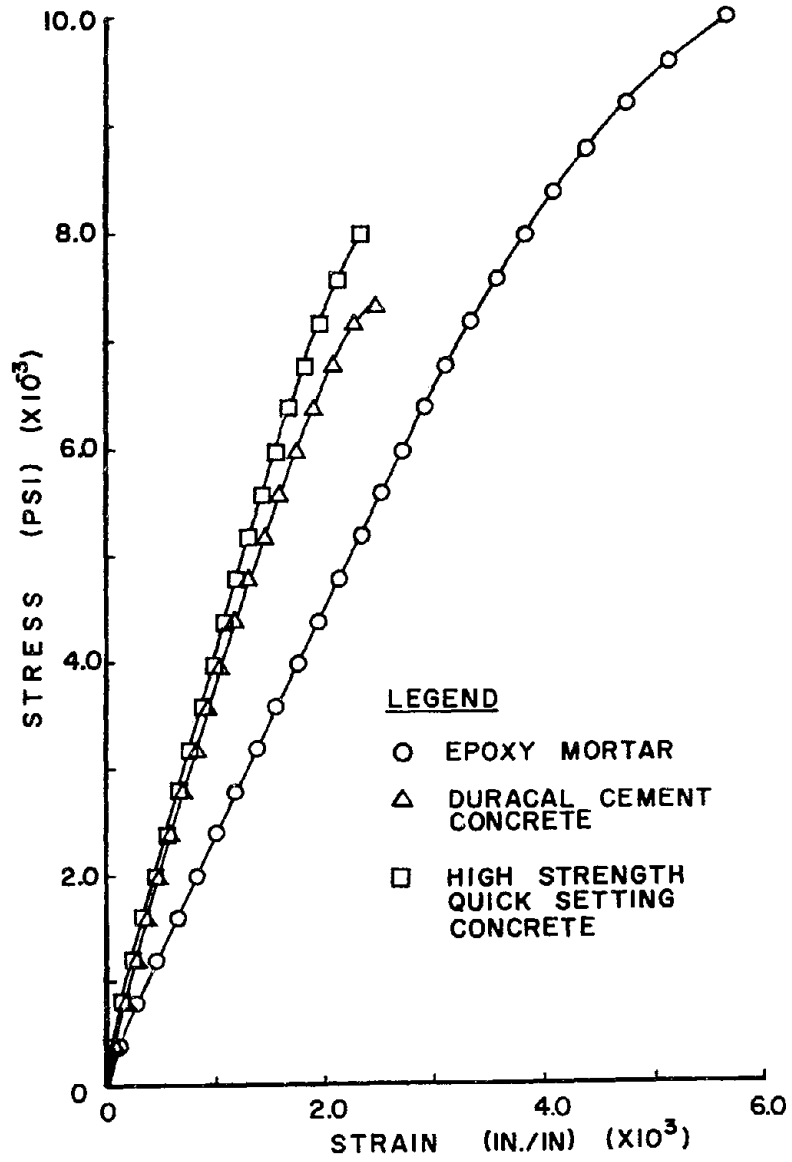


Figure 3. Stress vs. strain curves for high early strength materials at age 28 days.
 (1 ksi = 6.89 N/mm²)

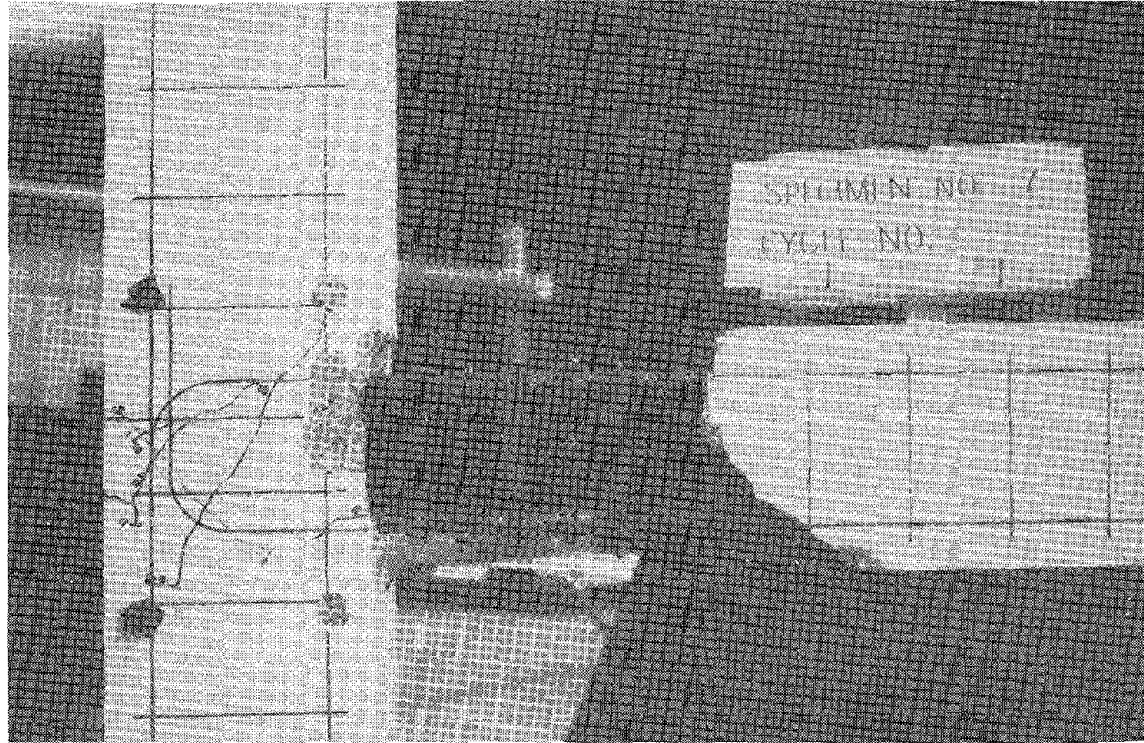


Figure 4. Specimen 7 in the upright position before repairs. Loose concrete was removed and stirrups were added after original testing.

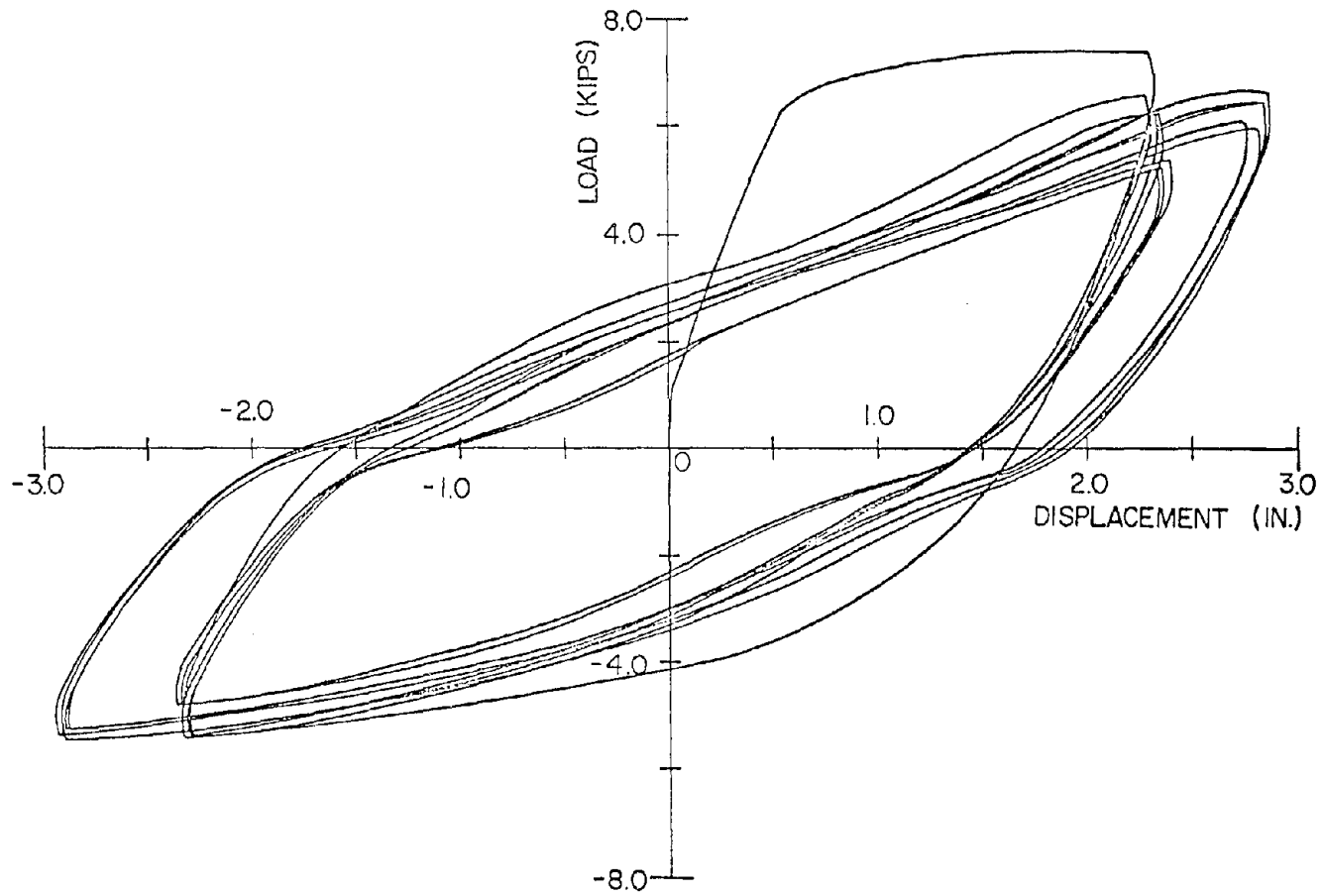


Figure 5a. Beam-tip force vs. deformation curves for original Specimen 2.
(1 kip = 4450 N and 1 in. = 2.54 cm)

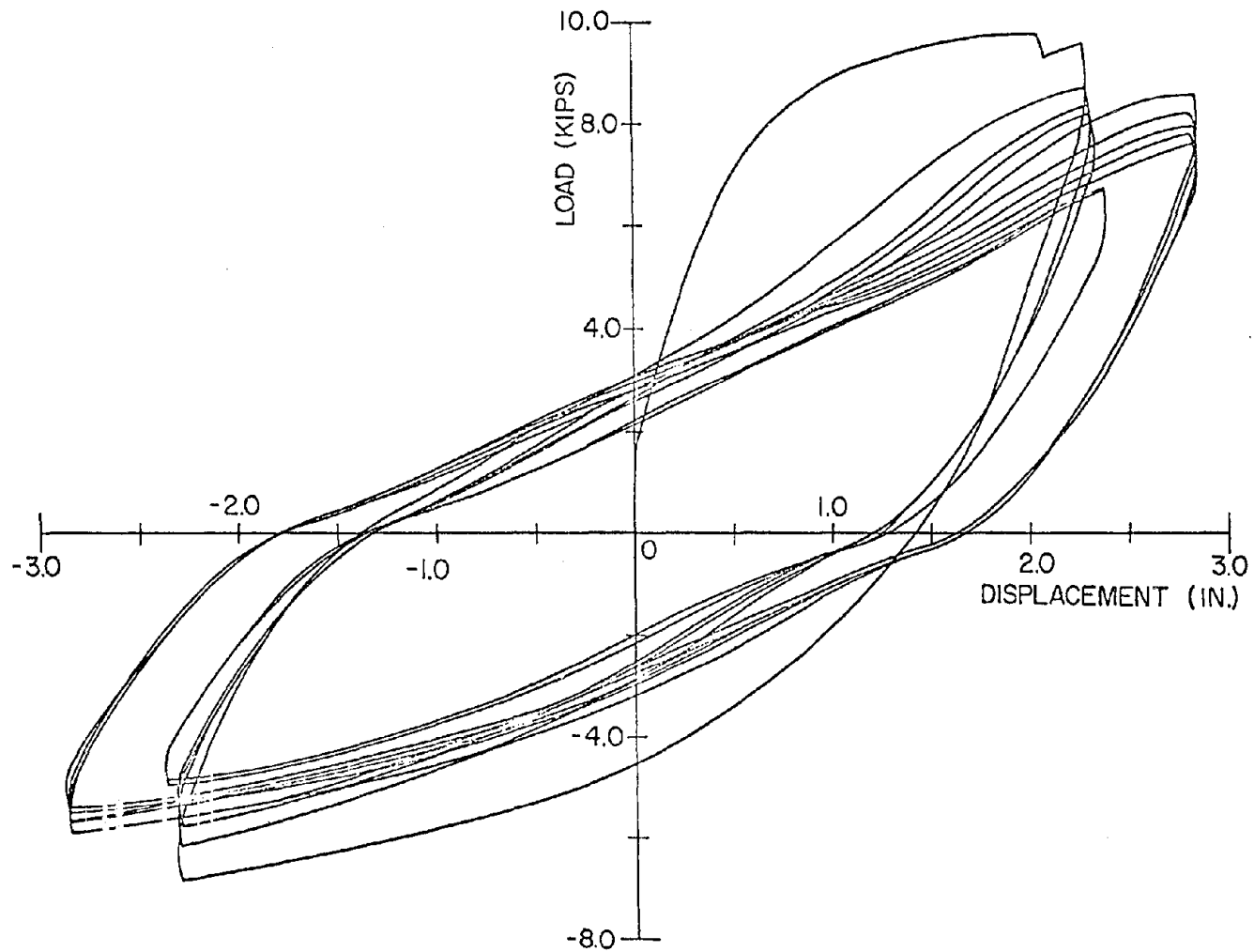


Figure 5b. Beam-tip force vs. deformation curves for repaired Specimen 2.
(1 kip = 4.45 kN and 1 in. = 2.54 cm)

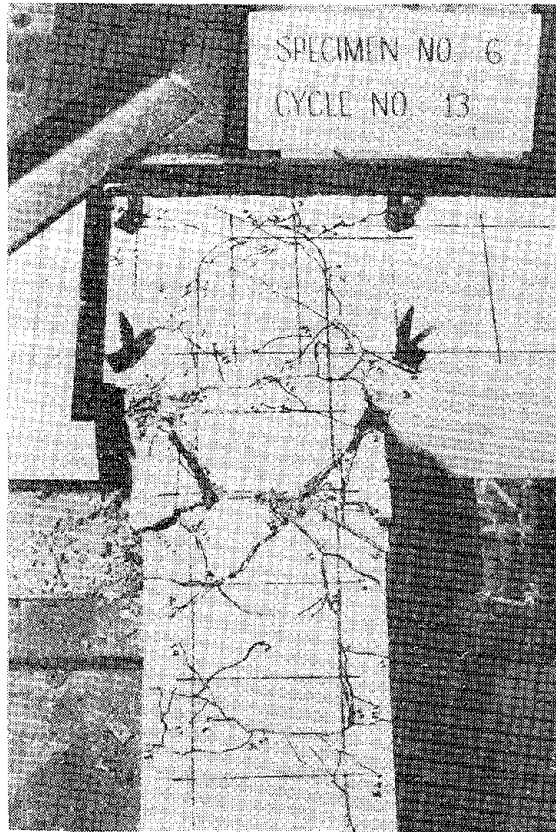


Figure 6a. Specimen 6 after original testing.

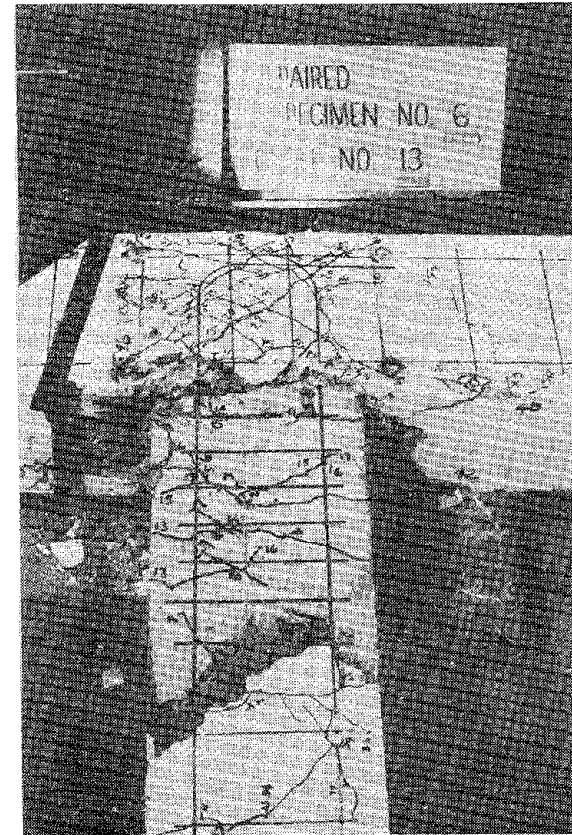


Figure 6b. Specimen 6 after retest.

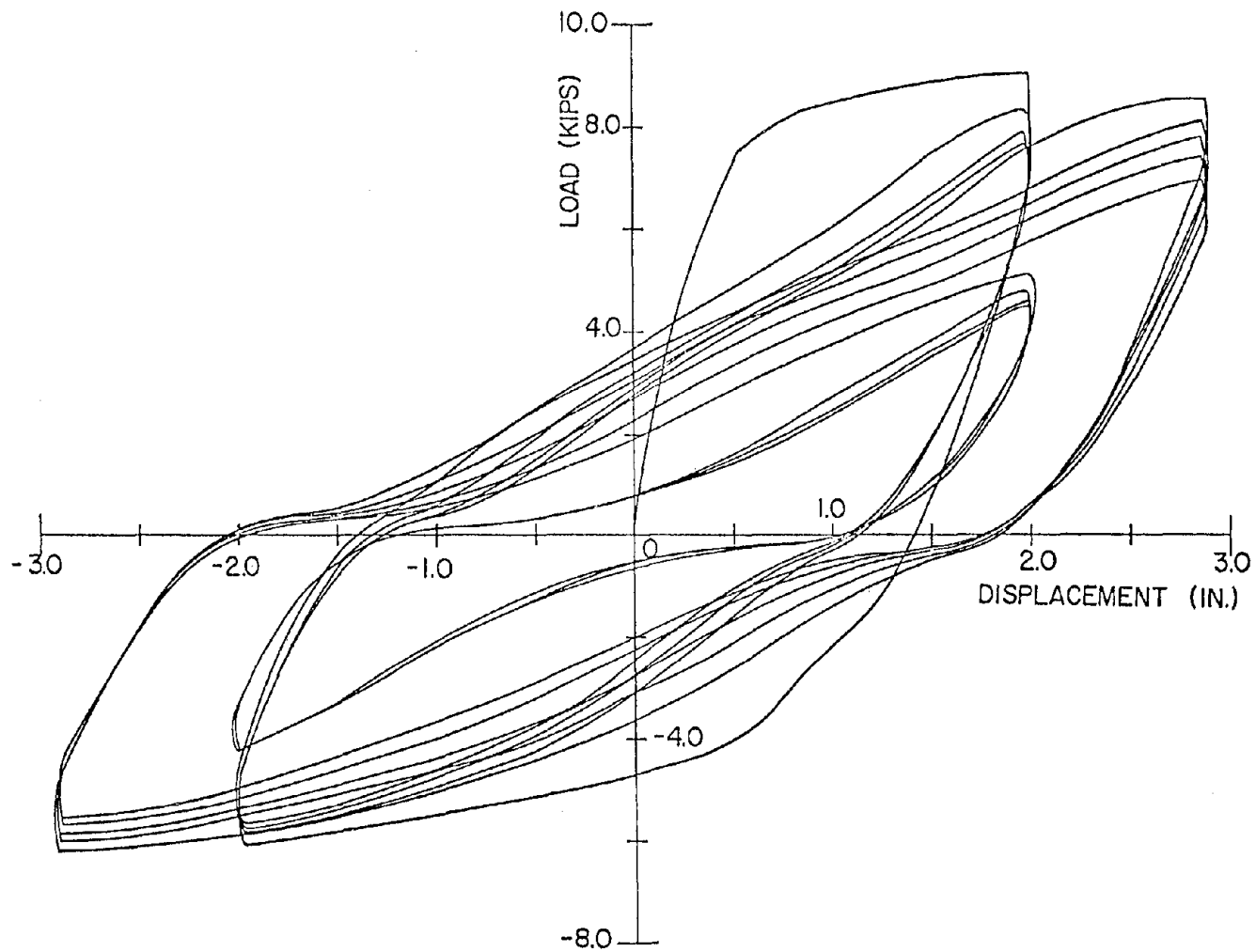


Figure 7a. Beam-tip force vs. deformation curves for original Specimen 6.
(1 kip = 4450 N and 1 in. = 2.54 cm)

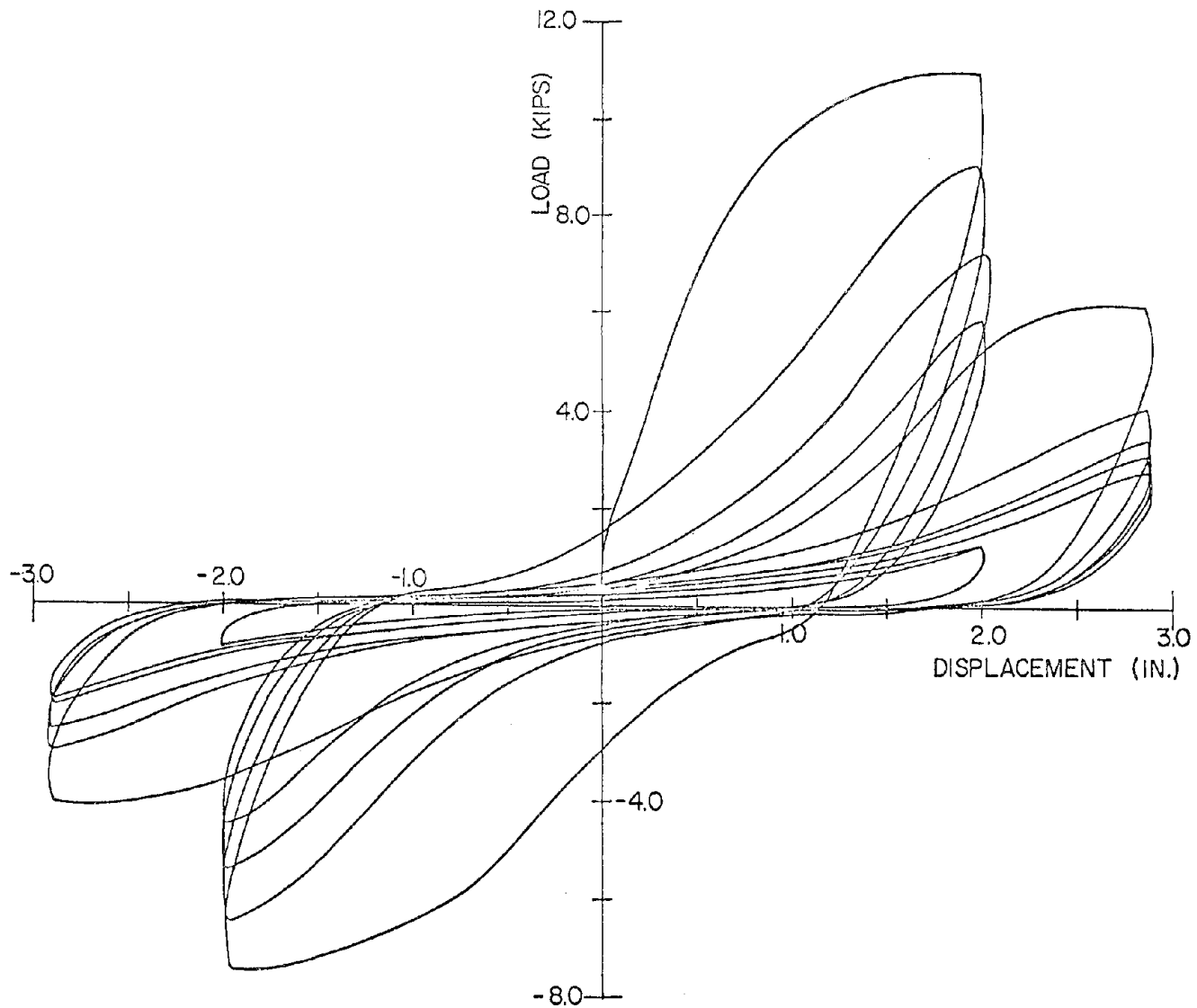


Figure 7b. Beam-tip force vs. deformation curve for repaired Specimen 6.
(1 kip = 4450 N and 1 in. = 2.54 cm)

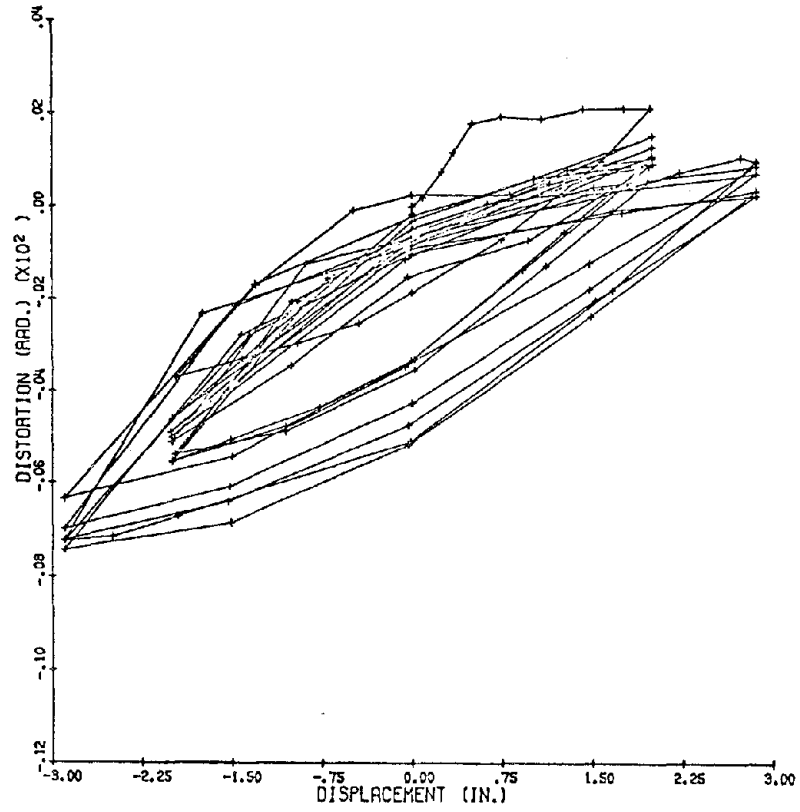


Figure 8a. Average joint distortion vs. beam-tip displacement for original Specimen 6. (1 in = 2.54 cm)

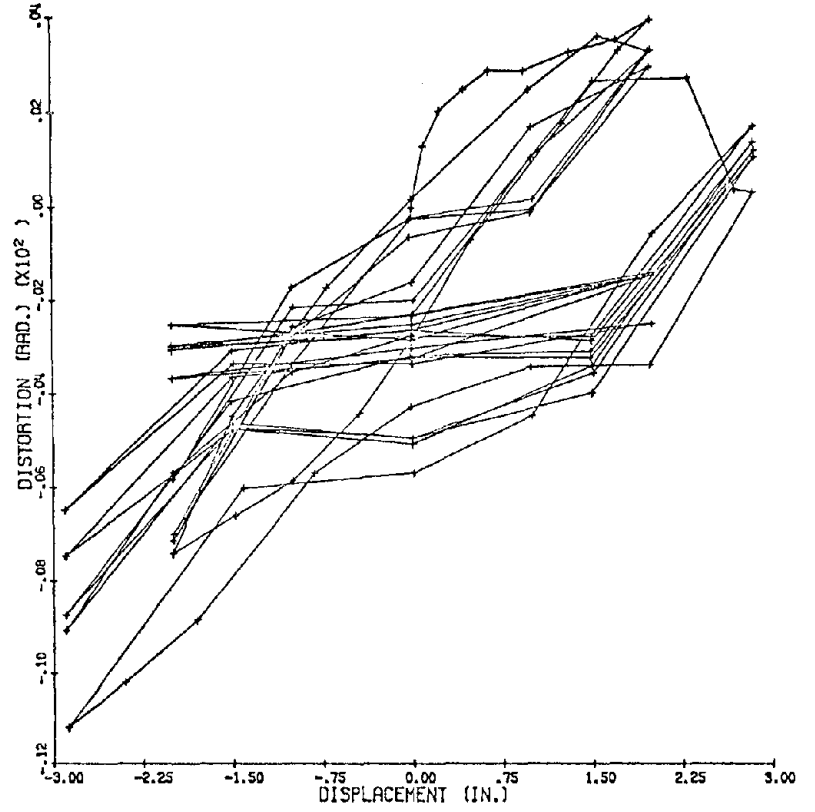


Figure 8b. Average joint distortion vs. beam-tip displacement for repaired Specimen 6. (1 in = 2.54 cm)

APPENDIX A

This appendix summarizes recent unpublished data developed by the senior author during his Ph.D. research. Complete data and analysis will be given in his dissertation to be completed in September 1975 (9). The primary objective of this investigation was to study the behavior of repaired reinforced concrete exterior beam-column subassemblages. The design of the original specimens was intended to model existing structures and the loading of each specimen was intended to simulate member response due to earthquake motions.

Design of Specimens. Two design criteria were used for the original specimens. The first design, referred to as "Type I Design" herein, used the 1971 American Concrete Institute (ACI) Building Code for nonseismic areas (excluding its Appendix A). This design was assumed to represent existing structures which were designed without considering seismic loading. The second design, referred to as "Type II Design" used the 1971 ACI Building Code including Appendix A (special provisions for the design of ductile moment-resisting space frames) along with recommendations from ACI-ASCE Joint Committee 352 for joints. Overall dimensions of the specimens and the details of the reinforcing steel for Type I and Type II designs are shown in Figs. A.1 and A.2 respectively. The primary difference in the members resulting from the two design criteria is the amount of shear reinforcement.

The specified concrete strength for the beam-column subassemblage was 4,000 psi (27.6 N/mm²). The nominal yield stress for the column's longitudinal reinforcement was 60,000 psi (423 N/mm²) and that for all the beam's main reinforcement was 40,000 psi (276 N/mm²). All shear reinforcement had a nominal yield of 40,000 psi (276 N/mm²).

Testing. The original and repaired specimens were tested in a horizontal position as shown in Fig. A.3. Rollers were placed vertically on each side of the column at both ends of the column to represent inflection points at the midstory height as the building deflects laterally. A constant axial force was applied to the columns and then the end of the beam was slowly deflected by a hydraulic actuator.

To obtain different degrees of damage during original testing, two displacement patterns were used to simulate moderate and severe earthquake loading as shown in Fig. A.4. Ductility as used in this paper is defined as beam-tip displacement divided by the displacement at the time of yielding of the beam's top bars. The uniform patterns illustrated in Fig. A.4 were utilized in studying the degradation characteristics of the specimens. For retesting, each repaired specimen was subjected to the same displacement pattern as used during original testing so that direct comparisons of the results

could be made.

Data Acquisition. For original testing, high elongation electrical resistance strain gages, applied to the reinforcing steel in and near the joint during construction, were used to indicate steel strains. During original testing and retesting, a continuous record of the beam-tip force vs. deformation was recorded and used to monitor the progress of the test. This data was later used to analyze the stiffness and load degradation, and energy dissipation capacity of the specimen. The shear distortion in the joint and the beam rotation measured relative to the column at a point 10 inches (25.4 cm) from the inside column face were both measured with Linear Variable Differential Transformers (LVDT).

Original Behavior. The type of design, column loading and the displacement pattern used for each specimen is given in Table A.1. The 40 kip (178,000 N) column load for Specimens 1 through 4 represented about 40 percent of the balanced axial load. For Specimens 2 and 4, a ductility of about five (instead of six) was attained during cycles 5 through 9 (see Fig. A.4(b)) due to actuator stroke limitation. The beam's shear span was decreased by moving the actuator in 5 1/2 inches (14 cm) for Specimens 5 through 8 to obtain a ductility of six during cycles 5 through 9 as shown in Fig. A.4(b).

For all the specimens, the primary damage occurred in the beam and most of the damage was attributed to flexural action. For the severe loading case minor crushing did occur in the beam's compression zone during the first quarter cycle of loading, but almost no drop in load resulted. X-type diagonal cracks were observed in the joint. Cracks could also be seen in the joint along the straight portion and around the hook of the beam reinforcement embedded in the joint indicating a loss of bond and high bearing stresses. A strain gage mounted on the reinforcing bar just before the hook indicated the bar was yielding at that location during cyclic motion. Specimens 5 through 8 had more cracks in the joint as compared to Specimens 1 through 4. However, it appeared the joints behaved well for all the specimens, especially the first four specimens which had a column load of 40 kips (178,000 N).

Repaired Behavior. Specimens 1 and 3 were repaired by epoxy injection technique after sustaining the moderate loading pattern in Fig. A.4(a). For Specimens 2 and 4, and 6 through 8, the removal and replacement technique was used to repair the specimens. (Specimen 5 was not repaired.) Table A.2 indicates the material used in each repair as well as their strengths at the time of retesting.

Briefly described below are observations made during the retest for each specimen.

- Specimens 1 and 3. Epoxy injected cracks remained closed. New cracks formed in the beam both within and adjacent to the repaired region. The joint continued to behave well.
- Specimen 2. Damage occurred in the repaired region. Overall behavior was similar to that of original testing. Joint continued to behave well.
- Specimen 4. Crushing occurred during the first quarter cycle and caused a sudden loss of the beam's cover in the compression zone. Flexural cracks in the repaired region offered little resistance to shear. Joint continued to behave well.
- Specimen 6. Repaired beam sustained minor flexural cracks. Major damage occurred in the joint. Cracks were also observed in the column.
- Specimen 7. The beam was repaired in two lifts with the second lift being the top one inch (2.54 cm) of the beam. Crushing occurred in the beam's compression zone during the first quarter cycle and caused partial loss of the beam's cover. Subsequent cycles caused separation of first and second lift at the epoxied construction interface. Joint showed additional cracking. Column continued to behave well.
- Specimen 8. Flexural cracks occurred in the repaired beam. No crushing was observed. Cracks were concentrated at the beam to column interface adjacent to the repaired region. Joint showed additional cracking. Column continued to behave well.

Table A.1. Design and Loading Parameters.
 (1 kip = 4450 N)

Specimen	Type of Design	Type of Loading	Column Load (kips)
1	II	Moderate	40
2	II	Severe	40
3	I	Moderate	40
4	I	Severe	40
5	II	Severe	0
6	I	Severe	0
7	I	Severe	0
8	I	Severe	0

Table A.2 Materials Used in Repair and Their Strengths at Time of Retest.
(1 ksi = 6.89 N/mm²)

Specimen	Sandblasted and Painted with Epoxy	Material	Compressive Strength (psi)
1	(Epoxy Injection)	Epoxy-Neat	12,000 (i)
2	Yes	High Early (Type III) Concrete	7,100
3	(Epoxy Injection)	Epoxy -Neat	12,000 (i)
4	No	High Strength Quick Setting Concrete	8,000
5	(Not Repaired)		
6	Yes	High Early (Type III) Concrete	7,000
7	Yes	Duracal Cement Concrete	6,000
8	Yes	Epoxy-Sand Mortar	9,700

(i) Supplied by Sika Chemical Corporation.

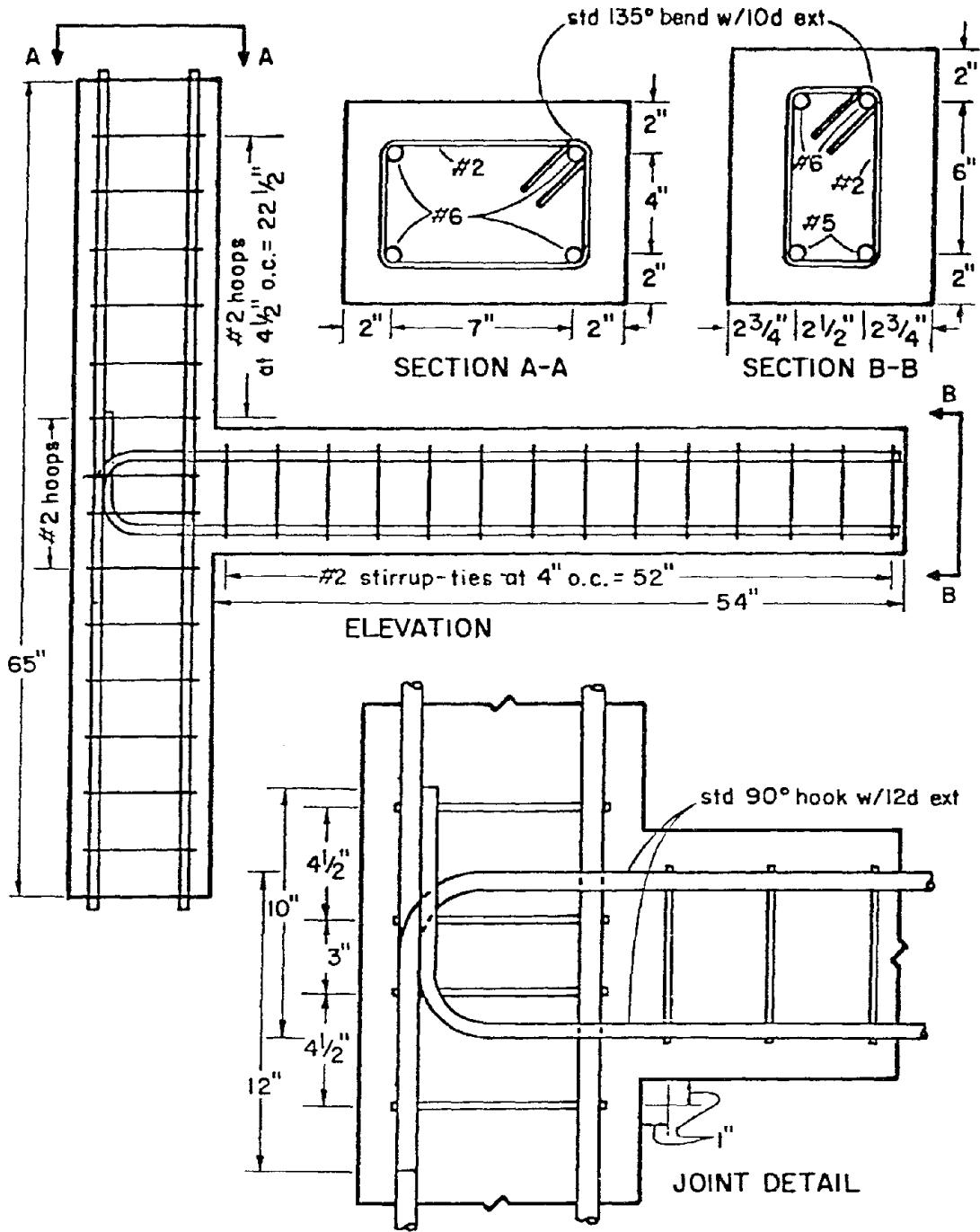


Figure A.1. Details of beam-column subassembly using Type I Design. (1 in. = 2.54 cm)

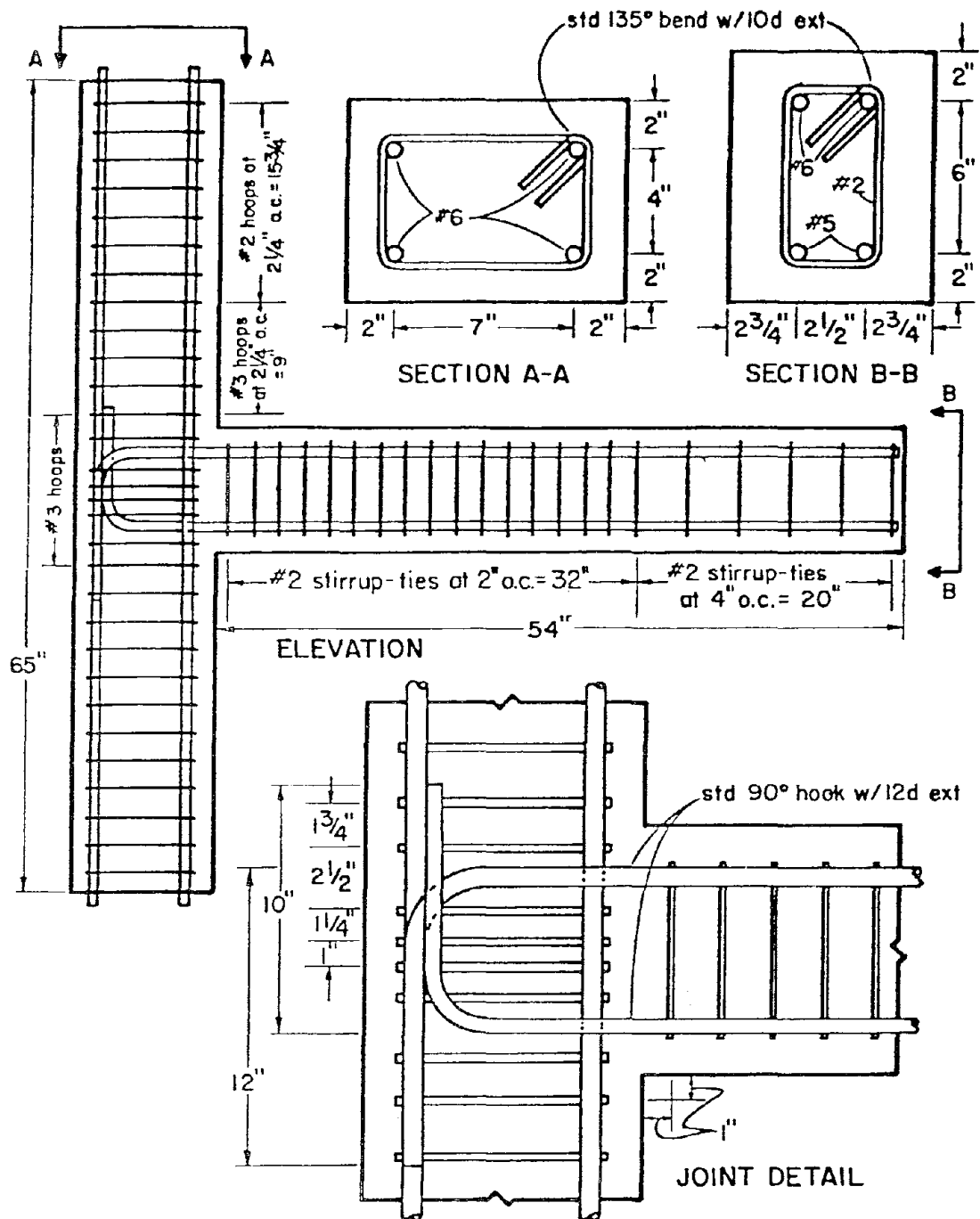


Figure A.2. Details of beam-column subassembly using Type II Design. (1 in. = 2.54 cm)

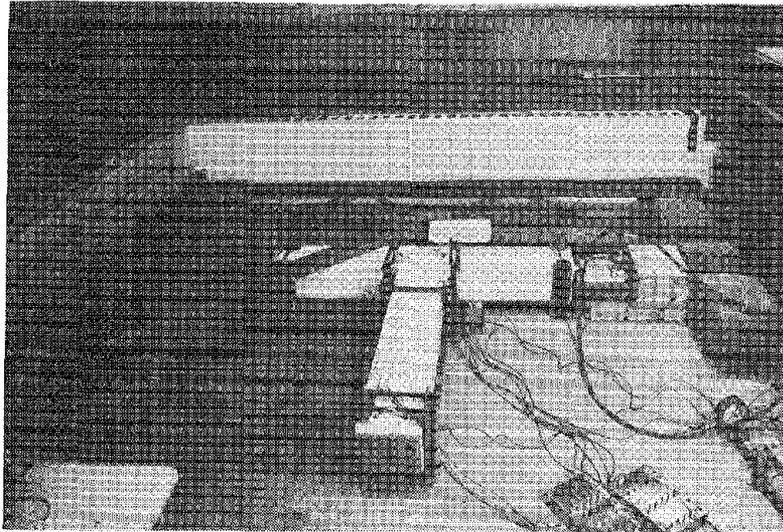


Figure A.3. Specimen in horizontal position during original testing and retesting.

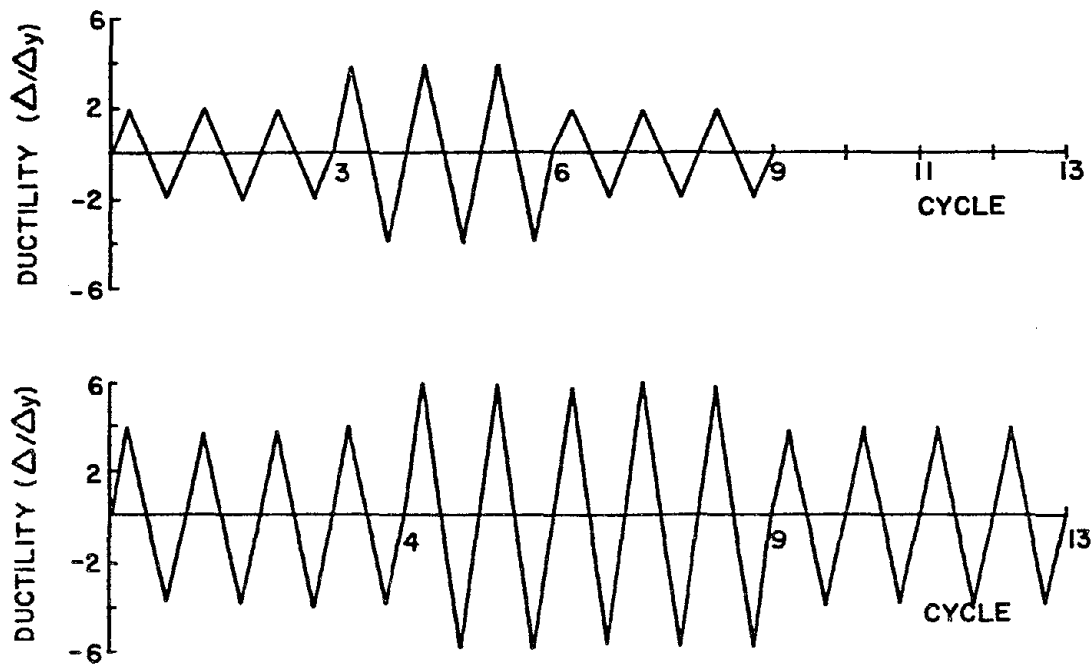


Figure A.4. Displacement pattern representing (a) moderate and (b) severe earthquake loading.



